SKELETON OF LATE PALEOCENE *PLESIADAPIS COOKEI*

DOUG M. BOYER and PHILIP D. GINGERICH

SKELETON OF LATE PALEOCENE *PLESIADAPIS COOKEI* (MAMMALIA, EUARCHONTA): LIFE HISTORY, LOCOMOTION, AND PHYLOGENETIC RELATIONSHIPS

DOUG M. BOYER
and
PHILIP D. GINGERICH

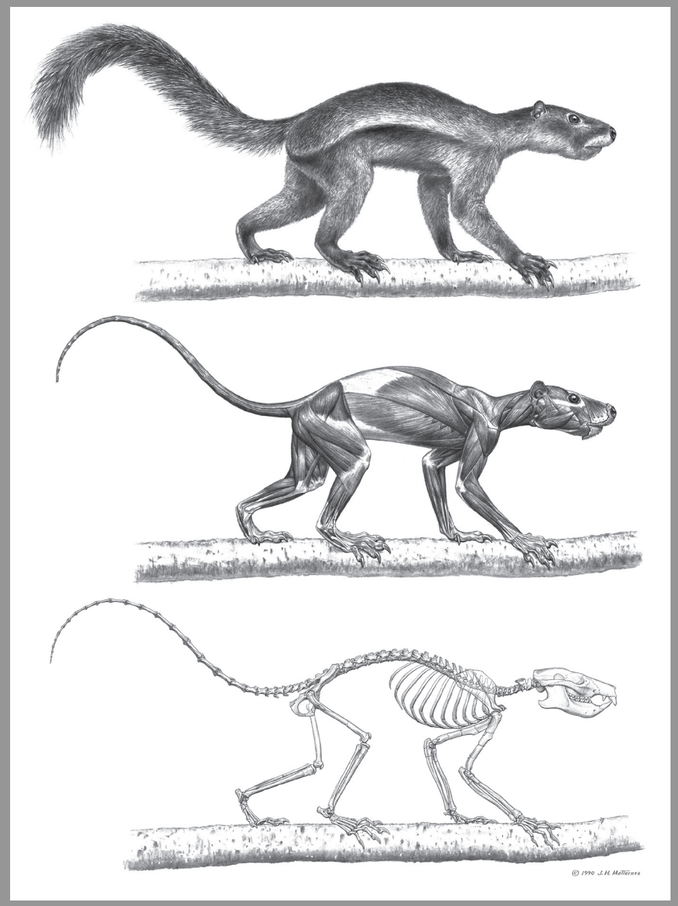

SKELETON OF LATE PALEOCENE *PLESIADAPIS COOKEI* (MAMMALIA, EUARCHONTA): LIFE HISTORY, LOCOMOTION, AND PHYLOGENETIC RELATIONSHIPS

PAPERS ON PALEONTOLOGY — RECENT NUMBERS

26. The Clarkforkian Land-Mammal Age and Mammalian Faunal Composition across the Paleocene-Eocene Boundary *by Kenneth D. Rose* (1981)

27. The Evolutionary History of Microsyopoidea (Mammalia, ?Primates) and the Relationship between Plesiadapiformes and Primates *by Gregg F. Gunnell* (1989)

28. New Earliest Wasatchian Mammalian Fauna from the Eocene of Northwestern Wyoming: Composition and Diversity in a Rarely Sampled High-Floodplain Assemblage *by Philip D. Gingerich* (1989)

29. Evolution of Paleocene and Eocene Phenacodontidae (Mammalia, Condylarthra) *by J. G. M. Thewissen* (1990)

30. Marine Mammals (Cetacea and Sirenia) from the Eocene of Gebel Mokattam and Fayum, Egypt: Stratigraphy, Age, and Paleoenvironments *by Philip D. Gingerich* (1992)

31. Terrestrial Mesonychia to Aquatic Cetacea: Transformation of the Basicranium and Evolution of Hearing in Whales *by Zhexi Luo and Philip D. Gingerich* (1999)

32. Fishes of the Mio-Pliocene Ringold Formation, Washington: Pliocene Capture of the Snake River by the Columbia River *by Gerald R. Smith*, *Neil Morgan*, *and Eric Gustafson* (2000)

33. Paleocene-Eocene Stratigraphy and Biotic Change in the Bighorn and Clarks Fork Basins, Wyoming *by Philip D. Gingerich (ed.) and others* (2001)

34. Form, Function, and Anatomy of *Dorudon atrox* (Mammalia, Cetacea): An Archaeocete from the Middle to Late Eocene of Egypt *by Mark D. Uhen* (2003)

35. The Tiffanian Land-Mammal Age (Middle and Late Paleocene) in the Northern Bighorn Basin, Wyoming *by Ross Secord* (2008)

36. Earliest Eocene Mammalian Fauna from the Paleocene-Eocene Thermal Maximum at Sand Creek Divide, Southern Bighorn Basin, Wyoming *by Kenneth D. Rose, Amy E. Chew, Rachel H. Dunn, Mary J. Kraus, Henry C. Fricke, and Shawn P. Zack* (2012)

37. Late Eocene Sea Cows (Mammalia, Sirenia) from Wadi Al Hitan in the Western Desert of Fayum, Egypt *by Iyad S. Zalmout and Philip D. Gingerich* (2012)

38. Skeleton of Late Paleocene *Plesiadapis cookei* (Mammalia, Euarchonta): Life History, Locomotion, and Phylogenetic Relationships *by Doug M. Boyer and Philip D. Gingerich* (2019)

Museum of Paleontology
The University of Michigan
Ann Arbor, Michigan 48109-1085

SKELETON OF LATE PALEOCENE *PLESIADAPIS COOKEI* (MAMMALIA, EUARCHONTA): LIFE HISTORY, LOCOMOTION, AND PHYLOGENETIC RELATIONSHIPS

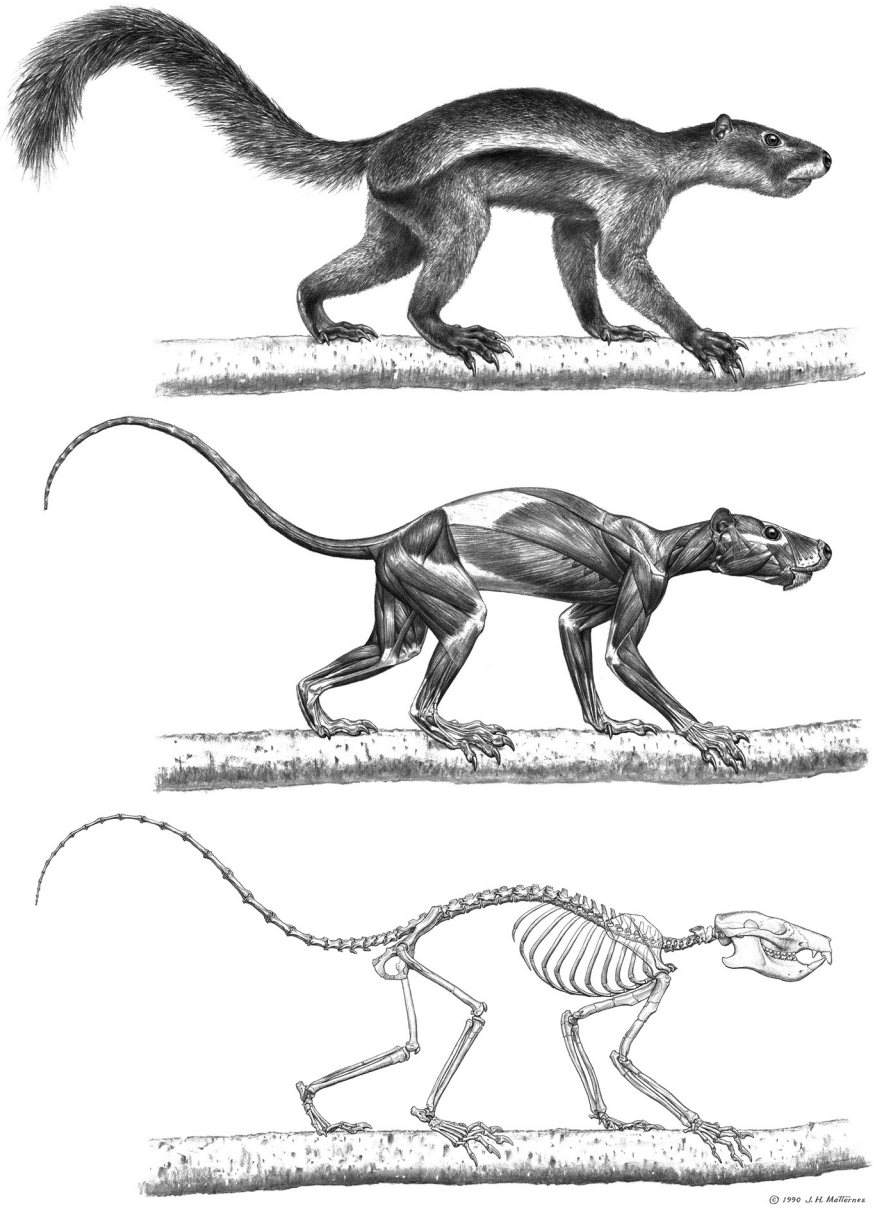

Frontispiece: Jay H. Matternes' restoration of the skeleton, musculature, and pellage of *Plesiadapis cookei* based on UM 87990. Images ©Jay H. Matternes. Used by permission of the artist.

SKELETON OF LATE PALEOCENE *PLESIADAPIS COOKEI* (MAMMALIA, EUARCHONTA): LIFE HISTORY, LOCOMOTION, AND PHYLOGENETIC RELATIONSHIPS

Doug M. Boyer

Department of Evolutionary Anthropology,
Biological Sciences Building, 130 Science Drive,
Duke University
Durham, North Carolina 27708
doug.boyer@duke.edu

Philip D. Gingerich

Department of Earth and Environmental Sciences
and Museum of Paleontology
University of Michigan
Ann Arbor, Michigan 48109-1085
gingeric@umich.edu

UNIVERSITY OF MICHIGAN
PAPERS ON PALEONTOLOGY NO. 38

2019

Papers on Paleontology No. 38

Museum of Paleontology
The University of Michigan
Ann Arbor, Michigan 48109-1085

Matt Friedman, Director

Jeffrey A. Wilson, Editor

TABLE OF CONTENTS

LIST OF FIGURES

LIST OF FIGURES (Cont'd)

LIST OF TABLES

APPENDIX FIGURES AND TABLES

APPENDIX I: CRANIAL AND DENTAL FIGURES AND MEASUREMENTS

APPENDIX II: POSTCRANIAL MEASUREMENTS

APPENDIX FIGURES AND TABLES (Cont'd)

APPENDIX FIGURES AND TABLES (Cont'd)

APPENDIX V: CRANIA OF OTHER NORTH AMERICAN AND EUROPEAN PLESIADAPIDAE

APPENDIX VI: CT SCAN DOCUMENTATION

ABSTRACT

Plesiadapis cookei is a large-bodied plesiadapiform euarchontan (and potential stem primate) known from many localities of middle Clarkforkian North American Land Mammal age, late Paleocene epoch, in the Clarks Fork Basin of northwestern Wyoming. Most specimens are gnathic and dental remains, but one specimen, University of Michigan Museum of Paleontology (UM) 87990, is a relatively complete skeleton preserving the skull, much of the axial skeleton, forelimbs, and hind limbs. Description, measurement, and illustration of the UM 87990 skeleton of *P. cookei* provides new information enabling analysis of proportions within the skeleton and comparisons across a range of primates and related mammals.

The skull of UM 87990 includes much of the upper and lower dentition, rostrum, braincase, and basicranium. The dental formula is 2.0.2.3 / 1.0.2.3. Composition of the auditory bulla as petrosal, ectotympanic, or entotympanic, is uncertain due breakage and some suture-like structures rimming the promontorium. *P. cookei* had a very small posterior carotid foramen and probably lacked a functioning internal carotid artery.

The axial skeleton of UM 87990 is represented by five cervical, 12 thoracic, and six lumbar vertebrae. The sacrum is complete with three vertebrae. There are 17 caudal vertebrae preserved, with at least three anterior positions missing. Thus there were at least 20 caudal vertebrae. Caudal vertebral proportions indicate the tail of *P. cookei* was relatively long. We expect the full plesiadapid vertebral formula to have been 7.13.6.3.24, matching the formula in *Tupaia* and the median formula in primates. Seven sternebrae are preserved, possibly representing the complete series. Ribs are slender and lack any notable anteroposterior expansion.

The pectoral girdle and forelimb of UM 87990 include clavicles, much of one scapula, humeri, ulnae, radii, and a number of carpal bones. Two sets of metacarpals, one set slightly longer than the other, were found in association with UM 87990. One set must have come from a partial skeleton of *Uintacyon* (UM 88187) that was preserved next to UM 87990. Manual proximal phalanges have long, low flexor sheath ridges. Intermediate phalanges have narrow, deep shafts, and distal articular surfaces suggesting flexed distal interphalangeal joints. Distal phalanges are all relatively long and distinctly falciform.

The pelvic girdle and hind limb of UM 87990 include well-preserved innominates, femora, tibiae, incomplete fibulae, and most tarsal bones (navicular and entocuneiform excepted). Metatarsals are identified based on their size and form in comparison to metatarsals described for other plesiadapids. Pedal phalanges are similar to manual phalanges but can be distinguished on the basis of size and a more neutrally flexed distal interphalangeal joint.

A principal components analysis of body proportions places *P. cookei* and other plesiadapiforms close to *Tupaia*, sciurids, and callitrichid primates. *P. cookei* is not particularly close to the lorisine slow climber *Nycticebus*, nor is it close to the colugo *Cynocephalus*. The postcranial skeleton of *P. cookei* suggests that it was a forest-dwelling arboreal climber primarily adapted, and possibly constrained, to large diameter vertical and horizontal supports. Headfirst descent of large supports was likely accomplished using claw-clinging with a reversed (supinated) foot. *P. cookei* would have been more cautious and less scansorial in its movements than smaller-bodied plesiadapids.

The body weight of *P. cookei* is predicted to be 1,799 to 2,052 g, based on long bone lengths and diameters of UM 87990. Brain weight is predicted to be close to 5 g based on a partial endocast and three-dimensional model. Comparison of observed with expected brain size for a mammal the size of *P. cookei* yields an encephalization quotient in the range of 0.257 to 0.281 and an encephalization residual in the range of −1.958 to −1.831. Both indicate that the brain of *P. cookei* was just over one-quarter of the size expected for an average living mammal of its body weight. A smaller than expected brain is a common feature of many Paleogene mammals.

We interpret UM 87990 to be a male individual of *P. cookei*, because the innominate has a relatively wide superior pubic ramus like that of male individuals in a range of rodents and primate species. UM 87990 has a fully erupted adult dentition, little tooth wear, and long-bone epiphyseal fusion limited to the elbow. We have no independent means of determining sexual maturity, and thus can only interpret UM 87990 as an advanced and nearly full-grown subadult, or as a full-grown young adult.

Cladistic analysis of craniodental characters and a geographic character indicates that Plesiadapidae is monophyletic, with the carpolestid *Elphidotarsius* forming the sister taxon of the group. *Pronothodectes* is paraphyletic but its species are the most basal within Plesiadapidae. *Chiromyoides*, and *Platychoerops* are monophyletic. *Plesiadapis* itself is polyphyletic, with *P. cookei* recovered as the sister taxon of *Platychoerops*. Our reconstructed phylogeny for the family is largely congruent with that of Gingerich (1976) based on stratophenetic methodology, but less resolved. A stratocladistic analysis run by adding a stratigraphic character to the craniodental and geographic character set is more resolved than our strict consensus using morphology and geography alone, and it is also more divergent from Gingerich's (1976) hypothesis in certain ways. Some notable results include recovery of *Nannodectes intermedius* as the common ancestor of all non-*Pronothodectes* plesiadapids and recovery of *Platychoerops antiquus* as ancestral to all later *Platychoerops* species.

On a broader scale, cladistic analysis of higher-level taxa, with scorings for Plesiadapidae revised based on optimization of the ancestral node at the species level, indicates that plesiadapids and carpolestids exhibit a greater number of identical character states than previously thought, though some previously proposed synapomorphies were refuted. Even so, analysis of combined data from dentition, cranium, and postcrania still robustly support a link between plesiadapids, saxonellids, and carpolestids (Plesiadapoidea) and does not contradict previous hypotheses suggesting a special relationship of plesiadapoids to euprimates (Euprimateformes).

INTRODUCTION

Plesiadapis is one of the most common mammals found in continental middle and late Paleocene fossil localities in Europe and North America. It has a stratigraphic range spanning the Selandian and Thanetian geological stages and ages of the Paleocene epoch, and is known on both continents from approximately 62 to 56 million years before present. *Plesiadapis* ranged through much of the Tiffanian and Clarkforkian land-mammal ages in North America. It survived longer in Europe, ranging through the early part of the Ypresian geological stage and age. In Europe it preceded and ranged through the Cernaysian and part of the Neustrian land-mammal ages (Vandenberghe et al., 2012).

Plesiadapis cookei Jepsen, 1930, is the largest and latest appearing species of Plesiadapidae known from the Paleocene of North America (Gingerich, 1976). Most recovered specimens are maxillae, dentaries, or isolated teeth, but University of Michigan Museum of Paleontology (UM) 87990 includes a partial cranium, dentaries, and much of the postcranial skeleton (Fig. 1). The skull of UM 87990 is the most complete known for a North American plesiadapid, and the skeleton of UM 87990 is the most complete known for the family. In some ways (for instance, in having most teeth in place) the new skull is even better preserved than the nearly complete skulls of *Plesiadapis tricuspidens*, a large-bodied species from the Paris Basin in France (Russell, 1964; Gingerich, 1976; Boyer et al., 2010a; 2012a,b). Many postcranial elements are known for *P. tricuspidens*, (Russell, 1964; Szalay et al., 1975), but most are isolated elements that were not preserved in association with cranial or dental remains nor with each other. The skull and skeleton of UM 87990 are important data for exploring the diet, life history, and locomotor behavior of *P. cookei*, and for testing phylogenetic hypotheses related to early primate evolution.

The diet of a mammal depends on body size and on the form and configuration of the dentition. The life history of a mammal depends on the state of development of critical characteristics and on the sequence of developmental events related to growth, survival, and reproduction during a life, from birth through death. A full understanding of life history requires a level of understanding of population biology that is beyond most paleontological studies. However, important characteristics that reflect aspects of life history can be inferred from fossils, such as brain size and form, encephalization (i.e., size of the brain in relation to body size), sexual dimorphism, and the rate and pattern of ontogenetic growth. The skeleton of UM 87990 enables a robust estimation of body size. UM 87990 includes much of the dentition of *P. cookei*, and parts not known in this specimen are preserved in other specimens of the species. UM 87990 preserves a partial endocranial cast documenting some aspects of brain morphology and enabling an estimate of encephalization. Sex can be predicted from the configuration of the pelvis. The stage of tooth eruption can be determined for UM 87990, which, with the stage of fusion of long bone epiphyses in the skeleton, enables both discussion of its ontogenetic stage of development and estimation of its rate of growth.

The habitual posture and locomotion of a mammal is related to its body size, to its trunk and limb proportions, and to the form of limb articulations and range of motion between articulating elements of the skeleton. Relative completeness of the UM 87990 skeleton enables determination of trunk and limb proportions, as well as assessment of likely habitual configurations of limb bone joints and their.

Previous analyses of the phylogenetic relationships of *Plesiadapis* have been based on its geological age relative to other taxa, on the configuration of the dentition as a whole, and on the form of individual teeth. Earlier analyses can now be extended by adding cranial characteristics of UM 87990 and a large number of postcranial traits. Generally speaking, the skeleton of *P. cookei* is relevant to assessing predictions generated by cladistic hypotheses that postulate plesiadapids to be a sister group of carpolestids and a close relative of crown group primates (Fig. 2; Bloch and Boyer, 2002; 2003; Kirk et al. 2003; Bloch and Silcox, 2006).

HISTORY OF STUDY

Study of the cranium and postcranial skeleton of *Plesiadapis* and its relatives has a long history, which is worth reviewing to place the present study in context. See below for a list of institutional abbreviations (AMNH, etc.).

Cranium

Cranial anatomy is known for seven plesiadapid species: (1) *Pronothodectes gaoi* (Boyer et al., 2012a); (2) *Nannodectes gidleyi* (Matthew, 1917; Simpson, 1935; MacPhee et al., 1983; Boyer et al. 2012a); (3) *Plesiadapis insignis* (Piton, 1940; Simpson, 1948; Russell, 1967; Gingerich, 1976); (4) *Plesiadapis tricuspidens* (Russell, 1959, 1964; Simons, 1960; Gingerich, 1971, 1976; Szalay, 1971, 1972b; Szalay and Delson, 1979; MacPhee and Cartmill, 1986; Szalay et al., 1987;

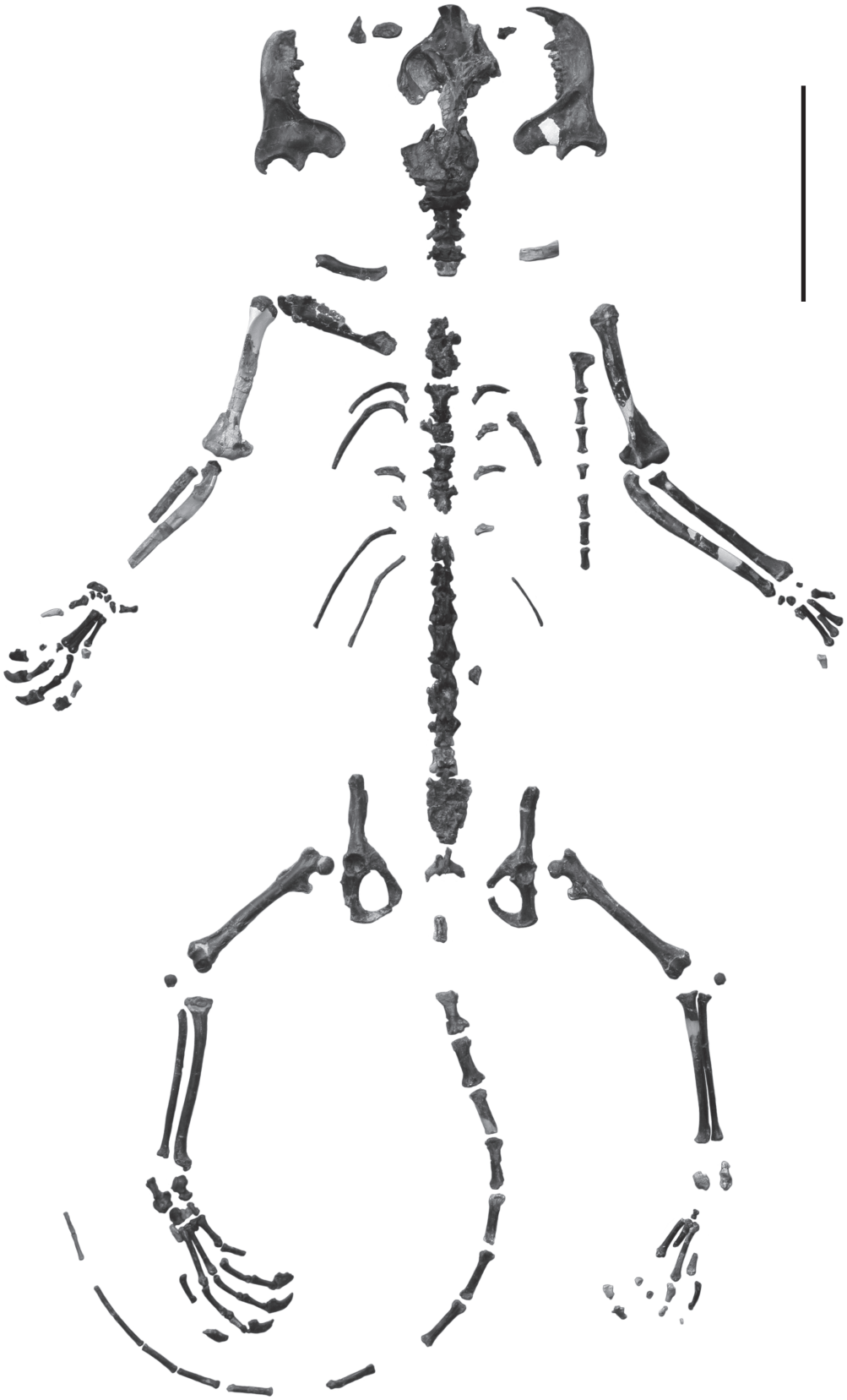

FIGURE 1.— Skeleton of *Plesiadapis cookei*, UM 87990), from locality SC-117 in the Clarks Fork Basin of Wyoming. Scale bar is 10 cm.

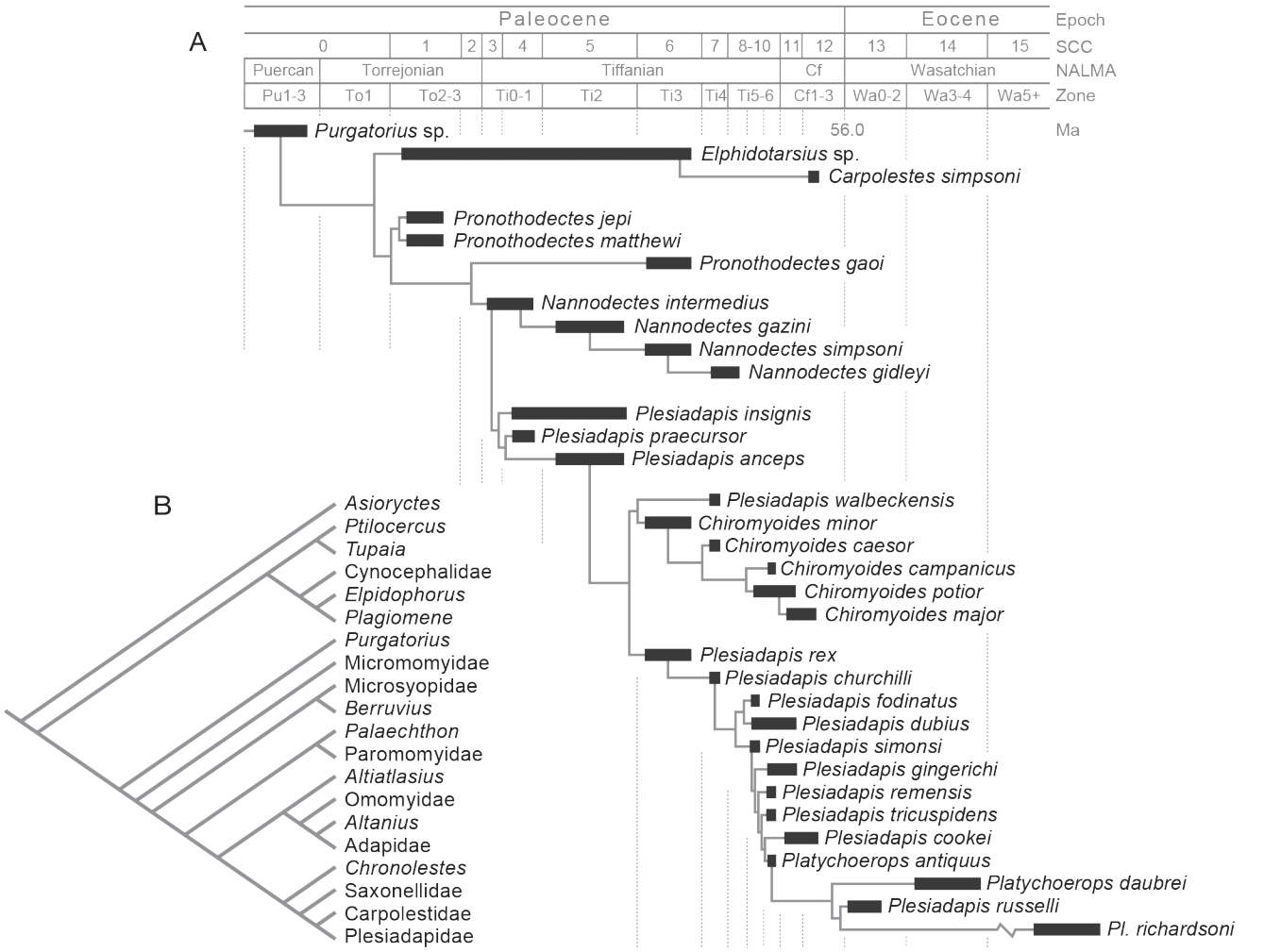

FIGURE 2.— Phylogenetic relationships of Plesiadapidae. **A**, Species-level phylogeny of 28 species of Plesiadapidae. This is a novel result from the current study where a cladistic character matrix consisting of 71 morphological characters (appendix tables A-IV-1 to A-IV-5), as well as a geographic character and stratigraphic character were analyzed using the stratocladistics software StrataPhy (Marcot and Fox, 2008). Note that the morphological character matrix is similar to that published in other studies (Boyer et al., 2012a, b) but modified to better represent morphology, correct errors, and with the addition of two new characters reflecting lower premolar features (appendix table A-IV-1 and A-IV-2: characters 70-71). The analysis recovered 716 equally parsimonious trees representing 30 distinct cladistic topologies. However, MacClade's (v4.08) computation of character debt found 12 out of these 716 to be of shorter length than the others. These 12 trees represented two topologies differing only in the position of *Nannodectes intermedius*. In addition, these 12 trees differed in whether *Pronothodectes matthewi*, *Pronothodectes jepi*, and *Platychoerops richardsoni* were ancestors or terminals. The tree depicted here is the strict consensus of the two topologies with ambiguous ancestralizations omitted. The strict consensus of the 30 distinct topologies recovered by StrataPhy differs from that shown in part A in several ways. 1) *Pr. jepi* and *Pr. matthewi* are not sisters but form a tritomy together with a clade comprising the rest of Plesiadapidae. 2) *Pronothodectes gaoi* is not distinguished from the node above it. That is, *Pr. gaoi*, *N. intermedius*, a clade of remaining *Nannodectes* species, and a clade of the remaining non-*Pronothodectes*, non-*Nannodectes* plesiadapids form a polytomy. 3) *Pl. richardsoni, Platychoerops russelli*, and *Platychoerops daubrei* form a tritomy. **B**, Relationship of Plesiadapidae to other supra-specific taxa of Euarchonta (Bloch et al. 2007). Note the hypothesized sister-group relationship of Plesiadapidae and Carpolestidae.

Kay et al., 1992; Bloch and Silcox, 2006; Boyer et al., 2010a; 2012a; Orliac et al., 2014); (5) *Plesiadapis anceps* (Gingerich, 1976; Boyer et al., 2012a); (6) *Nannodectes intermedius* (Gingerich et al., 1983; MacPhee et al., 1983; Boyer et al., 2012a); and (7) *P. cookei* (Gingerich and Gunnell, 2005; Boyer et al., 2010a; 2012a). Here we review chronologically the publications examining specimens pertaining to these species.

Historically there has been a great deal of attention paid to the tympanic bulla, the bone enclosing the middle ear cavity, and to the route, presence, and size of the internal carotid

neurovasculature. These are thought to provide important evidence bearing on the phylogenetic relationship of plesiadpiforms to extant primates. Specifically extant primates are apparently unique among mammalian orders in having a bulla that is developmentally comprised of the petrosal bone (MacPhee, 1981). If some plesiadapiforms shared this trait, it would be strong evidence of a close phylogenetic relationship. In addition, extant primates generally retain some component of the internal carotid system that reaches the endocranium via an intrabullar route. Even strepsirrhines that do not rely on the internal carotid artery for blood still receive sympathetic innervation for cranial structures through this route. Therefore, stem members of primates are thought to have retained a well developed internal carotid supply. In this context, reduction or loss of the internal carotid system counts as a strike against the hypothesis that a given fossil is a stem primate (e.g., MacPhee et al., 1983).

Matthew (1917) and Simpson (1935) provided the initial descriptions of parts of a plesiadapid skull and associated dentition (AMNH 17170–17173, 17379, 17387–17389, 17404) from the Mason Pocket locality in late Paleocene strata of the Nacimiento Formation, San Juan Basin, Colorado. Whereas Matthew (1917) referred to these specimens as a new species, *Nothodectes gidleyi*, Simpson (1935) considered them to belong to *Plesiadapis*, as *P. gidleyi*. Much later, Gingerich (1976) attributed these same specimens to *Nannodectes* as *N. gidleyi*. Matthew (1917) and Simpson (1935) were able to illustrate teeth at all positions in the dentition, including some deciduous teeth, but further details of cranial anatomy were limited to the palate, orbit, lacrimal, and basicranium. Simpson (1935) reported that the auditory bulla was completely ossified, small, and little inflated, with no external auditory meatus. He noted that the internal carotid artery did not enter anywhere along the medial side of the bulla, inferring that it probably entered at the posteroexternal corner of the bulla. No illustration of the basicranium was provided.

Piton (1940) named *Menatotherium insigne* for a skeleton from the maar lake at Menat in the Department of Puy-de-Dôme in central France. The specimen is crushed flat, and much of it is paper-thin. It originally included the whole body of the animal, not only the complete, articulated skeleton but also the body outline and hair, preserved as a coating of carbonaceous material. The principal part of the specimen is in the collection of the Faculté des Sciences of Clermont-Ferrand and shows the head and most of the body (Simpson, 1948). A less complete counterpart is in the Naturhistorisches Museum in Basel. Piton (1940) considered whether *Menatotherium* might be a rodent, like the first Menat mammalian skeleton reported by Launay (1908; see below), but he rejected this idea because *Menatotherium* retained upper canines not present in rodents. Piton finally interpreted *Menatotherium* as a tillodont because of what he (erroneously) thought were ever-growing incisors. Simpson (1948) restudied Piton's specimen and recognized that the enlarged incisors of *Menatotherium* resembled those of Plesiadapidae, but regarded the ordinal and family affinities to be uncertain. Russell (1967) used the clever trick of reversing left and right stereophotographs to generate a positive image of the dental impressions and was able to see the teeth of *Menatotherium insigne* in more detail than had been possible previously. Thus, he was able to identify it as an early species of *Plesiadapis*. Poor preservation of the cranium precluded any real description beyond the overall shape and absence of a postorbital bar.

Russell (1959) provided a preliminary description of a more complete plesiadapid skull, *Plesiadapis tricuspidens* (MNHN CR 125), from the locality of Berru near Reims in late Paleocene strata of the Paris Basin in northern France. As summarized by Gingerich (1976), Russell described the general form of the skull, interpreted it as preserving large premaxillae that contact the frontals, and otherwise focused on the basicranium. Russell (1959) stated that the skull preserved a posterior carotid canal, and that there were two subequal grooves on the promontorium for the promontorial and stapedial arteries. He also stated that the bullae appeared to have been derived from the petrosal. This contribution included a labeled sketch and corresponding photographs of the skull in dorsal and ventral views.

Simons (1960: fig. 1) reviewed the find of MNHN CR 125 and provided a reconstruction of the skull in lateral view that contains "correction for distortion." Simons (1960) noted the lack of a postorbital bar and presence of a relatively large antemolar dentition as distinctive features of this Paleocene "primate," contrasting it with what is found in extant primates.

Russell (1964) provided the most comprehensive description of a plesiadapid skull to date (*P. tricuspidens*, based on MNHN CR 125, 126, 966, 965, 4306) as a follow-up to his 1959 work. Figures 13–19 of Russell (1964) have been frequently relied upon as a reference for the cranial anatomy of *P. tricuspidens* (Gingerich, 1976; Bloch and Silcox, 2006). Russell (1964) was the only researcher to document the sutural and foraminal patterns in *P. tricuspidens* with original illustrations, although he provided no photographs. Due to the diagrammatic form of the illustrations and controversy concerning sutural patterns that followed, the lack of photographic evidence has become problematic. In fact, none of the cranial sutures, or foramina of the orbital region, have ever been adequately photographed. Russell (1964: figs. 14, 19) reconstructed the orbitotemporal region with a human- or tupaiid treeshrew-like pattern of foramina for cranial nerves, with separate foramina for ophthalmic (abbreviated "t.d.r." by Russell) and maxillary (abbreviated "t.r." by Russell) branches of the trigeminal nerve. Although Russell (1964: figs. 14, 19) also documented most major sutures, the alisphenoid/orbitosphenoid suture and the posterior termination of the orbitosphenoid/frontal suture were not illustrated or discussed.

Russell (1964) changed some of the interpretations he made in his original note from 1959. For instance, in 1964 he considered the stapedial artery to have been reduced relative to the promontorial branch or possibly absent.

Szalay (1971) concluded that the skull of *P. tricuspidens* had been incorrectly reconstructed in lateral view by Simons (1960) and Russell (1964), in which the tips of the upper and lower incisors were shown to meet one another while the cheek teeth were occluded. Szalay further suggested

that the premaxillae did not contact the frontal and provided a photographic dorsal view of the skull (fig. 2) showing transverse cracks (as interpreted by other authors) in the premaxillae looking very much like symmetrical sutures, intersecting the nasals before reaching the maxillae.

Gingerich (1971) published a comment in response to Szalay (1971), pointing out that Simons (1960) actually reconstructed the skull as Szalay (1971) proposed it should be reconstructed. Gingerich then challenged Szalay's (1971) interpretation that the premaxillae lacked a frontal contact.

Szalay (1972a) described the skull of a paromomyid plesiadapiform, *Phenacolemur jepseni* (AMNH 48005), and compared it to *P. tricuspidens* specimens MNHN CR 125 and MNHN CR 7377 (an isolated squamosal glenoid, petrosal, and ectotympanic), as well as to skulls of extant and fossil euprimates. This represented the first publication of MNHN CR 7377. Although the photographs Szalay provided of *P. tricuspidens* MNHN CR 125 are of high quality (Szalay, 1972a: figs. 5, 6), they reveal little about the carotid plexus pathway. His descriptions, however, are consistent with those of Russell (1964). Stereophotographic views of MNHN CR 7377 in Szalay (1972a: figs. 7–9) show a trough-like remnant of the carotid canal and a groove extending anteriorly from it onto the promontorium (labeled with an arrow in Szalay, 1972a: fig. 8).

Gingerich (1975a) announced a new specimen of *P. tricuspidens* from Berru. This specimen, which is not housed in an official repository, is called the "Pellouin skull" after the private collector who holds it to this day. Gingerich (1975a: fig. 2) provided stereophotographs of its right ear and suggested that its expanded external auditory meatus links it with tarsiiform euprimates.

Gingerich (1976) added descriptions of new specimens of *P. tricuspidens* and other *Plesiadapis* species. A frontal fragment from Berru was attributed to *P. tricuspidens* (YPM-PU 24618; Gingerich, 1976: fig. 34), and an edentulous rostrum fragment from 7-up Butte, a late Paleocene locality in the Medicine Rocks area of Montana, was attributed to *P. anceps* (YPM-PU 19642; Gingerich, 1976: fig. 32). He noted the *P. anceps* specimen shows a premaxilla-frontal contact like *P. tricuspidens*.

The descriptions on cranial anatomy in Gingerich (1976) are generally brief and serve more as an addendum and review than as a comprehensive reassessment of basicranial evidence. He provided overview stereophotographs of MNHN CR 125 (Gingerich, 1976: pl. 8a–c) and the Pellouin skull (Gingerich, 1976: pl. 9a–c). Gingerich (1976: pl. 9b) also noted that the ectotympanic bone of the basicranium has a "suspended ring" for attachment of the tympanic membrane that looks euprimate-like, which he illustrated with stereophotographs of the *P. tricuspidens* Pellouin skull. He also identified a vidian foramen in the Pellouin skull, but did not illustrate this morphology. He confirmed Russell's previous suggestion that there is a laterally positioned posterior carotid foramen and canal, noting their presence in the Pellouin skull.

Gingerich (1976) provided the first and only photographic documentation of the course of the internal carotid plexus in *P. tricuspidens*, with close-up, annotated stereophotographs of the right petrosal (Gingerich, 1976: pl. 9c). He provided additional evidence that a stapedial artery was absent by observing that there exists a bony ridge on the promontorium ventral to the fenestra vestibuli that would have blocked the course of the artery. He used the reconstruction from Szalay (1971) as a basis for reconstructing jaw musculature.

In addition, Gingerich (1976) used Szalay's reconstruction along with a dorsal profile of a partial endocast to estimate brain volume (Gingerich, 1976: fig. 35a). Figure 33 of Gingerich (1976) is a redrawing of part of figure 19 of Russell (1964) and represents the orbitotemporal region of *Plesiadapis*. It is labeled with equivalent, but different, terms. The sutural patterns depicted are similar to those in Russell's figure, but differ with respect to the relationship of the palatine/frontal suture to the postpalatine canal. Russell (1964) depicted the suture as entering the canal, whereas Gingerich (1976) showed the canal to be completely within the palatine. Finally, Gingerich (1976: pl. 9c) labeled a groove on the right promontorium of the Pellouin skull, which runs from posterolateral to anteromedial, as a "tympanic plexus groove." This groove is not visible on MNHN CR 125, and thus was not among those originally interpreted as a promontorial or internal carotid arterial route by Russell.

Gingerich et al. (1983) described a newly discovered crushed skull of *Nannodectes intermedius* (USNM 309902) from the Bangtail locality in south-central Montana. The description was brief and focused on the teeth. Gingerich et al. (1983) were mostly interested in biostratigraphic implications of the specimen and the fauna in which it occurred. The authors interpreted USNM 309902 as having existed in the earliest Tiffanian (Ti) North American Land Mammal Age (NALMA). If this temporal attribution is correct, USNM 309902 is the geologically oldest known plesiadapid cranium.

MacPhee et al. (1983) expanded on the description and discussion of the basicranium of USNM 309902 and re-analyzed the basicranium of *N. gidleyi* AMNH 17388. They did not illustrate the actual specimens, but provided a schematic illustration of a generalized "plesiadapid" petrosal that shows unique morphologies of both specimens (MacPhee et al., 1983: fig. 1). There is a mistake in the figure caption: two grooves are illustrated, "s1" and "s2." In the figure caption, the "s1" groove alone was said to characterize *N. intermedius*, whereas the "s2" groove alone was said to characterize *N. gidleyi*. However, inspection of the actual specimens indicates that the opposite is true (specimen numbers were switched in the figure caption). Nevertheless, their conclusions stand regarding the evidence these specimens provide of "variability" in expression of grooves on promontoria of plesiadapids. The "s1" groove was interpreted as a possible tympanic nerve route by MacPhee et al. (1983). It was noted that this is located in a much different position from the tympanic plexus groove photographed by Gingerich (1976) for the Pellouin skull and represents a different structure (although both could certainly have held tympanic plexus fibers).

MacPhee et al. (1983) noted that the "s2" groove has a similar location to a canal previously identified as the internal

carotid canal by both Russell (1964: fig. 15) in MNHN CR 125 and Gingerich (1976: pl. 9c). MacPhee et al. (1983) stated, however, that the groove does not connect to a foramen leading to an extratympanic space, implying that it could not have actually held a functioning internal carotid artery or nerve. They argued that this observation, combined with a lack of the "s2" groove on the other specimen, indicates that the internal carotid system is diminished in importance to the point that it was only sporadically retained in the adult plesiadapid specimens. MacPhee et al. (1983) also argued that bullar composition cannot be determined in fossil taxa lacking a suture between the bulla-forming bone and the promontorium of the petrosal (Russell, 1959, 1964; Gingerich, 1976), because only ontogenetic evidence can reveal whether a bulla started as an ossification separate from the petrosal bone.

MacPhee and Cartmill (1986) provided an expanded argument against any petrosal contribution to the auditory bulla based on further observations of the Pellouin skull (Gingerich, 1975a; 1976). They pointed out that although there is no visible suture between the petrosal bone and the bulla medial to the promontorium, there is no suture between the ectoympanic and lateral aspect of the bulla either. This means that it is not clear whether the bulla is petrosal, entotympanic, and/or ectotympanic in composition. It is important to note, however, that all of the specimens available to MacPhee and Cartmill (1986) lack the portion of the bulla medial to the annular component of the ectotympanic, where an ectotympanic suture is most likely to have been (given the results of more recent studies showing its position in other plesiadapiforms).

Paromomyid plesiadapiform basicrania that preserve the portion of the bulla medial to the annular component of the ectotympanic are interpreted as having an ectotympanic/entotympanic suture located in this portion (Kay et al., 1992; Bloch and Silcox, 2001). MacPhee and Cartmill (1986: fig. 17) also showed a radiograph of the Pellouin skull, which reveals the presence of extensive "cellules" inferred to communicate with the tympanic cavity. They suggested that presence of these "cellules," as a consequence of tympanic cavity pneumatic expansion, is a further indication that previously noted similarities between plesiadapids and modern lemuriforms are convergences (e.g., Gingerich, 1976). Finally, MacPhee and Cartmill (1986) documented a specific example of an animal convergent on plesiadapids and lemuriforms: the chinchillid *Lagostomus maximus* has a similarly constructed annular component to its external auditory meatus and an obliterated suture between the ectotympanic bulla and pars cochlearis of the petrosal.

Szalay et al. (1987: figs. 1, 2) provided a detailed description, stereophotographs (the same as those provided in Szalay, 1972a: figs. 7–9), and a reconstruction of a cranial fragment of *P. tricuspidens* (MNHN CR 7377). They suggested that it represents a young individual because sutures between the squamosal and petrosal are "clearly visible," as were sutures between the petrosal and the ectotympanic. The former are clearly illustrated. Whereas the suture between the mastoid part (pars canalicularis) of the petrosal and the ectotympanic is visible, it is not clear whether these sutures represent the "clearly visible" sutures to which the authors refer. Szalay et al. (1987) pointed out and illustrated additional features of *P. tricuspidens* that they argued are similarities with many modern primates: (1) a carotid canal supported by a dome-like, ventrolaterally projecting outgrowth from the petrosal that shields the cochlear fenestra (referred to as the "posterior septum" or *ps* later on); and (2) a ridge that projects from the roof of the tympanic cavity and extends posteromedially from the promontorium, holding the vestibular aqueduct.

Kay et al. (1992) described the then newly discovered paromomyid *I. graybullianus* (USNM 421608) and compared its morphology to that of *P. tricuspidens*, among other taxa. They reinterpreted the foramen rotundum identified by Russell (1964) in *P. tricuspidens* as a suboptic foramen (see Bloch and Silcox, 2006, and below, for more detailed discussion).

Bloch and Silcox (2001) described additional specimens of *I. graybullianus* and redescribed the original specimen, USNM 421608. They compared *I. graybullianus* to plesiadapids, providing illustrations and discussion of the morphology of a previously unpublished specimen of *P. cookei*, whose tympanic cavity is open due to breakage (UM 87990; Bloch and Silcox, 2001: fig. 7). They noted, but their figure does not clearly show, a groove they interpreted as carrying a branch of the internal carotid artery. This groove clearly differs from the small criss-crossing grooves for the tympanic plexus (which *are* visible in their figure 7). They also showed that *P. cookei* is similar to *P. tricuspidens* in having bony struts connecting the annular part of the ectotympanic to the external auditory meatus.

Bloch and Silcox (2001: p.192) indicated that the carotid canal and posterior carotid foramen is poorly known in plesiadapids and is only preserved in the Pelluoin skull of *P. tricuspidens* among all known plesiadapid cranial specimens.

Bloch and Silcox (2006) described the skull of another plesiadapiform, *Carpolestes simpsoni*, based on a number of specimens (UM 82670, 82688, 85177, 86273, 101923, 101963; USNM 482354). Again, comparisons were made with plesiadapids. Although no additional figures were included, they again discussed the controversy over the identification of foramina in the *P. tricuspidens* specimens that was initiated by Kay et al. (1992). They concluded that Kay et al. (1992) miscommunicated the nature of their disagreement with Russell (1964) and their reinterpretation of the morphology. The foramen Kay et al. (1992) reinterpreted as the suboptic foramen must actually correspond to what Russell (1964) identified as the "*t.d.a.*," (*trou dechire anterieur*: equivalent to the superior orbital fissure), based on Kay et al.'s description of its location and morphology. This means they considered Russell's "*t.r.*" (*trou rond*: equivalent to the foramen rotundum) to actually correspond to a sphenorbital fissure. Bloch and Silcox (2006) then argued that Kay et al.'s (1992) reinterpretation is less plausible than Russell's (1964) interpretation because the medial walls of the orbits are more widely separated in *P. tricuspidens* than in treeshrews possessing suboptic foramina, and because

Russell's "*t.r.*" is too ventrally and posteriorly displaced to represent a sphenorbital fissure.

Gingerich and Gunnell (2005) described additional aspects of the skull of *P. cookei* (UM 87990). The skull, which is associated with both dentaries, is preserved in pieces, of which there is a palatal/splanchnocranial fragment, a neurocranial fragment with well-preserved auditory bullae ventrally, and a frontoparietal fragment. Their reconstruction postulates a total length of 90 mm and bizygomatic breadth of 58 mm. They considered the overall morphology as being similar to that of *P. tricuspidens*. Gingerich and Gunnell (2005) also reconstructed the brain as being long and narrow, with large olfactory bulbs compared to modern primates. The rhinal fissure was identified and interpreted to indicate an unexpanded neopallium, suggesting neurological analogy with "olfactory reliant," sensory-deprived "basal insectivores" such as species of *Tenrec*. The foramen magnum diameters were given as 8.5 by 6.0 mm. The volume of the brain was estimated at 5 cc, which is less than a third the estimate of 18.7 cc derived by Gingerich (1976) from double integration of pictures of skulls of *P. tricuspidens*. The authors stated that 5 cc is a much more reliable estimate that is likely also to apply to *P. tricuspidens*.

Boyer et al. (2012a) described the first known cranial material of a species of *Pronothodectes*. The new material examined included a crushed cranium (UALVP 46685) and two isolated petrosals (UALVP 46687, 49105). They concluded that *Pronothodectes* shared similarities with *N. intermedius* and nonplesiadapid plesiadapiforms to the exclusion of *P. tricuspidens* and *P. cookei*, as expected for a more basal taxon of the family. In addition, they re-assessed the petrosal contribution to the bulla and concluded that previous interpretations of a petrosally derived bulla in plesiadapids could not be refuted. Finally, they provided a detailed framework for reconstructing tympanic neurovasculature and determining the homology and functional equivalence of intratympanic structures. We follow this framework and nomenclature here.

Finally, Orliac et al. (2014) described detailed aspects of endocranial anatomy of, *P. tricuspidens* (MNHN CR 125). They estimated endocranial volume, encephalization quotient, and the optic foramen index of Kay and Kirk (2000). Orliac et al. (2014) reassessed the foramina of the orbitotemporal region with the benefit of microCT data. Orliac et al. (2014) found *P. tricuspidens* to have an exceptionally small endocranium with midbrain exposure, and large olfactory bulbs, which they interpreted as primitive retentions, likening this primitive anatomy to that of stem-gliroids and lagomorphs.

They suggested that observed doming of the neocortex and a downwardly shifted olfactory bulb are specializations shared with euprimates. The optic foramin index is exceptionally small, suggesting a non-visually reliant animal. Their assessment of the foramina relating to the branches of the trigeminal nerve support Kay et al.'s (1992) re-assessment of Russell's (1964) identifications. That is, Orliac et al. (2014) found no evidence of a separate foramen rotundum and inferred that cranial nerves III, IV, V1, and V2 all exited through a sphenorbital fissure (previously interpreted as foramen rotundum by Russell, 1964; see above). They also examined what must correspond to Russell's (1964) "*t.d.a.*" and concluded that it must represent a suboptic venous channel as Kay et al. (1992) probably meant to suggest. In an unpublished dissertation upon which the present work is based, Boyer (2009) presented extensive evidence anticipating the conclusion of Orliac et al. (2014), using the same specimens examined by Russell (1964) and Gingerich (1976). The evidence of Boyer (2009) is included as Appendix V here.

Postcranium

Plesiadapidae is known from an extensive sample of postcranial specimens that has been accumulating with collecting efforts for over a century. The following is a summary of the previous studies of plesiadapid postcranial fossils, with a listing of the specimens figured and described in each. This section also serves to document the comparative sample employed to assist in the description and analysis of *P. cookei* UM 87990.

Previous researchers have focused on garnering evidence for positional behavior. The hypothesis that plesiadapiforms were arboreal has been evaluated through comparisons to extant primates and their close living relatives, treeshrews and dermopterans. Questions about the phylogenetic relatedness of plesiadapiforms to extant primates also have been evaluated through the lens of their inferred positional behaviors (e.g., Beard, 1993a, b). Furthermore, some researchers viewed the question of whether plesiadapiforms exhibited primate-like arboreality as a question about whether they provide important information about primate evolutionary origins. Cartmill (1974) suggested that a lack of primate-like arboreality rendered plesiadapiforms irrelevant to questions about primate origins whether or not cladistic analyses recovered them as stem primates. Anatomical regions that have undergone extensive scrutiny include the elbow and ankle joints. These joints can potentially convey information on mobility for rotating the hands (supination) and feet (inversion). In living arboreal primates, a high degree of mobility in supination and inversion is critical for grasping the variously angled branches they encounter in shrubs or trees. In clawed (non-grasping) arborealists, ankle rotational mobility is also important for "reversing" the feet and descending large tree trunks head first. Terrestrial animals tend to trade such mobility in favor of stability because of the more uniform substrate orientations they encounter.

Lemoine (1893) was the first to describe and illustrate postcranial elements of *Plesiadapis* (attributable to *P. tricuspidens*), from the locality of Cernay-les-Reims in northern France. He noted the presence of prominent flexor sheath ridges on the proximal phalanges.

The first postcranial skeleton of *Plesiadapis* was initially described as a "Tertiary squirrel" from the maar lake of Menat in central France and now housed in the École des Mines collection in Paris (Launay, 1908). This specimen, little more than a paper-thin impression on a bedding plane, originally included a complete, articulated skeleton with an outline of its fur and a bushy squirrel-like tail. Unfortunately the

skull and jaws were lost when the specimen was collected. In his brief description, Launay (1908: p. 395) mentioned the fur, the presence of claws on the feet, and an overall size matching that of a common squirrel, writing "tous ses charactères anatomiques sont également presque identiques à ceux d'un écureuil vulgaire." He noted that the proportions of the forearm to the arm as a whole are the same as that of a squirrel, but because the length of the humerus is not known, Launay must have been referring to diameters of the arm bones. Launay recorded lengths of the femur, tibia, and ulna as 46, 58, and 39 mm, respectively.

As mentioned above, Russell (1967) considered the cranium of *Menatotherium insigne* described by Piton (1940) from Menat to be *Plesiadapis*, an identification based on the Clermont-Ferrand specimen. Russell (1967) did not discuss the first École des Mines skeleton from Menat (i.e., Launay's "squirrel"), but its inferred early late Paleocene age predated the appearance of rodents in the fossil record by several million years, making identification as a rodent very unlikely. Following examination of the Clermont-Ferrand specimen and the École des Mines specimen, Gingerich (1976) concluded that both represent *Plesiadapis insignis* (see below).

Gregory (1920: p. 70; pl. XXVII), in his monographic treatment of *Notharctus*, illustrated and discussed a humerus of *N. gidleyi* (AMNH 17379) that he considered to be "tupaioid" in its morphological characteristics. The humerus was part of a larger accumulation of associated craniodental and postcranial remains originally discovered in 1916 by Walter Granger at the Mason Pocket locality in the Nacimiento Formation of the San Juan Basin in southern Colorado. This locality is within the Tiffanian (Ti) 4 biozone of the Paleocene (Gingerich, 1976; Lofgren et al., 2004). Simpson (1935) redescribed AMNH 17379 and additional postcranial remains from Mason Pocket, which he attributed to *Plesiadapis gidleyi* (now *Nannodectes gidleyi*; see Gingerich, 1975b). Simpson (1935: figs. 5–8, 11) attributed to AMNH 17379 a complete dentary with all teeth; axial elements including an atlas, other cervical vertebrae, two thoracic vertebrae, six lumbar vertebrae, a sacrum, and two caudal vertebrae; and appendicular elements including a left scapula, right humerus, right radius, left ulna and metacarpal, a proximal right femur, proximal and distal ends of a right tibia, right astragalus, left calcaneum, and pedal phalanx. Simpson (1935: figs. 9–10) also described parts of other cervical vertebrae (AMNH 17388) and a nearly complete left innominate and left distal femur (AMNH 17409). Simpson (1935) mentioned the existence of many isolated intermediate phalanges, but he was not convinced they belonged to *P. gidleyi* and he did not figure them. Based on the skeletal morphology preserved in AMNH 17379 and AMNH 17409, Simpson concluded that *P. gidleyi* was closer in form to "lemurids" than to tupaiids, but that *N. gidleyi* must have occupied an ecological niche very different from that of "lemurid" (notharctine) euprimates. All of the bones described by Simpson (1935) and many more were observed and measured during the course of the present study.

Teilhard de Chardin (1922: pl. 1:33) figured a distal humerus belonging to *Plesiadapis remensis* from Cernay-les-Reims and concluded that plesiadapids were "sciuroid" in their ecology.

Piton (1940) described *Menatotherium insigne* on the basis of a complete, articulated skeleton from Menat that was crushed flat and paper-thin, preserving the body outline and hair as a coating of carbonaceous material. The principal slab, in the collection of the Faculté des Sciences of Clermont-Ferrand, shows the head and most of the body (Simpson, 1948). Russell (1967) identified this as an early species of *Plesiadapis*, but did not illustrate the skeleton and wrote little about it. The Clermont-Ferrand specimen and the specimen from École des Mines lacking the skull allowed later researchers to estimate limb lengths and indices for *P. insignis* (see below). The small size of *P. insignis*, its similarity in form to early-occurring North American *Plesiadapis*, and contextual information from the deposits that yielded the specimen suggested to Gingerich (1976) and others that this specimen was probably contemporaneous with North American Tiffanian-1 index taxon *Plesiadapis praecursor*, making it the oldest skeleton of a plesiadapid known at the time (older than those from Cernay and Mason Pocket).

In a description of his collecting efforts at the Mouras (Berru) Quarry, near Cernay-les-Reims and the city of Reims Russell (1964: pp. 289–293) listed elements recognized as pertaining to *P. tricuspidens*, some of which were indicated as being associated with single individuals. He did not, however, provide descriptions or illustrations of these fossils, except for the claws. He compared the claws to those of the flying lemur *Cynocephalus*, noting that they were similar in being mediolaterally narrow and dorsoventrally deep.

Simons (1964: p. 56, fig. 3) provided a composite drawing of a skeleton of *P. tricuspidens* based on Russell's new fossils. It is difficult to determine which of these bones were used in the composite because the bones were reconstructed to varying degrees. However, the femur and tibia appear to correspond with MNHN R 408 and MNHN R 410, respectively, incomplete elements considered by Russell (1964) to pertain to the same individual. Because MNHN R 410 lacks both its proximal and distal ends, reported total hind limb length and crural indices represent estimates. Simons (1964) considered *Plesiadapis* to have been a treeshrew-like or tree-squirrel-like arborealist, and reiterated Russell's (1964) observation regarding similarity between the claws of *Plesiadapis* and *Cynocephalus*. Napier and Walker (1967) also suggested that plesiadapids were treeshrew-like or squirrel-like in their locomotion.

Szalay (1972b: p. 34) calculated a brachial index (93), crural index (93), and intermembral index (81) for *P. tricuspidens* based on the figure in Simons (1964), which appears have been based on incomplete hind limb elements. Our own calculations, based on the femur (MNHN R 408) and fragmentary tibial shaft (MNHN R 410), yield a crural index of about 92–93. Thus Simons' (1964) reconstruction and Szalay's (1972b) estimates appear to have been fairly accurate.

Szalay and Decker (1974: figs. 3–5, 8–12) described and illustrated an astragalus (AMNH 89533) and calcaneum

(AMNH 89534) from the middle Paleocene Saddle Locality in Wyoming and attributed them to *Plesiadapis* cf. *P. gidleyi*. The Saddle Locality was later determined to preserve *P. anceps* and *Nannodectes gazini* (Gingerich, 1976), and it therefore seems that these tarsal specimens should now be referred to one of these two taxa. Szalay and Decker (1974) also illustrated bones from other localities, including an astragalus (no number provided) and a calcaneum (MNHN R 611) of *P. tricuspidens*. We were able to locate the figured astragalus at the MNHN, but it was not associated with an accession number nor the number "47," was to have been written on the specimen (Szalay and Decker, 1974: fig. 6). Russell (1964: p. 291) listed MNHN R 5347 as an astragalus of *P. tricuspidens*, which suggests to us that Szalay and Decker's (1974) 'no number' astragalus is MNHN R 5347. Szalay and Decker (1974) indicated that the articulation between the astragalus and calcaneum was highly mobile and would permit a substantial degree of inversion and eversion. They inferred such mobility to be requisite in an arboreal setting, where substrates may occur in a variety of orientations and descent of large tree trunks is often necessary, requiring hind-foot reversal. The mid-tarsal joint was also identified as a point of axial mobility (for inversion/eversion) and mobility in plantar- and dorsiflexion.

Szalay et al. (1975) described, figured, and analyzed *P. tricuspidens* fossils from the Berru collection listed by Russell (1964) as well as vertebral specimens of *N. gidleyi* (AMNH 17379) beyond those illustrated by Simpson (1935). The *N. gidleyi* illustrations of Szalay et al. (1975: fig. 1) represent reconstructions of complete, undistorted elements rather than faithful depictions of the preserved morphology. Szalay et al. (1975) considered the anatomy of the *N. gidleyi* vertebrae to be lacking the appropriate comparative context and thus uninformative for phylogenetic or functional considerations.

Szalay et al. (1975: figs. 2, 4, 5) concluded that *Plesiadapis* possessed a spherical, rather than cylindrical, humeral capitulum based on specimens of *P. tricuspidens* (MNHN BR-3-L and MNHN BR-4-L) as well as those attributed *Na. gidleyi*, and *P. walbeckensis*. This shape was considered especially similar to that of Euprimates; otherwise plesiadapid humeri were more similar to those of arctocyonids than to those of Paleocene "insectivorans." Szalay et al. (1975: figs. 2–3) figured four ulnae for which no numbers were given (now known to be MNHN BR-7-L, MNHN R 452, MNHN R 1521, MNHN R 443, respectively). Szalay et al. (1974: fig. 6) also reconstructed a nearly complete and undistorted ulna lacking only the styloid process, based on MNHN R 546. They agreed with Simpson's (1935) assessment that *Plesiadapis* and *Notharctus* have similar ulnae, based on their shared shallow trochlear notch, proximal bowing of the shaft, and relatively small olecranon process. Szalay et al. (1975: fig. 4) considered radius MNHN R 550 to be especially primate-like because of the oval perimeter of its proximal articular surface. They figured two distal phalanges (p. 148, fig. 7), unnumbered at the time, but revealed by later researchers to be MNHN R 5313 and MNHN R 613 (Beard, 1989, p. 132). Szalay et al. (1975) noted that the bones are claw-like and did not add any information to Russell's (1964) assessment. They questioned Russell's (1964) attribution of abundantly preserved cheiridial elements from Berru to *Plesiadapis*, noting the presence of similarly-sized arctocyonids from the locality.

Szalay et al. (1975: p. 150) suggested that the plesiadapid innominate generally matches the "primitive eutherian condition." This conclusion was apparently based on several partial innominates of *P. tricuspidens*, including MNHN CR 448 (Szalay et al., 1975: fig. 8), MNHN CR 409 and MNHN CR 413 (Szalay et al., 1975: fig. 9), as well as innominates of *N. gidleyi* AMNH 17409 and *P. walbeckensis* (no number given). In fact, they considered *Tupaia* to have a more primate-like innominate than plesiadapids. Szalay et al. (1975), however, suggested that a proportionally large acetabulum is a special similarity between plesiadapids and euprimates.

Szalay et al. (1975: p. 151) described the femur of *P. tricuspidens* based on MNHN BR-15-L, MNHN BR-16-L, MNHN CR 408, MNHN CR 438, MNHN CR 444, MNHN CR 450 and "an additional half dozen fragmentary bones." They concluded the *P. tricuspidens* femur is fundamentally different those of fossil notharctine euprimates, noting that some of these differences unite plesiadapids with lorisines. Some of the distinct features of the plesiadapid femur mentioned by Szalay et al. (1975) include the low angle between the femoral neck and shaft, the distinct constriction of the femoral neck relative to the femoral head, a large medially projecting lesser trochanter, a distally positioned third trochanter, and an anteroposteriorly shallow patellar groove. Szalay et al. (1975) noted the existence of the crushed tibia and fibula of MNHN CR 410, but regarded Simpson's (1935) description of the tibia of *N. gidleyi* as adequate for understanding the morphology of the plesiadapid tibia more generally.

Szalay et al. (1975) listed what they considered to be four derived primate characteristics of the astragalus and calcaneum, including a pronounced groove for the tendon of flexor digitorum fibularis on the plantar surface of the calcaneal sustentaculum, an astragalus with a continuous navicular and sustentacular facet, a proximodistally long tibial trochlea, and a "helical-shape" (p. 156) to the posterior astragalocalcaneal articulation. These characterizations and interpretations of the astragalus and calcaneum were apparently based on earlier observations by Szalay and Decker (1974) and were supported by a broader assessment of tarsal variation among what they considered to be condylarth, palaeoryctoid, primate, and adapid "morphotypes." (Szalay et al., 1975: tables I-II). They illustrated some of the morphotypes they reference using an astragalus MNHN R 610 (Szalay et al., 1975: fig. 12) and calcaneum MNHN R 611 (Szalay et al., 1975: fig. 13) attributed to *P. tricuspidens*.

Szalay et al. (1975: p. 162) concluded that the forearm was habitually flexed and axially mobile, and that the "upper hindlimb" had a "capacity for strong retraction," but lacked leaping adaptations. They reiterated functional inferences from Szalay and Decker (1974) regarding the ankle joint. All of the fossils mentioned in Szalay et al. (1975) were restudied, photographed, and measured in the course of the current work.

Gingerich (1976) provided photographs and measurements of limb bones of the specimen of *P. insignis* from Menat (p. 35, table 6; p. 84, fig. 36 and table 12; pls. 11–12). Furthermore, he mentioned the existence of a distal humerus of *Platychoerops* UCMP 103829. He remeasured the postcranial elements of *P. tricuspidens* depicted in Simons (1964) and calculated brachial (95), crural (100), and intermembral (88) indices that differ slightly those given by Szalay (1972b). However, as mentioned above, the length of the tibia of *P. tricuspidens* is not actually known. Gingerich (1976) reported the same three indices for *P. insignis* as 86, 91, and 72, respectively. Gingerich (1976) was the first to extensively compare plesiadapids to sciurid rodents, the lack of which he regarded as a shortcoming of previous treatments by Gregory (1920), Simpson (1935), and Szalay et al. (1975). He concluded that the limb proportions were similar to those of *Marmota* and other terrestrial sciurids. Furthermore, he interpreted the robustness of the limbs as more consistent with a terrestrial, rather than arboreal, habitus. His interpretation of the evidence from the humerus, ulna, and radius of *N. gidleyi* (AMNH 17379) supported this conclusion. Specifically, the large teres major tuberosity on the humerus was noted to be consistent with digging proclivities. Furthermore, Gingerich interpreted the morphology of the ulna and radius to indicate a limited capacity for pronation and supination. He noted that the distal humeri of *Plesiadapis* (as figured by Teilhard de Chardin, 1922) and *Platychoerops* UCMP 103829 differ from that of *N. gidleyi* in having more expanded supinator crests. He also noted that the shallow olecranon fossa of the humerus of these larger forms would have prevented full extension of the elbow, consistent with Szalay et al.'s (1975) view.

Russell (1962) suggested that plesiadapids were likely capable of climbing trees when in danger, but that they were predominantly terrestrial. Simons (1967) and Van Valen (1971) considered it likely that at least some, if not all, plesiadapid species were terrestrial. However, these assessments were not based on detailed examinations of the postcranium like that of Gingerich (1976).

Gingerich (1976) concluded that the available evidence supported a terrestrial habit for plesiadapids. Although he acknowledged that there probably were more arboreally adapted plesiadapiforms, which may even have included some species of plesiadapids, he favored for terrestriality as the modal substrate.

Szalay and Drawhorn (1980) further discussed the diagnostic and functional features of archontan (i.e., treeshrew, dermopteran, chiropteran, euprimate, plesiadapiform) astragali and calcanea. Among the plesiadapids, they figured an unnumbered YPM astragalus of *Plesiadapis rex* (Szalay and Drawhorn, 1980: p. 145, fig. 6. IIIA–E), which Beard (1989) later identified as YPM-PU 23977. Szalay and Drawhorn (1980: p. 152, fig. 9. III.A–E, IV.A–E) also provided the first detailed figures of the astragalus and calcaneum of AMNH 17379, still attributed by them to *P. gidleyi*. The same figure also includes the astragalus and calcaneum of the primitive arboreal treeshrew *Ptilocercus lowii*. The intent of the figure design is not stated, but presumably it was meant to illustrate two taxa that come close to Szalay's view of the "archontan morphotype." Szalay and Drawhorn (1980: fig. 11. III.A–E, IV.A–E) also illustrated tarsals of *P. tricuspidens* (MNHN R 610–611) next to tarsals of *Cynocephalus volans*. Why Szalay and Drawhorn (1980) chose to re-illustrate the calcaneum MNHN R 611 (see above), but not the astragalus MNHN R 5347, is not stated. There do appear to be differences between MNHN R 610 and MNHN R 5347 (see below), but Szalay and Drawhorn (1980) did not mention any of the differences or what such differences might mean. We could not find a reference to Szalay and Drawhorn's (1980) figure 11 in their text, but presumably the figure was intended to illustrate similarity between *Plesiadapis* and *Cynocephalus*. Szalay and Drawhorn (1980) argued that *Cynocephalus* has mobility in its ankle joint to an extreme that is only of use in arboreal settings.

Szalay and Dagosto (1980) provided a more detailed functional assessment of the plesiadapid and plesiadapiform distal humerus than previously given. The work is elegant in its assessment of functional properties using qualitative comparative morphology combined with quantitative comparisons. Szalay and Dagosto (1980: fig. 3) provided the first illustrations of a humerus of *P. walbeckensis* from the Walbeck fissure fillings in Germany, the existence of which was first mentioned by Szalay et al. (1975). Walbeck is roughly correlative with Ti3 (Gingerich, 1976; Vandenberghe et al., 2012). The authors did not provide a catalogue number for the specimen. Szalay and Dagosto (1980) described a second "archontan," AMNH 89519, from the Mason Pocket locality—but then suggested that it may not be an archontan. The authors reiterated their view that the spherical capitulum on the humerus of plesiadapids and euprimates may link the two groups both behaviorally and phylogenetically. They further described the ulnar trochlea of the humerus as possessing a lateral ridge and suggested that this ridge is homologous to the central keel of euprimate humeri. Szalay and Dagosto (1980: p. 32) challenged Gingerich's (1976) conclusions concerning plesiadapid terrestriality and stated that the features identified as linking plesiadapids and marmots are primitive features found in most "relatively unspecialized" mammals. Further, they regarded the plesiadapid humeral capitulum and radial head to be significantly more spherical and rounded, respectively, than those of marmots. They argued that the arboreal rodent *Ratufa*, although generally similar to a marmot, is a better analogue for *Plesidapis* because of its more spherical capitulum and more rounded radial head. Szalay and Dagosto (1980) hypothesized that plesiadapiforms could be viewed as claw-climbing arborealists analogous to modern callitrichid euprimates. We did not directly observe any of the specimens newly illustrated by Szalay and Dagosto (1980).

Gunnell and Gingerich (1987) published an abstract on the then new specimen of *P. cookei* (UM 87990) described here, which they interpreted as adapted to a claw-climbing, arboreal lifestyle. Later, Gingerich and Gunnell (1992) published a photograph of the specimen mounted in a vertical posture on a large tree trunk as part of an exhibition in the Hall of Evolution in the University of Michigan's Exhibit Museum.

Szalay and Dagosto (1988) described entocuneiforms and first metatarsals of archontans and euprimates and discussed the evolution of euprimate pedal grasping. They figured the first known entocuneiforms for a plesiadapid, including an isolated specimen from the Bison Basin Saddle locality (AMNH 92011) that they identified on the basis of its similarity to craniodentally associated elements from the Berru locality (Szalay and Dagosto, 1988: figs. 6–7). Szalay and Dagosto (1988) did not provide a number for the Berru specimen, but Beard (1989) recognized it as part of MNHN R 416. Szalay and Dagosto (1980: pp. 9–10) considered the distinctive features of the entocuneiform to be its large plantar-projecting "plantar process" and a facet for MT I that is mediolaterally broad, relatively flat, and saddle-shaped. They viewed the bone as morphologically similar to that of the extant treeshrew *Ptilocercus lowii*. *Ptilocercus* is capable of grasping with a divergent hallux that exhibits mobility at the metatarsal-entocuneiform joint (Sargis, 2001), and Szalay and Dagosto suggested that the same activity could be inferred for plesiadapids. However, no first metatarsals had yet been described for any plesiadapid.

Gunnell (1989: pp. 41–48) discussed the astragalus, calcaneum, and cuboid of *Plesiadapis*, illustrating specimens for which no species identification nor specimen number was given. Judging from the scale, these belong to the *P. cookei* skeleton described here (UM 87990). Gunnell (1989: figs. 16–17, p. 45) compared the astragalus and calcaneum to those of *Marmota*, acknowledging that the astragalus and calcaneum indicate a high degree of mobility, as argued by Szalay and Decker (1974). However, he noted that mobility of the ankle does not necessarily argue for an arboreal habitus, as indicated by the mobile foot of terrestrial *Marmota* (convincingly argued by Jenkins, 1974). However, Gunnell (1989) noted that an on-going study with Gingerich indicated an arboreal habitus for the skeleton of *P. cookei*.

Beard (1989: pp. 20–89, figs. 1–16) described and illustrated a skeleton of *N. intermedius* USNM 442229, which likely represents the same individual as the skull USNM 309902 (see previous section). USNM 442229 includes the following bones: left scapula, right humerus, right ulna, left radius, right scaphoid, right lunate (but see Boyer et al., 2013), left pisiform, right capitate, both hamates, left metacarpal I, right metacarpal II (but see Boyer et al., 2013), right metacarpal III, four proximal manual phalanges, four intermediate manual phalanges, several distal manual phalanges, left tibia, left cuboid, left hallucal metatarsal, four non-hallucal metatarsal fragments, and two pedal intermediate and two pedal distal phalanges. All of these fossils, plus additional elements associated with the specimen but not described by Beard (1989), were observed, measured, and in some cases μCT-scanned in the course of our study. In addition, Beard (1989: pp. 89–101, figs. 17–18) described isolated elements from Cedar Point Quarry attributed to *P. rex*, including YPM-PU 23976, a proximal humeral fragment (not figured); YPM-PU 23975, a distal tibial fragment; YPM-PU 23977, a right astragalus, and UM 94816, a left astragalus. Of these, we were only able to restudy UM 94816.

Beard (1989: pp. 101–132, figs 19–21) also described a number of previously unstudied bones of *P. tricuspidens*, relying on Russell's (1964) documentation of their association with the partial skeleton mentioned above (Table A-II-48).

We were able to directly observe, photograph, and measure many elements of the skeleton of *P. tricuspidens* in the course of this study. However, we were not able to relocate all of the bones observed and listed by Beard (1989) (Table A-II-48).

According to Beard (1989), associations documented for elements of *N. intermedius* by Dr. P. Houde, who originally discovered and prepared the specimen, indicate that in *N. intermedius,* the pedal phalanges are longer and more robust than the manual phalanges. This was later found to be true for micromomyid (Bloch and Boyer, 2007) and paromomyid plesiadapiforms (Boyer and Bloch, 2008), although not for carpolestid plesiadapiforms (Kirk et al., 2008). The specimen of *N. intermedius* includes the first described carpal bones for a plesiadapid, including the only described scaphoid for a plesiadapiform, as well as the first known metacarpal I, 'pollical' proximal phalanx, and metatarsal I. Beard (1989) concluded that carpals of *N. intermedius* and *P. tricuspidens* are nearly identical in structure, information used by Bloch and Boyer (2007) and Boyer and Bloch (2008) to confirm identification of elements in accumulations of semi-articulated to merely dentally-associated plesiadapiform bones.

Beard's (1989) comparative observations strongly emphasized similarities to the extant dermopteran *Cynocephalus*. His structural and functional analyses demonstrated that plesiadapiforms did indeed have a capacity for axial rotation of the forearm. This information, plus documentation of a robust, divergent pollex and hallux, suggested that plesiadapids were arborealists (e.g., Beard, 1989: p. 420, table 6; p. 457). Beard (1989: p. 458) inferred that plesiadapids "spent most of their time in above-branch arboreal postures" based on comparisons of their forearm and phalangeal characteristics with those of extant dermopterans and extinct paromomyid plesiadapiforms. Beard (1990: fig. 1) showed the articulated metacarpals of digits I–III of *N. intermedius* based on USNM 442229 as evidence of a divergent pollex.

Godinot and Beard (1991: fig. 1–2) published an extensive description and comparison of fossil primate hands that included a composite digit ray of *P. tricuspidens* using specimens MNHN R 5305 (metacarpal II or metacarpal V — the authors appear to have disagreed on the designation), MNHN R 5303 (proximal phalanx), MNHN R 5341 (intermediate phalanx), and MNHN R 5361 (distal phalanx). They interpreted the metacarpophalangeal joint as having a capacity for extreme dorsiflexion, the proximal interphalangeal joint as having greater capacity in palmarflexion and limited dorsiflexion, and the distal interphalangeal joint as having a neutral range of flexibility. Godinot and Beard (1991) suggested that the large flexor tubercle on the distal phalanx indicates a robust tendon of flexor digitorum profundus. Godinot and Beard (1991) also noted that dorsoventrally deep phalanges would have resisted forces imposed by powerful contraction of this muscle. Thus, they concluded that *P. tricuspidens* could have forcefully

driven its claws into substrates, such as tree branches, and clung to them. They noted that the metacarpophalangeal morphology of *P. tricuspidens* is most similar to that of *Daubentonia* among primates, implying a correlation between the need for extreme dorsiflexion at the metacarpophalangeal joint and clawed terminal phalanges. They also stated that habitually dorsiflexed metacarpophalangeal joints of *P. tricuspidens* match postures used by lorisines when on large diameter supports, but differ from postures used by lorisines when grasping small supports.

Beard (1993a) presented results of a cladistic analysis of Archonta that recovered plesiadapiforms as stem dermopterans. More specifically, plesiadapids formed the outgroup to a clade Beard called "Eudermoptera" (= Paromomyidae + Cynocephalidae). One apparent synapomorphy supporting a dermopteran clade that included plesiadapiforms was a triquetrum that contacts both the scaphoid and lunate on its radial aspect. Evidence for this trait in plesiadapiforms relied on an interpretation of scaphoid and lunate morphology present in *N. intermedius* USNM 442229 (Beard, 1993a: fig. 10.8). Stafford and Thorington (1998) and Sargis (2004) questioned the validity of this trait for both extant dermopterans and plesiadapiforms.

Runestad and Ruff (1995) tested the hypothesis of Gingerich (1976) that the "robustness" of plesiadapid limbs was evidence of terrestriality in this group and the hypothesis of Beard (1993b) that paromomyid plesiadapiforms were gliders. They did this by regressing limb lengths against limb cross-sectional areas for comparative samples of extant gliding, nongliding arboreal, nongliding terrestrial, and fossorial rodents and marsupials. Runestad and Ruff (1995) found that gliders had the longest limb bones relative to cross-sectional areas of their limb bones, and that nongliding terrestrialists had the relatively shortest limb bones (i.e., the most robust limbs). They analyzed previously described plesiadapid bones including those of *P. tricuspidens* (MNHN BR-3-L, MNHN R 450, MNHN BR-16-L, MNHN R 444), *N. intermedius* (USNM 442229), and *N. gidleyi* (AMNH 17379), and found that these taxa had limbs that were shorter than those of extant gliders, arboreal nongliders and paromomyids, but similar in proportional length to those of terrestrial sciurids. Although the authors did not discuss the significance of this finding, the results support the view of Gingerich (1976).

Hamrick (2001) studied third-digit proportions based on metacarpal, proximal phalanx, and intermediate phalanx lengths for archontan mammals, plotting these on ternary diagrams that show the relative contribution of these three elements to digit length as positions in an equilateral triangle. Hamrick (2001: fig. 2) included measurements from undescribed bones of *P. cookei* specimen UM 87990 and found them to cluster near scandentians and far from modern primates. Hamrick (2001: p. 349) concluded that "origin of the [crown] primates early in the Cenozoic era coincided with an evolutionary change in digital ray pattern formation ultimately yielding a grasping, prehensile hand."

Bloch and Boyer (2002) added *P. cookei* and other plesiadapiforms to Hamrick's (2001) archontan ternary diagram of third-digit proportions. They showed that non-plesiadapid plesiadapiforms plot with euprimates and suggested that *P. cookei* is derived in having scandentian-like proportions. This contradicted Hamrick's (2001) suggestion that euprimates to the exclusion of plesiadapiforms acquired a developmental change that led to changes in finger proportions. Rather, Bloch and Boyer (2002) concluded that, if there were a developmental patterning change allowing long fingers, it must have occurred in the ancestor of a clade comprised of euprimates and plesiadapiforms (but probably excluding dermopterans and treeshrews).

Youlatos and Godinot (2004) used multivariate methods to demonstrate that *P. tricuspidens* is more similar to the arboreal squirrels (e.g., *Ratufa*) than to the terrestrial ones, as had been suggested by Szalay and Dagosto (1980). Youlatos and Godinot (2004) did not include information on robustness of the limbs, which may explain why their results contrasted with those of Runestad and Ruff (1995).

Much of the MNHN material listed in Youlatos and Godinot (2004: table 1, p. 105) has been figured or mentioned elsewhere, including ulnae (MNHN R 546 and 443), radii (MNHN R 550), femora (MNHN BR-16-L, MNHN R 408, MNHN R 444), and ungual phalanges (MNHN R 5361, 5381, 5309). In addition, Youlatos and Godinot analyzed several new MNHN ulnae (MNHN R 411 and 615), radii (MNHN R 553 and 597), a femur (MNHN R 407), and claws (MNHN R 612–613). They also included newly recognized uncatalogued specimens of radii and ungual phalanges. There were several issues with accession numbers and identifications associated with specimens used by Youlatos and Godinot (2004) that were clarified by our collections work. Youlatos and Godinot (2004) listed "MNHN R 542" as a proximal ulna, but Russell (1964: p. 309) listed "MNHN R 542" is a partial humerus of *Pleuraspidotherium aumonieri*. We could not find a specimen with this description and number at the MNHN, but we did find a proximal ulna with the similar number "MNHN R 452" that seems to be the specimen to which Youlatos and Godinot (2004) intended to refer. Youlatos and Godinot (2004) also listed "MNHN R 2527," which we could not locate, and Russell (1964) did not list. Youlatos and Godinot (2004) listed "MNHN R 5370" as a claw, but Russell (1964) and later Beard (1989) identified this bone as a metapodial. Youlatos and Godinot (2004) also listed "MNHN R 549" as a claw, but we could not locate this element in collections, and Russell (1964: p. 309) listed MNHN R 549 under *Pleuraspidotherium* and identified it as a fragmentary ulna. It seems likely that the specimen Youlatos and Godinot (2004) called "MNHN R 549" is actually MNHN R 589, listed by Russell (1964: p. 291) as a distal phalanx and described in more detail by Beard (1989). Despite problems with specimen numbers, we have little doubt that Youlatos and Godinot (2004) correctly identified bones of *P. tricuspidens* in their study.

Bloch and Boyer (2007: p. 562) discussed morphological and functional features of the plesiadapid postcranium, referring to new observations of "a skeleton of *Plesiadapis cookei*… in the process of being described." This is skeleton UM 87990, which is one referred to by Gunnell and Gingerich

(1987), Gunnell (1989), Gingerich and Gunnell (1992), Hamrick (2001) and Bloch and Boyer (2002), and described in detail in this monograph. Bloch and Boyer (2007) stated that *P. cookei* differs from other plesiadapids in morphology of the humerus, claws, and digital proportions. They suggested that these differences reflect a greater tendency toward suspensory postures in *P. cookei*. A layout of this skeleton in anatomical position was also provided (Bloch and Boyer, 2007: p. 545, fig. 3D).

Bloch et al. (2007) presented a cladistic analysis of plesiadapids and other euarchontans. Their analysis recovered the clade "Sundatheria," a grouping of extant scandentians and dermopterans also supported by genetic evidence at the time (Murphy et al., 2001), as the sister taxon to Primates (but see more recent studies, e.g., Janecka et al., 2007). Plesiadapiforms were nested within Primates as the paraphyletic stem of Euprimates, with a subgroup of plesiadapiforms (Plesiadapoidea) united as the monophyletic sister taxon to Euprimates. Plesiadapoidea includes *Chronolestes* and Saxonellidae as serial outgroups to a clade formed by Plesiadapidae and Carpolestidae. Bloch et al. (2007: p. 1163) suggested that aspects of morphology shared by *Ptilocercus*, *Cynocephalus* and plesiadapiforms were primitive for Euarchonta, including elongated fingers (i.e., 'prehensile hand proportions'). Bloch et al. (2007) also suggested that the specialized grasping of carpolestids might be primitive for Plesiadapoidea as a possible synapomorphy of Euprimateformes (Plesiadapoidea + Euprimates), even though the states of traits related to hallucal grasping were equivocal in their character state optimization analysis. If correct, their inference implies that the less specialized grasping foot and shorter fingers of the hand in plesiadapids were secondarily derived rather than retention of the primitive condition.

Boyer and Bloch (2008: pp. 239–240, table 11.1) presented length measurements for individual elements of *N. gidleyi* (AMNH 17379, metacarpal III, two proximal phalanges and three intermediate phalanges), *N. intermedius* (USNM 442229, metacarpal III, six proximal phalanges and four intermediate phalanges), and *P. cookei* (UM 87990, metacarpals II and III, both metatarsal IIIs, six proximal phalanges and five intermediate phalanges), as well as cross-sectional area measurements for the intermediate phalanges. Boyer and Bloch (2008: figs. 11.11–11.12) plotted other measurements of the intermediate phalanges of these plesiadapids. They published the first photograph of an intermediate phalanx of *P. cookei* (p. 249, fig. 11.12) and the first illustrations of its distal ulna and radius (p. 256, fig. 11.19). Furthermore, they plotted indices from limb measurements of *P. cookei* (UM 87990; p. 265, fig. 11.27). Boyer and Bloch (2008) calculated the brachial index of *P. cookei* to be 101 and the intermembral index to be 89, but they did not give a crural index. These values differ from those of *P. tricuspidens* given by Gingerich (1976), indicating a proportionally longer forearm in *P. cookei*. Generally, the data Boyer and Bloch (2008) present and their interpretations are supportive of previous suggestions that plesiadapids were arboreal, and that *P. cookei* may have had more suspensory/antipronograde tendencies than other plesiadapids.

Kirk et al. (2008) presented an analysis of digit III proportions using ternary diagrams, including data for the plesiadapiform specimens studied by Boyer and Bloch (2008). Kirk et al. (2008) confirmed that some plesiadapids and other plesiadapiforms had euprimate-like hand proportions but suggested that *P. cookei* had proportions indicative of a terrestrial lifestyle. They further showed that many clades of mammals (i.e., carnivorans, rodents, and marsupials) have arboreal members with euprimate-like intrinsic hand proportions, as does the scandentian *Ptilocercus lowii*. They concluded that euprimates are not unique among mammals in their elongate finger proportions. They also found evidence consistent with conclusions of Bloch et al. (2007) that plesiadapiforms and euprimates are not even unique among the clade Euarchonta in their hand proportions due to the primate-like proportions exhibited by *Ptilocercus*.

Boyer et al. (2013) reviewed primate hand proportions, building on the dataset of Kirk et al. (2008) and examining finger and hand lengths relative to body mass. Plesiadapiforms were found to have manual prehensility proportions similar to most extant primates, whereas Paleogene euprimates exhibit what they coined "hyper-prehensility" with extremely high finger to metacarpus length proportions — as seen only in tarsiers and aye-ayes among extant taxa (Boyer et al., 2013). Boyer et al. (2013) also made a detailed case for re-interpretation of certain elements in *N. intermedius* (USNM 442229), arguing that bones interpreted by Beard (1989) and Godinot and Beard (1991) as metacarpal II and a lunate are in fact metacarpal V and a metacarpophalangeal sesamoid, respectively. This reinterpretation has implications for the degree of pollical abduction and nature of the radiocarpal joint in *Nannodectes*.

OBJECTIVES

We provide a complete description of the only known skull and skeleton of *P. cookei* (UM 87990), discovered in 1986 in late Paleocene-aged strata of the Clarks Fork Basin (Gunnell and Gingerich, 1987; Gingerich and Gunnell, 1992, 2005; Bloch and Silcox, 2001). We seek to understand both the functional and phylogenetic implications of *P. cookei* and other plesiadapids in three separate sections of this monograph: the first section (in Chapters II through IV) focuses on systematics and description and comparison of cranial and postcranial morphology, with a functional interpretation of the latter. The second section (Chapter V) is a consideration of life history of *P. cookei*. The third section (Chapter VI) is a cladistic evaluation of the phylogenetic relationships of *Plesiadapis* among mammals with a discussion its implications for early primate evolution. Six appendices include different types of supporting data: Appendix I provides descriptions and images, as well as tables of measurements relating to the cranium and mandible; Appendix II provides similar for the postcranial skeleton; Appendix III provides information for estimation of body

weight; Appendix IV provides data used in the cladistic analysis; Appendix V provides detailed descriptions and comparisons of all known and available plesiadapid skulls; Appendix VI provides basic metadata on high resolution x-ray computed tomography scans and used to image and study skeletons as well as digital objective identifiers (DOIs) pointing to open access copies of all the scan datasets.

INSTITUTIONAL ABBREVIATIONS

AMNH — American Museum of Natural History, New York, New York, U.S.A.
MNHN — Muséum Nationale d'Histoire Naturelle, Paris, France
SBU — Stony Brook University, Stony Brook, New York, U.S.A.
UALVP — University of Alberta Laboratory for Vertebrate Paleontology, Edmonton, Alberta, Canada
UM — University of Michigan Museum of Paleontology, Ann Arbor, Michigan, U.S.A.
USNM — United States National Museum of Natural History, Smithsonian, Washington, D.C., U.S.A.
YPM-PU— Yale Peabody Museum–Princeton University collection, Yale University, New Haven, Connecticut, U.S.A.

GENERIC ABBREVIATIONS

C. — *Chiromyoides* (Plesiadapidae)
I. — *Ignacius* (Paromomyidae)
N. — *Nannodectes* (Plesiadapidae)
P. — *Plesiadapis* (Plesiadapidae)
Pl. — *Platychoerops* (Plesiadapidae)
Pr. — *Pronothodectes* (Plesiadapidae)

ANATOMICAL TERMINOLOGY

Cranial anatomical terminology follows Boyer et al. (2012a), who followed MacPhee (1981) for tympanic region terms and *Miller's Anatomy of the Dog* (Evans, 1993), *Nomina Anatomica* (1983), and *Nomina Anatomica Veterinaria* (1994) for the remainder of the skull.

Postcranial anatomical terminology follows Szalay and Dagosto (1980), Beard (1989), as well as *Nomina Anatomica* (1983), *Miller's Anatomy of the Dog* (Evans, 1993), and *Nomina Anatomica Veterinaria* (1994) for different regions of the skeleton. We deviate from Beard (1989) in applying the directional terms "radial" and "ulnar" to the radius in addition to the carpal bones. Beard (1989) chose to use a human anatomical reference for the radius, but this creates a confusing situation for *Plesiadapis* because we reconstruct the radius to be pronated in resting position. This problem is compounded in discussions of articulations of the radius with the humerus and ulna. Even disregarding the problem of establishing the anterior surface of the radius, using "mediolateral" terminology is confusing because the axis of the radius shaft exhibits torsion (see Radius description). As a result, the mediolateral axis of the proximal end nearly corresponds to the dorsopalmar axis of the distal end.

Because of the relevance of plesiadapiforms to studies by anthropologists, human-primate carpal terminology is used, following previous treatments of Plesiadapidae (Beard, 1993a).

The terms "superior" and "inferior" are considered equivalent to "cranial" and "caudal" for the clavicle, scapula, innominate, and sacrum, in contrast to what is generally considered appropriate for anatomy of quadrupedal domesticated mammals (*Nomina Anatomica Veterinaria*, 1994). This is done to permit use of detailed anatomical references such as "supraspinus fossa," "infraglenoid tuberosity," and "anterior superior iliac spine" (Nomina Anatomica, 1983). Furthermore, use of this terminology follows that in recent treatments of other euarchontan mammals (e.g., Sargis, 2002a, b).

In discussions of cervical, trunk, and sacral vertebrae, "craniocaudal" terminology is used as specified in the *Nomina Anatomica Veterinaria* (1994) and as used in recent treatments of other euarchontan mammals (Sargis, 2001). However, for caudal vertebrae, we use "proximodistal" terminology to avoid confusing references to "caudal caudal vertebrae."

MATERIAL EXAMINED

Crania.— The principal cranium described here is that of *P. cookei* (UM 87990). In addition, nearly all known specimens referable to Plesiadapidae and representing a major or critical portion of the cranium were examined for this study. The one exception that could not be located is MNHN CR 7377, an isolated squamosal glenoid, petrosal, and ectotympanic of *P. tricuspidens* from the locality of Berru near the city of Reims in northern France.

The cranium of *P. cookei* is compared to those of other species of *Plesiadapis*, mainly *P. tricuspidens* (crania MNHN CR 125, 126, 965, 4306, the Pellouin skull; and isolated petrosals MNHN BR 1371, 17414–17419), and the edentulous partial rostrum of *P. anceps* (YPM-PU 19642).

The cranium of *P. cookei* is compared to those of other plesiadapid genera including *Pr. gaoi* (UALVP 46685, 46687 and 49105), *N. intermedius* (USNM 309902), and *N. gidleyi* (AMNH 17388),

Postcrania.— Postcranial elements of *P. cookei* are compared to those of other species of *Plesiadapis*, including *P. rex* from Cedar Point Quarry in Wyoming, *P. churchilli* from Divide Quarry in Wyoming and Wannagan Creek in North Dakota, and *P. tricuspidens* from Berru near the city of Reims in northern France (see tables for specimen numbers).

Postcranial elements of *P. cookei* are compared to those of other plesiadapid genera including a partial skeleton of *N. intermedius* (USNM 442229, USNM 309900, USNM 399898) from the Bangtail locality of Montana, a partial skeleton of *N. gidleyi* (AMNH 17388, AMNH 17379, AMNH 17409) from the Mason Pocket locality of Colorado, and to isolated

specimens referred to *Pr. gaoi* from the Paskapoo Formation of Alberta;

These comparisons serve the usual role of highlighting probable species and generic-level differences but they also help in evaluating whether all of the elements included in UM 87990 are correctly attributed to *P. cookei*. Qualitative and quantitative comparisons are also made to various extant taxa. Specimen numbers for extant specimens are given in the descriptive and comparative text and in the tables.

METHODS

Digital photography and microscopy.— Cranial and small postcranial specimens were studied under a binocular light microscope. Anatomical identities of cranial sutures and foramina were established through comparison to extant and fossil skulls. Cranial morphology was photo-documented using a Nikon Coolpix 4500 camera mounted on a copy stand or tripod.

Postcrania morphology was photo-documented using a Canon SLR digital camera mounted on a copy stand. For more detailed morphology, we used a continuously-calibrated (for pixel scale) digital camera mounted on a steREO Discovery V12 Zeiss microscope with a 0.63x objective lens and 10x ocular lens, motorized focus and zoom, and capacity for reflected and transmitted illumination of objects in the object field (maximum = 36.5 mm) via two Zeiss LCD 2500 light boxes. Measurements were taken from the resulting photographs (on structures such as cranial foramina) with digits recorded to the nearest hundredth of a millimeter using the measurement software Axiovision 4.4 (though precision is probably much less than this and on the order of ±2%). In some cases, for small specimens that could not be imaged with the Zeiss microscope, camera lucida drawings were made and measured.

Prior to photography, all specimens were whitened with ammonium chloride salt or magnesium powder to remove tonal contrasts due to the mottled coloration of the fossil or glare off the surface. After whitening, dark and light areas on a specimen correspond predominantly to shadows and highlights, respectively, and reveal the specimen's shape more effectively. All externally visible morphological structures pertinent to the description are labeled on the figures. Many cranial features are labeled with numbers. Other bones are identified with abbreviations.

Italicized numbers following figure citations in the description below correspond to morphological features labeled in some or all of the cited figures.

High resolution x-ray computed tomography (microCT or μCT).— MicroCT data were acquired from Pennsylvania State University for the cranium of UM 87990. The original scan consisted of 1435 slices spaced at 0.0614 mm, each slice having a pixel resolution of 0.0527 mm. During the scan, the specimen was embedded in florist foam to hold it in place. Additionally, the florist foam was saturated with water, which constituted a wedge to help improve contrast between matrix and bone. Scans of additional crania and cranial fragments were also acquired at PSU's Center for Quantitative Imaging and other facilities. These are archived in MorphoSource and listed with DOIs in Table A-VI-1. CT and μCT data on the postcrania of UM 87990 were acquired from Stony Brook University facilities. A medical scanner was used for larger bones, and a μCT40 machine was used for hand and foot bones and these scans were used in the images and analyses of the current study. They have not been archived for access by other researchers. Instead, since this study was completed, every bone was scanned at Duke University using a Nikon XTH 225 ST and archived on MorphoSource.org (Boyer et al., 2016). See Table A-VI-2 for a list of the elements scanned, scanning resolutions, and DOI links where each bone can be accessed.

Data were visualized with the software Amira 4.1.2-1 and Image J, which assisted in description of internal morphology. MicroCT data were particularly important for verifying identifications of various cranial foramina. Comparative μCT data were acquired for a number of other specimens (Tables A-I-1 through A-I-5).

MEASUREMENTS AND ANALYSIS

Crania.— Measurements were taken using digital calipers, digital photographs, camera lucida drawings, and bone reconstructions from scan imagery (Appendix I; Tables A-I-1 through A-I-9). Repeated measurements of foramina suggest standard errors of about one-twentieth of a millimeter (manufacturer's claimed accuracy is ±0.001 inches). Other cranial measurements tend to have higher errors of about one-tenth of a millimeter. These measurements were used to compare shape and size differences between crania of *P. cookei* (UM 87990) and other plesiadapids.

Postcrania.— Various measurements were taken (1) on physical specimens and casts using digital calipers, (2) on photographs using the software Sigma Scan Pro 5.0; or (3) on surfaces created from μCT scan images using the software Amira 4.1.2-1 and Aviso 5.0. These measurements are presented in tables of Appendix II organized by bone or region of a bone. Along with raw measurements, various shape ratios are presented. The names of these measurements and ratios are defined in Table A-II-1. Measurements recorded here are used to assist in descriptions of the shapes of bones and to compare shape and size differences among bones of *P. cookei* (UM 87990) and those of other taxa. In addition to providing a set of 'new' measurements, all measurements used and defined by Sargis (2002a, b) and Szalay and Dagosto (1980) are recorded here. Some or all of their data are incorporated into analyses. Various analyses were undertaken using the programs SPSS 11.0 and PAST.

Measurements and shape indices of *P. cookei* are compared to those of samples of *P. tricuspidens* and other plesiadapids using Student's t-test (Sokal and Rohlf, 1995). These analyses assume UM 87990 represents the mean for *P. cookei* and determine the probability that distributions of measurements for other plesiadapid samples have the same mean. When linear or area measurements are compared among taxa, the values were first natural-log transformed. This was done

because arithmetic variance in a measurement of biological populations is typically correlated with the population mean of that measurement. As a result, distributions of measurements of biological samples are expected to be right skewed, whether statistical power is available to test this or not (Sokal and Rohlf, 1995; Gingerich, 2000). Logarithms express metrical data in terms of proportions and thereby provide a data format that can be analyzed to meaningfully address biological questions. For instance, the observation that an elephant population has absolutely greater variance in body mass than a mouse population is not very informative. However, finding a difference in variance in logarithms of body mass would deserve further consideration.

Principal components (PC) analyses are used to compare various sets of measurements of *P. cookei* to those of samples of extant and fossil taxa. Specifically, PC analyses are undertaken on variables sampling aspects of the skeleton in six different ways, including variables sampling (1) the distal end of the humerus; (2) metacarpals; (3) astragalus; (4) calcaneum; (5) aspects of the vertebral column; and (6) combinations of long bone and body segment lengths. Size-standardized variables were created for these analyses by dividing each measurement for a given specimen by the geometric mean of all, or a subset, of the linear measurements for that specimen. This method of size-standardization has been shown to be successful by numerous researchers (e.g., Mosimann and Malley, 1979; Jungers et al., 1995; Hamrick et al., 1999). Any measurements that could conceivably have values of zero or less were excluded from geometric mean calculations (e.g., the distance that the greater trochanter of the femur projects proximal to the femoral head could easily be positive, zero, or negative in a taxon of any absolute size). Particular variable sets used to create geometric means are cited in relevant table legends below. The resulting geometric mean ratios were then natural-log transformed.

ACKNOWLEDGMENTS

Comparative analysis of the *P. cookei* skeleton described here (UM 87990) formed a substantial part of the first author's Ph.D. dissertation (Boyer, 2009) in the Department of Anatomical Sciences at Stony Brook University. The dissertation advisor was David W. Krause, the chair of the dissertation defense was Maureen A. O'Leary, and the dissertation committee included John G. Fleagle, William L. Jungers, and PDG. Maureen A. O'Leary encouraged us to assess features characterizing basal plesiadapids in a more organized, better documented, and more methodologically rigorous fashion than attempted initially. Preparation of UM 87990 was carried out by William J. Ryan and later Ellen Miller and William J. Sanders at the University of Michigan using acid reduction techniques later described in Bloch and Boyer (2001). William J Sanders supervised production of research quality casts of the specimen. Discussion with Jonathan I. Bloch, Marc Godinot, Gregg F. Gunnell, Jonathan M. G. Perry, Kenneth D. Rose, Ross Secord, Mary T. Silcox, B. Holly Smith, and many other researchers contributed substantially to our research.

We thank Marc Godinot, Pascal Tassy and Claire Sagne of the Museum National d'Histoire Naturelle in Paris, and Jean-Louis Pellouin in Reims for access to important comparative specimens of *Plesiadapis* and *Platychoerops*. Richard Fox and Craig Scott provided access to specimens at the University of Alberta Laboratory for Vertebrate Paleontology. Meng Jin provided access to specimens in the American Museum of Natural History. K. Christopher Beard provided access to undescribed material of *Chiromyoides caesor* and *N. gazini* in the Carnegie Museum of Natural History, Pittsburgh. John Fleagle provided access to specimens at Stony Brook University. Robert Emry and Nicholas Pyenson provided access to specimens in the United States National Museum of Natural History. Walter Joyce and Donald Brinkman provided access to specimens in the Yale Peabody Museum–Princeton University collection. In Chapter VI (Phylogeny), the character matrix of Bloch et al. (2007) was downloaded from Morphobank.geongrid.org. The character matrix of Bloch and Silcox (2006) was obtained from M. Silcox.

We are grateful to Alan Walker, Timothy Ryan, and others at the Center for Quantitative Imaging, Pennsylvania State University, for providing high-resolution μCT scans of UM 87990; and to Stefan Judex and Clinton Rubin at the Center for Biotechnology in the Department of Biomedical Engineering at Stony Brook University for providing high-resolution μCT scans of UM 87990 and comparative material.

This research was funded by a U. S. National Science Foundation [NSF] Graduate Research Fellowship, an Evolving Earth Foundation grant, an NSF Doctoral Dissertation Improvement Grant (BCS-0622544), and an American Society of Mammalogists grant, all to D. M. Boyer. Field research leading to discovery of UM 87990 was funded by NSF grant EAR-8408647 to P. D. Gingerich. Study of UM 87990 was advanced by NSF grant BCS-0129601 to P. D. Gingerich and G. F. Gunnell, and by NSF grant EAR-0308902 to D. W. Krause and J. I. Bloch. In addition, NSF BCS grants BCS-1317525 (to D. M. Boyer and E. R. Seiffert), BCS-1304045 (to D. M. Boyer and E. M. St. Clair), BCS-1440742 and 1558555 (to D. M. Boyer and G. F. Gunnell), and BCS-1552848 (to D. M. Boyer) provided support while preparing this work. Jukka Jernvall contributed to development of several publications whose conclusions were important for interpreting data presented here. These include Boyer et al. (2010a) and Boyer et al. (2012a,b). We wish to thank Jonathan I. Bloch and John Wible for careful review of an earlier version of this manuscript. Finally, we thank editor Jeffrey A. Wilson, illustrator Carol Abraczinskas, and composer Linda Garcia for their patience and hard work bringing this project to completion.

II

SYSTEMATIC PALEONTOLOGY

Class MAMMALIA Linnaeus, 1758
Order PROPRIMATES Gingerich, 1989
Superfamily PLESIADAPOIDEA Trouessart, 1897
Family PLESIADAPIDAE Trouessart, 1897

Plesiadapidae are Paleocene and early Eocene mammals with enlarged and procumbent central incisors, simple wedge-shaped lower premolars, and robust molars. Their upper central incisors are generally tricuspid, and lower central incisors typically have a distinct 'margoconid' on the dorsal surface near the base of the crown. Their upper molars have a distinct postprotocingulum, and last lower molars have an elongated talonid.

PLESIADAPIS Gervais, 1877

Plesiadapis cookei Jepsen, 1930
Fig. 1ff.

Plesiadapis cookei Jepsen, 1930, p. 525, pl. 10: 1–7.
Plesiadapis cf. *cookei*, Gazin, 1942, p. 218.
Plesiadapis cookei (in part), Gazin, 1956, p. 5, pl. 1: 5–8.
Plesiadapis cookei, Simpson, 1937, p. 2. Wood et al., 1941, p. 9. Wood, 1967, p. 23. Gingerich, 1976, p. 33, pl. 5: H, K; 6: B, I. Dorr and Gingerich, 1980, p. 109. Rose, 1981, pp. 59, 129, 132; fig. 25. Anemone and Dirks, 2009, p. 118; fig. 4.
Plesiadapis gingerichi (in part), Dawson and Beard, 1996, p. 304.
Plesiadapidae, large sp., Wilf et al., 1998, p. 520.

Holotype.— YPM-PU 13293, associated left upper incisor, right maxilla, left and right dentaries, and right lower incisor.

Type locality.— "Upper, or Clark Fork, Paleocene, Little Sand Coulee basin, R101W, T57N, probably Sec. 32, Park County" (Jepsen, 1930, pp. 525–526). This locality is in the uppermost Fort Union Formation in the Clarks Fork Basin of northwestern Wyoming. The type locality is labeled PU 13293 on the map in Fig. 3.

Age and distribution.— *Plesiadapis cookei* was initially regarded as an index fossil for the Clarkforkian land mammal age (Wood et al., 1941), but it is now known to have a more restricted range. The middle Clarkforkian '*Plesiadapis cookei*' and 'Cf-2' biozones were initially based on the stratigraphic range of *P. cookei* (Rose, 1981; Gingerich, 1983). In the most recent revision of Clarkforkian biozones, Secord et al. (2006) redefined the boundary between Cf-2 and Cf-3. *P. cookei* continues to mark Cf-2, but now also ranges upward into the lower part of Cf-3 (see below).

P. cookei is known from many localities straddling the Fort Union and Willwood formational boundaries in the Clarks Fork and northern Bighorn basins of northwest Wyoming (Jepsen, 1930; Rose, 1981; see map in Fig. 3). The species is also known from several additional North American basins, all in western Wyoming. These are, from north to south, the Purdy Basin in Togwotee Pass (Rose, 1981), the Green River Basin (Gazin, 1942, 1956; Dorr and Gingerich, 1980), the Great Divide Basin (Anemone and Dirks, 2009), and the Washakie Basin (Rose, 1981; Wilf et al., 1998).

Emended diagnosis.— In practice, specimens of *P. cookei* are easily distinguished from all other North American plesiadapid species on the basis of their absolutely larger tooth size. Postcranial elements are correspondingly absolutely larger as well. *P. cookei* differs from all other species of *Plesiadapis* (in which foregoing features can be assessed) in (1) having absolutely larger incisors and molars; (2) having an upper central incisor (I^1) with a relatively long anterocone and laterocone, a minute mediocone; (3) lacking a tooth at the upper second premolar position (P^2); and (4) having a zygomatic process of the maxilla that arises lateral to M^1 (arises lateral to M^2 in other species). Postcranially, UM 87990 differs from other plesiadapids in having (1) more slender long bones (i.e., their proximodistal length is greater relative to cross-sectional diameter of the midshaft region), (2) a more distally projecting acromion process of the scapula, (3) features of the astragalus and calcaneus indicating a more axially mobile lower ankle joint, (4) features of the calcaneus and cuboid indicating more powerful ability to evert the foot (or to resist inversive forces), and (5) intermediate phalanges that are mediolaterally narrower than dorsoventrally tall.

Referred specimens.— Thirty-two University of Michigan localities in the Sand Coulee (SC) area of the Clarks Fork Basin and the Foster Gulch (FG) and McCullough Peaks (MP) areas of the northern Bighorn Basin have yielded specimens of *P. cookei* (Table 1) These include the skeleton of UM 87990 described here from locality SC-117. Three additional Princeton localities in the Sand Coulee area have yielded five additional specimens in the YPM-PU collection. All of these specimens are plotted on the distribution map in Figure 3.

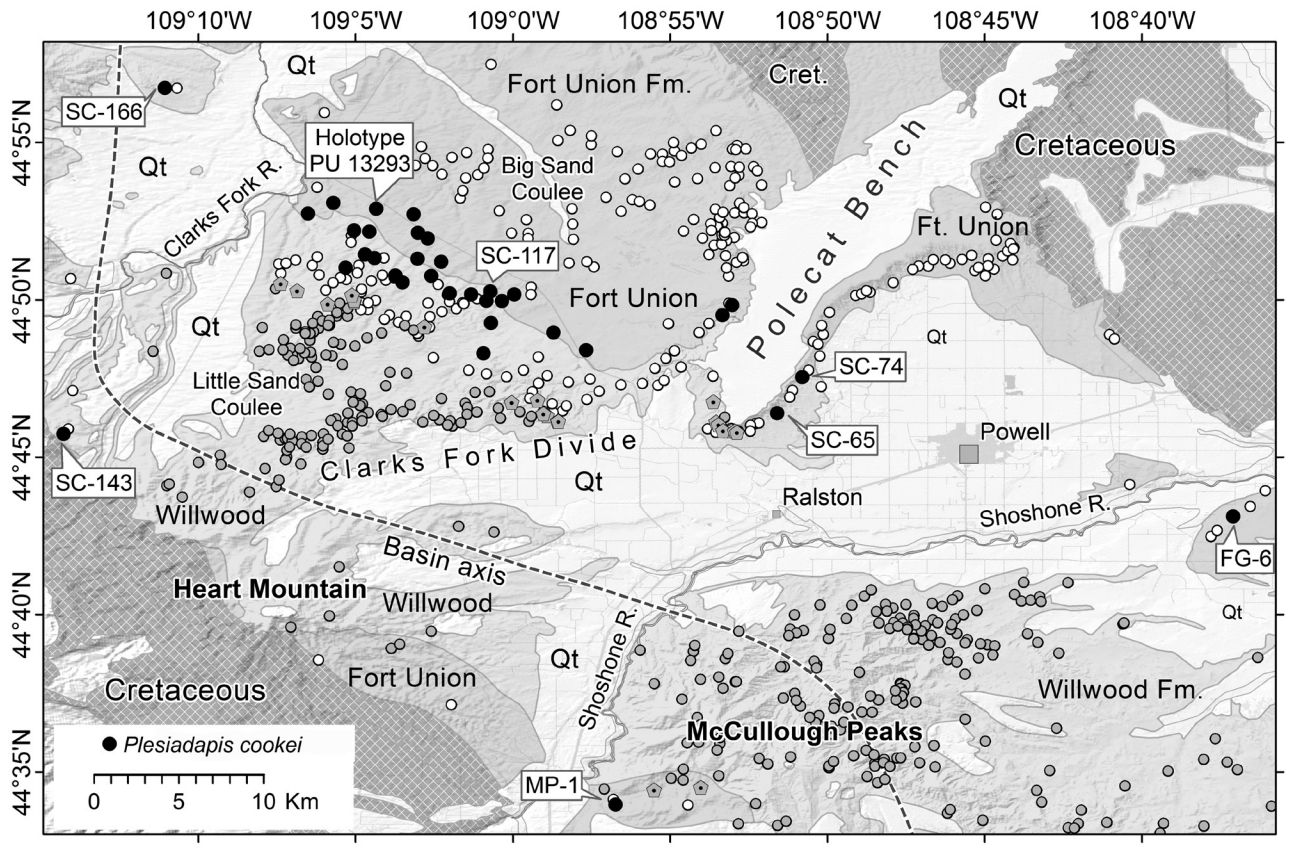

FIGURE 3.— Distribution of *Plesiadapis cookei*-bearing localities in the Clarks Fork and northern Bighorn basins of Wyoming. The principal settlement here is the town of Powell, Wyoming. Two geological formations yield fossils of interest here: the Paleocene Fort Union Formation and the overlying upper Paleocene and lower Eocene Willwood Formation. Open circles are University of Michigan [UM] localities yielding Paleocene mammals, and gray circles are UM localities yielding early Eocene mammals. Black circles are UM and old Princeton University localities yielding late Paleocene specimens of *Plesiadapis cookei*. Note that Clarks Fork Basin *P. cookei* is found in both uppermost Fort Union and lowermost Willwood strata.

STRATIGRAPHIC RANGE OF *PLESIADAPIS COOKEI*

Rose (1980, 1981) proposed a three-part subdivision of the Clarkforkian land-mammal age. He recognized the concurrent range zone of Rodentia and *Plesiadapis gingerichi* as early Clarkforkian, the stratigraphic range of *P. cookei* as middle Clarkforkian, and the *Phenacodus-Ectocion* acme zone as late Clarkforkian. The last was effectively the interval of Clarkforkian time following extinction of *P. cookei*. The three zones were subsequently abbreviated Cf-1, Cf-2, and Cf-3, respectively, without changing their definition (Gingerich, 1983).

Secord et al. (2006) revised Clarkforkian biostratigraphy by defining a new *Copecion* interval zone to replace the *Phenacodus-Ectocion* acme zone of Rose (1980, 1981), based on the first appearance of what Thewissen (1990) regarded as *Copecion brachypternus*. There are two motivations for this redefinition of Cf-3: it is preferred to recognize the start of an internal by the appearance, rather than the disappearance, of species; second, abundance can be influenced by taphonomic and local paleoenvironmental biases and has limited value for regional correlation. The phenacodontid *Copecion* was chosen to redefine Cf-3 because it makes its first appearance overlapping with *P. cookei* relatively late in Clarkforkian time. Redefinition of Cf-3 changes the definition of Cf-2 as well, from a range zone representing the stratigraphic range of *P. cookei* to an interval zone bracketed by the first appearance of *P. cookei* and the subsequent first appearance of *Copecion*.

Copecion is not common in Cf-3. Only 11 specimens are known from eight localities, comprising about 1% of ca. 1100 Cf-3 mammalian specimens in the UM collection, but its first occurrence provides an objective datum. The underlying Cf-2 biozone is well sampled (>2000 specimens in the UM collection), and *Copecion* has not been identified in this interval (as redefined). However, the earliest record of *Copecion*, UM 88181, comes from locality SC-117, which is the locality yielding the *P. cookei* skeleton described here (Fig. 5). Thus, following Secord et al. (2006), a substantial number of *P. cookei* specimens, including the UM 87990 skeleton, come from the early part of Clarkforkian zone Cf-3.

FIGURE 4.— University of Michigan locality SC-117 yielding UM 87990 skeleton of *Plesiadapis cookei*. White arrow shows where the skeleton was found. Collector is standing at the discovery site; view is toward the northwest. Rose (1981) mapped these strata as Willwood Formation, and beds near the top of the hill on the left side of the photograph include red paleosols.

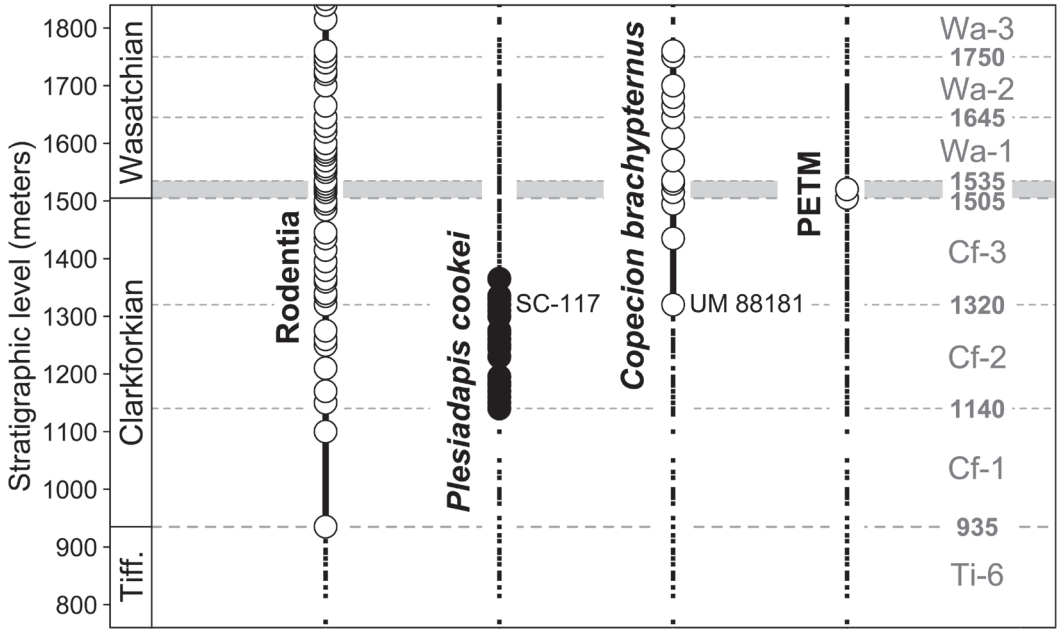

FIGURE 5.— Stratigraphic ranges of taxa defining the early, middle, and late Clarkforkian land-mammal age, Cf-1, Cf-2, and Cf-3, respectively, in the Clarks Fork Basin of northwestern Wyoming. Following Secord et al. (2006), the beginning of Cf-1 is defined by the first appearance of Rodentia (open circles), the beginning of Cf-2 is defined by the first appearance of *Plesiadapis cookei* (filled circles), and the beginning of Cf-3 is defined by the first appearance of *Copecion brachypternus* (open circles). The ends of Cf-1, Cf-2, and Cf-3 are marked, respectively, by the beginnings of Cf-2, Cf-3, and Wasatchian zone Wa-M during the onset of the Paleocene–Eocene thermal maximum (PETM; open circles). Meter levels are measured from the Cretaceous–Paleogene boundary at the base of the Fort Union Formation on Polecat Bench (see Fig. 3). Small dots mark stratigraphic intervals with mammalian samples. Note that a single specimen of *Copecion*, UM 88181 from UM locality SC-117, marks the beginning of Cf-3. On this basis the Cf-2 middle Clarkforkian taxon *P. cookei* is interpreted as ranging upward into Cf-3.

TABLE 1.— University of Michigan localities preserving *Plesiadapis cookei*, which yielded 190 specimens including the UM 87990 skeleton described here (locality SC-117). Most localities are in the Sand Coulee (SC) area of the Clarks Fork Basin, but several specimens are known from the Foster Gulch (FG) and McCullough Peaks (MP) areas of the northern Bighorn Basin. YPM-PU specimens 18046, 18118, 18138, 18312, and 19590 are from imprecisely known localities in the Clarks Fork Basin.

Locality	Specimens
FG-6	UM 74069; YPM-PU 17825
MP-1	YPM-PU 17973
SC-19	UM 63288, 64999, 65008, 65009, 65014, 65016, 65028, 65031, 65035, 65041, 69300, 69344, 69698, 80263, 80265, 80268, 80270, 80274, 80277, 82364, 82370, 82373, 85990, 85995, 98093, 98094, 98098, 108356, 112649, 112658, 112659, 112661
SC-20	UM 65049, 65050, 65053, 72892, 73704, 73891, 73892, 74040, 78914, 83004
SC-53	UM 111845
SC-61	UM 65716
SC-62	UM 65720, 69682, 71764, 82029, 98458, 101778, 102392
SC-65	UM 66125
SC-74	UM 66179, 80439
SC-91	YPM-PU 19846
SC-92	YPM-PU 19538, 19819; UM 66326, 98467, 101903
SC-98	UM 82352
SC-110	YPM-PU 17977
SC-115	UM 66701, 66702, 66703, 66704, 66705, 88177, 114565
SC-116	UM 66716, 66718, 66720, 66721, 67252, 73410, 73411, 98429, 98431, 98432
SC-117	UM 66725, 66730, 66731, 66734, 66739, 66741, 66746, 73414, 73415, 73417, 73653, 73655, 87798, 87804, 87809, 87990, 87992, 87994, 88001, 88004, 88172, 88183, 95858, 95868, 98073, 98074, 98075, 98076, 98077, 98083
SC-119	UM 66755
SC-120	UM 66765, 67018
SC-127	UM 66911, 66919
SC-134	YPM-PU 13293, 17893
SC-135	YPM-PU 13307, 13308
SC-136	YPM-PU 18056, 18093, 18097, 18098, 19547, 19551, 19621, 19623, 19624, 19851, 21009; UM 67187, 67190, 67203, 69235, 69906, 69913, 82025
SC-143	YPM-PU 13342, 17934, 17936, 17937, 17938, 17939, 17940; YPM 24616; UM 69934, 71016, 71031
SC-166	UM 68278. AMNH 16077 came from somewhere near this locality
SC-188	UM 68861, 68870, 69221, 71646, 71659, 73404, 82030, 94822, 109669, 109678, 109682, 109696, 109700, 109701, 109702, 109712, 109716, 109719, 109730
SC-189	UM 68875
SC-195	UM 69175, 69306
SC-201	UM 69265, 69271, 69313, 69319
SC-209	YPM-PU 21003
SC-220	UM 69995, 69999
SC-367	UM 63284, 63289, 65533, 65538, 69339, 69341, 80236, 80237, 98198
SC-368	UM 65662

III

CRANIAL MORPHOLOGY

Plesiadapis cookei is the largest and one of the latest-occurring North American plesiadapid species (Jepsen, 1930; Gingerich, 1976). The skull and postcranial skeleton (UM 87990; Fig. 1) described here are each the most complete known for a North American plesiadapid, and direct association of the skull with the rest of the skeleton make this specimen especially important for testing functional and phylogenetic hypotheses relating to early primate evolution. The new skull is similar its completeness to skulls of the large European species *P. tricuspidens* from the Paris Basin in France (Russell, 1964; Gingerich, 1976; Fleagle, 1999; Boyer et al., 2010a, 2012a, b). In some ways it is actually more complete than the European specimens (e.g., it retains most of its maxillary teeth). In other ways, it is not as well preserved as the Pelluoin skull and MNHN CR-125 due to more crushing of the neurocranium (see Boyer et al., 2010a).

The craniodental material of UM 87990 was preliminarily described by Gingerich and Gunnell (2005:187) as being preserved in five pieces: a palatal/splanchnocranial piece, a neurocranial piece with well-preserved auditory bullae, a frontoparietal piece, and two dentaries. Following additional preparation, the three skull pieces were glued together. Gingerich and Gunnell (2005) did not include in their count some additional pieces that are also part of the skull, including fragment of the left squamosal and zygomatic sutured together, an anterior piece of a left premaxilla, and a fragment of the right nuchal crest. The last two elements are illustrated here as isolated bones. A fragment of the right zygomatic bone was removed since Gingerich and Gunnell's (2005) description, but was temporarily reattached for photography. Finally, the ventral part of the right ectotympanic bone was either intentionally or accidentally removed, sometime after it was illustrated in Bloch and Silcox (2001: fig. 7), at which point it appeared to be connected to the rest of the skull. This has not been reattached because, when separated, the annular part of the ectotympanic and more of the promontorium can be viewed and studied than would otherwise be possible. Thus the skull is now in seven pieces, which accounts for gluing together of some of the original 5 mentioned by Gingerich and Gunnell (2005), the addition of more pieces, and the two dentaries.

The skull suffered a substantial amount of brittle deformation following burial. This distorts the true dimensions to some extent as evaluated by Boyer et al. (2010a) who concluded that this deformation has reduced the original mediolateral and dorsoventral dimensions of the neurocranium quite substantially. We include the corrections to the estimate of the cranium's overall length from their study here. UM 87990 is interpreted to represent a young adult individual because the complete set of permanent teeth is present, fully erupted, but tooth crowns show little occlusal wear and many long bone epiphyses remain unfused (see Chapter V).

Table 2 is a list of numerical codes for cranial structures that match the numerical codes used in Boyer et al. (2012a). Table 3 is a list of abbreviations for cranial bones and anatomical structures that is also consistent with Boyer et al. (2012a)

DESCRIPTION

Nasal.— The nasals have been shifted out of anatomical position; thus their shape is apparent, but their contacts with other bones are not (Fig. 6). Their mediolateral width is fairly constant from anterior (average unilateral width = 4.9 mm) to posterior (average unilateral width = 4.5 mm), but there is possibly a slight midpoint constriction (Fig. 6). Due to breakage, shifting, and crushing of bone, it is not possible to determine whether the nasals were isolated from contact with the maxillae by premaxillae (Fig. 6:*1*), as they are in other plesiadapids. The nasals appear to have extended posteriorly to the level of M^1, but the exact termination point is uncertain due the skull's deformation.

Premaxilla and premaxillary dentition.— The anterior part of the right premaxilla is preserved (Fig. 7). Sutures with the nasal, maxilla, and opposing premaxilla are visible. The nasal suture is straight and simple (Figs. 6, 7:*1*). The maxillary suture is observable just posterior to I^2 (Fig. 7:*2*). It is relatively straight and oriented dorsoventrally before turning dorsally to curve posteriorly. A strip of bone exists along this sutural edge, with an anteroposterior width of up to about 2 mm, and this appears to have received the maxilla on its lateral side. A higher magnification view of this surface reveals anteroposteriorly directed grooves and ridges, marking the early stages of what would likely have become pronounced 'inter-locking' of bones along the maxillary/premaxillary suture in an older individual (Fig. 7B: inset). Whether the incisive foramen is contained completely within the premaxilla or at the juncture with the maxilla cannot be determined because of some breakage in this region (Fig. 7). Even so, the symphyseal surface for the right premaxilla is present (Fig. 7:*3*), as well as some surface for palatal contact with the maxilla (Fig. 7:*2*).

The premaxilla has alveoli for just two teeth, interpreted as I^1 and I^2, with the latter preserved in place (Fig. 7). I^1 is not

TABLE 2.— List of numbered cranial features and the illustrations where they appear.

No.	Feature	Illustration
1	Premaxilla/nasal suture	Figs. 6–7, 9–11
2	Premaxilla/maxillary suture	Figs. 6–7, 9–11
3	Premaxillary symphysis	Figs. 6–7
4	Lacrimal/frontal suture in orbit	Figs. 6, 9
5	Lacrimal/zygomatic suture in orbit	Fig. 6
6	Maxilla/frontal suture on forehead	Fig. 6
7	Maxilla/palatine suture at level of M1 in palate)	Fig. 10
8	Notch between pterygoid process of palatine and M3 alveolus marking lesser palatine nerve route	Fig. 10
9	Maxilla/palatine suture at level of M3 in palate	Fig. 10
10	Dorsal communication of M3 alveolus with orbital cavity	Figs. 6, 8, 10
11	Infraorbital foramen	Figs. 8–11
12	Zygomatic/maxillary suture	Figs. 6, 8–11
13	Edge of orbital excavation on zygomatic bone	Figs. 6, 8–11
14	Expansion of ventral surface of zygomatic for masseter attachment	Fig. 10
15	Metopic suture	Figs. 6, 11–12
16	Ridges of frontal trigon	Figs. 6, 11
17	Frontal/parietal suture, most anterior part	Figs. 6, 9, 11
18	Cross-sectional view of frontal parietal contact	Fig. 12
19	Endocranial surface of frontal, depressions for olfactory bulbs	Fig. 10
20	Frontal/parietal suture on endocranial surface	Fig. 10
21	Base of left pterygoid process of palatine	Fig. 10
22	Postpalatine torus	Fig. 10
23	Postpalatine spine	Fig. 10
24	Sagittal crest	Figs. 6, 9, 11–13, 16
25	Nuchal crest	Figs. 6, 9, 13, 16
26	Parietal/?interparietal suture on dorsum of skull	Fig. 13
27	Glenoid fossa	Figs. 9–10
28	Postglenoid process	Figs. 9–10
29	Postglenoid foramen	Fig. 10
30	Entoglenoid process	Figs. 9–10
31	Basisphenoid entopterygoid process	Figs. 10, 12
32	Alisphenoid ectopterygoid process	Figs. 10, 12
33	Canal leading to sphenorbital fissure	Figs. 12
34	Possible vidian canal	Figs. 12
35	Pars cochlearis of petrosal	Figs. 10, 15
36	Pars canalicularis of petrosal	Fig. 10
37	Tympanic processes of auditory bulla	Figs. 10, 15
38	Digastric fossa, stylomastoid foramen area (?)	Figs. 9–10
39	Paroccipital process (mastoid process) of petrosal	Figs. 9–10, 16
40	Tubular external auditory meatus	Figs. 9–10, 15–17
41	Crista tympanica	Figs. 15, 17
42	Bony struts supporting crista tympanica	Fig. 17
43	Sagittal ridge of bone on basioccipital	Fig. 10
44	Occipital condyles	Figs. 9–10, 16
45	Hypoglossal foramen	Fig. 10
46	Jugular foramen	Fig. 10
47	Jugular processes	Fig. 10, 16
48	Foramen magnum	Fig. 16
49	Sagittal contact between right and left exoccipitals	Fig. 10, 16
50	Sutural contact between remnants of supraoccipital and exoccipital	Fig. 16
51	Wedge-shaped depression on exoccipitals, where supraoccipital is lost	Fig. 16

TABLE 3.— Anatomical abbreviations for the cranium.

Abbrev.	Feature
Cranial bones	
Boc	Basioccipital
Bul	Bulla forming bone
De	Dentary
Ect	Ectotympanic
Eoc	Exoccipital
Fr	Frontal
Lc	Lacrimal
Mx	Maxilla
Ns	Nasal
Pa	Parietal
Pal	Palatine
Pmx	Premaxilla
Ptr	Petrosal
Soc	Supraoccipital
Sq	Squamosal
Zy	Zygomatic
Miscellaneous osteological feature	
ac	Aperture for cochlear fenestra
av	Aperture for vestibular fenestra
bs	Bullar suture (?)
cc	Cochlear canaliculus: visible as the most posterior "septum" on medial aspect of promontorium. Houses a canal that connects the spiral cochlea to endocranial space (see MacPhee, 1981). HRxCT data was used in most cases to evaluate the presence of this feature.
eam	External auditory meatus
ec	Epitympanic crest
g1	Groove with a lateral route that likely holds the internal carotid plexus and possibly a remnant of the internal carotid artery
g2	Groove with a slightly more medial route that may hold internal carotid plexus fibers that approach the s1
g3	Groove that leads to the s2, which likely contains contributions from the tympanic plexus, but is probably mainly responsible for transmitting a small vein (MacPhee, 1981)
g4	Groove frequently present, alternative or additional, for tympanic plexus fibers to reach routes 1–3
g5	Groove frequently present that leads from a point ventral to the fenestra vestibuli dorsolaterally, toward the epitympanic crest
ica	Internal carotid artery
icp	Internal carotid (neurovascular) plexus
pcf	Posterior carotid foramen
ps	Posterior septum (and internal carotid canal): laterally curving septum of bone that shields the fenestra cochlea dorsally and holds a canal that leads to the posterior carotid foramen ventrally
s1	First (anterior) septum: most lateral septum extending anteriorly from promontorium (tubal canal forms between s1 and epitympanic crest)
s2	Second (medial secondary) septum: forms medial to s1, projects anteromedially from promontorium. g3 typically leads to the ventral or medial aspect of this septum
s3	Third septum: projects medially between s2 and raised ridge of cochlear canaliculus, more posteriorly
tca	Tympanic canaliculus: Foramina and groove on or near ridge of cochlear canaliculus in tympanic cavity marking the entrance of the tympanic nerve from extracranial space, and the re-entrance of the nerve into the promontorium as it moves laterally to contribute to the tympanic plexus. Associated canals do not communicate with cochlea.

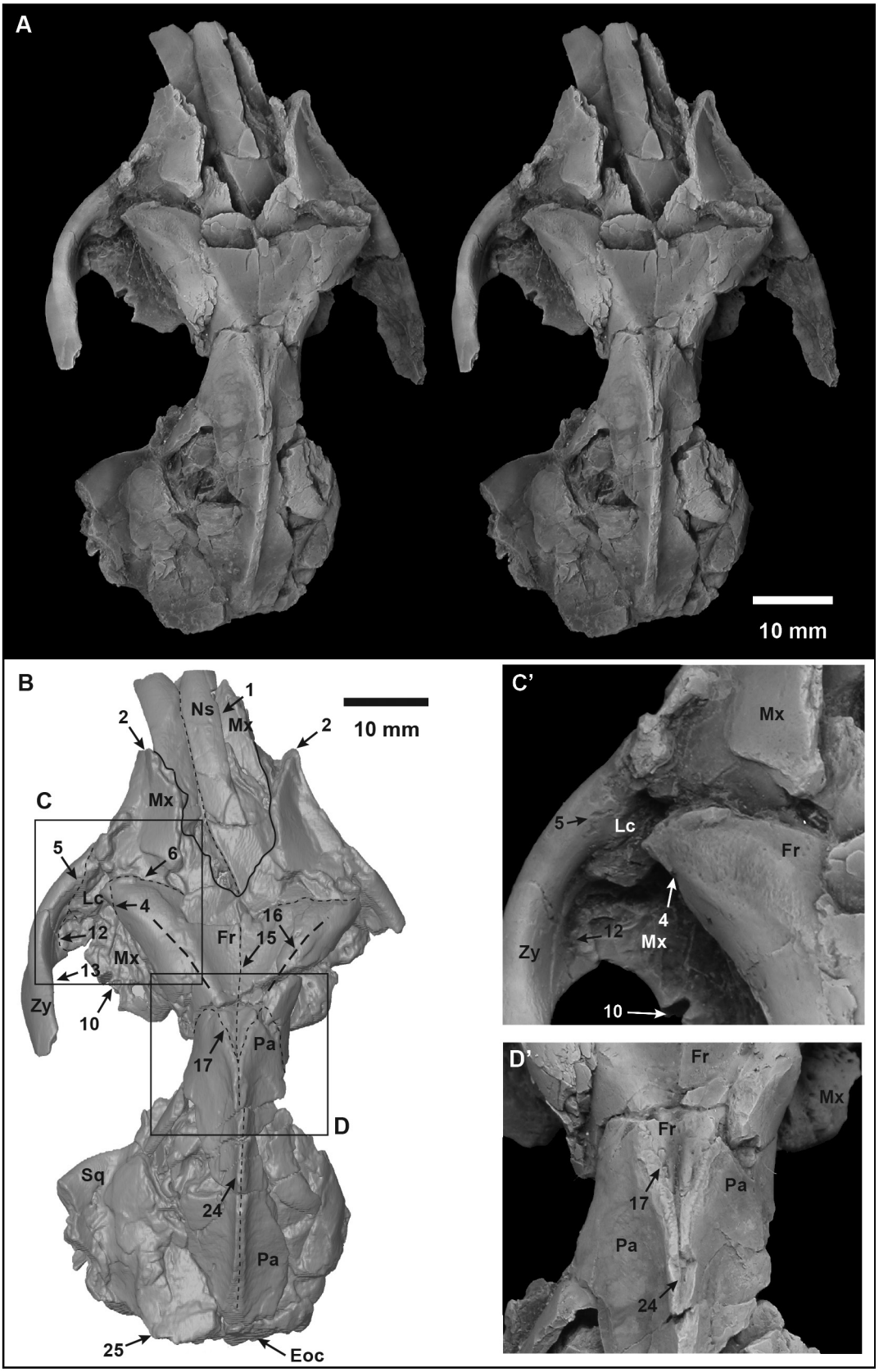
A
10 mm
B
10 mm
Ns
Mx
1
2
2
C
Mx
5
6
Lc
4
12
Mx
13
Zy
10
16
15
Fr
17
Pa
D
Sq
24
Pa
25
Eoc
C'
Mx
5
Lc
Fr
4
12
Mx
Zy
10
D'
Fr
Mx
Fr
17
Pa
Pa
24

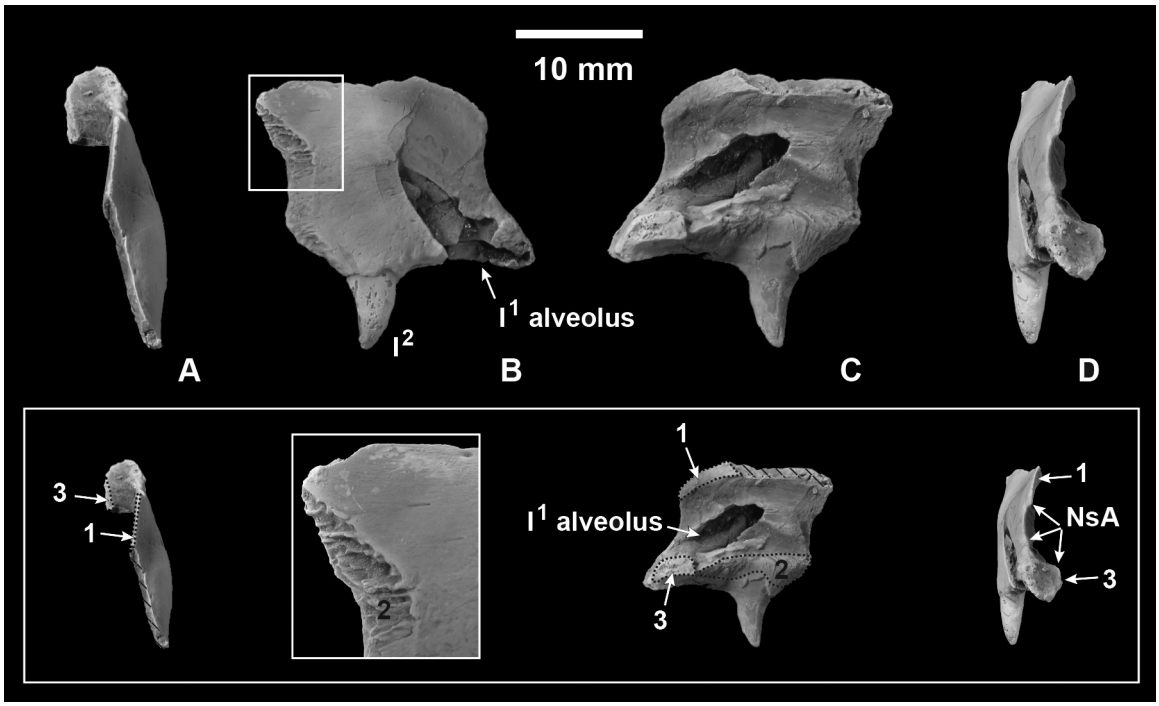

FIGURE 7.— Premaxilla of *Plesiadapis cookei* (UM 87990). **A**, right premaxilla in dorsal view (anterior at top). **B**, same in lateral view (anterior at right). **C**, same in medial view (anterior at left). **D**, same in anterior view (dorsal at top). Corresponding labeled or enlarged photographs are shown in the lower panel. Dashed lines encircle sutural surfaces, and hatching indicates broken surfaces. Abbreviations: *1*, premaxilla/nasal suture; *2*, premaxilla/maxillary suture; *3*, premaxillary symphysis; *NsA*, nasal aperture.

preserved; however, this tooth is known for other individuals of the species (see below). The right I^2 is a simple caniniform tooth. It has a single apical cusp with a distinct crest extending between the apex of the cusp and the base of the crown on the distal side of the tooth. The crown is slightly compressed buccolingually relative to its mesiodistal dimensions. I^2 measures 4.1 mm in mesiodistal length and 2.9 mm in mediolateral width.

Lacrimal.— The lacrimals have been almost completely destroyed by crushing and shearing that have shifted the rostrum posteriorly, displacing the anterolateral margins of the frontal laterally and ventrally into the orbit. On the left side, a small portion of the lacrimal, as well as the frontal and zygomatic sutures, are visible within the orbit (Figs. 6:*4*, *5*; 9:*4*). These visible bits of suture demonstrate that the facial process of the lacrimal did not extend far anteriorly.

Maxilla and maxillary dentition.— The right and left maxillae are preserved with P^4 and $M^{1–2}$ present on both sides, P^3 present on the right side, and alveoli for M^3 present on both sides (Figs. 8–10). This specimen is the first to demonstrate the upper dental formula of *P. cookei*, showing it to lack the upper canine and P^2. Thus, the formula is 2.0.2.3 (two incisors, no canine, two premolars, and three molars). Crowns of the teeth are well preserved with almost no wear, as expected for a young individual (Figs. 8–10).

The anterior margin of the maxilla is preserved. It contacts the premaxilla and reveals a diastema separating I^2 and P^3 that can be estimated confidently to be 14 mm. Anterior parts of the maxillae, as well as their zygomatic, palatal, and alveolar processes are well preserved (Figs. 6, 9–10). The orbital process is crushed (Fig. 9), and thus, the contributions of the maxillae to the orbital mosaics are poorly delimited (Fig. 9). Frontal contact with the maxilla occurs in an interval between the nasal or premaxilla and lacrimal on the dorsum of the skull, measuring 8.9 mm on the left side (Fig. 6:*6*).

The maxilla contacted the palatine along a slightly convoluted suture at the level of M^1 (Fig. 10:*7*). The length of the

FIGURE 6.— Cranium of *Plesiadapis cookei* (UM 87990) in dorsal view. **A**, Stereophotograph. **B**, High-resolution CT of cranium in dorsal view; reconstruction without parallax (boxes show positions of enlargements in C and D). Fine dashed lines are traces of sutures, coarse dashed lines represent temporal crests, and solid lines indicate major discontinuities on the surface of the specimen. **C**, Anteromedial wall of orbit. **D**, Orbitotemporal region. Abbreviations: *1*, premaxilla/nasal suture; *2*, premaxilla/maxillary suture; *4*, lacrimal/frontal suture in orbit; *5*, lacrimal/zygomatic suture in orbit; *6*, maxilla/frontal suture on forehead; *10*, dorsal communication of M^3 alveolus with orbital cavity; *12*, zygomatic/maxillary suture; *13*, edge of orbital excavation on zygomatic bone; *15*, metopic suture; *16*, ridges of frontal trigon; *17*, frontal/parietal suture; most anterior part; *24*, sagittal crest; *25*, nuchal crest; *Eoc*, exocipital; *Fr*, frontal; *Lc*, lacrimal; *Mx*, maxilla; *Ns*, nasal; *Pa*, parietal; *Sq*, squamosal; *Zy*, zygomatic.

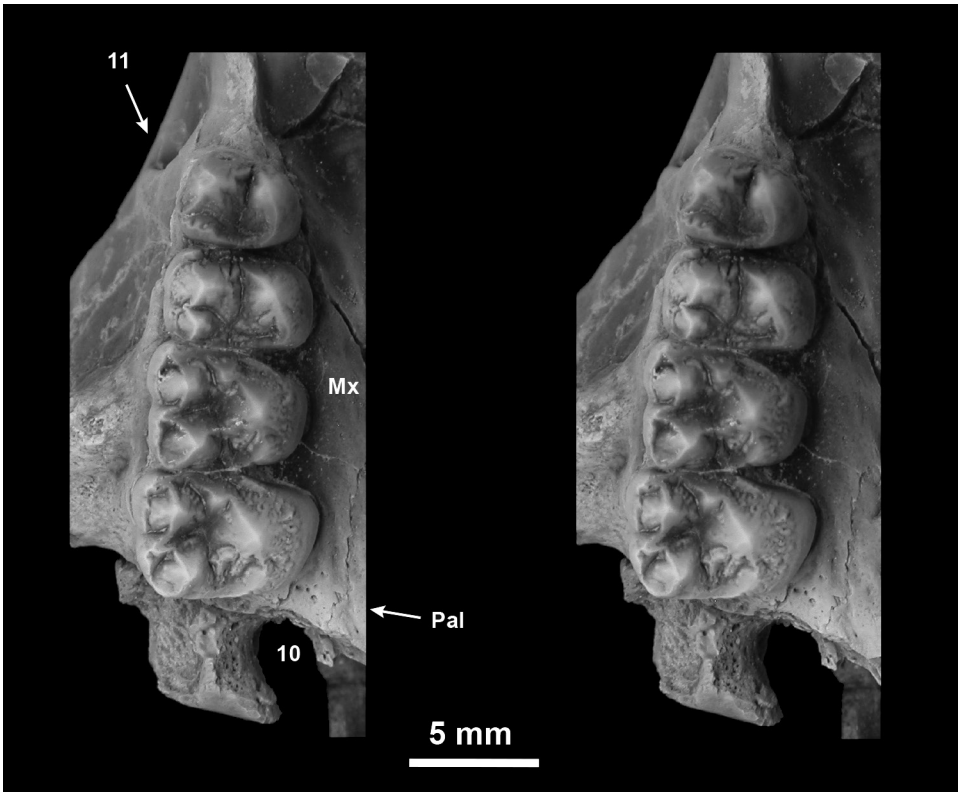

FIGURE 8.— Maxillary teeth of *Plesiadapis cookei* (UM 87990). Stereophotograph shows the right maxilla with P^3–M^2 in occlusal view. Note the absence of P^2, lack of paraconule on $P^{3–4}$, and dilambdodont morphology of molars with mesostyles. These features form a suite of diagnostic characters for *Plesiadapis cookei*. Abbreviations: *10*, dorsal communication of M^3 alveolus with orbital cavity; *11*, infraorbital foramen; *Mx*, maxilla; *Pal*, palatine.

palatal part of the maxilla is 30.2 mm, measured from its contact with the palatine at the M^1 level to the most anterior point. In ventral view, a notch can be seen on the left side of the skull separating the M^3 alveolar process from the pterygoid process of the palatine (Fig. 10:*8*). The palatine/maxilla contact continues from its apex, medial to M^1, and runs posteriorly through the lateral side of this notch, which would have held the lesser palatine nerve and vessels in life (Fig. 10:*9*). If M^3 had been preserved, the length of the tooth row from P^3 to M^3 would have measured about 23 mm. Some of the M^3 alveoli may have breached the dorsal surface of the alveolar process of the maxilla and communicated with the orbital cavity (Figs. 6, 8, 10:*10*). On the left side, it appears that one or both buccal roots communicated, but the lingual root did not (Figs. 6, 10); on the right side only the lingual root did (Fig. 8). This variable pattern may indicate that any apparent dorsal communication between the M^3 alveoli and the orbit in this specimen is actually the result of postmortem breakage.

The alveolar processes were rotated and translated medially during preservation so that the right and left tooth rows are slightly angled toward one another (Fig. 11B); thus, the original inter-tooth row distance has been artificially constricted. The average unilateral breadth of the palate, as preserved, measures 5.5 mm at the level of I^2, 7.7 mm at the anterior margin of P^2, and 13.6 mm at the level of M^3. These first two measurements reveal an anteriorly tapering snout. Though no intermaxillary suture is visible externally, the unilateral width of the maxilla measured from the median sagittal plane is 15.1 mm including the alveolar process. The zygomatic process

FIGURE 9.— Cranium of *Plesiadapis cookei* (UM 87990) in left lateral view. **A**, stereophotograph. **B**, high-resolution CT (reconstruction shown without parallax). **C**, lateral splanchnocranium. **D**, basicranium. Fine dashed lines represent sutures and solid lines indicate major discontinuities on the surface of the specimen. Hatches indicate broken surfaces. Abbreviations: *1*, premaxilla/nasal suture; *2*, premaxilla/maxillary suture; 4, lacrimal/frontal suture in orbit; *11*, infraorbital foramen; *12*, zygomatic/maxillary suture; *13*, edge of orbital excavation on zygomatic bone; *17*, frontal/parietal suture; most anterior part; *24*, sagittal crest; *25*, nuchal crest; *27*, glenoid fossa; *28*, postglenoid process; *30*, entoglenoid process; *38*, digastric fossa; stylomastoid foramen area (?); *39*, paroccipital process (mastoid process) of petrosal; *40*, tubular external auditory meatus; *44*, occipital condyle; *Bul*, auditory bulla; *Eoc*, exoccipital; *Fr*, frontal; *Lc*, lacrimal; *Mx*, maxilla; *Ns*, nasal; *Pa*, parietal; *Sq*, squamosal; *Zy*, zygomatic.

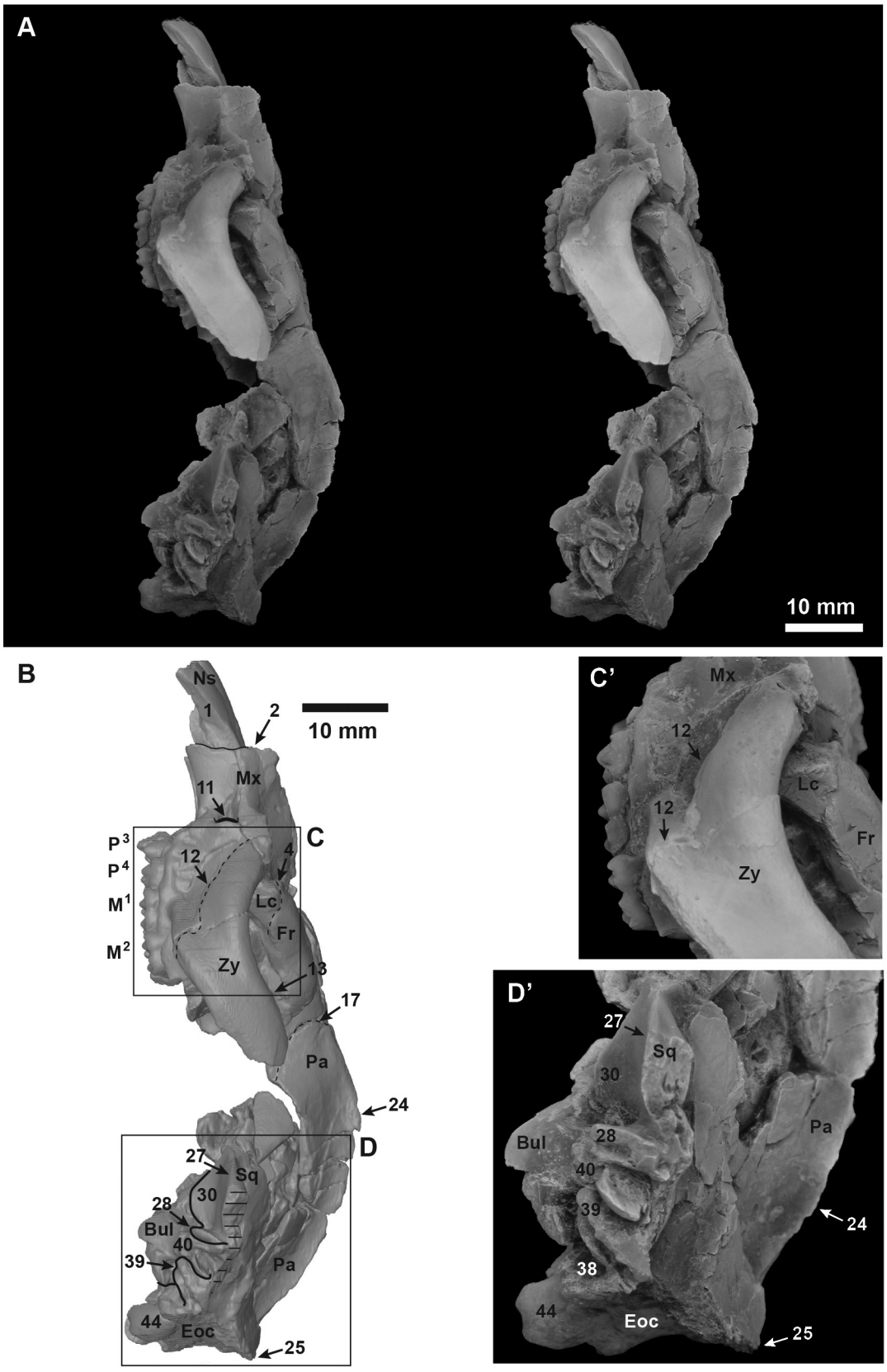
A
10 mm
B
Ns
1
2
10 mm
Mx
11
C
P3
P4
M1
M2
12
4
Lc
Fr
Zy
13
17
Pa
24
D
27
Sq
30
28
Bul
40
39
Pa
44
Eoc
25
C'
Mx
12
Lc
12
Fr
Zy
D'
27
Sq
30
Pa
Bul
28
40
39
24
38
44
Eoc
25

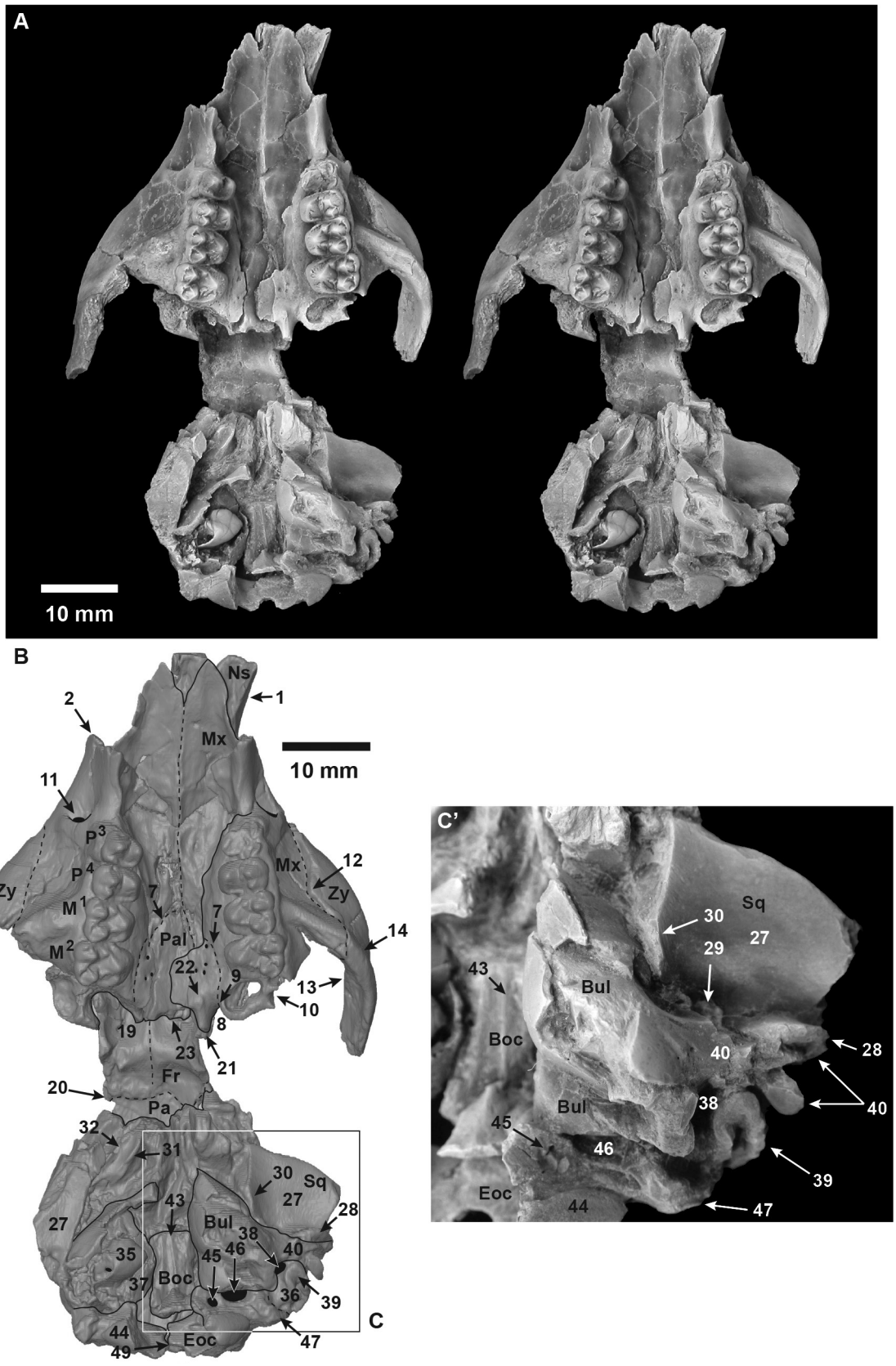
A
10 mm
B
10 mm
Ns
1
2
Mx
11
P3
P4
M1
M2
Zy
7
Pal
22
9
13
10
8
19
23
21
Fr
20
Pa
32
31
30
Sq
27
43
Bul
38
28
40
45
46
35
37
Boc
36
39
44
49
Eoc
47
C
12
14
C'
30
Sq
27
29
43
Bul
Boc
40
28
38
45
46
39
Eoc
44
47

projects laterally another 11 mm. The right infraorbital foramen, situated just anterior to P^3, is 2.7 mm high and 1.5 mm wide (Figs. 8, 10, 11:*11*). The left infraorbital foramen is visible but damaged.

Zygomatic.— The right and left zygomatics are fairly well preserved, with the left being more complete. Sutural contact with the lacrimal and maxilla measures 18.4 mm on the left side (Figs. 6, 9–11:*12*). This contact is straight and slopes laterally and posteriorly from its most anterodorsal point (Figs. 6, 9–11:*12*). The dorsoventral depth of the element decreases steadily laterally and posteriorly. At the lateral edge of the orbital excavation (Figs. 6, 9–11:*13*), the zygomatic is 7.9 mm deep. There is no evidence of a postorbital process in this vicinity. The ventral surface of the anterior end of the zygomatic is expanded transversely for attachment of the superficial masseter, as is the zygomatic process of the maxilla at its suture with the zygomatic (Fig. 10:*14*). This expansion measures 2.4 mm. The total anteroposterior length of the element along its ventral margin is 24.9 mm. The posterior end has a fragment of the zygomatic process of the squamosal still attached to it. The suture between these two elements measures at least 14.2 mm.

Frontal.— The frontals are visible on the dorsum of the skull; in this region they clearly contact the maxillae and lacrimals (Fig. 6:*4*,*6*). The contacts between the frontals and the premaxillae (if any) and the nasals are broken and obscured. Furthermore, breakage makes it difficult to assess the existence and/or nature of contacts with the palatine, orbitosphenoid, alisphenoid, and parietal. A metopic suture is prominent (Fig. 6, 11:*15*) and extends from the anterior end of the frontals to the parietals. The anteroposterior length of the frontal is 21 mm, and the unilateral width, from the metopic suture to the lacrimal suture, is roughly 15.3 mm. The frontals exhibit distinct ridges (temporal crests) that run medially from their anterolateral margin, where they contact the lacrimals, toward the metopic suture. The temporal crests meet the metopic suture at the posterior end of the frontals, where they contact the parietals (Fig. 6:*16*). Thus, they would have formed a distinct 'trigon' on the forehead. There is no sign of postorbital processes on these bones.

MicroCT imaging shows the frontal is a thin plate of bone anteriorly that thickens posteriorly and is densely trabeculated (Fig. 12B). No major diploic cavities or ethmoid foramina could be identified. The most anterior point of contact between the parietal and frontal is a few millimeters anterior to the apex of the posteriorly converging temporal crests, to the point of maximum mediolateral constriction of the orbitotemporal region (Fig. 6, 9:*17*). This suture is only visible via microCT, which reveals that the parietal overlaps the frontal (Fig. 12:*18*). Thus, although much of the neurocranium has an "outer shell" of parietal, the frontal extends quite far posteriorly beneath it. Most likely, the frontal forms at least the anterior part of the endocranial surface, the topology of which reflects that of the brain, mainly the olfactory bulbs (Fig. 10:*19*). In fact, the posterior part of the frontal's endocranial surface and the endocranial expression of its suture with the parietal are exposed to visual inspection (Fig. 10:*20*). This region has been described by Gingerich and Gunnell (2005).

Palatine.— The palatal processes of the palatines are visible and well preserved (Fig. 10). The base of the left pterygoid process is preserved (Fig. 10:*21*). More of the posterior parts of the palatine also may be present but shifted dorsally and posteriorly into the neurocranium (Fig. 10). On the palate, the palatines terminate at the choanae in a swollen rim of bone, also referred to as a postpalatine torus (Fig. 10:*22*). The outer margin of the torus reaches the lateral margin of the pterygoid processes and is sharply angled, with the anterior part of it following a straight, transversely-running course, and the lateral parts following a straight, anteroposteriorly-running course. Prior to postmortem shifting of the palatines, the inner margin of the horizontal process of the palatine—which forms the direct boundary to the choanae—would have been biconcave with a postpalatine spine present (Fig. 10:*23*). This posterior termination of the palatal part of the palatine bone is at the level of the posterior margin of M^3.

Parietal.— Much of what can be said about the parietals has been described in the context of the frontal. The sutures with the alisphenoid and squamosal are obscured by breakage. The right and left elements meet along a straight suture to form a single sagittal crest (Figs. 6, 9, 11–13, 16:*24*). Right and left parietals appear to end short of the nuchal crests (e.g., Fig. 13:*25*), such that a different bone forms the posterior margin of the dorsal aspect of the skull (Fig. 13:*26*). However the identity of the particular bone that forms this region is not obvious (see below). It appears that the parietals were free of foramina for ramus temporalis branches of the stapedial artery and for emissarial venae comitantes. However, this assessment

FIGURE 10.— Cranium of *Plesiadapis cookei* (UM 87990) in palatal or ventral view. **A**, stereophotograph. **B**, high-resolution CT reconstruction (shown without parallax). Fine dashed lines represent sutures, and solid lines indicate major discontinuities on the surface of the specimen. **C**, left glenoid and bulla. Abbreviations: *1*, premaxilla/nasal suture; *2*, premaxilla/maxillary suture; *7*, maxilla/palatine suture at level of M^1 in palate; *8*, notch between pterygoid process of palatine and M^3 alveolus marking lesser palatine nerve route; *9*, maxilla/palatine suture at level of M^3 in palate; *10*, dorsal communication of M^3 alveolus with orbital cavity; *11*, infraorbital foramen; *12*, zygomatic/maxillary suture; 13, edge of orbital excavation on zygomatic bone; *14*, expansion of ventral surface of zygomatic for masseter attachment; *19*, endocranial surface of frontal; depressions for olfactory bulbs; *20*, frontal/parietal suture on endocranial surface; *21*, base of left pterygoid process of palatine; *22*, postpalatine torus; *23*, postpalatine spine; *27*, glenoid fossa; *28*, postglenoid process; *29*, postglenoid foramen; *30*, entoglenoid process; *31*, entopterygoid process of pterygoid; *32*, alisphenoid ectopterygoid process; *35*, pars cochlearis of petrosal; *36*, pars canalicularis of petrosal; *37*, tympanic processes of auditory bulla; *38*, digastric fossa, stylomastoid foramen area (?); *39*, paroccipital process (mastoid process) of petrosal; *40*, tubular external auditory meatus; *43*, sagittal ridge of bone on basioccipital; *44*, occipital condyles; *45*, hypoglossal foramen; *46*, jugular foramen; *47*, jugular processes; *49*, sagittal contact between right and left exoccipitals; *Boc*, basioccipital; *Bul*, auditory bulla; *Eoc*, Exoccipital; *Fr*, frontal; *Mx*, maxilla; *Ns*, nasal; *Pa*, parietal; *Pal*, palatine; *Sq*, squamosal; *Zy*, zygomatic.

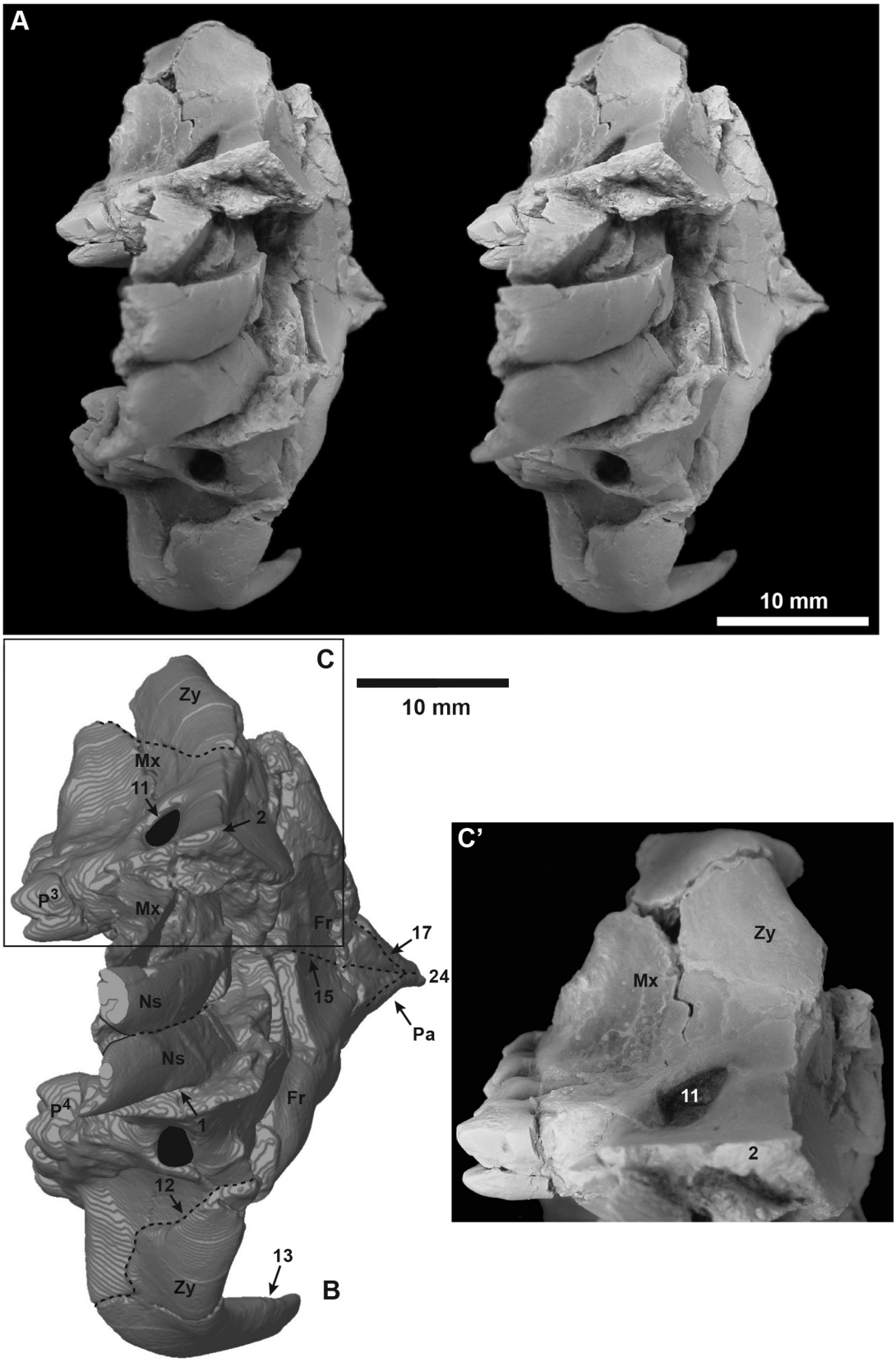
A
10 mm
C
10 mm
Zy
Mx
11
2
P3
Mx
Fr
17
24
15
Pa
Ns
Ns
P4
1
Fr
12
13
Zy
B
C'
Zy
Mx
11
2

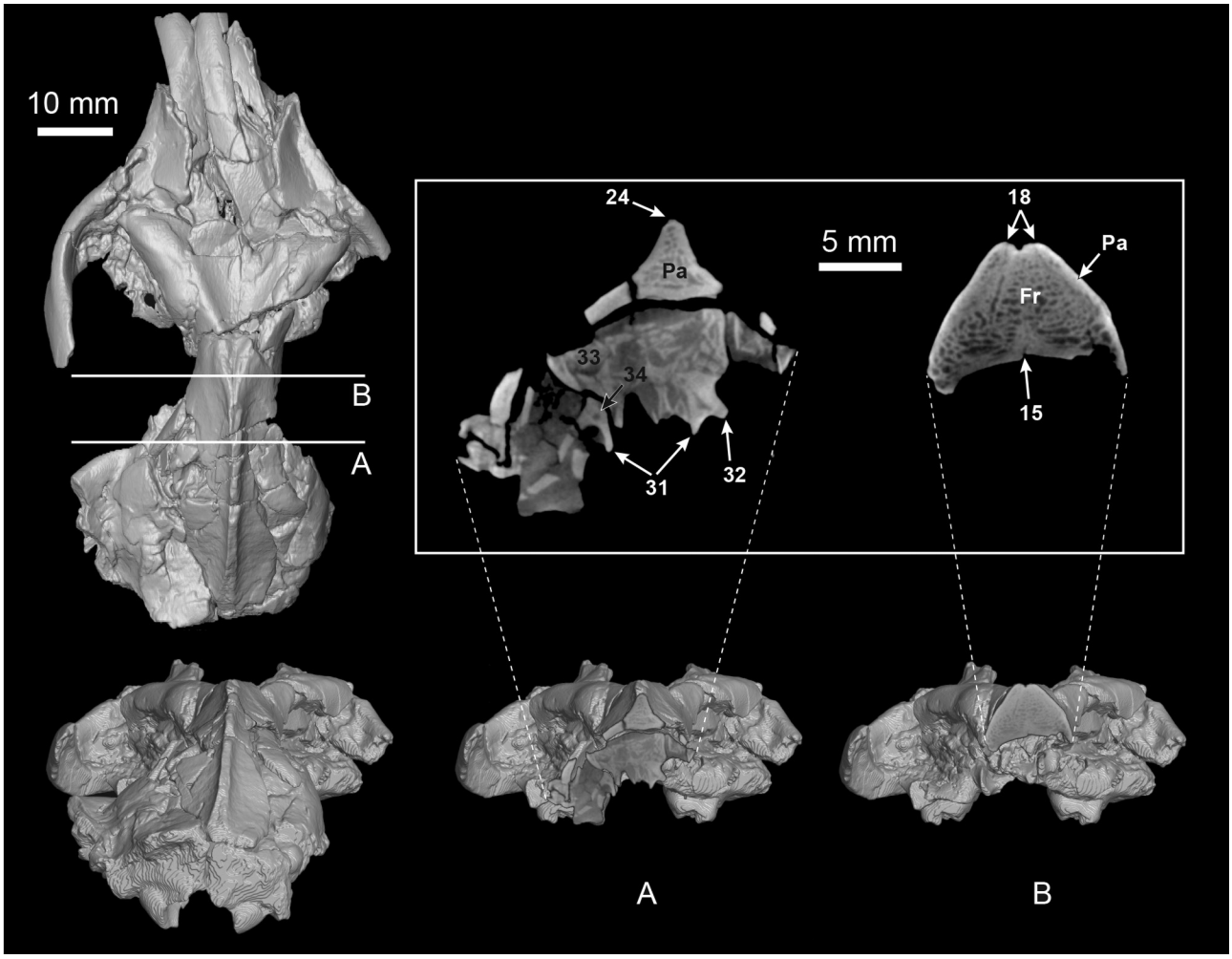

FIGURE 12.— Cranium of *Plesiadapis cookei* (UM 87990) with internal information revealed by high-resolution CT data. Top left, cranium reconstruction in dorsal view (perpendicular to slice orientation), showing position of cross-sections in A and B. Bottom left, cranium rotated into posterodorsal view. **A**, skull reconstruction in posterodorsal view with bone posterior to posterior cross-section removed. Enlargement of this cross-section (box) shows sphenoids that have been crushed into the cranium. **B**, skull reconstruction in posterodorsal view with bone posterior to anterior cross-section removed. Enlargement of this cross-section (through orbitotemporal region close to point of maximum orbitotemporal constriction; box) shows suture with parietal onlapping onto frontal. Abbreviations: *15*, metopic suture; *18*, cross-sectional view of frontal/parietal contact; *24*, sagittal crest; *31*, entopterygoid process of pterygoid; *32*, alisphenoid ectopterygoid process; *33*, canal leading to sphenorbital fissure; *34*, possible vidian canal; *Fr*, frontal; *Pa*, parietal.

FIGURE 11.— Cranium of *Plesiadapis cookei* (UM 87990) in anterior view. **A**, stereophotograph. **B**, high-resolution CT anterior view reconstruction shown without parallax. Fine dashed lines represent sutures and solid lines indicate major discontinuities on the surface of the specimen. **C**, right splanchnocranium. Abbreviations: *1*, premaxilla/nasal suture; *2*, premaxilla/maxillary suture; *11*, infraorbital foramen; *12*, zygomatic/maxillary suture; *13*, edge of orbital excavation on zygomatic bone; *15*, metopic suture; *17*, frontal/parietal suture, most anterior part; *24*, sagittal crest; *Fr*, frontal; *Mx*, maxilla; *Ns*, nasal; *Pa*, parietal; *Zy*, zygomatic.

is questionable because the elements have suffered so much breakage. The length of the sagittal crest is roughly 41 mm (this measurement includes the fragment shown in Fig. 13, which is not attached to the specimen in other figures).

Squamosal.— The left glenoid fossa and part of the right glenoid fossa are intact (Figs. 9, 10:*27*). Fragments of the neurocranial portion of the squamosal are preserved, but sutural contacts are obscured through crushing. Although examination of physical specimens hints that meaningful morphology of the alisphenoid or petrosal contact might be preserved, microCT data show their internal morphology to be shifted, sheared, and crushed. The left postglenoid process of the squamosal (Figs. 9, 10:*28*) is situated lateral

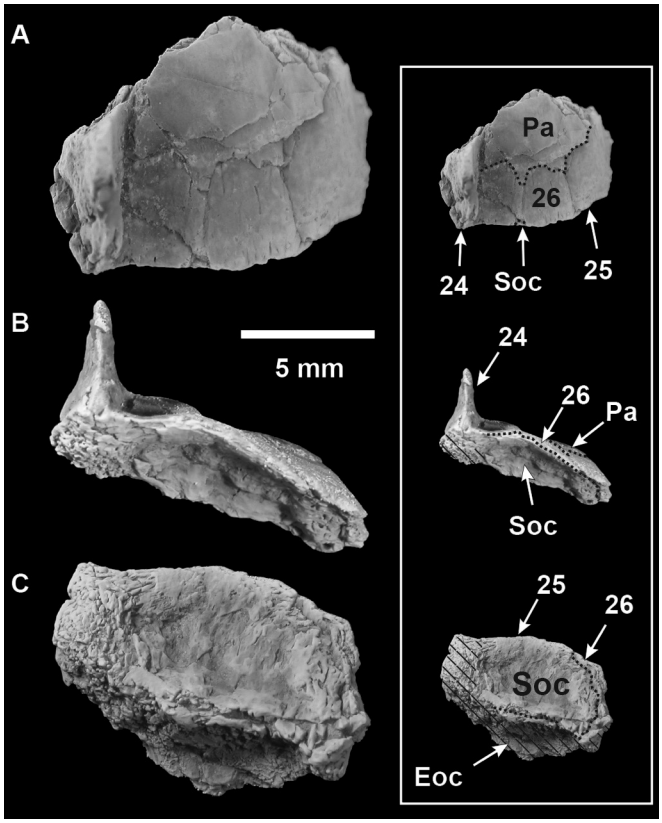

FIGURE 13.— Nuchal crest of the cranium of *Plesiadapis cookei* (UM 87990). Fragment of right nuchal crest in dorsal view (**A**, anterior to top), posterior view (**B**, dorsal to top), and ventral view (**C**, anterior to bottom). Corresponding photographs are labeled (box). Fine dashed lines represent sutures, and hatched areas indicate broken surfaces. Abbreviations: *24*, sagittal crest; *25*, nuchal crest; *26*, parietal/?interparietal suture on dorsum of skull; *Eoc*, exocipital; *Pa*, parietal; *Soc*, supraoccipital.

to the postglenoid foramen (Fig. 10:*29*). It projects straight ventrally by about 3.7 mm, and is separated from the glenoid by a shallow, transverse trough on the joint surface (Fig. 9:*28*). The entoglenoid process is quite large, projecting ventrally beyond the glenoid fossa by 2.5 mm (Figs. 9, 10:*30*). It slopes medially and is oriented anteroposteriorly at roughly 90 degrees from the orientation of the postglenoid process. The glenoid is rather flat and anteroposteriorly longer (11.5 mm) than mediolaterally wide (10.1 mm). MicroCT imagery seems to reveal a sinus within the squamosal medial to the anterior half of the left glenoid.

Alisphenoid, pterygoid, and basisphenoid.— Fragments of the alisphenoid and pterygoid are preserved, but they have been shifted into the endocranium during preservation (Figs. 10, 12:*31–32*). The boundary between the two bones is not discernable, but the bases of the entopterygoid (pterygoid) and ectopterygoid (alisphenoid) processes are visible. MicroCT imagery reveals a cylindrical trough (most clearly on the left side) on the endocranial surface above the pterygoid processes that would have held the ophthalmic and/or maxillary divisions of cranial nerve V (trigeminal nerve; Fig. 12:*33*). Where it is not distorted, the trough has a diameter measuring 1.9 to 2.1 mm. At the convergence of the pterygoid crests is a canal that may represent the former location of the vidian nerve (Fig. 12:*34*). The foramina connecting this canal to extracranial space are minute and asymmetrical. The interpretation of their function is thus tentative. More posteriorly, microCT imagery of the fragmented remains of the basisphenoid suggest the presence of a large sphenoidal sinus, but the fossil is damaged in this region and this interpretation is tentative.

Petrosal.— The pars cochlearis is preserved for both petrosals, but the left pars cochlearis is obscured beneath a crushed bulla (Fig. 10:*35*). The pars canalicularis (Fig 5:*36*) is best preserved on the left side, upon which the description is based. We identify surface anatomy of the tympanic cavity (Fig. 14) following the terminology used in the reconstruction by Boyer et al. (2012a: fig. 17). The maximum diameter of the fenestra vestibuli ('oval window') is 1.32 mm (Fig. 15:*av*). Spiral cochlea length is 19 mm (Coleman and Boyer, 2012). The width of the pars cochlearis of the right side is 4.4 mm, whereas its dorsoventral depth, as measured from the endocranial surface, is about 5.5 mm. The ventral surface of the pars cochlearis ('promontorium') is criss-crossed by grooves of varying diameters (Fig. 15). Several bony ridges (or septa) extend out from the promontorium at varying angles, some of which are only apparent with microCT. Ventral to the fenestra vestibuli on the lateral aspect of the promontorium is a large, anterodorsally directed *g1* groove, measuring 0.40 mm in diameter (Fig. 14, 15:*g1*). At its posteriormost point, it is associated with the posterior septum (MacPhee, 1981), which covers the aperture for the fenestra cochleae ("round window," Fig. 15:*ac*) and contains the internal carotid canal in its ventral margin (Fig. 15:*ps*).

The anterodorsal continuation of *g1* onto the promontorium appears equivalent to what has been termed *g5* for other plesiadapids (Fig. 14, 15:*g5*). There are other grooves on the lateral aspect of the promontorium, one of which extends laterally from the lateral side of the anterior apex of the posterior septum of the promontorium (Fig. 15:*tng*). Where this groove emerges from the fossula for the fenestra cochleae, it deepens and runs approximately parallel and laterodorsal to *g1*. It passes under a bridge of bone (becoming a fully enclosed canal, briefly) on the petrosal and continues for a short distance before becoming shallow and disappearing just anterior and ventral to the anterior apex of the fenestra vestibuli. A foramen for an intrapetrous canal is present near the fenestra cochleae (Fig. 15B-F). The intrapetrous canal appears to lead medially to a foramen on the medial side of the promontorium. Because of its location and morphology, this foramen resembles the tympanic canaliculus (Boyer et al., 2012a; Fig. 15C:*tca*).

Another groove courses more ventromedially than *g5*, starting near the anterolateral margin of the posterior septum. This is the first of two grooves attributed to *g2* (Fig. 14, 15A, B, E, F:*g2*), the second of which is more medially positioned (Fig. 15A, B, D:*g2*). The first g2 groove approaches a septum that is only visible with microCT imagery (Fig. 15B). This

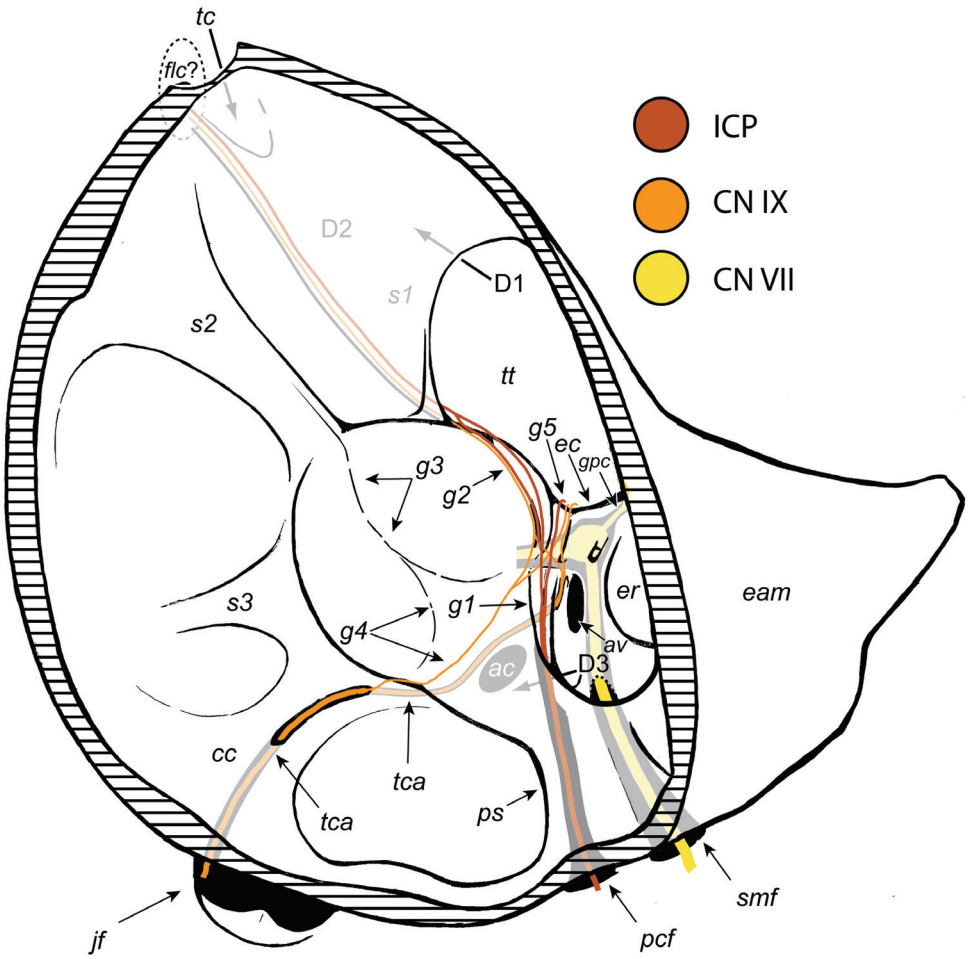

FIGURE 14.— Reconstruction of the plesiadapid middle ear based on all available specimens. Note that the middle ear of *Plesiadapis tricuspidens* differs from this figure in having a more tubular external auditory meatus and a more flaring annular component of the ectotympanic. Furthermore, only *Pronothodectes gaoi* and a single specimen referable to *P. tricuspidens* seem to exhibit the *s3* septum. This reconstruction illustrates some of the observed variations in the pattern of the tympanic plexus in different specimens. Grooves marking major routes followed by cranial nerve IX and the internal carotid plexus include the following: *g1*, a lateral route that begins at the posterior carotid foramen and proceeds through a short canal to the lateral aspect of the promontorium (this likely held the internal carotid plexus and possibly a remnant of the internal carotid artery); *g2*, a slightly more medial route that seems to stem anteriorly from the groove *g1* and probably held fibers of the internal carotid plexus (this groove approaches the septum *s1* and probably represents sympathetic fibers that join with cranial nerves after entering the endocranial space through the foramen lacerum, anterodorsal to the opening of the tubal canal); *g3*, route that leads to septum *s2*, which likely contained contributions from the promontory nerve plexus and may also have held a small vein (MacPhee, 1981); *g4*, a frequently present alternative or additional route for tympanic plexus fibers to reach routes *g1–g3* and *g5*; *g5*, a groove that sometimes seems to be an anterior continuation of *g1* and is dorsolateral to *g2* (this is relatively broad and may represent the place of assembly of the main part of the tympanic plexus). Groove *g5* reaches the apex of the epitympanic crest and then continues dorsolaterally on the anterior face of the epitympanic crest. The deep petrosal nerve likely stemmed from this point to meet the greater petrosal nerve, which probably emerged lateral and dorsal to *g5*, from the hiatus Fallopii. Abbreviations: *ac*, aperture for cochlear fenestra; *av*, aperture for vestibular fenestra; *cc*, cochlear canaliculus; *CN VII*, fibers of facial nerve; *CN IX*, fibers of the ninth cranial nerve (glossopharyngeal); *D1–3*, bullar cavity diverticula of MacPhee (1981); *eam*, external auditory meatus; *ec*, epitympanic crest; *er*, epitympanic recess; *flc?*, probable position of foramen lacerum (= anterior carotid foramen); *gpc*, greater petrosal nerve canal (leads to hiatus Fallopii); *icp*, internal carotid plexus; *jf*, jugular foramen; *pcf*, posterior carotid foramen; *s1*, first (anterior) septum (*S2* of Russell, 1964), most lateral septum extending anteriorly from the promontorium (tubal canal forms lateral to *s1*; *D1* and *D2* are separated by *s1*); *s2*, second septum (probably equivalent of medial secondary septum of MacPhee (1981; *S1* of Russell, 1964), forms medial to *s1* and projects anteromedially from the promontorium (*g3* usually leads to the ventral or medial aspect of this septum); *s3*, third septum, projects medially between the septum *s2* and, more posteriorly, the raised ridge of the cochlear canaliculus; *tc*, tubal canal; *tca*, tympanic canaliculus: foramina and groove on or near ridge of cochlear canaliculus in tympanic cavity marking the entrance of the tympanic nerve from extracranial space, and the re-entrance of the nerve into the promontorium as it moves laterally to contribute to the tympanic plexus (associated canals do not communicate with cochlea); *tt*, tegmen tympani.

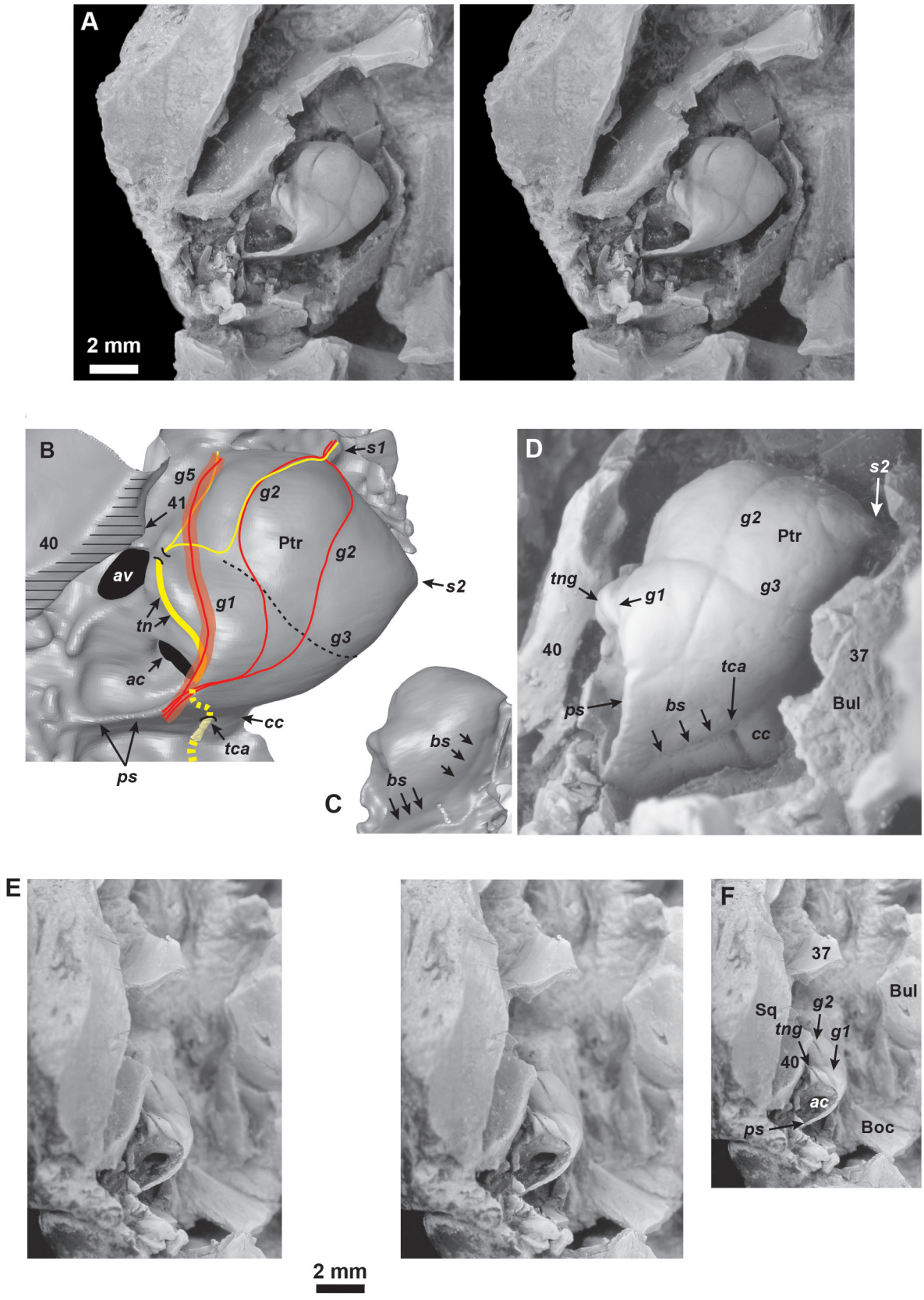
A
2 mm
B
s1
g5
41
g2
Ptr
g2
40
av
s2
g1
tn
g3
ac
cc
tca
ps
C
bs
bs
D
s2
g2
Ptr
tng
g1
g3
40
37
tca
ps
bs
Bul
cc
E
2 mm
F
37
Bul
Sq
g2
tng
g1
40
ac
ps
Boc

septum is the most anterior and lateral of those preserved on the specimen. It appears equivalent to *s1* (Fig. 14) and to MacPhee's (1981) anterior septum, which marks the course of the main bundle of neurovasculature of the internal carotid plexus as it approaches the foramen lacerum to gain entrance to the endocranium. The second *g2* groove, which converges toward the main *g2* groove, seems to have held a nerve that originated from the posterior edge promontorium near the point where the internal carotid plexus enters the tympanic cavity and then coursed toward the anterior septum. Thus, this more medially positioned second *g2* groove is also likely to have communicated with the internal carotid plexus, especially considering the fact that the internal carotid plexus frequently consists of two nerve bundles (MacPhee, 1981). Yet another groove crosses the promontorium at a right angle to the two *g2* grooves (Fig. 15:*g3*). This *g3* groove starts from near where the tympanic nerve groove ends on the lateral side of the promontorium. The *g3* groove then crosses to the medial side of the remnant of a second bony ridge or septum that extends anteromedially from the promontorium (Fig. 15:*s2*, this septum is located medial to the anterior septum). UM 87990 has no grooves that meet the definition of the *g4* groove present in some plesiadapid specimens (see Boyer et al., 2012a; Fig. 14).

The lateral walls of the auditory bulla (Figs. 9, 10:37) have been crushed concentrically toward the promontorium such that septa and tympanic processes have been crushed and obscured. The posterior septum is broken and the posterior wall of the bulla is destroyed, so no posterior carotid foramen is visible. On the medial side, the ridge above the cochlear canaliculus (Fig. 15:*cc*) is just barely visible. The cochlear canaliculus itself is visible with microCT. Additionally, as mentioned earlier, the groove and foramen that typically occupy the ventral aspect of this ridge, which appear to relate to the tympanic nerve, are visible. Running anteriorly and posteriorly from the foramen for the tympanic canaliculus is a distinct foramen-lined groove, which may represent a bullar suture (bs) (Fig. 15:*bs*).

A fragment of the pars canalicularis is preserved on the left side. It is relatively short anteroposteriorly. There is a deep groove that abuts the jugular process of the exoccipital and appears to lead to the stylomastoid foramen; it may also represent the digastric fossa (Fig. 10:*38*). Lateral to this groove is a prominent tubercle that probably buttressed the posterior aspect of the ectotympanic tube and would be identified as a mastoid process in that case (Fig. 10:*39*). If the pars canalicularis of the petrosal had any posterior exposure in the pristine skull, it is not apparent from the fossil (Fig. 16).

Ectotympanic.— The ectotympanic bone is preserved bilaterally (Fig. 10). Although the right side is fragmentary, it exposes morphology not visible on the left side (Fig. 17). The left side reveals that the external auditory meatus is'tubular' because its diameter is narrow compared to its mediolateral length (Figs. 9, 10, 15:*40*). The right ectotympanic preserves a narrow crista tympanica that extends medially around the base of the external auditory meatus (Figs. 15, 17:*41*). The crista tympanica defines the medial or proximal end of the external auditory meatus. On the left side, the tube of bone forming the external auditory meatus extends roughly 12 mm laterally from what remains of the crista tympanica. The tube is wider at its base and narrows laterally so that it reaches a minimum diameter of 4.8 mm directly posterior to the postglenoid foramen. The annular component of the ectotympanic is solidly braced against the outer tube by a series of bony struts (Fig. 17:*42*). There is no "recessus dehiscensce" (*sensu* Bloch and Silcox, 2001) separating the annular component of the ectotympanic from the outer tubular component. The annular component does not flare substantially beyond the struts of the annular bridge. However, at least some bone has been lost from this margin because the crista tympanica typically has a concentric projection toward the middle of the external auditory meatus, as in *N. intermedius* USNM 309902 (Figs. A-V-4D and A-V-5). What remains of the annular component of the external auditory meatus in UM 87990 lacks the concentrically projecting lip typically associated with this projection.

Whether the ectotympanic is limited to the lateral part of the skull and bullar cavity or comprised most or all of the bulla is unknown due to breakage and the absence of any informative sutures (Fig. 10).

Basioccipital, exoccipital, and supraoccipital.— The basioccipital, paired exoccipitals, and supraocciptal are fairly well preserved, with apparent sutures distinguishing the latter two

FIGURE 15.— Right promontorium of *Plesiadapis cookei* (UM 87990). **A**, stereophotograph in ventral view. **B**, high-resolution CT in ventral view (reconstruction shown without parallax). **C**, high-resolution CT reconstruction in ventromedial view; a fragment of the tympanic process (37) has been removed digitally to show the continuation of a foramina-lined groove that may represent a suture. **D**, close-up of promontorium in same view as the image in C. **E**, stereophotograph in lateral view (ventral to right, anterior to top). **F**, same view as E. The thick red line represents the main course of the internal carotid plexus, and the thin red lines represent branches stemming from this. Yellow lines represent components of the tympanic plexus. The fine dashed line is groove *g3*. Hatches indicate broken surfaces. Abbreviations: *37*, tympanic processes of auditory bulla; *40*, tubular external auditory meatus; *41*, crista tympanica; *ac*, aperture for cochlear fenestra; *av*, aperture for fenestra vestibuli; *Boc*, basioccipital; *bs*, bullar suture; *Bul*, auditory bulla; *cc*, cochlear canaliculus; *g1*, groove with lateral route that likely holds internal carotid plexus and possibly remnant of internal carotid artery; *g2*, groove with slightly more medial route that may hold internal carotid plexus fibers that approach *s1*; *g3*, groove that leads to *s2*, which likely contains contributions from the tympanic plexus but was mainly responsible for transmitting a small vein; *g5*, groove frequently present that leads dorsolaterally toward epitympanic crest from a point ventral to the vestibular fenestra; *ps*, posterior septum; *Ptr*, petrosal; *s1*, first (anterior) septum (most lateral septum extending anteriorly from promontorium; tubal canal forms between s1 and epitympanic crest); *s2*, second septum (forms medial to *s1* and projects anteromedially from the promontorium); *Sq*, squamosal; *tca*, tympanic canaliculus; *tn*, tympanic; *tng*, tympanic nerve groove.

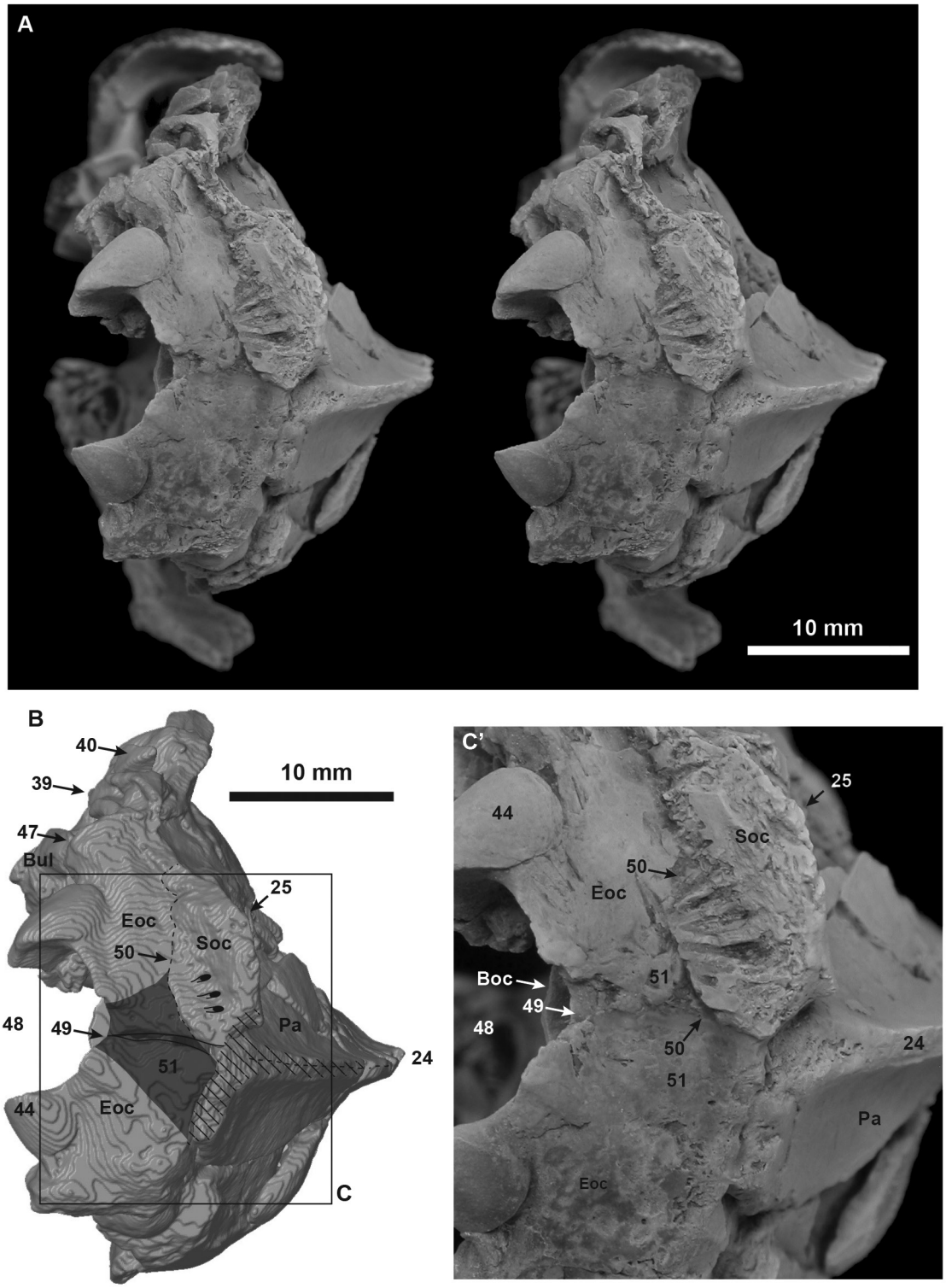

FIGURE 16.— Cranium of *Plesiadapis cookei* (UM 87990) in posterior view. **A**, stereophotograph. **B**, high-resolution CT reconstruction (shown without parallax). **C**, close-up of the posterior surface. Dashed lines represent sutures and hatched areas represent broken surfaces. Area in solid gray represents former site of supraoccipital bone. Abbreviations: *24*, sagittal crest; *25*, nuchal crest; *39*, paroccipital process (mastoid process) of petrosal; *40*, tubular external auditory meatus; *44*, occipital condyle; *47*, jugular process; *48*, foramen magnum; *49*, sagittal contact between right and left exoccipitals; *50*, sutural contact between remnants of supraoccipital and exoccipital; **51**, wedge-shaped depression on exoccipitals where supraoccipital is lost; *Boc*, basioccipital; *Eoc*, exoccipital; *Pa*, parietal; *Soc*, supraoccipital.

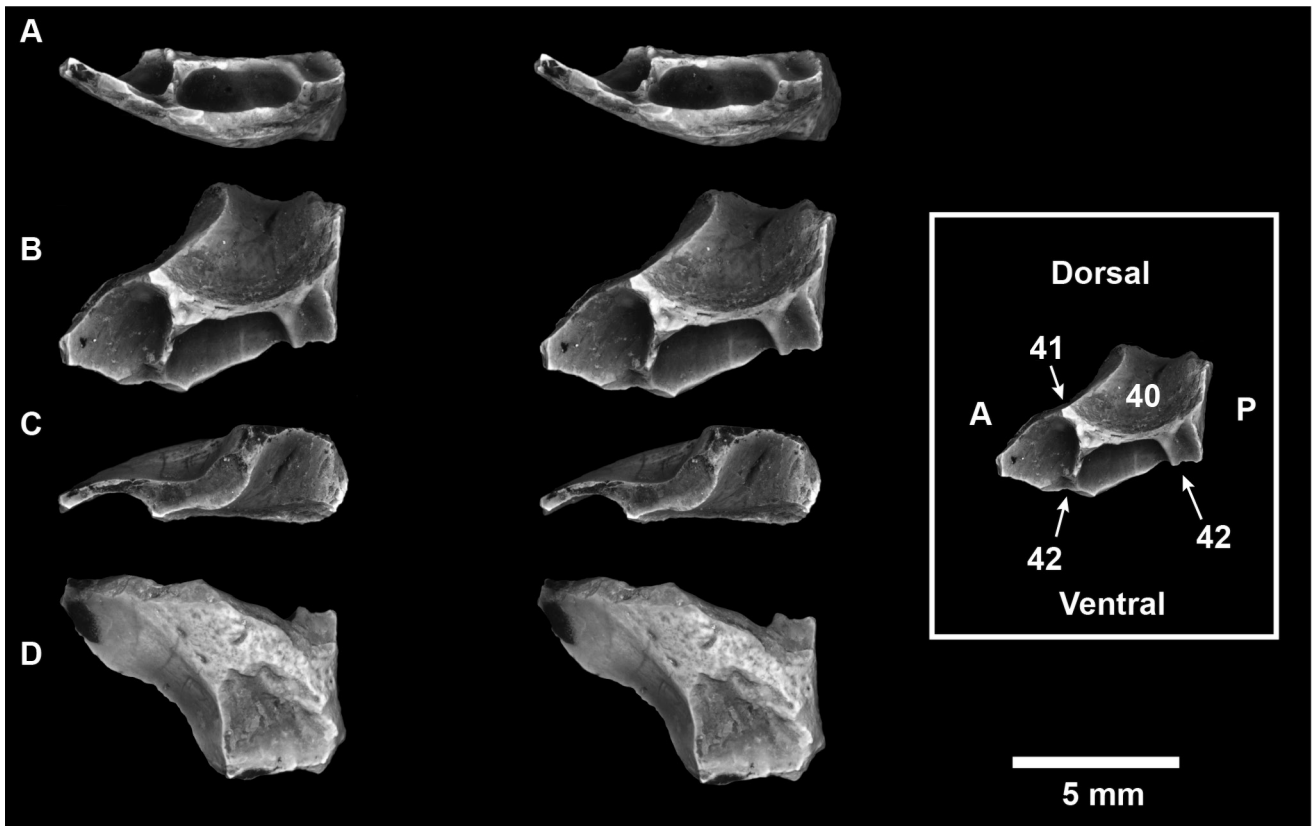

FIGURE 17.— Ectotympanic fragment of *Plesiadapis cookei* (UM 87990). Images are stereophotographs of right ectotympanic. **A**, ventral view (medial to top); **B**, medial view (dorsal to top, with labeled view in the box to the right); **C**, dorsal view (medial to bottom); and **D**, lateral view (dorsal to bottom). Abbreviations: *40*, tubular external auditory meatus; *41*, crista tympanica; *42*, bony struts supporting crista tympanica; *A*, anterior; *P*, posterior.

bones (Fig. 16:*50*). The basioccipital is crushed dorsally into the endocranium, but its dimensions can be measured (Fig. 10). Its anteroposterior length is 14.4 mm. Mediolaterally, the anterior end measures 4.7 mm, and it narrows to roughly 4.4 mm at its midpoint. The posterior width and dorsoventral thickness cannot be measured due to breakage. The basioccipital is marked by a longitudinal ridge along its midline (Fig. 10:*43*).

The right and left exoccipitals preserve both occipital condyles (Fig. 9, 10, 16:*44*), the left hypoglossal foramen (Fig. 10:*45*), the posterior margins of both posterior lacerate foramina (or jugular foramina; Fig. 10: *46*), both jugular processes (Figs. 10, 16:*47*), and the majority of their contribution to the posterior surface of the skull (Fig. 16). The suture marking contact with the basioccipital is completely obscured. Each occipital condyle is 5.1 mm high and 4.5 mm wide. The hypoglossal foramen is 1.8 mm by 1.60 mm and has two smaller foramina inset within it. The left jugular foramen is 2.9 mm in maximum diameter. The jugular processes do not project posteriorly beyond the condyles, as they do in certain other taxa, instead they project laterally beyond the condyles by 2.4 mm on both sides. The foramen magnum appears undistorted and is 6.4 mm high and 9.1 mm wide (Fig. 16:*48*). The dorsal rim of the foramen magnum is comprised mainly of right and left exoccipitals, which almost meet in the midline and may have actually touched in the pristine skull (Fig 16:*49*). Given that the exoccipitals and supraoccipital appear generally undistorted overall, the mediolateral diameter of the back of the skull between posteriormost projections of the exoccipital jugular process can be measured at 21.7 mm.

The supraoccipital is fragmentary (Figs. 16, 19) and is preserved on the posterior sides of the nuchal crests. This bone was thin and overlaid the exoccipitals (Figs. 10, 16, 19:*50*). The region of contact between the missing pieces of supraoccipital can be seen as a wedge-shaped, rugose depression on the exoccipitals (Fig. 16:*51*). The apex of this wedge points ventrally and would have reached the middle of the dorsal rim of the foramen magnum, riding over the suture between the two exoccipitals. Viewed laterally, the back of the skull is concave due to strong development of the nuchal crest (Figs. 9, 13). The height of the supraoccipital from the top of the foramen magnum to the top of the nuchal crest is at least 9.9 mm. As discussed above, the identity of the bone forming the inner core and dorsal/anterior surface of the nuchal crest is not

clear. It appears to be exoccipital, but an interparietal element could also be present.

Dentary.— The right and left dentaries are well preserved (Fig. 18; Tables A-I-5–A-I-8). The right side retains teeth in all positions, indicating a lower dental formula of 1.0.2.3: I_1, $P_{3–4}$, and $M_{1–3}$. The tooth crowns are similar to those in other specimens referred to *P. cookei*. The P_4 crown has previously been described as being simple, with only a protoconid and a hypoconid (Gingerich, 1976; Rose, 1981). However, this specimen and other *P. cookei* specimens in which this tooth position is unworn show that the P_4 possesses an entoconid and a talonid basin. Furthermore, the protoconid comprises the distal margin of a trigonid basin formed by an encircling crest (Figs. 18, 19) with an incipient paraconid in its mesial aspect (see also Boyer et al., 2010a). This morphology is reminiscent of that in *Platychoerops* from the early Eocene of Europe.

COMPARISONS

Dentition

Plesiadapis cookei *and* Plesiadapis tricuspidens.— UM 87990 shows that *P. cookei* has a different dental formula from *P. tricuspidens* because it lacks P^2 (2.0.2.3/1.0.2.3 vs. 2.0.3.3/1.0.2.3, respectively; Fig. 19; see also Boyer et al., 2010a). The upper central incisors (I^1) of *P. cookei* differ from those of *P. tricuspidens* in several ways. *P. tricuspidens* retains the mediocone and the centroconule crest typical of I^1 in earlier *Plesiadapis* species, whereas *P. cookei* has lost both of these features (Fig. 20). Furthermore, the remaining cusps of I^1 in *P. cookei* are reduced relative to its crown height and occlusal dimensions, as reflected in incisor shape indices #2 and #3 (Table A-I-8; Fig. A-I-2; see also Boyer et al., 2010a; fig. 7). Finally, I^1 teeth of *P. cookei* are much larger than those of *P. tricuspidens*, even though these two species are of similar cranial and postcranial dimensions. *P. tricuspidens* retains a P^4 paracone that is lost in *P. cookei* (Gingerich, 1976). In the lower dentition, the P_4 of *P. tricuspidens* has a simple conical crown lacking a paraconid and a trigonid basin, both of which are present in *P. cookei* (Fig. 21). Compared to the M_2 of *P. tricuspidens*, the M_2 of *P. cookei* is absolutely larger, relatively longer, and has a more buccolingually expanded trigonid, with a larger and better-developed entoconid (Fig. 21), as well as greater occlusal relief and complexity (Boyer et al., 2010a: fig. 4, table A5).

Plesiadapis cookei *and* Platychoerops.— The lower dental formula is similar in *Plesiadapis cookei* and *Platychoerops*, but the upper formula is not because it varies within *Platychoerops* species. *Platychoerops daubrei* has three maxillary premolars, based on isolated P^2s attributed to that species by Gingerich (1976), but *Pl. richardsoni* appears to lack P^2 and canines. Thus, it appears to have had the same maxillary formula as *P. cookei*.

Although the loss of the mediocone and centroconule crest on I^1 of *P. cookei* represent similarities to *Platychoerops*, the I^1 of *P. cookei* retains a laterocone and a rounded anterocone of moderate size. In *Pl. daubrei* the laterocone is lacking and there is a large, pointed, projecting anterocone (Fig. 20). On the other hand, proportions of I^1 in *P. cookei* are more like those of *Platychoerops* than *P. tricuspidens* (i.e., shape indices #2–3 in Table A-I-8 and in figure 7 of Boyer et al., 2010).

P. cookei lacks the paraconule present on P^4 in other species of *Plesiadapis*, but a paraconule is again present in different form in *Pl. daubrei* (Gingerich, 1976). Upper molars are more bunodont and less selenodont and lack the highly crenulated enamel of *Pl. daubrei*.

In the lower dentition, the P_4 of *P. cookei* has a small paraconid and occasionally a small trigonid basin (Table A-I-7), both of which are more strongly developed in *Pl. daubrei*. P_4 of *Pl. daubrei* is relatively large and much more molarized than that of *P. cookei* (Fig. 21). M_2 of *P. cookei* has a buccolingually expanded trigonid like that of *Pl. daubrei*, but the shape of the crown differs in being more angular and more selenodont in *Pl. daubrei*, with greater relief (Fig. 21; see also Boyer et al., 2010a: fig. 4, table A5).

Cranium

The crania of *P. cookei* and *P. tricuspidens* are similar in size and in most morphological features. UM 87990 appears to be much smaller than specimens of *P. tricuspidens* (e.g., MNHN CR 125, Fig. 19), but this is an artifact of breakage. Skulls of the two species are very similar in size (Table 4; see also Boyer et al., 2010a).

Crania of the two species are notably similar among known plesiadapid skulls in their laterally expanded, tubular external auditory meati, and in the minimal exposure of the molar roots on the dorsal surface of their maxillae (Appendix V).

P. cookei differs from *P. tricuspidens* in having proportionally broader nasals (Table 5: N/GM), a more anteriorly situated maxillary zygomatic process, and a proportionally smaller glenoid fossa (Table 5: Gld/GM). In addition, *P. cookei* appears to differ from *P. tricuspidens* in having an ectotympanic ring that does not flare as substantially beyond its attachment to the bullar part of the ectotympanic, a more posteriorly projecting nuchal crest, and a more anterior root to the zygomatic process. Interestingly, most features separating *P. cookei* from *P. tricuspidens* also separate smaller North American plesiadapids, including *P. anceps*, *N. intermedius*, *N. gidleyi*, and *Pr. gaoi* (Appendix V), from European *P. tricuspidens*. An exception is the position of the zygomatic process of the maxilla, which arises lateral to M^1 in *P. cookei*, unlike any other plesiadapid except in speices of *Chiromyoides* and *Pl. richardsoni*.

Auditory bulla

P. cookei is similar to many other plesiadapids in having a laterally positioned carotid groove with a diameter in the range of 0.30 to 0.40 mm (Fig. 14:*g1*, 28; Tables A-I-3, A-I-4). This morphology, as well as the presence of *g2* grooves, demonstrates an intratympanic route for the internal carotid plexus of *P. cookei*.

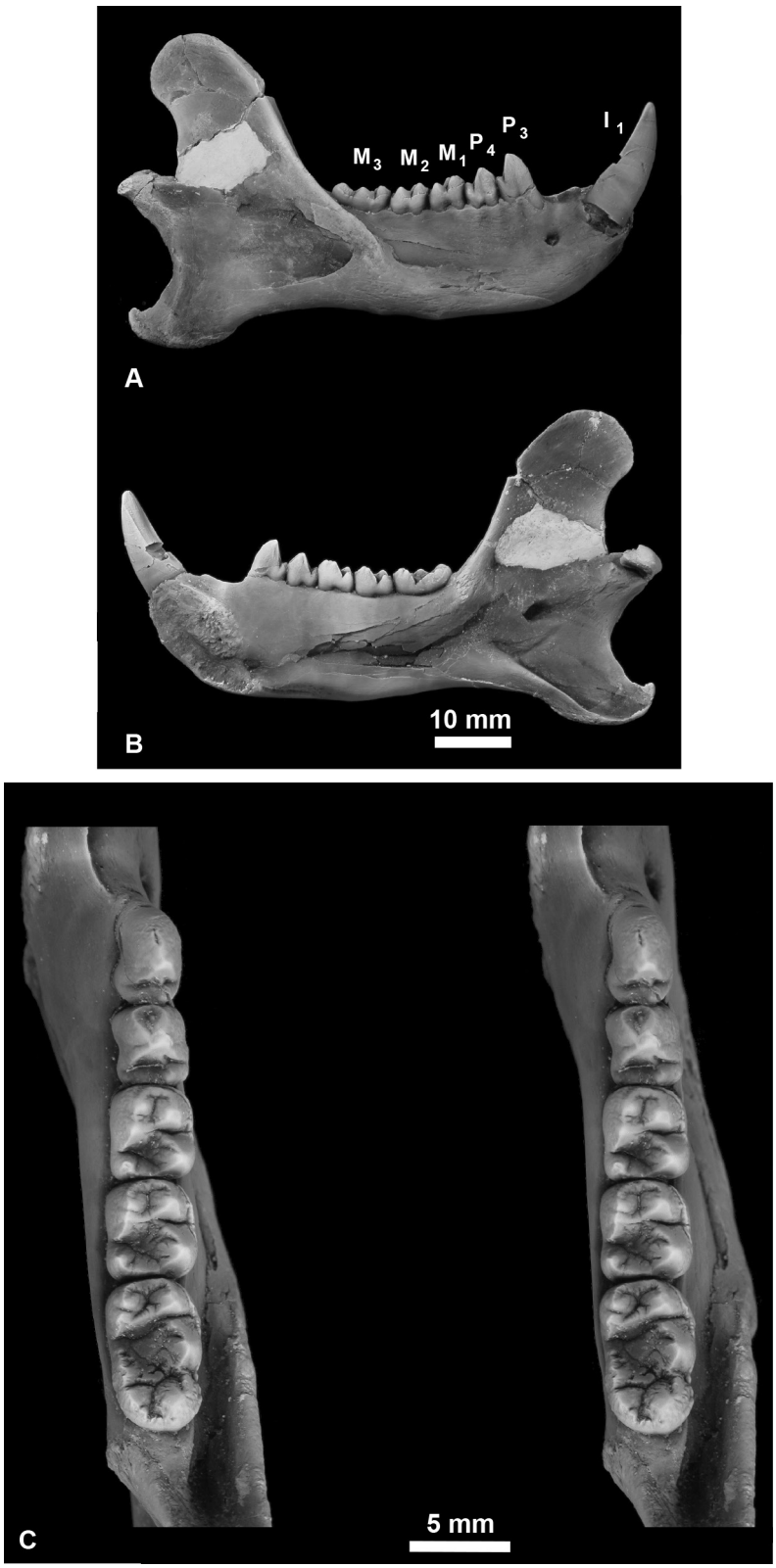

FIGURE 18.— Dentary of *Plesiadapis cookei* (UM 87990). **A**, right dentary in buccal view. **B**, right dentary in lingual view. **C**, stereophotograph of right dentary in occlusal view. Note lack of margoconid on I_1 in images A and B. Note trigonid basin on P_4 in stereophotograph images C.

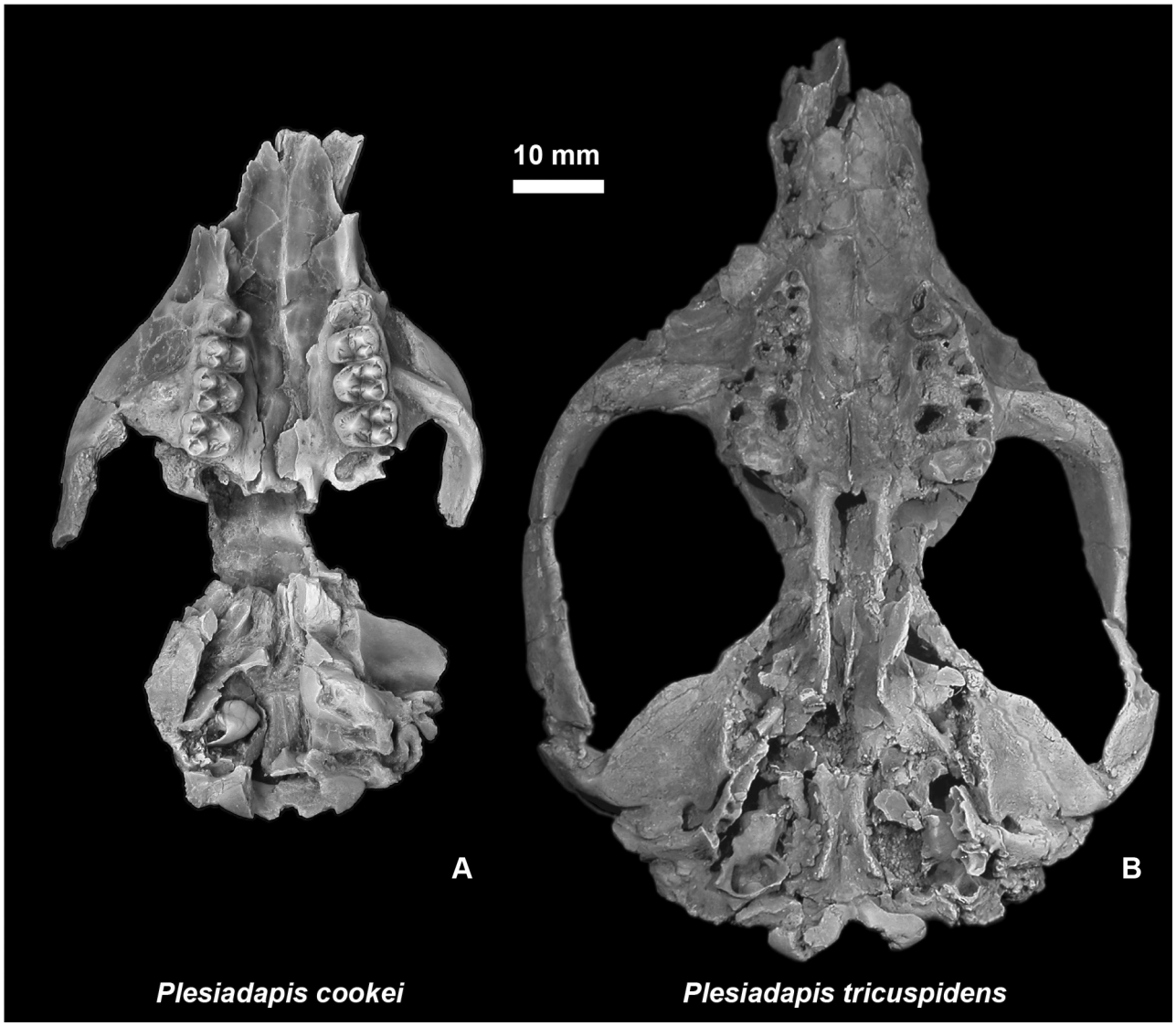

FIGURE 19.— Crania of *Plesiadapis cookei* and *P. tricuspidens* compared at the same scale. **A**, *Plesiadapis cookei* (UM 87990) in ventral view. **B**, *Plesiadapis tricuspidens* (MNHN Cr-125) in ventral view. The great difference in size apparent here is mainly an artifact of different modes of brittle deformation. The geometric mean of 39 measurements of the cranium of *P. cookei* is 10.7 mm, and the geometric mean of 39 measurements of *P. tricuspidens* is 10.6 mm (see appendix Table A-I-2).

Compared to other plesiadapids (Fig. 14; Appendix V), the *g2* grooves diverge from the *g1* groove more proximally (Fig. 15). The divergence of the two *g2* grooves from one another on the promontorium is also unusual and is not observed in other plesiadapid specimens (Appendix V).

The rostral tympanic process in UM 87990 is unique among the comparative sample of plesiadapids in exhibiting a 'suture-like' line of foramina (Fig. 15D; Appendix V). Comparative rodent specimens of *Marmota* and *Lagostomus* (Figs. 22–24) show neurovasculature invading the middle ear cavity at the petrosal/ectotympanic boundary, creating a line of foramina at this sutural boundary. This extant morphological pattern makes it tempting to interpret the line of foramina in *P. cookei* as the remnant of a suture between the petrosal and ectotympanic (or entotympanic) as well, which would mean that the auditory bulla is not petrosal in origin. Unfortunately, microCT imaging of UM 87990 does not provide any more insight on whether foramina marking the boundary between the pars cochlearis of the petrosal and its rostral process represent a suture, because this area appears as solid bone. Admittedly, the resolution of the scan may be too coarse to allow visualization of such a suture.

Even if there is no suture present in the specimen, the foramina could still mark the location of a suture that has

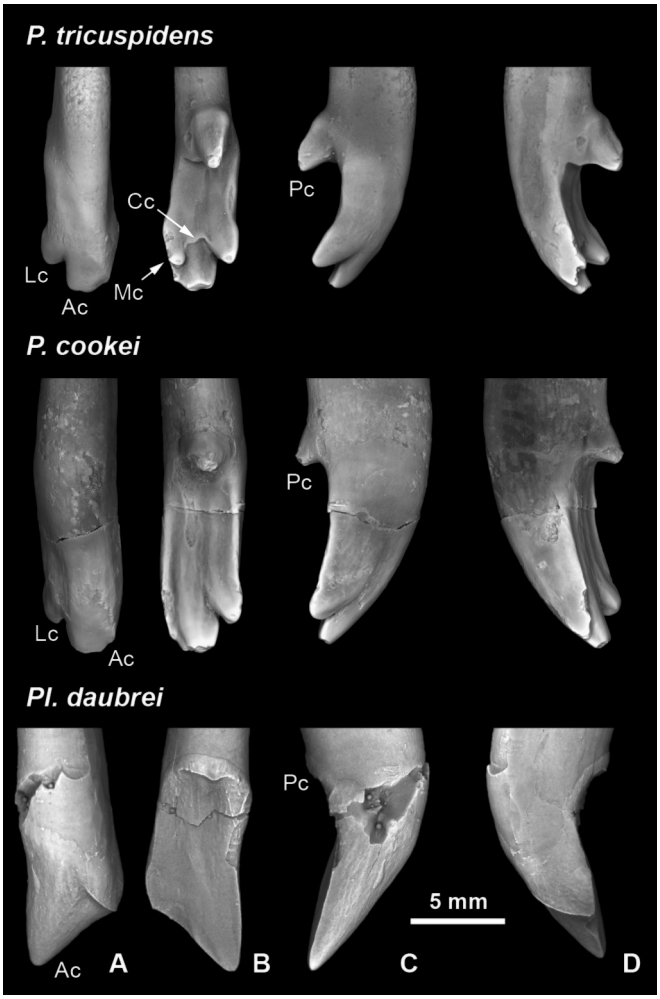

FIGURE 20.— Upper central incisors (I^1) of *Plesiadapis* and *Platychoerops*. *P. tricuspidens* is shown in the top row (unnumbered specimen from MNHN Berru collection); *P. cookei* is shown in the middle row (UM 66725);, and *Pl. daubrei* is shown in the lower row (MNHN Mut 17158). Each incisor is shown in anterior (**A**), posterior (**B**), lateral (**C**), and medial (**D**) views. Note that despite being smaller overall, *P. tricuspidens* has a posterocone (*Pc*) that is larger, and an anterocone (*Ac*) and laterocone (*Lc*) that are the same size as those in *P. cookei*. Furthermore, *P. cookei* lacks the mediocone (*Mc*) and centroconule crest (*Cc*) of *P. tricuspidens*. The small cusps and simplified form of I^1 in *P. cookei* make it very similar to I^1 of *Platychoerops*, which is interpreted to have lost the *Lc* (Gingerich, 1976). See appendix Figure A-I-2 and Table A-I-8 for quantification of these features.

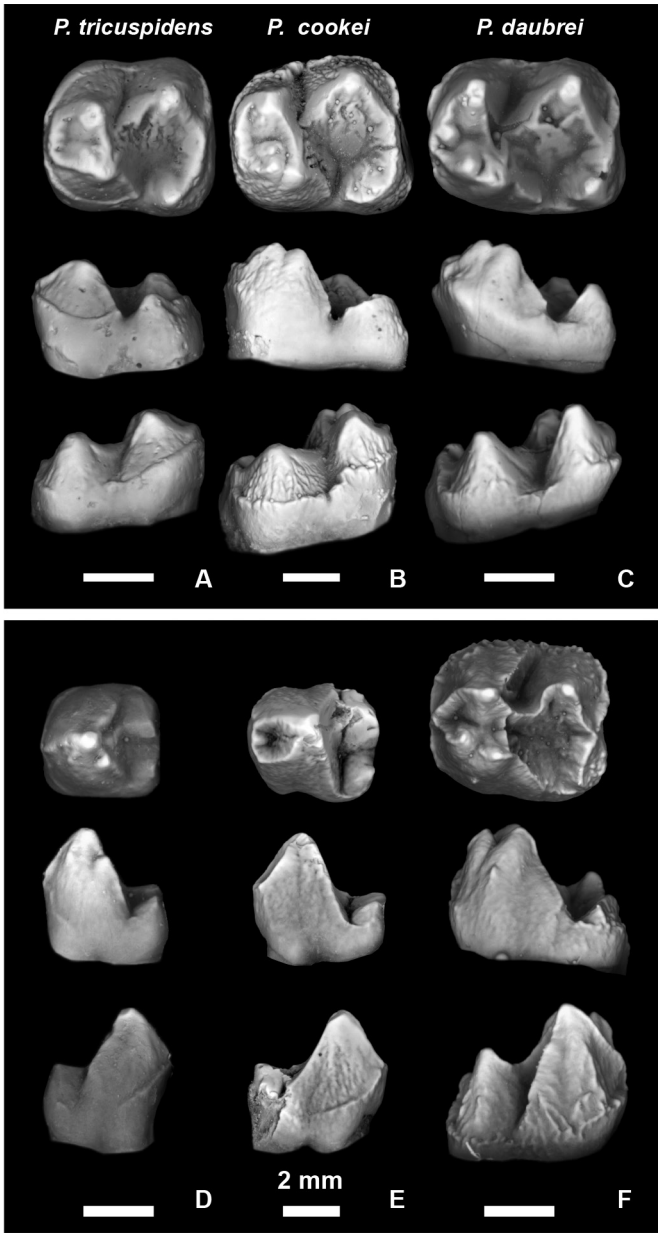

FIGURE 21.— Mandibular teeth of *Plesiadapis* and *Platychoerops*. A–C, right M_2 in occlusal, medial, and lateral view. D–F, right P_4 in occlusal, medial, and lateral view. **A**, *Plesiadapis tricuspidens* (unnumbered specimen from MNHN Berru collection). **B**, *Plesiadapis cookei* (UM 66719). **C**, *Platychoerops daubrei* (MNHN AL-5164). **D**, *P. tricuspidens* (MNHN R 129). **E**, *P. cookei* (UM 69265). **F**, *Pl. daubrei* (MNHN AL-J). Molars are scaled to the buccolingual width of talonid. Premolars are scaled to the molar of the same taxon. Note that M_2 of *P. cookei* and M_2 of *Pl. daubrei* are relatively longer, have more buccolingually expanded trigonids, and have larger, better-developed entoconids than M_2 of *P. tricuspidens*. Note too that P_4 is virtually unworn in all three taxa, but only P_4 of *P. tricuspidens* lacks a trigonid basin (even though it has metaconid). In addition, P_4 of *P. cookei* has a rudimentary paraconid, visible in occlusal view. Scale bars are all 2 mm.

been almost completely fused through internal remodeling. For instance, the tympanic canaliculus foramen is among the many other tiny foramina that form this boundary. If the entrance point for these nerves corresponds to the boundary between bulla-forming bone and a separate petrosal, then the morphological pattern would be extremely similar to that of the extant rodents *Marmota* (Fig. 22) and especially *Lagostomus* (Figs. 23–24). However, these nerves are perfectly capable of

TABLE 4.— Size comparisons of plesiadapid crania as a proportion (%) of crania of *Plesiadapis tricuspidens* (CR 125) and *P. cookei* (UM 87990). Cranial estimates are based on a measured length of 106.36 mm for MNHN CR 125 (*P. tricuspidens*) and an estimated length of 105.83 mm for UM 87990 (*P. cookei*). The number in parentheses following each percentage is the number of cranial measurements available for estimating cranial length in a given specimen.

	Nannodectes intermedius	*Pronothodectes gaoi*	*Nannodectes gidleyi*	*Plesiadapis anceps*	*Plesiadapis tricuspidens*	*Plesiadapis tricuspidens*	*Plesiadapis tricuspidens*	*Plesiadapis cookei*
Reference specimen	USNM 309902	UALVP 46685	AMNH 17388	YPM-PU 19642	MNHN CR 965	Pellouin Skull	MNHN CR 125	UM 87990
Proportion (%) of CR 125	48% (14)	58% (21)	53% (11)	83% (6)	93% (4)	101% (30)	100% (39)	99% (39)
Estimated cranial length	50.7 mm	61.1 mm	56.9 mm	87.9 mm	98.5 mm	106.9 mm	106.3 mm	105.8 mm
Proportion (%) of UM 87990	48% (14)	58% (21)	59% (11)	65% (6)	91% (4)	101% (30)	101% (39)	100% (39)
Estimated cranial length	50.4 mm	61.2 mm	62.3 mm	69.2 mm	96.2 mm	106.5 mm	106.3 mm	105.8 mm

TABLE 5.— Selected shape variables for comparison of plesiadapid crania (equivalent to Table 2.6 of Boyer, 2009; and Table A5 of Boyer et al., 2012a). Specimen number, element, and locality are given for each taxon. Shape variables are explained in Table A-I-1.

	Nannodectes intermedius	*Pronothodectes gaoi*	*Nannodectes gidleyi*	*Plesiadapis anceps*	*Plesiadapis tricuspidens*	*Plesiadapis tricuspidens*	*Plesiadapis tricuspidens*	*Plesiadapis cookei*
	USNM 309902	UALVP 46685	AMNH 17388	YPM-PU 19642	MNHN CR 125	MNHN CR 965	Pellouin	UM 87990
	Skull	Skull	Skull	Rostrum	Skull	Skull base	Skull	Skull
Shape variable	Bangtail	DW-2	Mason Pocket	7-up Butte	Berru	Berru	Berru	SC-117
Av/GM	—	0	—	—	0	—	—	0
Cl/GM	3	3	—	—	2	—	—	2
EAM-S	—	1	—	—	3	—	3	3
Gld/GM	0	1	1	—	1	—	1	1
N/F	—	2	—	2	1	—	—	1
Nc/GM	0	0	—	—	0	—	0	0
Nc/Nr	1	0	—	1	0	—	—	0
Nc/Pmx	—	1	—	0	0	—	—	—
Pcsa/GM	0	0	—	—	0	—	—	0
Pmx/GM	—	0	—	—	0	—	—	—

obtaining access to the intratympanic cavity via "intrapetrous" canals, as discussed by MacPhee (1981) for *Microcebus*, and as we have observed in a specimen of *Eulemur* (SBU efr-3562). From observations on *Indri* and paromomyid plesiadapiforms (Figs. 25–27), the line of foramina observed in UM 87990 cannot be regarded as evidence of a non-petrosal bulla even if they do represent a suture or boundary between different bony laminae. It is also relevant to note that UM 87990, the only plesiadapid specimen to exhibit this line of foramina, is also ontogenetically younger than other specimens whose skulls are discussed in Appendix V.

Consideration of the ectotympanic bulla of rodents such as *Marmota* and *Lagostomus* raises the question of the medial extent of the ectotympanic-derived bone in *P. cookei*. No visible suture exists anywhere on the bulla or on the external auditory meatus to delimit a boundary between ectotympanic and bulla-forming bone (nor is such morphology convincingly well preserved in other plesiadapids; Appendix V). Thus, the homology of the auditory bulla of *Plesiadapis*—ectotympanic, entotympanic or petrosal—is still an open question.

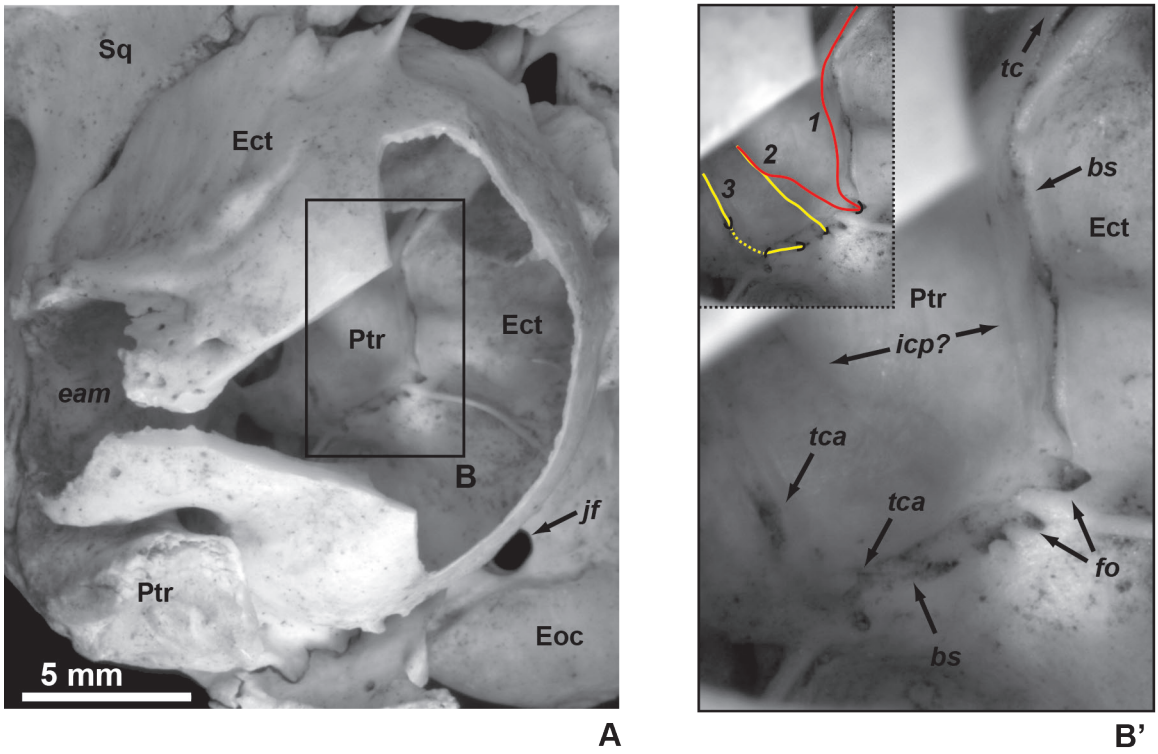

FIGURE 22.— Basicranium of the North American marmot *Marmota monax* (Boyer collection). **A**, right basicranium in ventral view. **B**, enlargement of suture between petrosal and ectotympanic bones, with reconstruction of neurovascular pathways. Anterior is at the top in both figures. *1* and *2*, branches of the internal carotid plexus; *3*, tympanic nerve. Stapedial artery is functional and enters bulla posteromedially. Given that this artery is the only remnant of the internal carotid system, it is likely that the nerve plexus related to it also entered medially. Foramina apparent on medial side of promontorium lead to grooves (*2*) that course laterally, and one that leads to *s2* (*1*). In *Marmota s2* is apparently not homologous to that in plesiadapids because in *Marmota* it leads to the tubal canal (as *s1* does in plesiadapids and euprimates). The internal carotid plexus should send branches toward the tubal canal. Thus the particular route of these grooves is another point supporting interpretation of them. The most posteriorly situated groove (*3*) likely relates to the tympanic plexus as it leads from the jugular foramen, courses laterally in a groove that is sometimes shallowly floored by the petrosal (and thus forms a canal at these points), and probably goes toward site of formation of tympanic plexus. Morphology relating to the tympanic nerve of *Marmota* is thus similar to that in *Lagostomus* (see below), plesiadapids and even some euprimates (MacPhee, 1981). Abbreviations: *bs*, bullar suture; *eam*, external auditory meatus; *Ect*, ectotympanic; *Eoc*, exoccipital; *fo*, foramen; *icp?,* internal carotid plexus?, possible route of the internal carotid plexus; *jf*, jugular foramen; *Ptr*, petrosal; *Sq*, squamosal; *tc*, tubal canal; *tca*, tympanic canaliculus.

Internal carotid artery

Functionality of the internal carotid artery in extant primates is reflected in the relative and absolute size of the posterior carotid foramen (Kay et al., 1992). Estimates of the functionality of the internal carotid artery have been based on the diameter of the posterior carotid foramen (Kay et al., 1992; Boyer et al., 2016), the internal carotid plexus canal, and the groove for the internal carotid plexus on the promontorium (Bloch and Silcox, 2006). For plesiadapid crania that do not preserve the posterior carotid foramen, the groove for the internal carotid artery, which is equivalent to the g1 groove here, can be measured instead (Bloch and Silcox, 2001; Boyer et al., 2012a; see Tables A-I-3, A-I-4).

Figure 28 illustrates the allometric relationship of posterior carotid foramen diameter to skull length in extant primates that have a functional internal carotid artery (shaded convex polygon), extant primates with a non-functional carotid artery (open convex polygon), and several fossil species (filled squares). The plesiadapid *N. intermedius* falls within the polygon bounded by extant primates with a non-functional internal carotid artery. The plesiadapids *Pr. gaoi*, *P. tricuspidens*, and *P. cookei* also have a small posterior carotid foramen, but they fall outside this region because they have a longer skull. Because all plesiadapids have a posterior carotid foramen that is smaller than that of any extant species with a functional internal carotid artery (regardless of cranial length), it is unlikely that any had a functional internal carotid artery.

Skull length can be measured directly only in *P. tricuspidens* (MNHN CR 125; 106 mm). Skull length in *P. cookei* (UM 87990) was estimated to be nearly the same, based on 39 different cranial measurements (Table 4). Estimation of size difference from multiple measurements assumes that skull shape is constant, but we know there are numerous proportional differences distinguishing *P. tricuspidens* from

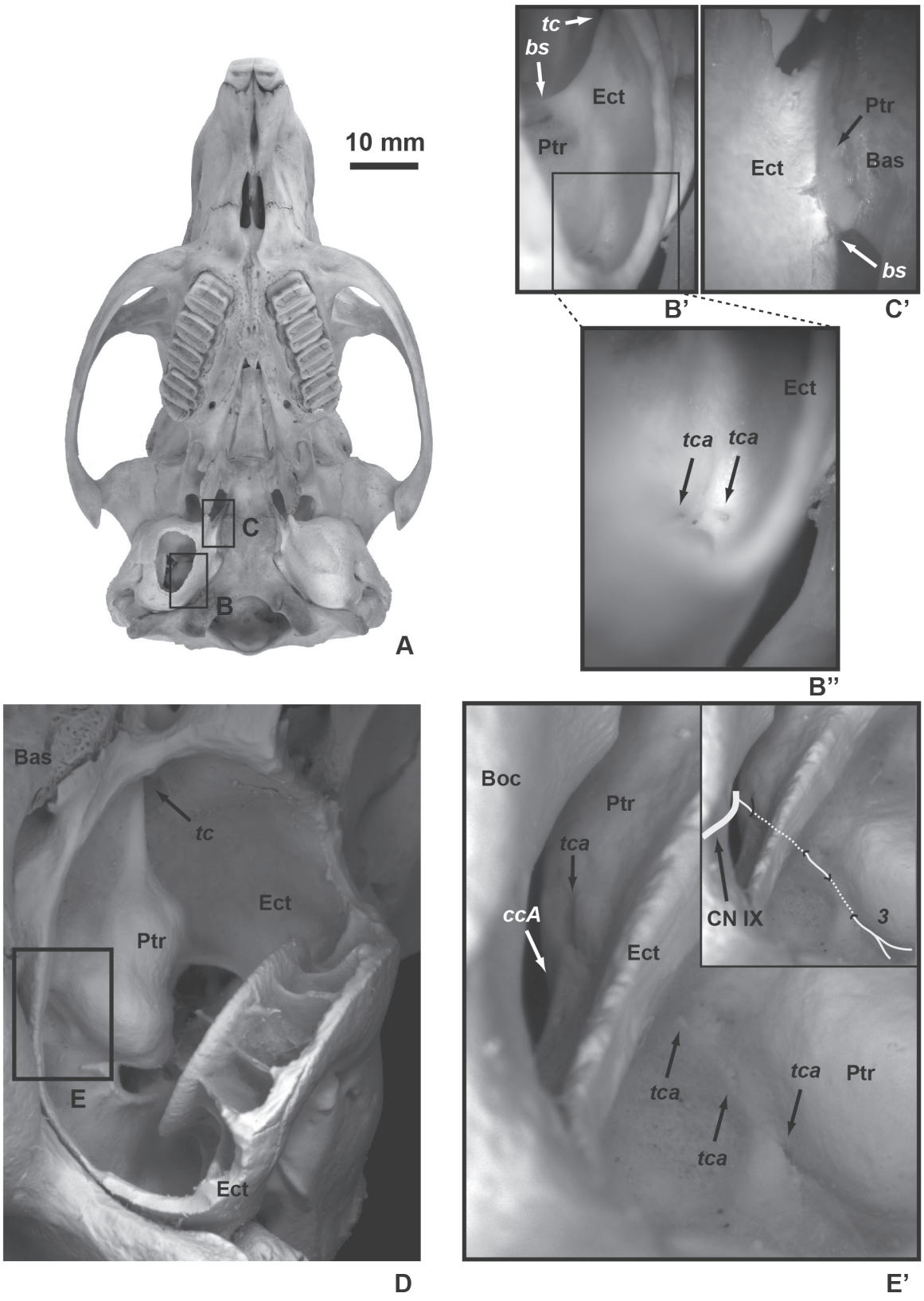
10 mm
C
B
A
tc
bs
Ect
Ptr
B'
Ptr
Ect
Bas
bs
C'
Ect
tca
tca
B''
Bas
tc
Ect
Ptr
E
Ect
D
Boc
Ptr
tca
ccA
CN IX
3
Ect
tca
tca
tca
Ptr
E'

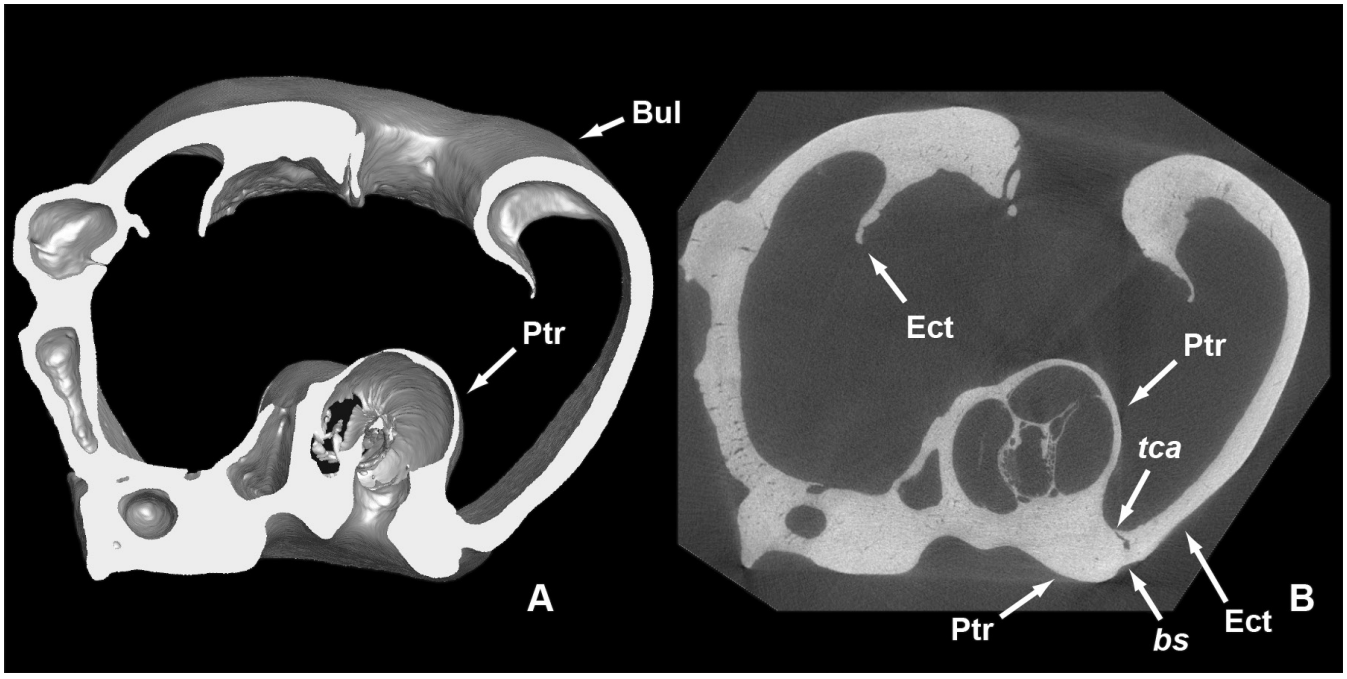

FIGURE 24.— Petrosal and ectotympanic of *Lagostomus maximus* (AMNH 41527). **A**, anterior view of the left petrosal and ectotympanic based on a surface reconstruction of high-resolution CT data. **B**, anterior view of high-resolution CT slice. High-resolution CT imagery shows that, despite color differences visible at the ectotympanic/petrosal boundary (Fig. 23B′–C′, there is no internally visible density difference or sutural surface. However, the tympanic canaliculus can be traced through the medial process and it appears to follow the ectotympanic/petrosal boundary. Abbreviations: *bs*, bullar suture; *Bul*, auditory bulla; *Ect*, ectotympanic; *Ptr*, petrosal; *tca*, tympanic canaliculus.

FIGURE 23.— Basicranium of the South American plains viscacha *Lagostomus maximus* (A–C, specimen UMMZ TS13; D–E, specimen AMNH 41522). **A**, ventral view of the skull. **B**, enlargement of the right tympanic cavity. **C**, inset of anterior end of bulla. There is a distinct color difference visible near where petrosal/ectotympanic boundary must be in B and C. Note that in the enlargement of B the more medial (farther right) *tca* foramen represents the opening of the tympanic canaliculus into the tympanic (bullar) cavity. The *tca* foramen to the left is the beginning of a shallow canal that represents the continued lateral course of branches of the tympanic nerve. **D**, ventral view of left petrosal with the bulla cut away. **E**, enlargement of the medial aspect of the promontorium. *Lagostomus,* unlike *Marmota,* has grooves on the promontorium relating back to the tympanic canaliculus in the wall of the jugular foramen (the internal carotid plexus apparently does not enter the tympanic cavity from a medial position in *Lagostomus*). The *tca* foramen farthest to the left in E represents the initial opening of the tympanic canaliculus into the bullar cavity. The next foramen to the right represents the beginning of the canal for the continued course of the nerve, and that farthest to right represents the end of this short, shallowly-floored canal. Grooves and canals leading across the promontorium appear similar in morphology to those of this region in plesiadapids and in *Marmota*. Abbreviations: *Bas*, basisphenoid; *Boc*, basioccipital; *bs*, bullar suture; *ccA*, aperture for cochlear canaliculus; *CN IX*, cranial nerve IX; *Ect*, ectotympanic; *Ptr*, petrosal; *tc*, tubal canal; *tca*, tympanic canaliculus.

P. cookei and other North American plesiadapids (Appendix V). These shape differences, which are present in various regions of the skull (e.g., mediolateral width of the posterior extent of the nasals), mean that using measurements from MNHN CR 125 to estimate skull length in North American specimens that are more fragmentary than UM 87990 could yield more biased results. For the data plotted in Figure 28, we used skull measurements of *P. cookei* to reconstruct cranial lengths for North American specimens with substantially fewer than 39 comparable measurements (e.g., there are only 14 measurements available for *N. intermedius*) by calculating the geometric mean percent difference between one of the North American specimens and *P. cookei* for all comparable cranial measurements (Table 4). The length estimate is then the mean percent difference multiplied by the length of the *P. cookei* skull (105.8 mm). We used geometric mean differences because ratios of arithmetic means are asymmetrical and yielded inconsistent estimates of size when we interchanged reference specimens. That is, the direction of comparison affected results: when the size of *P. cookei* was calculated as an arithmetic mean of percent differences from *P. tricuspidens*, it was estimated to be slightly larger, but the opposite was true if *P. tricuspidens* was calculated as a simple mean of percent differences from *P. cookei*. When geometric mean percentages were used, then *P. cookei* was shown to be slightly smaller than *P. tricuspidens* in both comparisons.

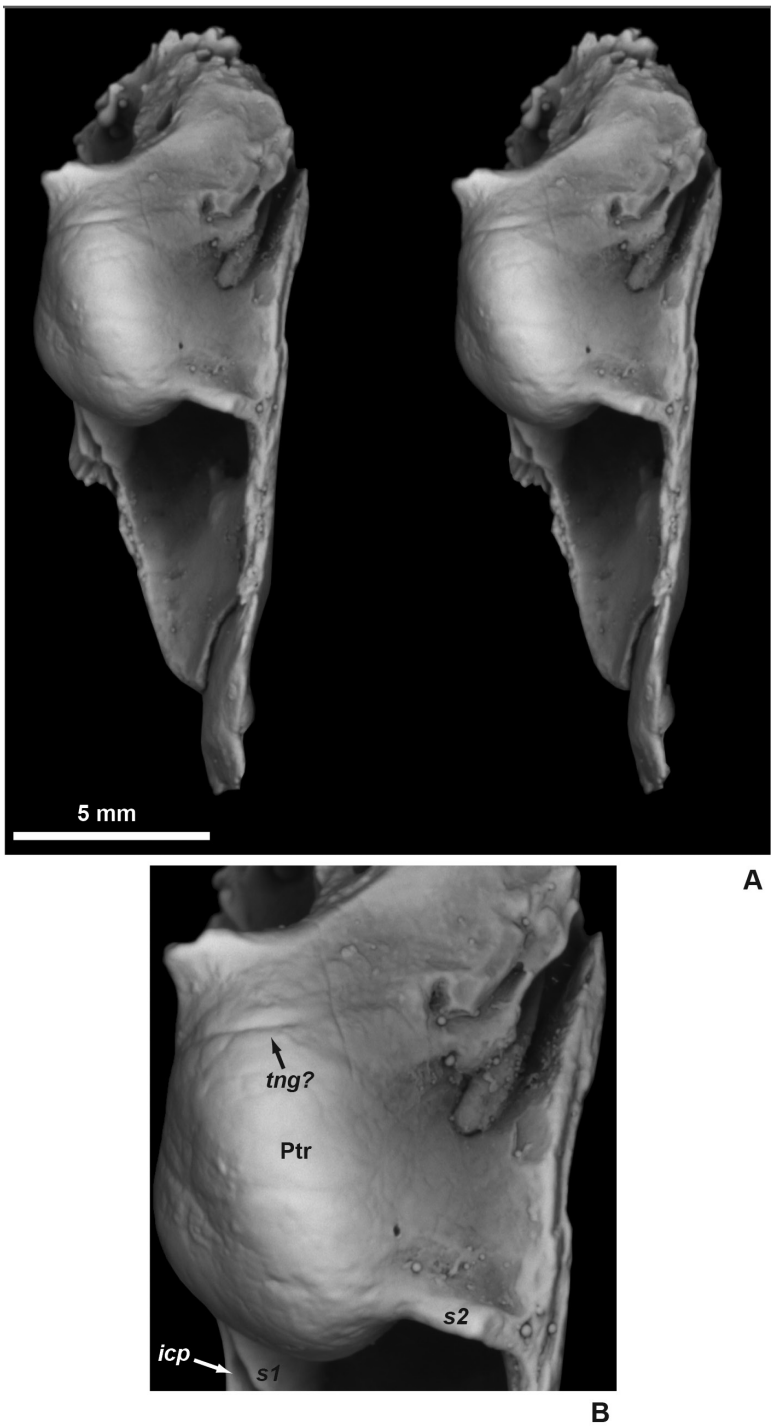

FIGURE 25.— Petrosal of *Indri indri* (AMNH 185638). **A**, Stereophotograph of the left petrosal in medial view, with a broken bulla and medial tympanic process. **B**, Enlarged image of the promontorium. Anterior is at the bottom in both images. The broken medial process appears to include two bony laminae and looks just like the broken medial process of taxa that have a non-petrosal bulla, as well as that of plesiadapids (Figs. 23–24). Euprimates, including *Indri*, have a petrosal bulla, meaning that multiple laminae cannot be taken as evidence of multiple bones in this region. Abbreviations: *icp*, internal carotid plexus; *Ptr*, petrosal; *s1*, first (anterior) septum, which is the most lateral septum extending anteriorly from promontorium (tubal canal forms between *s1* and the epitympanic crest); *s2*, second septum, which forms medial to *s1* and projects anteromedially from the promontorium (*g3* typically leads to the ventral or medial aspect of this septum); *tng*?, tympanic nerve groove?

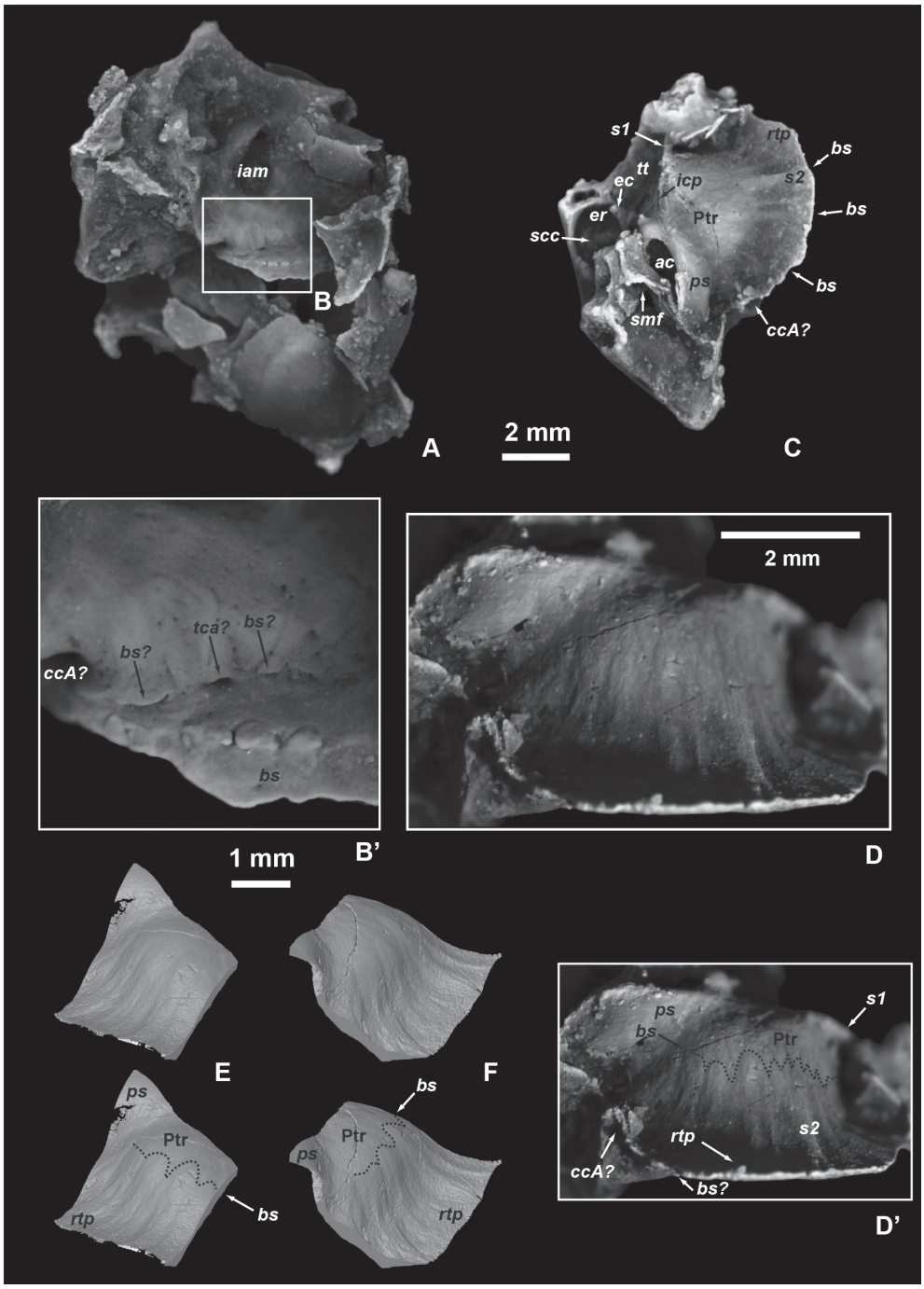

FIGURE 26.— Basicranium of *Ignacius clarkforkensis* (USNM 482353). **A**, left ear region in dorsal view (anterior at right, lateral at top). **B**, enlargement of the medial edge of the medial tympanic process. Note the apparent sutural groove in addition to sutural surface for the ectotympanic (as identified by Kay et al., 1992, and Bloch and Silcox, 2001). **C**, right ear in ventral view (anterior at top). **D**, right ear in medial view with a dashed line highlighting the subtle margin of ridges on the medial process that may represent a former suture (ventral at top). **E**, high-resolution CT reconstruction of right ear in anteromedial view (ventral at top). **F**, high-resolution CT reconstruction of right ear in posterior view (ventral at top). E and F illustrate the course of the boundary between ridges of the medial tympanic process and the promontorium. Abbreviations: *ac*, aperture for cochlear fenestra; *bs*, bullar suture; *cc*, cochlear canaliculus; *ccA*, aperture for cochlear canaliculus; *ec*, epitympanic crest; *er*, epitympanic recess; *iam*, internal acoustic meatus; *icp*, internal carotid plexus; *ps*, posterior septum; *Ptr*, petrosal; *rtp*, rostral tympanic process; *s1*, first (anterior) septum (tubal canal forms between *s1* and epitympanic crest); *s2*, second septum formed medial to *s1*; *scc*, semicircular canal; *smf*, stylomastoid foramen; *tca*, tympanic canaliculus; *tt*, tegmen tympani.

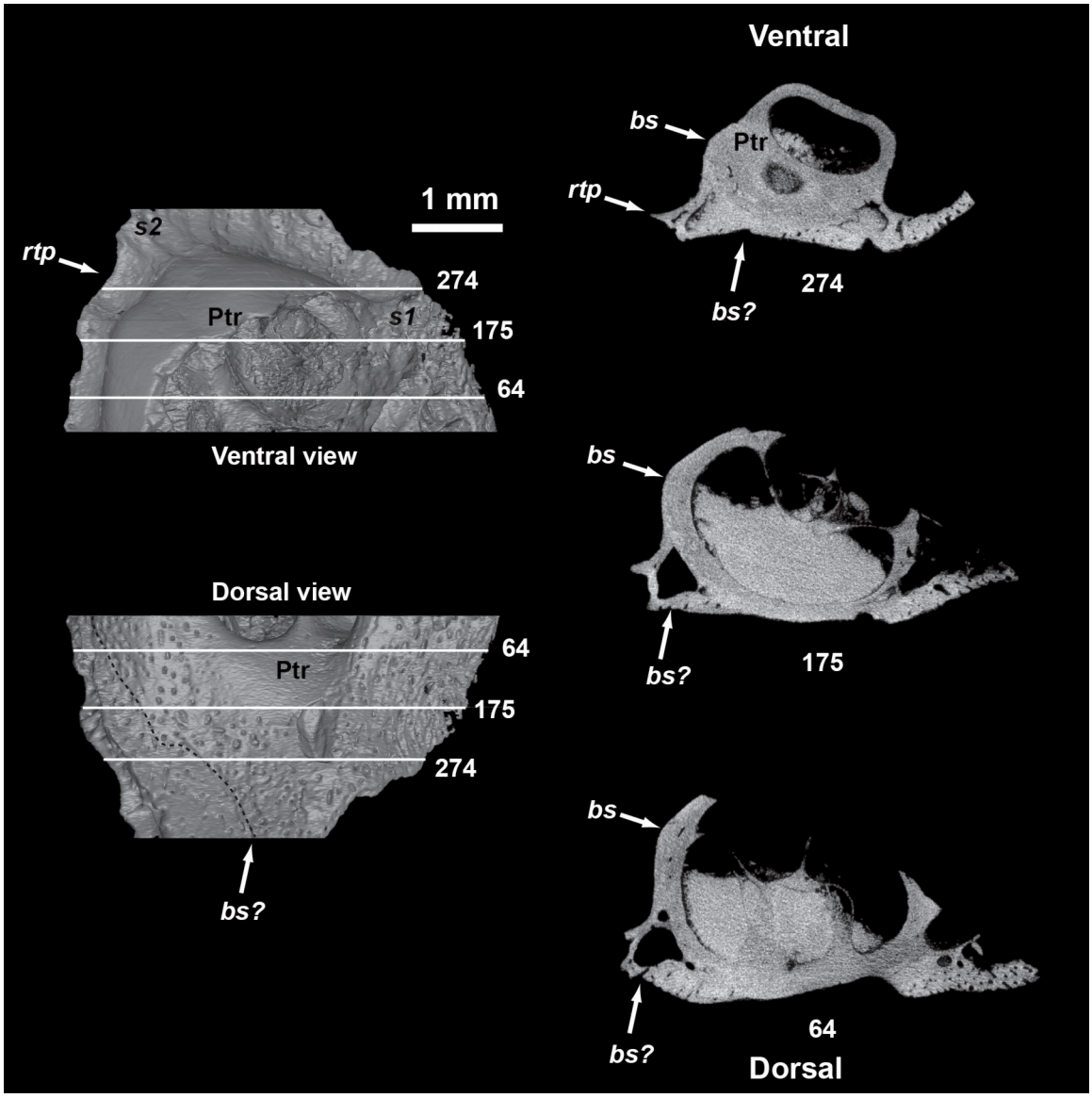

FIGURE 27.— Basicranium of *Acidomomys hebeticus* (UM 108207). This is a left promontorial fragment of the petrosal with high-resolution CT surface reconstructions at left, and individual slices at right. Slices 64, 175, and 274 are shown here (slice numbers increase anteriorly). Medial is to left in all images. This individual is a juvenile with very porous bone, retaining unshed deciduous teeth and unerupted adult teeth. These images were acquired to evaluate whether grooves illustrated for the adult *Ignacius* specimen in Fig. 26B (*bs?*) and Fig. 26D–F (*bs*) are in fact sutures. There is a density difference between the dorsal region of bone and the cochlea containing bone. Structures illustrated for *Ignacius* in Fig. 24D–F appear to be sutural in that they are a meeting of two different types of bone, but that in Fig. 24B appears to be a meeting of two different outgrowths from same bone. The bone forming the medial process of the petrosal appears to extend over the entire dorsal surface of bones housing the cochlea in this specimen, and thus likely represents part of the temporal bone (see text). Abbreviations: *bs*, bullar suture; *Ptr*, petrosal; *rtp*, rostral tympanic process; *s1*, first (anterior) septum; *s2*, second septum, which forms medial to *s1*.

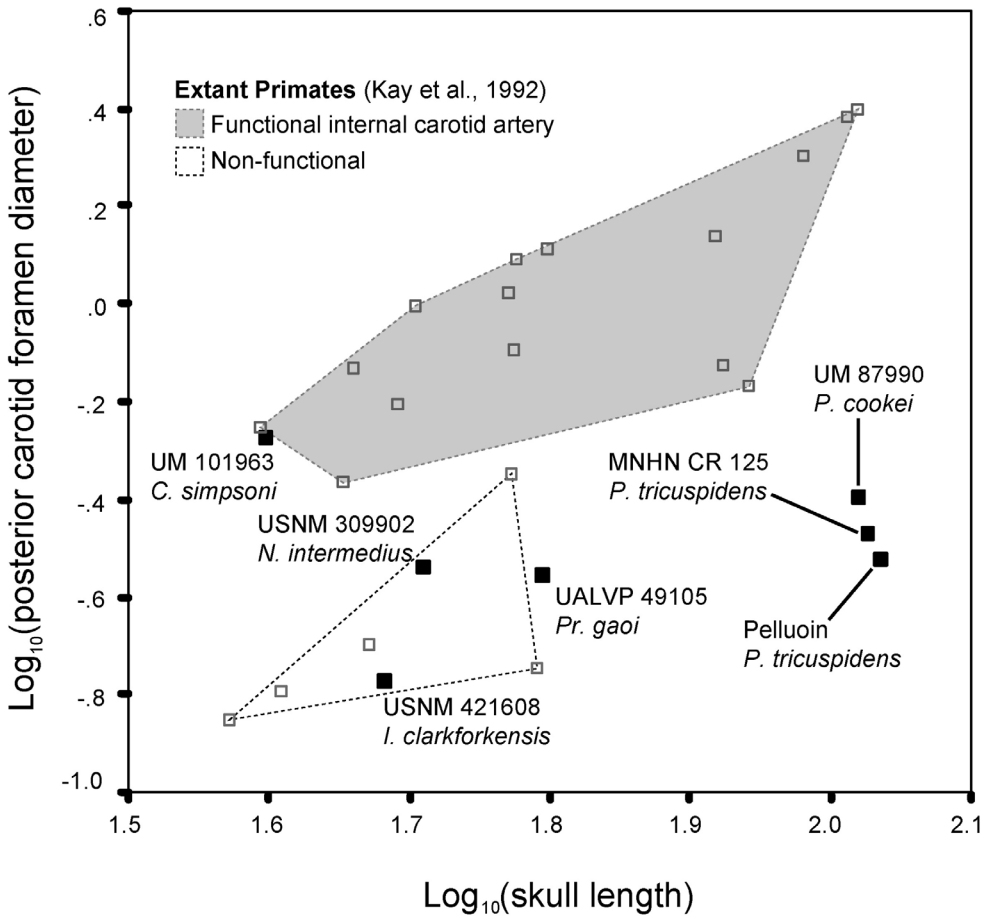

FIGURE 28.— Plot of posterior carotid foramen sizes of selected plesiadapiforms (solid squares) relative to those of extant primates (open squares) measured by Kay et al. (1992). The ordinate represents the diameter of the posterior carotid foramen or the width of the *g1* groove for the internal carotid plexus (which are equivalent; Bloch and Silcox, 2001, 2006). The posterior carotid foramen (or *g1* groove) for all plesiadapids is smaller than that of extant primates that have a functional internal carotid artery. It is also smaller than that of *Carpolestes simpsoni* (Bloch and Silcox, 2006), but larger than that in *Ignacius* (Kay et al., 1992). Skull length estimates for fragmentary specimens were based on *Plesiadapis tricuspidens* and *P. cookei* and were generated as described in the text (see appendix Table A-I-9). The method for generating skull length estimates here is simple, but skull length is not critical for interpretation of the functionality of the carotid foramen in this sample. Foramina of taxa with functional arteries are generally larger than those of taxa with non-functional arteries regardless of skull length.

IV

POSTCRANIAL MORPHOLOGY

The skeleton of *P. cookei* described here (UM 87990) was found in a lens-shaped deposit of freshwater limestone mixed with bones of a similar-sized carnivoran *Uintacyon rudis*. Late Paleocene and early Eocene miacids such as *U. rudis* were arboreal claw-climbers with mobile limb joints (Rose, 1990, 2001). Teeth and cranial bones of *Plesiadapis* and *Uintacyon* are very different, but postcranial elements are somewhat similar. Thus an initial obstacle in this study was distinguishing postcranials of the two genera.

The skeletons of *P. cookei* and *U. rudis* were prepared using acid reduction techniques described in Bloch and Boyer (2001). Information about bone distributions, bone associations, and in situ articulation was not recorded during preparation. Thus there is uncertainty about whether some postcranial elements belong to *P. cookei* or to *U. rudis*. Preparation and documentation of skeletal–dental associations in other plesiadapiform taxa has helped resolve some questions (Beard, 1989; Bloch et al., 2007; Boyer et al., 2013). Some skeletal elements are easily identified as belonging to *P. cookei*, because they are well known among plesiadapiforms (e.g., Szalay et al., 1975). However, identification of the less frequently preserved elements included in UM 87990 was more difficult. The problem is greatest for metapodials II–V, some carpals (the trapezium, trapezoid, and hamate), some tarsals (the mesocuneiform and ectocuneiform), vertebrae, and ribs. We attempt to justify attribution of these elements to *P. cookei* in the following sections of this chapter. Evidence for attribution of hand bones has also been presented in Boyer et al. (2013).

The postcranial skeleton of *P. cookei* is logically divided into four regions: the vertebral column or axial skeleton, the thorax comprising the sternebrae and ribs, the forelimbs including the hands, and the hind limbs including the feet. We describe bones of the postcranial skeleton region by region and element by element, with comparisons inserted where appropriate. Measurement abbreviations are listed in appendix Table A-II-1. Measurements of the postcranial skeleton are provided in the Appendix II tables.

The descriptions of individual bones are followed by interpretations of the functional implications of each bone's morphology. We then end with a functional interpretation of the skeleton as a whole.

DESCRIPTION

Vertebral column

Much of the vertebral column is preserved but very little positional information was recorded as UM 87990 was prepared. Identification of vertebrae as cervical, thoracic, lumbar, sacral, or caudal is straightforward, but identification of individual vertebrae to position within the neck, thorax, lumbus, sacrum, and tail is more difficult. Our assessments are based on morphological features and on morphological and metrical trends. For instance, the sixth cervical vertebra is identified as such based on the presence of a hypertrophied ventral transverse process (equivalent to "anterior tubercle" using human terminology). The first thoracic vertebra is identified as T1 because it has a body with a shallower dorsoventral depth than any other preserved thoracic vertebra. There are probably mistakes in this seriation but these are hopefully not too serious. Recovery of more complete specimens and better comparative data in the future will illuminate any such misidentifications.

Comingling of bones of *Uintacyon* with the skeleton of *Plesiadapis* means that some vertebrae may not actually belong to *P. cookei*. Misattribution of vertebrae is less likely to be a problem for more complex vertebrae of the thorax and lumbus than it is for more simple distal vertebrae of the tail. A number of lines of evidence were used to deduce the attribution of vertebrae to UM 87990. First, a good number of vertebrae of *Uintacyon* remain associated with its skull, which is still partly embedded in limestone, thus cervical and thoracic atributions are relatively secure. In addition, *N. gidleyi* and *N. intermedius* preserve vertebrae from all regions of the vertebral column, and these were helpful in corroborating the identification of vertebrae of UM 87990 as those of *P. cookei*.

We do not know how many vertebrae were present in the complete vertebral column of *Plesiadapis*. The median number of vertebrae at each position in mammals is seven cervical, 13 thoracic, six lumbar, four sacral, and 20 caudal vertebrae, for a vertebral formula of 7.13.6.4.20 (Flower and Gadow, 1885; see also appendix Table A-II-2). The median formula for primates differs in having fewer sacral and more caudal vertebrae (7.13.6.3.24), which is also the formula for the treeshrew *Tupaia glis* (Table A-II-2). UM 87990 preserves five cervical, 12 thoracic, and six lumbar vertebrae. The sacrum is complete with three vertebrae. There are 17 caudal vertebrae preserved, with at least three of the most proximal positions missing. Thus, there were at least 20 caudal vertebrae. Given the euarchontan affinities of *P. cookei*, and its demonstrable differences from the treeshrew *Ptilocercus lowii* in lumbar vertebral number (Sargis, 2001), and from the dermopteran *Cynocephalus volans* in caudal

and sacral vertebral number (Table A-II-2), we expect the full plesiadapid vertebral formula to match the formula in the treeshrew *Tupaia* and the median formula in primates: 7.13.6.3.(>20). The number of preserved sternebrae (7) represents the complete sternebral series, which also supports the conclusion that there 13 thoracic vertebrae (see below for details). Although it is possible that *P. cookei* could have had more thoracic vertebrae (and sternebrae) than were preserved and was more similar to *P. lowii* and *C. volans* in this regard, we find this unlikely because increased numbers of thoracic vertebrae tend to be features reflecting dorsostability of the thorax (Granatosky et al., 2014). As discussed below, *P. cookei* does not exhibit any other 'dorsostable' features in the thorax, unlike *P. lowii* and *C. volans*.

Cervical vertebrae

Five of an expected seven cervical (C) vertebrae of UM 87990 are preserved (Fig. 29). Cervical vertebrae are identified by their short craniocaudal length and their distinctive morphology, including on some the presence of a transverse foramen for the vertebral artery. Measurements are given in appendix Tables A-II-3 and A-II-4.

Atlas.— The atlas or cervical vertebra C1 is well preserved (Fig. 29A). The right transverse process is broken lateral to the canal for the vertebral artery. The dorsal ("posterior") arch is craniocaudally longer than the ventral ("anterior") arch. It is shortest at the midline and becomes longer, or more expanded, laterally (Fig. 29A). The dorsal arch has a small tubercle for attachment of the rectus capitis posterior minor muscle. The foramen for entrance of the vertebral artery is located between the lateral aspect of the axis facet and the dorsal arch. This foramen leads to a canal that pierces the atlas from ventral to dorsal, lateral to the vertebral foramen (for the spinal cord). At the beginning of its course, the canal has an opening on the ventrolateral aspect of the atlas. The canal then traverses medially and cranially though the dorsal arch of the atlas to open within the vertebral canal just above the occipital articular facets of the lateral masses of the atlas. The middle part of the vertebral artery canal has another opening on the dorsolateral surface of the dorsal arch.

Axis.— The axis or C2 is fragmentary (Fig. 29B), missing the cranial and caudal tips of its spinous process, the postzygapophyses, the tips of the transverse processes, and the caudal centrum epiphysis. The body is also severely crushed. It seems likely that its spinous process would have projected cranially prior to breakage. A substantial portion of the caudal projection of the spinous process is intact. The dorsal edge of the spinous process is preserved near the craniocaudal midpoint. The transverse foramina are preserved, as are the roots of the transverse processes, which form the lateral edges of the foramina. The odontoid process is preserved. It has craniolaterally facing depressions for the alar ligaments.

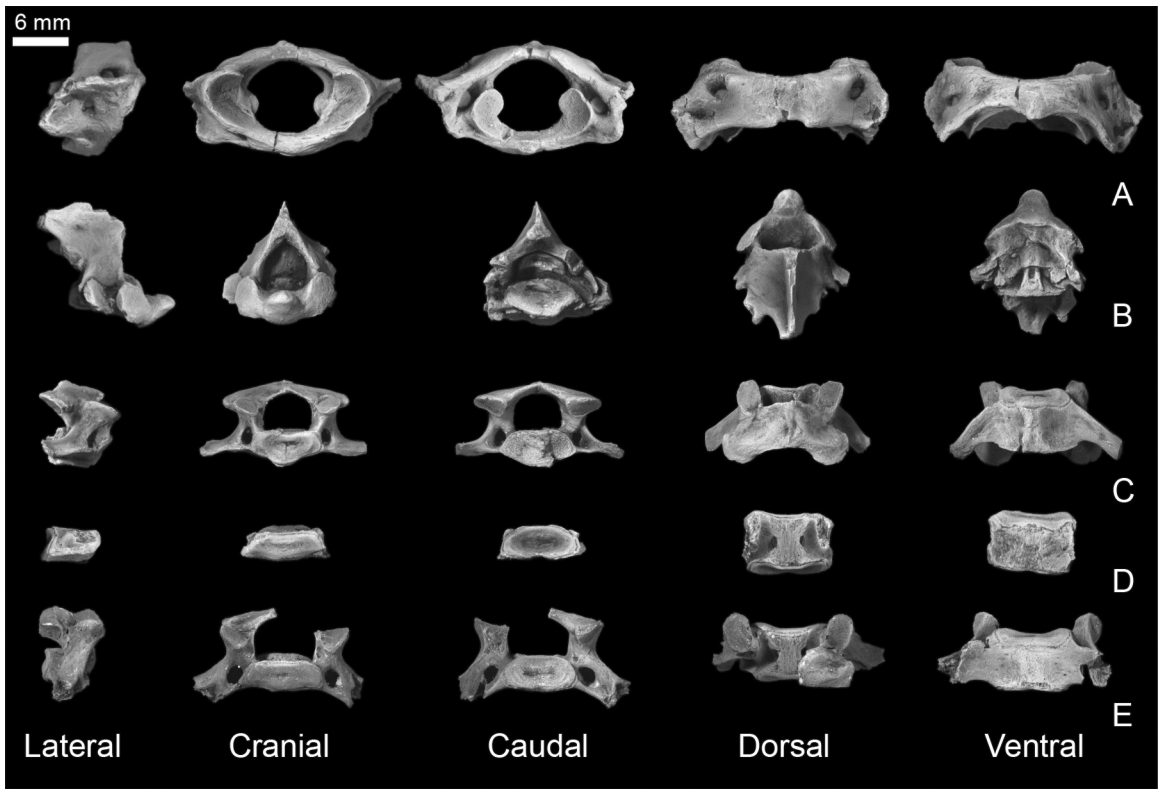

FIGURE 29.— Cervidal vertebrae of *Plesiadapis cookei* (UM 87990). **A**, atlas (C1). **B**, axis (C2). **C**, cervical C3? **D**, cervical C4? **E**, cervical C6? All are shown in lateral, cranial, caudal, dorsal, and ventral view.

As is often the case, the axis is the longest of the cervical vertebrae, even without accounting for what is likely to have been a significant amount of craniocaudal crushing, the loss of the caudal centrum epiphyis, or the length of the odontoid process.

Third cervical vertebra (C3).— Three other cervical vertebrae are preserved. One is identified as C3 (Fig. 29C), although it could also represent C4. It is not C5 or C7 because it does not articulate well with the vertebra identified as C6. It is almost perfectly preserved. Each lamina of the vertebra is craniocaudally expanded relative to its mediolateral width, which is one reason that it is assigned to C3 rather than C4. The spinous process appears to have been weakly developed. The prezygapophyses are oriented dorsally whereas the postzygapophyses face ventrally. The centrum is rectangular with a distinct midline ventral ridge. Its cranial facet faces cranially and is angled slightly ventrally. Within the vertebral canal, the dorsal surface of the centrum is marked by two foramina. The transverse processes are long and narrow, projecting caudolaterally. These contain transverse vertebrarterial foramina.

Fourth cervical vertebra (C4).— Another cervical vertebra is represented by the centrum alone (Fig. 29D). It is considered to be C4, even though it cannot be articulated with C3 due to the missing caudal epiphysis of C3. There is slight mismatch between the caudal epiphysis of 'C4' and C6, which is taken as additional evidence that it is correctly identified as C4 (and not C5). The C4 centrum is even more 'rectangular' than that of C3, because the dorsal and ventral surfaces are parallel to one another, and there is no midline ridge on the ventral surface. Like C3, there are two foramina on the dorsal surface. The cranial centrum facet faces slightly ventrally, like that of C3. The caudal facet faces slightly dorsally; however it has a dorsal lip, which makes the surface cylindrically concave.

Sixth cervical vertebra (C6).— The last of the preserved cervical vertebrae is identified as C6, mainly because of the presence of broken roots of hypertrophied, ventrally-directed transverse processes that typically characterize this position (Fig. 29E). The left half of the pedicle and lamina are also broken away, as are the tips of the transverse processes. The prezygapophyses are oriented slightly more medially than the dorsally facing facets of C3, whereas the postzygapophyseal facets are oriented slightly more laterally than the ventrally facing facets of C3. The transverse vertebrarterial foramina are preserved. The centrum is basically identical in shape and morphology to that of C4.

Comparisons.— The atlas of *P. cookei* is similar to that of *N. gidleyi*, *N. intermedius*, tupaiids, and *Sciurus* in most respects. It differs from these taxa in having a ventral arch that is more craniocaudally expanded compared to the dorsal arch. This makes it slightly more similar to the condition in *Ptilocercus*, dermopterans and chiropterans (Sargis, 2001). Sargis (2001) suggested that a more expanded atlas in *Ptilocercus*, as compared to that of *Tupaia*, reduces neck mobility.

In most preserved features, the axis of *P. cookei* is similar to that of *N. intermedius*. One notable difference is that *N. intermedius* has a proportionally larger vertebral canal. However, this is true throughout the vertebral column and also distinguishes vertebrae of *N. gidleyi* from those of *P. cookei*. It is likely an allometric effect of absolute size differences between the three plesiadapids.

C3, C4, and C6 in *P. cookei* have morphology similar to that preserved in *N. gidleyi* and *N. intermedius*, although these taxa appear to have slightly more prominent ventral midline ridges on their vertebrae. Plesiadapids are also morphologically similar to *Ptilocercus* and arboreal tree squirrels in (1) having vertebral bodies of the cervical vertebrae that are mediolaterally wide relative to their craniocaudal length and (2) lacking pronounced spinous processes. On the other hand, species of *Tupaia* and terrestrial rodents (e.g., *Rattus*) have mediolaterally narrower vertebral bodies and more pronounced spinous processes. These differences have been related to contrasts in head mobility among various taxa (Argot, 2002). The tupaiid-like form is thought to retain greater mediolateral mobility due to the presence of a narrower body. *Cynocephalus* is an interesting case because it has cervical centra that are similar to those of plesiadapids in most respects, but it has prominent spinous processes on all of its cervical vertebrae, unlike plesiadapids (Stafford, 1999).

Thoracic vertebrae

Twelve of an expected 13 thoracic (T) vertebrae of UM 87990 are preserved (Fig. 30). Thoracic vertebrae were identified as thoracic by the presence of rib facets on the body or on transverse processes, or in some cases by the orientation of the zygapophyseal facets. The craniocaudal position of a vertebra in the series, other than whether it comes before or after the diaphragmatic position, is difficult to determine due to extensive postmortem deformation that prevents assessment through articulation or detailed measurements. Centrum length, height, and overall size often increase progressively from cranial to caudal. The first thoracic vertebra is craniocaudally shorter than the others, but there is no clear pattern of increase in the remaining prediaphragmatic vertebrae (Fig. 30B–I; Table A-II-5). This is demonstrated beyond any doubt by the only two vertebrae preserved in articulation (Fig. 30E), in which the more cranial one is slightly, but definitely, longer. However, the two postdiaphragmatic thoracic vertebrae (Fig. 30J–K) are longer than the ten vertebrae cranial to them.

First thoracic vertebra (T1?).— The bone interpreted as the first thoracic vertebra lacks the neural arch due to breakage (Fig. 30A). The centrum is distinctive in being reniform in transverse section, low or shallow dorsoventrally, and broad transversely, with a facet for a rib head more or less filling each corner. The dorsal surface of the centrum has a conspicuous depression on each side lateral to the midline. The ventral surface of the centrum is smooth.

Second thoracic vertebra (T2?).— The bone interpreted as the second thoracic vertebra has an intact neural arch (Fig. 30B). Much of the centrum is missing, but what remains is reniform in cross section, low and wide like that of T1. Rib facets are not as large relative to the size of the centrum as in T1. Prezygapophyses arise from laminae of the neural arch and face upward and slightly lateral. Postzygapophyses arise higher

on the arch and face downward and medially. The neural spine is not preserved.

Third thoracic vertebra (T3?).— The bone interpreted as the third thoracic vertebra is similar to T2 but the centrum is longer and greater in height (Fig. 30C). It has no ventral midline keel. Prezygapophyses face upward and slightly laterally, whereas postzygapophyses face downward.

Fourth thoracic vertebra (T4?).— The bone interpreted as the fourth thoracic vertebra is not well preserved (Fig. 30D). The shallowness of the centrum suggests that this vertebra might belong farther forward in the series, but the keeled ventral surface of the centrum is more like later vertebrae.

Fifth thoracic vertebra (T5?).— The bone interpreted as the fifth thoracic vertebra remains in articulation with the sixth (Fig. 30E). The centrum is more circular in cross-section than that of more cranial centra, with a faintly-raised ventral midline keel. Pedicles for the neural arch arise from the cranial half of the centrum. A relatively long diapophysis is preserved on the right side, arising from the corresponding lamina of the neural arch and ending in a crescentic articular facet for a rib tuberculum. The neural arch itself is damaged by breakage. The ventral surface of the centrum has a broad but shallow keel.

Sixth thoracic vertebra (T6?).— The bone interpreted as a sixth thoracic vertebra remains in articulation with the fifth (Fig. 30E), which it resembles in size and form. The postzygapophysis is well preserved on the right side. It projects a little more caudally than the centrum, but breakage precludes judging its angle relative to the centrum. The centrum of T6? has a broad but shallow keel like that of T5?.

Seventh thoracic vertebra (T7?).— The bone interpreted as the seventh thoracic vertebra (Fig. 30F) is poorly preserved, with a relatively small cylindrical centrum and a narrow ventral midline keel.

Eighth thoracic vertebra (T8?).— The bone interpreted as the eighth thoracic vertebra (Fig. 30G) has a cylindrical centrum like that of T7?, but with a broader ventral midline keel like that on T5? and T6?. The diapophysis is preserved on the left side, with a small mammillary process or metapophysis rising above the tubercular facet.

Ninth thoracic vertebra (T9?).— The vertebra interpreted as the ninth thoracic vertebra (Fig. 30H) is one of the better preserved thoracic vertebrae. The centrum resembles that of the preceding vertebra, but with a narrow ventral midline keel. The neural arch is intact, extending caudally past the end of the centrum. The base of the neural spine is preserved, rising above this caudal extension. Diapophyses are present on both sides, each surmounted by a distinct metapophysis above the tubercular facet.

Tenth thoracic vertebra (T10?).— The bone interpreted as the tenth thoracic vertebra (Fig. 30I) is like T9?, but the centrum is more 'D'-shaped in cross section. The caudal extension of the neural arch is also different in being divided, with two distinct downward and medially-facing postzygapophyses. The diapophyses are shorter and more elevated than those of T8? and T9?.

Eleventh thoracic vertebra (T11?).— Between T10? and T12? there must have been a diaphragmatic vertebra, which we therefore indicate as T11? even though it was not preserved. A diaphragmatic vertebra has dorsolaterally angled prezygapophyseal facets, like the vertebrae more cranial to it, and ventrolaterally facing postzygapophyseal facets, to articulate with dorsomedially facing prezygapophyseal facets of the vertebrae more caudal to it, including the lumbar, sacral and proximal part of the caudal region. Although it is possible that more than one vertebra intervened between what we have called T10 and T12, inferring only one is the most conservative position to take.

Twelfth thoracic vertebra (T12?).— The bone interpreted as the twelfth thoracic vertebra (Fig. 30J) has a centrum with a hexagonal caudal epiphysis. The postzygapophyses differ from those of T10? in facing downward and laterally rather than downward and medially.

Thirteenth thoracic vertebra (T13?).— The bone interpreted as the thirteenth thoracic vertebra (Fig. 30K) is similar to that identified as T12.

Comparisons.— The first three thoracic vertebrae exhibit dorsoventrally shallow articular surfaces of the centrum, whereas those of T4?–T10? are deeper. The centrum of T12? cannot be measured cranially, and T13? cannot be measured caudally, but together they are the deepest caudally and deepest cranially (respectively) in the thoracic region. Centrum mediolateral widths are even less patterned. T1? is wider cranially than all vertebrae that follow until T13?. Caudally it is the widest of any vertebra in the thoracic region. Of the vertebrae with preserved diapophyses, the most caudal ones are mediolaterally narrower than the more cranial ones (i.e., Fig. 67E vs. 67H–I). Of those with intact laminae and spinous processes, the more caudal vertebrae have more vertically oriented processes. The prediaphragmatic spinous processes all appear to have been longer dorsoventrally than they were craniocaudally.

The thoracic vertebrae have zygapophyses with rounded margins, although T12? appears to have postzygapophyses that are slightly more angular, or square. The postzygapophyses of T13? are too broken for meaningful comment. The postdiaphragmatic neural spine of T12? is broken, but it appears to have been vertically oriented, suggesting that it was the anticlinal vertebra. The neural spine of T13? is badly broken, but its caudal and dorsocaudal margins are intact, revealing that it was cranially oriented and probably shorter dorsoventrally than it was long craniocaudally. The two postdiaphragmatic vertebrae preserve the roots of large accessory processes (anapophyses).

Thirteen is the modal number of thoracic vertebrae in mammals, although this may be slightly above average for small generalized, terrestrial to arboreal mammals (Table A-II-2). Thirteen is the number seen in tupaiid treeshrews, but this is one less than the number present in *Ptilocercus* (14) and in some *Cynocephalus* (14; Sargis, 2001). It is generally thought that a longer thorax represents an emphasis on stabilization rather than mobility (Sargis, 2001). The presence of an anticlinal vertebra within the thoracic region and the presence of large anapophyses indicates that this region had

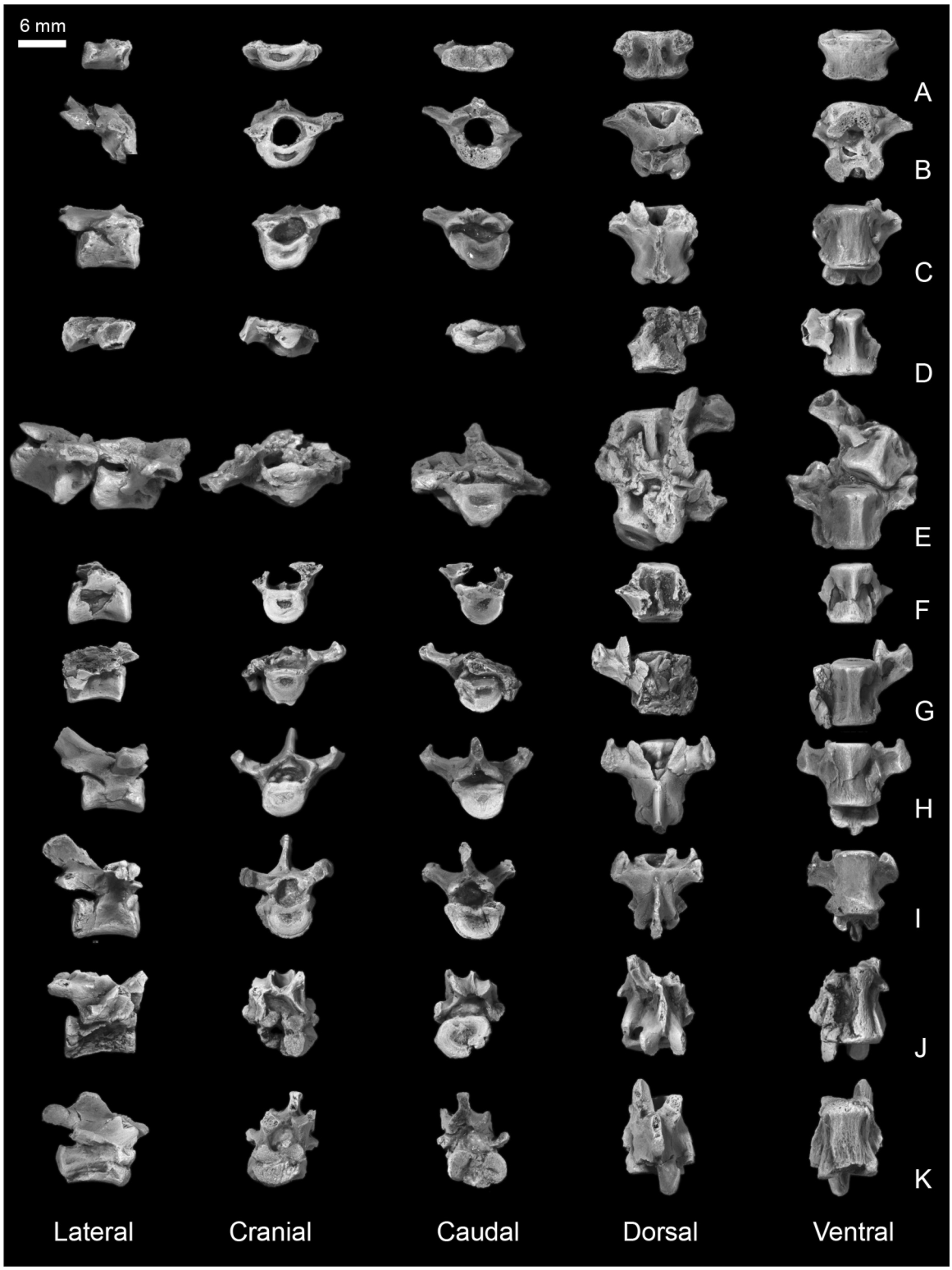

FIGURE 30.— Thoracic vertebrae of *Plesiadapis cookei* (UM 87990). **A**, thoracic T1? **B**, thoracic T2? **C**, thoracic T3? **D**, thoracic T4? **E**, thoracic T5–6? **F**, thoracic T7? **G**, thoracic T8? **H**, thoracic T9? **I**, thoracic T10? **J**, thoracic T12? **K**, thoracic T13? All are shown in lateral, cranial, caudal, dorsal, and ventral view. Vertebrae in images A–I are pre-diaphragmatic vertebrae. Vertebra in image J appears to be postdiaphragmatic and anticlinal. Vertebra in image K is postdiaphragmatic.

pronounced mobility in dorsiflexion and extension, but was restricted in axial rotation or mediolateral flexion. Animals that sometimes use a bounding, asymmetrical gait, and which therefore do not require dorsostability, are characterized by such features (e.g., *Sciurus*, tupaiid treeshrews, many arboreal quadrupedal primates). Apes, humans, lorises, sloths, *Cynocephalus* and some opossums lack a thoracic anticlinal vertebra, and do not engage in quadrupedal bounding gaits (Boyer and Bloch, 2008). The thoracic region of *P. cookei* therefore indicates that it was *not* restricted to slow, cautious locomotion. However, it does not confirm frequent use of bounding gaits either.

The lack of a pronounced serial increase in vertebral centrum dimensions distinguishes *P. cookei* from *Eulemur* and *Tupaia* among members of the available sample (Table A-II-2), which could mean it was not as agile as these taxa. Overall, *P. cookei* appears most similar to the scansorial phalangerid marsupial *Trichosurus vulpecula* in the number of thoracic vertebrae (13), the position of its anticlinal vertebra (T11?), and in patterns of change in the length and height of thoracic vertebral centra (Table A-II-2).

Looking at other plesiadapids, there are at least two basic differences between thoracic vertebrae of *P. cookei* and those of *N. gidleyi* and *N. intermedius*. As mentioned previously, the vertebral canal is proportionally larger in the smaller taxa. In addition, the neural spines of at least *N. intermedius* are craniocaudally narrower for their proximodistal lengths compared to those of *P. cookei*.

Lumbar vertebrae

Six lumbar (L) vertebrae of UM 87990 are preserved (Fig. 31). One may be missing, based on a lack of precise articulation and a size difference between the first two vertebrae of the preserved series (Table A-II-5; Fig. 31A, B). As interpreted here, the lumbar centra increase in all dimensions sequentially from cranial to caudal. The spinous processes appear to become longer dorsoventrally and narrower craniocaudally from cranial to more caudal positions. The transverse processes are small, arise from the vertebral body (not the pedicle), and are cranially positioned on L1 and L3. On the remaining lumbar vertebrae, the transverse processes are larger, arise from the base of the pedicle, and are positioned at the craniocaudal midpoint of each element. All transverse processes project cranioventrally to some degree. The accessory anapophyses are largest on L1 and appear to decrease sequentially, although breakage makes it difficult to be certain just where the anapophyses disappear.

First lumbar vertebra (L1?).— The bone interpreted as the first lumbar vertebra (Fig. 31A) has a relatively elongated centrum that is reniform to 'D'-shaped in cross section. Short transverse processes arise from the lateral surface of the centrum near its cranial end. The neural arch is robust, with laminae rising dorsally from the cranial half of the centrum. The neural spine is long craniocaudally and short dorsoventrally, projecting slightly cranially. Prezygapophyses project cranially and postzygapophyses project caudally near the apex of the neural arch. The former are not well preserved, but the latter are robust, rounded, and face ventrally and laterally. Prominent anapophyses flare caudolaterally, paralleling the postzygapophyses, and both project caudally well past the caudal end of the centrum.

Second lumbar vertebra (L2?).— The bone interpreted as the second lumbar vertebra (Fig. 31B) is similar to L1? but has the postzygapophyses intact. These are surmounted by robust mammillary processes or metapophyses that wrapped around prezygapophyses of the proceding vertebra to some extent. The postzygapophyses of L2? are more gracile and flatter than those of L1?, and the anapophyses are more gracile.

Third lumbar vertebra (L3?).— The bone interpreted as the third lumbar vertebra (Fig. 31C) is similar to L1? and L2?, but is compressed and broken in a way that obscures details of morphology. Here again the preserved right prezygapophysis is surmounted by a robust metapophysis. The transverse process preserved on the right side is longer and directed more cranially than that on preceding lumbar vertebrae.

Lumbar L4?.— The bone interpreted as the fourth lumbar (Fig. 31D) is similar to L3? but differs in having a caudal centrum that is more flattened dorsoventrally, in having prezygapophyses that are more gracile and more vertical, and in lacking the prominent caudally directed anapophyses of preceding vertebrae.

Lumbar L5?.— The bone interpreted as the fifth lumbar vertebra (Fig. 31E) is similar to L4? but has a more prominent metapophysis preserved above the left prezygapophysis. There is a rudimentary anapophysis preserved on the right side of the centrum. It is possible that we have switched L4? and L5? in our identifications.

Lumbar L6?.— The bone interpreted as the sixth lumbar vertebra (Fig. 31F) is distinctive in having the most dorsoventrally flattened lumbar centrum, with a cranial epiphysis that is reniform in outline and a caudal epiphysis that is more pentagonal in outline. The neural arch is deformed, making it difficult to be certain of other differences.

Comparisons.— The lumbar zygapophyses increase in size from L1? to L3?, but appear of roughly equivalent size from L3? to L6?. The prezygapophyses face dorsomedially and are concave. The postzygapophyses face ventrolaterally, and are slightly convex. The caudal margins of the postzygapophyses appear square from a dorsal view.

Though the spine of UM 87990 has thoracic region features indicating patterns of mobility consistent with a bounding gait, certain lumbar features indicate it may not have been a rapid or frequent bounder. These features include prezygapophyses and mammillary processes that are relatively small; and spinous process that are craniocaudally long (Sargis, 2001; Boyer and Bloch, 2008). Active bounders, like *Tupaia* (Jenkins, 1974), have prezygapophyses with prominent mammillary processes or metapophyses, and large ventrally projecting transverse processes (Boyer and Bloch, 2008). These traits presumably correlate with the use of a bounding gait, because they increase the area available for epaxial musculature, enhancing powerful extension (and possibly also flexion) of the spine (Boyer and Bloch, 2008). Furthermore, taxa that

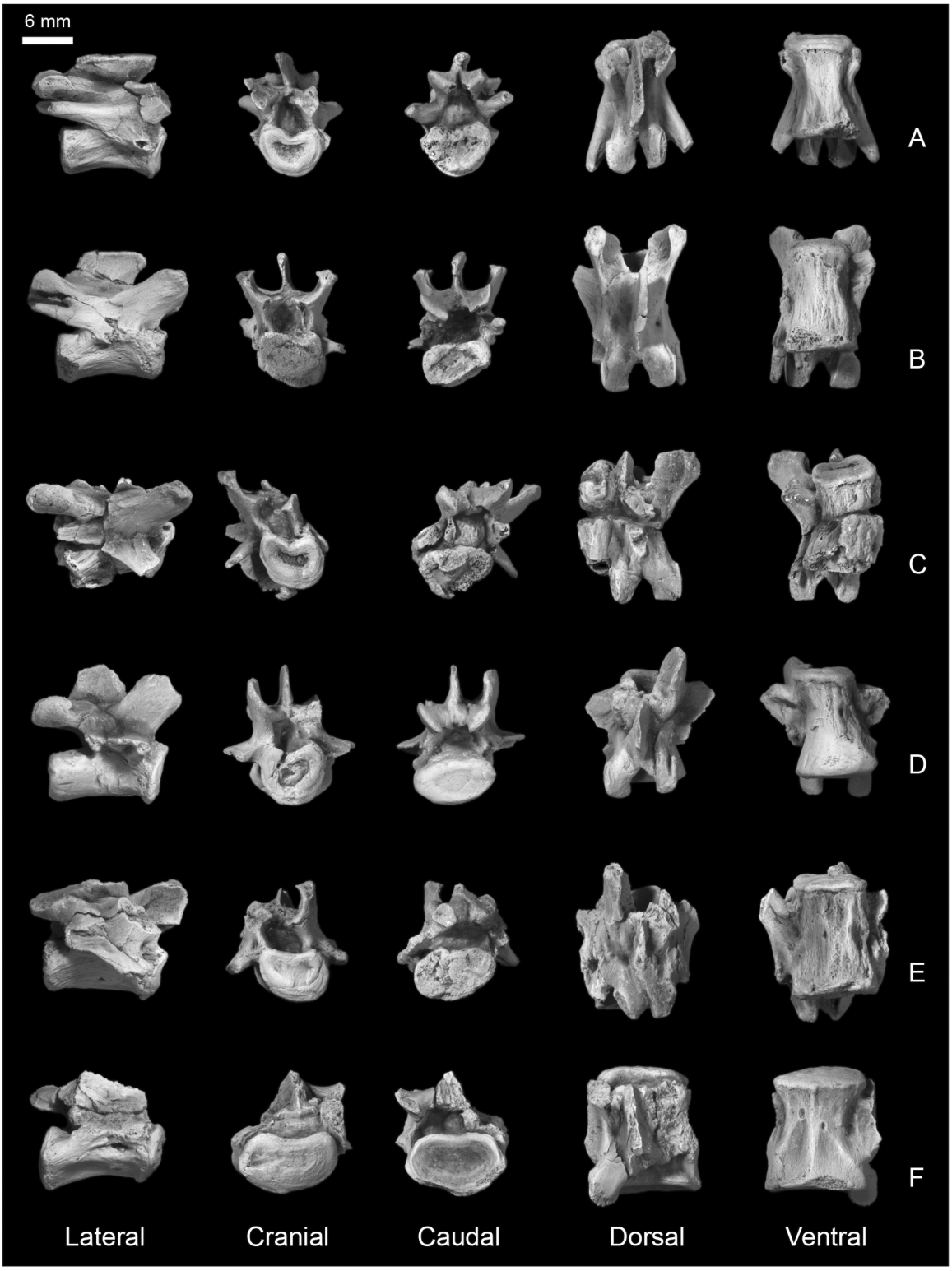

FIGURE 31.— Lumbar vertebrae of *Plesiadapis cookei* (UM 87990). **A**, lumbar L1? **B**, lumbar L3? **C**, lumbar L4? **D**, lumbar L5? **E**, lumbar L6? **F**, lumbar L7? All are shown in lateral, cranial, caudal, dorsal, and ventral view.

rely on a bounding gait increase the length of the lumbus relative to the thorax (Sargis, 2001; Shapiro and Simons, 2002). The lumbar region of *P. cookei* is estimated to have been 81% the length of the thoracic region. This contrasts with agile scansorial treeshrews in which the lumbar region is 94% the length of the thoracic region (Table A-II-2).

P. cookei is similar in its lumbar vertebral morphology to smaller plesiadapids, though these smaller taxa have proportionally larger vertebral foramina and narrower spinous processes. The lumbar spinous process proportions of *N. intermedius* suggest that it utilized an agile bounding gait like tree squirrels and tupaiid treeshrews (Boyer and Bloch, 2008). In contrast, those of *P. cookei* are similar to ptilocercid treeshrews and cynocephalid dermopterans in being more craniocaudally expanded (Sargis, 2001). *Cynocephalus* differs from all of the taxa mentioned in having caudally projecting lumbar spinous processes (Boyer and Bloch, 2008).

Sacrum

The sacrum of UM 87990 is crushed and missing one of its prezygapophyses as well as the tips of its spinous processes (Fig. 32; Tables A-II-6 and A-II-7). It includes three vertebrae, denoted as S1–S3.

Sacral S1–S3.— The auricular processes for articulation with the innominates span the lateral surfaces of the first two vertebrae. The pleurapophyses or costal processes of the third vertebra are fused to those of the second. Individual pleurapophyses are separated by spinal nerve foramina. Each vertebra has a separate spinous process. Although the spinous processes are broken, enough remains to say that the first process was superiorly (cranially) oriented and was the largest of the three. The second spinous process was probably the smallest, although it also appears to be the most fragmentary. The third process is slightly smaller than the first and is oriented vertically. The laminae of the three vertebrae are separated by 'interzygapophyseal intervertebral gaps' that communicate with the vertebral canal. The form of the prezygapophysis preserved on the first sacral vertebra is similar to those of the later (more inferior) lumbar vertebrae. The postzygapophysis of the third sacral vertebra is similar to, although smaller than, those of the inferior lumbar vertebrae. It is also similar to that of the most proximal of the preserved caudal vertebrae (see below).

Comparisons.— The orientation and large size of the spinous process of the first sacral vertebra is similar to that of the inferior lumbar vertebrae. This similarity suggests that the sacrum was integrated into the relatively rigid segment formed superiorly (cranially) by the inferior lumbar vertebrae. In highly agile taxa such as treeshrews, *Sciurus*, and richochetal rodents (Gambaryan, 1974), the spinous process of the first sacral vertebra is often reduced. This morphology is associated with a relatively large range of flexibility at the lumbosacral joint, important for agile locomotor behaviors. The presence of a large first sacral spinous process thus may indicate less flexibility and less agile locomotion.

However, there is some evidence that the reduction of this

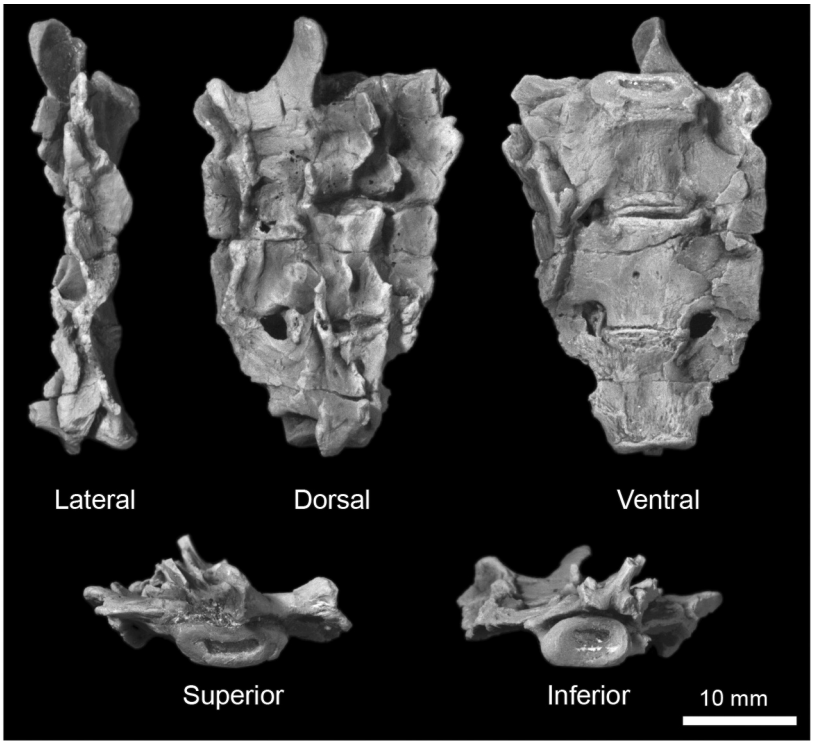

FIGURE 32.— Sacrum of *Plesiadapis cookei* (UM 87990). This element includes three co-ossified vertebral centra, S1–S3. Sacrum is shown in lateral, dorsal, ventral, superior, and inferior view.

process only correlates with agility in taxa that mainly use pronograde postures: a brief survey of primate taxa that frequently use orthograde postures reveals them to have a large, cranially-oriented first sacral spinous process, even including those that also exhibit agile (e.g., *Callithrix*) or acrobatic (e.g., *Galago*) locomotor behaviors. Given independent evidence suggesting a somewhat agile locomotor repertoire in *P. cookei* (e.g., position of the anticlinal vertebra), the sacral spinous process size and orientation may be an indicator of substantial reliance on orthograde postures. On the other hand, *P. cookei's* lumbar region does not suggest agility as great as that in *Eulemur, Tupaia, Sciurus, Callithrix* or *Galago*, and thus the sacrum spinous process features may also be reflective of reduced mobility.

The sacra of *N. intermedius* and *N. gidleyi* are virtually identical to that of *P. cookei* in the morphological features mentioned above. The paromomyid plesiadapiform *Ignacius clarkforkensis* differs in having a reduced first spinous process (Boyer and Bloch, 2008). All treeshrews exhibit a condition like *Ignacius* (Sargis, 2001). *Cynocephalus* exhibits the plesiadapid condition (a large first sacral spinus process).

Caudal vertebrae

There are 17 caudal (Ca) vertebrae attributed to UM 87990 (Fig. 33; Table A-II-8).

Second or third caudal vertebra (Ca1, 2, or 3).— The bone interpreted as the first, second, or third caudal vertebra (Fig. 33A) has a complete vertebral canal, pre- and postzygapophyses, cranially projecting transverse processes, and the broken base of a spinous process. The centrum is missing but it would have been relatively short craniocaudally and wide mediolaterally. The short centrum and caudally projecting transverse processes are indicative of a position at the base of the tail.

Fourth or fifth caudal vertebra (Ca4? or Ca5?).— The bone interpreted as the fourth caudal vertebra (Fig. 33B) has a relatively short but thick centrum with a small but complete neural canal. It is substantially longer than the preceding vertebra, but less elongated than the next of the preserved vertebrae.

Sixth caudal vertebra (Ca6?).— The vertebra interpreted as the sixth caudal (Fig. 33C) is much longer than the preceding two. It has a naturally incomplete vertebral canal (the laminae do not meet in the sagittal plane). The pre- and postzygapophyses did not articulate directly with those of more proximal and distal vertebrae. There is a set of cranioventrally projecting transverse processes and a set of caudoventrally projecting processes.

Seventh caudal vertebra (Ca7?).— The vertebra interpreted as the seventh caudal (Fig. 33D) is very similar to Ca6?. It differs in being absolutely longer, proportionally narrower, and in having absolutely and proportionally smaller transverse processes.

Eighth through twelfth caudal vertebrae (Ca8?–Ca12?).— The vertebrae interpreted as the eighth, ninth, tenth, eleventh, and twelvth caudal vertebrae (Fig. 33E–I) are identified on the basis of increasing length and/or decreasing prominence of zygapophyses and transverse processes. The centrum diameters of these vertebrae do not appear to vary greatly or systematically through the region. Ca11? and Ca12? (Fig. 33H, I) are very similar to one another and it is possible that their identifications have been reversed. If not, Ca12 is the longest preserved caudal vertebra.

Thirteenth through twentieth caudal vertebrae (Ca13–Ca20?).— The vertebrae interpreted as the thirteenth through twentieth caudal vertebrae (Fig. 33J–Q) are elongated rods of bone identified on the basis of the assumption that centrum length, width, and height decreased from more proximal to more distal positions in this region of the tail (Table A-II-8).

Comparisons.— The caudal vertebrae of *P. cookei* show that it had a relatively long tail (Fig. 33; Table A-II-8). A proportionally long tail is a feature of arboreal specialists. Stafford (1999) showed that *Ptilocercus lowii* has a significantly longer tail proportionally than more scansorial-to-terrestrial scandentians. He also documented that *Ratufa*, the arboreally committed tree squirrel, has a longer tail than more versatile sciurid rodents. Boyer and Bloch (2008) showed a sample of quadrupedal arboreal primates to have relatively longer tails than some rodents and tupaiids.

Looking at the first ten caudal vertebrae, the tail of *P. cookei* is proportionally longer (standardized against trunk length) than that of *Tupaia* and *Sciurus*, and similar to those of many euprimates (Table A-II-2). It is also similar in proportional length to that of *Cynocephalus*; however, considering the whole tail (instead of just the first ten vertebrae) reveals *Cynocephalus* to actually have a short tail (Stafford, 1999; Boyer and Bloch, 2008). This is due to an abrupt and drastic serial decrease in vertebral length distal to Ca10 in *Cynocephalus* and a reduced number of caudal vertebrae (Table A-II-2). The tail of *P. cookei* has a more typical gradual decrease in vertebral length through the tail, and at least three more vertebrae than the tail of *Cynocephalus*. *N. intermedius* preserves Ca6 and Ca7, which appear virtually identical to those of *P. cookei*. *N. gidleyi* preserves two of the first three caudal vertebrae, which also appear similar to the one preserved in *P. cookei*.

Sternebrae and ribs

The mammalian thoracic cavity is an expandable protective enclosure shielded by bone that primarily houses the lungs and heart. Contraction of the diaphragm and external intercostal muscles expands the cavity, drawing air into the lungs when breathing. Relaxation of the diaphragm as well as contraction of the internal intercostal muscles and abdominal core helps expel this air. The 'backbone' of the thorax is the dorsal midline vertebral column itself. A cage-like enclosure is formed by the ribs, generally 13 on each side in mammals (in humans there are 12), extending laterally and ventrally from the dorsal midline. Pairs of left and right ribs are connected to a corresponding thoracic vertebra by synovial joints that move continuously as the rib cage expands and contracts. This movement is facilitated (and the rib cage is completed ventrally) by stiff but flexible cartilages that link the distal ends of cranial ribs to a ventral sternum composed of ossified 'rib spacers' or sternebrae. Ribs and sternebrae ossify during

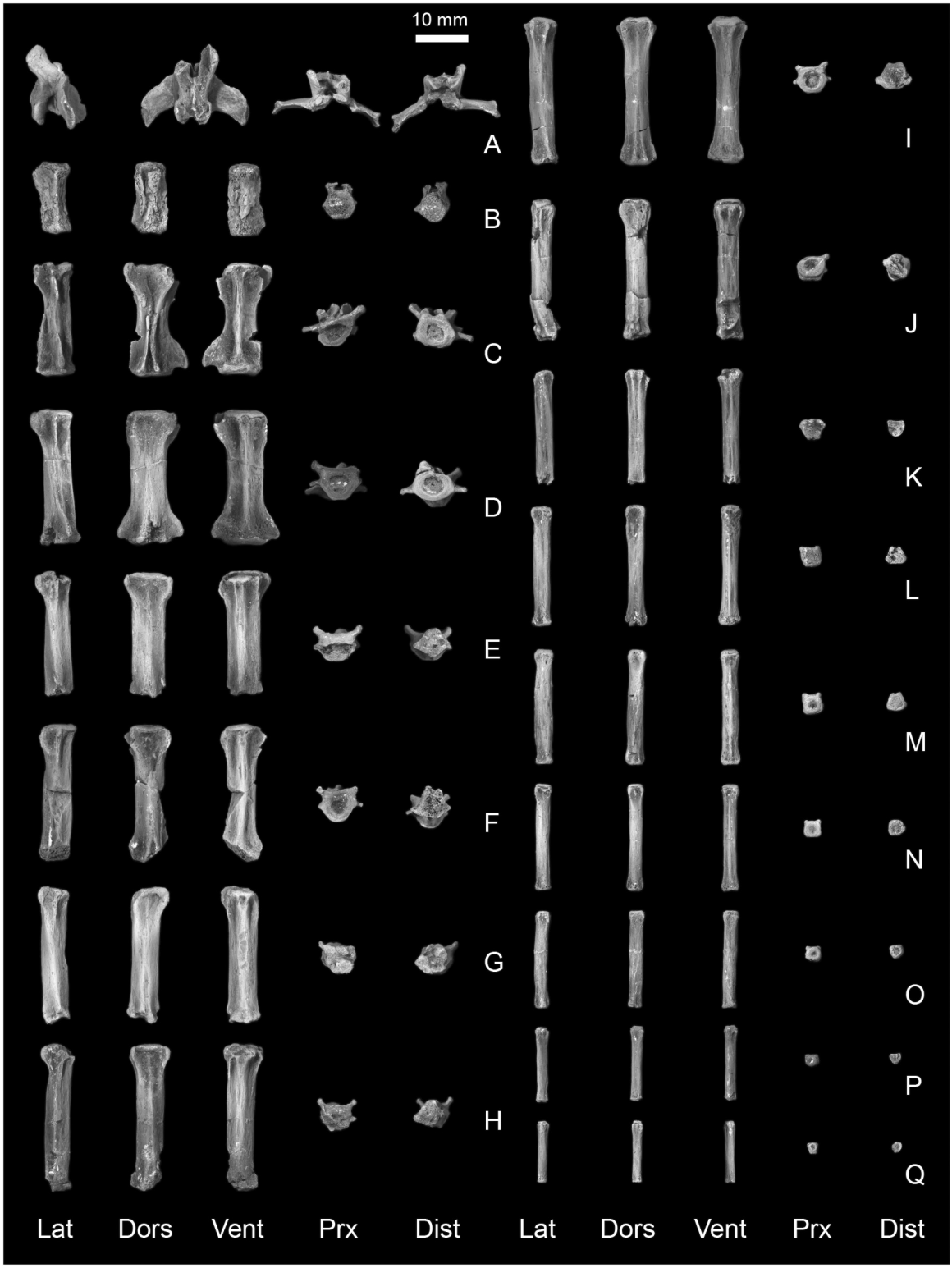

FIGURE 33.— Caudal vertebrae of *Plesiadapis cookei* (UM 87990). **A**, caudal Ca1, 2 or 3. **B**, caudal Ca4? **C**, caudal Ca6? **D**, caudal Ca7? **E**, caudal Ca8? **F**, caudal Ca9? **G**, caudal Ca10? **H**, caudal Ca11? **I**, caudal Ca12? **J**, caudal Ca13? **K**, caudal Ca14? **L**, caudal Ca15? **M**, caudal Ca16? **N**, caudal Ca17? **O**, caudal Ca18? **P**, caudal Ca19? **Q**, caudal Ca20? All elements are shown in lateral, dorsal, ventral, proximal, and distal view.

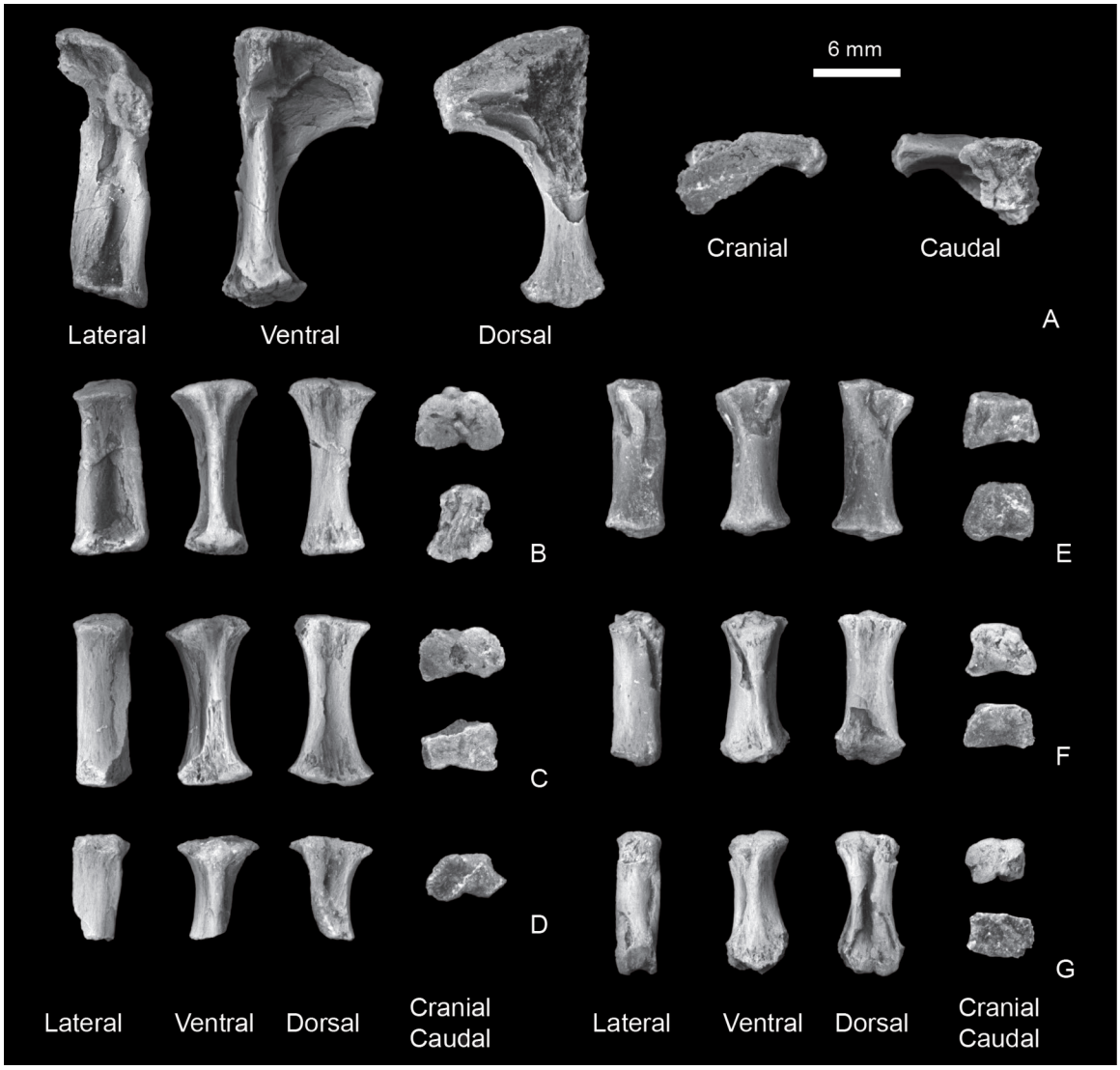

FIGURE 34.— Sternebrae of *Plesiadapis cookei* (UM 87990). **A**, manubrium or first sternebra. **B**, sternebra St2? **C**, sternebra St3? **D**, sternebra St4? **E**, sternebra St5? **F**, sternebra St6? **G**, sternebra St7? The last of these, St7?, appears to be the ultimate sternebra because its inferior end does not look like the superior or inferior surfaces of other sternebrae. It compares well to the ultimate sternebra of articulated museum specimens of primates, treeshrews, and squirrels. Elements in A–C and E–G are shown in lateral, ventral, dorsal, cranial, and caudal view. Element in D is shown in lateral, ventral, dorsal, and cranial view.

development and hence are commonly found when skeletons are preserved.

Sternebrae

Seven sternebrae are preserved with UM 87990. These are illustrated in Figure 34 and numbered St1 through St7. Measurements are listed in Table A-II-9. Sternebrae are ventral midline bones, and all are more or less bilaterally symmetrical, although there is often some variation and some departure from symmetry.

Manubrium sterni or sternebra St1.— The manubrium sterni or first sternebral element of UM 87990 is distinct in form and easily recognized because it is the largest sternebra and it flares widely into a 'T' at its cranial end (Fig. 34A). The specimen at hand has the left side of this 'T' intact but much of the right costal process is broken away. The cranial surface of the left costal process has a slight depression for articulation with the left clavicle. Lateral to this the left costal process is roughened where the first costal cartilage connected the manubrium and the left first rib (the same would be true for the right side if this were preserved). The caudal surface of St1 is roughened where St1 connected to St2 and to costal cartilages of the left and right second ribs.

The cranial margin of the manubrium is convex. The

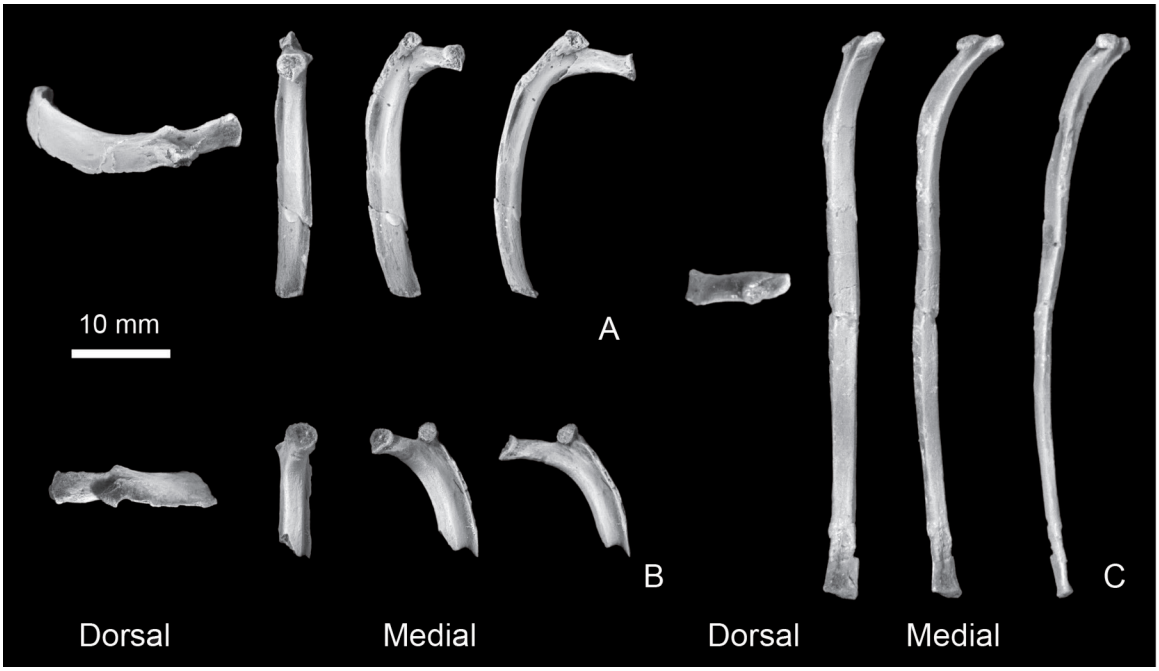

FIGURE 35.— Ribs of *Plesiadapis cookei* (UM 87990). **A**, most cranial of the left ribs recovered. **B**, most cranial of the right ribs recovered. **C**, one of the most caudal ribs of the left side. All are shown, from left to right, in dorsal, medial, cranial, and caudal view. Note that the ribs are gracile with no indication of craniocaudal expansion or imbrication.

dorsal surface is flat. The ventral surface is marked by a strong midline keel. The keel is narrowest at its root. Thus, a transverse cross-section through the manubrium reveals it to be shaped like an 'I-beam.' The articular surface between the manubrium and the next sternebra is somewhat oblique. Thus, when articulated, the manubrium and next sternebra formed an obtuse angle projecting ventrally.

Sternebrae St2?–St7?.— The remaining sternebrae of UM 87990 (Fig. 34B–G) are all similar to each other in size and form. Each is elongated and blocky with smooth dorsal, ventral, and lateral surfaces, and roughened cranial and caudal ends where each articulated with the next sternebra and with costal cartilages. Cranial sternebrae have a ventral keel, but this is muted on more caudal sternebrae. The last sternebra differs from the others in having a caudal end that is rounded instead of flat, with a longitudinal groove on its dorsal surface. We interpret this as the xiphoid process of the terminal sternebra.

Comparisons.— The manubrium sterni of *P. cookei* appears more similar to that of *Tupaia glis* than to those of many euprimates in having a stronger keel and in forming a strong angle with the next sternebra.

Ribs

Twelve ribs and rib fragments are attributed to UM 87990 (Fig. 35; Table A-II-10). Six appear to be left ribs and six appear to be right ribs. Cranial ribs have the rib head and rib tuberculum distinctly separated for articulation with correspondingly separated rib articulatins on anterior thoracic vertebrae. All of the ribs are slender and most exhibit a crest along their caudal borders. This crest is most expansive near the rib angles and becomes less pronounced more ventrally. On the medial surface of these crests is a groove for the intercostal neurovasculature. One or two of the more caudal floating ribs (T10–13) are preserved. They have a simple rib head with no tuberculum, and have a shorter and straighter rib body.

Comparisons.— The ribs of *P. cookei* compare best to those of tupaiid treeshrews and other plesiadapiforms (Boyer and Bloch, 2008) among euarchontan mammals. Ptilocercid treeshrews, dermopterans, and many euprimates have ribs that are much more craniocaudally expanded (Sargis, 2001; Granatosky et al., 2014) than those of *P. cookei*. *N. gidleyi* preserves rib fragments showing it to be similar to *P. cookei* in this regard (Table A-II-10).

Pectoral girdle and forelimb

Clavicle

The right and part of the left clavicle are preserved (Fig. 36A; Table A-II-11). No clavicle has been previously described for a plesiadapid. However, a skull and partial skeleton of *N. gidleyi* (AMNH 17388) preserves parts of right and left clavicles (Appendix V), and thus allows confirmation that the clavicles described here do in fact belong to *P. cookei* (and not *Uintacyon*). The clavicle of UM 87990 has a strong inferior (caudal) convexity to its shaft when viewed ventrally or dorsally. The medial end is relatively straight, with a

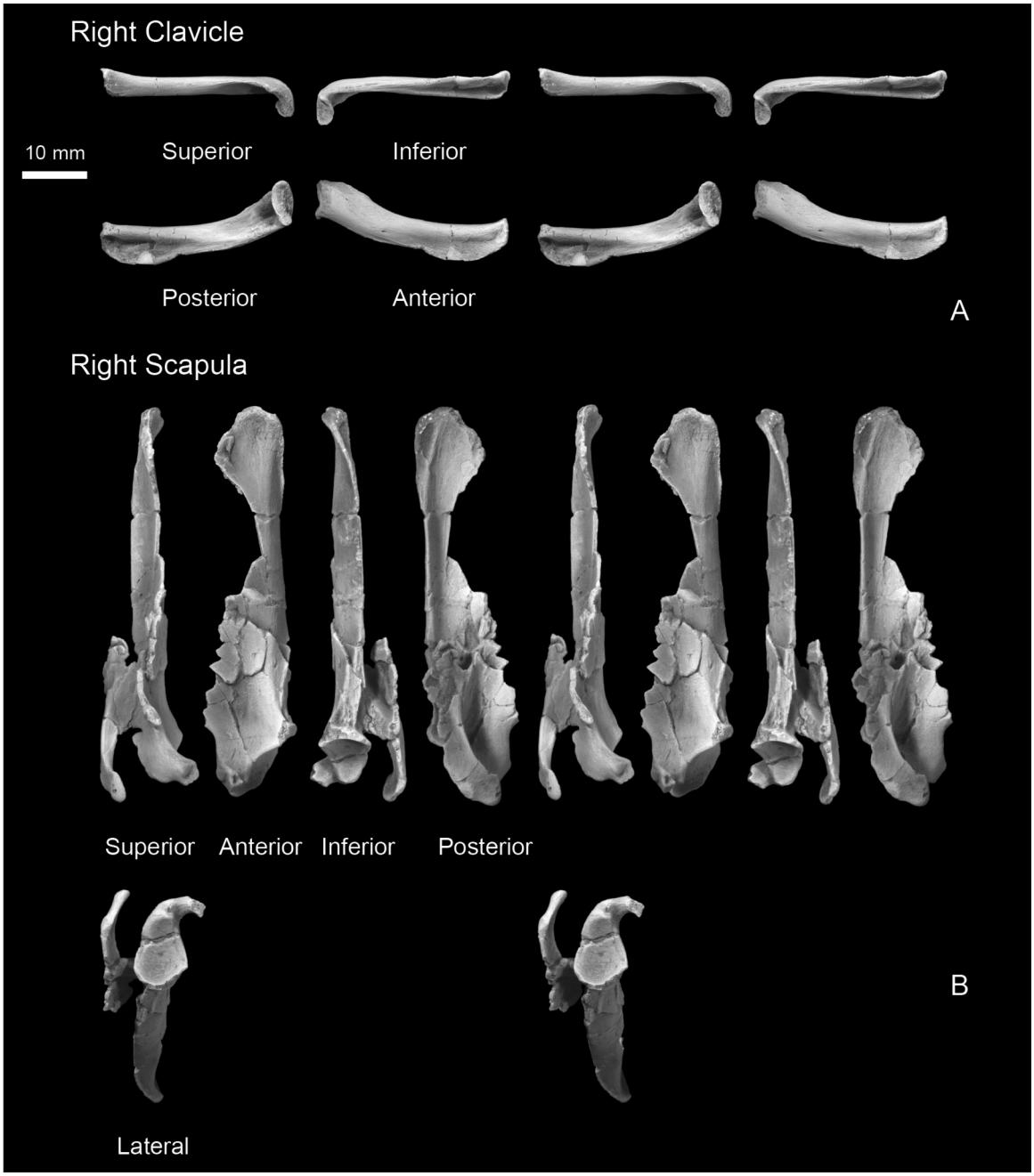

FIGURE 36.— Clavicle and scapula of *Plesiadapis cookei* (UM 87990). **A**, stereophotographic images of right clavicle, shown in superior, inferior, posterior, and anterior views. **B**, right scapula, shown in superior, anterior, inferior, posterior, and lateral views. The left clavicle is represented by the middle third of its shaft, but this is not illustrated.

roughened articular surface for the sternum. This articular surface is triangular in shape, possibly because it is poorly preserved. The lateral end of the clavicle is distinctly curved, and the articular facet for the acromion process of the scapula is narrowly elliptical (6.8 mm by 3.5 mm). The shaft of the clavicle is expanded superoinferiorly (craniocaudally) and is quite unusual in this respect.

The clavicle measures 4.9 mm in superoinferior depth and 2.9 mm in dorsoventral thickness at midshaft. The medial third of the inferior surface of the bone is marked by a prominent crest. The bone is marked by substantial depressions superior to the crest on both ventral and dorsal surfaces. On the dorsal surface, this depression continues as a groove to the medial edge of the lateral third of the bone. The lateral part

of the clavicle lacks such prominent crests. Bone surrounding the acromial articular surface is raised and roughened. This roughened area extends medially for about a quarter of the clavicle's length on the superior surface, and extends medially for about half the clavicle's length on the inferior surface.

The great superoinferior depth of the clavicle of *P. cookei* suggests ample room for attachment of muscles and ligaments of the pectoral girdle. Specifically, the inferior flange on the medial side probably served to increase the insertion area of the clavicular head of pectoralis major on its anterior surface. On the dorsal surface, the most lateral part of the groove above the inferior flange probably served as the attachment site of the subclavius muscle. The roughened areas on the lateral aspect of the bone undoubtedly refect the attachment points of the trapezius muscle (superiorly) and the deltoid muscle (inferiorly).

Comparisons.— Comparing the clavicle of *P. cookei* to that preserved for *N. gidleyi* in AMNH 17388 reveals general similarity, even with regard to the unusual cross-sectional proportions (Table A-II-11; Appendix V). This is different from, for instance, humans and treeshrews, which have clavicles with rod-like shafts. If the unusual morphology of the clavicle reflects some basic aspect of locomotion, posture, or feeding in *P. cookei*, then these behaviors were most likely shared by *N. gidleyi*.

Scapula

The right scapula of *P. cookei* is the most complete scapula known for a plesiadapid (Fig. 36B; Table A-II-12). All that is missing is the inferior margin of the spine (possibly including a metacromion process), most of the coracoid process, the part of the scapular blade that held the supraspinous fossa, and part of the infrapinous fossa. The glenoid is shallowly concave and mediolaterally narrower than it is superoinferiorly long. The glenoid faces somewhat laterally relative to the blade. The coracoid process projects anteriorly. It is marked by two tuberosities, one on its superior surface and the other laterally, just superior to the glenoid fossa. The acromion is mediolaterally narrow and superoinferiorly elongate. It projects nearly parallel to the scapular spine, and extends laterally beyond the glenoid fossa. It reaches superiorly to the level of the coracoid process. The superolateral tip of the acromion is slightly swollen and smooth, representing the articular surface for the clavicle. Medial and inferior to the clavicular articular surface, the bone becomes raised and rugose. If there had been a metacromion process, it would normally have extended inferiorly, inferomedial to this rugosity; however the bone is broken here.

The inferior margin of the scapular blade is oriented at an obtuse angle of ~125° with respect to the glenoid fossa. The inferior margin of the blade, just medial to the glenoid, is fractured and its morphology is somewhat obscured. However, a distinct pit is visible on the anteroinferior surface that probably represents what is often referred to as an 'infraglenoid' tuberosity (the attachment point of the long head of the triceps brachii muscle). About three-quarters of the distance from the glenoid fossa to the inferior angle of the scapula, the inferior border curves anteriorly and an inferodorsally-facing surface is developed above the inferior margin. The superior edge of this inferodorsally facing surface meets the inferior margin of the infraspinous fossa. This surface extends down to the inferior angle, and appears to represent the attachment site of the teres major muscle (George, 1977). The inferior angle itself is blunt and dorsoventrally thick. More superiorly, what remains of the scapular blade (the part representing the fragmentary infraspinus fossa) is deeply concave dorsally.

Comparisons.— Comparison of the scapula of *P. cookei* to that of other plesidapids does not reveal much, due to the fragmentary nature of the other specimens. The acromion process of *N. intermedius*, USNM 442229, differs from that of *P. cookei* in that the acromion projects superiorly and is therefore oriented almost perpendicular to the scapular spine, instead of parallel to it, as in *P. cookei*. As a result, the acromion also differs in not extending laterally (or distally) beyond the glenoid in *N. intermedius*. Because of the configuration of its acromion, it seems that the shoulder of *N. intermedius* should be more mobile in abduction than that of *P. cookei*.

Interestingly, comparison of the scapulae of these plesiadapids to that of *Tupaia glis* reveals that *P. cookei* and *T. glis* are more similar to each other than either is to *N. intermedius*. This includes aspects of the acromion as well as the blade.

Humerus

The right and left humeri of *P. cookei* are preserved (Fig. 37; Tables A-II-13 and A-II-14). The left side is in much better condition. Both have had segments of their shafts reconstructed with paste epoxy. The left humerus also has some epoxy in a broken part of the medial keel of its trochlea. The proximal epiphyses remain unfused on both humeri.

The greater and lesser tuberosities are well developed. The greater tuberosity is positioned more proximally than the lesser tuberosity, but neither extends above the top of a globular humeral head. The greater tuberosity has a distinct depression on its proximal surface (probably for the supraspinatus muscle) and another depression on its posterolateral surface (probably for the infraspinatus muscle). The greater tuberosity is continuous with the deltopectoral crest. The deltopectoral crest projects anterolaterally from the humeral shaft and reaches its apex at ~40% of the shaft length.

The lesser tuberosity projects medially. Distally, the lesser tuberosity is continuous with the medial border of the humeral shaft, which swells into the teres major tubercle. This tubercle is large and covers the middle portion of the shaft.

The supinator crest begins to flare laterally and posteriorly at the proximal edge of the distal third of the shaft. It ends at the distal end of the humerus, on the lateral epicondyle. The distal end of the humerus can be separated into medial and lateral epicondyles, articular surfaces for the radius (capitulum) and ulna (trochlea), and the fossae bounding these articular surfaces both anteriorly and posteriorly. The lateral epicondyle does not extend appreciably lateral to the capitulum, and it is marked by a shallow depression for a radial collateral ligament. The medial epicondyle (entepicondyle), on the other hand, projects medially to a substantial degree and its medial surface, which probably formed an attachment point for digital flexors, is oriented mediodistally. A

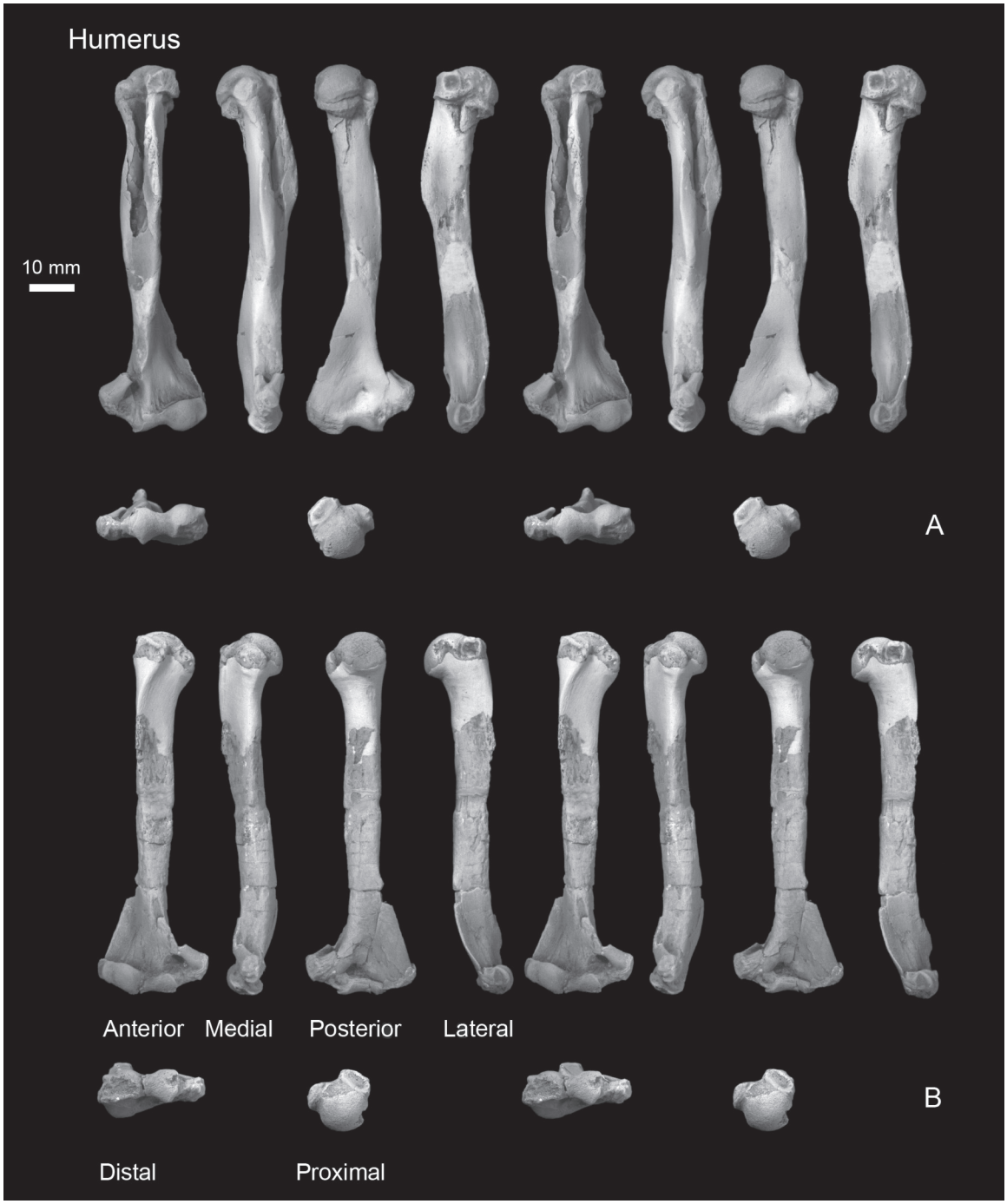

FIGURE 37.— Humerus of *Plesiadapis cookei* (UM 87990). Stereophotographs. **A**, left humerus. **B**, right humerus. Both are shown in anterior, medial, posterior, lateral, distal, and proximal views. Note that a segment of the left shaft is reconstructed just proximal to the supinator crest. Enough of the shaft remains to be certain that the original length has not been changed and that the proximal segment is correctly oriented with respect to the anteroposterior anatomical plane of the distal segment. The proximal quarter of the right humerus shaft is missing. It is not clear how much evidence supports the details of its reconstruction.

strut between the medial epicondyle and the shaft (more proximally) encloses a large, elliptical entepicondylar foramen. The capitulum is separated from the trochlea by a deep constriction of the articular surface, often referred to as the 'zona conoidea.' The capitulum appears 'sub-spherical' as a result of (1) constriction of the zona conoidea and (2) having a radius of curvature that first decreases and then increases lateral to the zona conoidea. The lateral edge of the capitulum is marked by a groove running proximodistally, but the articular surface extends laterally beyond this groove: this articular region, lateral to the capitulum is referred to as the lateral flange (e.g., Beard, 1989). The surface of the capitulum faces proximally, anteriorly, and distally but does not continue onto the posterior surface of the bone.

The anterior surface of the humerus, just proximal to the capitulum, is excavated to form a substantial supracapitular fossa. The humeral trochlea is mediolaterally narrower than the capitulum. Its radius of curvature increases medially from the zona conoidea to its medial margin, or 'keel' (Szalay and Dagosto, 1980; Beard, 1989). The posterior and anterior aspects of the trochlea are roughly equal in the degree to which they are developed. Superior to the trochlea on the posterior side of the humerus is a noticeable, but fairly shallow olecranon fossa. Medial to the trochlea on the posterior surface of the medial epicondyle is a dorsoepitrochlear fossa, for attachment of the ulnar collateral ligament. The rotational axis for the ulna and radius on the distal articular surfaces, as well as the mediolateral axis of the entire distal end of the humerus, is rotated lateral to the proximal end by ~32º. Thus, the medial epicondyle actually projects somewhat anteriorly, and the 'anterior' surface of the distal humerus faces somewhat laterally.

Comparisons.— Comparing the humerus of *P. cookei* to other plesiadapids shows it to differ from smaller forms including *Pr. gaoi, N. intermedius*, and *N. gidleyi* in having much greater lateral deviation of its distal end (Table A-II-13: LD); whereas *P. tricuspidens, P. remensis*, and *Pl. daubrei* appear to have the distal end of the humerus oriented like that of *P. cookei*. Although all known plesiadapids have a prominent medial keel on the ulnar trochlea of the humerus, *P. cookei* differs from *Pr. gaoi, P. rex, P. tricuspidens* and *Pl. daubrei* in lacking a lateral keel on its trochlea. This feature is present in many euprimates, but is also found in the primitive arboreal treeshrew *Ptilocercus lowii* (Sargis, 2002a). In taxa possessing a lateral keel, the trochlea is more easily distinguished from the zona conoidea lateral to it. The specimens of *Nannodectes* are like *P. cookei* in lacking the lateral keel. *P. cookei* differs from *P. rex*, but is similar to other plesiadapids for which the distal humerus is known in having a dorsoepitrochlear fossa. Finally, *P. cookei* appears to differ from at least *P. tricuspidens* in having a more gracile humerus (Table A-II-13: note higher SSV). Furthermore, although the left humerus of *P. cookei* is absolutely longer than any complete elements known for *P. tricuspidens*, almost all of the fragmentary humeri of *P. tricuspidens* have greater midshaft diameters than those of *P. cookei*, further implying that the humerus is a more gracile bone in UM 87990 than in any known individual of *P. tricuspidens*.

Radius

The left radius and the distal epiphysis of the right radius are preserved (Fig. 38A; Tables A-II-15 and A-II-16). These two elements have been glued to one another with paste epoxy as if they originally belonged to the same bone. To correct this, a medical CT image was manipulated to estimate the morphology of the actual element. The diaphysis was separated in the surface reconstruction, inverted, and repositioned on the epiphysis (Fig. 39). In the following description, the terms 'ulnar' and 'radial' are used in place of lateral and medial (see Anatomical Terminology). The 'ulnar side' of the radius is that which contacts the ulna at the distal radioulnar joint, and to which the interosseous membrane attaches. The radial side is the opposite side (i.e., the side that the pollex is on; also equivalent to the pre-axial side).

Overall, the radius is a slender element with a slight dorsoulnar convexity to its shaft. The radioulnar axis of the distal end exhibits ~40° of torsion relative to the proximal end (radial head). That is, when the proximal end of the radius is articulated with the humerus in a fully pronated position, the manus would have been supinated by ~40° (full supination is equal to 180°; see below). Furthermore, the manipulated CT image reveals that the distal articular surface faced ventrally and ulnarly.

The central fossa of the radial head for articulation with the humeral capitulum is spherically concave. However, the proximal end of the radius (radial head) appears oval, or even slightly rectangular in proximal view. The radial head is mediolaterally wider than it is dorsoventrally deep (Table A-II-15:BSV). This is due to the fact that the spherical depression of the central fossa is flanked radially by a broad 'lateral lip.' At this point, it is convenient to note that the terminology of Beard (1989) is followed in this section, because it allows for more detailed descriptions of morphology. In fully or semipronated positions the 'lateral lip' of the radial head articulates with the zona conoidea, which is on the medial side of the capitulum. In terms of radioulnar directions, the 'lateral lip' is on the radial side of the radial head. Opposite the lateral lip, on the ulnar side of the bone, the radial head is rimmed by a proximally projecting crescentic ridge that would have articulated with the lateral flange of the capitulum during pronated forearm postures. Beard (1989) referred to this as the 'medial crescent.'

The ventral and ulnar aspects of the radial head exhibit an articular surface for the ulna, referred to as the 'rim of the radial head.' Distal to the rim of the radial head, the circumference of the bone decreases to form the radial neck. Then the cross-section increases abruptly at the tuberosity for biceps brachii on the ventral surface. Farther distally, the shaft cross-section becomes more elliptical with the major axis oriented almost dorsoventrally. The dorsal margin of this elliptical shaft is continuous with the radial side of the bone, whereas the ventral side corresponds to the ulnar side. The peak of the dorsal arch of the shaft is marked by a tuberosity for the pronator teres muscle. This point is located at about two-thirds the length of the shaft from the proximal end. Starting from the ulnar side of the proximal end, a crest crosses the dorsal

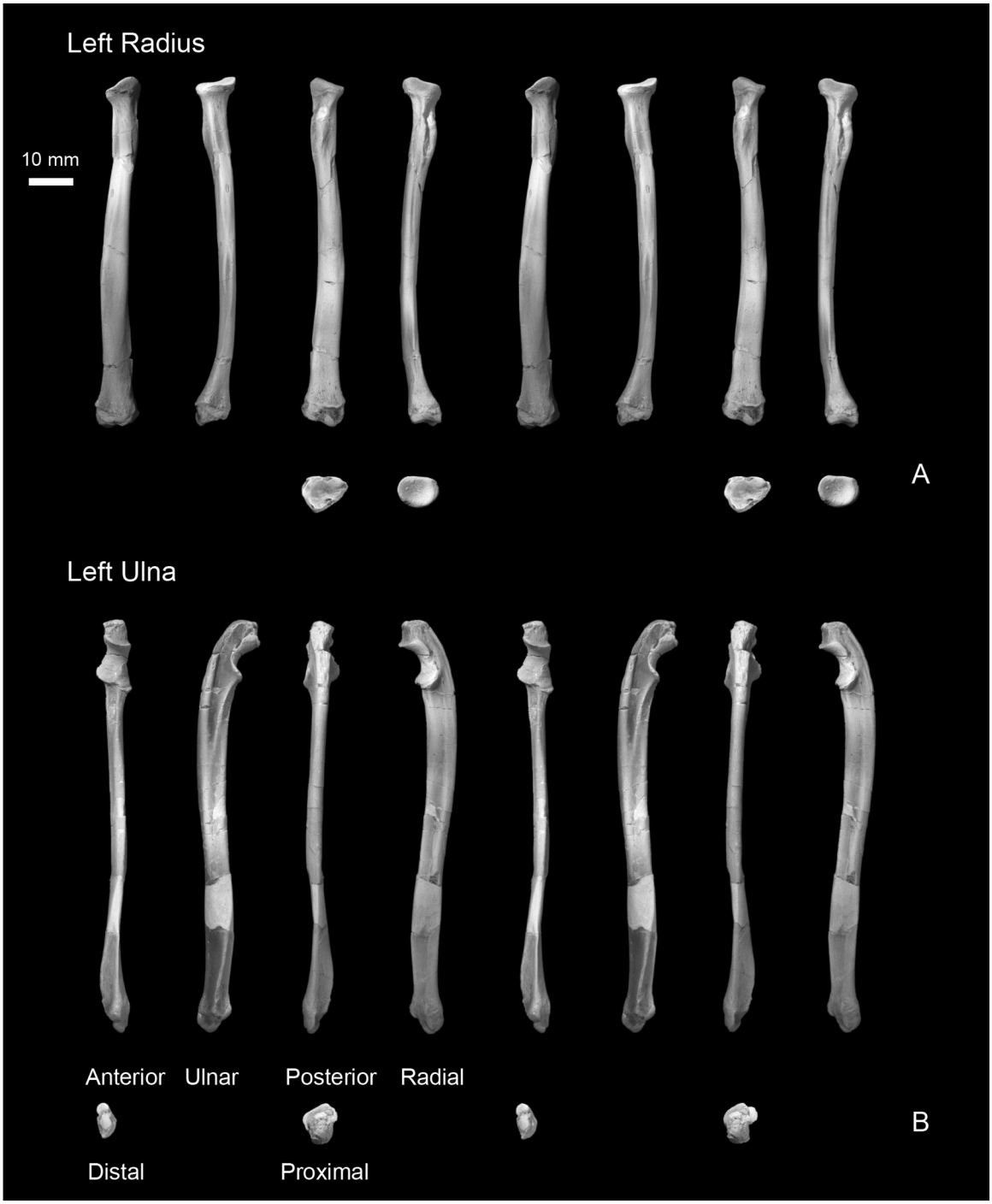

FIGURE 38.— Radius and ulna of *Plesiadapis cookei* (UM 87990). **A**, stereophotographs of left radius. **B**, stereophotographs of left ulna. Both are shown in anterior, ulnar, posterior, radial, distal, and proximal views. Note that the distal epiphysis of the right radius has been attached to the diaphysis of the left radius. Thus this element does not correctly represent the true morphology of the radius of *P. cookei* (see Fig. 39). A distal segment of the ulnar shaft is missing and reconstructed. It is not clear how much evidence supports the details of its reconstruction.

margin of the shaft to meet the pronator teres tuberosity. This crest probably delimits the radial edge of the compartment for the digital extensor musculature. The ulnar margin of the shaft of the radius develops a distinct crest for the interosseous membrane toward its distal end. The shaft swells abruptly to accommodate the distal articular surface.

The dorsoradial margin of the distal epiphysis is marked by three tuberosities that formed the bony boundaries of the three extensor tendon compartments that cross the proximal carpal joint. From radial to ulnar these tuberosities correspond to the styloid process, Lister's tubercle, and a frequently present but unnamed tubercle (Stern, 1988; Fig. 39). The first extensor compartment would have been located radial and ventral to the styloid process. The distal articular surface itself is triangular in distal view (Fig. 39). The radial margin forms a vertex of the triangle, and the ulnar surface is the opposing base of the triangle. The distal articular surface is marked by a faint dorsoventral ridge reflecting the respective positions of the scaphoid and lunate on either side of it. Ulnar to the lunate area, the articular surface extends onto the radial shaft for contact with the ulna.

Comparisons.— The radius of *P. cookei* is similar to that of other plesiadapids (Tables A-II-15 and A-II-16). The radial head is essentially the same shape as it is in the other taxa for which it is known (Table A-II-15). The distal end is also similar among all taxa for which it sufficiently known, although it is too fragmentary in both *Nannodectes* specimens to be confident in this assessment. The distal end appears to be physiologically supinated (i.e., to exhibit torsion) relative to the proximal end to a similar degree in *N. intermedius* and *P. tricuspidens*. The pronator teres tuberosity is equally noticeable in *N. intermedius*, the only other specimen for which it is preserved. Two points of interesting variation include the following: (1) *P. cookei* has a more gracile radial shaft than do *P. tricuspidens* and *N. intermedius* (Table A-II-15: inverse of SSV); and (2) *N. intermedius* has a larger radial head for its shaft length (Table A-II-15: inverse of RSV) as compared to either *P. cookei* or *P. tricuspidens*, possibly suggesting proportionally shorter limbs for *N. intermedius*.

Ulna

A nearly complete left ulna and a proximal fragment of the right are preserved (Fig. 38B; Tables A-II-17 and A-II-18). Unfortunately, a segment of the shaft of the left side is missing, and the exact length is unknowable, although it can be estimated using the left radius. This was done during preparation of the skeleton and the missing segment of the ulna has been reconstructed with paste epoxy (Fig. 38B). Neither side preserves enough of the olecranon process to estimate its total length. Thus the total length given in Table A-II-17 is likely an underestimate.

Overall, the ulna is slender and rod-like. The proximal end has a pronounced posterior (or dorsal) convexity to it. This shape is accentuated by the slight anterior cant of the olecranon process. The distal end bends posteriorly, creating an anterior convexity in this region. The element thus appears 's-shaped' in lateral profile. However, the distal curvature may be an artifact of the reconstruction of the shaft in this region to some degree. The shaft is mediolaterally narrower than anteroposteriorly deep for most of its length. The trochlear notch for articulation of the ulna is saddle-shaped, being anteriorly concave proximodistally, and convex mediolaterally. Viewed anteriorly, the proximal and distal margins of the trochlear notch obliquely intersect the proximodistal axis of the ulna (i.e., the medial sides of the proximal and distal margins are situated more proximally than the lateral sides). The facet for the radial head is lateral to and confluent with the trochlear notch. It is pyriform (pear-shaped) in profile, with the apex of the 'pear' pointing proximally. It extends beyond the distal margin of the trochlear notch. The radial facet is fairly flat, but it is gently saddle-shaped in the same way as the trochlear notch. Its surface faces anterolaterally.

There is a deep groove on the medial side of the ulna, posterior to the trochlear notch, which appears to have extended some distance proximally onto the olecranon. This groove continues distally for approximately half the length of the shaft. Distal to the trochlear notch, the groove is paralleled and accentuated by a more anteriorly situated ridge that extends distally from the notch for ~1 cm. Anterolateral to this ridge is a flattened, anteriorly-facing surface that probably received the brachialis muscle insertion. The lateral aspect of the shaft also has a proximodistally running groove. It is not as pronounced as the medial groove and is sharper. The groove on the lateral aspect of the shaft is more distinctive distally than proximally.

Toward the distal end of the shaft on its anterior aspect, two distally diverging ridges develop. The lateral one approaches the distal radial facet, and the other passes medial to it before meeting up with a surface that is contiguous with the radial facet and the carpal facet more distally. The more lateral of the two ridges appears to be the interosseous crest, and the medial one probably represents the medial edge of the area of origination for the pronator quadratus muscle (George, 1977). The distal end is marked by an anterodistally-facing, convex facet for the distal radius and the lunate (see below). Distal to this, the styloid process has a convex, anterodistomedially-facing facet for the triquetrum and pisiform of the proximal carpal row.

Comparisons.— The ulna of *P. cookei* differs little from those of other plesiadapids (Tables A-II-17 and A-II-18). None of the shape indices in Table A-II-17 reveal any quantitative differences. Qualitatively, comparing more subtle aspects of the morphology, it can be stated that the ulna of *P. cookei* seems to be unusual in the shallowness of the longitudinal groove marking the lateral side of its shaft for origination of extensor musculature, but it is difficult to say whether this reflects individual variation. The ulna of *P. cookei* also appears more slender than those of other plesiadapids; however, as mentioned, this is not borne out by any shape variables (Table A-II-17: e.g., NSV and SSV).

Scaphoid

The right scaphoid is preserved (Figs. 40A; Table A-II-19). It was originally identified by comparison to the scaphoid of

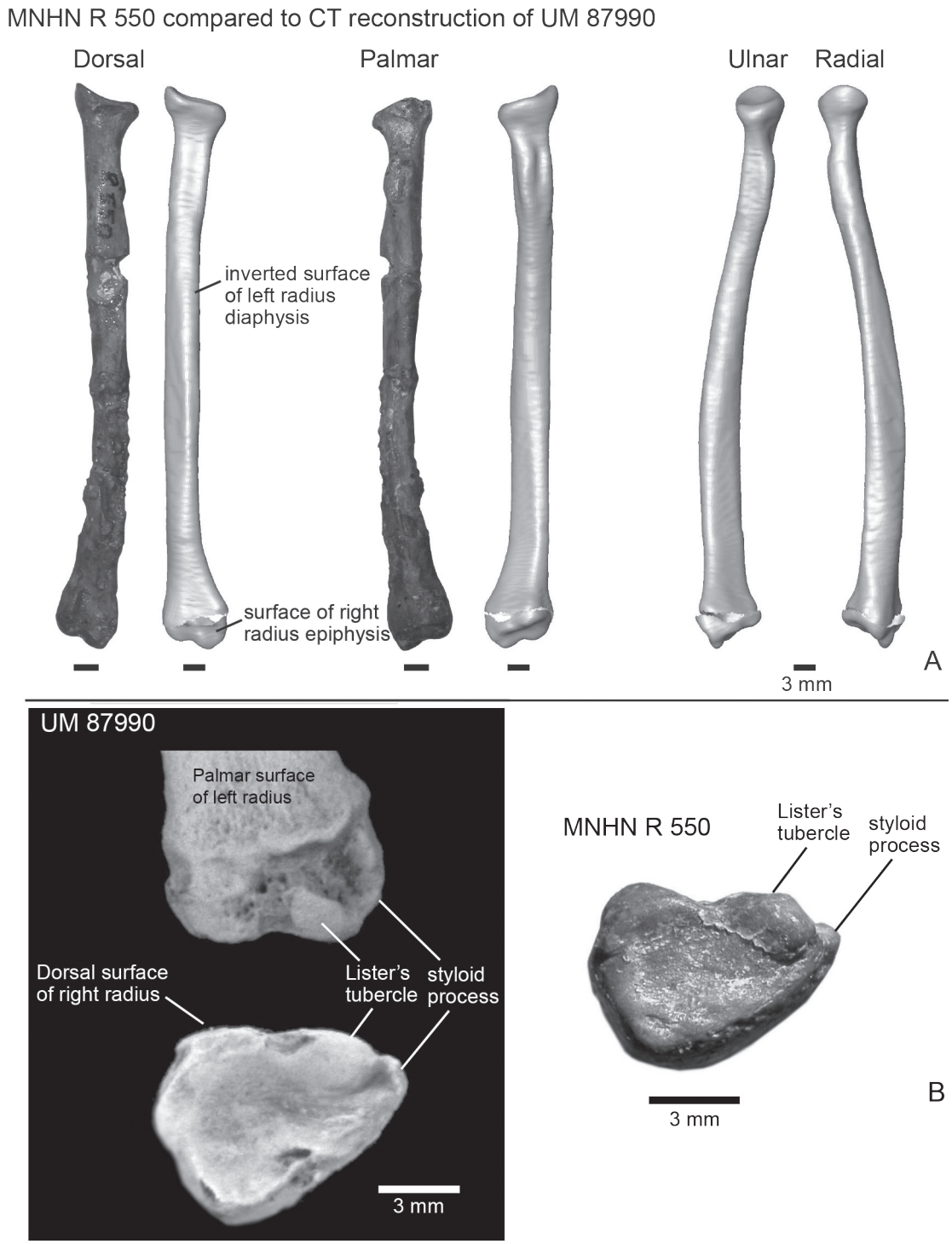

FIGURE 39.— Reconstruction of the right radius of *Plesiadapis cookei* (UM 87990) using high resolution CT imagery. **A**, comparison of right radii of *P. cookei* (CT images of UM 87990) and *P. tricuspidens* (photographs of MNHN R 550). The former is shown in dorsal, palmar, ulnar, and radial views. The latter is shown in dorsal and palmar views. The diaphysis of the CT reconstruction of the left radius of UM 87990 was separated from the right distal epiphysis and inverted to represent the right diaphysis. These two segments were then repositioned as they are thought to have been in life. Note the similarity between the distal ends of the photograph of *P. tricuspidens* and the reconstructed radius of *P. cookei*. The distal articular surfaces face ulnarly and palmarly to a similar degree. **B**, detailed comparisons of the distal epiphyses of the radii of *P. cookei* and *P. tricuspidens*. The styloid process, Lister's tubercle and a more ulnarly positioned tubercle allow confident identification of the *P. cookei* element as belonging to the right side.

N. intermedius USNM 442229 (Beard, 1993a) and to a scaphoid associated with the paromomyid *Acidomomys hebeticus* (Boyer and Bloch, 2008). Boyer et al. (2013) noted that this bone is almost identical in size and shape to an undescribed scaphoid UCMP 229399 associated with other plesiadapid postcranials from the UCMP Mutigny collection, including a humerus UCMP 102829 that probably represents *Pl. daubrei* (Gingerich, 1976). Aside from being 'boat-shaped,' as the etymology of the bone's name suggests, with a convex proximal articular surface forming the 'hull of the boat' and the concave distal articular surface forming the 'boat's interior' the scaphoid of *P. cookei* could also be described as 'barbell-shaped' because the ventral (palmar) tubercle is quite large and distinct from the articular surface for the radius. On the proximal surface, the radius facet is triangular to pyriform in outline (Fig. 41:5), with a vertex of the triangle (or the apex of the pear) pointing radially. The radius facet meets the lunate facet (Fig. 41:3) at its ulnar margin and the two surfaces form an angle of ~90º with one another. The lunate facet meets the facet for the distal carpals at its distal margin (Fig. 41:2), and these two surfaces form an angle of around 100º. It is also apparent in ulnar view that the distal carpal articular surface of the scaphoid is not entirely parallel to the radius facet. In fact, the average tangent of the concave distal articular surface differs from that of the proximal radius surface by ~45°, such that these surfaces deviate in their orientation, from proximal or distal, to somewhat dorsal with respect to one another.

In distal view, the distal articular surface of the scaphoid is triangular in outline (Fig. 40A); its radial apex reaches the radiodistal tip of the scaphoid tubercle and continues onto it. Dorsal to the distal carpal surface is a flat, distally-facing shelf (Fig. 41:1) that may have articulated with bones of the distal carpal row during extremely dorsiflexed postures of the mid-carpal joint. The smooth, articular bone of the radial margin of the distal carpal articular surface continues proximally onto the radial and ventral aspects of the scaphoid tubercle (Fig. 41). A prepollex or radial sesamoid (Haines, 1955) may have articulated here. In addition to the scaphoid tubercle, there is another tuberosity situated radioventral to the lunate surface. The tuberosity is thus located ulnar to the scaphoid tubercle. A distinct groove is present between the two tuberosities. This groove probably held tendons of the flexor compartment (e.g., flexor pollicis longus).

Comparisons.— The scaphoid of *P. cookei* is quite similar to that of *N. intermedius* (Fig. 41). This is significant because Beard (1993a) interpreted *N. intermedius* as having a facet for the lunate on its 'distal surface' as well as a facet for the triquetrum on its lateral surface. This interpretation appears to be incorrect, as implied by the description above and as illustrated in Figure. 41. The interpretation used here is supported by a number of other lines of evidence presented by Boyer et al. (2013). Beard's (1993a) interpretation was plausible when originally proposed because (1) the *N. intermedius* scaphoid is incompletely preserved, allowing for more speculation about the missing morphology; (2) the morphology of the bone he identified as the lunate fit expectations of what it should be under that interpretation of the scaphoid morphology, and (3) a less complete carpus was available for assessing whether this interpretation was plausible in an articulated specimen.

Lunate

The lunate is typical in form; that is, it resembles a 'crescent moon' when seen in radial or ulnar view (Fig. 40B). The proximal end is convex and the distal end is concave to accomodate the distal carpal row (Fig. 42A). Its maximum dorsoventral depth is 5.1 mm, and its mediolateral width is 2.3 mm. In dorsal view, it appears wedge-shaped because the scaphoid facet is shorter (1.8 mm) than the ulnar side (2.5 mm). Therefore, when articulated with the scaphoid, its distal surface faces slightly radially: together the combined distal surfaces of the lunate and scaphoid form a 'cup' for the distal carpals (Figs. 40B, 42A:2). Additionally, the shelf-like distally facing facet on the scaphoid is continued ulnarly by similar morphology of the lunate (Figs. 40B, 42A:4). The radius articular surface for the lunate is also visible in dorsal view (Figs. 40B, 42A:6). It arcs from the radiodistal edge of the lunate, down to the lunate's proximoulnar margin, where it contacts the dorsal edge of a small, ulnar facing facet for the distal part of the distal radial facet of the ulna (Figs. 40B, 42A:3). This facet for the ulna can be seen more clearly from ulnar view. This view also shows that the lunate is mainly non-articular on the ulnar side. Its proximal surface has the facet for the ulna. Distal to this there is a non-articular gap, and farther distal still there is a strip-like facet for the triquetrum, which faces laterodistally (Fig. 40B, 42A:1).

Comparisons.— Comparing the lunate described here to that described for *N. intermedius* by Beard (1989; Fig. 42A, C), one must conclude that the two bones are very different. This is surprising given: (1) the similarity of the scaphoids of these two taxa (Fig. 41); and (2) the good fit between the scaphoid and the lunate described here. These two observations are part of the evidence that the bone described as the lunate of *N. intermedius* by Beard (1989), USNM 442229, is incorrectly identified as such (Boyer et al., 2013). Boyer et al. (2013) noted additional issues for the bone Beard (1989) identified as a lunate. We also discuss these issues and provide illustrations (Fig. 42) below.

If we were to accept Beard's identification of the lunate in USNM 442229, this would imply that USNM 442229 preserves a second lunate of equivalent chirality. This second "lunate" was preserved in association with an intermediate phalanx (Fig. 42D). Two "lunates" from the same side of the body would be the only evidence that USNM 442229 represents more than one individual. Alternatively, if we reconsider the identity of these bones, sesamoids are a likely option as there are multiple sesamoids of the same 'chirality' in the hand and foot and they have morphology similar to the bone Beard (1989) identified as the lunate. Direct comparison to pedal sesamoids of *Sciurus carolinensis* SBU MRd-10 (Fig. 42B) supports this view.

Triquetrum

Left and right triquetra are both preserved (Fig. 40C; Table A-II-20). They are subrectangular in dorsal view due to

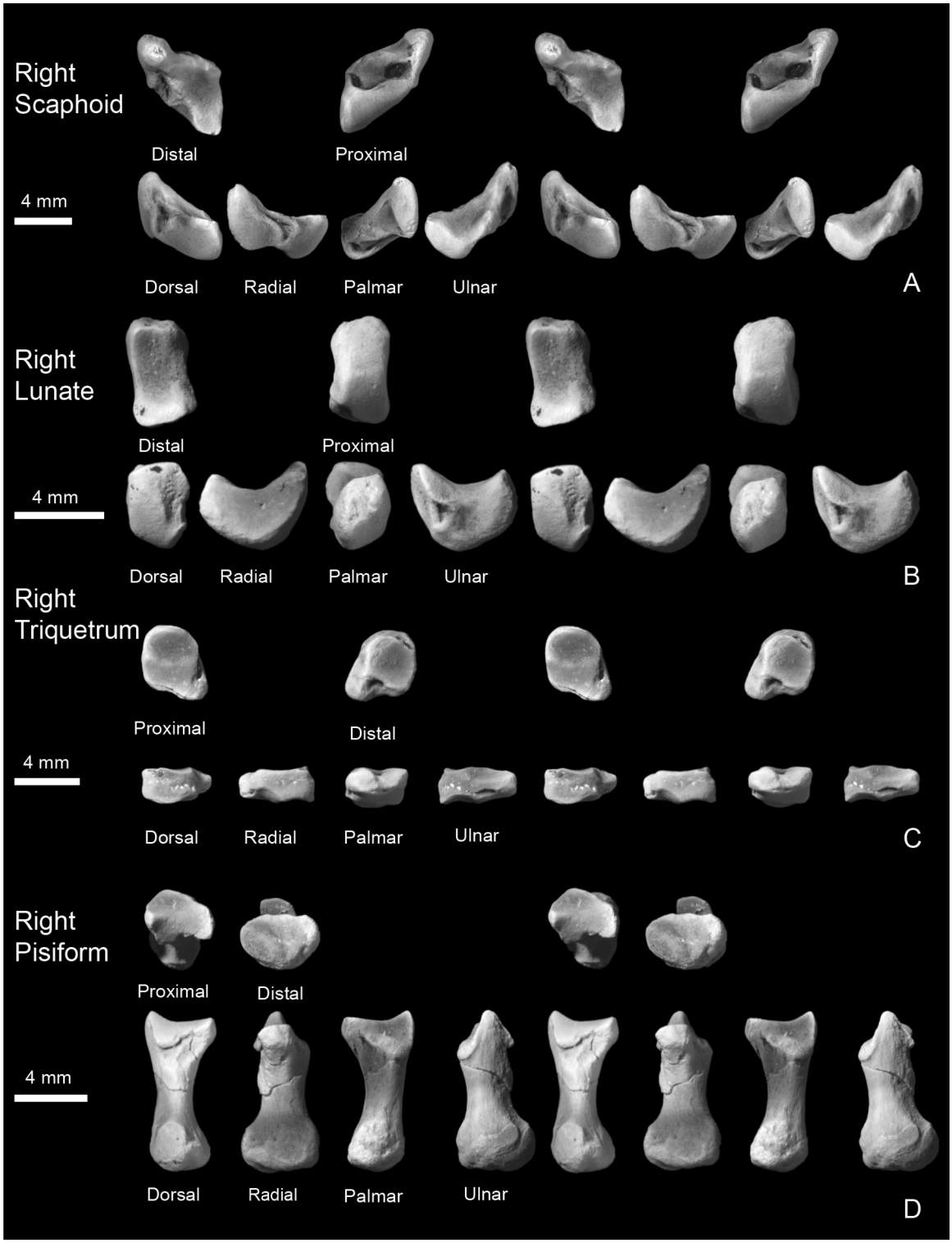

FIGURE 40.— Proximal carpal bones of *Plesiadapis cookei* (UM 87990). Stereophotographic images of the proximal row of carpal bones. **A**, right scaphoid. **B**, right lunate. **C**, right triquetrum. **D**, right pisiform. All are shown in dorsal, radial, palmar, ulnar, proximal, and distal views.

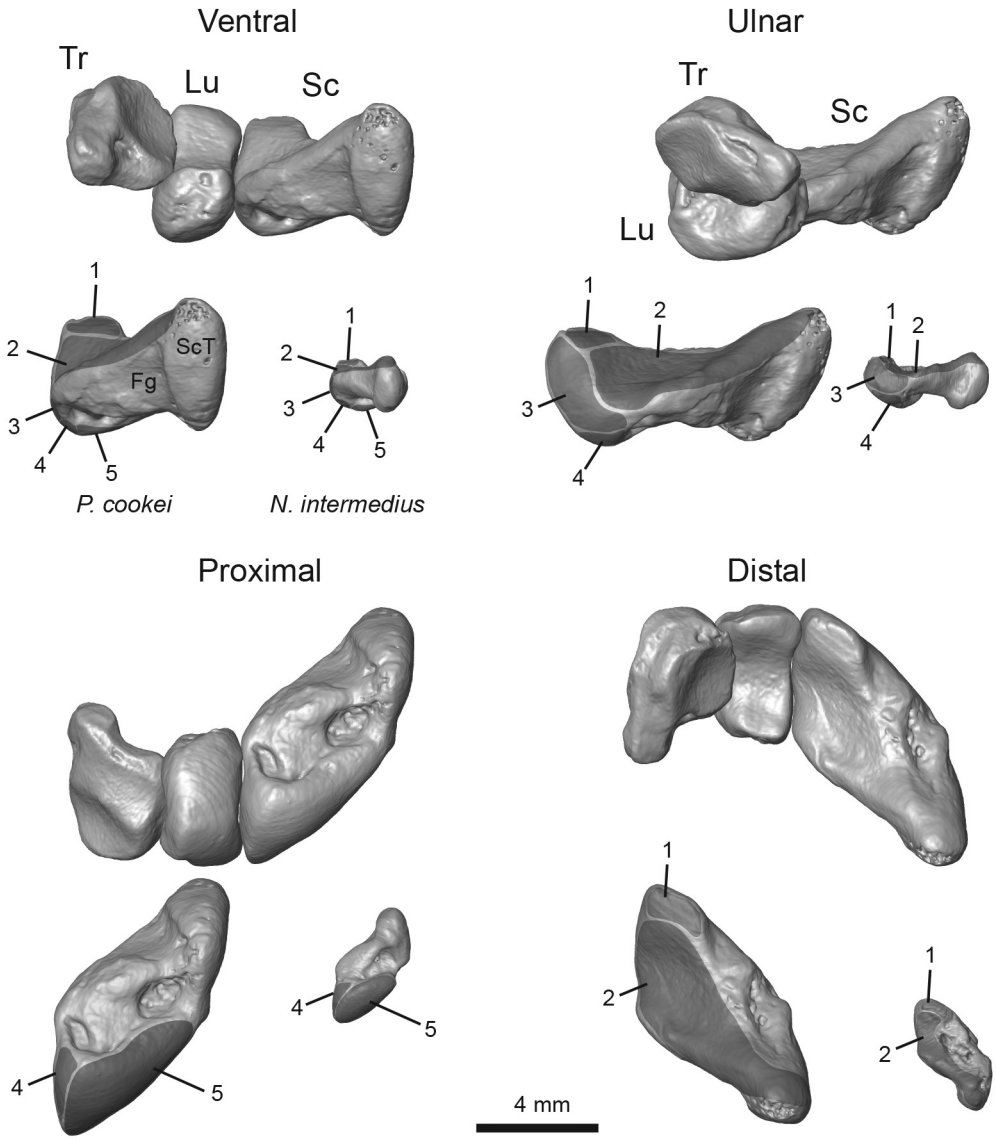

FIGURE 41.— Articulation of proximal carpal bones of *Plesiadapis cookei* (UM 87990), and a comparison to the scaphoid of *Nannodectes intermedius* (USNM 442229). Images are high-resolution CT reconstructions. Articular surfaces and other regions are identified with gray shading and labeled with numbers on the scaphoids: *1*, shelf-like facet that may contact distal carpal row during dorsiflexed postures of the midcarpal joint; *2*, articular surface for distal carpal bones including hamate, capitate, centrale, trapezoid and trapezium; *3*, lunate facet; *4*, possibly a non-articular area or extension of lunate facet (this appears to be the area that Beard, 1989, interpreted as the triquetrum facet in *N. intermedius*, which is almost certainly incorrect); and *5*, radius articular facet. Abbreviations: *Fg*, flexor tendon groove; *Lu*, lunate; *Sc*, scaphoid; *ScT*, scaphoid tubercle; and *Tr*, triquetrum.

proximodistal dimensions that are narrow compared to their radioulnar dimensions. They are squarish-to-oval in proximal and distal views. The proximal end is completely covered by articular surface. Dorsal and ventral facets are separated by a radioulnarly oriented ridge. The dorsal facet articulates with the distal facet of the ulnar styloid process. The ventral facet articulates with the pisiform. Both facets are dorsoventrally concave. The ulna facet is additionally radioulnarly concave. In other words, this surface is spherically depressed. The pisiform facet is additionally radioulnarly convex. Thus the pisiform facet is saddle-shaped. The ulnar, dorsal, and ventral surfaces of the bone are non-articular.

The radial surface articulates with the lunate. This articular surface is proximodistally flat, but dorsoventrally convex. The facet is oriented at a right angle to the proximal facet for the ulna. Thus, when the medial facet of the triquetrum

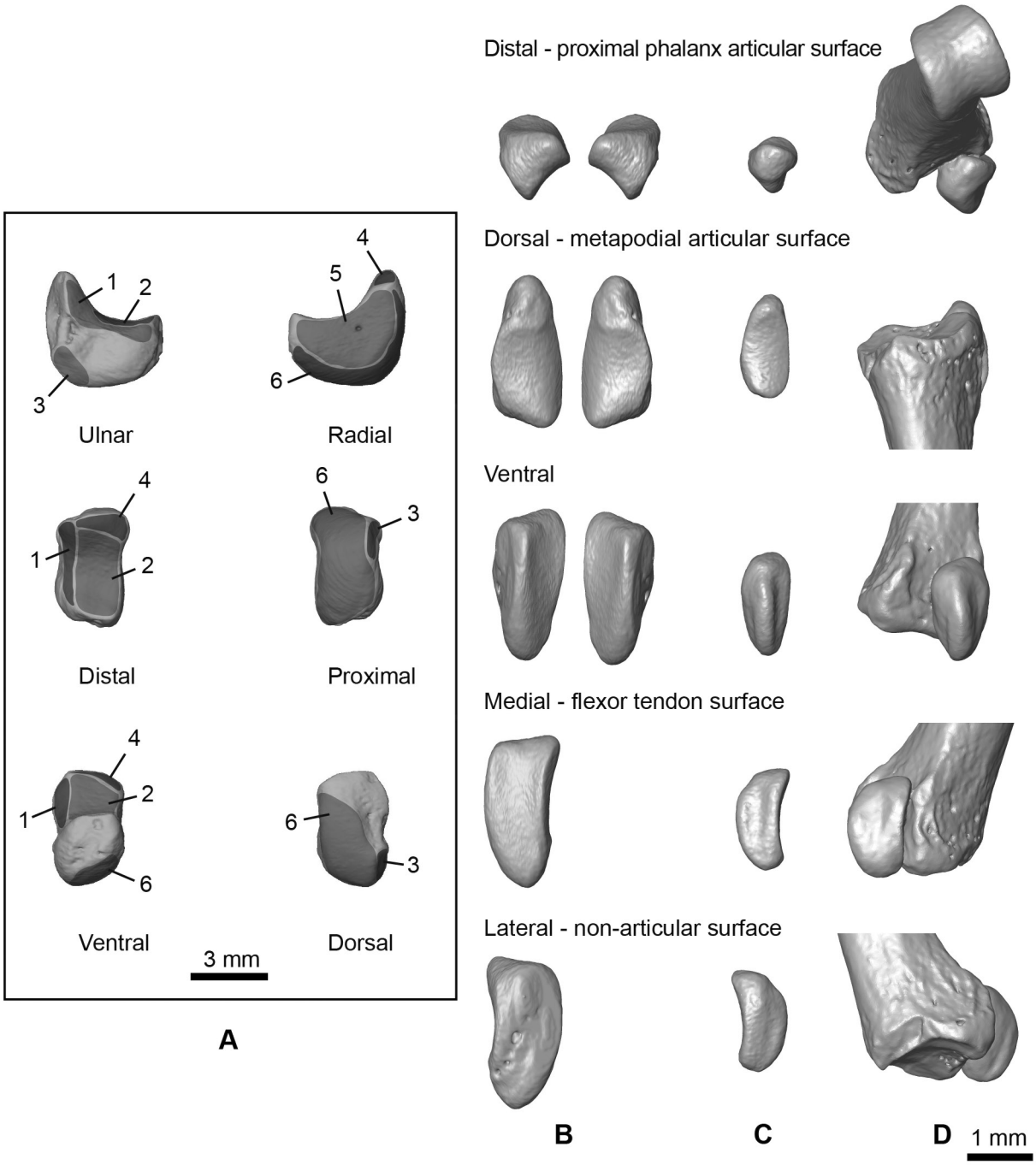

FIGURE 42.— Lunate of *Plesiadapis cookei* (UM 87990). Surface reconstructions of lunates and sesamoids are based on high-resolution CT data. **A**, right lunate of *P. cookei* (UM 87990). Articular surfaces and other regions are identified with gray shading and labeled with numbers: *1*, triquetrum facet; *2*, hamate facet; *3*, ulna facet; *4*, shelf-like facet that may contact distal carpal row during dorsiflexed postures of the midcarpal joint; *5*, scaphoid facet; and *6*, radius facet. **B**, medial and lateral pedal sesamoids of *Sciurus carolinensis* (SBU MRd-10). **C**, "lunate" of *Nannodectes intermedius* (USNM 442229; Beard, 1989). Note the similarity of this bone to the leftmost pedal sesamoid of *Sciurus*. **D**, second 'lunate' adhering to an intermediate phalanx of USNM 442229 (not mentioned in Beard, 1989). Although slightly different, the bones of *N. intermedius* in C and D appear to represent sesamoids from the same side.

is articulated with its facet on the lunate, the bone's true mediolateral axis is revealed to be oblique to that being used for descriptive purposes (Figs. 40C, 41) by ~45°. The distal facet thus faces obliquely toward the radius. The triquetrum completes a deeply cupped mid-carpal joint (to which the distal surfaces of the lunate and scaphoid also contribute), in which sit the hamate, capitate, and centrale. Aside from its radial orientation, the distal facet (for the hamate) is characterized by being shallowly, spherically concave and equal in its radioulnar and dorsoventral dimensions. Ventral to this facet, still on the distal surface of the triquetrum, is a nutrient foramen. Ventral and lateral to the foramen is a tubercle that supports the pisiform facet on its proximal surface.

Comparisons.— The only other plesiadapid for which the triquetrum is known is *P. tricuspidens*. The two taxa are fairly similar in the morphology of their triquetra, which helps confirm they are correctly attributed to *Plesiadapis* in both cases. *P. tricuspidens* differs in having a proximodistally proportionally thicker element (Table A-II-20: TrL-V), suggesting that its hands may have exhibited less ulnar deviation than those of *P. cookei*. Furthermore, *P. tricuspidens* has a much larger tubercle on its ventro-ulnar aspect. Finally, *P. tricuspidens* differs in exhibiting a nutrient foramen on its proximal aspect (lateral to the pisiform facet) as well as on its distal aspect. Whether these types of differences are also found at the intraspecific level is unknown. However, as the right and left triquetra of *P. cookei* are identical, it can, at least, be said that these differences are beyond what is expected for intra-individual variation.

Pisiform

The right pisiform is preserved (Fig. 40D; Table A-II-21). It is quite large, but confidently attributed to *P. cookei* because the articular facet for the triquetrum matches the pisiform facet on the triquetrum described above. Furthermore, it is quite similar to the pisiform described for *N. intermedius* (Beard, 1989) although much larger (Table A-II-21). When articulated with the rest of the proximal carpal row, the pisiform tubercle projects roughly parallel to the proximal articular surface of the other carpals (see below) and at almost 90° to the scaphoid tubercle (i.e., if the pisiform is considered to project ventrally, then the scaphoid tubercle can be described as projecting distally).

The triquetrum facet of the pisiform is reciprocally saddle-shaped compared to the corresponding facet on the triquetrum. This facet is dorsally and slightly distally oriented. The ulna facet is pyriform and gently concave. It is proximally and (slightly) dorsally oriented. The pisiform has a distinct shaft that is narrower than the proximal end. The distal end is swollen proximodistally, relative to the shaft, for attachment of the flexor carpi ulnaris, hypothenar muscles, and pisohamate ligament (Haines, 1955; George, 1977).

Comparisons.— *P. cookei* is similar to *N. intermedius* in its pisiform morphology. The only notable difference is a shorter shaft relative to facet size and shaft diameter in *N. intermedius* (Table A-II-21: BSV and SSV). If these animals utilized similar postures and behaviors in life, a larger pisiform might have been an allometric consequence required to maintain equivalent abilities in ventriflexion in the absolutely larger animal.

Trapezium

A bone identified as a possible left trapezium is preserved in UM 87990 (Fig. 43A). This element is not known for any other plesiadapid or plesiadapiform. It is identifiable as a trapezium mainly by its match to the proximal articular surface of the first metacarpal (MC I). However, it has a morphology dramatically different from that seen in trapezia of extant and fossil euprimates as well as extant dermopterans and treeshrews (Boyer et al., 2013: fig. 17), which gives some pause to the attribution. Future discoveries will be required to confirm our identification of this bone and its attribution to *P. cookei*.

The facet for MC I is reniform or 'kidney-shaped' in distal view (Fig. 44A:2). It measures 3.73 mm by 1.91 mm, and its surface area is 5.6 mm^2. In ulnar and radial view, the outline of the trapezium is trapezoidal. This is due to dimensions that differ on the dorsal side of the bone (1.97 mm) compared to the ventral side (3.00 mm). The ulnar surface has a proximal facet for the trapezoid (Fig. 44A:3) that slopes distally toward the dorsal side. The proximodistal axis of the trapezium deviates from the plane of the trapezoid facet by ~45° in a radial direction.

Trapezoid

Possible right and left trapezoids are preserved (Fig. 43B). Like the trapezium, these are the only examples of this bone known for any plesiadapiform and there are similar uncertainties about its attribution. The distal articular facet is rectangular in distal view and measures 4.13 mm by 2.15 mm. Its surface area is 8.2 mm^2 (Table A-II-22). It is gently saddle-shaped, with a concave dorsoventral profile and convex radioulnar profile. In radial or ulnar view, it is true to its name-sake in having a trapezoidal outline, with a narrower proximal end than distal end. The radial surface articulates with the trapezium. This surface is also saddle-shaped with a concave dorsoventral profile and a convex proximodistal profile. The ulnar surface for articulation with either the capitate or the centrale (or both?) is helical at its distal end, such that toward its dorsal margin it forms an obtuse angle with the second metacarpal facet. Ventrally this facet is at an acute angle to the metacarpal facet. The proximodistal length of the bone is 2.4 mm. Only the dorsal surface of the trapezoid is largely non-articular.

Hamate

A left hamate is preserved (Fig. 43C; Table A-II-23). There is some doubt about whether this bone is correctly attributed to *P. cookei* given that the hamates of *N. intermedius*, *P. tricuspidens*, and even extant treeshrews appear more similar to each other than any are to the hamate associated with *P. cookei* (Boyer et al., 2013, 2016). Nonetheless, all these taxa have fairly conservative morphology and there are no distinctive features that allow us to effectively rule out the possibility that this bone belongs to *P. cookei*. The most rigorous way to evaluate this attribution would be to do a broad quantitative analysis comparing hamates of plesiadapiforms and miacid carnivorans, but we have not done this.

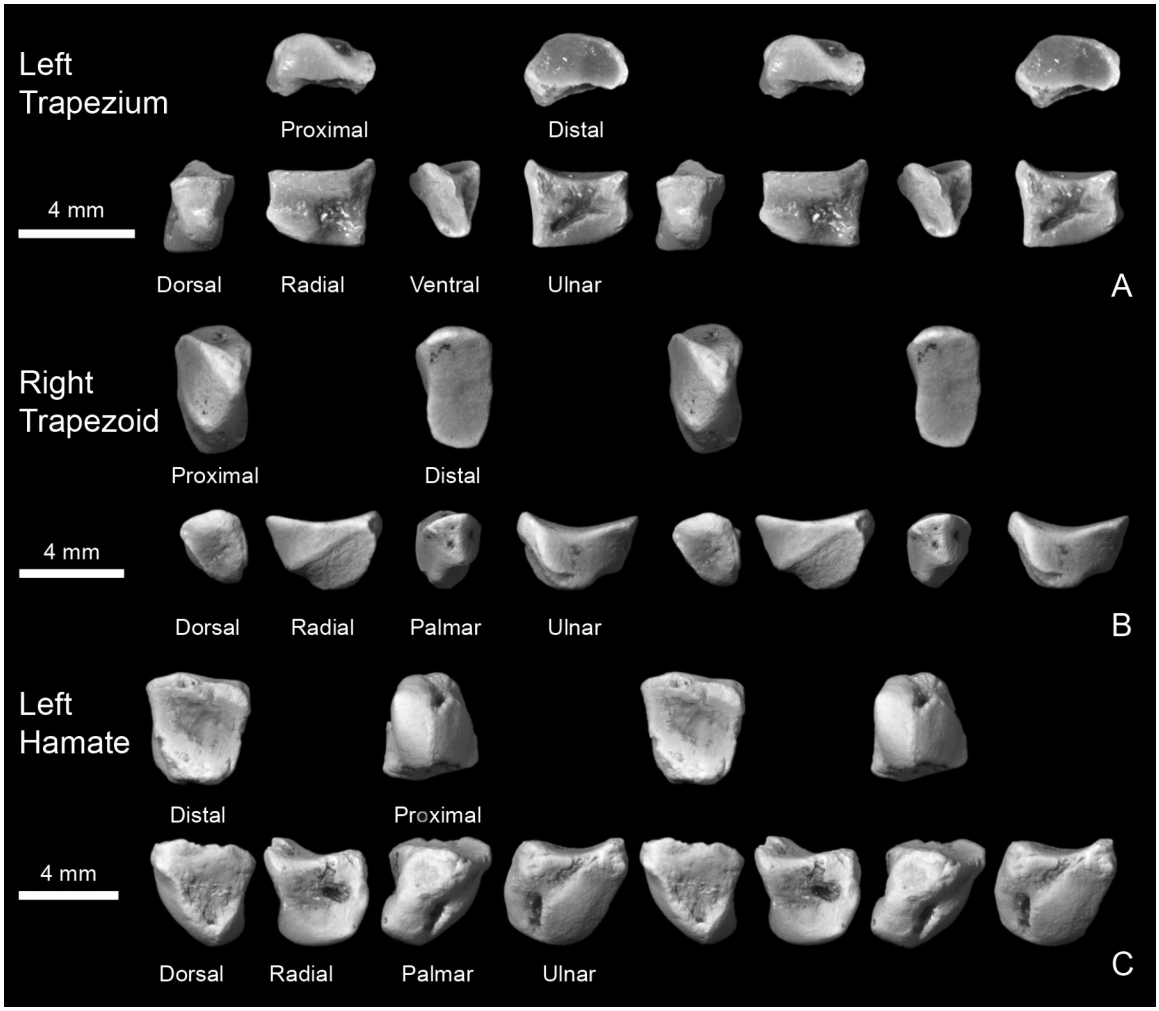

FIGURE 43.— Distal carpal bones of *Plesiadapis cookei* (UM 87990). Stereophotographic views of the distal row of carpals. **A**, left trapezium. **B**, right trapezoid. **C**, left hamate. All are shown in dorsal, radial, palmar, ulnar, distal, and proximal views.

In dorsal view, this hamate has the shape of a right triangle with the distal and radial surfaces forming legs of the 'triangle,' and the ulnar surface forming the hypotenuse (Figs. 43C; Table A-II-23). The distal surface for the fourth and fifth metacarpals is dorsoventrally concave. It has a surface area of 10.7 mm^2. In distal view, the distal articular surface is 'trapezoid' shaped, with the dorsal margin radioulnarly wider than the ventral margin. The maximum radioulnar width of the dorsal margin of the distal surface is slightly narrower than the dorsoventral depth of the distal surface. The ulnar surface is gently convex and articulated with both the triquetrum (distally) and lunate (proximally), and possibly even with the scaphoid in some postures (proximally and radially), although there is no clear demarcation between regions touched by one bone versus the other.

The distal margin of the triquetrum facet has a lip protruding beyond it, which would have served to limit radial translation of the hamate with respect to the triquetrum. The radial surface of the hamate (for articulation of the capitate) is proximodistally concave. Toward its proximal base, the radial surface is dorsoventrally convex. This convexity appears to be the boundary between the capitate facet, which occupies the more ventral part of the radial side, and an accessory facet dorsal to it that faces slightly dorsad (Fig. 45B:5). The proximal surface has a narrow facet that extends onto the ventral surface and appears to have received the scaphoid in certain postures (Fig. 45B:3). On either side of the ventral expression of the scaphoid facet, nutrient foramina separate it from the other ulnar and radial surface facets.

Comparisons.— As mentioned above, the hamate of *P. cookei* differs in several respects from those known for *P. tricuspidens* and *N. intermedius*. The radioulnar width of the distal end in the hamate of *P. cookei* is narrower relative to its dorsoventral depth (Table A-II-23: DEV). The capitate articular surface is concave instead of flat. Finally, the proximal margin has a more distinctive facet for the scaphoid

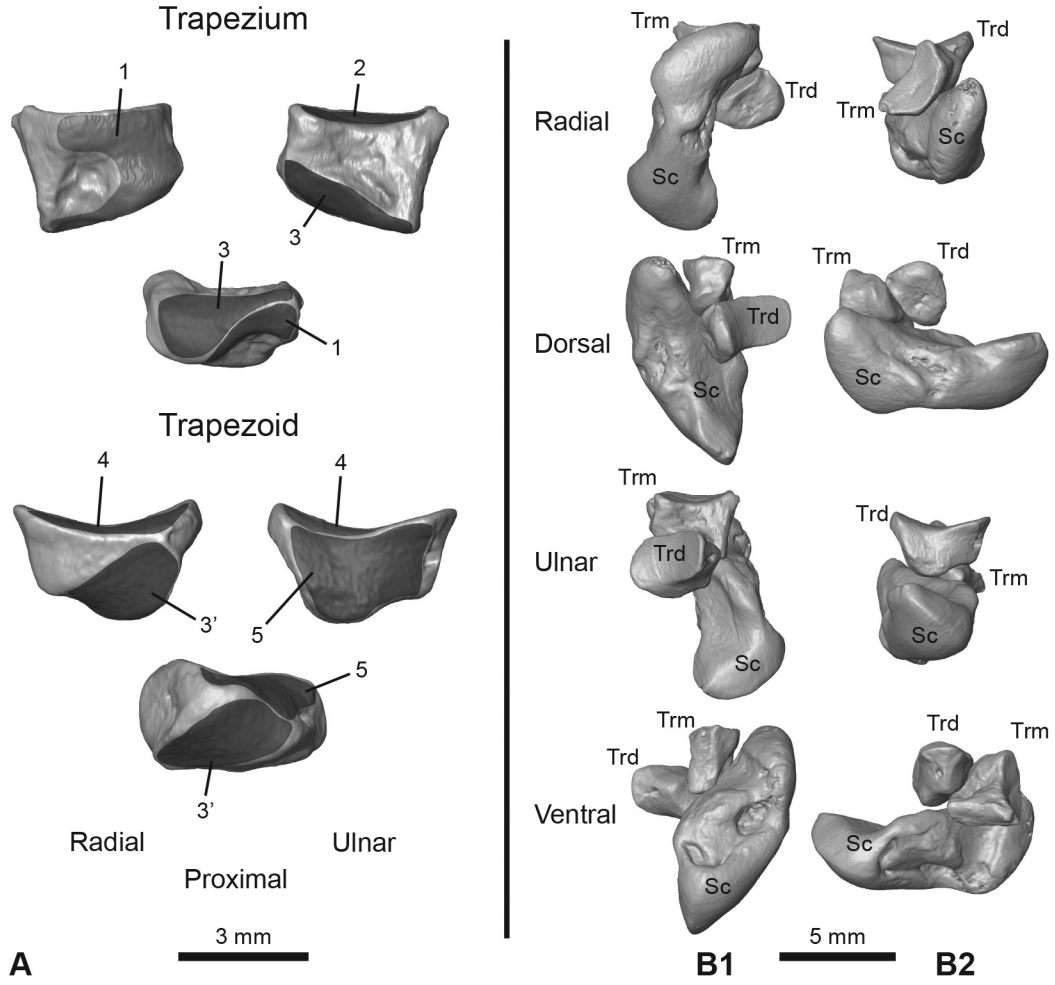

FIGURE 44— Articulation of distal carpal bones of *Plesiadapis cookei* (UM 87990). Images are based on high-resolution CT data. **A**, right trapezium and trapezoid. Articular surfaces are illustrated with gray shading and labeled with numbers: *1*, scaphoid facet; *2*, MC I facet; *3–3′*, corresponding facets of trapezoid and trapezium; *4*, MC II facet, and *5*, capitate and/or centrale facet. **B1**, scaphoid (*Sc*), trapezium (*Trm*), and trapezoid (*Trd*) articulated and oriented in several views with respect to idealized anatomical planes of the trapezium (as used in Fig. 43). **B2**, same bones as in B1 articulated and oriented in several views with respect to idealized anatomical planes of the trapezoid (as used in Fig. 43). Note the wide separation between the facets for MC I and MC II. These did not contact in the articulated hand.

than that in either *N. intermedius* or *P. tricuspidens* (Fig. 45B:3). The greater development of the proximal scaphoid facet may suggest more frequent reliance on abducted hand postures, because in order for this facet to solidly contact the scaphoid, the hamate must be abducted with respect to it.

Metacarpals

There are two distinct metacarpal morphologies associated with UM 87990. We refer to these as ‘set 1’ metacarpals (Fig. 46; Table A-II-24) and ‘set 2’ metacarpals (Fig. 47; Table A-II-24). The two sets are similar in size and morphology (Fig. 48), but they are not identical.

Metacarpal associations.— UM 87990 includes a total of 15 metacarpals, of which 10 are complete and measureable (Table A-II-24). There are two MC I’s, which are left and right mirror images of one another. There are three examples of MC II, two lefts and a right. There are two examples of MC III, two rights. There are three examples of MC IV, one left and two rights. Finally, there are three examples of MC V, one left and two rights. The presence of several pairs of metacarpals of the same position and same side indicates that a minimum of two individual animals are represented.

The base of right MC III fits together with the base of a right MC IV, an association that initiated what we have called, ‘set 1’, metacarpals. There is also a good fit between the bases of one example of left MC II (when digitally reversed) and a right MC III and MC IV, an association that we have called, ‘set 2’, metacarpals. Comparing these two sets, metacarpal III of ‘set 2’ is 16% longer than that of ‘set 1’. The remaining MC II is 90% as long as that of ‘set 2’, indicating that it belongs to ‘set 1’.

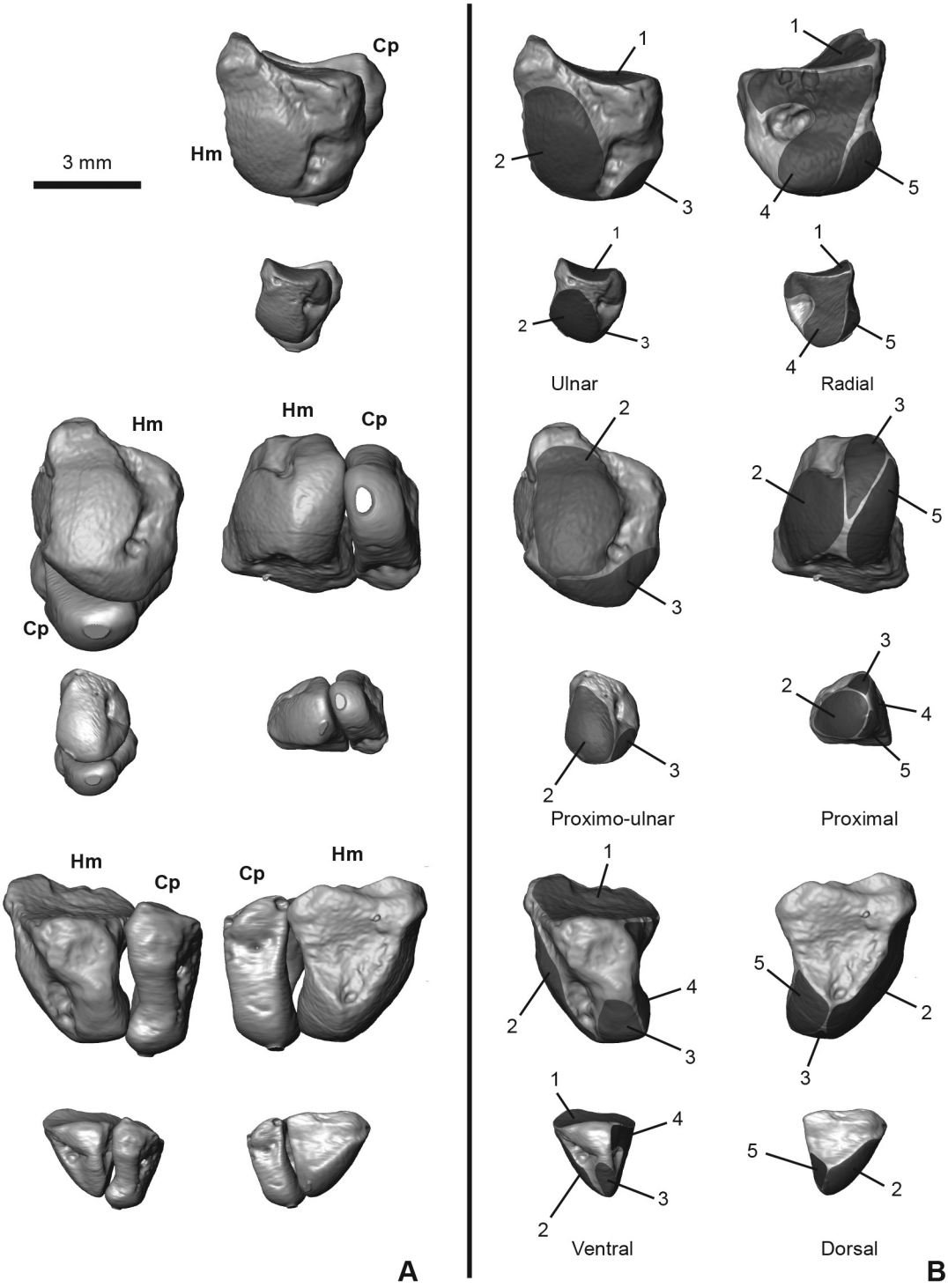

FIGURE 45.— Articulation of carpal bones in *Plesiadapis cookei* (UM 87990) and *Nannodectes intermedius* (USNM 442229). Images based on high-resolution CT data. Six sets of views are provided of the two taxa, with *P. cookei* elements positioned above the corresponding view for elements of *N. intermedius*. **A**, view of the two specimens showing the capitate and hamate articulated. Note that the capitate is not known for *P. cookei*. The surface reconstruction of the hamate of *P. cookei* is articulated with a surface reconstruction of that belonging to *N. intermedius* scaled upward by a factor 1.74. **B**, hamates in six views. Articular surfaces are illustrated with gray shading and labeled with numbers: *1*, MC IV and V facet; *2*, triquetrum facet; *3*, possible ventral accessory facet for scaphoid and/or lunate; *4*, capitate facets; and *5*, possible dorsal accessory facet for scaphoid and/or lunate. Abbreviations: *Hm*, hamate; *Cp*, capitate.

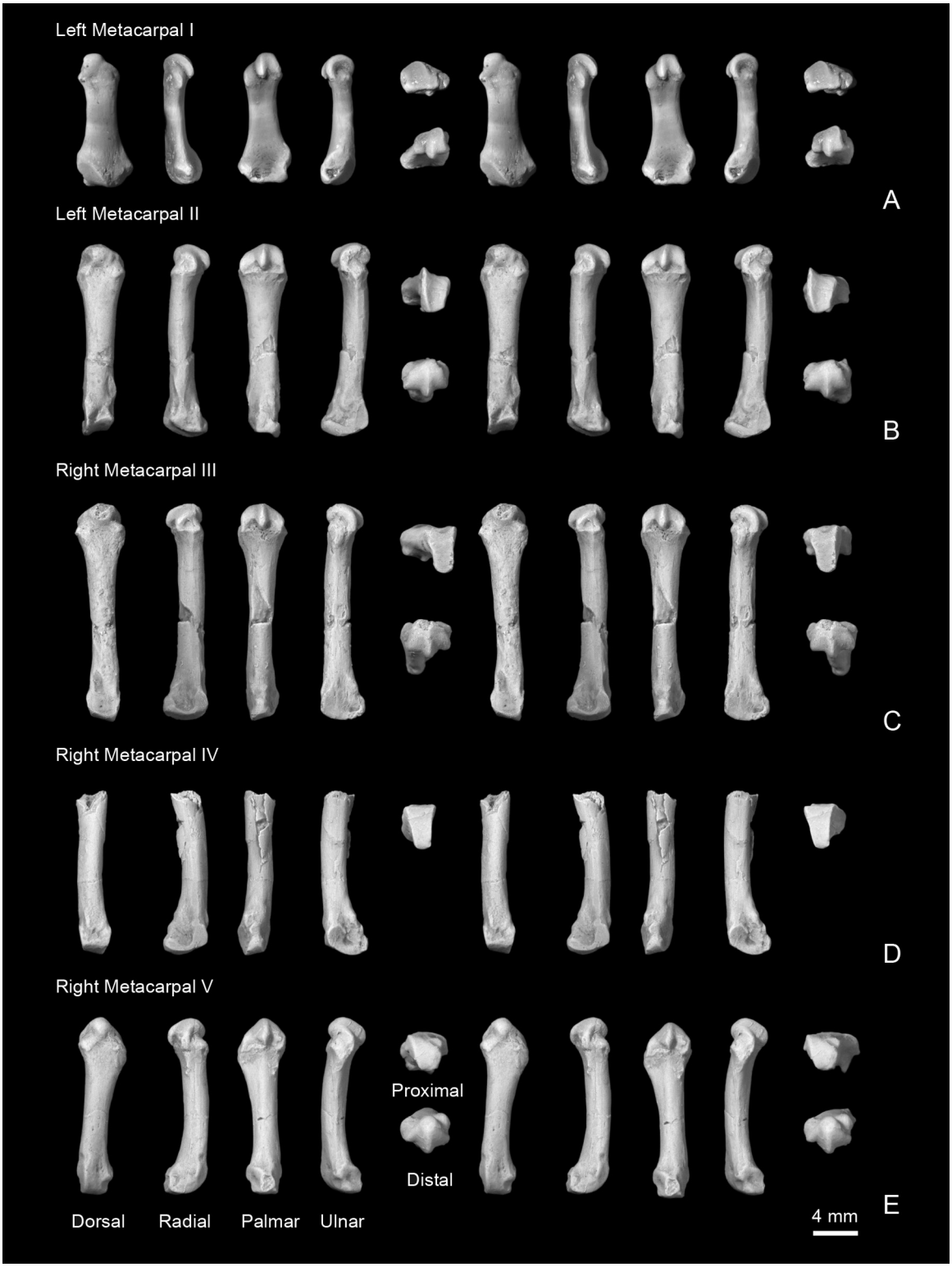

FIGURE 46.— 'Set 1' metacarpals of *Plesiadapis cookei* or *Uintacyon rudis* (UM 87990). Stereophotographic views of 'set 1' metacarpals. **A**, left MC I (pollical metacarpal). **B**, left metacarpal MC II. **C**, right metacarpal MC III. **D**, right metacarpal MC IV. **E**, right metacarpal MC V. All are shown in dorsal, radial, palmar, ulnar, distal, and proximal views. Also preserved are proximal fragments of a right MC II and a left MC III. 'Set 1' metacarpals are shorter and more robust than 'set 2' metacarpals.

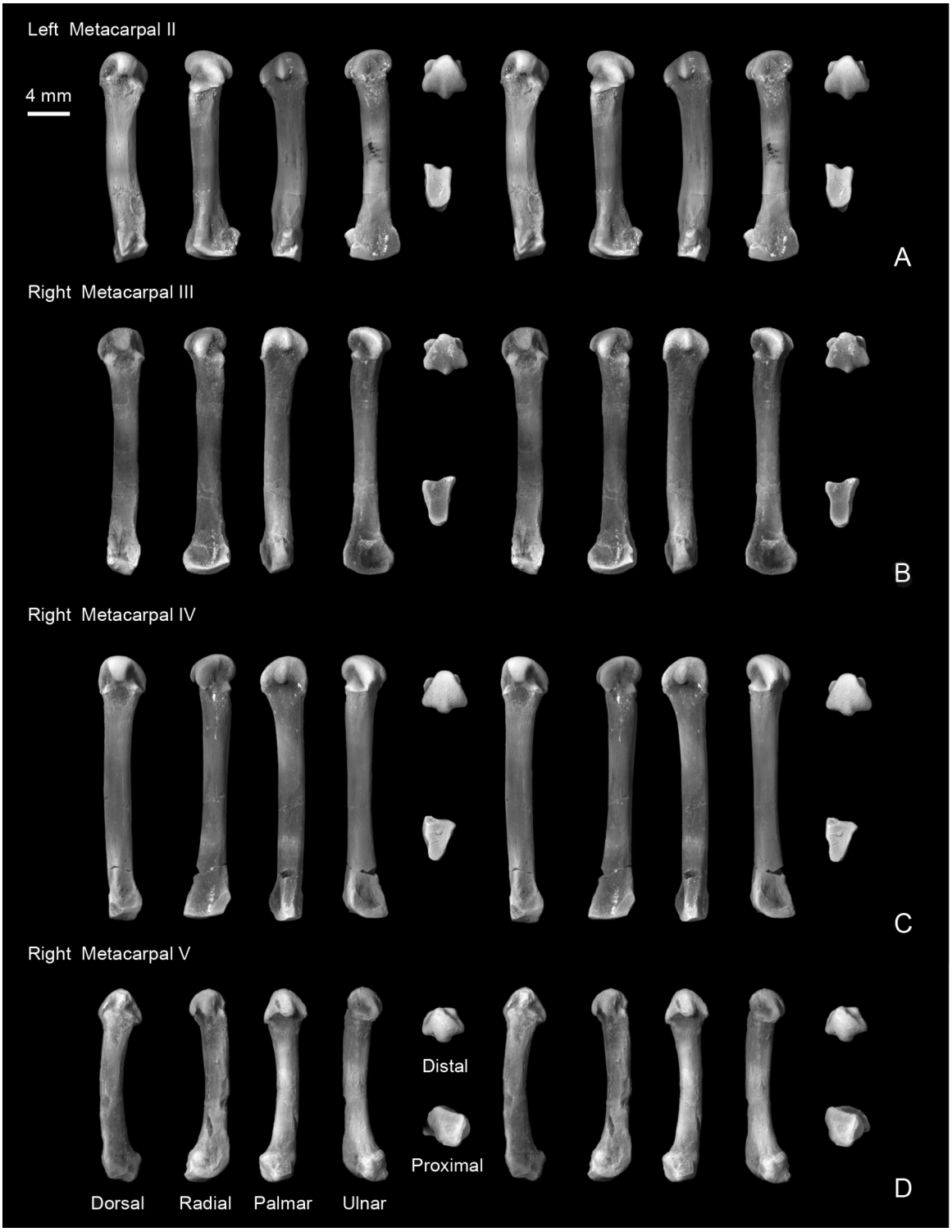

FIGURE 47.— 'Set 2' metacarpals of *Plesiadapis cookei* or *Uintacyon rudis* (UM 87990). Stereophotographic views of 'set 2' metacarpals. **A**, left metacarpal MC II; **B**, right metacarpal MC III; **C**, right metacarpal MC IV; and **D**, right metacarpal MC V. All are shown in dorsal, radial, palmar, ulnar, distal, and proximal views. 'Set 2' metacarpals are longer and more gracile than 'set 1' metacarpals.

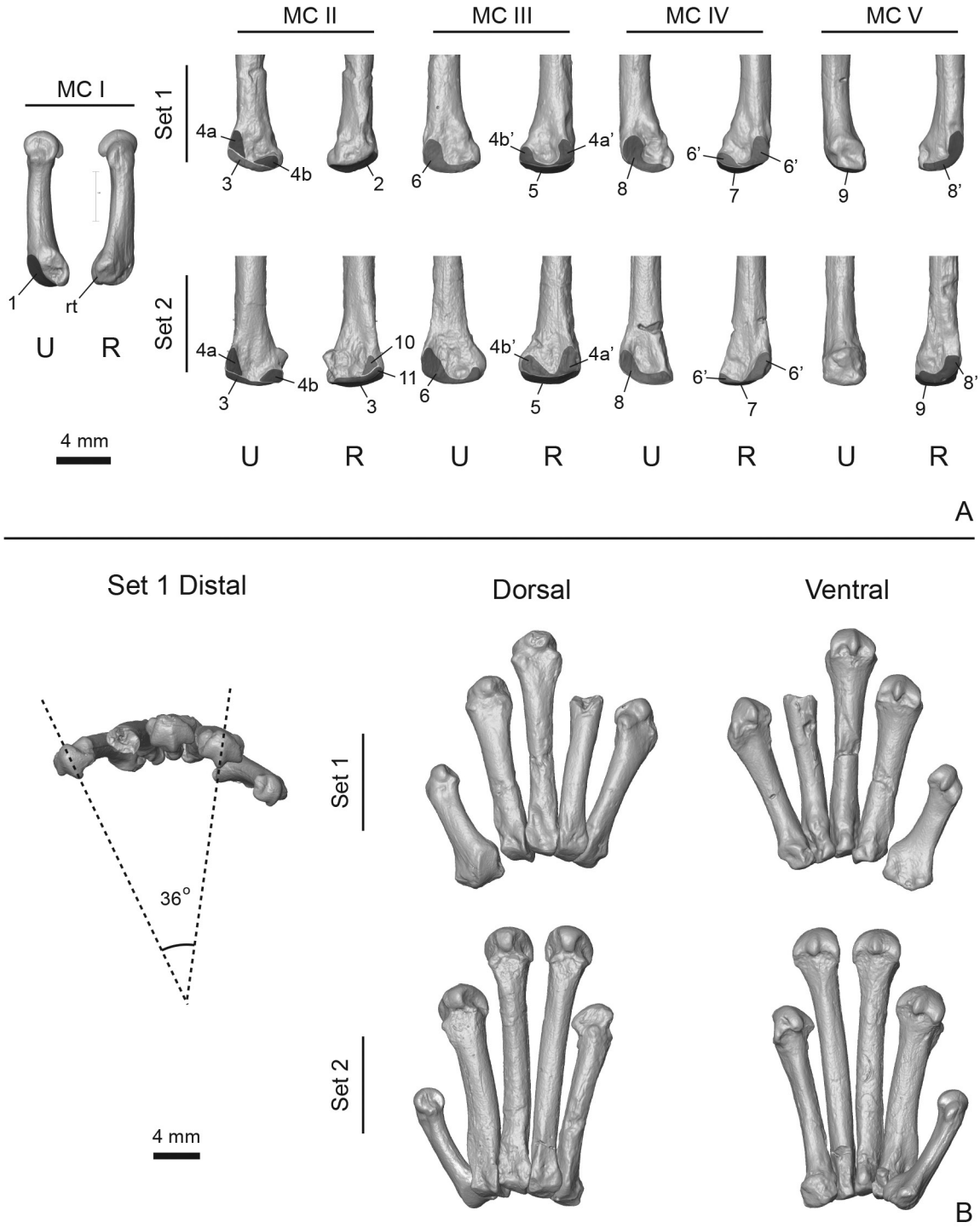

FIGURE 48.— Comparison of 'set 1' and 'set 2' metacarpals of the right manus of *Plesiadapis cookei* and *Uintacyon rudis* (UM 87990), showing interpretation of articular relationships. Surface reconstructions are based on high-resolution CT data. **A**, 'set 1' and 'set 2' metacarpals in radial (*R*) and ulnar (*U*) views. Articular surfaces are illustrated with gray shading and labeled with numbers: *1*, trapezium facet; *2*, trapezoid facet; *3*, capitate facet of MC II; *4a–4a'* dorsal MC II–III facet; *4b–4b'*, ventral MC II–III facet; *5*, capitate facet of MC III; *6–6'*, MC III–IV facets; *7*, hamate facet of MC IV; *8–8'*, MC IV–V facets; *9*, hamate facet of MC V; *10*, ?MC I–II facet of "set 2" MC II; and *11*, ?trapezium facet of 'set 2' MC II. **B**, reconstructions of the right metacarpus of *P. cookei*. One uses the 'set 1' elements, the other uses 'set 2' elements, and both incorporate the only preserved, undoubted pollical metacarpal of UM 87990. The 'set 1' recontruction is also shown in distal view at left. The angle between the axis of flexion at the distal facet of MC II and MC V is shown, illustrating that the metacarpus supported a convergent hand. Abbreviation: *rt*, radial tubercle for abductor pollicis muscle tendon.

Of the two examples of MC V that are complete, the longer of the two differs from the shorter by 13% (meaning the shorter is 88% of the longer). These proportions match the proportional differences of MC II and III and indicate that the longer MC V is a 'set 2' metacarpal and the shorter MC V is a 'set 1' metacarpal.

UM 87990 includes identical, left and right MC I's, which can be identified to set by comparing their length to the lengths of 'set 1' and 'set 2' MC III and MC V, and by then referencing proportions in other plesiadapids. The length ratio of the MC I to the 'set 1' MC III is 0.57, and the ratio to 'set 1' MC V is 0.73. The proportions to 'set 2' MC III length and MC V length are 0.49 and 0.64, respectively. AMNH 17379 (*N. gidleyi*) has an MC I to MC III length ratio of 0.58, and USNM 442229 (*N. intermedius*) has an MC I length to MC V length ratio of 0.76. These proportions indicate that the MC I's of UM 87990 belongs to the 'set 1' group of metacarpals (assuming it is the MC I of a plesiadapid).

In addition to having absolute length differences, 'set 1' and 'set 2' metacarpals II, III, and V have different shapes to their distal ends (or 'heads'). The heads of 'set 1' are notably shallower in a dorsoventral direction (Table A-II-24; DED/DEW).

Metacarpal I.— The left pollical metacarpal (MC I) is illustrated in Figures 46A and 48. This is unambiguously identified as such by its similarity to the previously described pollical metacarpals of *N. intermedius* USNM 442229 and *N. gidleyi* AMNH 17379 (Beard, 1989, 1990). The proximal end is marked primarily by a dorso-ulnarly facing facet for the trapezium. The facet is convex in longest dimension and slightly concave in its narrowest direction. These two curvatures form a saddle-shaped surface. The proximal end of the bone is much greater in mediolateral dimensions than it is in dorsoventral dimensions. This is due mainly to a pronounced, radially projecting tuberosity. The ulnar side of the bone has a flattened area that is smooth and looks like an articular facet. Beard (1989) interpreted this feature on *Nannodectes* as a point of contact between MC I and MC II; however, these bones do not seem to have actually contacted one another (see trapezium and trapezoid sections above; and Boyer et al., 2013).

The shaft of the pollex (MC I) is absolutely short compared to those of the other metacarpals (Table A-II-24). It is also short relative to its cross-sectional area (Table A-II-24: SSV). The cross-sectional shape of the shaft is more elliptical than that of the other metacarpals. The distal end has three ventral ridges, or keels. The radial side keel is more proximally restricted than the median and ulnar-side keel, contributing to a distal profile that is asymmetrical in the greater slope of the radial side. The distal articular surface is centered over the median and ulnar keels. It extends onto the dorsal side of the distal end where it is hemispherically convex.

Beard (1989) previously described the plesiadapid MC I as having lateral torsion of the distal end. This is also true for MC I of *P. cookei*: the long axis of the proximal facet represents the dorsoventral axis of the articulated hand in certain trapezium postures. In a metacarpal with no torsion, the dorsopalmar axis of the shaft and distal end are aligned with the dorsoventral axis of the proximal facet. However, the dorsoventral axis of MC I is laterally rotated some 45° from the dorsoventral axis. The bone is oriented according to the distal end anatomical planes in Figure 46A and 48. Thus the existence of this torsion can be appreciated by asymmetrical positioning of the proximal end facet in the dorsal view of the bone in Figure 46A.

Metacarpal II.— MC II of metacarpal 'set 1' (Figs. 46B, 48) is represented by the complete bone on the left side and by a fragment of the proximal end of the bone on the right side. The complete metacarpal has a straight shaft that becomes progressively wider mediolaterally from its proximal end to its distal end. This is especially noticeable just beyond the proximal articular surface, because the girth of the shaft increases abruptly there. The proximal articular surface for the trapezoid slopes so that its ulnar edge projects farther proximally than its radial edge. The articular surface for the trapezoid also faces slightly dorsally relative to the metacarpal shaft. The trapezoid facet is saddle-shaped and has a surface area of 7.7 mm^2 (Table A-II-22). The ulnar side of the proximal facet is separated into ventral and dorsal regions. Both regions probably articulated with both MC III (distally) and the capitate (proximally).

The strip of articular surface connecting the dorsal and ventral facets articulated with the capitate. The radial side of the proximal end appears to be devoid of articular facets. Both the radial and ulnar sides of the proximal end are flat, without any substantial convexity or concavity. In ventral view, the distal end has three prominent keels: lateral, medial, and median. The radial side of the distal end profile slopes away from its distal apex more gradually than the ulnar side. In dorsal and lateral view, it can be seen that the distal articular surface extends onto the dorsal side of the element and is hemispherically convex. This hemispherical articular surface is flanked laterally by deep collateral ligament pits. The proximolateral margins of the pits are large tuberosities.

MC II of metacarpal 'set 2' (Fig. 47A) is similar to MC II of 'set 1', just described, but they clearly come from two different individuals (both are left side elements) and from two different species. Differences that distinguish MC II in the two sets include the following: (1) the 'set 2' MC II is a larger, more slender bone (Table A-II-24); (2) the trapezoid facet has a larger surface area of 9.5 mm^2 (Table A-II-22); (3) there appear to be facets on the radial side of the proximal end, possibly for MC I and/or the trapezium; (4) the dorsoventral depth of the 'set 2' MC II head is absolutely and proportionally larger than that of the 'set 1' MC II (Table A-II-24); (5) the 'set 2' MC II shaft is bowed laterally and does not increase in width so continuously or dramatically from proximal to distal; (6) the proximal end trapezoid facet also does not face dorsally to any substantial degree.

Metacarpal III.— MC III of 'set 1' (Figs. 46C, 48) is represented by the complete bone on the right side and by a fragment of the proximal end of the bone on the left side. MC III of 'set 1' is similar to MC II of 'set 1' in many respects.

Points of similarity include the flatness of the radial and ulnar side facets on the proximal end and the overall morphology of the distal end. The two differ in other aspects of proximal end morphology and shaft length (MC III is longer). The ulnar side of the proximal end of MC III does not project so far proximally relative to the radial side as it does in the 'set 1' MC II. There two radial side facets on the proximal end, a dorsal one and ventral one. The dorsal one is larger than the ventral one. The dorsal radial side facet is smaller than the ulnar facet on the 'set 1' MC II with which it likely articulates.

Despite this size difference, the distal margins of the corresponding facets on MC III and MC II match. The smaller, ventrally-located radial-side facet on MC III probably articulated with the ventral facet on the ulnar side of MC II. The ulnar side of MC III has a dorsal facet and ventral facet that match those of the 'set 1' MC IV. Unlike MC II, the proximal end of MC III is mediolaterally wider than the shaft. Specifically, the dorsal radial-side proximal facet projects laterally farther than the shaft just distal to it, and the dorsal ulnar-side facet is flush with the shaft distal to it. The proximal end of the capitate facet has a surface area of 7.1 mm^2 (Table A-II-22).

The 'set 2' MC III is similar to the 'set 1' MC III in many respects (Figs. 46C, 47B). It differs in being a larger and more slender element, and in having an absolutely and proportionally deeper distal end (Table A-II-24). The proximal end also differs in having its radial side facet flush with, instead of flaring beyond, the shaft distal to it. The proximal end capitate facet of the 'set 2' MC III has a surface area of 8.5 mm^2 (Table A-II-22).

Metacarpal IV.— MC IV of 'set 1' (Figs. 46D, 48) is fragmentary and missing its distal end. The proximal end facet for the hamate, like the carpal facets on MC II and III, projects farther proximally on its ulnar side. MC IV differs from MC II and is similar to MC III in having a proximal end that is mediolaterally wider than the shaft just distal to it. However, it is more like the 'set 2', MC III in having the radial side proximal facet flush with the shaft beyond it, whereas the ulnar side proximal facet is more flaring. On the other hand, the 'set 1' MC IV differs from MC III and is actually similar to the 'set 1' MC II in having a carpal facet that faces dorsally relative to its shaft. The radial side proximal facets match the corresponding ulnar side facets on the 'set 1' MC III perfectly, indicating that the two bones articulated. The ulnar side of the proximal end of MC IV is concave, unlike those of MC II's and III's, which are flat.

Furthermore, the ulnar side facet is not differentiated as distinctly into dorsal and ventral regions. The dorsal part of the ulnar side facet is elliptical in outline, similar to the dorsal proximal facets on other metacarpals, but the ventral extension of this facet is proximodistally proportionally thicker than in the other metacarpals. Finally, MC IV differs from MC II and III in having a shaft that bows slightly ulnarly instead of radially. The proximal end hamate facet of MC IV has a surface area of 6.8 mm^2 (Table A-II-22).

The 'set 2' MC IV is represented by complete right and left side elements (Fig. 47C). They are essentially similar to the 'set 1' MC IV, but differ in being slightly larger and apparently more slender. The proximal end hamate facet of the 'set 2' MC IV has a surface area of 8.5 mm^2 (Table A-II-22). The bone is similar to the other 'set 2' metacarpals in having a dorsoventrally deep distal end. It differs from the 'set 2' MC III in being slightly longer, indicating an ectaxonic metacarpal pattern. Additionally, the mediolateral asymmetry of the head is mirrored compared to MC II and III of both sets (i.e., the ulnar side of the distal end is more gradually sloping than the radial side).

Metacarpal V.— The 'set 1' MC V is similar to the other 'set 1' metacarpals in the proportional dorsoventral depth of its distal end (Fig. 46E; Table A-II-24). It is further similar to other described metacarpals (of both sets) in most aspects of the distal end morphology (i.e., spherical shape of the dorsal aspect of the distal articular facet, presence of pits for collateral ligaments with tuberosities flanking these pits). Although identification of the other metacarpal positions is relatively straightforward, bones with morphology nearly identical to that described here as MC V were previously described as MC II by Beard (1989, 1990) and Godinot and Beard (1991) for both *N. intermedius* and *P. tricuspidens*. However, Boyer et al. (2013) present evidence suggesting alternative interpretations. We follow Boyer et al. (2013) here.

The 'set 1' MC V (Fig. 46E) proximal end is distinct in having a hamate facet that is dorsoventrally convex with a large amount of its surface facing dorsally relative to the shaft. The hamate facet has a surface area of 6.0 mm^2 (Table A-II-22). The radial-side facet of the proximal end faces slightly proximally as it arcs from the dorsal aspect of the bone to the ventral aspect. Taken as a whole, this arcing, proximally-facing facet is slightly convex. This convexity matches the concavity on the ulnar facet of MC IV. The ulnar side of MC V does not appear to have any distinctive facets, although Beard (1989, 1990) described and illustrated it as having an articulation with MC I in *N. intermedius* USNM 442229.

The 'set 1' MC V shaft narrows distal to the facets of the proximal end and then broadens dramatically as it approaches the distal end. More specifically, this MC V is distinctive among other metacarpals and the 'set 2' MC V in that the ulnar margin of the distal end of the shaft flares much more than the radial margin. The asymmetry of the head of MC V is similar to that of MC IV in being opposite the asymmetry of MC II and III. The asymmetry of the head of MC V differs from that in MC IV in being even more pronounced. The distal end of MC V shows torsion relative to the proximal end, so that its ventral surface faces slightly radially. The 'set 2' MC V is represented by the complete right side element and the proximal end of the left (Figs. 47D, 48). It is similar to the 'set 1' MC V (Fig. 48). The two bones differ in that the 'set 2' MC V is longer and more slender, it has a larger surface area for the hamate (7.5 mm^2; Table A-II-22), it does not show the dramatic ulnar flaring of the distal part of the shaft; and it does not show the extreme asymmetry in the distal end profile.

Metacarpal attribution.— The metacarpals of UM 87990 cannot all belong to one individual animal, and two forms are represented at most metacarpal positions. We are confident

of our association of metacarpals into the two sets recognized here, but attribution of one or the other set of metacarpals to *P. cookei* is more difficult.

We first attempted to resolve this by comparing the areas of articular surfaces of the distal carpals to corresponding articular surfaces of the proximal metacarpals (Table A-II-22). This comparison indicates that there is a closer correspondence between the distal carpals and 'set 1' metacarpals than between the distal carpals and 'set 2' metacarpals. The problem with this comparison is that the capitate distal facet is reconstructed, and the trapezoid and hamate are only tentatively referred to *P. cookei* (Boyer et al., 2013).

We then attempted to determine whether 'set 1' or 'set 2' metacarpals belong to *P. cookei* using multivariate comparisons of metacarpal measurements (Table A-II-24), and univariate comparisons of metacarpal shape variables (Table A-II-25).

In panels A and B of Figure 49, the 'set 2' MC III of *P. cookei* is closer to *P. tricuspidens* as a model than is the 'set 1' MC III. The opposite is true in panels C and D, where the 'set 1' MC III of *P. cookei* is closer to the model than is the 'set 2' MC III. The result depends on how the measurements are scaled in tables A-II-24 or A-II-25, and there is no clear reason to prefer one over the other.

In panels A and B of Figure 49, the 'set 1' MC V of *P. cookei* is closer to *P. tricuspidens* as a model than is the 'set 2' MC V. The opposite is true in panels C and D, where the 'set 2' MC V of *P. cookei* is closer to the average for MC V of *P. tricuspidens* than is the 'set 1' MC V. Here again the result depends on how the measurements are scaled. Adding to the uncertainty, MC V links 'set 1' metacarpals to *P. tricuspidens* and hence to *Plesiadapis*, whereas MC III links 'set 2' metacarpals to *P. tricuspidens* and hence to *Plesiadapis*.

The key to metacarpal attribution appears to be metacarpal head shape, based on the head shape variable HSV of Table A-II-24. Ln HSV values are plotted for each of the species preserving measurable metacarpals in Figure 50, where filled triangles represent MC I, filled circles represent MC II–IV, and filled diamonds represent MC V. The heads of MC I are the narrowest and have the lowest HSV values, at or below the HSV values for MC II–IV (lighter shading in Fig. 50). Heads of MC V are consistently wider than those of MC I and are high (darker shading) in the HSV range for MC II–IV.

The HSV value for MC I in UM 87990 'set 1' is higher than those for *N. intermedius* and *N. gidleyi*, but similarly near the lower end of the range for MC II–IV. MC I is not preserved in UM 87990 'set 2' metacarpals nor in *P. tricuspidens*. The HSV values for MC II–IV metacarpals in 'set 1' are much closer to the ranges of these values for MC II–IV in *P. tricuspidens*, *N. intermedius*, and *N. gidleyi* than are the HSV values for MC II–IV in the 'set 2' metacarpals. Similarly, the HSV value for MC V in 'set 1' is much closer to the ranges of these values for MC V in *P. tricuspidens* and *N. intermedius* than is the HSV value for MC V in the 'set 2' metacarpals. The differences are illustrated by arrows in Figure 50.

Boyer et al. (2013) regarded 'set 1' MC I and V as representing *P. cookei* with 'reasonable certainty.' Here we go farther and, on the basis of head shape, regard all of the UM 87990 'set 1' metacarpals as representing *P. cookei*. A conservative approach, pending discovery of hands unambiguously associated with *P. cookei* teeth, would be to include both sets of UM 87990 metacarpals, 'set 1' and 'set 2', in any future analysis of the hand of *Plesiadapis*.

A final piece of evidence arguing for the attribution of all 'set 1' metacarpals to *P. cookei* is the proportional length differences between MC I and V compared to the other metacarpals. Specifically, MC I/MC III and MC I/MC V ratios match those of *Nannodectes* species best when only 'set 1' bones are used.

Proximal phalanges

Phalanges of the hand and foot of UM 87990 can only be distinguished by comparing them directly, and hence all are described here together.

Proximal phalanx I.— Three elements referable to proximal phalanx I are preserved. These include proximal bases of what appear to be both hallucal proximal phalanges (one is illustrated in Fig. 51A), and a third fragmentary base and shaft of the left pollical proximal phalanx. The elements are too fragmentary for meaningful quantification of their morphology, although a few measurements are given in Table A-II-26. The bones are recognizable by comparison to previously identified proximal first phalanges of *P. tricuspidens* and *N. intermedius* (Beard, 1989). Hallucal and pollical elements are distinguished here for the first time based on the much larger size of the hallucal elements. The proximal end of this bone is distinct among the proximal phalanx sample in the asymmetry of tubercles that flank and extend ventral to the proximal articular surface. The medial side tubercle is blunt and proximally restricted, and the lateral side tubercle is pointed and proximally extended beyond its partner (Fig. 51A). The shaft of the pollical element is also distinct among the proximal phalanges of the sample in being strongly dorsally curved, in having a more triangular cross-section and a more dramatic difference between the proximal and distal end shaft diameters.

Comparisons.— The proximal phalanx of the first digit is preserved in *P. tricuspidens, N. intermedius*, and *N. gidleyi* (Table A-II-26). The right and left elements of *N. intermedius* and *P. tricuspidens* are almost identical in their proportions. However, that of *N. gidleyi*, though fitting the description of this element generally and being roughly the same length as that of *N. intermedius*, is much more slender (*N. intermedius* SSV = 1.57, *N. gidleyi* SSV = 1.79, *P. tricuspidens* SSV = 1.60: see Table A-II-26). The *N. gidleyi* element also has smaller proximal and distal ends than those of *N. intermedius*. The more robust versions of these bones seem likely to represent pedal elements.

Proximal phalanges II to V.— The other 11 preserved proximal phalanges are fairly similar to each other in most respects (Figs. 51, 52). The morphological differences that do exist may reflect differences between manual and pedal elements. Previous postcranial associations for *P. tricuspidens*, *N. intermedius* (Beard, 1989), and other plesiadapiforms (Bloch and Boyer, 2007; Boyer and Bloch, 2008) suggest that the manual phalanges are shorter than the pedal elements (as is typical for most mammals). Two of the complete phalanges

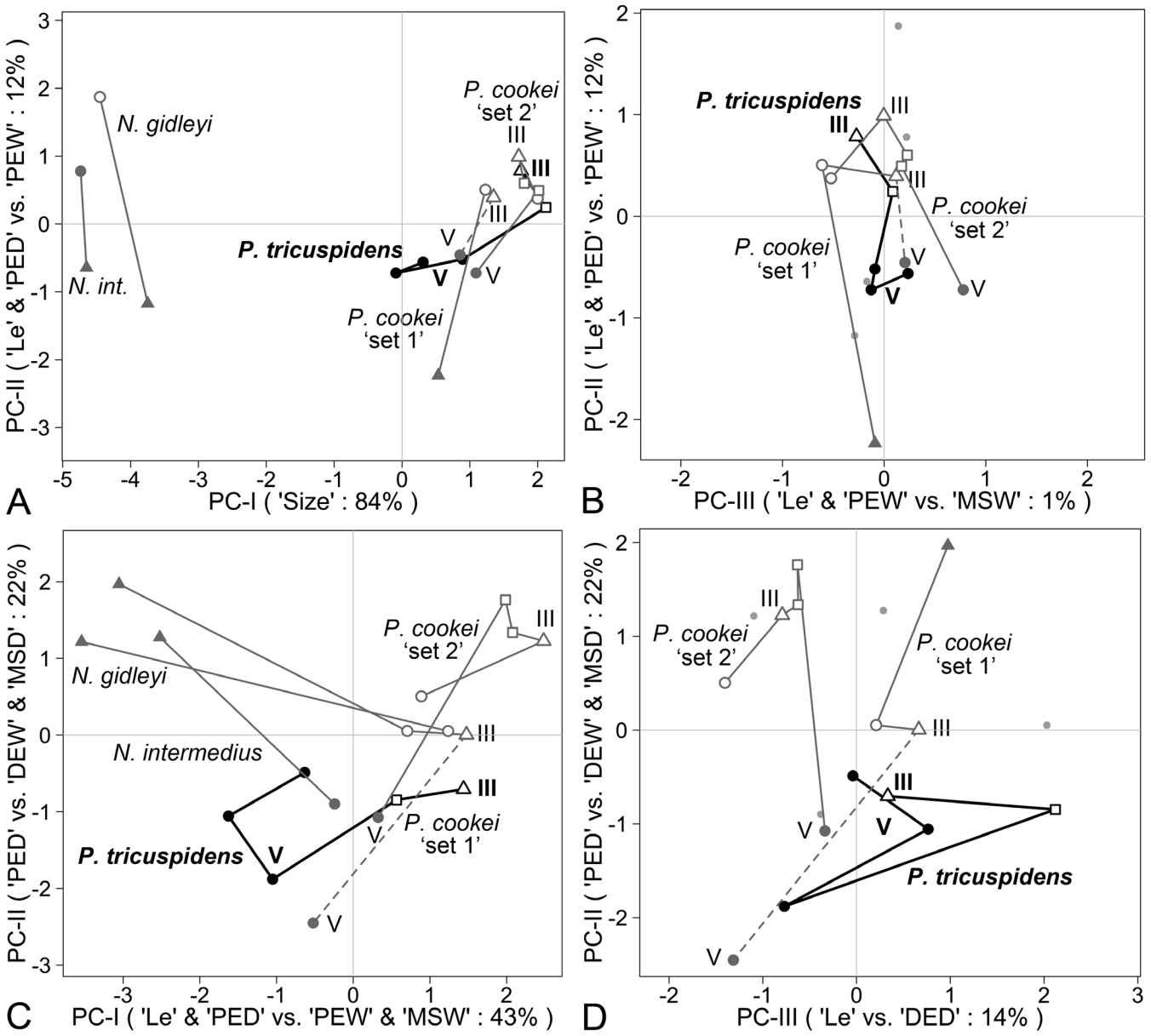

FIGURE 49.— Principal components analysis of metacarpal size and shape. Lines connect metacarpals of the same individual or set. *Plesiadapis tricuspidens* is highlighted in bold as a model. Symbols are: MC I, solid triangle; MC II, open circle; MC III open triangle; MC IV, open square; and MC V, solid circle. Panels A and B are based on measurements in Table A-II-24, and panels C and D are based on shape variables expressed as proportional differences in Tale A-II-25. **A**, plot of PC-I on the abscissa, including 84% of total variance and expressing size, versus PC-II on the ordinate, including 12% of total variance and contrasting metacarpal length and proximal end depth versus proximal end width. **B**, plot of PC-III, including 1% of total variance and contrasting metacarpal length and proximal end width compared to midshaft width, versus PC-II, including 12% of total variance and contrasting metacarpal length and proximal end depth compared to proximal end width. **C**, plot of PC-I on the abscissa, including 43% of total variance and contrasting metacarpal length and proximal end depth compared to proximal end width and midshaft width, versus PC-II on the ordinate, including 22% of total variance and contrasting proximal end depth compared to distal end width and midshaft depth. **D**, plot of PC-III, including 14% of total variance and contrasting metacarpal length compared to distal end depth, versus PC-II, including 22% of total variance and contrasting proximal end depth compared to distal end width and midshaft depth. Note that in panels A and B, MC III of UM 87990 'set 2' is closer to the model than is MC III of UM 87990 'set 1,' whereas in panels C and D, MC III of UM 87990 'set 1' is closer to the model than is MC III of UM 87990 'set 2.' However, in panels A and B, MC V of UM 87990 'set 1' is closer to the model than is MC V of UM 87990 'set 2,' whereas in panels C and D the MC V of UM 87990 'set 2' is closer to the average for the three examples of *P. tricuspidens* MC V than is MC V of UM 87990 'set 1.' See Figure 50 for a simpler and more convincing identification of UM 87990 metacarpals.

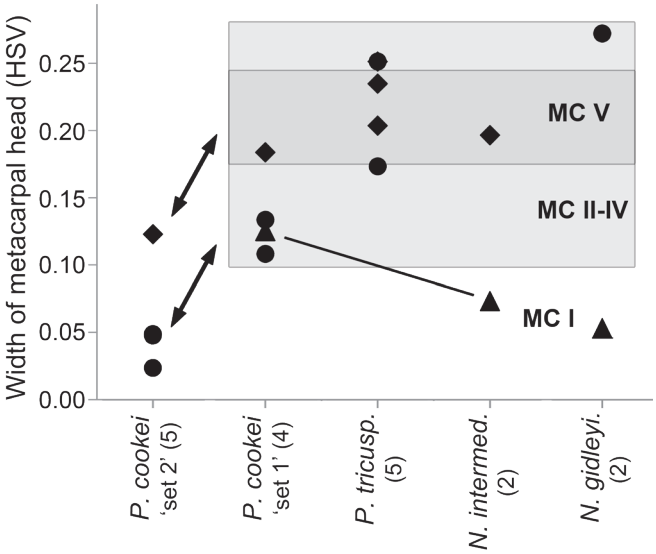

FIGURE 50.— Comparison of metacarpal head shapes in plesiadapids. The head-shape variable plotted here is HSV, where HSV = ln (DEW / DED), DEW is distal mediolateral width, and DED is distal dorsoventral depth (Table A-II-24). Metacarpals MC I are represented by triangles; MC II–IV by circles, and MC V by diamonds. Note that metacarpal heads of plesiadapids, including the UM 87990 'set 1' metacarpals attributed to *P. cookei*, are relatively wide compared to their depth (HSV value is high). UM 87990 'set 2' metacarpals have lower HSV values (arrows) than expected for homologous metacarpals of a plesiadapid. Head shape provides the strongest evidence that metacarpals of 'set 1' belong to *P. cookei*. UM 87990 'set 2' MC II–V with narrower heads probably belong to *Uintacyon rudis*.

preserved in UM 87990 are distinctly shorter than the remaining four (Table A-II-26). The two shorter phalanges also appear to be more dorsoventrally curved, to have stouter shaft diameters for their length, and to have absolutely and proportionally shallower dorsoventral dimensions of the proximal and distal ends. Natural logarithm shape ratios constructed to quantify these differences show that among the *P. cookei* sample, as well as among other plesiadapids, the more robust, shorter proximal phalanges probably belong to the hand (have a greater SSV: Table A-II-26). However, the dorsoventral dimensions of the proximal and distal ends to not appear to consistently differentiate proximal phalanges into manual and pedal groups (BSV and HSV: Table A-II-26).

In general, all proximal phalanges have a proximal articular surface that is spherically concave. Relative to the shaft, the proximal articular surface faces proximally and slightly dorsally. A pair of tubercles flanks the proximal articular surface laterally and extends proximoventrally. These tubercles are usually asymmetrical, with one being larger, blunter, and extending farther proximally than the other. Distal to the proximal end, the shaft first narrows mediolaterally to near its midpoint and then widens slightly just proximal to the distal articular surface. The dorsoventral dimensions of the shaft tend to decrease continuously from the proximal to distal end. Often times the shaft curves away from the side with the larger proximal tubercle. The ventral surface of the shaft is usually marked by prominent flexor sheath ridges. Although these ridges are impressive in covering almost the entire length of the shaft, they are subtle in their ventral projection. Their presence is more distinctly highlighted by the groove formed where they meet the ventral surface of the shaft (Figs. 51 and 52).

The distal articular surfaces of the proximal phalanges are distinctive in having two longitudinal grooves that separate three trochleae, as can be seen in ventral and distal views of these bones. The lateral trochleae are mediolaterally narrower than the median one. They also tend to have a larger radius of curvature. One of the lateral trochleae is usually larger, or projects farther distally than the other. Typically, this larger trochlea is on the opposite side of the larger, blunt proximal tubercle. As can be seen in lateral and dorsal views, the distal articular surface has its largest radius of curvature on its ventral aspect, a narrower one distally, and almost no expression of the distal articular surface on its dorsal aspect. The lateral aspects of the distal end are pitted for collateral ligaments.

Comparions.— Compared to other plesiadapids, the proximal phalanges of *P. cookei* cannot be shown to differ in any easily quantifiable fashion. Smaller *Nannodectes* species seem to exhibit less pronounced lateral trochleae on the distal articular surfaces and to have proportionally slightly wider shafts. Some of the proximal phalanges from the French Berru locality have prominent ventrally projecting flexor sheath ridges (e.g., MNHN R 503; MNHN unnumbered 'Divers coll.' specimen: see Table A-II-26). Although they are identified as plesidapids, this noted morphologic difference makes them more like known paromomyid plesiadapiforms (Beard, 1989; Boyer and Bloch, 2008).

Intermediate phalanges

Seven intermediate phalanges are included in UM 87990 (Fig. 53; Table A-II-27). Four of these are complete. As for the lateral proximal phalanges, these elements are all generally similar except with regard to a few features that may reflect differences between bones of the hand and foot. Previous studies (Beard, 1989; Bloch and Boyer, 2007; Boyer and Bloch, 2008) suggested that the manual elements are shorter. Although only one of the intermediate phalanges identified as a manual element can be measured for its total length (Fig. 53; Table A-II-27), three others are complete enough to indicate that they would have been much shorter than three others identified as pedal elements. These shorter elements, identified as belonging to the hand, also appear to have smaller midshaft dimensions and to have proximal ends that are proportionally smaller in their dorsventral dimensions.

Natural logarithm shape ratios constructed to quantify these differences show that within the *P. cookei* sample, as well as among other plesiadapids, the more robust, and shorter intermediate phalanges also have slightly shallower dorsoventral dimensions of the proximal end (have a greater SSV, and lower BSV, respectively: Table A-II-27), and are probably from the hand. Unfortunately, the dorsoventral dimensions of

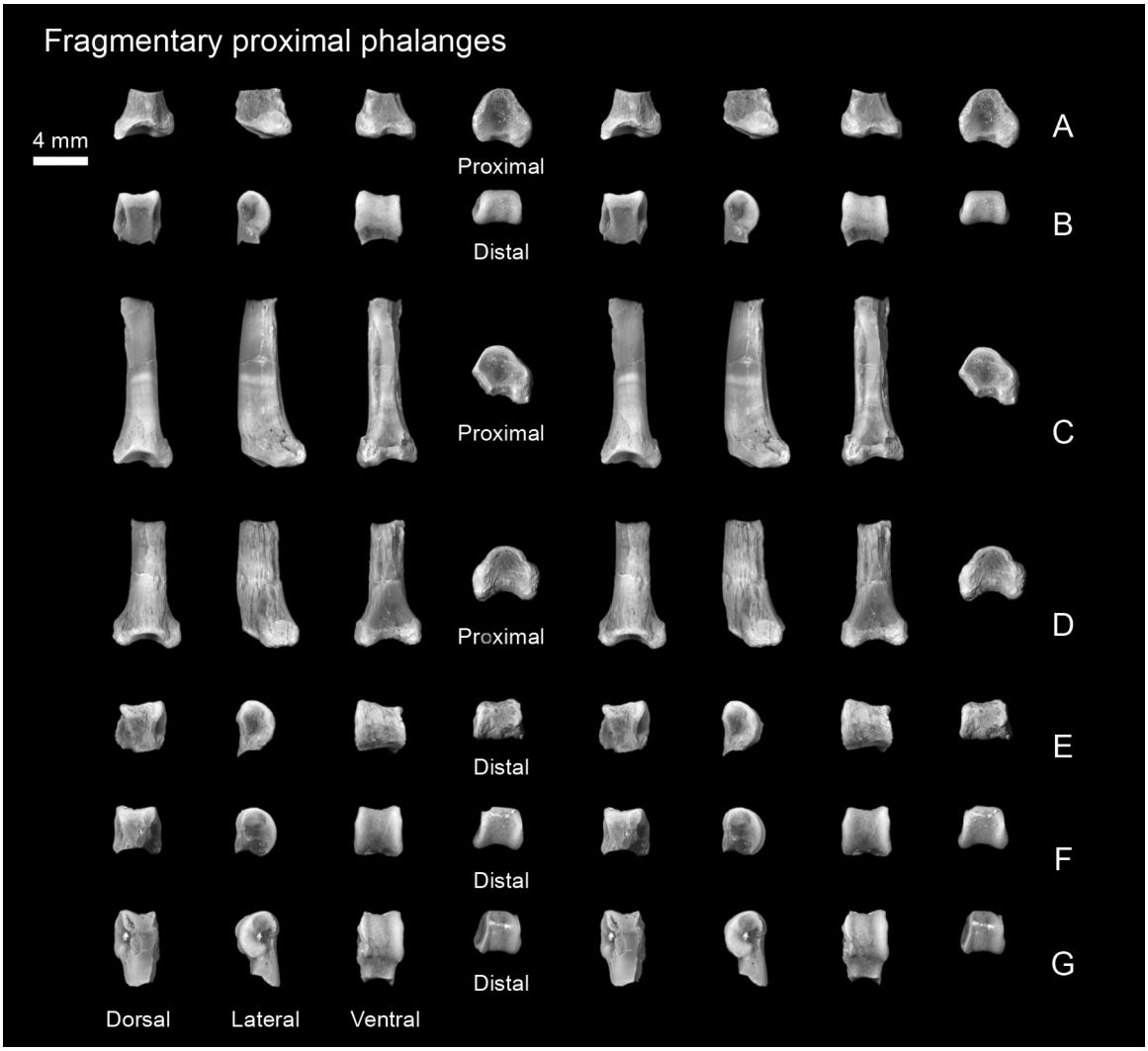

FIGURE 51.— Incomplete proximal phalanges of *Plesiadapis cookei* (UM 87990). Stereophotographs of incomplete proximal phalanges. **A**, proximal end of the proximal phalanx of a left hallux. **B**, distal end of a proximal phalanx. **C–D**, proximal ends of proximal phalanges. **E–G**, distal ends of proximal phalanges. All are shown in dorsal, lateral, ventral, and distal or proximal views. Also preserved are a proximal fragment of the proximal phalanx of a right hallux, and the badly eroded shaft of what may be the proximal phalanx of a pollex.

the proximal and distal ends cannot be used in a similar manner to differentiate proximal phalanges into manual and pedal groups (BSV and HSV: Table A-II-27).

Intermediate phalanges generally have a cylindrically concave proximal articular surface. This surface is often marked by three longitudinal (dorsoventral) grooves that fit the three trochleae of the proximal phalanges. The dorsal and ventral margins extend proximally roughly equal distances relative to the proximodistal axis of the shaft. However, the ventral margin is usually slightly more proximally projecting, which makes the proximal articular surface face slightly dorsally, relative to the shaft axis. The proximal end is usually slightly greater in its dorsoventral depth than its proximodistal width, with a couple of exceptions for certain manual elements.

The ventral surface is marked by prominent tubercles that project ventrally. These appear to be either the flexor sheath tubercles or insertion points for the flexor digitorum superficialis tendons. Beyond the proximal end, the shaft shape is similar to that of proximal phalanges, narrowing in its mediolateral dimension until roughly the proximodistal midpoint of the shaft, and narrowing in its dorsoventral dimension for the entire length of the shaft.

For much of the shaft length, the dorsoventral dimension is greater than the mediolateral dimension. The shafts are essentially straight, except for the three longest (probably pedal) elements, which show a slight amount of dorsal convexity (Boyer and Bloch, 2008). The distal ends of the intermediate phalanges have a single groove down the center

of their distal articular surface, rather than two grooves as seen in the proximal phalanges. In lateral profile it can be seen that distal articular surface has a fairly constant radius of curvature and ~180° of arc to it, although one phalanx (Fig. 53G) appears to have well over 180°. The articular surfaces, seen in dorsal and lateral view, have a greater amount of ventral-facing area than dorsal-facing area, although they are not as restricted in the amount of dorsal area as the proximal phalanx distal articular facets.

Comparisons.— The intermediate phalanges of *P. cookei* differ substantially from other plesiadapids in their proximal end dimensions (Table A-II-27: BSV). The dorsoventral depth of the proximal end is greater relative to its mediolateral width than for other sampled plesiadapids as well as many extant arboreal mammals (Boyer and Bloch, 2008). Boyer and Bloch (2008) showed extant taxa that use their phalanges for antipronograde, or suspensory activities (including *Cynocephalus*, *Daubentonia*, bats, and sloths) to share this feature with *P. cookei* and to a lesser degree with *P. tricuspidens*.

Distal phalanges

Ten distal phalanges are preserved in UM 87990, of which three are virtually complete (Fig. 54, Table A-II-28). These phalanges are all distinctly falciform (Koenigswald et al., 2012) and quite similar to each other. There is no morphological basis for distinguishing manual and pedal claws. There are, however, two phalanges in the sample (Fig. 54A, D) that appear similar to one another and different from the others. They have a mediolaterally wider flexor tubercle with two processes that project proximally from the lateral aspects of the proximal margin. If there is any significance to this distinctive morphology, it may be that these two phalanges represent first (preaxial) digits.

The distal phalanges can be described as relatively large, 'hook-like' claws with narrow shafts and pronounced flexor tubercles. More specifically, the proximal articular surface is much higher dorsoventrally than it is wide mediolaterally. It is marked by a central ridge, which meets the central groove of the corresponding distal facet on the intermediate phalanges. Dorsal to the proximal articular surface is a vertically expanded area for insertion of the extensor tendon (the extensor tubercle). Ventral to the proximal articular surface is another larger vertically expanded area, possibly for contact with a distal sesamoid. Distal to this, on the ventral surface of the claw, are two nutrient foramina, positioned side by side with a thin rod of bone separating them. Distal to these foramina is the flexor tubercle.

The flexor tubercle is usually slightly longer proximodistally than it is wide mediolaterally, and its mediolateral width is typically greater than that of the claw shaft to which it attaches. The ventral surface of the flexor tubercle is typically separated proximodistally into three regions. The most proximal part is flat to slightly convex, continuous with the rod-like bony process separating the nutrient foramina, and faces slightly proximally. The middle part of the flexor tubercle can be further subdivided into right and left pits. These pits face ventrally to slightly proximally. They presumably represent the actual attachment points for the flexor digitorum longus tendon. Finally, the third, distal part of the flexor tubercle is strongly convex. The proximal end of the third part faces ventrally, and the distal part faces distally.

Distal to the flexor tubercle, the ventral margin of the claw shaft arches first dorsally and then strongly ventrally. The tip of the claw shaft is usually more ventrally situated than the ventral margin of the flexor tubercle. The dorsal surface of the claw, as viewed laterally, is slightly concave between the extensor tubercle and the main shaft. Otherwise, the shaft is smoothly convex for its entire length. The proportionally great lengths of the claw shafts obscure the fact that they are also quite deep dorsoventrally. This point is best appreciated by looking at the claw in dorsal or ventral view, so that its mediolateral narrowness can be seen.

Comparisons.— *P. cookei* has the deepest and narrowest claws, on average, compared to those of other plesiadapids (Table A-II-28). Means of the claw shape variable (CSV), representing claw depth relative to width, are 1.07, 0.95, 1.00, 0.84, and 0.89 for the five species *P. cookei*, *P. tricuspidens*, *P. churchilli*, *N. intermedius*, and *Pr. gaoi*. An analysis of variance of CSV for the five species showed that there are significant differences between groups (ANOVA with $df = 23$, $F = 4.942$, and $p = 0.007$). Deeper and narrower claws in *P. cookei* compared to those in other plesiadapids are consistent with the idea that *P. cookei* was more of a commited arborealist and less scansorial than the other plesiadapids (Bloch and Boyer, 2007). Claws of *P. churchilli* on the other hand are significantly wider and shallower than those of *P. cookei* ($p = 0.003$). The one claw of *Pr. gaoi* is also relatively wide, like those of *P. churchilli*, and looks more like a claw of a scansorial mammal.

Digit proportions

Digit proportions can be described using the phalangeal index, the ratio of the sum of the lengths of the intermediate and proximal phalanges to the length of the metacarpal of the third digit ray (Hamrick 2001; Kirk et al. 2008). Depending on which set of metacarpals is used, the value of *P. cookei* is estimated to have a combined length of the intermediate and proximal phalanges that is 130% the length of the third metacarpal for 'set 1', or 108% the length of the third metacarpal for 'set 2'. Previous studies have computed the value for UM 87990 using 'set 2'.

Comparisons.— *N. intermedius* and *N. gidleyi* have combined lengths of intermediate and proximal phalanges that are about 130% the length of the third metacarpal (Kirk et al. 2008), and *P. insignis* (an articulated specimen: see Gingerich, 1976: 141, pl. 12) is estimated at 140%. These values are similar to the estimate for *P. cookei* based on 'set 1' metacarpals. The phalangeal index value for *P. tricuspidens* (Tables A-II-24, A-II-26, and A-II-27) is estimated at ~111%, closer to the estimate for *P. cookei* based on 'set 2' metacarpals.

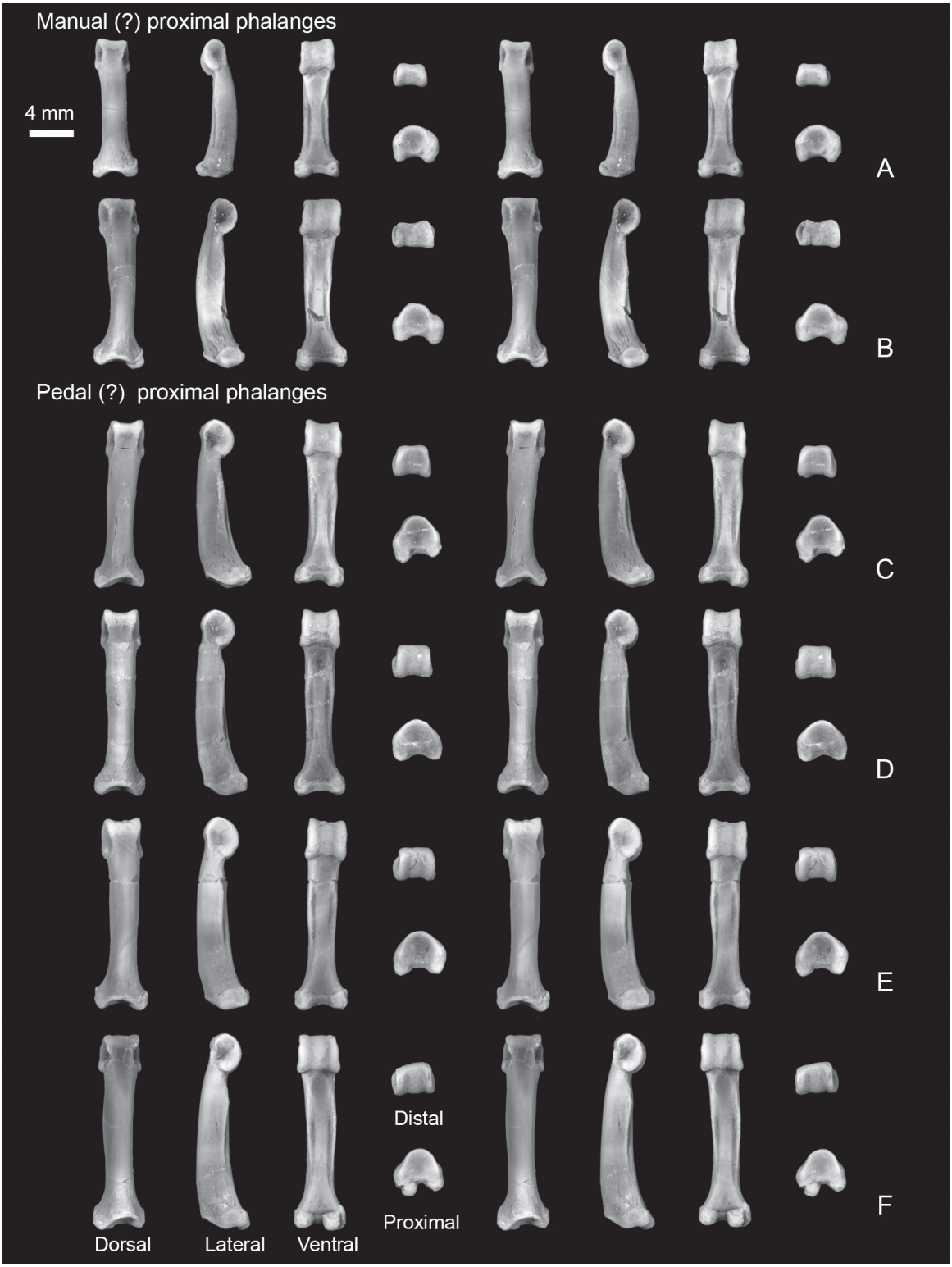

FIGURE 52.— Complete proximal phalanges of *Plesiadapis cookei* (UM 87990). Stereophotographs. **A–B**, possible manual proximal phalanges. **C–F**, possible pedal proximal phalanges. All are shown in dorsal, lateral, ventral, distal, and proximal views.

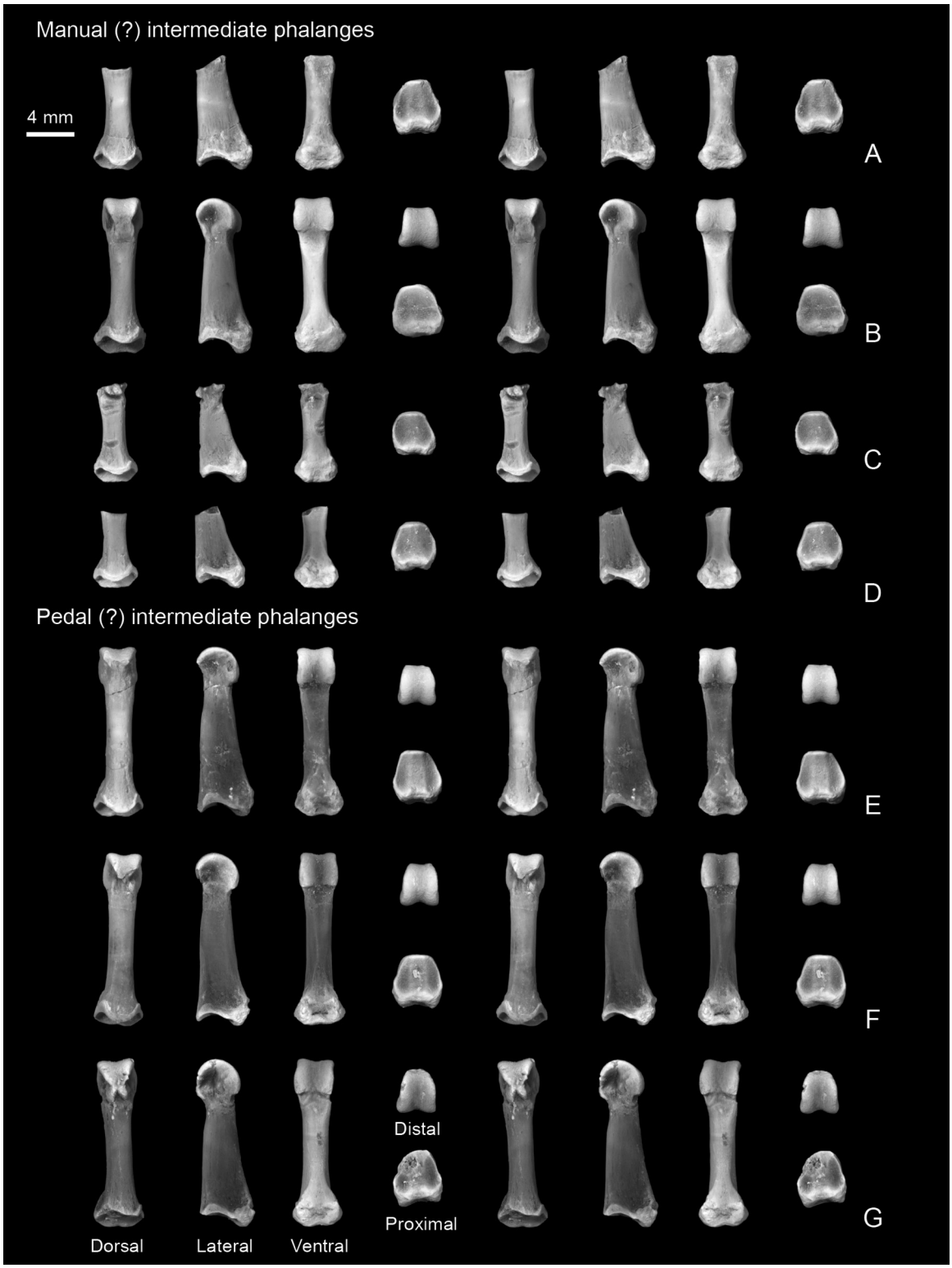

FIGURE 53.— Intermediate phalanges of *Plesiadapis cookei* (UM 87990). Stereophotographs. **A–D**, Possible manual intermediate phalanges. **E–G**, Possible pedal intermediate phalanges. All are shown in dorsal, lateral, ventral, distal, and proximal views.

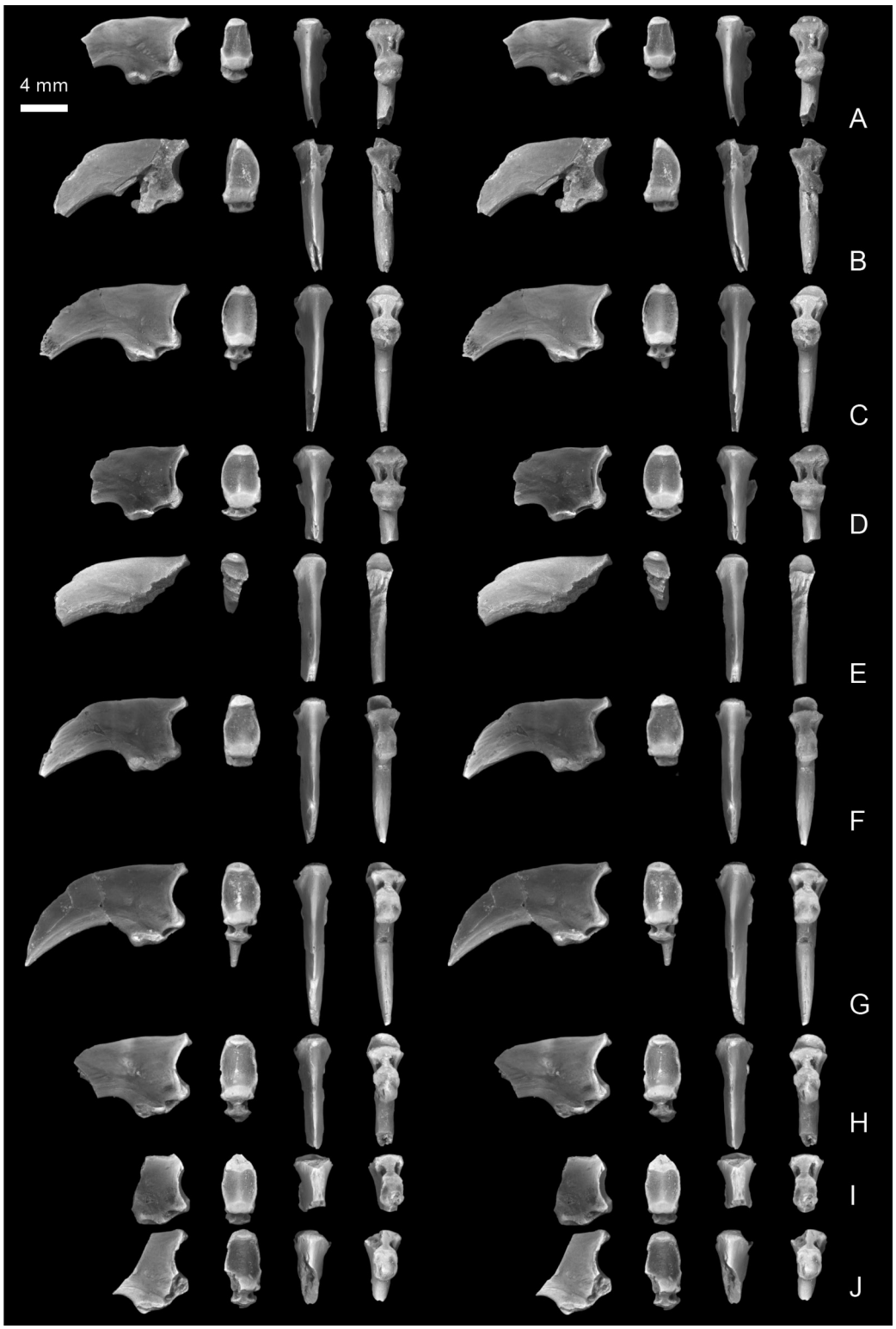

FIGURE 54.— Distal phalanges of *Plesiadapis cookei* (UM 87990). Stereophotographs. All are shown in lateral, proximal, dorsal, and ventral views. Note the narrow width and great depth of all distal phalanges relative to their length.

Pelvic girdle and hind limb

Innominate

Both innominates of UM 87990 are preserved (Fig. 55; Table A-II-29). Both are slightly broken and distorted in different ways, but consideration of both sides allows a view of the complete element. The ilium is the longest of the three bones comprising the innominate. It forms the superior margin of the acetabulum and then tapers in its cross-sectional dimensions superiorly. Moving superiorly from the acetabular area, the posterior margin begins to flare as the posterior inferior iliac spine is reached. This is also the beginning of a roughened facet for the ala of the sacrum, the auricular facet. The anterior surface also flares slightly as the auricular facet is approached, but there is no distinct spine associated with its beginning. A sharp crest runs superoinferiorly separating the posterior and anterior surfaces of the ilial shaft. The crest starts posterior to a small raised roughened area, just superior to the acetabulum (where the anterior inferior iliac spine would be) and runs to the anterior superior iliac spine at the superior tip of the iliac blade. This crest thus separates the gluteal surface of the iliac crest (posteriorly) from the iliacus surface (George, 1977). Starting at the posterior inferior iliac spine the gluteal surface becomes anteroposteriorly wider as it is followed to the superior margin of the blade, and the iliacus surface narrows slightly.

The lunate facet of the acetabulum is typical in its form, with a gap that opens anteroinferiorly toward the obturator foramen. The sutures between the different bones of the innominate are barely visible, but it can be seen that the ischium forms the longest arc of the lunate facet (~10.5 mm), the ilium continues the facet for a slightly shorter distance (~9.7 mm), and the pubis has the shortest contribution (~6.1 mm). The acetabulum appears to have fairly shallow margins. Superior buttressing of the acetabulum is evident (note that other authors refer to this as 'cranial buttressing': e.g., Beard 1989). The anteroposterior dimension of the acetabulum is roughly equal to its superoinferior dimension. Therefore, the acetabulum has a circular, rather than elliptical, outline.

The superior pubic ramus forms an angle of ~150º with the ilium. Its anterior margin is slightly convex at the level of the acetabulum. At the apex of this convexity, the ramus

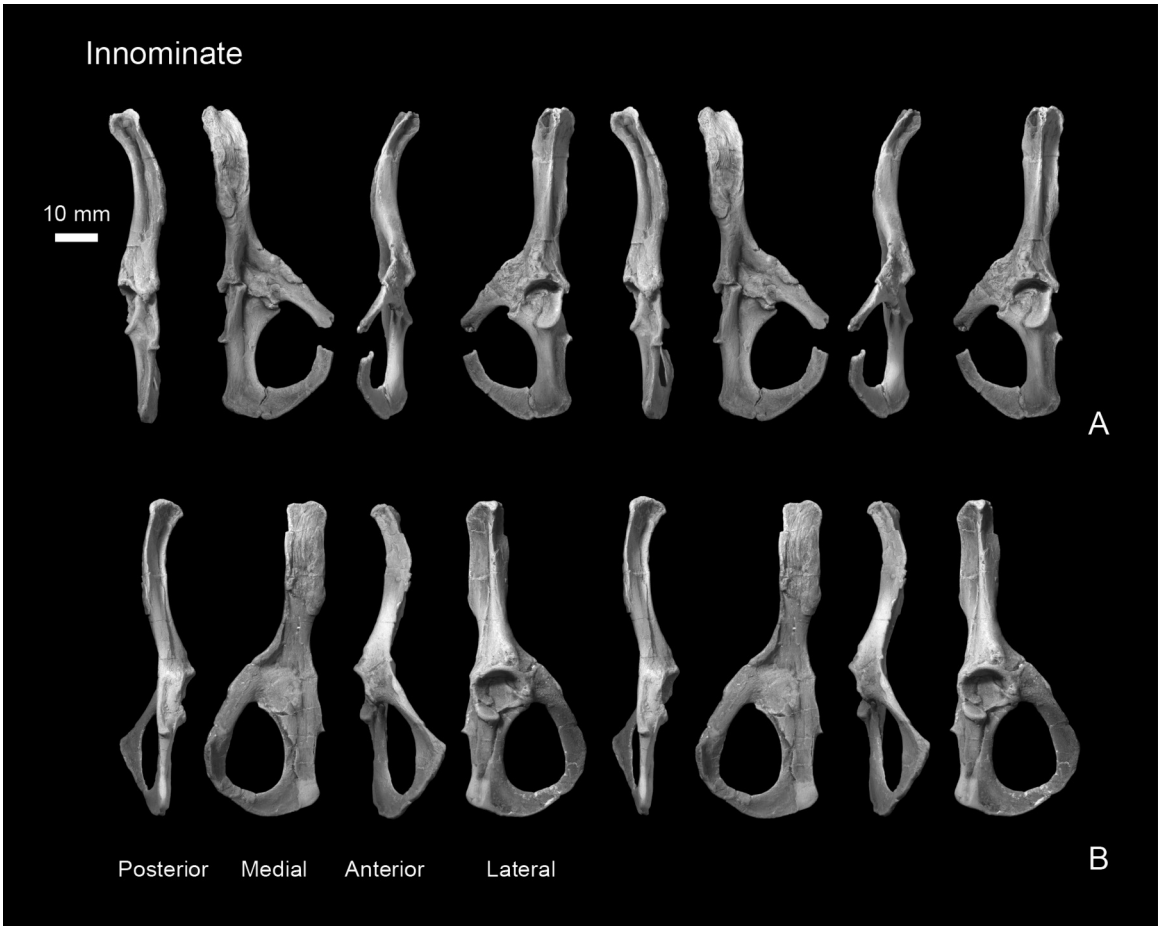

FIGURE 55.— Innominates of *Plesiadapis cookei* (UM 87990). Stereophotographs. **A**, left innominate. **B**, right innominate. Both are shown in posterior, medial, anterior, and lateral views. Note that the tip of the right ischial tuberosity is reconstructed.

flares mediolaterally, creating a broad attachment area for the pectineus muscle that is ~13 mm long, or a little less than two-thirds the total length of the superior pubic ramus. A ridge projects anteriorly from the inferior margin of the pubic portion of the acetabulum and then arcs inferiorly to follow the pubic ramus. The external surface of the ramus is concave posterior to this ridge. The ridge forms the rim of a depression encircling the obturator foramen. The obturator externus muscle probably occupied this depression.

Because of the large angle formed between the ilium and pubic ramus, the pubic symphysis ends up forming quite far posteriorly and is quite short superoinferiorly. It is situated ~6 mm inferior to the level of the ischial spine. The superior pubic ramus is wider anteromedially than it is posterolaterally. Its inferior border (forming the edge of the obturator foramen) diverges from the superior border dramatically and reaches the level of the inferior margin of the pubic symphysis. The segment of pubis (or ischium) just inferior to the pubic symphysis is the narrowest segment of the bone forming the rim of the obturator foramen.

The ischial ramus is fairly straight. It is just a little over half the length of the ilium. The posterior surface of the ramus is convex until the ischial spine is reached at about 2 mm below the inferior margin of the acetabulum. The posterior surface is then concave until it peaks at the ischial tuberosity. The tuberosity is narrow mediolaterally. The ridge forming the edge of attachment area for the obturator externus muscle crosses from the inferior margin of the ischial tuberosity to the anterior margin of the ischial ramus.

Comparisons.— The innominate of *P. cookei* does not appear to differ very much from those known for other plesiadapids. However, these other specimens are not very complete. Nevertheless, some relevant observations can be made from the available material. The known innominate fragments of *P. tricuspidens* are larger than those of *P. cookei* (Table A-II-29). This is interesting considering that most of the known forelimb elements are roughly the same size in the two species, with those of the *P. cookei* specimen usually exhibiting greater proximodistal lengths.

The acetabula of all specimens show some cranial buttressing. The acetabulum of *N. gidleyi* appears to be more elliptical and less circular in outline than acetabula of *P. tricuspidens* and *P. cookei* (although the acetabula of *N. gidleyi* exhibit damage that make them unmeasurable). Another point of interest in the three innominates of *N. gidleyi* is the much more distal positioning of the ischial spine, relative to acetabular dimensions (Table A-II-29: IspV). Thus, in *N. gidleyi,* the obturator internus muscle had a greater component of force directed inferiorly. This muscle could therefore contribute more to flexion of the limb than it could in the other taxa.

Femur

Both femora of UM 87990 are preserved (Fig. 56; Tables A-II-30 to A-II-32). The left element is in better condition. The right element is missing the apophysis of the greater trochanter, has a noticeably displaced proximal epiphysis, and has a crushed distal shaft segment.

The femur is slender and straight with a slightly anteriorly convex bend to its shaft. The femoral head is globular. Its articular surface has a narrow extension that covers the posterior aspect of the ridge connecting the head to the greater trochanter. The fovea capitis femoris is positioned close to the inferior rim of the epiphysis and slightly posterior of the anteroposterior midpoint. The femoral head sits on a femoral neck that projects at ~145° from the femoral shaft. The greater trochanter extends to the proximal level of the femoral head. It is canted slightly anteriorly. A deep trochanteric fossa is present on its posterior surface. The distolateral edge of the fossa meets a faint ridge, the intertochanteric crest that arcs medially across the posterior surface of the femur to meet the lesser trochanter. The lesser trochanter is positioned quite far distally, such that the femoral shaft becomes noticeably constricted distal to the head and greater trochanter, but proximal to the lesser and third trochanters. The lesser trochanter projects medially and somewhat proximally, at an angle paralleling the femoral neck. It is relatively large and projects medially beyond the femoral head on the left side. The third trochanter is comparatively small in its lateral projection. It is positioned slightly farther distally than the lesser trochanter, and has a laterally facing rugosity for the gluteus superficialis muscle (George, 1977; Sargis, 2002b).

The femoral shaft is smooth, lacking any expression of the linea aspera (a ridge sometimes running down the posterior surface of the shaft), and is mediolaterally wider than it is anteroposteriorly deep. The distal epiphyseal suture is distinctly visible. The shaft lacks any significant torsion and the condyles face posterodistally relative to the proximal end, instead of facing laterodistally or mediodistally. The patellar groove is shallow and only slightly longer proximodistally than wide mediolaterally, giving it a 'square' appearance in anterior view. The medial margin of the patellar groove projects anteriorly to a greater extent than the lateral margin. In addition, most aspects of the medial side of the distal end are slightly larger than those of the lateral side. For example, the medial condyle is longer proximodistally and wider mediolaterally than the lateral condyle. The medial and lateral epicondyles have notable pits for the collateral ligaments. In addition, the lateral epicondyle has a pit that is more crescentic in form, and positioned below the collateral ligament pit. This crescentic pit is probably for the origin of the popliteus muscle.

Comparisons.— The femur of plesiadapids does not exhibit very much variation in the species for which it is known. Most aspects of the description given for *P. cookei* apply equally to *P. tricuspidens*, *N. gidleyi*, and a newly recognized specimen of *N. intermedius* (tables A-II-30 to A-II-32). The femoral head of *P. cookei* differs from the description of femoral heads given by Beard (1989) for other plesiadapids, which he characterized as being spherical, having a centrally placed fovea capitis femoris, and as lacking a lateral extension of its articular facet. These features distinguish plesiadapids from non-plesiadapid plesiadapiforms (Beard, 1989: fig. 76). Although we agree that plesiadapids differ from non-plesiadapids to a degree, based on our observations of the entire collection of *P. tricuspidens* in Paris and *N. gidleyi*,

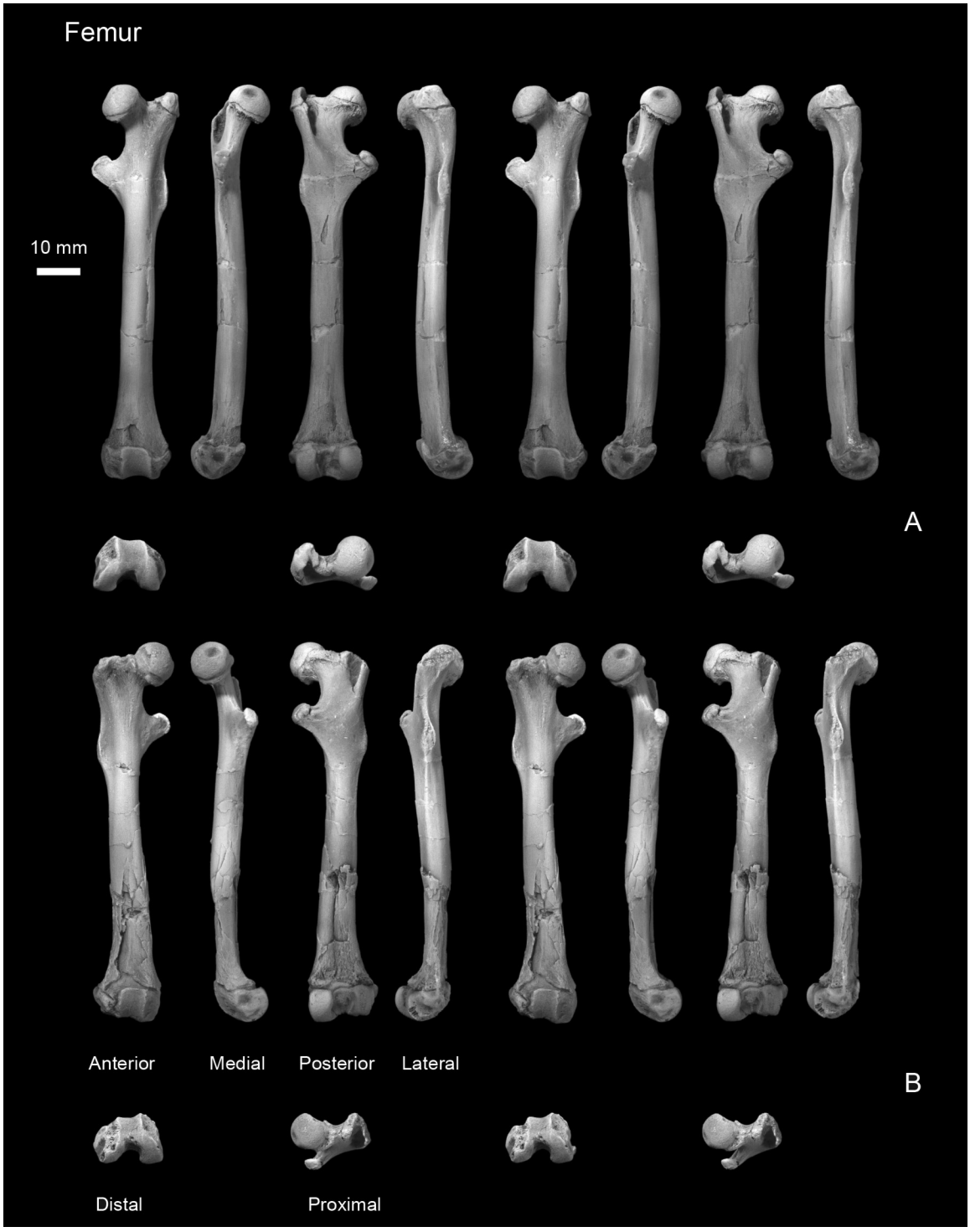

FIGURE 56.— Femora of *Plesiadapis cookei* (UM 87990). Stereophotographs. **A**, left femur. **B**, right femur. Both are shown in anterior, medial, posterior, lateral, distal, and proximal views.

almost all appear to exhibit the three features that they were said to lack. We would modify Beard's (1989) assessment to say that, plesiadapids differ from non-plesiadapids in having a femoral head with a slightly less posteriorly positioned fovea capitis femoris, and a smaller lateral extension of the articular surface. It is important to be clear that these features are just less developed, not absent, because of the functional implications (see below).

The large sample of *P. tricuspidens* from the Berru locality in France enables a statistical comparison of size and shape differences beween *P. cookei* and *P. tricuspidens* (Table A-II-32; two-tailed *t*-tests assuming equal variances). The two samples differ in femur length, with *P. cookei* being significantly longer (Ln [Le]: $t = 2.721$, 9 d.f., $p = 0.012$); in femoral shaft shape, with *P. cookei* being more slender (SSV: $t = 3.139$, 9 d.f., $p = 0.006$); in relative size of the femoral head, with *P. cookei* having a proportionally smaller femoral head (HShV: $t = 6.451$, 8 d.f., $p < 0.001$); and in the position of the lesser trochanter, with *P. cookei* having a more proximally positioned lesser trochanter (LTPV: $t = 3.191$, 8 d.f., $p = 0.006$).

There are, on the other hand, no differences in the absolute mid-shaft cross-sectional area (Ln [MSW * MSD]: $t = 0.170$, 16 d.f., $p = 0.434$), in the area of the femoral head (Ln [HMW * HMD]: $t = 0.045$, 12 d.f., $p = 0.482$), or in the absolute proximodistal distance between the lesser trochanter and femoral head (Ln [LTP]: $t = 0.360$, 12 d.f., $p = 0.362$). Thus, it is principally the longer femoral shaft distal to the lesser trochanter in *P. cookei* that makes it different from *P. tricuspidens* in femoral size and shape.

Tibia

Both tibiae are preserved (Fig. 57; Tables A-II-33 and A-II-34). The right element is in better condition, with both epiphyses and the shaft complete. The bone is narrow and rod-like, and it lacks a raised cnemial crest. The shaft has a pronounced sigmoid curvature, with the proximal half bowed medially and the distal half curved laterally. The proximal end is wider than it is deep. The medial condyle is smaller than the lateral condyle and more distally positioned, so that the tibial plateau is stepped. The condyles face proximally with respect to the proximal segment of the shaft. However, due to the sharp lateral curvature in the first part of the shaft, the condyles face laterally by 25° or so with respect to the more distal segment of the shaft.

Both condyles are shallowly concave. They are separated by an intercondylar eminence on which the lateral intercondylar tubercle projects farther proximally. The medial condyle appears to have a deeper concavity, as a result of its more distal position with respect to the lateral condyle and the intercondylar eminence. The intercondylar eminence is truncated in its posterior projection leaving an intercondylar notch between the posterior margins of the condyles for the posterior cruciate ligament. The proximodistal thickness of the medial condyle is less than that of the lateral condyle due to buttressing of the lateral condyle for articulation with the fibula on its distal aspect.

The anterior surface of the proximal end of the tibia is marked by a distinct, shallow groove for attachment of the patellar ligament. This groove is located ~2 mm below the proximal lip of the tibial plateau and forms a convex arc that is ~5 mm long. The tibial tuberosity is located just distal to this but is barely visible. The anteromedial side of the tibial shaft is convex due to the curvature of the shaft. It is also relatively rugose. This rugosity extends for a little over half the length of the shaft. The lateral and posterior surfaces of the shaft are strongly concave, extending about a third of the way distally down the shaft. They are separated by a sharp ridge that would have held the interosseous membrane. Most of the distal two-thirds of the shaft is subcircular in cross-section, with the anteroposterior dimension being slightly greater.

Just proximal to the distal articular surface the cross-section of the tibial shaft becomes more triangular because of an anterolaterally projecting crest. Slightly posterior to this crest the interosseous crest gains prominence again. Thus, the distal end of the shaft has a distinct lateral surface formed between these two crests. The surface is slightly concave and would have articulated with the fibula. This is usually referred to as the fibular notch. The surface of the fibular notch is relatively rugose.

The distal articular surface for the astragalus is flat and slants by ~20° to face laterally from distal. It also faces posteriorly of distal by somewhat less than 20°. The anteroposterior length of the astragalar facet is greater than its mediolateral width. The medial malleolus projects beyond the distal articular surface by ~2 mm. Its lateral surface forms an obtuse angle with the distal articular surface. The medial malleolus is quite long anteroposteriorly (5 mm), or about half the anteroposterior length of the entire facet, even if short proximodistally. In distal view, the anteroposterior axis (formed where the malleolus and distal articular surface meet) shows medial torsion relative to the proximal end of the tibia. The lateral surface of the medial malleolus is also distinctive in being laterally convex, possibly indicating that it met a concave surface on the astragalus. In anterior view the medial malleolus appears to have a 'sharp' tip. This is due to the presence of two prominent depressions on its distomedial surface.

Comparisons.— The tibia is a rare element in the French collections of *P. tricuspidens*, and a single specimen is available for comparison from the Berru assemblage (MNHN BR 218). The proximal end is all that is preserved, but this still exhibits distinctive morphology. Both species of *Nannodectes*, however, preserve tibiae. All of these specimens are basically similar. The *Nannodectes* specimens preserve distal femora, and thus the proportions of the femoral and tibial condyles can be compared among them. In *N. intermedius*, only the medial condyles are available, and the ratio between the medial femoral and tibial condyle lengths is 0.89, the same as the ratio in *P. cookei*. In *N. gidleyi* both sets of condyles are present: the medial femoral and tibial condyles have a ratio of 0.97, whereas the lateral ones have a ratio of 0.82. The pattern is the same in *P. cookei*, suggesting a looser fit between the lateral condyles than the medial ones. However, the slightly tighter fit between both medial and lateral condyles of *N. gidleyi* may suggest a less axially mobile

FIGURE 57.— Tibiae of *Plesiadapis cookei* (UM 87990). Stereophotographs. **A**, left tibia. **B**, right tibia. The former is shown in anterior, medial, posterior, and lateral views, and the latter is shown in anterior, medial, posterior, lateral, distal, and proximal views. The left tibia is missing its epiphyses. A segment of the proximal part of the shaft was reconstructed on the left side (evidence for this reconstruction is unknown).

knee joint, and possibly a greater degree of agile pronograde locomotion. An additional difference between *N. gidleyi* and other plesiadapids — a convex, rather than concave lateral condyle, as seen in tree squirrels and treeshrews — is also consistent with agile pronograde locomotion.

Fibula

Fragmentary right and left fibulae are preserved with UM 87990 (Figs. 58, 59; Table A-II-35). The right fibula has an undistorted complete diaphysis. The left fibula is broken, with the proximal end offset (seemingly due to postmortem breakage). The epiphyses are missing from both fibulae. The proximal end of the shaft, where the epiphysis would have sutured, is expanded anteromedially to posterolaterally, but it is narrow perpendicular to this. Thus the proximal shaft can be described as blade-like. Approximately 2 mm distal to the proximal end, the shaft depth narrows to about two-thirds its proximal end depth. Farther distally, the shaft continues to narrow gradually until just prior to reaching the distal end,

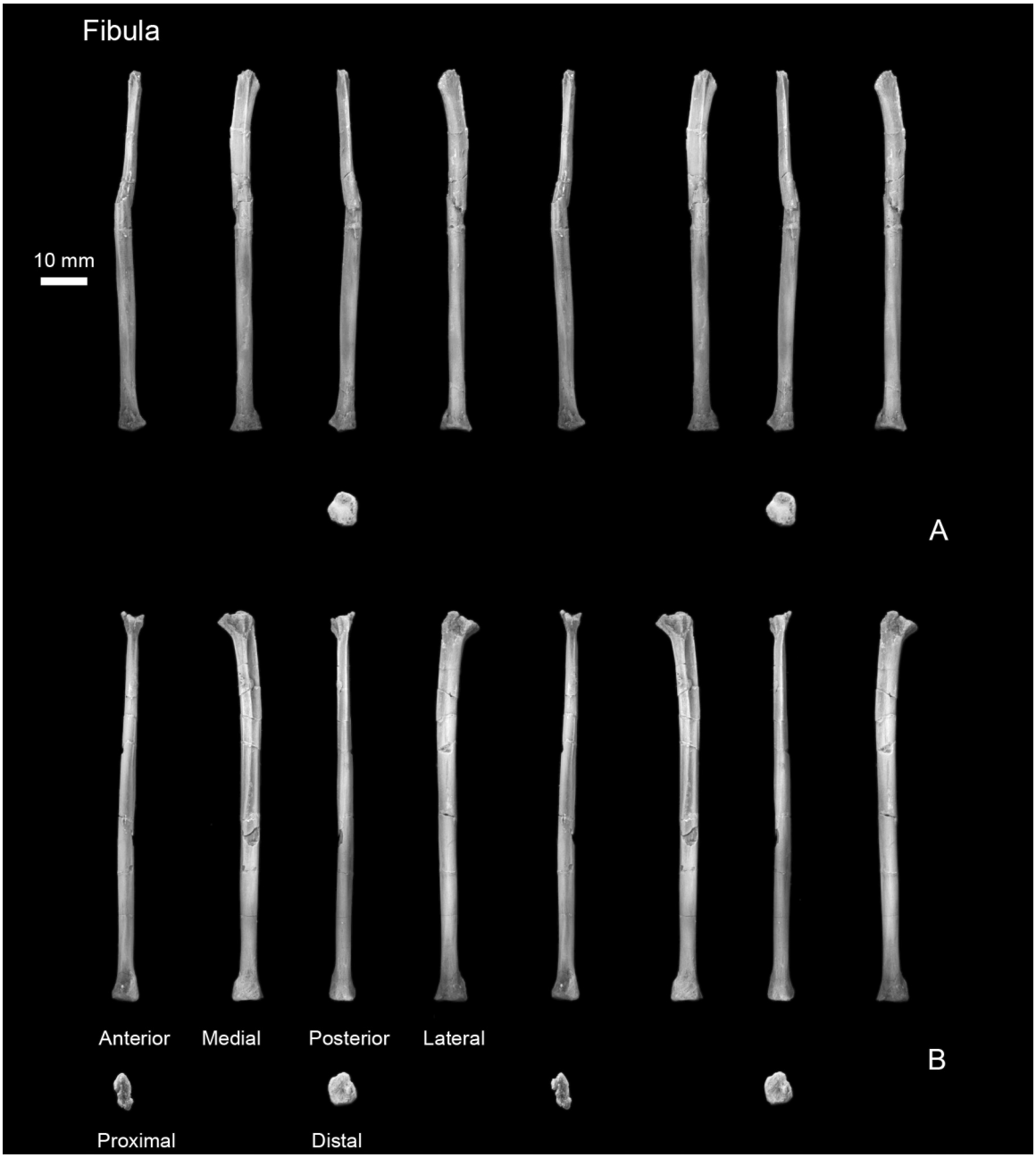

FIGURE 58.— Fibulae of *Plesiadapis cookei* (UM 87990). Stereophotographs. **A**, left fibula. **B**, right fibula. The former is shown in anterior, medial, posterior, lateral, and distal views, and the latter is shown in anterior, medial, posterior, lateral, proximal, and distal views. Both fibulae are missing their epiphyses.

where it flares out in all directions and develops an anteromedially oriented rugosity, which would have contacted the fibular notch of the tibia, just posterior to the tibia's crest for the anterior tibiofibular ligament.

The anteromedial edge of the blade of the fibula's proximal end is concave, whereas the posterior margin is convex. The proximal end of the anterolateral surface has a proximodistally oriented crest toward the anterior margin, which separates this bone into a smaller, more anteriorly-facing surface, and a more laterally-facing posterior surface. The more anterior surface is that typically referred to as the 'anterior surface with medial and lateral lips' (Stern, 1988), and the larger, more posterior surface is equivalent to the peroneal surface. The peroneal surface is slightly concave at the proximal end, but becomes convex farther distally.

The posteromedial surface is marked by a sharp, posteromedially projecting crest that separates this surface into anterior and posterior regions of roughly equal anteroposterior

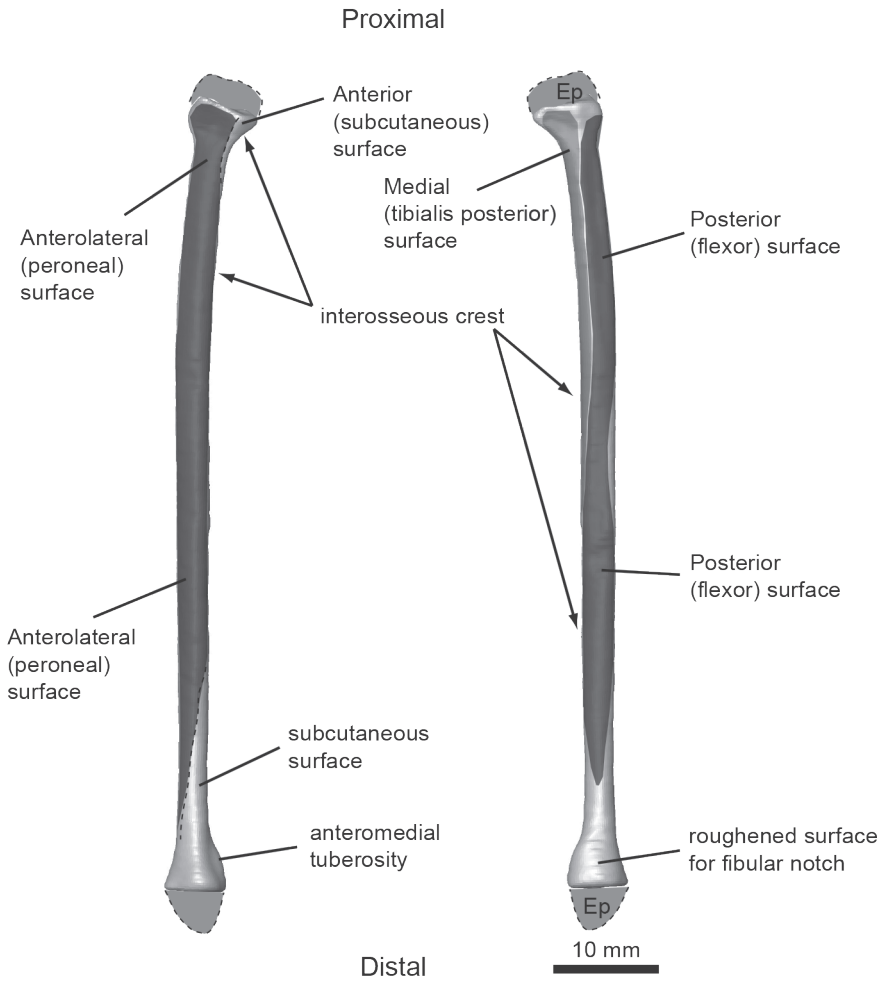

FIGURE 59.— Reconstruction of the right fibula of *Plesiadapis cookei* (UM 87990). Reconstruction is based on CT data. The image is shaded and labeled to aid in understanding statements made in its description. Abbreviation: *Ep*, epiphysis (reconstructed).

dimensions. The surface posterolateral to this crest is that typically referred to as the posterior, or 'flexor surface,' whereas the more anteromedial one is that referred to as the medial or 'tibialis posterior surface' (Stern, 1988). Followed distally, the crest separates these two surfaces and arcs anteriorly, converging on another crest, the interosseous crest, which has its proximal origin from the medial lip of the anterior surface.

Comparisons.— The only other plesiadapid fibula available for comparison is MNHN BR-11-L, a distal fibula of *P. tricuspidens* (Beard, 1989). We were unable to locate and study this specimen. Beard (1989) mentioned the presence of a distal articular surface for the tibia being present, and suggests that this articulation was synovial rather than syndesmotic. As described above, this was not the case in *P. cookei*. Thus, the two taxa had different distal fibulae, or our interpretations differ.

Astragalus

UM 87990 preserves a complete right and fragmentary left astragalus (Figs. 60A and 61; Tables A-II-36 to A-II-38). The astragalus of plesiadapids is relatively well known (Szalay and Decker, 1974). Most descriptive features of these published specimens also apply to the astragalus of *P. cookei*.

The most distinctive feature of the right astragalus is its mediolateral asymmetry. On the astragalar body, the dorsal facet for the tibia (the lateral tibial facet) slopes steeply medially. This occurs because the fibular facet (which meets the lateral margin of the lateral tibial facet) is much deeper dorsoventrally (4.9 mm) than the dorsoventrally oriented facet for the medial malleolus (medial tibial facet; 3.4 mm). As a further result of this asymmetry, the angle between the fibular and lateral tibial facets is slightly acute (84°), and the lateral and medial facet angle is obtuse (115°).

The lateral and medial margins of the lateral tibial facet are farthest apart distally and converge proximally, so that the facet is triangular. It forms an arc of ~90° and is shallowly grooved distally. The medial edge of the lateral tibial facet extends onto the neck of the astragalus. The medial and lateral

margins of the lateral tibial facet also curve in the transverse plane so that they are laterally convex. The lateral convexity of the facet margins results in the medial tibial facet being concave, matching the convex surface of the medial malleolus of the tibia (see above). The medial tibial facet is triangular, with one of the apices of the triangle meeting the distal edge of the lateral tibial facet. Its dorsal and ventral margins thus diverge proximally and the whole surface curves ventrally in the sagittal plane, giving the facet a paisley or curved teardrop shape.

The surface supporting the fibular facet is square to rectangular in shape. The articular area itself is restricted to the dorsal half of this surface. This facet also has a paisley shape; however, it is more like the lateral tibial facet in having the largest girth distally, with margins that converge proximally. Ventral to the facet itself is a divot for the astragalofibular ligament. The apex of the triangular surface of the fibular facet stops short of the proximal margin of the lateral tibial facet, after the two facets diverge around a prominent superior astragalar foramen.

On the proximal surface of the astragalus, plantar to the superior astragalar foramen, the area between the two facets increases and develops into an expansive concavity. This concavity leads to the flexor fibularis groove on the plantar side of the astragalus. In plantar view, the surface of this groove is triangular, with a proximodistally oriented medial margin formed by the edge of the medial tibial facet, and a more obliquely running facet on the lateral margin formed by the proximal part of the posterior astragalocalcaneal (ectal) facet.

Lateral to the flexor fibularis groove, the ectal facet is rectangular, with its narrowest dimension oriented mediolaterally. It is saddle-shaped with a proximodistal concavity and mediolateral convexity. The first curvature of the saddle is more pronounced than the second and forms an arc of ~45°. The lateral margin of the ectal facet meets the surface for the fibular facet at an angle of just over 90°. The axis of the ectal facet diverges from that of the lateral tibial facet by ~20°, so that the latter is oriented more medially. At the mediodistal margin of the contact between the ectal facet and the flexoris fibularis groove is a deep sulcus separating this structure from the middle astragalocalcaneal (sustentacular) facet. This sulcus leads medially to the inferior astragalar foramen (which leads to the superior astragalar foramen).

Medial to the inferior astragalar foramen is the proximal extension of the sustentacular facet, the medial edge of which meets the medial tibial facet. This facet is proximally concave, where it occupies the sulcus beneath a platform holding the flexor fibularis groove. Followed distally it becomes convex as it also diverges slightly laterally, wrapping around the neck of the astragalus. Because this 'strip-like' facet wraps obliquely around the 'cylindrical' neck of the astragalus, it is often referred to as 'helical' in its shape (Szalay and Decker, 1974). Distally it meets the facets for the spring ligament and navicular bone.

In dorsal view the neck of the astragalus is oriented at an angle with respect to the body, so that the neck projects medially. Distal to the neck is the head, which is occupied by the distal end of the sustentacular facet, the spring ligament facets, and the navicular facets mentioned above, on its ventrolateral, ventromedial, and distal surfaces, respectively. In dorsal view, the head is much wider than the neck. The medial and lateral edges of the navicular facet appear to flare dorsally and proximally with respect to the middle part of the facet. Thus, in distal view, the facet appears reniform. The lateral side of the navicular facet faces distally with respect to the proximodistal axis of the lateral tibial facet. The mediolateral long axis of this side of the facet is parallel to the plane of the lateral tibial facet of the astragalus. The medial part of the navicular facet (the other half of the 'kidney' shape) faces mediodistally, and its mediolateral long axis is oriented dorsomedial to plantolateral with respect to the lateral tibial facet.

Comparisons.— The astragalus of *P. cookei* differs from those of other plesiadapids in at least two notable ways. First, it has a more proximodistally expanded proximal end to its medial tibial facet. In fact, this expansion almost appears pathological because, as a consequence, the concave part of the sustentacular facet into which the sustentaculum of the calcaneus must insert has been narrowed substantially. The concavity is actually too narrow for the calcaneal element to fit into it easily and flushly contact the astragalar surface. The increase in the proximodistal depth of the medial tibial articular surface and consequent narrowing of the concavity of the proximal part of the sustentacular facet appears to also be correlated with proximoventral expansion of the flexor fibularis groove surface. Expansion of the flexor fibularis groove surface could conceivably have been the progressive result of high stresses on this surface caused by the flexor fibularis tendons that run under it. Second, and less likely as a result of pathology, in *P. cookei* the astragalar neck is proportionally longer compared to the astragalar body than it is in other plesiadapids.

Calcaneum

UM 87990 preserves a complete right and a fragmentary left calcaneum (Figs. 60B, 62; Tables A-II-39 to A-II-41). Plesiadapid calcanea are relatively well known (Szalay and Decker, 1974). Most features of these published specimens also apply to the calcaneum of *P. cookei*.

The most distinctive feature of the calcaneum of *P. cookei* is the large peroneal tuberosity on the lateral side, which covers 40% of the proximodistal length of the bone. This arises from the tuber proximal to the distal end of the ectal facet, but it does not project distally beyond the calcaneocuboid facet as it does in some plesidapiforms and *Deccanolestes* (Godinot and Prasad, 1994). The dorsoplantar depth of the peroneal tubercle is relatively large. The lateral surface of the tubercle is marked by a deep groove that crosses it obliquely from dorsoproximal to plantodistal.

The calcaneal tuber and posterior calcaneoastragalar (ectal) facet together make up a little less than two-thirds of the length of the bone. The tuber is deep dorsoventrally relative to its proximodistal length. The proximal end is mediolaterally wider than the shaft of the tuber distal to it. The medial side of the tuber projects more strongly medially than the

FIGURE 60.— Astragalus and calcaneum of *Plesiadapis cookei* (UM 87990). Stereophotographs. A, right astragalus. B, right calcaneum. Both are shown in dorsal, plantar, proximal, distal, medial, and lateral views.

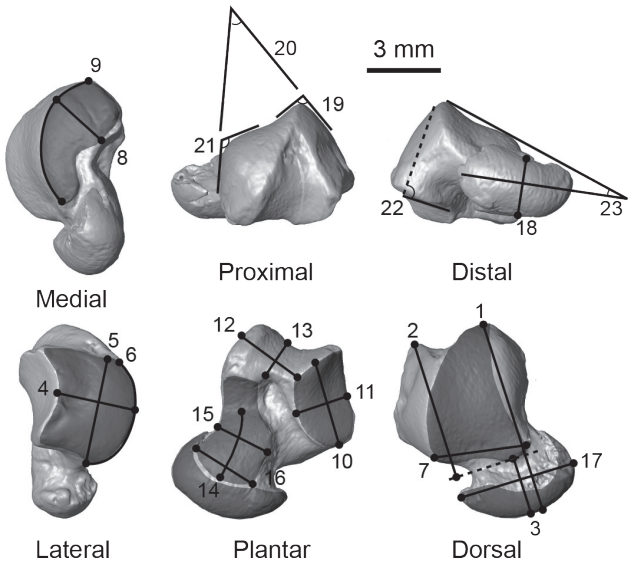

FIGURE 61.— Measurements of the astragalus. See appendix Table A-II-36 through A-II-38 for descriptions of the measurements, and Figure 75 for a principal components analysis of P. cookei in the context of primates, dermopterans, and other mammals.

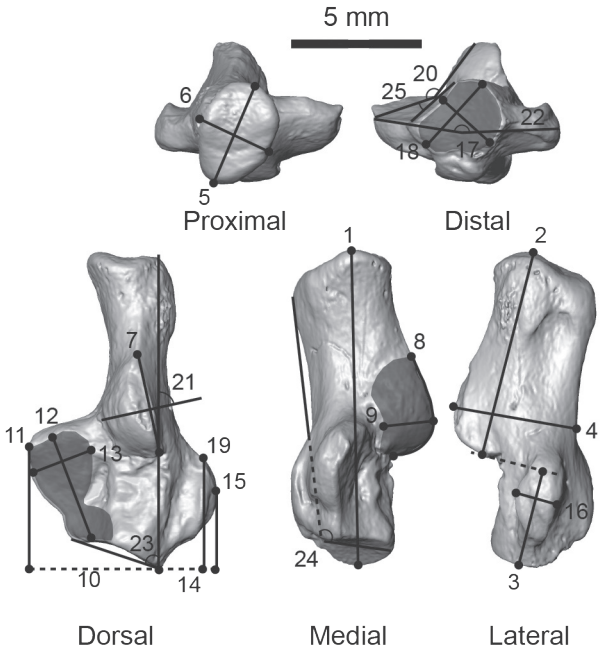

FIGURE 62.— Measurements of the calcaneum. See appendix Tables A-II-39 through A-II-41 for descriptions of measurements.

lateral side projects laterally. The ectal facet is shaped like a segment of a cone with its tip truncated (i.e., a narrowing cylinder). The axis of ectal facet points almost medially relative to the proximodistal axis of the calcaneum, but deviates mediodistally by ~15°.

A small fibular facet is located lateral to the ectal facet and faces laterally. The middle and anterior calcaneoastragalar facets (proximal and distal sustentacular facets) are located mediodistal to the ectal facet and separated from it by a nonarticular sulcus. The proximal sustentacular facet is shallowly cylindrically concave, with an axis paralleling that of the ectal facet. The surfaces of the ectal facet and proximal sustentacular facet are not parallel but rather deviate from parallel by ~30° (i.e., they form an angle of ~150° with each other). Distally, the distal sustentacular facet is fairly flat and continuous with the proximal one. Its entire surface is rotated medially with respect to the proximal sustentacular facet, so that it comes close to paralleling the surface of the ectal facet. Given the change in sustentacular facet surface angle from proximal to distal, this facet can be described as 'helical' in form like its convex counterpart on the astragalus, a descriptor often used for calcaneal facets in plesiadapiforms (e.g., Szalay and Decker, 1974).

The proximal end of the proximal sustentacular facet is confluent with a facet that covers the proximal side of the sustentaculum. This flat, square facet is the 'sustentaculum tali' that would normally contact the proximal extension of the sustentacular facet of the astragalus in other plesiadapids, although it cannot do so in UM 87990 (see above).

The calcaneocuboid facet is saddle-shaped in UM 87990, being strongly concave mediolaterally, and slightly convex dorsoventrally due to a subtle pit in the facet on its plantar aspect, just dorsal to the anterior plantar tuberosity (see Beard, 1989). The calcaneocuboid facet is oriented oblique to the long axis of the calcaneum, and faces 15° or 20° medially. The main notable features of the plantar surface are (1) the anterior plantar tubercle, which is centrally located but flares medially, and (2) the deep groove running medial to the anterior plantar tubercle on the plantar surface of the sustentaculum.

Comparisons.— Three features that make *P. cookei* unique among plesiadapids suggest an increased capacity for, and control of, inversion and eversion movements at the lower ankle joint: (1) a proportionally longer astragalar neck and calcaneal head (NVar: Table A-II-36; DVar: Table A-II-39), (2) a larger angular difference between the proximal and distal parts of its calcaneal sustentacular facet, and (3) a longer calcaneum ectal facet length and arc length (Cc-08: Table A-II-39), but an astragalar ectal facet length that is average among the *P. tricuspidens* sample (Ast-10: Table A-II-36). Features 1and 2 indicate that the helical sustentacular facets are proportionally longer and that their surfaces encompass a larger arc. Thus, a greater amount of inversion-eversion rotation was possible. Feature 3 suggests that the calcaneal ectal facet was proportionally larger compared to the astragalar ectal facet in *P. cookei* than it was in *P. tricuspidens* and possibly other species. This greater offset enabled the astragalus ectal facet to rotate through a larger arc on the calcaneum ectal facet, which would have been necessary to accommodate the more extensively rotating helical sustentacular facets.

Additional differences between *P. cookei* and other plesiadapids concern morphology related to muscles that control inversion-eversion. The peroneal tuberosity and groove for

the peroneous longus tendon crossing it are larger and deeper, respectively, in *P. cookei* than in *P. tricuspidens*, suggesting a stronger peroneous longus muscle, the main function of which is to evert the foot (Boyer et al., 2007). Likewise, the groove on the plantar aspect of the calcaneum for the flexor fibularis (as well as tibialis posterior and flexor tibialis) tendon(s) is broader and better defined in *P. cookei* than it is in *P. tricuspidens*, suggesting that these muscles—responsible for both plantarflexion and inversion—were better developed. *P. cookei* also differs from other plesiadapids in development of the plantar pit of the calcaneocuboid joint. This pit is said to control the movement of the cuboid, enabling it to rotate more effectively on the calcaneum (Beard, 1989), as it does during inversion and eversion.

Cuboid

The right cuboid is preserved in UM 87990 (Figs. 63A, 64; Table A-II-42). It has the shape of an elongated rectangular cube. Much of the proximal end for articulation with the calcaneum is flat, with a slight convexity. The distal surface of the cuboid is oriented ~58° laterally relative to the proximal calcaneal facet, but it has a dorsoventral axis that parallels the axis of the calcaneal facet. The medial side of the proximal articular surface curves slightly distally.

When the calcaneum and cuboid are in closest-packed position, the medial surface of the cuboid forms a continuation of the distal sustentacular facet of the calcaneum, providing more contact area for the astragalus. However, a change of surface orientation creates a strong convexity at the proximal peak of the cuboid, marking the point of contact with the plantar pit of the calcaneum (see above).

There is a medially-facing facet for the navicular on the medial side of the cuboid. It is distal to and confluent with the proximal articular facet for the astragalus. Distal to and confluent with the navicular facet, there is a convex facet for the ectocuneiform. The tangent of its surface faces distomedially, and slightly dorsally. Distal to the ectocuneiform facet is a recessed non-articular area, leading up to the distal end of the bone. The dorsal surface of the cuboid is proximodistally concave and non-articular. In anterior view, the lateral surface is marked by a blunt, tubercle-like projection. This tubercle can be followed to the ventral surface where it serves to form the proximal boundary of a deep, broad, mediolaterally-running groove for the tendon of the peroneus longus muscle. This groove has a greater girth medially than laterally.

The distal articular surface is triangular in distal view. The facet has dorsolateral, medial and ventral surfaces. The medial surface, which abuts the ectocuneiform, is notched. The medial two-thirds of the distal surface itself is shallowly, dorsoventrally concave for articulation with MT IV. The lateral third, where MT V fits, is shallowly convex.

Comparisons.— P. cookei differs from other plesiadapids in having a proportionally broader peroneus longus groove (PgV: Table A-II-42). A larger groove for the peroneous longus tendon may indicate more forceful control over eversion of the foot.

Ectocuneiform

A left ectocuneiform is present (Fig. 63B, 64). No other plesiadapids have an ectocuneiform preserved; thus attribution of this element to *P. cookei* cannot be confirmed with comparative information. However, it seems to fit with the cuboid, which clearly belongs to *P. cookei* based on comparative information (see above). Furthermore, it is quite similar to the ectocuneiform of another plesiadapiform, *Ignacius clarkforkensis* (Boyer and Bloch, 2008).

The ectocuneiform is square in lateral or medial view, and mediolaterally narrow (2.9 mm) compared to its dorsoplantar (4.8 mm) and proximodistal (4.7 mm) dimensions. It is dorsoventrally wedged, with its dorsal surface wider mediolateraly than its ventral surface. The proximal surface is concave and slopes medially relative to its proximodistal axis, and the distal surface is slightly concave and faces directly distal. The proximal surface is notched on its medial side, and the distal surface has a shallow notch on its lateral side. The dorsal surface is smooth and non-articular. The plantar surface is notched for the continued course of the peroneus longus tendon. The dorsolateral corner of the proximal end has a proximolaterally facing surface for contact with the distal tip of the dorsodistomedially-facing surface of the medial side of the cuboid. The plantoproximal corner of the lateral side has a tiny facet for contact with a corresponding facet on the cuboid (Fig. 64). Distal to these two contacts with the cuboid is a concave articular area that seems to also fit the cuboid more distally. In order for these more distal facets to align, the distal metatarsal surface of the ectocuneiform (for MT III) must be inset slightly proximal to the metatarsal facet of the cuboid. The medial side of the ectocuneiform has distinctive articular facets along the dorsal and proximal margins for the mesocuneiform, and along its distal margin for MT II).

Mesocuneiform

The right mesocuneiform is present (Figs. 63C, 64). It is slightly smaller than the ectocuneiform and triangular in dorsal view. The mesocuneiform is trapezoidal in lateral view, with smaller dorsoplantar dimensions proximally (4.0 mm) than distally (5.0 mm). The proximal articular surface faces laterally, toward the ectocuneiform, relative to the proximodistal axis of the bone, and the distal end faces distally. As with the ectocuneiform, the mesocuneiform is wedge-shaped, with a dorsal surface that is mediolaterally broader than the plantar surface. The lateral surface for articulation with the ectocuneiform is flat, and the medial surface for articulation with the entocuneiform is concave. The bone is quite short proximodistally, and the length of its lateral side is only 2.8 mm. Thus, when articulated with the ectocuneiform, its distal metatarsal facet was inset proximally compared to that of the ectocuneiform (and also compared to the entocuneiform (based on entocuneiforms for other plesiadapids described by Szalay and Dagosto, 1988).

Metatarsals

Metatarsal I.— The right hallucal metatarsal (MT I), like the pollical metacarpal, is a robust bone (Figs. 65A, 66; Table

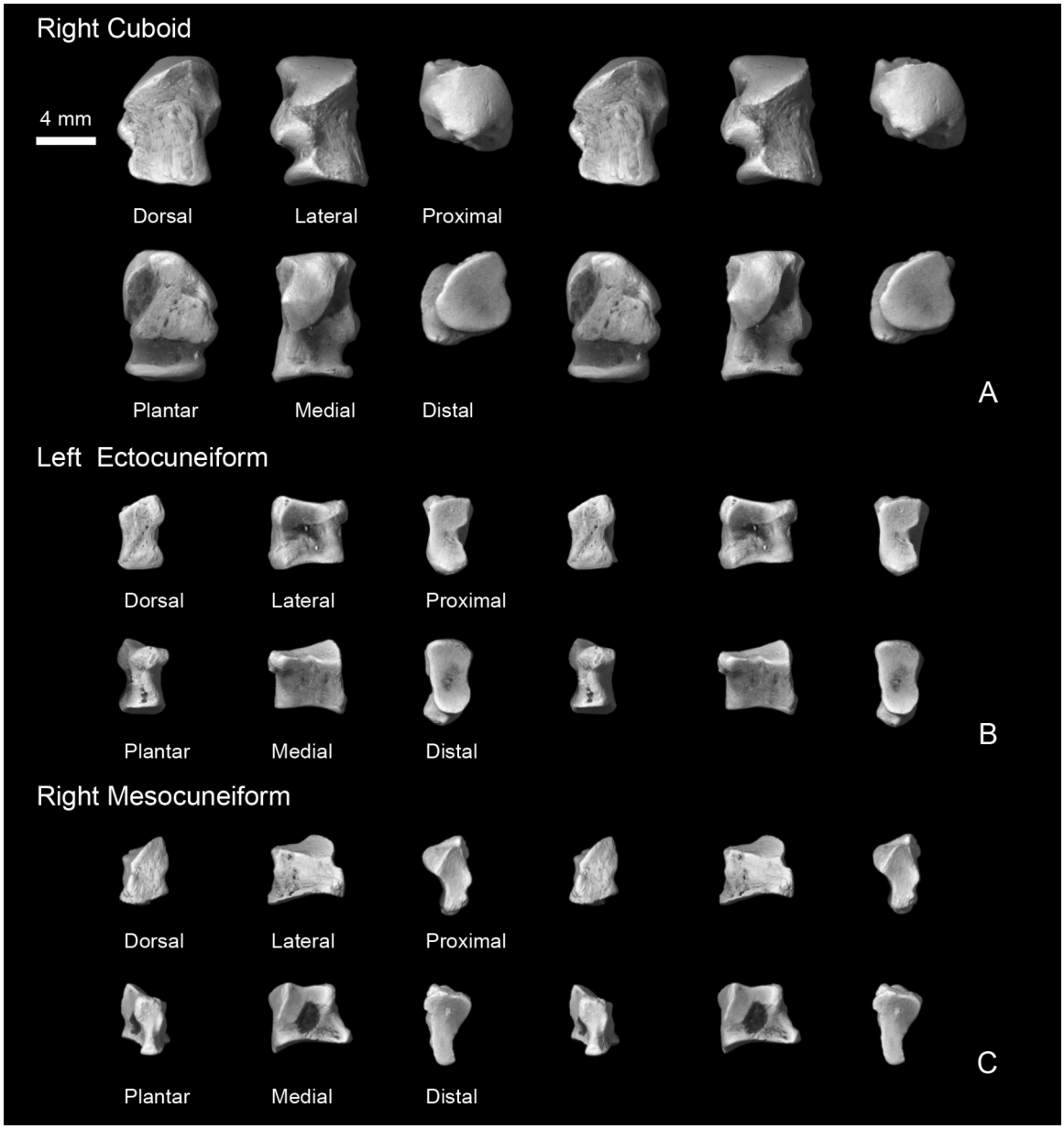

FIGURE 63.— Distal tarsal bones of *Plesiadapis cookei* (UM 87990). Stereophotographs. **A**, right cuboid. **B**, left ectocuneiform. **C**, right mesocuneiform. All are shown in dorsal, lateral, proximal, plantar, medial, and distal views.

A-II-43). The entocuneiform facet is dorsoplantarly convex and mediolaterally concave, giving the joint a distinct saddle shape. This facet is roughly equal in its mediolateral and dorsoventral dimensions. The facet is flanked by proximoventrally projecting tubercles on its lateral and medial sides. The entocuneiform facet is essentially perpendicular to the metatarsal shaft and therefore faces proximally.

The lateral side tubercle is the peroneal tubercle that received the tendon of the peroneous longus muscle. The medial side tubercle is larger than the peroneal tubercle. The shaft narrows from the proximal end going distally. Near the midpoint of the shaft, the cross-sectional shape is roughly circular. The shaft expands mediolaterally from the midpoint to the distal articular surface. The ventromedial aspect of the shaft is marked by a strong, longitudinally running groove.

The articular surface of the distal end of MT I is similar to that of the pollical metacarpal MC I in having three keels, in the asymmetry of its profile, in the form of its articulation with the hallucal proximal phalanx, and in the ratio of its mediolateral width to dorsoventral depth (Tables A-II-24, A-II-43; SSV). Furthermore, the hallucal metatarsal is similar to the pollical metacarpal in the torsion formed between the dorso-

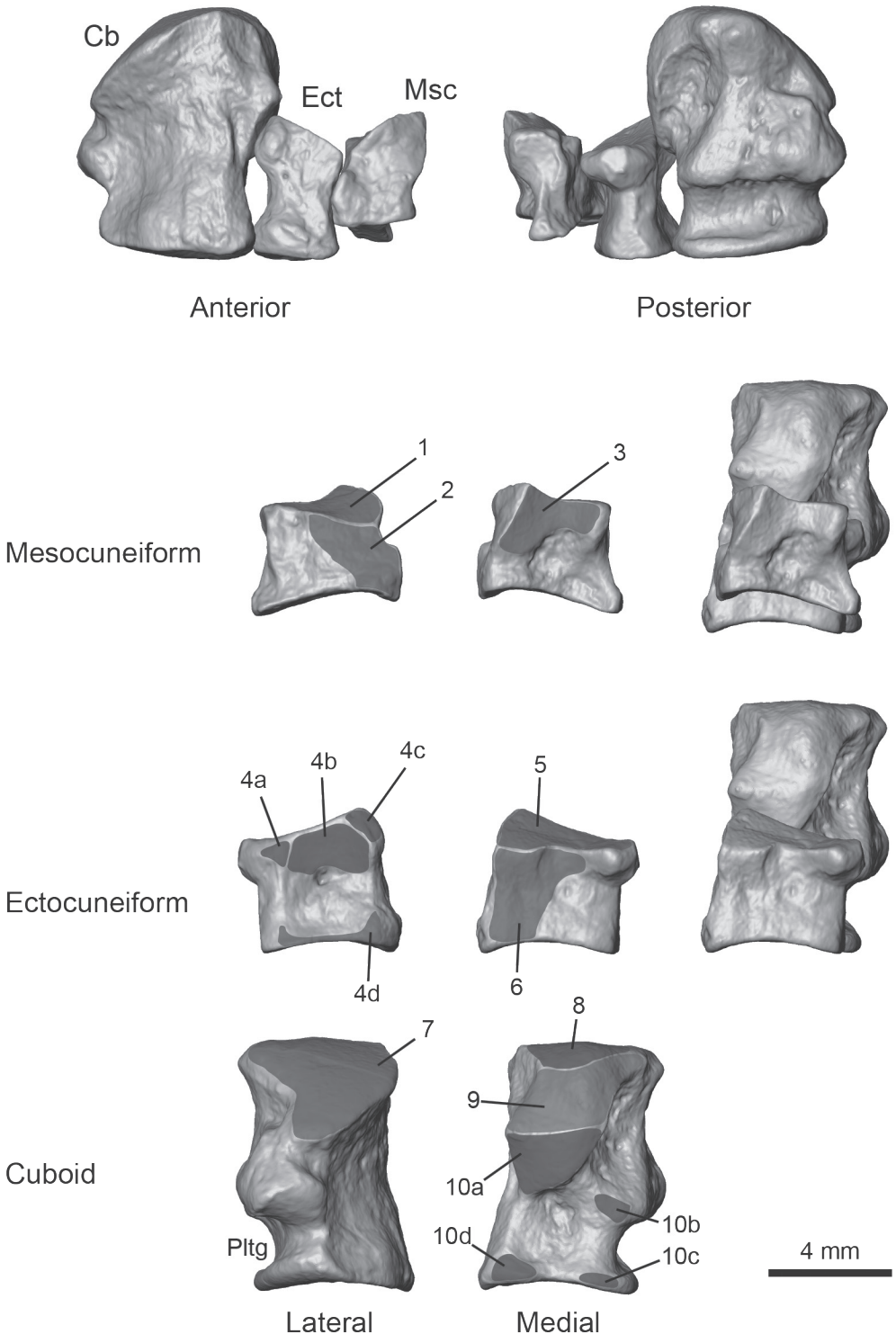

FIGURE 64.— Articulation of distal tarsal bones of *Plesiadapis cookei* (UM 87990). Images are based on high-resolution CT data. Articular areas are shown in gray and labeled with numbers: *1*, navicular articular facet of mesocuneiform; *2*, ectocuneiform facet; *3*, entocuneiform facet; *4a–d*, cuboid; *5*, navicular facet of ectocuneiform; *6*, mesocuneiform facet; *7*, calcaneum facet; *8*, astragalus facet; *9*, navicular facet; and *10a–d*, ectocuneiform facets of cuboid. Facet *4a* typically contacts *10b*. Facet *4b* seems only to engage *10a* when the ectocuneiform is shifted proximally or dorsally relative to the cuboid. Facet *4c* contacts *10a* when the bones are positioned as shown in the figure. *4d* contacts *10c–d*. Abbreviations: *Cb*, cuboid; *Ect*, ectocuneiform; *Msc*, mesocuneiform; *Pltg*, peroneus longus tendon groove.

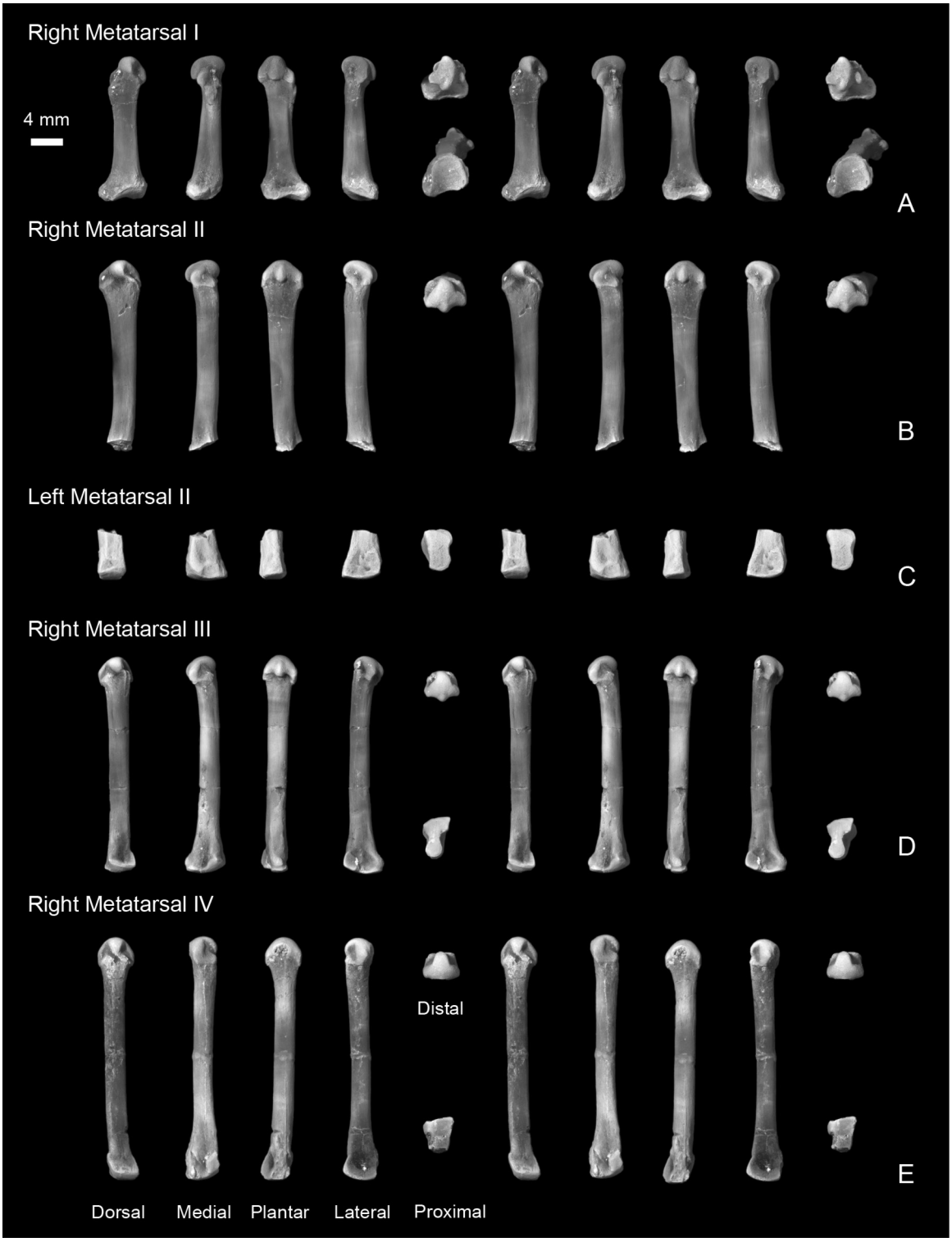

FIGURE 65.— Metatarsals of *Plesiadapis cookei* (UM 87990). Stereophotographs. **A**, right MT I (hallucal metatarsal). **B**, right MT II. **C**, left proximal fragment of MT II. **D**, right MT III. **E**, right MT IV. Elements in A, D, and E are shown in dorsal, medial, plantar, lateral, distal, and proximal view. Element in B is shown in dorsal, medial, plantar, lateral, and distal view. Element in C is shown in dorsal, medial, plantar, and lateral view.

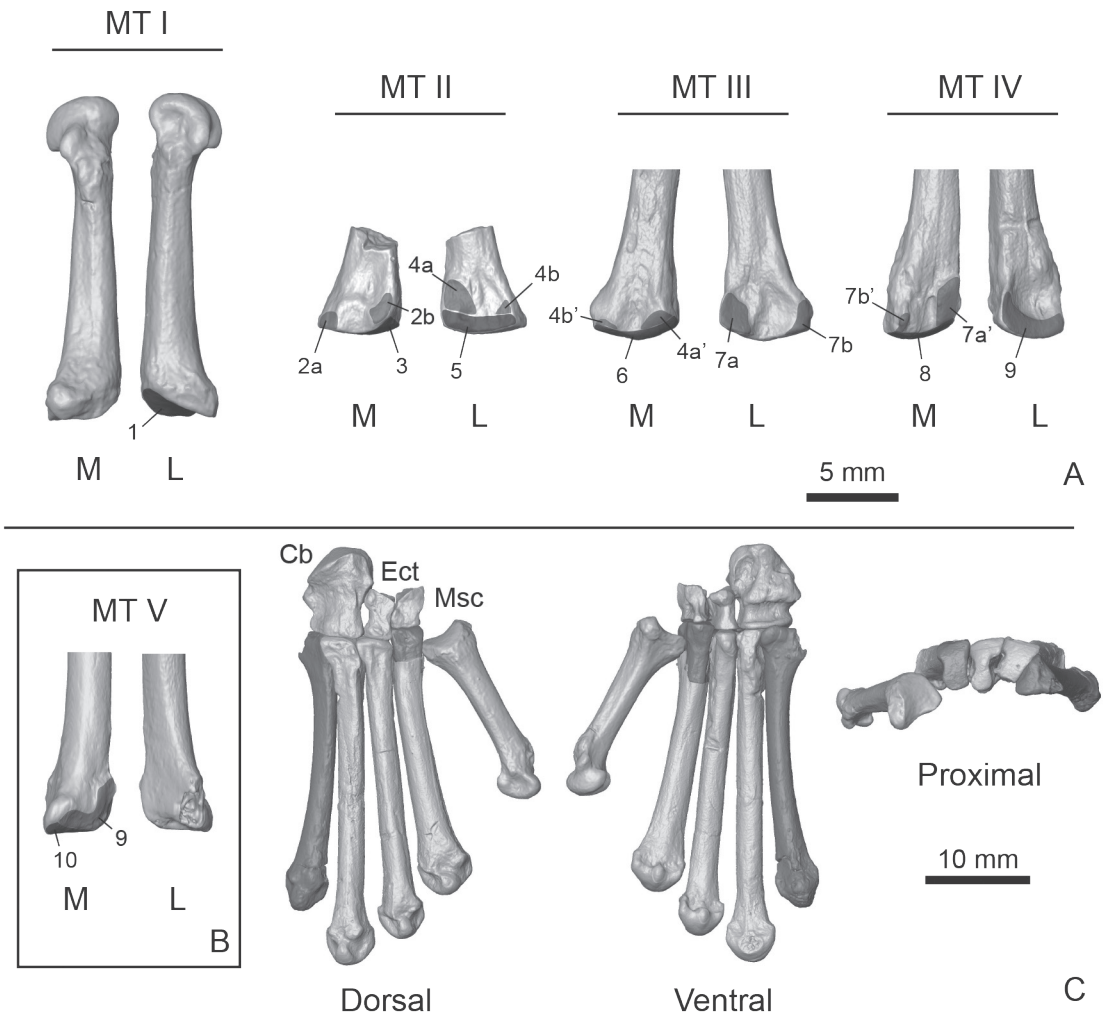

FIGURE 66.— Articulation of metatarsals of *Plesiadapis cookei* (UM 87990). Images are based on high-resolution CT data. **A**, metatarsals in medial (*M*) and lateral (*L*) views. Articular surfaces are illustrated with gray shading and labeled with numbers: *1*, entocuneiform facet; *2a–b*, entoceuniform facets of MT II; *3*, mesocuneiform facet; *4a–4a′*, dorsal MT II–III facet; *4b–4b′*, dorsal MT II–III facet; *5*, ectocuneiform facet of MT II; *6*, ectocuneiform facet of MT III; *7a–7a′*, dorsal MT III–IV facet; *7b–7b′*, ventral MT III–IV facet; *8*, cuboid facet of MT IV; *9*, MT IV–V facet; *10*, cuboid facet of MT V. **B**, high-resolution CT reconstruction of MT V belonging to cf. *P. churchilli* (P77.33.517). Lateral view shows this bone to be missing its peroneal tubercle. Otherwise the bone is well enough preserved to reveal that the proximal MT V fragment included in UM 87990 does not belong to *P. cookei* (Fig. 66). MT IV is also preserved in P77.33.517. Thus scans of the bones of cf. *P. churchilli* could be magnified together until the size of its MT IV equaled that of UM 87990. The magnified MT V of cf. *P. churchilli* was then used in reconstructing the foot of *P. cookei*. **C**, Composite reconstruction of the metatarsus of *P. cookei*. Abbreviations: *Cb*, cuboid; *Ect*, ectocuneiform; *Msc*, mesocuneiform; *MT*, metatarsal.

ventral axis of its proximal end and the dorsoplantar axis of the distal end. The main differences between the two bones are that the hallucal metatarsal is larger, more slender, and has a proximal facet that is mediolaterally broader and faces more proximally and less dorsally.

Metatarsal II.— There are two bones that appear to represent MT II (Figs. 65B–C, 66; Table A-II-43): a right element that preserves everything but the proximal end and a left element that is only the proximal end. It is not certain that these both represent the same taxon, however no information contradicts this possibility and they are treated as belonging to *P. cookei*. Some of the justification for identifying this bone as MT II, specifically, must be done in a comparative context that considers all preserved metatarsals together. The results of these analyses are presented below.

The lateral margin of the proximal surface of MT II, which articulates with the mesocuneiform, projects slightly farther proximally than the medial margin. This proximal facet is slightly convex, but basically flat, and articulates well with the mesocuneiform. The medial side of the proximal end has two facets: one dorsal and one ventral. The dorsal facet faces dorsomedially, and the ventral facet faces ventromedially. Together these two

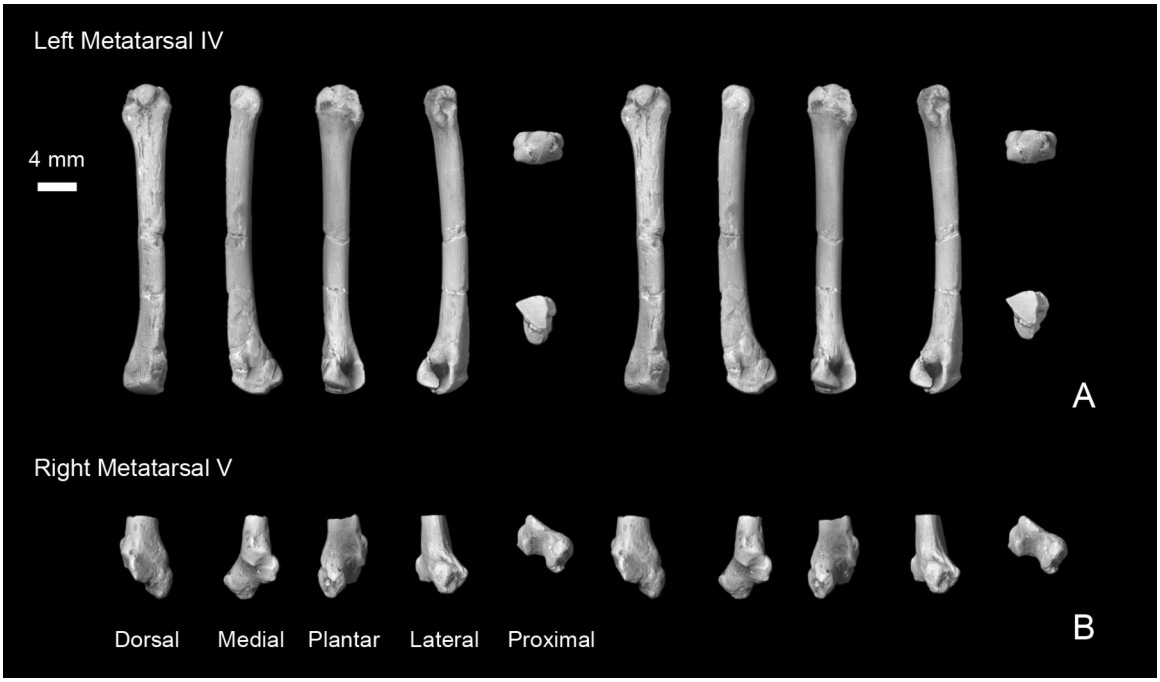

FIGURE 67.— Metatarsals of UM 87990 that do not appear to belong to *Plesiadapis cookei*. Stereophotographs. **A**, left MT IV. **B**, right proximal fragment of MT V. Element in A is shown in dorsal, medial, plantar, lateral, distal, and proximal view. Element in B is shown in dorsal, medial, plantar, lateral, and proximal view.

facets form a convex surface for articulation with the entocuneiform. The lateral margin has a flat, parasagittally oriented articular surface, which additionally faces slightly distally. The borders of facets here are not distinctly delimited. However, this surface would have contacted the distal end of the medial aspect of the ectocuneiform proximally, and the medial side of MT III distally.

The shaft of MT II becomes progressively wider mediolaterally from its proximal to its distal end. The distal end is bowed away from the more lateral digits and toward MT I. The distal articular surface is similar to those of the metacarpals. It differs in being larger and in having a smaller dorsoplantar depth for its mediolateral breadth (a lower HSV; Table A-II-43). The head is asymmetrical, with a more gradually sloping medial aspect to the distal profile, as is true also for MC II and III. Although it is fragmentary, enough is preserved to determine that it would have been longer than any of the metacarpals of 'set 1', and about the same length as the 'set 2' MC III and IV.

Metatarsal III.— MT III is represented by the complete right side element and by the proximal half of the left side element. It is quite different from MT II in that it is longer and more gracile, its proximal end is more asymmetrical, and its distal end is narrower (Figs. 65D, 66; Table A-II-43). The lateral side of the proximal articular surface of MT III (for the ectocuneiform) projects farther proximally than the medial side. The articular surfaces on the medial and lateral aspects of the proximal end of the bone have nonarticular gaps that separate each side into dorsal and ventral articular regions. These nonarticular 'gaps' appear as notches on the lateral and medial sides of the bone in proximal view. The medial side of the proximal articular surface has a dorsally positioned, distal extension onto the medial side of the shaft, representing a point of articulation with MT II. The medial side of the proximal end also has a ventrally positioned, proximodistally narrow facet for MT II. The lateral side of the proximal end has two distinctly developed facets for MT IV. The more dorsal of these faces ventrodistally, whereas the more ventral one faces slightly dorsally. Together these facets form a concave surface that cups the medial side of MT IV. The shaft of MT III is straight, changing little in its cross-sectional dimensions along its length. The distal end is similar to that of MT II, except that it is absolutely mediolaterally narrower and dorsoplantarly shallower, but proportionally dorsoventrally deeper (i.e., it has a lower HSV; Table A-II-43).

Metatarsal IV.— MT IV is the only metatarsal position represented by two morphs. The 'set 1' morph (Figs. 65E, 66) is a right side element that is similar in length to MT III and has a similar distal end morphology. Furthermore, the right side MT III and MT IV articulate smoothly. On the other hand, the, 'set 2', morph (Fig. 67A) is a left side element that is longer than MT III and the right side MT IV. The distal end morphology is difficult to assess due to breakage but it appears to have been absolutely and proportionally mediolaterally wider with more prominent tubercles flanking collateral ligament pits.

The proximal end of the 'set 1' MT IV is in some ways similar to that of MT III. The lateral side of the proximal articular surface (for the cuboid) projects farther proximally than the medial side. The medial side of the proximal articular surface of the 'set 1' MT IV has a dorsally positioned distal extension onto the medial side of the bone. However, this extension is much greater in MT IV than in MT III. This difference represents the existence of a much more extensive articulation between MT III and IV than between MT II and III. There is a non-articular gap separating the dorsally located medial side facet on MT IV from a ventrally placed one. As for dorsal facets, the ventral facet is larger than the corresponding medial side facet on MT III. The lateral side of the proximal end of MT IV differs from that of MT III in having a continuous concave articular surface for the more lateral metatarsal (MT V) with no nonarticular gaps separating it into dorsal and ventral regions.

In most respects the proximal end of the 'set 2' MT IV is similar to that of the, 'set 1', element. However, it is diagnostically different in the morphology of the medial side, dorsal facet for MT III. Specifically, this facet is larger and strongly concave in the, 'set 2', MT IV (instead of slightly convex). As a result of these differences in articular surface morphology, the 'set 2' MT IV, which is a left side element, will not articulate securely with the left side MT III.

Metatarsal V.— Only a proximal fragment of the right MT V is preserved (Fig. 67B). It is identifiable as MT V by its large peroneal tuberosity. However, it clearly did not belong to *P. cookei*, as revealed by MT V elements preserved with two other plesiadapid skeletons (Table A-II-43). Although not described by Beard (1989), a proximal base and distal shaft of an MT V of *Nannodectes intermedius* USNM 442229 are preserved. A specimen of cf. *P. churchilli* (SMM P77.33.517) from Wannagan Creek in North Dakota also preserves this element (Fig. 66B, C). The plesiadapid MT V is revealed to be treeshrew or dermopteran-like by these specimens. The UM 87990 MT V does not fit this pattern and does not even articulate well with the 'set 1' MT IV. Presumably, it articulates with the 'set 2' MT IV better, however the MT V facet on MT IV is too broken to assess this possibility.

Assessment of metatarsal association and attribution.— As discussed in the previous descriptions, all of the metatarsals except one left MT IV and one right MT V appear to belong to *P. cookei*. This interpretation is not as thoroughly supported as those for the metacarpals because: (1) there are fewer and less complete metatarsals than metacarpals in UM 87990; and (2) there are fewer complete comparative metatarsal specimens available. The most speculative of the attributions for the metatarsals described above is that of MT II, given its fragmentary nature and its unusual morphology (compared to MT III and IV). However, this attribution is actually supported by comparisons to *N. intermedius* material. Measurements of proximal and distal fragments of MT I–V preserved with *N. intermedius* USNM 442229 show that MT II in USNM 442229 is similar to the element identified as MT II in UM 87990 in being more robust than MT III and IV (Table A-II-43). An additional similarity between MT II of USNM 442229 and UM 87990 is that both have a distal end that is proportionally dorsoventrally shallower than those of the other metatarsals. These same proportional features also appear to characterize the MT II of *Dryomomys szalayi* UM 41870, although quantitative data are not available for comparison (Boyer and Bloch, 2008).

The identification of MT III and IV in *P. cookei* is supported by the similarity of the proximal ends of these bones to those of MT III and IV of USNM 442229. Dentally-associated skeletal remains of cf. *P. churchilli* (SMM P77.33.517) from Wannagan Creek of North Dakota also include fairly complete proximal ends of MT III and IV. Again, these are nearly identical to those of *N. intermedius* and *P. cookei*. As discussed above, the same cf. *P. churchilli* specimen also includes a nearly complete MT V. A composite plesiadapid foot can thus be assembled (Fig. 66C) using information from these three specimens along with information from the tarsals.

FUNCTIONAL INTERPRETATION

Functional interpretation of the postcranial morphology of *P. cookei* is considered by anatomical region, starting with the vertebral column and then continuing with the thorax, the forelimb and the hind limb.

Vertebral column proportions

Table A-II-2 includes the lengths of the neck, thorax, lumbus, sacrum, and tail (C-l, T-l, L-l, S-l, and Ca-l, respectively) for *P. cookei* and fifteen comparative taxa. These include the Paleocene plesiadapiform *Ignacius clarksforkensis* and fourteen extant taxa. The extant taxa include *Tupaia*, *Cynocephalus*, eight relatively small primates, the sciurids *Sciurus* and *Spermophilus*, the wrist-winged marsupial glider *Petaurus*, and the marsupial brushtail possum *Trichosurus*. The relative proportions of vertebral segments can be compared in a principal components analysis, which is summarized in Figure 68. Panel A in this figure is a scatter plot of principal component scores with PC-I on the abscissa and PC-II on the ordinate. Panel B is a scatter plot of principal component scores with PC-III on the abscissa and PC-II on the ordinate. PC-I represents 41% of the variance, PC-II 32% of the variance, PC-III 19% of the variance, and the three PC axes together account for 92% of the total variance.

Loadings for each variable indicate that PC-I in Figure 68A represents a contrast of taxa with a relatively longer thorax (on the left) compared to taxa with a relatively longer tail (on the right). PC-II in Figure 68A represents a contrast of taxa with a relatively longer tail (near the base of the panel) compared to taxa with a relatively longer neck (near the top of the panel). *Cynocephalus*, with a relatively long cervical series and short caudal series (Stafford, 1999), is in its own region of the morphospace.

PC-III in Figure 68B represents a contrast of taxa with a longer sacrum (on the left) compared to taxa with a relatively longer neck and thorax (on the right). PC-II in Figure 68B is

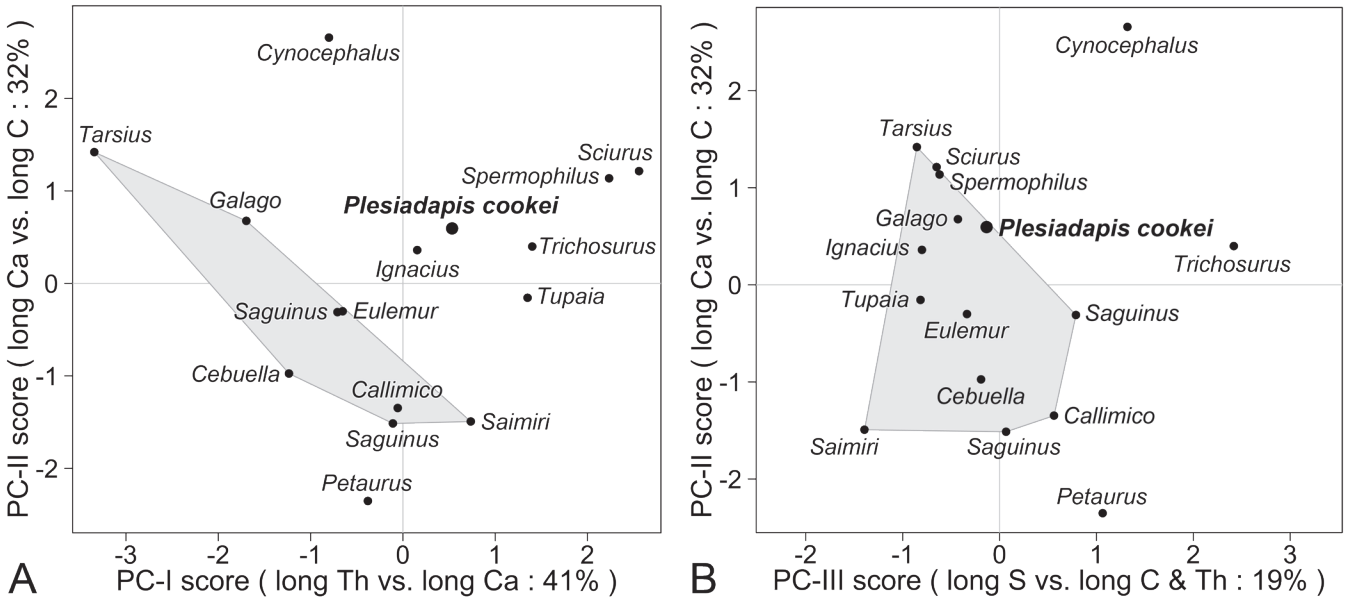

FIGURE 68.— Principal component scores calculated from vertebral column lengths C-l, T-l, L-l, S-l, and Ca-l (cervix length, thorax length, lumbus length, sacrum length, and cauda length) for *Plesiadapis cookei* and 15 comparative taxa in Table A-II-2. **A**, scatter plot of PC-I on the abscissa and PC-II on the ordinate. **B**, scatter plot of PC-III on the abscissa and PC-II on the ordinate. Measurements were standardized before analysis by transforming to logarithms and subtracting the mean ln value for each taxon. Convex polygons link euprimates in the comparative sample. In simplest terms, loadings indicate that PC-I contrasts taxa with a longer thorax, on the left, versus taxa with a longer tail, on the right (41% of variance). PC-II contrasts taxa with a longer tail, below, versus taxa with a longer neck, above (32% of variance). PC-III contrasts taxa with a longer sacrum, on the left, versus taxa with a longer cervix and thorax, on the right (19% of variance). A similar analysis of cranial length and 30 individual vertebral lengths yielded a similar result for *P. cookei* (Table 4 and appendix Tables A-II-3 through A-II-8) and these comparative taxa. Note the central position of *Plesiadapis cookei* in both plots, reflecting its generalized vertebral proportions.

that same as PC-II in Figure 68A (and folding on a vertical axis between the two panels enables visualization in three-dimensions). *P. cookei* is centrally located in both plots, reflecting its generalized mammalian vertebral proportions.

Profiles showing the lengths of the first 18 individual caudal vertebrae and the cumulative length of caudal vertebrae normalized by sacrum length are shown in Figure 69A-B. The tail of *P. cookei* is more like tails of the tree shrew *Tupaia* and tamarin *Saguinus* in its pattern of changing vertebral length (Fig. 69A). It is also more like tails of the tree shrew *Tupaia* and tamarin *Saguinus* in cumulative length Fig. 69B; for mammals with more than 18 caudal vertebrae).

Long tails are typically found in arboreal and scansoreal mammals where they function as stabilizers when running and leaping. They also serve as visual aids in communication. These two possibilities make it difficult to interpret the function of the tail in *P. cookei*, and it may have been used in both stabilization and communication.

The vertebral column of *P. cookei* indicates that it was a generalized mammal with no clear specializations in terms of neck, thorax, lumbus, sacrum, or tail size or proportions.

Thorax

The thorax of *P. cookei* is not well preserved, but the elements known, sternebrae (Fig. 34) and ribs (Fig. 35), have features expected in a generalized mammal. The ribs of *P. cookei* show no sign of the craniocaudal expansion found in ribs of animals requiring dorsostability. Examples of primates that do have expansion for dorsostability include the slow-climbing lorisoids *Arctocebus*, *Perodicticus*, and *Loris* (Jenkins, 1970) as well as *Cheirogaleus medius* (Granatosky et al. 2014). Among non-primate euarchontans, the more cautious and arboreally committed of the scandentians exhibits craniocaudally expanded ribs (i.e., *Ptilocercus lowii*: Sargis, 2001), but the more scansorial tupaiids do not. Cynocephalid dermopterans exhibit craniocaudally expanded ribs (Boyer and Bloch, 2008). This feature likely reflects the part of their habitus that is analogous to that of quadrumanus suspensory sloths that also have pronounced craniocaudal expansion of the ribs.

Pectoral girdle and forelimb

Clavicle.— Functional clavicles connecting the scapulae to, and separating them from, the sternum are present in arboreal, fossorial, volant, and all other mammals where the forelimbs must be both powerful and have a large range of mobility (Trotter, 1885; Flower and Gadow, 1885). *P. cookei*, with its robust clavicles, is clearly in this category.

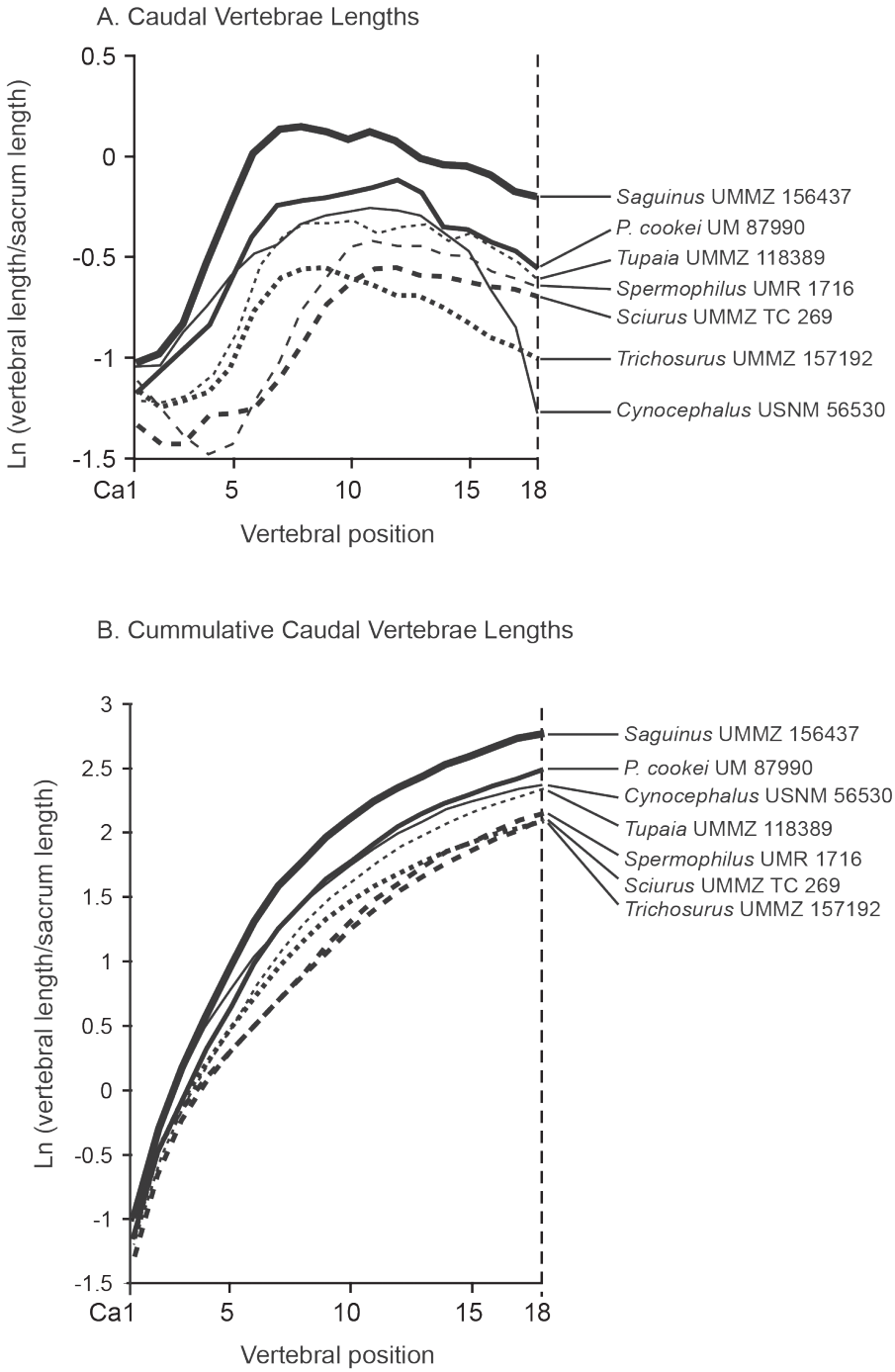

FIGURE 69.— Comparison of caudal proportions in *Plesiadapis cookei* (UM 87990) and other mammals. **A**, proportional length of the first 18 caudal vertebrae of *Plesiadapis cookei*, *Cynocephalus,* and a subset of the comparative sample (all standardized to sacrum length). Note that the last several vertebrae in the tail of *Cynocephalus* decrease in length more rapidly than those of other taxa, reflecting its shorter tail. *P. cookei* has proportionally long distal caudal vertebrae (starting at Ca6), second to the euprimate *Saguinus*. The profile is similar to that of *Saguinus* and *Tupaia*. **B**, cumulative proportional length shows that by the 18th caudal vertebra, *P. cookei* has the second longest tail relative to its sacrum (for calculation of the tail length of *P. cookei*, missing Ca2–3 were each assumed to be the same length as Ca1, and missing Ca5 was represented by the average of Ca4 and Ca6). *Cynocephalus* has the third longest tail at Ca18, but this represents the tip of its tail. Other taxa in the sample, including *P. cookei,* have additional vertebrae. The *P. cookei* profile is again similar to that of *Saguinus* and *Tupaia*.

Scapula.— The narrow, shallowly concave surface of the scapular glenoid and its articulation with a much larger, convex humeral head indicates that the shoulder joint was mobile. However, mobility in abduction may have been limited by the acromion process because it extends so far beyond the glenoid. This mobility-restricting scapular similarity of *P. cookei* to *Tupaia* might be considered to indicate greater terrestriality in *P. cookei*.

Humerus.— The humeral head, with its low but large tuberosities, suggests that the shoulder was mobile. The large deltopectoral crest suggests the ability for powerful adduction and extension of the humerus, as does the large, distally-positioned teres major tuberosity (e.g., Gingerich, 1976). The flaring supinator crest provides ample area for origins of the brachialis musclature anteriorly and the triceps musculature posteriorly. The posterior arc of the supinator crest gave the muscles that attached to it (extensor carpi radialis and brachioradialis) a point of origination situated posterior to the brachial-antebrachial joint. This would have given these muscles the mechanical capacity to powerfully maintain tightly flexed elbows.The deep supracapitular fossa is consistent with this capacity because it provides a depression for the radial head to move into as the forearm is 'fully-flexed,' and allows a more acute angle to be formed between the arm and forearm than if it were not present.

The sub-spherical shape of the capitulum suggests that the radius could rotate around its proximodistal axis and contribute to supination and pronation of the hand. The capacity for axial mobility in the forearm partly explains the pronounced medial epicondyle: the large size and medial projection of the epicondyle increased the area of attachment and leverage for the major pronators of the forearm that arose from it. The conical shape of the ulna trochlea suggests that this joint was capable primarily of flexion and extension. The relatively shallow olecranon fossa and posterior restriction of the capitulum suggest that fully extended forearm postures were unstable or impossible. Lateral rotation of the distal end implies that the forearms were typically somewhat abducted during pronograde postures (Fig. 70).

Measurements from Szalay and Dagosto (1980) were augmented to enable comparison of the distal humerus of *P. cookei* to distal humeri of other plesiadapids and other mammals (mainly euarchontans; Fig. 71 and Table A-II-44). A version of the data in Table A-II-44, with some additional taxa, was analyzed by Boyer et al. (2010b: fig. 7), who found similar results. Six size-standardized variables were analyzed with principal components analysis (PCA). In terms of distal humerus morphology, *P. cookei* lies in the zone of overlap of Plesiadapidae and Eocene adapid and omomyid euprimates (Fig. 71). Primitive eutherian mammals and non-primate euarchontans are generally well-separated from *P. cookei*.

Radius.— The spherical depression of the central fossa of the radial head suggests that the radius was axially mobile, as does the corresponding morphology of the humeral capitulum. A distally positioned, dorsally elevated pronator teres muscle attachment would provide a large area and lever arm for this muscle to resist substrate reaction forces causing supination, whereas the supinator muscle, attaching along the ulnar margin of the pronator teres attachment, could resist the opposite motion. Together, these muscles, as well as biceps brachii and some of the muscles originating from the supinator crest, could stabilize or rotate the humeroradial joint. The shallow distal articular surface suggests a mobile radiocarpal joint. The orientation of this joint surface suggests a ventriflexed, abducted proximal carpal row. Pronounced tubercles delimiting the extensor compartments are consistent with a mobile wrist joint in which extreme hand postures (primarily extremes of dorsiflexion and abduction) could have caused the extensor tendons to strain their boundaries if not reinforced by bony buttresses.

Ulna.— The ulnar trochlea complements the morphology of the humerus and radius in the rather flat form and lateral orientation of its radial facet, which permitted the head of the radius to rotate on it. An anteriorly (ventrally) projecting olecranon process suggests habitually flexed forearms that may have limited the capacity for full extension, depending on the undistorted size of the olecranon process (Szalay et al., 1975). The only notable muscle scars are the groove on the medial surface of the proximal end of the ulna, which likely provided a large area for insertion of the flexor carpi ulnaris muscle (George, 1977), and the ridge denoting the edge of the attachment for what was probably a well-developed pronator quadratus muscle (George, 1977). The presence of a distinct, convex distal radial facet reinforces the idea that there was substantial axial mobility of the radius with respect to the ulna. Its location on the dorsal aspect of the ulna is consistent with the morphology of the radius, suggesting that the wrist was maintained in a semi-supinated orientation most of the time.

Scaphoid.— The most salient functional features of the scaphoid are its dorsally inclined distal articular surface for the capitate, centrale, and probably hamate (in certain postures); the shelf-like surface on its dorsal aspect (that probably reflects hyperextended postures of the midcarpal joint); and its prominent tubercle, the large size of which may have helped increase the volume of the carpal tunnel and served as a 'windlass' mechanism (Hamrick, 1997) while the pollex was strongly abducted (as in pollical grasping).

Lunate.— The extent and orientation of the facets of the lunate, like those of the scaphoid, suggests a habitually dorsiflexed carpus, and the capacity for a large amount of dorsiflexion.

Triquetrum.— The small size and narrow proportions of the triquetrum suggest a hand that was habitually ulnarly-deviated, or adducted toward the ulna (Godinot and Beard, 1991).

Pisiform.— A pisiform that projects at 90° from the scaphoid tubercle suggests a habitually dorsiflexed hand and possibly pronograde postures (Fig. 35). The large size of the pisiform suggests a capacity for powerful ventriflexion (using flexor carpi ulnaris) from an initially dorsiflexed posture, and is also suggestive of pronograde postures.

Trapezium.— When the trapezium is articulated with the scaphoid and trapezoid in what would seem to be an

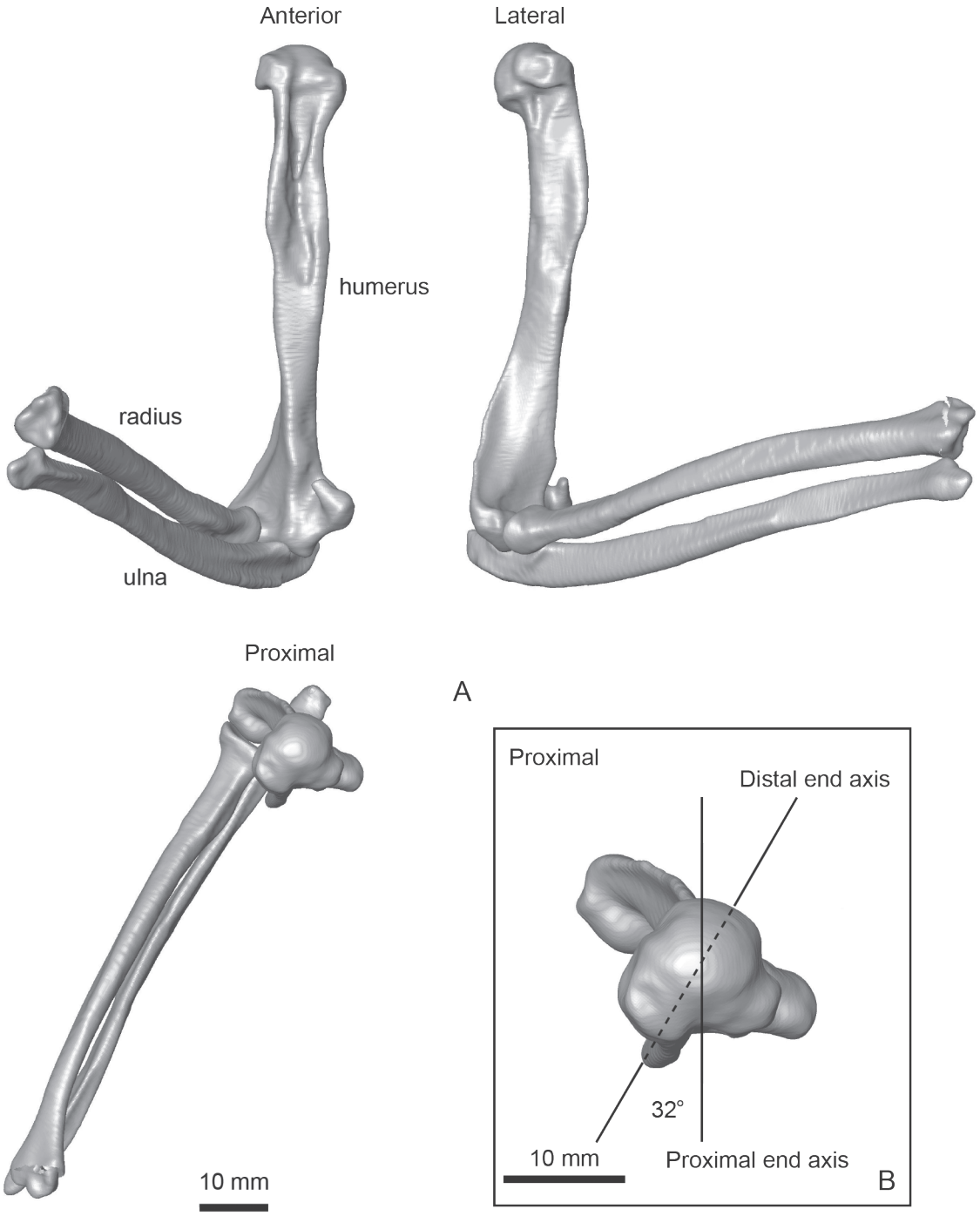

FIGURE 70.— Articulated forelimb of *Plesiadapis cookei* (UM 87990). Surface reconstructions of the humerus, radius, and ulna are based on CT images. **A**, humerus, radius, and ulna shown in anterior, lateral, and proximal views, and articulated so that respective joint surfaces are maximally overlapping. Note that the forearm is flexed and projects laterally relative to the proximodistal and anteroposterior axes of the proximal end of the humerus, respectively. **B**, proximal view of humerus. Note that the axis of the distal end is rotated 32° lateral to the axis of the proximal end, which explains the lateral projection of the radius and ulna.

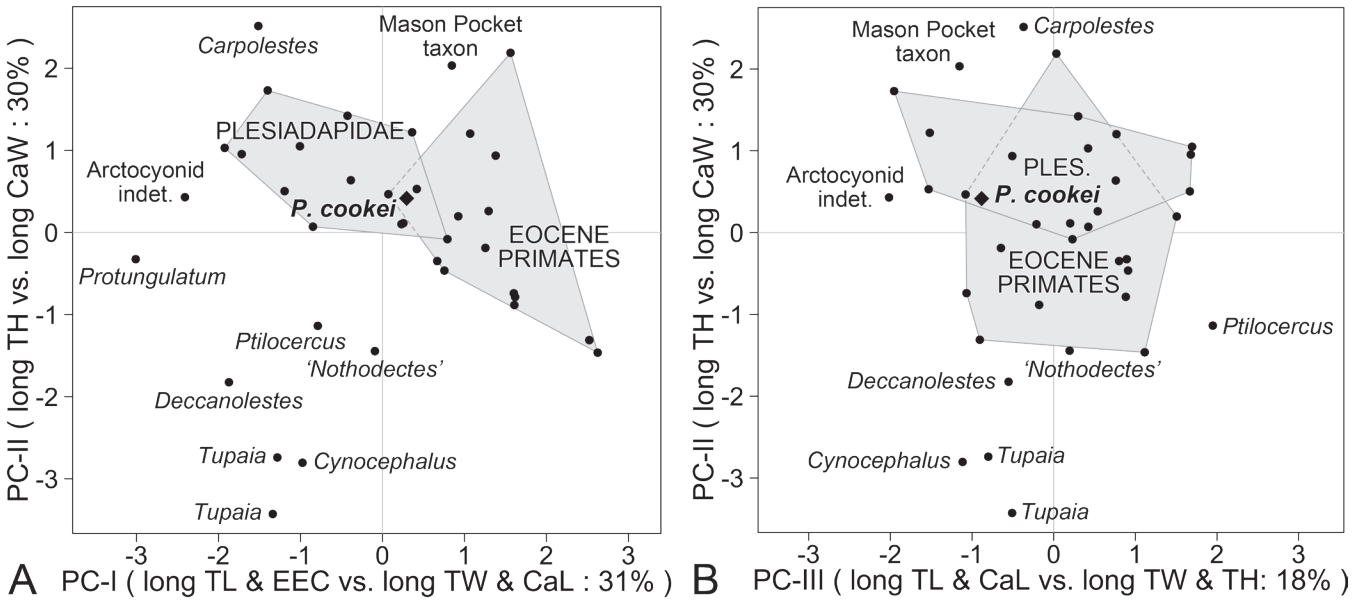

FIGURE 71.— Principal component scores calculated from distal humerus measurements TW, TH, CaW, TL, CaL, and EEC (trochlea width, trochlea height, capitulum width, trochlea length, capitulum length, and entepicondyle width) for *Plesiadapis cookei* and 37 comparative taxa in Table A-II-44. **A**, scatter plot of PC-I on the abscissa and PC-II on the ordinate. **B**, scatter plot of PC-III on the abscissa and PC-II on the ordinate. Measurements were standardized before analysis by transforming to logarithms and subtracting the mean ln value for each taxon. Convex polygons link plesiadapids and link Eocene euprimates in the comparative sample. In simplest terms, loadings indicate that PC-I contrasts taxa with a longer trochlea and wider entepicondyle, on the left, versus taxa with a wider trochlea and longer capitulum, on the right (31% of variance). PC-II contrasts taxa with a higher trochlea, below, versus taxa with a wider capitulum, above (30% of variance). PC-III contrasts taxa with a longer trochlea and longer capitulum, on the left, versus taxa with a wider trochlea and higher trochlea, on the right (18% of variance). Note that the polygons of plesiadapids and Eocene primates overlap, and *P. cookei* (diamond) falls in this zone of overlap. The position of '*Nothodectes'* (AMNH 17379) may indicate that it does not belong to *Nannodectes gidleyi*. Another humerus not plotted here (because it is incomplete) is also associated with *N. gidleyi*. It is nearly identical to that of *N. intermedius* and seems more likely than that of '*Nothodectes* to have been a component of the skeleton of *N. gidleyi.*' Some taxa such as *Saxonella* fall within the convex polygon of Plesiadapidae and/or Eocene primates.

anatomically natural position (Fig. 72), the MC I facet of the trapezium faces radially and ventrally compared to the MC II facet of the trapezoid. This suggests the presence of a divergent pollex. Furthermore, the MC I facet is broadly separated from the MC II facet when the two bones are articulated, indicating that MC I and MC II did not contact each other in the articulated hand (Figs. 40, 41, and 72). Beard (1989) recognized that *N. intermedius* had a widely divergent pollex. However, he considered MC I and II of *N. intermedius* to have had a relatively immobile contact with one another, based on study of the metacarpals alone. This interpretation now seems unlikely given the overall similarity between elements of *P. cookei* and *N. intermedius* and re-identification of Beard's 'MC II' as 'MC V' (discussed above; see also Boyer et al., 2013). The convex, slightly incongruent articulation between trapezoid and trapezium suggests the presence of substantial mobility at the trapezoid-trapezium-scaphoid joints, meaning MC I could have moved quite extensively relative to the other metacarpals.

This inferred mobility is similar to the mobility in the pollex of many euprimates (Napier, 1961). It differs in detail, however, in that hand types defined by Napier (1961) as

FIGURE 72.— Articulated forelimb and hand of *Plesiadapis cookei* (UM 87990). Surface reconstructions are based on high-resolution CT data. **A**, right carpus and metacarpus. The capitate and centrale are not preserved for UM 87990 (this view illustrates how preserved bones of the carpus and metacarpus can be fit together, despite missing elements). **B**, various views of carpus. Note in radial view that the proximodistal axis of the articular surfaces for the metacarpals face dorsally relative to the articular surface of the radius. This suggests the hand was habitually dorsiflexed. **C**, reconstructed right forearm with metacarpals. Joint surfaces are positioned so that they are maximally overlapping. Note that because of the palmar orientation of the distal articular surface of the radius, the degree of natural dorsiflexion is muted from what is indicated by analysis of the carpal bones alone. **D**, views from 'C' with the right humerus included. Note that the palmar surface of the hand is somewhat supinated relative to the humerus, reflecting torsion between the proximal and distal ends of the radius. Abbreviations: *Hm*, hamate; *Hum*, humerus; *Lu*, lunate; *MC I*, pollical metacarpal; *MC III*, third metacarpal; *MC V*, fifth metacarpal; *Ps*, pisiform; *Rd*, radius; *Sc*, scaphoid; *Tr*, triquetrum; *Trd*, trapezoid; *Trm*, trapezium; and *Uln*, ulna.

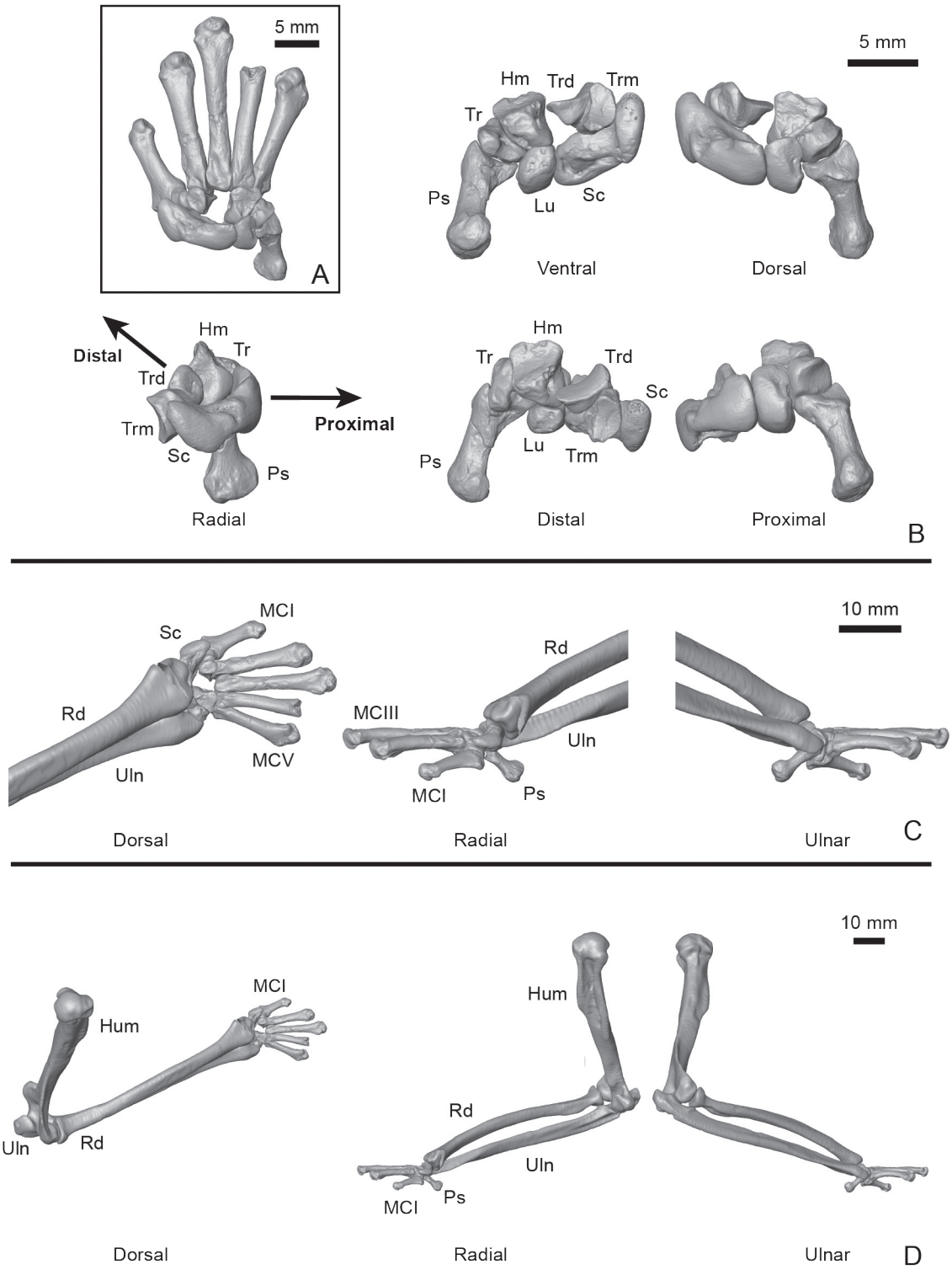
5 mm
A
5 mm
Hm
Trd
Trm
Tr
Ps
Lu
Sc
Ventral
Dorsal
Distal
Hm
Tr
Trd
Trm
Sc
Ps
Proximal
Radial
Hm
Tr
Trd
Sc
Ps
Lu
Trm
Distal
Proximal
B
10 mm
MCI
Sc
Rd
MCV
Uln
Rd
MCIII
Uln
MCI
Ps
Dorsal
Radial
Ulnar
C
10 mm
MCI
Hum
Uln
Rd
Hum
Rd
Uln
MCI
Ps
Dorsal
Radial
Ulnar
D

'opposable' obtain their mobility at the carpometacarpal joint, not at an intercarpal joint or joints. The carpometacarpal joint of the first digit in *P. cookei* does not appear highly mobile due to the very close fit between the opposing facets of MC I and the trapezium. Therefore, if the trapezium has been correctly identified in *P. cookei*, its articular relationships and overall morphology suggests a different mechanism for generating pollical mobility as compared to extant euarchontans.

Trapezoid.— The saddle-shaped facets for the trapezium and MC II suggest that both bones were mobile with respect to the trapezoid.

Hamate.— The three proximal carpal articular surfaces of the hamate suggest it to have been a highly mobile bone (along with the rest of the distal carpal row), meaning that it was capable of assuming many positions and articular configurations with respect to the rest of the carpus. Such wrist mobility is typically seen only in arboreal animals specialized for grasping supports at a variety of angles (e.g., lorisids; Boyer et al. 2013, 2016)

Pollical metacarpal.— Beard (1989) estimated that MC I of *N. intermedius* diverged from the second metacarpal by 73°. This is in the range of lorisiform euprimates with specialized grasping capacities. He also suggested that there was limited mobility at the carpometacarpal joint due to what he interpreted as a facet between MC I and MC II. He considered these features and torsion of the metacarpal shaft to have enabled advanced 'pseudo-opposability' of MC I (Napier, 1961). As mentioned (see trapezium and trapezoid comparisons above), we disagree with this assessment based on our interpretations of the relationship between the trapezium and trapezoid, and our assessment of the mobility at the trapezium-trapezoid-scaphoid joints of *P. cookei*. We agree that MC I was divergent, but we estimate the divergence to have been only ~24° (an estimate that is poorly constrained), which is more divergence than is seen in many treeshrews, dermopterans, and platyrrhines (Boyer et al., 2013: fig.18).

The large radial tuberosity on the proximal end of MC I in *P. cookei* seems likely to have received the tendon of the abductor pollicis longus muscle, a ventriflexor of the wrist and abductor of the wrist and pollex.

Metacarpus.— The wedge-shaped proximal ends of MC II–IV articulate to produce a pronounced transverse metacarpal arch (Fig. 48B). Napier (1961) explained that this gives the hands the capacity for convergence (i.e., when the proximal interphalangeal joints flex, the finger tips converge on each other), which enhances grasping ability. The extensive dorsally-facing part of the distal articular surfaces indicates the capacity for stable 'hyper-dorsiflexed' finger postures as are used in pronograde and orthograde quadrupedal locomotion (Jenkins, 1974).

Proximal phalanx I.— Although it is shorter than the other proximal phalanges, this bone is still substantial in length indicating an important role in clinging and grasping, which is consistent with implications of morphology observed in the digit I metapodials. The projecting lateral process of the proximal end of proximal phalanx I may have served to increase the attachment area and mechanical advantage for intrinsic flexor and adductor musculature of the hand.

Proximal phalanges II–V.— Several features of the proximal phalanges and metacarpals suggest a metacarpophalangeal joint that was (1) mobile in abduction-adduction, axial rotation, and flexion-extension; and (2) most stable in a dorsiflexed position, where the greatest overlap in corresponding joint surface area is formed (see also Boyer et al., 2013). Features supporting this interpretation include the concave spherical shape and dorsal orientation of the proximal phalanx proximal articular surface, as well as the convex spherical shape and dorsal orientation of the metacarpal distal articular surface. The orientation of the distal articular surface of the proximal phalanx, its differential radius of curvature, and the presence of extensive flexor sheath ridges suggest habitual ventriflexion of the proximal interphalangeal joints (Godinot and Beard, 1991; Boyer et al., 2013).

Intermediate phalanges.— The dorsoventrally deep shafts of the intermediate phalanges suggest that they were resistant to parasagittal stresses imposed by the weight of the body during antipronograde clinging postures, or possibly stresses due solely to the force of contraction of the digital flexor muscles. The form and orientation of the distal articular surfaces suggest that the distal phalanges would have had a large range of flexibility and could have attained substantially dorsiflexed configurations (unlike the intermediate phalanx at the proximal interphalangeal joint). However, when joint surfaces are maximally overlapped, the distal phalanx is strongly ventriflexed (Godinot and Beard, 1991).

Distal phalanges.— Like the intermediate phalanges, the distal phalanges also exhibit proportionally large dorsoventral depth. Thus, we infer that the distal phalanges were also capable of resisting parasagittal bending moments. The strongly curved claw shafts, and large distally positioned extensor tubercles suggest a capacity for strongly clinging to or grappling on varied substrates.

Hand proportions.— We consider the most likely phalangeal-metacarpal ratio for *P. cookei* to be ~130% (using 'set 2' metacarpals). Other smaller-bodied plesiadapids are in this range as well. Kirk et al. (2008) demonstrated that this value is typical for arboreal animals with prehensile hands. The lower value of *P. tricuspidens* at 111% is seen in partially terrestrial animals. However, there is little other evidence of terrestriality in *P. tricuspidens*. It may be that the elongation of digits in plesiadapids was influenced to an important degree by the distal phalanx, which seems to be proportionally larger in large plesiadapids compared to smaller ones. Unfortunately, we did not have an adequate comparative dataset to examine when and how long claws contribute to digit length in mammals. A less interesting possibility for *P. tricuspidens* is that the 'species mean' approach we are obliged to use skews the estimates of digit length relative to metacarpal length. The values computed for other plesiadapids reported here are all based on craniodental-postcranial associations of one or two individuals. As discussed in more detail later, there is also some evidence that the low values for *P. tricuspidens* are the result of using the digit V proximal phalanges instead of digit III/IV.

Pelvic girdle and hind limb

Innominate.— The narrow ilium of the innominate suggests that *P. cookei* had relatively small gluteal muscles and limited capacity for forceful extension of the thigh (George, 1977; Sargis, 2002b). A distinct depression for the obturator externus muscle (an external rotator) and a robust attachment area for pectineus (an internal rotator) may indicate that rotational movements were important components of locomotor behavior. This is further suggested by the position of the ischial spine, which forms a trochlea for the obturator internus muscle very close to the acetabulum (~2 mm inferior to it). Thus the major effect of contraction would be lateral rotation and abduction of the thigh. When the spine is more inferiorly positioned, the muscle can have more of an effect in flexion of the thigh (Gambaryan, 1974).

The hamstrings were probably not well-developed, as surmised from the narrow dimensions of the ischial tuberosity. Furthermore the fact that the ischium does not display any retroflexion suggests against the importance of vertical leaping in its locomotor repertoire (Fleagle and Anapol, 1992). Finally, the inferior position and narrow dimensions of the pubic symphysis are not typical of highly active, hind limb driven animals (Boyer and Bloch, 2008). The cranial buttressing of the acetabulum may indicate the use of orthograde postures in which body weight was directed through the cranial part of the lunate facet, as suggested by other authors (e.g., Beard, 1989).

Femur.— The femur of *P. cookei* reinforces the functional signal inferred from the innominate. The femur appears specialized for behaviors that emphasize medial and lateral rotation of the bone, rather than flexion and extension. The shape of the femoral head and the asymmetry introduced by the position of the fovea capitis femoris indicate that the articular surfaces of the femur and acetabulum correspond most closely when the femur is flexed, abducted, and rotated laterally. The motions that maintain the closest fit between the joints are adduction–abduction and medial–lateral rotation.

Abduction from a flexed, medially rotated position engages the lateral extension of the femoral condyle with the inferior aspect of the lunate facet (Fig. 73: position 4). From this position, no more abduction was possible, but lateral rotation, followed by extension, allowed the condyles to shift farther caudally. Relatively small greater and third trochanters, and a medially projecting (rather than posteriorly projecting) lesser trochanter are further indicative that the femur was not flexed and extended forcefully using the gluteal musculature (Sargis, 2002b). However, the expansive trochanteric fossa and expanded area distal to the intertrochanteric crest for the obturators and quadratus femoris, respectively, would have given the limb a capacity for powerful abduction and lateral rotation of a flexed, adducted thigh. The large, medially projecting lesser trochanter would have provided a large lever arm for the iliopsoas muscle, from a somewhat extended, abducted, medially rotated posture. Iliopsoas would also have served to flex, adduct, and laterally rotate the femur.

The proximally restricted patellar groove and distally extensive condyles suggest that full extension of the knee was infrequent or impossible, and that a flexed knee was a habitual posture. Relatively shallow femoral condyles suggest extension of the knee was not particularly forceful (Beard, 1989; Sargis, 2002b) when it occurred. The pattern of buttressing of the margins of the patellar groove is consistent with a posture wherein the femur was habitually flexed and abducted, and the knees were flexed (Boyer and Bloch, 2008).

Tibia.— Most features of the tibia of *P. cookei* argue against both leaping and running. These include the anteroposteriorly relatively shallow tibial plateau, a concave lateral tibial condyle, the absence of a prominent cnemial crest, a proximally situated groove for the patellar tendon, and an ungrooved astragalar articular surface (Boyer and Bloch, 2008).

The relative lengths of the tibial and femoral condyles (Tables A-II-31, 33) have implications for mobility at the knee (Sargis, 2002b). The ratio between the lengths of the medial femoral and tibial condyles is 0.9, whereas that between the lateral condyles is 0.75. A lateral tibial condyle that is enlarged, and a corresponding lateral femoral condyle that is reduced, compared to one another or to the medial condyles, suggests that *P. cookei* had an enhanced capacity to rotate the tibia axially on the femur, with the medial condyle serving as the axis of rotation and translation occurring between the lateral condyles.

The relatively large pit for the popliteus tendon on the femur may indicate that this muscle had an important role in causing or maintaining a certain degree of medial rotation. The dramatic concavity of the posterior surface of the proximal tibial shaft may indicate a robust tibialis posterior muscle or flexor digitorum tibialis. The former of these muscles is a plantar flexor and invertor, whereas the latter is typically the most important muscle for flexing the digits during powerful grasping in certain primates (Boyer et al., 2007). The concavity of the lateral surface would have held part of the attachment of tibialis anterior, a dorsiflexor and pedal invertor, but this surface is not unusual in its proportional size or morphology.

The distal end of the tibial shaft is notable in the roughened surface of the fibular notch and the strong crest forming the anterior border of the fibular notch. These features suggest a syndesmosis with the fibula and an especially robust anterior tibiofibular ligament. The distal articular surface of the tibia is notable for its flat surface for articulation with the astragalus, and for the convex lateral surface of the medial malleolus. These features suggest that the astragalus may have been able to pivot medially and laterally on the tibia, with its medial surface sliding around the convex lateral surface of the medial malleolus. This motion would result in abduction and adduction of the foot relative to the tibia. The distomedial pits of the medial malleolus reflect a robust deltoid ligament that attached the tibia to the navicular, astragalus, and calcaneum, thus helping to maintain the integrity and stability of this joint.

Fibula.— A striking feature of the fibula is the blade-like crest projecting posterolaterally from the proximal end. This crest extends the posterior or 'flexor surface' of the fibula proximally, far beyond its limit in humans, for instance. This

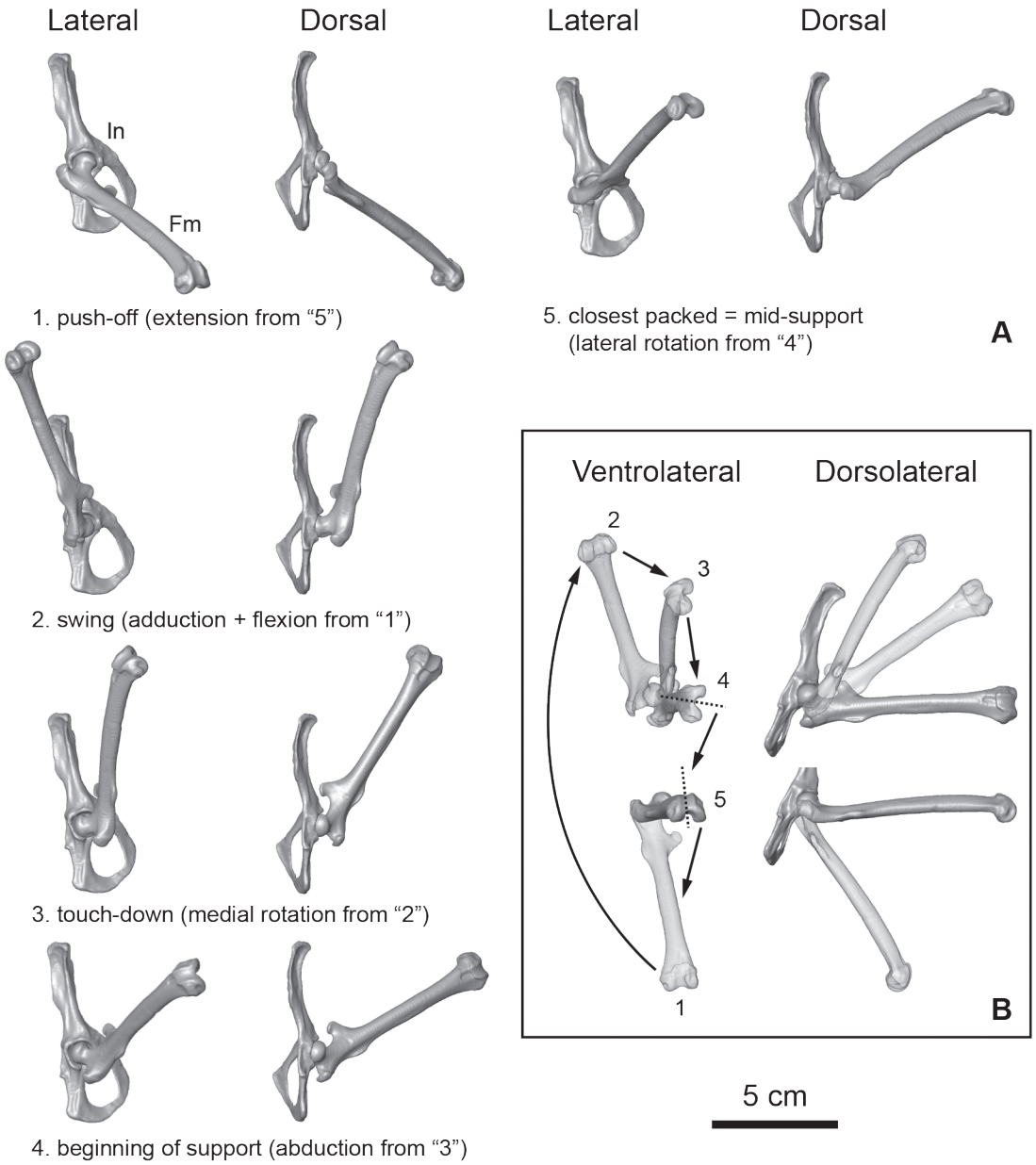

FIGURE 73.— Articulated innominate and femur of *Plesiadapis cookei* (UM 87990). Images are based on CT data. **A**, major increments of change in femoral orientation and articulation with the innominate during a gait cycle. Step 5 shows a closest-packed posture suggesting that the usual or average posture of the femur is one in which it is flexed, abducted and slightly laterally rotated. Steps 1–5 show how abduction-adduction, mediolateral rotation, and flexion-extension movements combined during a gait cycle to bring the thigh through a large positional and angular excursion, while keeping the joint surfaces of the acetabulum and femur in maximal overlap. Going from the closest-packed position of the hip to pushing off from the substrate (steps 5 | 1) required simple extension the abducted femur. During the swing phase (1 | 2) the thigh was adducted and flexed without any axial rotation. At touch down (2 | 3) the femur was probably medially rotated, especially if the tibia and foot were incorporated into increasing the length of the stride (see below). The beginning of the propulsive phase (3 | 4) likely entailed abduction until the posterolateral extension of the femoral head articular surface abutted the acetabulum. From here, lateral rotation would have brought the femur back to its closest packed position while also causing the body to swing forward (anteriorly) and ventrally on the tibae (4 | 5). From the closest packed position the femur could have extended again (steps 5 | 1), pushing the body forward again. **B**, summary of movements in different planes through the gait cycle. Abbreviations: *Fm*, femur; *In*, innominate; *Ectf*, ectal facet; *Stcf*, sustentacular facet.

crest would greatly augment the area of origin for both the flexor digitorum fibularis muscle on the posteromedial side of the crest and the peroneus longus muscle on the opposite side (anterolateral). Functions associated with these muscles, such as forceful flexion of the digits and eversion of the foot, may have been enhanced. The rugose tuberosity for the fibular notch on the medial aspect of the distal end suggests a strong tibiofibular syndesmosis, and thus limited mobility between the tibia and fibula.

Astragalus.— The functional features of the astragalus have been discussed at length for plesiadapids and plesiadapiforms (Szalay and Decker, 1974; Szalay, 1984; Chester et al., 2015). However a few observations and interpretations can be added here. Beard (1989) speculated on the nature and degree of mobility between the astraglus and tibia, but study of these elements in a single individual allows a better assessment of their mobility.

Articulation and manipulation of the astragalus and tibia of UM 87990 show that when the tibia is fully dorsiflexed on the astragalus, the shaft of the tibia forms an angle of slightly less than 90° with the head and neck of the anteriorly projecting astragalus. When the astragalus is plantarflexed by rotating it through the full 90° of arc formed on the lateral tibial facet, there are two other conjunct motions that occur because of the slanting surface of the lateral tibial facet and the laterally concave surface of the medial tibial facet (Fig. 74): (1) the astragalus inverts (rotates laterally on its proximodistal axis) by a full 90°; and (2) the distal end of the astragalus rotates medially (around a dorsoplantar axis) by a full 90°. The angle between the astraglar neck and tibia changes by somewhat less than 90°. Thus the act of 'plantar-flexion' of the astragalus on the tibia, results in relatively little true plantar flexion (see discussion below for the broader significance of these features for positional behaviors).

To compare *P. cookei* with other plesiadapids and other mammals, 18 linear and five angular measurements were taken on the astragalus (Fig. 61; Tables A-II-36 to A-II-38). The linear measurements were standardized against absolute size in the usual way (see Materials and Methods) using a geometric mean of astragalus measurements Ast01, 04–15, and 17–18. Angles were measured in degrees and analyzed in both degrees and radians; analyses in degrees and radians yielded the same result.

Principal components analysis of the size-standardized linear measurements of astragali (Fig. 75) indicates, first, that plesiadapiform astragali are similar to each other, and second, that plesidadapiform astragali are well-separated from those of euprimates and dermopterans. Plesiadapiform astragali differ from those of euprimates principally in being shorter and in having a wide flexor fibularis groove (PC-I). Plesiadapiform and primate astragali together differ from those of the dermopteran *Cynocephalus* principally in having a wider ectal facet and a relatively short astragalar body (PC-II). The third principal component (PC-III) does not separate any of the taxa of interest. The euprimates closest to plesiadapiforms in Fig. 75A are lorises, a similarity that supports Beard's (1989) interpretation of plesiadapiforms as slow, cautious arborealists.

Principal components analysis of angular measurements of astragali (Fig. 76) indicates, again, that plesidadapiform astragali are similar to each other, and well separated from those of euprimates and dermopterans. Plesiadapid astragali all plot in the lower part of the plesiadapiform polygon in Fig. 76A. Plesiadapiform astragali differ from those of euprimates principally in having larger angles between the fibular facet and medial tibial facet and between the medial and lateral tibial facets, and in having a smaller angle between the ectal and fibular facets (PC-I). The second and third principal components (PC-II and III) do not separate any of the taxa of interest. The euprimate closest to plesiadapiforms in Fig. 76A is *Galago*, a similarity that weakens Beard's (1989) interpretation of plesiadapiforms as slow, cautious arborealists.

Calcaneum.— Functional features of the plesiadapid calcaneum have been discussed at length by other authors (Szalay and Decker, 1974; Chester et al., 2015). The most important feature cited is the helical form of the calcaneal astragalar facets, which allow the astragalus to rotate the dorsal surface of its distal end to face medially at the same time as it moves proximally on the calcaneum. The result is inversion of the mediolateral axis of the lower ankle joint and the entire foot (Fig. 77). This inversion is illustrated in the context of the entire hind limb in Figure 78, which shows a posture possibly utilized while descending the trunks of large-diameter trees.

Hind foot reversal is an ability exhibited by many species of arboreal mammals including carnivorans, euarchontans, gliroids, marsupials, multituberculates, and others (Jenkins and McClearn 1984). It has apparently great adaptive value in allowing the claw tips to face ventrally while the foot is plantar-flexed, thereby allowing an animal to engage its claws while clinging upside down on a vertical substrate. Although many primates are capable of hind foot reversal, it is unclear whether they rely on this for headfirst descent on inclined substrates (Meldrum et al. 1997). The mechanism exhibited by *P. cookei* is similar to that of tree squirrels, treeshrews, and euprimates, where most of the inversion happens at the lower ankle joint, with additional rotation accomplished at the transverse tarsal joint, and rotation at the knees augmenting reversal (Meldrum et al., 1997). Marsupials, on the other hand, accomplish much of their rotation at the talocrural joint (Szalay, 1984). Likewise, multituberculates appear to have utilized rotation at the talocrural joint, combined with plantar flexion and inversion at the subtalar joints to complete hind foot reversal (Jenkins and Krause 1983; Krause and Jenkins 1983).

To gauge the similarity of the calcaneum of *P. cookei* and other plesiadapiforms to those of dermopterans, primates, scandentians, and other mammals, 19 measurements were made on 54 calcanea. The measurements are illustrated in Figure 62, and listed in Tables A-II-39 and A-II-40. These were standardized for size in the usual way, subtracting the mean of log-transformed Cc-1, 4–7, 9–11, and 17–18 from the natural log value of each measurement. The resulting size variables were then compared using principal components analysis. Principal axes I and II separate plesiadapiforms, dermopterans, scandentians, and primates (Fig. 79A).

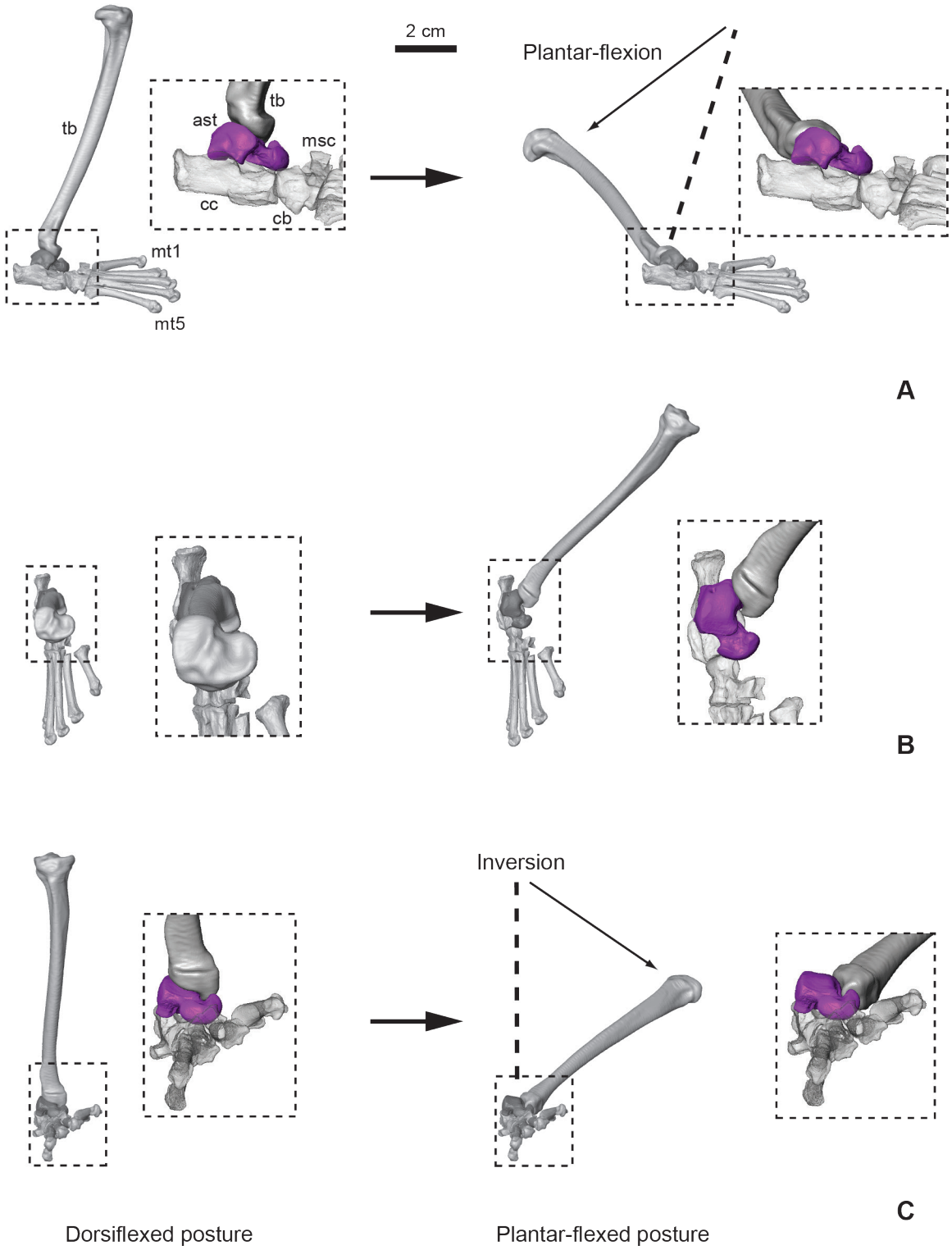
2 cm
Plantar-flexion
tb
ast
tb
msc
cc
cb
mt1
mt5
A
B
Inversion
C
Dorsiflexed posture
Plantar-flexed posture

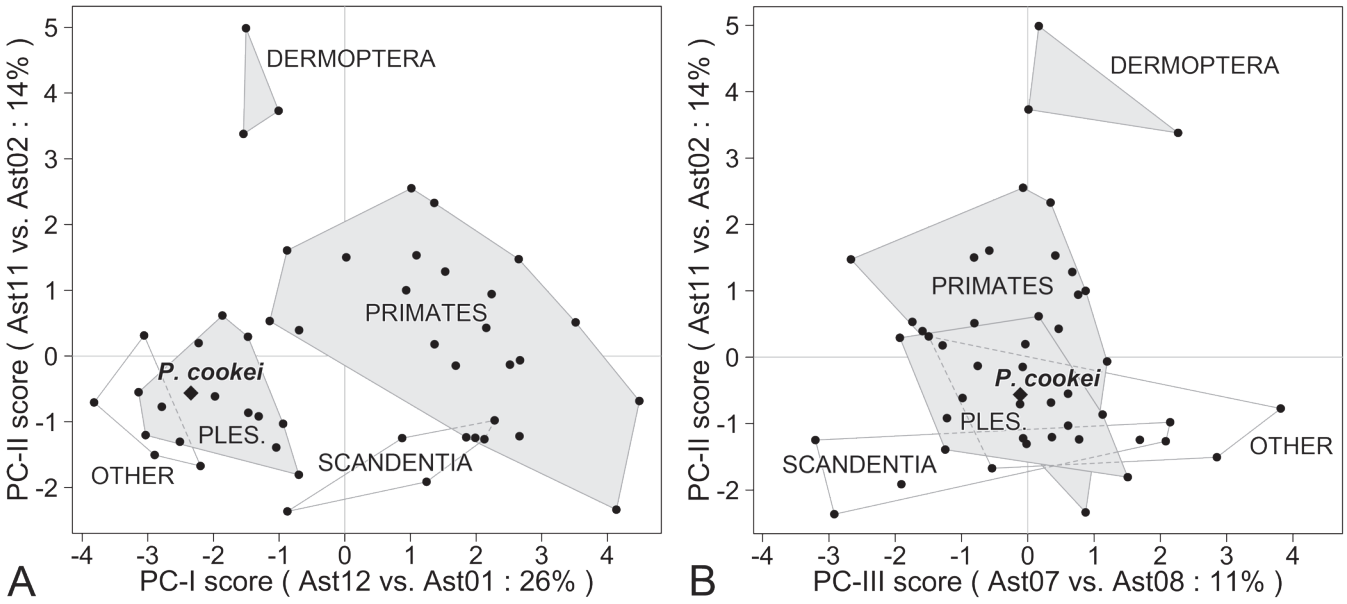

FIGURE 75.— Principal components analysis of 18 size-standardized astragalus shape variables (calculated from measurements in Tables A-II-36 and A-II-37). **A**, scatter plot of PC-I on the abscissa and PC-II on the ordinate. **B**, scatter plot of PC-III on the abscissa and PC-II on the ordinate. Measurements were standardized before analysis by transforming to logarithms and subtracting the mean ln value of Ast-1, 4–15, and 17–18. In simplest terms, loadings indicate that PC-I contrasts taxa with a wide flexor fibularis groove, on the left, versus taxa with a long astragalus, on the right (26% of total variance). PC-II contrasts taxa with a wide ectal facet, below, versus taxa with a long astragalar body, above (14% of variance). PC-III contrasts taxa with a wide lateral tibial facet, on the left, versus taxa with a high medial tibial facet, on the right (11% of variance). Plesiadapiformes are well separated from Primates and Dermoptera on PC axes I and II, and *Plesiadapis cookei* (diamond) falls near the center of Plesiadapiformes on all three shape axes. 'Other' here includes *Deccanolestes*, *Procerberus*, and *Protungulatum*.

FIGURE 74— Articulated tibia and foot of *Plesiadapis cookei* (UM 87990). Images are based on high-resolution and medical CT data. The transition from dorsiflexion to plantar flexion is shown in three views. **A**, lateral view of a partly inverted foot. Note that the metatarsals and tibia form a slightly acute angle when dorsiflexed in the image on the left. They form an obtuse angle, augmented by ~60º when plantar-flexed in the image on the right. **B**, dorsal view of a partly inverted foot. Note that the anteroposterior axis of the tibial plateau is parallel to the proximodistal axis of the metatarsals in the dorsiflexed image. The anteroposterior axis of the tibia points out of the plane of the page in the plantar-flexed image. Thus the proximodistal axis of the foot now points mediodistal relative to the tibia. **C**, anterior view of the partly inverted foot. The proximodistal axis of the tibia is offset from the mediolateral plane of the foot by 60–70º (close to neutral) in the dorsiflexed image. The mediolateral plane of the foot is aligned with the proximodistal axis of the foot in the plantar-flexed image. The complex motion that occurs at the tibioastragalar joint is a consequence of the complexity of the joint surface. Specifically, the medially-concave medial tibial facet and the obliquely-oriented lateral tibial facet lead to these conjunct motions. Abbreviations: *ast*, astragalus; *cb*, cuboid; *cc*, calcaneum; *msc*, mesocuneiform; *mt1*, first metatarsal; *mt5*, fifth metatarsal; and *tb*, tibia.

P. cookei falls in a generalized position in a region where these groups overlap.

We made a similar principal components analysis of six angles measured on the same calcanea. The angles are illustrated in Figure 62, and the resulting measurements are listed in Table A-II-41. In this case, principal axes I and II do not clearly separate plesiadapiforms, dermopterans, scandentians, and primates (Fig. 79B). *P. cookei* falls in a generalized position in a region where these groups overlap, but the analysis of calcaneal angles is not very informative.

Cuboid.— The orientation of the proximal and distal facets on the cuboid indicate habitual abduction of the foot with respect to the proximal tarsus. The cuboid facet on the calcaneum is medially rotated by ~15°, but subtracting the ~60° angle between the proximal and distal cuboid facets reveals that the metatarsal facet would have faced 45° laterally with respect to the axis of the calcaneum. Manipulation of the articulated calcaneum and cuboid reveal that they do not rotate very extensively, contrary to Szalay and Decker (1974) and Beard (1989), who described movements at this joint in other plesiadapids and plesiadapiforms. There is much more mobility in abduction and adduction of the cuboid on the calcaneum, thereby reducing or increasing the 45° of abduction that occurs in the closest packed position. In an inverted foot position, mobility in abduction–adduction of the foot translates to

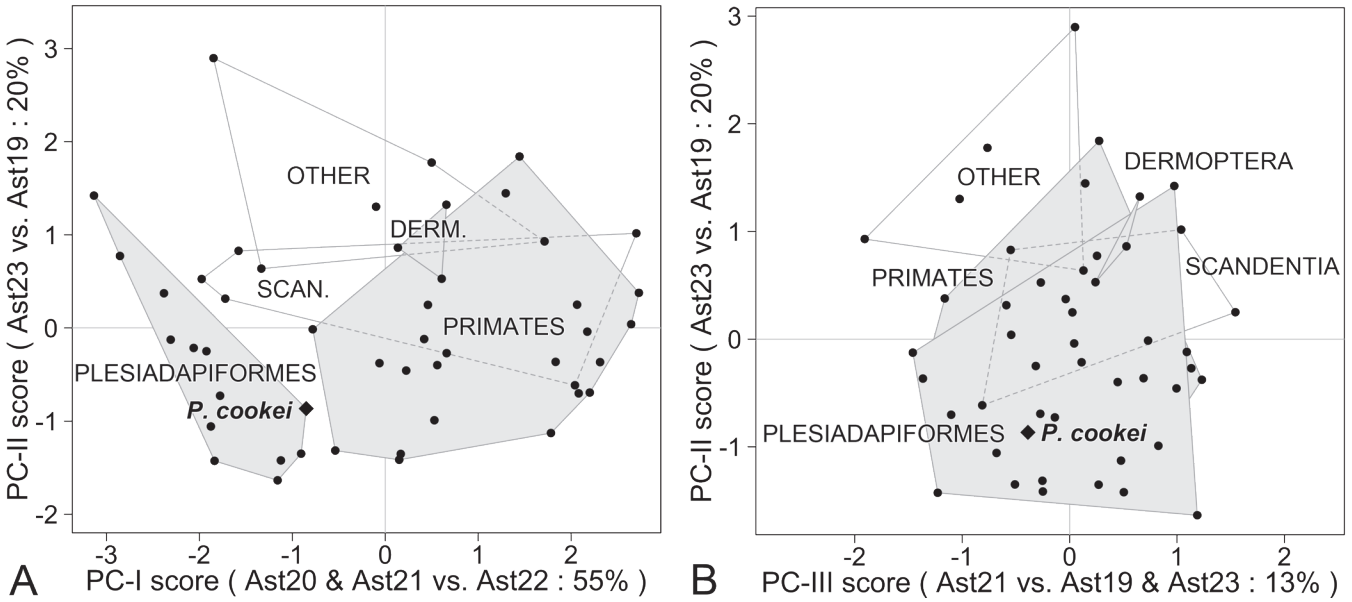

FIGURE 76.— Principal components analysis of five astragalus angles (A-II-38). **A**, scatter plot of PC-I on the abscissa and PC-II on the ordinate. **B**, scatter plot of PC-III on the abscissa and PC-II on the ordinate. In simplest terms, loadings indicate that PC-I contrasts taxa with larger angles between the fibular facet and medial tibial facet and between the medial and lateral tibial facets, on the left, versus taxa with a larger angle between the ectal and fibular facets, on the right (26% of total variance). PC-II contrasts taxa with a larger angle between the major axis of the head and plane of the lateral tibial facet, below, versus taxa with a larger angle between the fibular facet and lateral tibial facet, above (14% of variance). PC-III contrasts taxa with a large angle between the medial and lateral tibial facets, on the left, versus taxa with large angles between the fibular facet and lateral tibial facet and between the major axis of the head and plane of the lateral tibial facet, on the right (11% of variance). Plesiadapiformes are well separated from Primates and Dermoptera on PC axis I, but separations between other groups are not so clear. 'Other' here includes *Deccanolestes*, *Procerberus*, and *Protungulatum*.

plantarflexion–dorsiflexion relative to the more proximal limb elements (i.e., relative to the long axis of the tibia).

Ectocuneiform.— The presence of an MT II facet on the ectocuneiform indicates that the tarso-metatarsal joint of MT III was distally positioned relative to that for MT II. Thus the foot would not have been as mobile as that of *Cynocephalus,* stepsirrhine euprimates, and other taxa that have tarsometatarsal joints II–V lying in a single plane perpendicular to the proximodistal axis of the foot. In having a proximally inset MT II, it is more like a tupaiid, squirrel or callitrichine.

Metatarsal I.— The large size of the medial proximal tubercle relative to the lateral peroneal tubercle of MT I may indicate the presence of a large tibialis anterior tendon, which is a dorsiflexor and invertor of the foot. The strong groove on the medial side of the shaft may have received fibers of an opponens hallucis muscle (Straus, 1930; George, 1977). The saddle-shaped facet for the entocuneiform, the lateral torsion of the distal end relative to the proximal end, and evidence for the presence of a muscle that could pull the hallux more fully into opposition are consistent with previous interpretations that the hallux was specialized for grasping in a way essentially similar to that of euprimates and the treeshrew *Ptilocercus* (Szalay and Dagosto, 1988; Sargis et al., 2007).

Goodenberger et al. (2015) made more explicit quantitative comparisons between *P. cookei*, other plesiadapiforms, and other euarchontans. One feature they quantified is termed the 'physiologic abduction angle' (PAA), which is high (obtuse) when the angle between the plane of the proximal entocuneiform articular surface deviates from being perpendicular to the shaft and faces medially. The effect of high PAA is that when the MT I is articulated with the entocuneiform, the MT I shaft diverges strongly medially and is 'abducted' in its closest packed position. *P. cookei*, *Carpolestes simpsoni*, and other non-primate euarchontans actually exhibit deviation in the opposite direction of euprimates. That is, the entocuneiform facet orientation relative to the shaft is acute (80–90°), which suggests slight adduction in a closest packed position (Goodenberger et al., 2015: fig. 3, table 2).

Bloch and Boyer (2002) noted that the MT I divergence in *C. simpsoni* is accomplished through a medially facing MT I facet on the entocuneiform as well as through strong plantar orientation of the MT I facet. In terms of shaft proportions, *P. cookei* exhibits a robust MT I shaft like that of *Ptilocercus* or *C. simpsoni*, whereas tupaiid treeshrews and dermopterans have a more slender shaft (Goodenberger et al., 2015: fig. 3). In terms of torsion of the shaft, Goodenberger et al. (2015: table 2) reported the MT I distal end to be rotated 17° lateral of plantar. This matches *P. cookei* with scandentians that range from 14° (*Tupaia*) to 15° (*Ptilocercus*). *C. simpsoni* was shown to exhibit greater, euprimate-like torsion at 39° lateral of plantar.

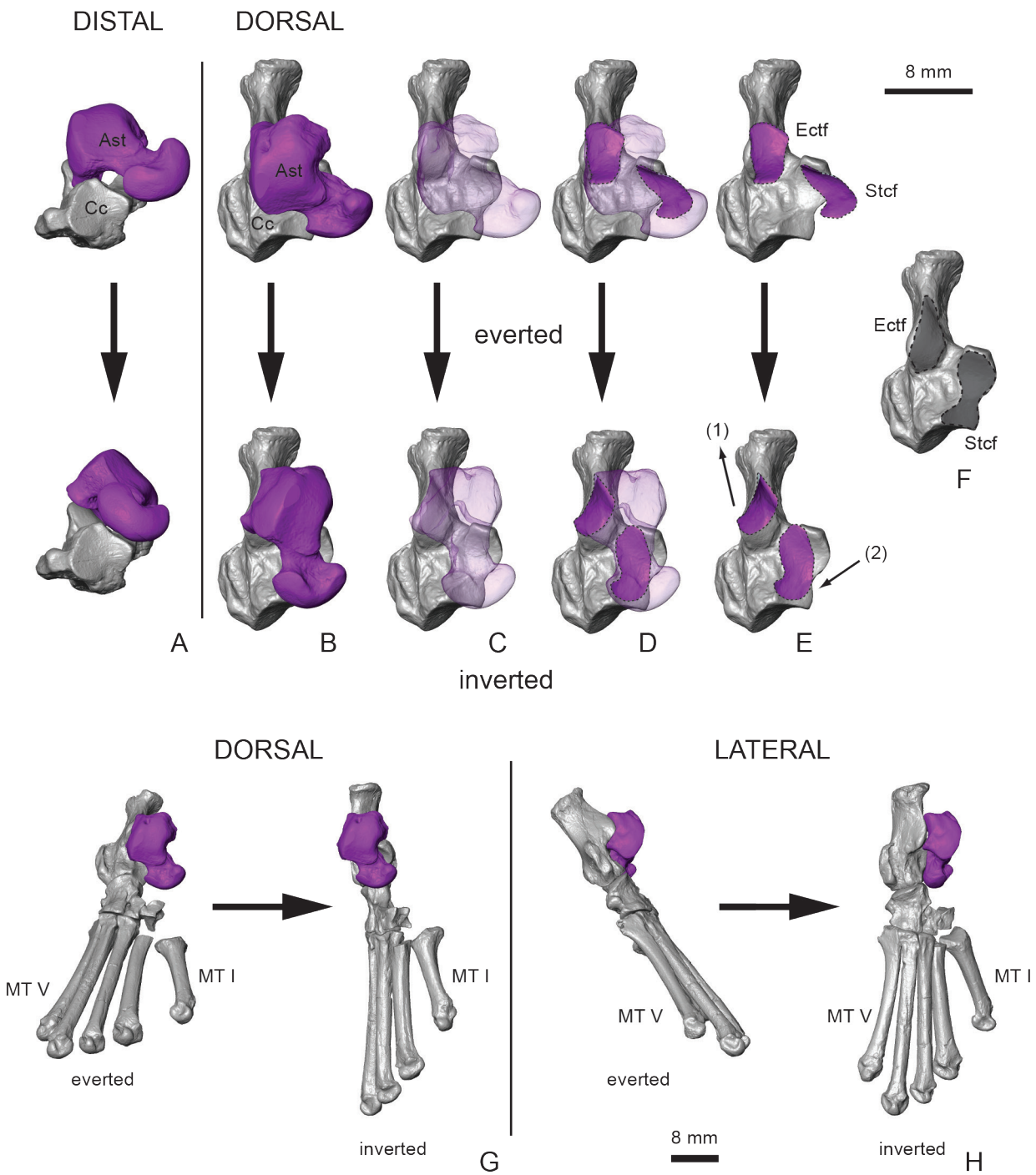

FIGURE 77.— Articulated astragalus, calcaneum, and foot of *Plesiadapis cookei* (UM 87990) to show movement and the degree of inversion possible at the astragalocalcaneal joint. Images are based on high-resolution CT data. **A**, everted (top) and inverted (bottom) astragalocalcaneal joint in distal view, with calcaneum orientation held constant. **B**, everted (top) and inverted (bottom) astragalocalcaneal joint in dorsal view. **C**, everted (top) and inverted (bottom) astragalocalcaneal joint as in B, with the astragalus made transparent to show the astragalocalcaneal articular surface. **D**, everted (top) and inverted (bottom) astragalocalcaneal joint as in C, with calcaneal facets on the astragalus highlighted. **E**, everted (top) and inverted (bottom) astragalocalcaneal joint as in C with calcaneal facets on the astragalus shown in relation to astragalar facets on the calcaneum. Inversion is accomplished by: (1) plantar-flexion and medial translation of the calcaneum at the posterior astragalocalcaneal joint (ectal facets); and (2) simultaneous medial translation and lateral rotation of the calcaneum at the anterior astragalocalcaneal joint (sustentacular facets). **F**, calcaneum in dorsal view with the astragalus removed and astragalar facets highlighted. **G**, astragalus in dorsal view showing the change in foot position with inversion (left to right) at the astragalocalcaneal joints. H, astragalus in lateral view showing the same change in articulation at the astragalocalcaneal facet. Note that inversion also leads to substantial conjoint plantar-flexion of the foot. Abbreviations: *Ast*, astragalus; *Cc*, calcaneum ; *Ectf*, ectal facet; *Stcf*, sustentacular facet.

All euprimates except *Homo sapiens* (15°) have greater torsion according to Goodenberger et al. (2015: table 2).

Body proportions

Body proportions can be quantified by calculating limb indices expressed as percentages. The first and most general of these, the limb-trunk index (Ltr-I; Table A-II-1), is a measure of average forelimb and hind limb length as a proportion of trunk length. The value we calculate for *P. cookei* is 79, which is intermediate between 58 and 89 calculated for *P. insignis* and *Ignacius clarkforkensis*, respectively (Table A-II-45). Unfortunately, we do not have limb-trunk index values for an extant comparative sample.

The brachial index (Br-I) compares forearm length to arm length (radius length divided by humerus length). The value we calculate for *P. cookei* is 101, which is close to that estimated for *P. tricuspidens* (Br-I = 99), and intermediate between 84 and 112 calculated for *P. insignis* and *Carpolestes simpsoni*, respectively (Table A-II-45). A brachial index of 101 is in the range of brachial indices for both lemurs and lorises (98–119) but well below the value for indriids (108–122; Jungers, 1979), gliding mammals (such as *Glaucomys* and *Cynocephalus* ~116), and suspensory sloths (Boyer and Bloch, 2008).

The crural index (Cr-I) compares anatomical leg length to thigh length (tibia length/femur length). The value we calculate for *P. cookei* is 99, which is intermediate between 94 and 104 calculated for *P. insignis* and *Ignacius clarkforkensis*, respectively (Table A-II-45). A crural index of 99 is slightly greater than that of lemurs and lorises (87–99), and substantially greater than the value for indriids (87–88; Jungers, 1979).

The intermembral index (Int-I) compares forelimb length to hind limb length by expressing humerus length + radius length as a proportion of femur length + tibia length. The value we calculate for *P. cookei* is 88, which is greater than the range of 71–80 calculated for *P. insignis*, *Nannodectes intermedius*, and *Ignacius clarkforkensis* (Table A-II-45). An intermembral index of 88 is higher than that for sciurids (68–78; Wood, 1962), *Ptilocercus* (80; Ankel-Simons, 2007), *Tupaia* (73–75; Novacek, 1980; Ankel-Simons, 2007), and lemurs (64–72; Jungers, 1979), but within the range of intermembral indices for lorises (87–90; Jungers, 1979). It is also close to that observed for gliding dermopterans (Boyer and Bloch, 2008). Quadrumanus suspensory taxa tend to have much higher indices (Fleagle 1999; Boyer and Bloch, 2008).

The humerofemoral index (Hf-I) compares anatomical arm length to leg length (humerus length/femur length). The value we calculate for *P. cookei* is 87, which is slightly less than that estimated for *P. tricuspidens* (Hf-I = 92) and greater than the range of 74–84 calculated for *P. insignis*, *Nannodectes intermedius*, and *Ignacius clarkforkensis* (Table A-II-45). A humerofemoral index of 87 is within the range for sciurids (75–105; Wood, 1962).

The radiotibial index (Rt-I) compares forearm length to leg length (radius length/tibia length). The value we calculate for *P. cookei* is 89, which is higher than the range of 67–76 calculated for *P. insignis*, *Nannodectes intermedius*, and *Ignacius clarkforkensis* (Table A-II-45). It is also higher than the range for sciurids (63–70; Wood, 1962).

It is simple but inefficient and often questionable to compare body proportions using indices. Indices are inefficient because they compare measurements in pairs or in small groups, and they are often difficult to interpret because they are ratios dependent on their denominators as well as their numerators. The indices compared here suggest that *P. cookei* may have been most like lorises in overall body proportions.

We sought to test this inference of similarity to lorises with a multivariate comparison. Lengths of the trunk (thorax length + lumbus length), humerus, radius, MC III, femur, tibia, and MT III for *P. cookei* and two other plesiadapiforms are listed in Table A-II-46. Lengths of these body segments for 17 comparable mammalian species are listed in Table A-II-47. All were standardized for analysis by transforming to logarithms and subtracting the mean ln value for each specimen. A principal components analysis of the resulting variables for all 20 genera and species is illustrated in Figure 80.

When PC-II is plotted against PC-I in Figure 80A, and PC-II is plotted against PC III in Figure 80B, much of the area in each plot is occupied by primates. This is not surprising considering that 11 of the 20 species analyzed are primates. PC-I contrasts taxa with a relatively long tibia such as *Tarsius* on the left in Figure 80A, versus taxa with a long humerus and radius such as *Bradypus* on the right. PC-II contrasts taxa with a relatively long MT III such as *Tupaia* near the bottom of both plots, versus taxa with a long femur and tibia such as *Tarsius* and *Galago* near the top of both plots. PC-III contrasts taxa with a relatively long MC III such as *Ateles* on the left in Figure 80B, versus taxa with a long trunk such as *Nycticebus* on the right.

P. cookei has principal component scores near zero, average for the axis, on PC-I and PC-III. It differs from expectation for an average mammal on PC-II, where it falls with mammals having MT III relatively long and the femur and tibia relatively short. *P. cookei*, and plesiadapiforms in general, resemble extant *Tupaia*, sciurids, and callitrichid primates in body segment proportions. *P. cookei* is not particularly close to the one lorisine slow climber, *Nycticebus*, nor is it near *Cynocephalus*.

Summary

The postcranial skeleton of *Plesiadapis cookei*, in terms of morphology and relative proportions, has implications for joint mobility, habitual posture, substrate preference, and habitual behavior. The skeleton as a whole suggests that *P. cookei* was an arborealist primarily adapted (or restricted) to large diameter vertical and horizontal supports. This reconstruction suggests life in a habitat including tree trunks of the forest understory and proximal branches of the forest canopy. Headfirst descent of large supports was likely accomplished using claw-clinging with a reversed (supinated)

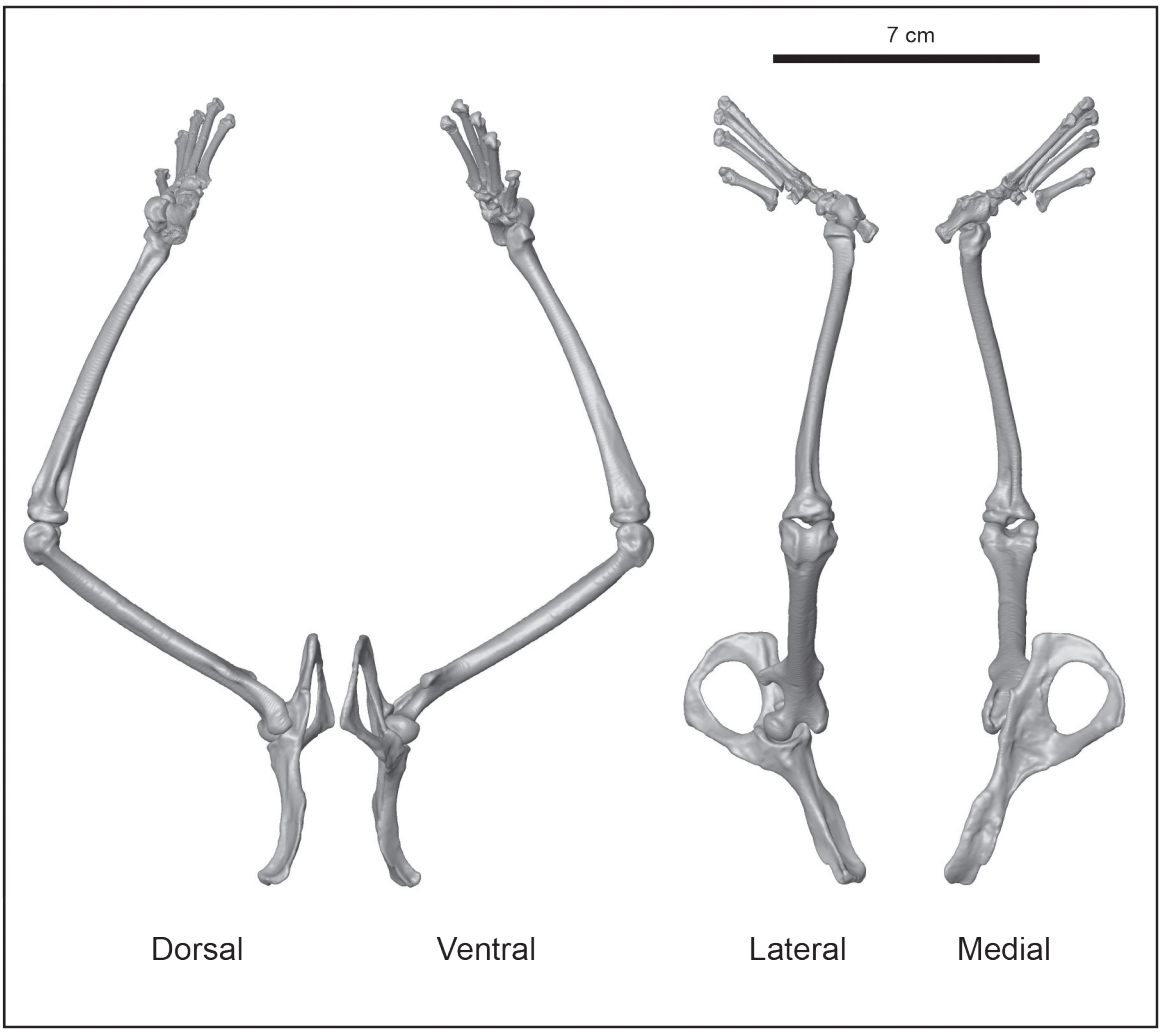

FIGURE 78.— Articulated hind limb of *Plesiadapis cookei* (UM 87990). Images are based on high-resolution CT and medical CT data. Reconstruction illustrates a posture possibly utilized in vertical descent of large-diameter tree trunks. It is likely that further inversion of the foot could have been accomplished by rotations at the transverse tarsal joint and between metatarsals and distal tarsals.

foot. *P. cookei* would have been more cautious and less scansorial in its movements than smaller-bodied plesiadapids, which may be a simple allometric consequence of its larger body size. Previous suggestions that *P. cookei* may have have been more terrestrial (Hamrick 2001) are inconsistent with its gracile limbs and its greater digital prehensility than appreciated previously. Earlier suggestions that *P. cookei* may have used sloth-like suspensory postures (Bloch and Boyer, 2007; Boyer and Bloch, 2008) are inconsistent with morphological evidence suggesting habitually sprawled limbs and dorsiflexed hands and feet (see above), quite the opposite of the medially approximated limbs and ventriflexed hands and feet expected for suspensory animals. A more extensive and detailed discussion of these morphofunctional observations and interpretations is presented in Chapter VII.

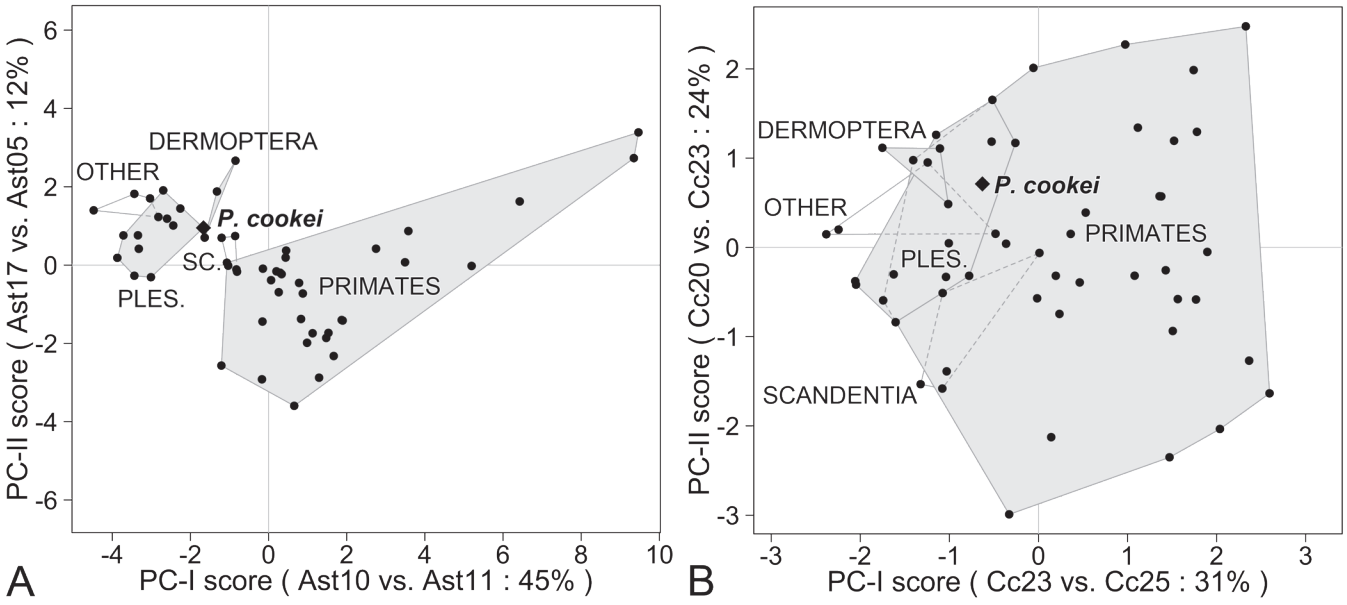

FIGURE 79.— Principal components analyses of calcaneum shape variables and calcaneal angles. **A**, scatter plot with PC-I on the abscissa and PC-II on the ordinate for 19 size-standardized shape variables (calculated from measurements in Tables A-II-39 and A-II-40). Measurements were standardized before analysis by transforming to logarithms and subtracting the mean ln value of Cc-1, 4–7, 9–11, and 17–18. In simplest terms, loadings indicate that PC-I contrasts taxa with a long medial projection of the sustentaculum from the lateral margin of the ectal facet, on the left, versus taxa with a long distal calcaneum measured from the medial apex of the sustentaculum, on the right (45% of total variance). PC-II contrasts taxa with a large calcaneocuboid facet measured perpendicular to the sustentacular facet, below, versus taxa with a calcaneal tuber that is high proximally, above (12% of variance). Note that *P. cookei* (diamond) falls at the nexus of primates, scandentians, and dermopterans. Primates on the far right are *Tarsius* and *Galago*. **B**, scatter plot with PC-I on the abscissa and PC-II on the ordinate for six calcaneal angles (Table A-II-41). Loadings indicate that PC-I contrasts taxa with a large mediolateral angle between the calcaneocuboid facet and tuber axis, on the left, versus taxa with a large angle between the proximal and distal parts of the sustentacular facet (parallel to their axes), on the right (31% of total variance). PC-II contrasts taxa with a large angle between the ectal facet surface and the proximal sustentacular facet surface (parallel to their axes), below, versus taxa with a large mediolateral angle between the calcaneocuboid facet and tuber axis, above (24% of variance). Primates that overlap Plesiadapiformes in calcaneal angle are all *Cebus*. 'Other' here includes *Deccanolestes*, *Procerberus*, and *Protungulatum*.

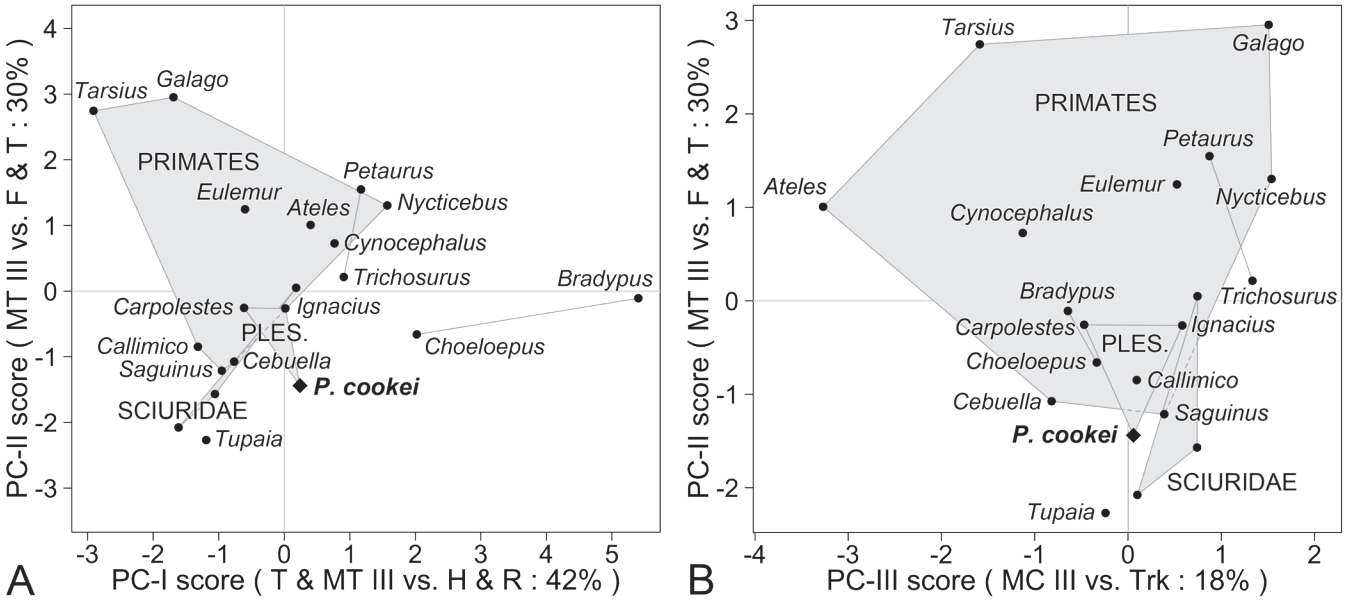

FIGURE 80.— Principal components analysis of body segment lengths in *Plesiadapis cookei* (UM 87990) compared to those of other mammals. Measurements of trunk, humerus, radius, MC III, femur, tibia, and MT III lengths in Tables A-II-46 and A-II-47 were standardized before analysis by transforming to logarithms and subtracting the mean ln value for each specimen. **A**, scatter plot with PC-I on the abscissa and PC-II on the ordinate. In simplest terms, loadings indicate that PC-I contrasts taxa with a long tibia and MT III, on the left, versus taxa with a long humerus and radius, on the right (42% of total variance). PC-II contrasts taxa with a long MT III, below, versus taxa with a long femur and tibia, above (30% of variance). **B**, scatter plot with PC-III on the abscissa and PC-II on the ordinate. Loadings indicate that PC-III contrasts taxa with a long MC III, on the left, versus taxa with a long trunk, on the right (18% of total variance). Note that *P. cookei* (diamond) falls near the average on axes I and III, but differs from most taxa here in having a longer MT III and shorter femur and tibia. It resembles *Tupaia* and Sciuridae in these proportions.

V

LIFE HISTORY

Recovery of a nearly complete skeleton of a single individual of *Plesiadapis cookei* (UM 87990) allows estimation of important life history parameters such as body and brain weight, sex, tooth eruption, and ontogenetic stage.

BODY WEIGHT AND ENCEPHALIZATION

Encephalization in *Plesiadapis cookei*

The first study of body weight, brain morphology, and brain size in *P. cookei* was by Gingerich and Gunnell (2005), based on UM 87990 (Fig. 81). Body weight, estimated from long bone lengths and diameters, was about 2,175 g. The brain was described as small and narrow, with a smooth neocortex and considerable midbrain exposure. A model of the brain had a volume of about 5 cm^3, indicating a brain weight of about 5 grams. Additional information on the brain of UM 87990 was published when the brain of *P. tricuspidens* was analyzed by Orliac et al. (2014).

Gingerich and Gunnell (2005) combined the 5 g estimate of brain weight with the 2,175 g estimate of body weight for *P. cookei* to yield an encephalization quotient or EQ of 0.25. The EQ for a mammal is the ratio of observed or estimated brain weight to the brain weight expected for an average mammal of the same body weight living today. Following Jerison (1973: p. 61), the expected value is based on an empirical allometric log-log scaling relationship of brain weight to body weight in living mammals. EQ = 0.25 for *P. cookei* indicates that its brain was about one quarter the size expected for a living mammal of its body weight.

Quotients are useful for understanding how an encephalization residual compares to expectation. However, encephalization quotients are unsuitable for comparison between species because the quotients are proportions on a non-uniform scale. Encephalization quotients underestimate differences in relative brain size for quotients smaller than one, and they overestimate differences in brain size when quotients are greater than one. This is evident in the asymmetry of EQ distributions plotted by Silcox et al., (2009b: fig. 9). It is better to make comparisons as encephalization residuals (ER) in the original allometric (logarithmic) framework (Gingerich, 2016).

The most intuitive scale for encephalization studies is a log base-2 or halving-doubling scale. Brain weight compared to body weight is different in terrestrial (*T*), aquatic (*A*), and volant (*V*) mammals, and it is important to distinguish these and identify the source sample. Similarly, the allometry of brain weight and body weight is different for terrestrial mammals as a class (*C*), as orders (*O*), as families (*F*), or as genera (*G*). The source sample and the taxonomic scale can be indicated by attaching subscripted *T*, *A*, or *V*, and *C*, *O*, *F*, or *G*, as for example, EQ_{TC}, for terrestrial mammals as a class.

Here we consider the relative brain size of *P. cookei* in the context of terrestrial mammals as a class. The expected size of the brain for a comparison of terrestrial mammals as a class is given by:

$$E_e = 0.740\ P_i - 4.004$$

where E_e is $\log_2$ of the expected weight in grams and P_i is $\log_2$ of the observed body weight in grams for species *i* (Gingerich, 2016: p. 26). Use of $\log_{10}$ transformation instead of $\log_2$ transformation would make the intercept –1.205 instead of –4.004 (Gingerich, 2016: p. 25). Similar equations of Martin (1981) and Eisenberg (1981) relating brain size to body size are based on smaller samples compromised in mixing terrestrial, aquatic, and volant mammals.

The encephalization residual is then the difference between observation and expectation:

$$ER_{TC} = E_i - E_e$$

where E_i is $\log_2$ of the the observed brain weight in grams for species *i* (E_i is $\log_{10}$ of observed brain weight if $\log_{10}$ was used to calculate E_e). ER_{TC} will be positive when $E_i > E_e$ and negative when $E_i < E_e$.

We employ the body weight estimation algorithm of Gingerich (1990). The original Basic program has been rewritten as an R script (see Appendix III), where the reference sample is again that of Alexander et al. (1979) for 36 species of mammals that span much of the range of mammalian body sizes. Alexander et al. (1979) published the body weights, and Professor Alexander generously made the long bone lengths and widths available for analysis in the 1990 study. We used the rewritten R script to calculate body weights for *P. cookei* and for other plesiadapid species of interest (Table 6).

The long bone measurements for *P. cookei* reported here (Table A-III-1) differ from those reported by Gingerich and Gunnell (2005) in being smaller, notably in metacarpal length, metatarsal length and diameter, and humerus diameter. Consequently, the revised geometric mean estimate of body weight for *P. cookei* is smaller at 1,799 g (Table 6). A related approach to body weight estimation involves multiple regression of body weight on a whole set of long bone

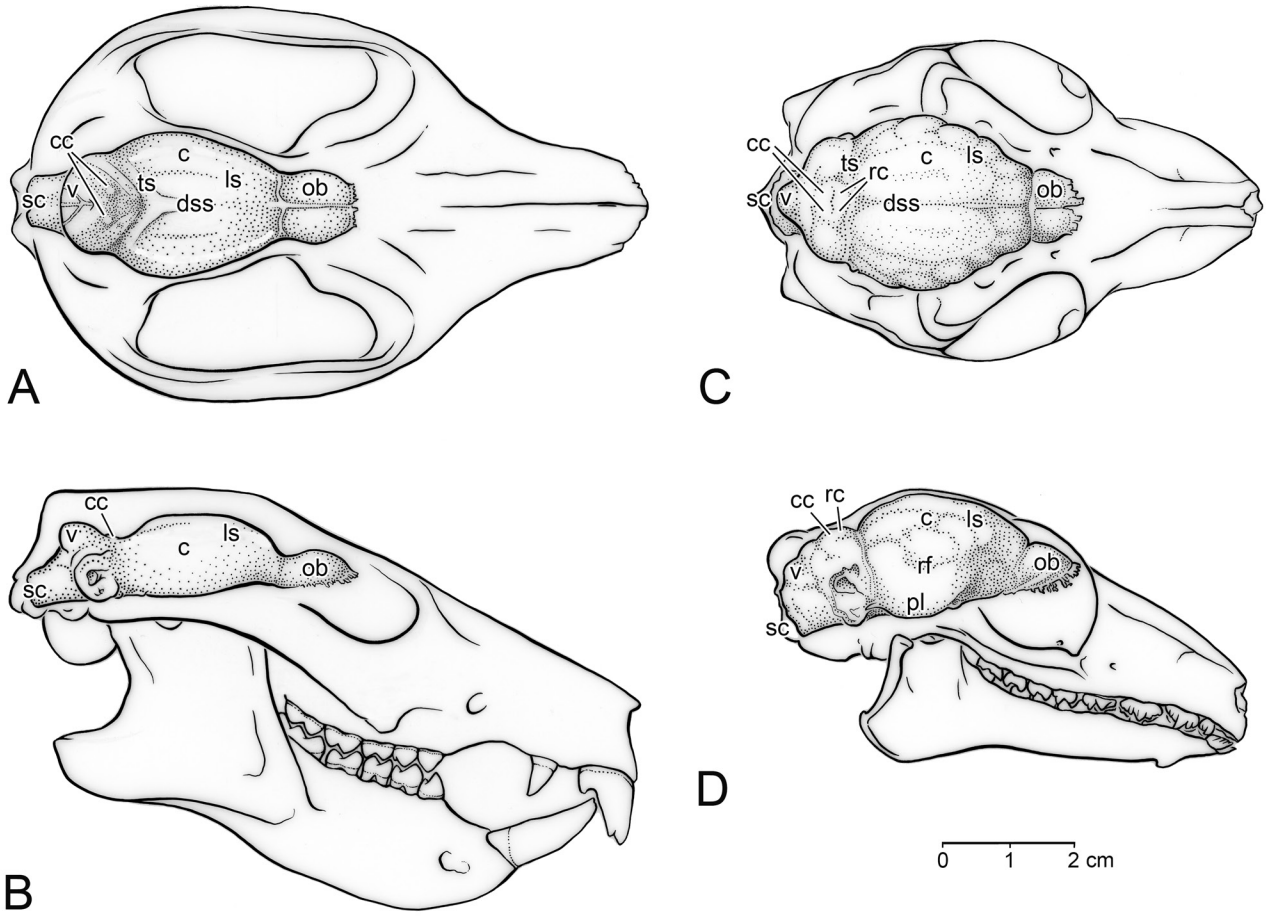

FIGURE 81.— Skull and brain of late Paleocene *Plesiadapis cookei* (A–B) compared to those of the smaller extant flying lemur *Galeopterus variegatus* (C–D). Each is shown in dorsal and right lateral view. **A–B**, *P. cookei*, UM 87990, from locality SC-117 in the Clarks Fork Basin, Wyoming. **C–D**, *G. variegatus*, UMMZ 117122, from Selangor, Kuala Lumpur, Malasia. Note the small size of the brain in *P. cookei*, the relatively large olfactory bulbs, the long smooth cerebrum, and the extensive midbrain exposure with distinct impressions of the caudal colliculi. *G. variegatus* has an expanded neocortex above the rhinal fissure, numerous sulci within the neocortex, and midbrain exposure due to enlargement of the corpora quadrigemina. Illustrations are by Bonnie Miljour. Abbreviations: *c*, cerebrum; *cc*, caudal colliculi of midbrain; *dss*, dorsal sagittal sinus; *ls*, lateral sulcus; *ob*, olfactory bulb; *pl*, piriform lobe; *rc*, rostral colliculi of midbrain; *rf*, rhinal fissure; *sc*, spinal cord; *ts*, transverse sinus; *v*, vermis of cerebellum.

measurements. Multiple regression of body weight on all 11 long bone lengths and diameters yields a weight estimate of 2,052 g, and multiple regression of body weight on the six long bone lengths yields a weight estimate of 2,050 g. The multiple regression estimates for body weight in *P. cookei* are very similar, and the estimate for multiple regression of body weight on the 11 long bone lengths and diameters, 2,052 g, is better than the other two because it explains more of the variance in weight.

The body weight estimate of 2,052 g for *P. cookei* yields an ER_{TC} estimate of −1.816 and a corresponding EQ_{TC} value of 0.284 ($EQ = 2^{ER}$). The new weight for *P. cookei* is about 120 g lighter than that calculated by Gingerich and Gunnell (2005), and the new ER_{TC} value is about 0.18 units larger. But even so, ER_{TC} of −1.816 and EQ_{TC} of 0.284 indicate that the brain of *P. cookei* was very small relative to the size of its body.

The small size of the brain of *P. cookei,* with an ER_{TC} in the range of −1.816, and its long narrow form, retention of midbrain exposure, and smooth neocortex all indicate a small and primitive brain. A similarly primitive living relative, the colugo or flying lemur *Galeopterus variegatus* (Fig. 81C–D), has an endocranial volume and brain weight estimated at 7 g (UMMZ 117122; Fig. 81) and an adult body weight of 1,300 g (Davis, 1962). This yields $ER_{TC} = -0.843$ and $EQ_{TC} = 0.557$, indicating a relative brain size double that of that of *P. cookei*. The 6.2 g brain weight and 810 g body weight that Pirlot and Kamiya (1982) reported for *G. variegatus* are both small. If the Pirlot and Kamiya weights represent an adult *G. variegatus*, then the ER_{TC} value for the species could be as high as −0.513 ($EQ_{TC} = 0.701$), increasing the difference from

TABLE 6.— Plesiadapid body weight estimates (grams) derived from measurements of individual long bones. Estimates are based on a reference sample of 36 mammalian species ranging in size from a shrew to an elephant (Alexander et al., 1979; Gingerich, 1990). Plesiadapid long bone length and diameter measurements are listed in Table A-III-1. Long bone diameters for *P. insignis* (parentheses) are not included in calculating a weight for the species because the bones are distorted by compression. Results are expressed in terms of the geometric mean (*GM*; bold) and a confidence interval ranging from the maximum of minimum estimates (*Min*) to the minimum of maximum estimates (*Max*). Body weights for *Plesiadapis cookei* based on (a) multiple regression of weight on lengths and diameters for 26 species, excluding artiodactyls, and (b) multiple regression of weight on lengths alone for 26 species, excluding artiodactyls, are 2052 g and 2050 g, respectively. Multiple regression estimates were not attempted for plesiadapids lacking the full set of long bone measurements. Abbreviations: *F*, femur; *H*, humerus; *Mc*, third metacarpal; *Mt*, third metatarsal; *R*, radius; *T*, tibia; *U*, ulna. For each bone: *D*, parasagittal (anteroposterior) diameter; *L*, length.

Taxon	H-L	U-L	Mc-L	F-L	T-L	Mt-L	H-D	U-D	Mc-D	F-D	T-D	Mt-D	GM	Min	Max
P. cookei	2934	2752	1432	2465	1687	1330	2394	—	1321	1984	1670	953	**1799**	1321	3206
P. tricuspidens	2434	2488	1635	1777	—	—	3178	—	1492	1729	—	—	**2034**	1754	3286
P. rex	—	—	—	—	—	—	498	—	—	—	—	—	**498**	274	906
P. churchilli	—	—	—	—	—	—	—	—	—	923	—	290	**517**	485	1090
P. insignis	425	241	372	543	248	—	(1,691)	—	—	(1,573)	(1,170)	—	**348**	148	766
N. intermedius	—	347	365	—	229	—	352	—	174	415	266	172	**276**	218	426
N. gidleyi	—	—	406	—	—	—	—	—	161	599	403	—	**354**	315	394
Pr. gaoi	—	—	776	—	—	—	994	—	472	—	—	489	**650**	548	1146

P. cookei. The geological age of *P. cookei* is also undoubtedly an important factor influencing its brain size.

The individual body weight estimates in Table 6 tell us something about the body proportions of *P. cookei*. If the skeletal proportions of *P. cookei* matched those of an average living mammal, then each long bone length and diameter would yield the same weight estimate. However the humerus length for *P. cookei* yields a weight of 2,934 g, which is substantially greater (63% greater) than the geometric mean weight of 1,799 g. The ulna length for *P. cookei* yields a weight of 2,752 g, which is 53% greater than 1,799 g. The femur length for *P. cookei* yields a weight of 2,465 g, which is 37% greater than 1,799 g. Finally, the metatarsal diameter yields a weight of 953 g, which is substantially less (47% less) than 1,799 g. These comparisons indicate that *P. cookei* had a relatively long humerus, ulna, and femur compared to those of an average living mammal, and relatively slender metatarsals.

Encephalization in *Plesiadapis tricuspidens*

Orliac et al. (2014) estimated the endocranial volume of *P. tricuspidens* to be about 5.2 cm^3 and the brain weight to be 5.2 g. They used a body weight estimate for *P. tricuspidens* from Boyer (2009; the weight Orliac et al. reported as 2,039 g should have been 2,034 g or the 2,035 g reported here). Together the 5.2 g brain weight and 2,035 g body weight yield an encephalization residual $ER_{TC} = -1.751$ and an encephalization quotient $EQ_{TC} = 0.297$. Both are close to the estimates given above for *P. cookei*.

Here again, the individual body weight estimates in Table 6 tell us something about the body proportions of *P. tricuspidens*. Most of the individual estimates are close to the geometric mean, but the humerus diameter yields a weight of 3,178 g, which is 56% greater than the geometric mean weight of 2,034 g. Comparing weight estimates, the lengths of the humerus, ulna, and femur do not show the same degree of elongation seen in *P. cookei*. The body weight and encephalization of *P. tricuspidens* are close to those of *P. cookei*, but the limbs are less elongated and the humerus is more robust.

Orliac et al. (2014) found that *P. tricuspidens* retained a very small and simple brain, with midbrain exposure and minimal encephalization and neocorticalization like that of stem rodents and lagomorphs.

Encephalization in *Plesiadapis* compared to that of Eocene primates

The advantage of UM 87990 for understanding relative brain size in *P. cookei* is its association of a three-dimensional model of the brain with a much of a postcranial skeleton. This permits reliable estimation of both brain weight (5 g) and body weight (2,052 g) in the same individual animal, and, as outlined above, calculation of an encephaziation residual ($ER_{TC} = -1.816$) and corresponding encephalization quotient ($EQ_{TC} = 0.284$). Gingerich and Gunnell (2005) showed that the size of the brain relative to body size in *P. cookei* places it within the range of early Paleogene archaic ungulates and within the range of living basal insectivores. An encephalization residual of −1.816 is well below that of any living primate.

Comparison of encephalization in Paleocene *P. cookei* with encephalization in Eocene primates is complicated because: (1) endocranial casts are available for relatively few Eocene primates; (2) few postcranial elements have been described and measured for these species; and (3) confusing numbers of body weight proxies and encephalization allometries have been used to compare endocasts. Description and

measurement of better skeletons would greatly improve body weight estimation.

Ramdarshan and Orliac (2016) provided measurements for the tarsioid primates *Tetonius homunculus*, *Necrolemur antiquus*, and *Microchoerus erinaceus*, and the adapoid *Adapis parisiensis* that enable calculation of an encephalization residual comparable to that for *P. cookei*. Following Ramdarshan and Orliac (2016), *Tetonius*, *Necrolemur*, and *Microchoerus* have ER_{TC} values of −0.458, +0.306, and −0.807, and *Adapis* has an ER_{TC} value of −0.697. This range, from −0.807 to +0.306 starts a full doubling larger than the value for *P. cookei* (−0.807 − −1.816 = +1.009). Surprisingly, the encephalization of *Necrolemur* is also a full doubling greater than that of closely related *Microchoerus* (0.306 − −0.807 = +1.113).

Harrington et al. (2016) described and published measurements for an excellent series of virtual endocasts of *Notharctus*, *Smilodectes*, and *Adapis*. Estimates of brain weight were then combined with a range of tooth size, cranial length, and area of the astragalar ectal facet proxies for body weight to calculate encephalization quotients. Harrington et al. (2016: abstract) concluded that "regardless of the body mass prediction method used, … the average EQ of adapiforms was similar to that of plesiadapiforms." Gilbert and Jungers (2017: p. 86) discussed the Harrington et al. (2016) evidence, and concluded "an increase in brain size characterizes the origin of euprimates [Tarsioidea and Adapoidea], as noted previously by many authors."

Partial skeletons with long-bone lengths and diameters are known for *Notharctus*, *Smilodectes*, and *Adapis*, which, when studied, promise to yield more reliable estimates of body weight and, from these, more reliable estimates of encephalization. More reliable estimates of encephalization for adapoids will test the proposition that substantial increase in relative size of the brain was required in any transition from a *Plesiadapis*-like plesiadapiform to a *Tetonius* or *Notharctus*-like euprimate (Gingerich and Gunnell, 2005; Orliac et al., 2014).

Body weight in other plesiadapids

If we rank the plesiadapid species in Table 6 by their estimated body weight, *P. tricuspidens* and *P. cookei* are similar in size and much larger than the remaining six species. These are, from largest to smallest, *Pronothodectes gaoi*, *P. churchilli*, *P. rex*, *N. gidleyi*, *P. insignis*, and *N. intermedius*. None of these six species has a cranium preserving an endocranial cast, so nothing is known about their brain morphology or size.

Gingerich and Gunnell (2005), Yapuncich et al. (2015), and others have shown that body weight predictions for a species can vary substantially depending on the body-weight proxy and the reference sample. We attempted to quantify the relative magnitude of this variation by calculating coefficients of variation for predictions based on long bone lengths, long bone diameters, and both combined (Table A-III-2). The coefficients of variation for *P. cookei* weight estimates, based on lengths, based on diameters, and based on lengths and diameters combined, are virtually identical at 33, 34, and 34, respectively. Coefficients of variation for weights in *P. tricuspidens* of 21, 43, and 29, respectively, tell a different story. In *P. tricuspidens* estimates based on diameters are more than twice as variable as those based on lengths. It is not clear why the coefficients of variation should be so different. However, the *P. tricuspidens* data are average values for several individuals. Thus, the greater variability includes some population variability.

P. cookei is predicted to be about the same size as *P. tricuspidens*, but much larger than other plesiadapids. Here we compare differences in cranium-based predictions of size (Table 3) to differences in postcranium-based predictions of size. Cranium-based estimates of relative size are made in two ways: (1) by assuming an isometric relationship between skull size and body mass; and (2) using regression based on an extant sample (from Silcox et al., 2009a). Skull lengths treated isometrically and masses predicted using postcranial dimensions are consistent in suggesting 1) that *P. cookei* and *P. tricuspidens* were close in size and 2) that these species were between 5 (based on postcrania) and 9 (based on crania) times the mass of *N. intermedius,* the smallest species for which skull length and mass was predicted. However, masses predicted using skull length via regressions from Silcox et al. (2009a) suggest *P. cookei* and *P. tricuspidens were* more than ~17 times the mass of *N. intermedius* (Tables 3, A-III-2).

SEX OF UM 87990

Every mammal has a sex, male or female, and dimorphism related to sex is common in mammals. Males and females often differ in secondary characteristics that extend beyond primary differences in the genitalia. A thorough investigation of sexual dimorphism in *P. cookei* would require a sample of skeletons to ensure representation of both sexes, but here we are limited to the skeleton of UM 87990. Mammalian dimorphism is often expressed in the size of the canine teeth, which might enable inference of the sex of an individual skeleton, however *P. cookei* lacks canines. Mammalian dimorphism is also often expressed in the innominate, which is present in UM 87990.

Guilday (1951) found that innominates of meadow voles, *Microtus pennsylvanicus*, collected by barn owls could be sexed by comparing the length and width of the pubic ramus. For Guilday, the single best measurement for distinguishing sexes was the width of the pubic ramus at its narrowest point, measured between the superior and inferior borders. Males have a shorter and wider pubic ramus than in females.

There is a common pattern of sexual dimorphism in the pelvis of mammals that has been studied, in one way or another, by a long series of authors. Dunmire (1955) extended Guilday's observations to a wider range of rodent species. Bernstein and Crelin (1967) made a similar comparison of innominates in laboratory rats and found, echoing Guilday, the width of the pubis to be the most salient difference between sexes. Brown and Twigg (1969) studied pelves in a range of murids and cricetids, and concluded that innominates of females have a longer and thinner pubis than those of males. Black (1970) used an index of pubis length to ischium length

to distinguish sexes in the primates *Cebus albifrons*, *Saimiri sciureus*, and *Saguinus nigricollis*. She found that females consistently have a relatively longer pubic ramus. These results are all consistent.

Leutenegger (1973) found no significant sexual dimorphism in pelves of the African lorises *Perodicticus potto* and *Arctocebus calabarensis*, but he did not measure the width of the pubic ramus. Steudal (1981) measured pelves of large samples of ceboid, cercopithecoid, and hominoid primates. She found significant dimorphism in some species, but again did not measure the width of the pubic ramus. Pissinatti et al. (1992) found the width of the pubic ramus to overlap in male and female *Leontopithecus rosalia* but also to differ significantly in a statistical sense between the sexes. Tague (2003) studied dimorphism in pelves of the marsupial *Didelphis virginiana* but did not measure width of the pubic ramus. Finally, St. Clair (2007) studied pelvic dimorphism in *Microcebus griseorufus* and found females to have significantly longer and more gracile pubic rami. She did not measure the width of the pubic ramus. Again, when dimorphism of the public ramus is studied, results are consistent with the early findings of Guilday.

Gingerich (1972) studied the ontogeny of pelvic dimorphism in *Saimiri sciureus* to test (and refute) the idea of Bernstein and Crelin (1967) that juvenile pelvic morphology is female. Bernstein and Crelin considered male morphological features to be acquired during development. The debate about development does not concern us here, but Gingerich's measurements for *S. sciureus* can be used to place the innominate of UM 87990 in morphological context and then evaluate the sex of this specimen of *P. cookei* (Fig. 82). *S. sciureus* is one species illustrating a consistent and widely distributed pattern of pelvic dimorphism in mammals; other species could also be used as models to test this in *P. cookei*.

The distal end of the pubic ramus and the pubic symphysis are incomplete in UM 87990, and so the index most frequently used to distinguish male and female innominates, the ratio of pubis width to length, cannot be quantified here. However, the width of the superior pubic ramus and its relationship to ilium length, the second relationship used to distinguish sexes, is preserved in UM 87990. Ilium length and pubic ramus width can be measured most accurately on the right side in UM 87990, where these are 44.0 mm and 4.8 mm, respectively. The *P. cookei* ilium is longer than any *S. sciureus* individual measured, but its pubic ramus width is well within the range and approximately twice the width expected for a female. This leads us to conclude that this specimen of *P. cookei* is likely to be male (Fig. 82).

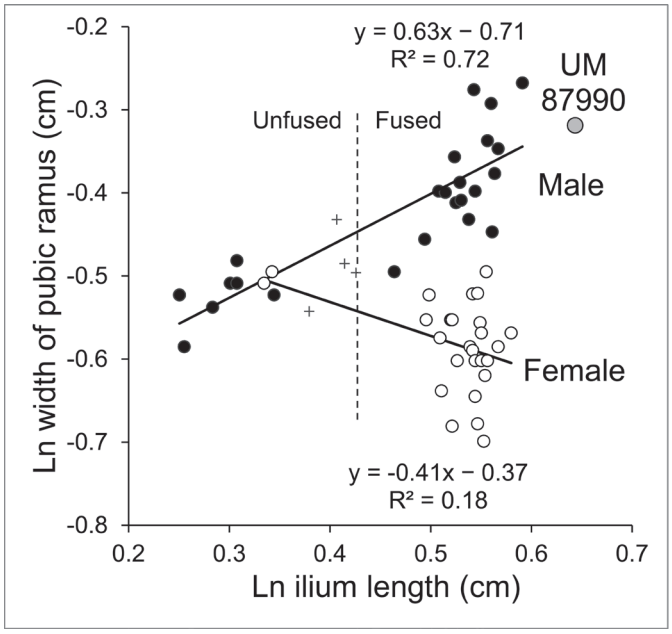

FIGURE 82.— Innominate of *Plesiadapis cookei*, UM 87990 (larger gray circle), interpreted in relation to ontogeny of sexual dimorphism in the squirrel monkey *Saimiri sciureus*. Smaller filled circles are male and open circles female *S. sciureus* (juveniles represented by a plus sign are unsexed). The ilium, ischium, and pubis of *S. sciureus* fuse when the ilium is about 1.55 cm long (0.44 on a scale of natural logarithms). The UM 87990 innominate is larger than innominates of *S. sciureus*, but has the pubic ramus width expected for a male. Innominate measurements for *S. sciureus* are from Gingerich (1972).

SEQUENCE OF TOOTH ERUPTION AND RATE OF GROWTH

The only *P. cookei* specimen with teeth erupting is UM 67190, which includes fragmentary dentaries. No deciduous teeth are present, but left and right P_4 are partially erupted (Rose, 1981). Specimens of other *Plesiadapis* species confirm that $P^{3–4}$ and $P_{3–4}$ are the last teeth to erupt (Gingerich, 1976; Bloch et al., 2002). Rapidly growing mammals such as the tree shrew *Tupaia* have three sets of teeth that erupt sequentially: (1) deciduous teeth, (2) molars, and (3) teeth including P^4 and P_4 that replace deciduous precursors. In more slowly growing mammals, the third of these sets, the set of replacement teeth, moves forward in time to overlap with eruption of molar teeth in the second set (Smith, 2000). *Plesiadapis*, with P^3/P_3 and P^4/P_4 erupting late, was clearly in the category of *Tupaia*-like rapidly-growing mammals with three sets of teeth that erupted sequentially.

ONTOGENETIC STAGE OF DEVELOPMENT OF UM 87990

The commonly recognized stages of mammalian ontogeny are (1) *neonate*, retaining an umbilical cord or early in lactation; (2) *nestling*, having limited locomotor and sensory development; (3) *suckling*, mammal before weaning; (4) *juvenile*, weaned but smaller than a subadult; (5) *subadult*: young mammal not fully grown that may or may not be sexually mature; (6) *adult*: fully grown and sexually mature; and

(7) *old adult*: mammal with extreme tooth wear (Kunz et al., 1996). Some stages may overlap, some depend on life history (precocial mammals rarely have a nestling stage), and some are not easily recognized in fossils. Generally speaking, neonates, nestlings, and sucklings have only 'milk' teeth (or, in altricial mammals, no teeth at all) and long bones not fully formed. Juvenile mammals have first molars, M^1 and M_1, erupted and additional cheek teeth erupting. Subadults have most permanent teeth in place and long bone diaphyses approaching definitive size. Adults have a fully erupted dentition and may or may not have fused epiphyses on long bone diaphyses. Finally, old adults show advanced tooth wear and most have fused epiphyses on long bones.

Tooth eruption and wear

Gingerich (1976) reported that the dental formula of *Plesiadapis cookei* is 2.0.3.3 / 1.0.2.3, which, with recovery of the cranium of UM 87990, we have corrected to 2.0.2.3 / 1.0.2.3. The upper incisors of UM 87990 were not recovered, and so we cannot say anything directly about their stage of eruption. However, the fact that the all other observable adult teeth are fully erupted suggests that the upper first incisor I^1 was almost certainly fully erupted as well.

The ventral or palatal view of the cranium of UM 87990 shows that all of the upper cheek teeth were fully erupted (Fig. 10). All of the cheek teeth have roots that seem largely complete anchoring them into the maxillae, with the possible exception of the last upper molars (left and right M^3), which are missing on both sides of the palate. The posterior portion of the maxilla is well preserved on the left side of the palate, and alveoli for the left M^3 are largely intact. The fact that the tooth itself is missing suggests that the roots may not have been fully formed, enabling the tooth to slip out of its alveoli after death. Maxillary bone surrounding the right M^3 is less well preserved, but the fact that the right M^3 is also missing supports the suggestion from the left side that the roots of the right M^3 too may not have been fully formed.

Lateral, medial, and occlusal views of the dentaries of UM 87990 show that all of the lower cheek teeth, like the uppers, were fully erupted (Fig. 18). None of these teeth have any substantial wear, which shows that little time passed during their emergence and reinforces interpretation of *Plesiadapis* as a rapidly growing mammal.

Epiphyseal fusion

Growth of the long bones and fusion of epiphyses provides additional information about the ontogenetic stage of development of UM 87990. In the shoulder, the proximal epiphysis of the humerus is unfused. In the elbow, both the distal epiphysis of the humerus and the proximal epiphyses of the ulna and radius are fused. In the wrist, the distal epiphysis of the radius is unfused. Metacarpal epiphyses are fused, as are those of the manual phalanges. In the hip, the ilium, ischium, and pubis are united to form an innominate. Traces of those sutures are barely visible, indicating that the innominate has achieved full size; here too the proximal epiphysis of the femur is unfused. In the knee, the suture of the distal epiphysis of the femur remains visible and the proximal epiphyses of the tibia and fibula are unfused. In the ankle, distal epiphyses of the tibia and fibula are unfused. Metatarsal epiphyses are fused, as are those of the pedal phalanges.

These observations provide a partial sequence of limb joint fusion for *P. cookei* that can be abbreviated E–(A–H–W–K–S), where the joints represented are elbow (distal humerus, proximal radius and ulna), ankle (distal tibia and fibula), hip (femoral head), wrist (distal radius and ulna), knee (distal femur and proximal tibia and fibula), and shoulder (proximal humerus), respectively. The elbow is the first of these joints to ossify fully, and the parentheses indicate that there is no evidence resolving the sequence among the later-ossifying hip, ankle, wrist, knee, and shoulder joints. Shigihara (1980) listed fully-resolved sequences of ossification for 24 genera of mammals, all of which ossify the elbow first. The most common of Shigihara's sequences was E–H–A–K–W–S represented by seven genera of primates, followed by E–H–A–W–K–S represented by six genera including primates and also the tree shrew *Tupaia* and hedgehog *Erinaceus*. The sequences E–A–H–W–K–S and E–A–H–K–W–S are represented by four genera and three genera, respectively that are principally artiodactyls. *P. cookei*, with only the elbow resolved relative to the remaining ossifications, could fit any of these patterns.

Ontogenetic stage of UM 87990

If we combine the observations of a fully erupted dentition, little tooth wear, and epiphyseal fusion limited to the elbow, we can interpret UM 87990 as either an advanced subadult or a young adult. Most mammals, including UM 87990, have the dentition (D) fully erupted before epiphyseal fusion (E) is complete, a sequence represented as D–E (Shigehara, 1980). Sexual maturity (S) can precede D and E, intervene, or follow D and E, yielding the sequences S–D–E, D–S–E, and D–E–S, respectively.

According to Shigehara (1980), the first sequence, S–D–E with sexual maturation occurring first, is found in the marsupial *Didelphis*, in domestic animals, and in catarrhine higher primates. The second sequence, D–S–E with sexual maturation occurring between completion of dental eruption and completion of epiphyseal fusion, is found in the insectivore *Suncus* and in rodents. The third sequence, D–E–S with sexual maturation occurring last, is found in the treeshrew *Tupaia*, in wild carnivorans, and in platyrrhine primates.

Thus, if a mammal with the body and brain size of *Didelphis* were a good model for *Plesiadapis* ontogeny, then we would expect UM 87990 to represent a sexually mature adult. Alternatively, if a mammal the body and brain size of *Suncus* and rodents were a good model for *Plesiadapis* ontogeny, then the sexual maturity of UM 87990 would be an open question. Finally, if a mammal with the body and brain size of *Tupaia* were a good model for *Plesiadapis* ontogeny, then we would expect UM 87990 to represent a sexually immature subadult. The sexual maturity of a mammal like *P. cookei* is not predictable when all we know is that is it has completed tooth eruption but not epiphyseal fusion. Given this uncertainty, we can only conclude that UM 87990 represents

either an advanced and nearly full-grown subadult or a full-grown young adult *P. cookei*.

DISCUSSION

The ontogenetic stage observed in UM 87990, with the adult dentition fully erupted, teeth almost completely unworn, and most long bone epiphyseal sutures open, is found in other plesiadapiform specimens. For example, the skeleton of *Carpolestes simpsoni* (UM 101963) described by Bloch and Boyer (2002) and skeletons of *N. intermedius* (USNM, USNM 442229) have adult dentitions but unfused epiphyses. Many of the postcranial specimens attributed to *P. tricuspidens* from Berru in France have unfused epiphyses.

Specimens of the paromomyid *Acidomomys hebeticus* (Bloch et al., 2002; Boyer and Bloch, 2008) were preserved at early stages of tooth replacement. Postcrania associated with these juvenile *A. hebeticus* have more porous bone those of plesiadapiform specimens with adult dentitions and from most postcrania attributed to *P. tricuspidens*. A paromomyid specimen of *Ignacius clarkforkensis* (UM 108210) with slightly worn adult teeth and partially fused epiphyses (Boyer and Bloch, 2008) has bone with a visually apparent density and texture differing from bone in the *A. hebeticus* specimens and resembling bone in UM 87990. This is another reason to interpret specimens with all of their permanent teeth, like UM 87990, as full-grown or nearly full-grown individuals, despite the persistence of some epiphyseal sutures.

Patterns of development are related to the timing of different life history events, which in turn are important correlates of life strategy (Smith, 1992). Rapid growth like that inferred for *P. cookei* is often associated with a relatively short life span. Sexual maturation and initiation of reproduction are delayed until full size is attained. UM 87990 represents what is probably a widespread mammalian baseline condition of rapid growth. Some derived mammals including later primates grow more slowly and have longer life spans, but the evolutionary origin of this strategy remains to be documented in the fossil record.

VI

PHYLOGENY

Information compiled in this study allows us to address several questions regarding phylogeny. First, what is the species-level phylogeny of Plesiadapidae? Second, how are plesiadapids related to other plesiadapiforms and euprimates?

The phylogenetic relationships of plesiadapid species have been studied comprehensively by Russell (1964), Gingerich (1976), Boyer (2009), and Boyer et al. (2012a, b). All of these assessments are based largely on craniodental traits. Gingerich (1976) also employed chronological data in a stratophenetic approach. Boyer (2009) and Boyer et al. (2012a, b) were the only authors to use cladistic algorithms. The latter studies were largely based on the information compiled here.

Higher-level phylogenetic relationships of plesiadapids were analyzed by Bloch et al. (2007) using a mixture of species-, genus-, and family-level taxa. They used a family-level operational taxonomic unit (OTU) to represent plesiadapids and based their scoring primarily on the literature available for the skull and postcranial skeleton of *P. tricuspidens* (e.g., Russell, 1964; Szalay et al., 1975; Gingerich, 1976), a humerus of *P. walbeckensis* (Szalay and Dagosto, 1980), and the postcranium of two species of *Nannodectes* (Simpson, 1935; Beard, 1989), as well as direct observations on the skeleton of *P. cookei* UM 87990. When different reference species showed variance in character states, Bloch et al. (2007) scored Plesiadapidae as polymorphic. Bloch et al. (2007) recovered Plesiadapidae and Carpolestidae as sister taxa. This grouping plus Saxonellidae and *Chronolestes* formed the sister taxon to Euprimates.

Ni et al. (2013, 2016) included three plesiadapid species in a matrix of 196 taxa and simultaneously evaluated the monophyly of those species and the position of plesiadapids in euarchontan phylogeny. They found intra-familial relationships consistent with Gingerich (1976), Boyer (2009), and Boyer et al. (2012a, b), with *P. tricuspidens* and *N. gidleyi* forming a clade, and *Pronothodectes matthewi* forming the sister taxon of that clade. Their results are also consistent with Bloch et al. (2007) in that Carpolestidae forms the sister taxon to Plesiadapidae. Their results differ from those of Bloch et al. (2007) in reconstructing most plesiadapiforms as more closely related to living dermopterans than to living primates.

With regard to the species-level phylogeny of Plesiadapidae, the main hypotheses to be tested relate to the monophyly of named genera and the relationships between genera. Specifically, we test the hypotheses that *Pronothodectes* is the most basal genus, that *Nannodectes* and *Plesiadapis* are sister taxa, and that *Chiromyoides* and *Platychoerops* emerge from within *Plesiadapis*. Some relationships of special interest are whether: (1) *Pr. gaoi* is more closely related to other species of *Pronothodectes* than to *P. rex* (Fox 1990, 1991; Gingerich 1991); (2) *P. walbeckensis* is actually part of an otherwise monophyletic *Chiromyoides* clade (Boyer et al. 2012a, b); (3) *Platychoerops* is more closely related to *P. cookei* than to *P. tricuspidens* (Russell 1964; Boyer et al. 2012a, b); and (4) *P. cookei* is more closely related to *P. dubius* and *P. fodinatus* than to *P. simonsi*, *P. gingerichi*, and *P. tricuspidens* (Boyer et al. 2012a, b).. The species-level analysis of this study (like others) relies on craniodental characters because most species have no postcrania and few have overlapping postcranial elements.

With regard to higher-level phylogeny, the main hypotheses to be tested are: (1) plesiadapids are close relatives of carpolestids; and (2) these taxa, plus saxonellids and *Chronolestes simul*, are the sister taxon to Euprimates. The latter hypothesis is most often supported by matrices that include substantial dental data (Bloch et al., 2007; Ni et al., 2013, 2016) and has been favored by specialists familiar with dental morphology (Simpson, 1937; Szalay, 1968; Gingerich, 1976; Fox, 1993; Van Valen, 1994). It is notable that two previous analyses lacking dental data (Bloch and Boyer, 2002; Bloch and Silcox, 2006) did not recover support for it.

Although dental data may have driven the grouping of plesiadapids and carpolestids in previous studies, we are most interested in the phylogenetic signal among postcranial and cranial data here. In the course of this study we re-assessed previous descriptions of cranial and postcranial morphology, as well as character scorings by Bloch et al (2007) and Bloch and Silcox (2006).

CLADISTIC METHODS

Given that our goal is to test both species-level and higher-level relationships of plesiadapids, the ideal approach might have been to compile a character-taxon matrix with adequate sampling of all species and all higher-level clades. Such a dataset would have allowed us to test both sets of hypotheses simultaneously. However, no such matrix is available in the literature. Systematics was not the primary goal of this study, so we could not justify building a new comprehensive matrix from scratch. Instead, here we run two sets of cladistic analyses that differ in the taxa and characters they utilize. One set of

analyses is designed to test the species-level relationships within Plesiadapidae. We attempt comprehensive, if not completely exhaustive taxonomic sampling of plesiadapid species and use a character matrix composed primarily of craniodental traits. The other is designed to test hypotheses of higher-level relationships, utilizes supraspecific OTUs, and has well-balanced sampling of dental, postcranial and cranial traits. We allow the species-level results to inform the analysis of supraspecific taxa by optimizing character states from the supraspecific matrix onto the root node of the tree resulting from the species-level analysis, and then using that optimization to represent Plesiadapidae in the supraspecific matrix. Details for each matrix and analysis follow

Species-level cladistic analysis

A phylogenetic tree was generated using parsimony analyses of a matrix consisting of 37 dental characters (Tables A-IV-1 and A-IV-2), 34 cranial characters (Tables A-IV-3, A-IV-4; A-IV-5) and a geographic character. These 72 characters were scored in 32 taxa (Table A-IV-2), including one outgroup (*Purgatorius janisae*) and two carpolestids (*Elphidotarsius*, *Carpolestes simpsoni*). Scoring of *Purgatorius janisae* was based on Rose (1975), Bloch et al. (2001), Clemens (2004), and Silcox and Gunnell (2008); scoring of *Elphidotarsius* was based on Bloch et al. (2001) and Silcox et al. (2001), scoring of *Carpolestes simpsoni* was based on Bloch and Gingerich (1998) and Bloch and Silcox (2006). We chose to use the genus *Elphidotarsius* as an OTU rather than its fragmentarily known composite species *E. florencae* and *E. wightoni* (Bloch et al., 2001; Silcox et al., 2001). The 29 plesiadapid species included were scored based on Gingerich (1976), Fox (1990), newly available data from the upper dentition of *Pr. gaoi* (Boyer et al., 2012a), an undescribed upper dentition of *Ch. caesor* (CM 72770), undescribed lower incisors of *Ch. caesor*, and undescribed central incisors of *Nannodectes gazini* (CM 76922, CM 76938). Scoring of dental formulae is based on Gingerich (1976) unless evidence from newly available specimens contradicts his reconstructions. For instance, Gingerich (1976) inferred that *P. cookei, Pl. russelli*, and other *Platychoerops* species lacked upper canines, but retained upper second premolars, based on the well-known morphology of *P. tricuspidens*. However, as discussed above, *P. cookei* UM 87990 actually lacks C^1 *and* P^2. Furthermore, it appears to us that the type of *Pl. richardsoni* YM 550 also lacks these teeth. Therefore, it cannot be assumed that *Pl. russelli* retained P^2.

The 72 x 32 character matrix was analyzed with PAUP v. 4.01 BETA (Swofford 2002) using a heuristic search of 10,000 replicates, with a random addition sequence and a "Tree Bisection and Reconnection" branch swapping algorithm.

Stratocladistic analysis

In order to take advantage of the potential phylogenetic information encoded in the rich stratigraphic record for plesiadapids, we also scored a stratigraphic character with 16 states (Figure 2A), added this to the 72 character matrix referenced above, and ran a stratocladistic analysis in the program STRATAPHY (Marcot and Fox, 2008). We used the default settings in STRATAPHY, allowing 1,000 trees in memory, executing 10 replicate searches, and allowing one heuristic ancestralization search. We ran this analysis three times. We utilized a variety of resources to determine the most appropriate stratigraphic intervals for known plesiadapids including Gingerich (1976), Bloch and Gingerich (1998), Gradstein et al. (2004), Woodburne (2004), and Secord (2008).

Character optimization

Cranial and postcranial characters discussed in the descriptions above and in Appendix V, as well as characters from Bloch et al. (2007), were optimized onto the ancestral node for Plesiadapidae using the newly generated species-level cladogram. A total of 26 cranial characters (Table A-IV-3) and 65 postcranial characters (Table A-IV-6) were optimized. An additional eight cranial characters (Table A-IV-6) were not part of Bloch et al. (2007) or Bloch and Silcox (2006) and were not, therefore, part of the optimization. The optimization represents only a 'down pass' step of the total optimization exercise (e.g., Wiley et al., 1991), because the ancestral state cannot be assumed as required for the 'up pass' step. Furthermore, inclusion of the sister taxon to the Plesiadapidae cannot be used to help reconstruct the ancestral condition of the family because this would allow results of the Bloch et al. (2007) cladistic analysis to influence the reconstruction. Instead, the ancestral node for Plesiadapidae is left polymorphic for characters that cannot be reconstructed as monomorphic through a 'majority rules' criterion on the 'down pass' step of the optimization.

Cladistic analysis of matrices using higher-level taxa

Selection of character matrix.— For the present study, we chose to use the character matrix of Bloch et al. (2007) with updates from Chester et al. (2015) to *Purgatorius* to test the position of Plesiadapidae among euarchontans because of its combined craniodental-and-postcranial dataset and extensive taxon sampling within Euarchonta. We chose the matrix of Bloch and Silcox (2006) to test the effects of new information on the cranium in isolation of other anatomical partitions. The character matrix of Bloch and Silcox (2006) is almost identical to that of Bloch et al. (2007) with 23 of its 24 characters overlapping.

Although we considered the possibility of using the matrix of Silcox et al. (2010), which was updated and used by Bloch et al. (2016), there are several issues that make the matrix of Slicox et al. (2010) less appropriate for the goal of this study. Primarily, it is less appropriate because it was designed to test relationships of animals *to* Euarchonta, not *within* Euarchonta. Some consequences of this design include increased sampling of taxa that can be considered outgroups to Euarchonta, and reduced sampling of plesiadapiform taxa that were sampled by Bloch et al. (2007). Another consequence is that several characters considered important for discussions of euarchontan relationships are omitted, even though the total number of characters is greater than in the Bloch et al. (2007) matrix. For instance, the form of the external auditory meatus and the

position of the posterior carotid foramen are not characters in this matrix.

There are overlapping characters between Chester et al. (2015) and Silcox et al. (2010). Therefore, it could be argued that updates to Silcox et al. (2010) applied by Bloch et al. (2016) should have been transferred to the version of Chester et al. (2015) that we built upon. However, the modifications that Bloch et al. (2016) made to the matrix of Silcox et al. (2010) relate primarily to crania of micromomyid plesiadapiforms, taxa we expect to have minor relevance to plesiadapid-carpolestid relationships. Although there is one change that Bloch et al. (2016) made to the matrix of Silcox et al. (2010) that affects plesiadapoids (character 107 describing the form of the fenestra rotunda was changed to 'shielded' for *Carpolestes simpsoni*), the version of this character in the matrices of Bloch et al. (2007) and Bloch and Silcox (2006) already scored the fenestra rotunda (or "cochlear fenestra") as shielded. See Bloch and Silcox (2006: table 3, character 23). Another reason updating the Chester et al. (2015) matrix with new micromomyid codings is not relevant at this time is that the results of both Silcox et al. (2010) and Bloch et al. (2016) are consistent with those of Chester et al. (2015) with respect to the relationships of plesiadapids to carpolestids and of plesiadapoids to euprimates. Therefore, we think that adding new plesiadapid scorings to Bloch et al. (2007; as modified by Chester et al. 2015) and Bloch and Silcox (2006) is a useful test. However, as a next step, it would be interesting to combine the new observations of Bloch et al. (2016) on micromomyids and the new observations on plesiadapids (and carpolestids) of the current study in a matrix including all the characters and taxa of both matrices.

Analysis of matrices.— We re-analyzed the matrices of Bloch et al. (2007) and Bloch and Silcox (2006) here to assess the effect of new cranial material alone on existing phylogenetic hypotheses (see acknowledgments for details on how we accessed these data). We examined and edited the matrices using the software MESQUITE. Parsimony analyses of the matrix of Bloch et al. (2007) were conducted using the same software and heuristic search settings as for species-level analyses, whereas the matrix of Bloch and Silcox (2006) was analyzed exhaustively.

We first reanalyzed the matrices of Bloch and Silcox (2006) and Bloch et al. (2007) without revising any character scorings in order to confirm that we could reproduce the results of the original authors. We were successful in recovering the exact same topologies and tree metrics. Next, we changed scorings for the Plesiadapidae OTU in both matrices, based on the results of the optimization described above. We also changed scorings for Paromomyidae and Carpolestidae where we disagreed with Bloch and Silcox (2006) and Bloch et al. (2007) based on re-assessment of the fossil evidence (see discussion in Chapters III and IV, Appendix V, and Boyer et al. 2012a). In the matrix of Bloch and Silcox (2006), eight character scorings were changed for Plesiadapidae (Tables A-IV-3, A-IV-4, and A-IV-7). Two character scorings were changed for both Carpolestidae and Paromomyidae (Table A-IV-7). In the matrix of Bloch et al. (2007), 18 character scorings were changed, representing 16 characters and three taxa (Tables A-IV-3 through A-IV-7). Seven of these characters encode postcranial morphology. The remaining nine characters encode cranial morphology. Eight of these characters are the same as those changed in the Bloch and Silcox (2006) matrix (Table A-IV-3 and A-IV-4). See results for listing and discussion of all of these changes.

RESULTS

Species level cladistic analysis

15,314 trees of 117 steps resulted from analysis of the 72-character matrix. The strict consensus of these is shown in Figure 83A. Plesiadapidae is monophyletic, with a clade comprised of *Elphidotarsius* sp. and *Carpolestes simpsoni* forming its sister taxon. *Pronothodectes* is the sister taxon to all other genera of the family. *Chiromyoides*, and *Platychoerops* are monophyletic, and *P. cookei* is recovered as the sister taxon of *Platychoerops*. In most respects, the results are congruent with, if less resolved than, the stratophenetic results of Gingerich (1976). It differs from recent species level cladistic results (Boyer et al., 2012a, b) in failing to recover a sister-taxon relationship between the clade formed by *P. dubius*, *P. fodinatus*, *P. cookei* and a clade formed by *Platychoerops* to the exclusion of *P. tricuspidens* and *P. remensis*. Furthermore, there is no longer unanimous support for *P. walbeckensis* as a sister taxon to *Chiromyoides* in the set of most parsimonious trees.

Stratocladistic Analysis

We ran a STRATAPHY search three times and obtained 716–724 trees and exactly 30 distinct topologies each time. The strict consensus tree was more resolved than that using only morphology, but broadly consistent with it. Key ways in which the stratocladistic consensus tree differed from the consensus tree based on morphology include (1) *Pronothodectes gaoi* was not consistently distinguished from all non-*Pronothodectes* plesiadapids, (2) unambiguous support for *P. walbeckensis* as a sister to the clade of all *Chiromyoides* species, and (3) *P. tricuspidens* and *P. remensis* were not recovered as sister taxa.

Because total character debt is calculated differently in MACCLADE v.4.08 and STRATAPHY, we also examined all 716 trees from the last iteration of our STRATAPHY analysis in MACCLADE v.4.08. We found that of these 716 trees, 12 (representing two topologies) were shorter than the others and equally parsimonious. These trees differed only in the position of *N. intermedius*, which was positioned either as the ancestor of a monophyletic clade of *Nannodectes* species, or as the ancestor of a non-*Pronothodectes*, non-*Nannodectes* plesiadapid clade. Within each topology, the there were six different trees representing differences in ancestralization of *Pronothodectes matthewi*, *Pronothodectes jepi*, and *Pl. richardsoni*. This is the result depicted in Figure 2A. *N. intermedius* is depicted as the common ancestor of both the *Nannodectes* lineage and other non-*Pronothodectes*,

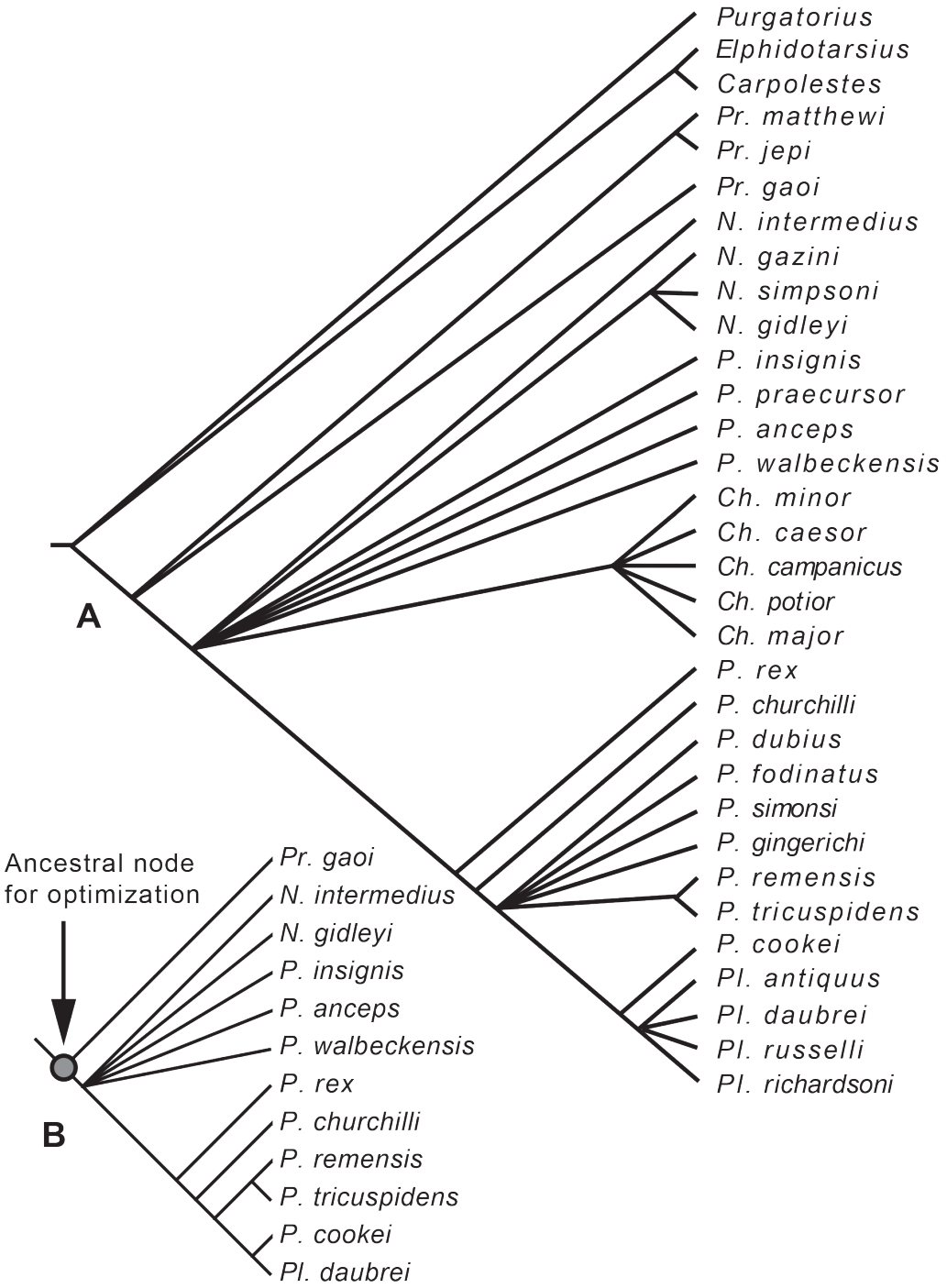

FIGURE 83.— Cladistic relationships of plesiadapid species. **A**, cladogram of all well-known plesiadapid species. The topology is the result of an analysis of 37 dental characters (appendix Tables A-IV-1 and A-IV-2), 34 cranial characters (appendix tables A-IV-3, A-IV-4 and A-IV-5), and a geographic character with two states (North American vs. European). Analysis of this matrix in PAUP using a heuristic search with 1000 replicates recovered ~15,000 equally parsimonious topologies for which the strict consensus is shown. Adding a stratigraphic character slightly changes and considerably resolves the topology (see Fig. 2). However, when considering the ancestral node for Plesiadapidae, character state reconstructions of cranial and postcranial characters from Bloch et al. (2007) do not change when adding stratigraphic information. **B**. cladogram representing taxa for which cranial and/or postcranial data are available, which were used to reconstruct the ancestral node for Plesiadapidae. Abbreviations: *Ch*, *Chiromyoides*; *N*, *Nannodectes*; *P*, *Plesiadapis*; *Pl*, *Platychaerops*; *Pr*, *Pronothodectes*.

non-*Nannodectes* plesiadapids. The three taxa with variable ancestralization are left as terminal taxa because this seems intuitively more plausible to us. The caption of Figure 2 also provides an explicit description of the consensus topology of the original 30 generated by STRATAPHY.

Character optimization

Table A-IV-3 is a list of characters scored based on the Description above and Appendix V. Internal carotid artery functionality was also scored (Tables A-IV-4 and A-IV-5). These character states were optimized onto the consensus cladogram recovered through the species level analysis (Fig. 83). The optimized state for the ancestral node is given in the last row of Tables A-IV-4 and A-IV-6. The PAUP-derived consensus cladogram (Fig. 83A) and the STRATAPHY- and MACCLADE-derived consensus topologies (Fig. 2A) yielded the same ancestral state optimization.

Various plesiadapid taxa differ from the reconstruction representing the ancestral node for Plesiadapidae. For instance, *N. gidleyi* differs in having an apparently relatively larger glenoid fossa (Table A-IV-5: c30) and an internal carotid plexus that probably did not have an intratympanic route. However, if the posterior carotid foramen is correctly identified in *N. gidleyi* (Appendix V), then the route for the internal carotid plexus was relatively laterally positioned on the basicranium, similar to that of other plesiadapids. *P. tricuspidens* differs in a number of respects illustrated in Figure 84: it exhibits a tubular external auditory meatus (Table A-IV-4: c3), a narrow nasal bone (Table A-IV-4: c16), a broad premaxilla/frontal contact (Table A-IV-5: c27), and an annular component to its ectotympanic that flares substantially beyond the bony struts connecting it to the bullar wall (Table A-IV-5: c28). Additionally, *P. tricuspidens* lacks exposure of molar tooth roots other than the distobuccal root of M^3 (Table A-IV-5: c29), has a proportionally larger glenoid fossa (Table A-IV-5: c30), and appears to have a less posteriorly projecting nuchal crest (Table A-IV-5: c31). *P. cookei* is similar to *P. tricuspidens* in the tubular form of its external auditory meatus and in the lack of dorsal exposure of most tooth roots in the orbit.

Major features shared by basally diverging and nested plesiadapids include a premaxilla that contacts the frontal bone, an apparently petrosal bulla, and an internal carotid artery that has a posterolateral entrance, is non-functional, and crosses the lateral aspect of the promontorium (see Chapter III and Appendix V). *Plesiadapis* has previously been considered to lack a lacrimal tubercle (e.g., Bloch and Silcox, 2001; Bloch et al., 2007; Bloch et al., 2016). However, as discussed in Appendix V, the best preserved lacrimal specimen of *P. tricuspidens* (MNHN CR 126) has a blunt lacrimal tubercle. We consider the presence of a lacrimal tubercle in MNHN CR 126 as evidence that it was generally present in plesiadapids and that is was previously considered lacking based on poor preservation. Optimization of postcranial traits from Bloch et al. (2007) reveals a few substantial differences in the scoring of basal plesiadapids compared to more derived forms. These are discussed in the next section.

Cladistic analysis of character matrices using higher-level taxa

Description of character state changes.— As mentioned above in the Cladistic Methods section, the scoring of cranial and postcranial characters for Plesiadapidae in Bloch and Silcox (2006) and Bloch et al. (2007) was changed as a result of the character optimization exercise discussed above (see Table A-IV-7). We also review the implications of these changes for similar characters in the matrix of Silcox et al. (2010) and Bloch et al. (2016).

For cranial character 3, 'Form of external auditory meatus,' Bloch and Silcox (2006) and Bloch et al. (2007) scored Plesiadapidae with a '1' indicating that the external auditory meatus is 'expanded into a tube.' However, the character optimization shows that the tube form, as seen in *P. tricuspidens* and *P. cookei* is derived, because basal species like *Pr. gaoi* (UALVP 46685) and *N. intermedius* (USNM 309902) exhibit the unexpanded, '0' state. This character was not included in the matrices of Silcox et al. (2010) or Bloch et al. (2016) but the discussion of Silcox et al. (2010: p.795) suggests they viewed it as expanded for plesiadapids.

For cranial character 5, 'Presence of branches of internal carotid artery,' Bloch and Silcox (2006) and Bloch et al. (2007) scored Plesiadapidae with a '2' indicating that 'evidence for the internal carotid system is absent.' Specimens of *Pr. gaoi* UALVP 46687, 49105, *N. intermedius* USNM 309902, *P. tricuspidens* (e.g., MNHN CR 125, Pellouin skull, various

FIGURE 84.— Plesiadapid skulls based on character state reconstructions. **A** and **B**, comparison of the reconstructed skulls of basal and derived Plesiadapidae, in ventral and dorsal views, respectively (left, based on ancestral node reconstruction; right, based on *Plesiadapis tricuspidens*. Numbers correspond to characters listed in appendix Table A-IV-3. The derived form was reconstructed using measurements from skulls of *P. tricuspidens*, which are complete enough to reveal overall cranial proportions. This reconstruction was then modified by using all available measurements and morphology from *Pronothodectes gaoi* (Table A-IV-7), which matches the ancestral node reconstruction in most respects (Tables A-IV-4 and A-IV-5). To transform the skull of *P. tricuspidens* into that of *Pronothodectes*, all bones were rescaled according to nasal length, but this re-scaling could have been done using a single dimension on any other bone preserved without distortion in both taxa. Where there is no morphological information on basal plesiadapids, the reconstruction was left similar to the derived form. Thus, these comparisons probably under-represent the full morphological disparity separating basal *Pr. gaoi*-like and derived *P. tricuspidens*-like plesiadapids. Numbers correspond to features in which derived *P. tricuspidens* (and in some cases *P. cookei*) differ from primitive ones (Table A-IV-3). **C**, size comparison of reconstructed skulls of basal and derived Plesiadapidae (dorsal view). The more derived skull is shown at 210% the size of the basal one, which approximates the difference in size between early *Nannodectes intermedius*-sized taxa and late *P. tricuspidens*. The only plesiadapid estimated to be larger is *P. cookei* (but see Chapters III and IV, Table 3, and Table A-I-9). The only smaller plesiadapids are *Pr. matthewi* and *N. gazini* (Gingerich, 1976). Most of the size range of Plesiadapidae is illustrated by the two reconstructed skulls.

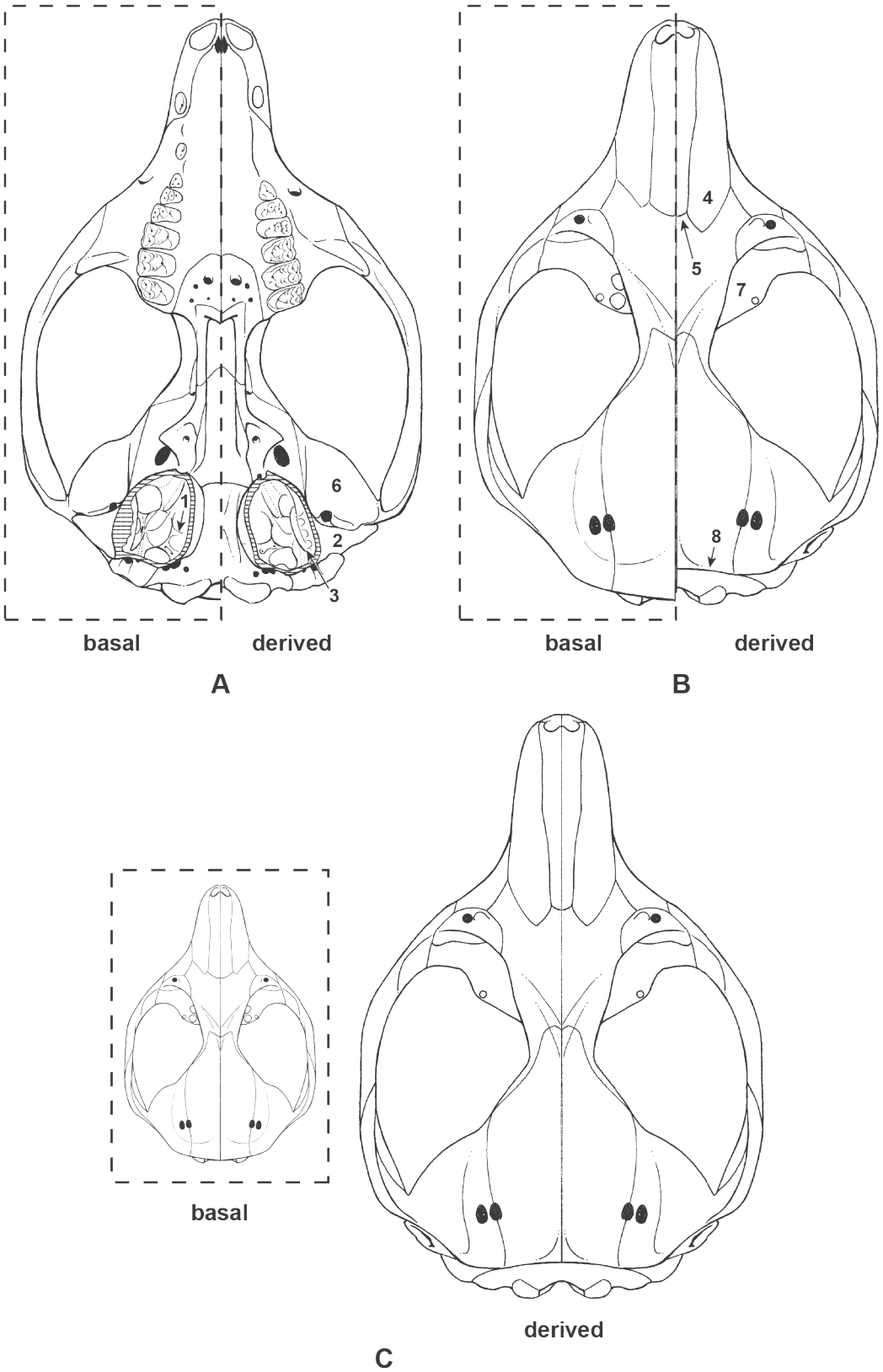
1
2
3
6
basal
derived
A
4
5
7
8
basal
derived
B
basal
derived
C

MNHN isolated petrosals), and *P. cookei* UM 87990 all show evidence that the internal carotid plexus entered the middle ear cavity. In many of these specimens, the internal carotid plexus left a groove on the lateral aspect of the promontorium (see Chapter III and Appendix V). These taxa are thus considered to exhibit the '0' state, 'groove for at least promontorial branch present.' Only *N. gidleyi* AMNH 17388 appears to lack evidence of the internal carotid plexus. Optimization of this character suggests that Plesiadapidae primitively exhibited state '0.' Silcox et al. (2010: appendix 2, character 104) and Bloch et al. (2016) also recognized Plesiadapidae as having state '0' for this trait in their matrix, but do not address their reason for differing from Bloch et al. (2007) here.

For cranial character 6, 'Position of posterior carotid foramen,' Bloch and Silcox (2006) and Bloch et al. (2007) scored Plesiadapidae '0' indicating that the foramen had a 'posteromedial position.' The same set of specimens mentioned for character 5 reveal that the posterior carotid foramen is directly adjacent to the stylomastoid foramen when preserved, which is a criterion for considering the foramen to have a 'posterolateral' position. Furthermore, in other taxa with the posteromedial state, the posterior carotid foramen is often medial to the medial edge of the promontorium. In the plesiadapids studied in Appendix V, the foramen is lateral to the medial edge of the promontorium. In fact, it is lateral to the entire promontorium. Therefore, this character is re-scored as '1,' 'posterolateral' for Plesiadapidae. This character was not included in the matrix of Silcox et al. (2010) or Bloch et al. (2016). However, Silcox et al. (2010: p. 795) state that the foramen was "further lateral" in plesiadapids suggesting a similar interpretation to that in the present study.

For cranial character 16, 'Flaring of nasals,' Bloch and Silcox (2006) and Bloch et al. (2007) scored Plesiadapidae '1' indicating that the nasals do not flare at their posterior extent and have a narrow contact with the frontal. Silcox et al. (2010: Appendix 2, character 71) and Bloch et al. (2016) present scorings and discussion indicating the same interpretation. *Pr. gaoi* UALVP 46685, *N. intermedius* USNM 309902, *P. anceps* YPM-PU 19642, and *P. cookei* UM 87990, however, have nasals that are proportionally much wider mediolaterally than those of *P. tricuspidens* MNHN CR 125 at their caudal end and even appear to flare slightly compared to the mediolateral width of these bones at their anteroposterior midpoint. Therefore, character optimization reveals primitive plesiadapids to have exhibited the '0' state, 'flaring nasals.'

For cranial character 18, 'Contact between lacrimal and palatine in the orbit,' Bloch and Silcox (2006) and Bloch et al. (2007) scored Plesiadapidae with a '1' indicating that the contact is 'obscured by maxillofrontal contact.' Silcox et al. (2010) and Bloch et al. (2016) also reflected this interpretation in their scoring (Silcox et al., 2010: Appendix 2, character 75). However, as discussed in the Description and Appendix V, the only plesiadapid specimens (*P. tricuspidens*: MNHN CR 126 and the Pellouin skull) that preserve this region relatively well are still too ambiguous to code the morphology with confidence. Therefore, we changed this character state to '?' for all plesiadapids.

For cranial character 19, 'Lacrimal tubercle,' Bloch and Silcox (2006) and Bloch et al. (2007) scored Plesiadapidae as 'absent.' However, as discussed in Appendix V, our own examination of the only plesiadapid specimen with a well-preserved lacrimal (*P. tricuspidens*: MNHN CR 126) reveals the presence of a poorly defined, blunt tubercle, similar in morphology to that described and illustrated for carpolestids by Bloch and Silcox (2006). Therefore, we changed the character state to 'present' for *P. tricuspidens*, which allows the Plesiadapidae to be represented by the 'present' state as well. Though Silcox et al. (2010) and Bloch et al. (2016) score the tubercle as present for plesiadapids, consistent with the conclusion of this study, it is not clear what evidence led them to differ from Bloch et al. (2007). Furthermore, as mentioned above, discussion in Bloch et al. (2016: p.74) suggests they viewed *Plesiadapis* as lacking a lacrimal tubercle.

For cranial character 21, 'Foramen rotundum,' Bloch and Silcox (2006), and Bloch et al. (2007) scored Plesiadapidae '1' indicating that the foramen is 'present.' Silcox et al. (2010) and Bloch et al. (2016) also discussed and scored Plesiadapidae as retaining a distinct foramen rotundum. As discussed in Appendix V, our own inspection of specimens of *P. tricuspidens* MNHN CR 125, CR 965 leads us to the alternate interpretation, also supported by Orliac et al. (2014). The foramen previously identified as the superior orbital fissure appears to be a suboptic foramen because it does not communicate with the endocranium, is variably present, and is located within the orbitosphenoid. The foramen previously identified as the foramen rotundum appears to be formed between the alisphenoid and orbitosphenoid. These observations suggest that the previously identified foramen rotundum is actually a sphenorbital fissure. Therefore, we changed the scoring for *P. tricuspidens* to the '0' state (absent). This allows Plesiadapidae to also be represented by a '0.'

For cranial character 23, 'Shielding of cochlear fenestra,' Bloch and Silcox (2006) and Bloch et al. (2007) scored Plesiadapidae, Carpolestidae and Paromomyidae as '2,' indicating that the fenestra is 'shielded by a bony septum.' Adapid euprimates, on the other hand were scored by them with a '1,' indicating that the fenestra is 'shielded by an arterial tube.' The bony shield referred to in cranial character 23 is the 'posterior septum' of MacPhee (1981). As discussed for plesiadapids and paromomyids in Boyer et al. (2012a) and Appendix V, a bony tube for the internal carotid plexus runs through the base of the posterior septum. This can be observed directly in *P. tricuspidens* (MNHN CR 125 and the Pellouin skull), *Pr. gaoi* UALVP 46685, UALVP 46687, UALVP 49105, and *I. graybullianus* (e.g., USNM 482353, USNM 421608). We cannot see how this differs from the state assigned to Adapidae. Therefore, we changed the scoring from '2' to '1' for plesiadapids, carpolestids and paromomyids.

Cranial character 24 of Bloch and Silcox (2006) is different than that of Bloch et al. (2007). For Bloch and Silcox (2006) it is 'Presence/absence of an auditory tube that runs through lateral wall of anterior chamber.' No similar character is included in Bloch et al. (2007). Bloch and Silcox (2006) scored carpolestids as having the 'present' state. Study of

the original specimen of *Carpolestes simpsoni* UM 101963 and discussion with J. Bloch lead us to conclude that the bone separating the carpolestid bulla into an anterior and posterior chamber (the 'platform bone' of Bloch and Silcox 2006), is in fact a piece of the ectotympanic bone that has been pushed out of place. Therefore, the carpolestid bulla is not divided into chambers, and carpolestids must be considered as exhibiting the 'absent' state for cranial character 24 of Bloch and Silcox (2006). No similar character was included in Silcox et al. (2010) or Bloch et al. (2016).

For postcranial character 4, 'Position of deltopectoral crest on humerus,' Bloch et al. (2007) scored plesiadapids as polymorphic (0,1), with some having a laterally positioned crest and others having an anteriorly positioned crest. They based this polymorphic scoring on *P. cookei* (UM 87990) exhibiting an anteriorly positioned crest, in contrast to *P. tricuspidens*, *P. walbeckensis*, and *N. intermedius* (USNM 442229), which exhibit a laterally positioned crest. Additional specimens including those of *Pr. gaoi* (UALVP 49114) and *P. rex* (UM 64588) are also observed to have a laterally positioned crest. This allows the ancestral node for Plesiadapidae to be optimized as having the lateral position state. No similar character was included in Silcox et al. (2010) or Bloch et al. (2016).

For postcranial character 10, 'Morphology of the ulnar trochlea on humerus,' Bloch et al. (2007) scored Plesiadapidae with the '0' state, indicating 'only a medial ridge present.' Silcox et al. (2010: Appendix 2, character 12) and Bloch et al. (2016) score this feature similarly. However, *Pr. gaoi* UALVP 49114, *P. rex* UM 64588, and many *P. tricuspidens* specimens exhibit a lateral ridge as well. These observations allow optimization of the ancestral node of Plesiadapidae as having a medial and lateral ridge (state '1').

For postcranial character 21, Bloch et al. (2007) scored plesiadapids '?,' indicating that it was not known whether any plesiadapid had a nail on any of its digits. Silcox et al. (2010: Appendix 2, character 60) and Bloch et al. (2016), similarly considered the form of the distal phalanx on the pedal digit I to be unknown. However, the skeleton of *Plesiadapis insignis* in Gingerich (1976) illustrates the presence of claws on all pedal digits, and all manual digits except for the pollex, which is obscured. Furthermore, the form of the hallucal and pollical proximal phalanges of *P. tricuspidens* and *Nannodectes* (see Chapter IV) suggest the presence of claws, rather than nails.

For postcranial character 30, 'Plantodistal process of entocuneiform,' Bloch et al. (2007) scored Plesiadapidae as polymorphic (0,1) indicating that some taxa have a 'strong' process, whereas others have one that is 'reduced or absent.' This was based on the observation that the entocuneiform attributed to the skeleton of *P. cookei* UM 87990 lacks a strong plantodistal process. However, our reassessment of this bone is that it is so different from the entocuneiform of other plesiadapids (*P. tricuspidens*: MNHN R 416, MNHN R 5359, MNHN R 5331; *P. anceps* AMNH 92011; see Szalay and Dagosto, 1988) and other plesiadapiforms (Sargis et al. 2007), that it must be tentatively considered as incorrectly attributed to UM 87990. Whether or not this is correct, the presence of a strong plantodistal process in *P. tricuspidens* and *P. anceps* allows us to re-score plesiadapids as having the '0' state only. Silcox et al. (2010) and Bloch et al. (2016) also considered the plantodistal process to be unequivocally present, though they did not explain why they differ from Bloch et al. (2007) on this point.

For postcranial character 32, Bloch et al. (2007) scored Plesiadapidae as polymorphic (0,1) for the presence of 'cranial buttressing' on the acetabulum. However, all plesiadapids known for this morphology (*N. gidleyi* AMNH 17409, AMNH 17379; *P. tricuspidens* MNHN R 448; *P. cookei* UM 87990) exhibit the '1' state as compared to, for instance, tupaiid treeshrews. We therefore re-scored the group in this way. Silcox et al. (2010) and Bloch et al. (2016) also considered the acetabulum to be unequivocally cranially butressed, though they did not explain why they differ from Bloch et al. (2007) on this point.

For postcranial character 54, 'Length of pubic symphysis,' Bloch et al. (2007) scored plesiadapids with the '0' state, indicating a 'long' pubic symphysis. However, the only plesiadapid with the symphyseal region of the innominate well enough preserved to make an assessment is *P. cookei* (UM 87990). In Chapter IV, we discuss its morphology, which appears to be more like that of *Cynocephalus volans*. *C. volans* has a 'short' pubic symphysis compared to those of paromomyid plesiadapiforms, which have a 'long' pubic symphysis (Boyer and Bloch, 2008). We therefore changed the scoring of postcranial character 54 to '1' (short) for *P. cookei*, which allows Plesiadapidae to also be represented by a '1.' No similar character was included in Silcox et al. (2010) or Bloch et al. (2016).

For postcranial character 58, 'Orientation of spinous process on axis,' Bloch et al. (2007) scored Plesiadapidae with the '0' state, indicating a 'caudal' orientation. Silcox et al. (2010: Appendix 2, character 64) and Bloch et al. (2016) scored plesiadapids similarly, apparently based on the axis of *P. cookei* UM 87990. Our study of this specimen suggests to us that it is broken cranially (see Chapter IV), meaning that whether or not there was a cranial orientation to the process is unknown. However, a specimen of *N. intermedius* USNM 442229 retains a prominent, cranially-oriented spine. Thus, we re-scored this character for Plesiadapidae with the '1' state, indicating a 'cranial' orientation.

Results of cladistic analysis.— A heuristic search of the rescored Bloch and Silcox (2006) matrix resulted in the same three most parsimonious trees and consensus (Fig. 85A) as recovered by the original authors. Treelength decreased from the original result, as did the consistency index (CI) and the retention index (RI) (Table A-IV-8).

Analysis of the Bloch et al. (2007) matrix, with the scoring changes described above and those of Chester et al. (2015), yielded the same results as analysis of the original matrix (Fig. 85B). Treelength decreased and CI decreased slightly compared to the version analyzed by Chester al. (2015; Table A-IV-8).

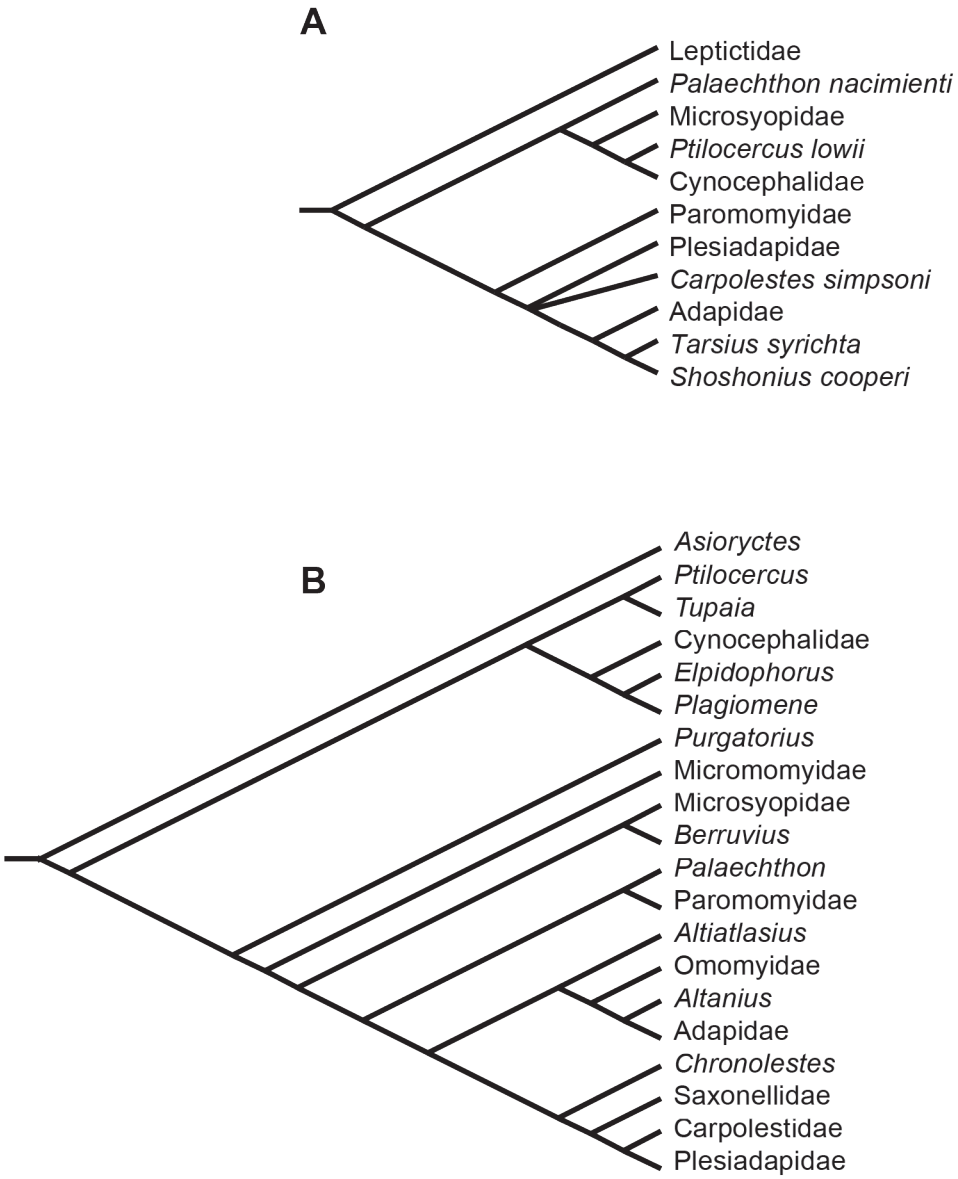

FIGURE 85.— Cladistic relationships of plesiadapid families. Most-parsimonious (MP) trees based on modified character matrices. **A**, MP tree 1 from analysis of the modified matrix of Bloch and Silcox (2006), with topology matching one of the MP trees of the original matrix. **B**, MP tree from analysis of modified matrix of Bloch et al. (2007).

VII

DISCUSSION AND CONCLUSIONS

In the preceding sections we reviewed the cranial morphology, postcranial morphology, life history characteristics, and phylogenetic relationships of *Plesiadapis cookei* based on study of UM 87990. Here we consider the functional, ecological, and phylogenetic significance of these observations.

CRANIAL MORPHOLOGY

The cranium of *P. cookei* is very similar to that of *P. tricuspidens* in most respects, and it appears to have been very similar in size. However, *P. cookei* differs from *P. tricuspidens* in having larger teeth, more molariform P^4 and P_4, no P^2, broader nasal bones, a zygomatic process of the maxilla that arises lateral to M^1, smaller glenoid fossa, possibly a less expanded annular component of the ectotympanic bone, and a more posteriorly projecting nuchal crest. The latter three features make *P. cookei* more similar to earlier-occurring North American plesiadapids such as *Pr. gaoi, N. intermedius*, and *P. anceps*. On the other hand, the large teeth of *P. cookei* and the anteriorly shifted maxillary zygomatic process differentiate it from many other plesiadapid species, including the taxa listed above, which have much smaller teeth for the size of their crania. The only other plesiadapids known to have the same zygomatic process position as *P. cookei* are species of *Chiromyoides* and the species *Pl. richardsoni*.

Our results suggest that some features of the orbitotemporal region (Fig. 86) and basicranium previously thought to unite some plesiadapids and carpolestids do not (see Table A-IV-3: characters *c6, c16, c18*, and *c21* of Bloch and Silcox, 2006). We reviewed the form and distribution of trigeminal nerve foramina and can confidently conclude that in *P. tricuspidens* there was no separate foramen for the maxillary branch of the trigeminal nerve. Both the ophthalmic and maxillary branches must have emerged through a sphenorbital fissure (Fig. 86, Chapter III, Appendix V; Boyer et al. 2012a). Previous interpretation of a foramen rotundum for the maxillary branch in *P. tricuspidens* was listed as evidence linking plesiadapids and carpolestids (Silcox et al., 2001; Bloch and Silcox, 2006). We also reviewed the pattern of contacts in the orbital mosaic, which had been argued to be similar in carpolestids and plesiadapids because the maxilla and frontal excluded contact between the palatine and lacrimal (Bloch and Silcox, 2006). We show that the primary specimens used for this interpretation are ambiguous in the sutural pattern they exhibit (Fig. A-V-24).

In the basicranium, the position of the posterior carotid foramen has been ambiguous (Bloch and Silcox, 2001, 2006; Bloch et al., 2007), and it is uncertain whether this canal held a patent artery or just carotid-plexus sympathetic nerves. Direct comparison among many plesiadapid taxa, as well as other plesiadapiforms and euprimates, confirms that the posterior carotid foramen was laterally positioned in plesiadapids, as it is in paromomyids, adapiforms, and extant lemuriforms (Fig. 14), and that the foramen was too small to hold a patent artery (Table A-I-9; Fig. 28). The lack of a patent internal carotid artery implies that encephalic blood was supplied by the vertebral artery (as in non-cheirogaleid lemurs) or by a rete mirable (as in dermopterans, cheirogaleids, and lorisiforms). In contrast, *C. simpsoni* appears to have a posteromedially positioned posterior carotid foramen and a functional internal carotid artery (Bloch and Silcox, 2006: table 3, character 6). One surprising result of measuring posterior carotid foramina among plesiadapids is that the widest observed foramen (belonging to *P. cookei*) is only 1.30 to 1.43 times the width of that in the rest of the plesiadapid sample (Table A-I-9), meaning that there is a lot of *proportional* variation in the diameter of this canal relative to cranium size, with the proportionally largest internal carotid plexus groove being found in the smallest species, *N. intermedius.*

Another longstanding ambiguity is whether the tympanic bulla was developmentally derived from the petrosal bone or from a distinct entotympanic element (e.g., Szalay et al., 1987; MacPhee et al., 1983; MacPhee and Cartmill, 1986; Kay et al., 1992; Bloch and Silcox, 2001, 2006; Bloch et al., 2007; Boyer et al., 2012a). We surveyed all available plesiadapid skulls and found anatomical patterns suggestive of an entotympanic bone ventrally overlapping the promontorium in *P. cookei* (Fig. 15C–D), the Pelluoin skull of *P. tricuspidens* (Fig. A-V-21E: 131), and specimens of *Pr. gaoi* (see figures in Boyer et al., 2012a). In addition, we observed features that look like a 'finished edge' to a limited rostral process on the petrosal in *Pr. gaoi* (section III, Appendix V, Figs. A-V-25 and A-V-26; Boyer et al., 2012a). However, when CT data were obtained, we could not verify the distinction between the bulla-forming bone and the petrosal. Thus, we tentatively accept previous interpretations that plesiadapids had a euprimate-like tympanic bulla derived from the petrosal bone. Another reason for uncertainty surrounding the presence of an entotympanic element is difficulty in determining the extent of the ectotympanic bone in currently available specimens.

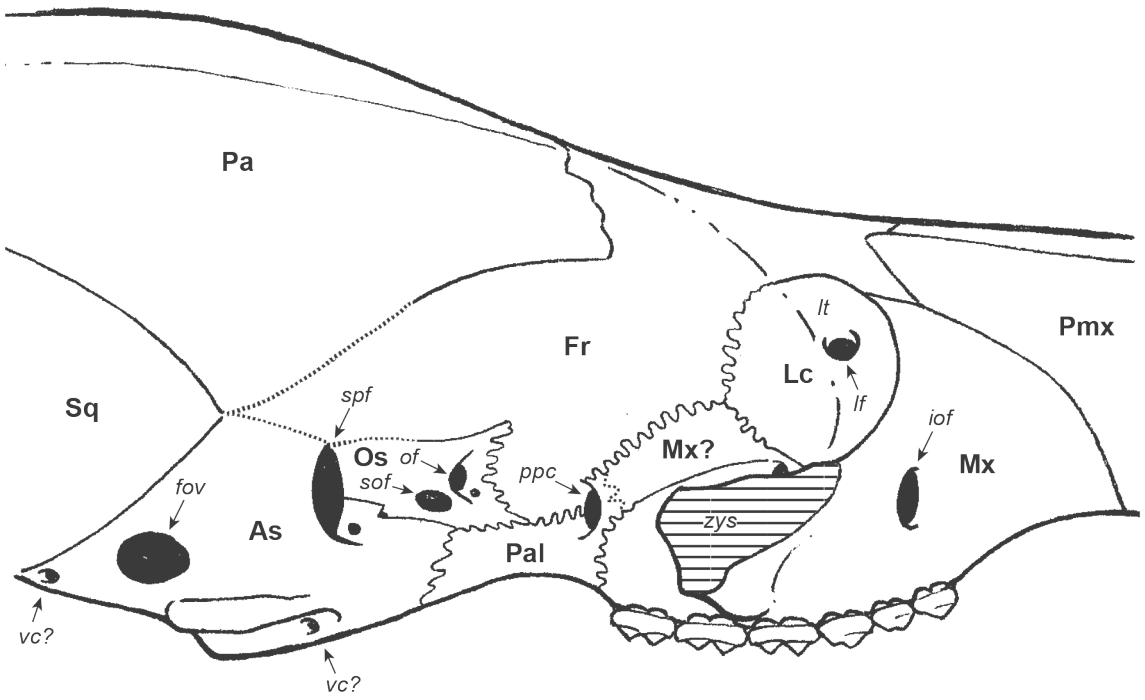

FIGURE 86— Reconstruction of orbitotemporal sutures and foramina in a generalized plesiadapid (hypothesized suture paths are shown as dotted lines). There appears to be some variability in the position of the alisphenoid/orbitosphenoid suture based on two specimens where it is interpreted as partly preserved. Drawing represents what is likely to be the average position. In MNHN CR 125 the suture is more ventrally located than shown here (photograph in Fig. A-V-13D'), whereas in MNHN CR 965 it is more dorsally located than shown here (Fig. A-V-17A, C'). Style of illustration is based on that in Russell (1964: fig. 19) and Gingerich (1976: fig. 33). Abbreviations: *As*, alisphenoid; *fov*, foramen ovale; *Fr*, frontal; *iof*, infraorbital foramen; *Lc*, lacrimal; *lf*, lacrimal foramen; *lt*, lacrimal tubercle; *Mx*, maxilla; *Mx?*, possible fragment of maxilla; *of*, optic foramen; *Pa*, parietal; *Pal*, palatine; *Pmx*, premaxilla; *ppc*, postpalatine canal; *sof*, suboptic foramen; *spf*, sphenorbital fissure; *Sq*, squamosal; *vc?*, possible entrance to vidian canal; *zys*, sutural surface on maxilla for zygomatic.

Although we can be reasonably sure that the annular ring for the tympanic membrane is ectotympanic, no obvious sutures separate this structure from the annular bridge or external auditory meatus. Furthermore, no sutures on the ventral aspect of the bulla are obvious, unlike in paromomyids, which have an obvious suture separating the entotympanic and ectotympanic (Kay et al., 1992; Bloch and Silcox, 2001). Based on similarities to rodents (Fig. 23) it is possible that the ectotympanic forms both the entire bulla as well as the annular component. We await better specimens and better images that might resolve the issue.

Although plesiadapids were thought to possess a nasal bone that narrows posteriorly, as in carpolestids (e.g., Bloch et al., 2016), it appears to be present in only *P. tricuspidens*. Other plesiadapids have nasals that are broader posteriorly, like paromomyids and micromomyids.

On the other hand, some features previously thought to differentiate plesiadapids and carpolestids are actually shared between them (see Table A-IV-3). Using *P. triscuspidens* as their examplar, previous studies differentiate plesiadapids from carpolestids (and other plesiadapiforms) based on its tubular external auditory meatus. However, ancestral state reconstruction here shows that the non-expanded external auditory meatus (c3) is primitive: *N. intermedius* and *Pr. gaoi* display this state. Although a posterior carotid foramen was recognized in plesiadapids by earlier workers (e.g., Gingerich, 1976; Bloch and Silcox, 2006), MacPhee et al. (1983) cast doubt on wheteher the internal carotid plexus extended across the promontorium. Therefore, grooves on the promontorium relating to the internal carotid plexus (*c5*) were not recognized by Bloch and Silcox (2006) or Bloch et al. (2007). In this study we outline strong evidence identifying grooves *g1–2* as the internal carotid plexus.

Previous work suggested plesiadapids lacked a lacrimal tubercle (*c19*) based on observation of *Plesiadapis tricuspidens* MNHN CR 125 (Bloch et al., 2007; Bloch et al., 2016). As described in Appendix V, we find evidence of a lacrimal tubercle in MNHN CR 126, suggesting again that plesiadapids were actually similar to, not differentiated from, carpolestids in this respect. Finally, since we reinterpret the carpolestid bulla as lacking accessory chambers (Bloch and Silcox, 2006: table 3, character 24), carpolestids are similar to plesiadapids in this feature as well.

POSTCRANIAL MORPHOLOGY

Several skeletal elements preserved in UM 87990 were not previously recorded in *Plesiadapis*, including the pollical metacarpal, scaphoid, lunate, pisiform, trapezoid, trapezium, ectocuneiform, hallucal metatarsal, and much of the vertebral column. Skeletal elements previously only known from fragmentary bones in *Plesiadapis* include the innominate and the tibia. New information on these elements has allowed significant progress in understanding the articular relationships of wrist bones, metacarpals, and metatarsals. Uncertainty remains regarding reconstruction of the wrist and hand, however, due to problems with associations and the lack of a complete wrist for a single plesiadapid individual.

Skeletal proportions

Digit proportions.— Newly determined digit proportions of *P. cookei* are consistent with arboreal habits, contrary to proportions calculated by Kirk et al. (2008). The relatively shorter fingers of *P. tricuspidens* are still puzzling, but we interpret this result as an artifact of misassignment of some of the finger bones to the foot in the MNHN sample. That is, the intermediate phalanges assigned to the hand by Beard (1989) may represent only the shortest digits of the hand, whereas some of the longer manual phalanges, and specifically those of the third digit, may be misidentified as pedal elements. Some of the incomplete phalanges assigned to the hand of *P. cookei* (Fig. 53C, D) would have been quite short and close to the length of the phalanges assigned to the hand of *P. tricuspidens*. But if there was variation in manual phalangeal length across digit rays, the shorter phalanges are not relevant for calculation of the phalangeal index because the phalangeal index uses the third digit ray, and phalanges of the third digit are usually the longest or close to the longest of the hand, not the shortest. An articulated specimen of *P. insignis* provides the only direct evidence of variation in manual digit ray length in plesiadapids. The lengths of bones of its third digit ray give a phalangeal index of 140, but phalanges from the fifth digit ray give a phalangeal index of 112, which is nearly identical to the value calculated for *P. tricuspidens*. It seems likely that *P. tricuspidens* (like *P. cookei, P. insignis*, and *Nannodectes*) will be found to have third digit phalangeal indices of around 130–140 when more-confidently identified digit rays are available. The numerical value of this index is lower than that most arboreal euprimates, but much higher than the index for many terrestrial mammals (Kirk et al., 2008). If, on the other hand, it turns out that *P. tricuspidens* truly does have very short fingers, this would not necessarily provide evidence contradicting an arboreal habitus (Kirk et al., 2008) nor overwhelm plentiful information from other parts of the skeleton suggesting arboreal habits (Youlatos and Godinot, 2004). It should be noted, however, that a more terrestrial habit would be consistent with the absolutely thicker and proportionally shorter limbs of *P. tricuspidens* as compared to *P. cookei* and extant arboreal mammals (Runestad and Ruff, 1995).

Postcranial proportions.— Body proportions of plesiadapids are compared to those of other mammals in the principal components plots of Figure 80, where the position of plesiadapids and other plesiadapiforms is consistent with their interpretation as 'callitrichid-like' or 'squirrel-like' arborealists (Bloch and Boyer, 2007; Boyer and Bloch, 2008). Suspensory taxa including *Cynocephalus* and sloths lie in a different part of the morphospace, which does not overlap with *P. cookei* or with plesiadapoids. This could be considered evidence against the suggestion of Bloch and Boyer (2007) and Boyer and Bloch (2008) that *P. cookei* had 'suspensory tendencies.' In this regard, limb proportions are consistent with evidence from vertebral proportions and analysis of joint mobility. That is, the vertebral column exhibits features not typically found in suspensory taxa, a short neck and a long tail (Stafford, 1999).

More phylogenetically focused comparisons of body segment lengths could be interpreted as supporting the hypothesis of suspensory tendencies for *P. cookei*. For example, suspensory taxa have higher brachial and intermembral indices than quadrupedal arboreal taxa (Boyer and Bloch, 2008). *P. cookei* has a greater brachial index and possibly intermembral index than other plesiadapids. Furthermore, the longer and more gracile humerus and femur of *P. cookei*, as compared to those of *P. tricuspidens*, are consistent with more frequent use of antipronograde postures in *P. cookei* (Jungers, 1985).

Posture and mobility

Limb mobility.— A skeletal reconstruction and life restoration of UM 87990 *P. cookei* is shown in Figure 87. The complete skeleton of a single individual provides an opportunity to consider the functional significance of mobility at several joints of the limbs. Analyses presented in Chapter IV indicate that *P. cookei* probably assumed postures in which the arm was either extended or flexed at the shoulder in the sagittal plane to some degree, but not substantially abducted or laterally rotated (i.e., the distal end of the humerus pointed caudally or ventrally, but not substantially laterally). As discerned in previous studies of *P. tricuspidens* (Szalay et al., 1975), it seems that the elbow was typically flexed by around 90º or more from a fully extended position. The forearm would have been abducted by ca. 30º, relative to the anteroposterior axis of the humerus. In the closest-packed configuration of the joints of the elbow and wrist, the manus was partly supinated and slightly dorsiflexed, although it had the capacity for a large range of dorsiflexion. The mechanical capacity for such a large range of dorsiflexion of the hand (and digits) is probably important for pronograde quadrupedalism, and possibly for descent on large-diameter vertical substrates (Jenkins, 1974).

A typical hind limb posture seemingly involved a femur that was abducted, flexed, and laterally rotated relative to the innominate. The knee would have been flexed, and the leg slightly abducted. The foot would have been dorsiflexed and slightly inverted, with the capacity for a wide range of inversion (Fig. 77). Abducted limbs result in a posture with sprawled hands and feet. Such a posture would have made *P. cookei* adept at navigating relatively large diameter substrates. A physiologically supinated hand and inverted

foot would have accommodated cylindrical substrates well (i.e., tree trunks and branches). Jenkins (1974) presented data on *Tupaia glis* showing it to adopt such supinated hand and inverted foot postures during quadrupedal locomotion on relatively narrow branches.

The inferred mobility, in the hind limb especially, would have been useful in ascending vertical substrates, because the hind limb has much of its mobility concentrated in a coronal plane, rather than a sagittal plane. Thus, extension of the hind limb would not tend to push the body farther away from the substrate. This is primarily related to the fact that the femur of *Plesiadapis* extended and flexed in a coronal plane. Because the knee would have been laterally rotated during much of the support phase of locomotion, flexion and extension of the knee also occurred mainly in a coronal plane. Finally, as explained in Chapter IV, although flexion and extension of the astragalotibial joint is limited, abduction-adduction and inversion-eversion are emphasized. It is important to keep the body close to the substrate during vertical climbing because the rotational moments created by gravity acting on body mass, around the hands and feet as anchoring points, increases with distance of the center of mass from the substrate (Cartmill, 1974, Jungers, 1976).

The hind limb of the treeshrew *Ptilocercus* resembles that of *P. cookei* in many respects (Sargis, 2002b). *Ptilocercus* is arboreally committed, engaging in vertical clinging and climbing behaviors (Le Gros Clark, 1926). Thus, features promoting mobility in the transverse plane are associated with orthograde postures and locomotion in *Ptilocercus lowii*. In contrast, the tupaiid treeshrews do not resemble *P. cookei* or *Ptilocercus lowii* in their hind limb morphology and do not frequently engage in orthograde clinging and climbing. Furthermore, the hind limb postures that Jenkins (1974) illustrated for *Tupaia* show the femur to be more sagittally oriented and sagittally mobile than suggested in the reconstructions presented here for *P. cookei.* So it seems reasonable to conclude that *P. cookei* moved more like *Ptilocercus* than *Tupaia*.

The reduced ability for plantarflexion in plesiadapids relative to treeshrews like *Tupaia* and many primates (see above) raises the question of how vertical descent postures could have been accomplished in plesiadapiforms, given the importance of hind foot reversal (Jenkins and McClearn, 1984; Meldrum et al., 1997). Beard (1989) suggested plesiadapiforms were not effective at descending vertical supports and proposed that gliding behaviors represented an alternative means for descending forest canopies. However, our reconstruction of the hind limb of *P. cookei* (Fig. 78) shows an approximation of a limb posture that could be used for vertical descents, with an abducted, extended femur, a knee flexed 90º, an astragalotibial joint plantarflexed 90º, and a fully inverted astragalocalcalcaneal joint. Further inversion of the foot could be accomplished by rotating the transverse tarsal joints and metatarsals, but just exactly how and how much these bones could be moved with respect to each other is difficult to constrain. Interestingly, the reconstructed posture of *P. cookei* depicted in Figure 78 is similar to cineradiography-based drawing of hind foot reversal in *Tupaia* in Jenkins (1974: p.102, fig. 6) except for the increased degree of abduction in the hind limb of *P. cookei*.

Differences from other plesiadapids.— The major features differentiating *P. cookei* from other plesiadapids are more gracile limb bones, in some cases proportionally longer limb bones, and proportionally narrower intermediate phalanges (Boyer and Bloch, 2008). In addition, *P. cookei* has features of the ankle that appear to give it more mobility than the ankle of other plesiadapids. The metacarpals of *P. cookei* and *P. tricuspidens* appear to be more robust than those of *Nannodectes*, although not proportionally shorter compared to the phalanges (see below). Finally, the vertebrae of *P. cookei* differ from those of *Nannodectes* in having features that suggest the vertebral column was more rigid and 'stable.' Overall, these unique features of *P. cookei* may correspond to a lifestyle that was more committed to arboreal settings and possibly orthograde postures.

Some researchers have suggested that *P. cookei* was behaviorally distinct from other plesiadapids: Bloch and Boyer (2007) and Boyer and Bloch (2008) suggested that *P. cookei* was not only an arborealist, but had morphology suggestive of 'suspensory tendencies.' Bloch and Boyer (2007) specifically mentioned features of the humerus, intermediate phalanges, and claws. Bloch et al. (2007) noted additionally that scapular morphology distinguishes *Plesiadapis* from other plesiadapiforms, but they did not provide details on these differences or their behavioral implications. Here, however, we find that differences between the scapulae of *P. cookei* and *N. intermedius* are consistent with a less mobile shoulder in *P. cookei* and do not clearly support the case for suspensory behavior in *P. cookei*. Although there are some differences between the humerus of *P. cookei* and those of *Nannodectes* and other plesiadapids, these were not quantified here and are not strongly suggestive of suspensory postures. In fact, some of the humeral morphology that has been quantified shows all plesiadapids to be similar in morphology of the distal humerus.

The greater degree of lateral torsion in the humeral shaft of large-bodied plesiadapids is opposite the medial torsion that is observed in suspensory primates and xenarthrans. In contrast, the intermediate phalanges of *P. cookei* resemble those of suspensory bats, sloths, and *Cynocephalus* (Boyer and Bloch, 2008). The aye-aye *Daubentonia* also exhibits intermediate phalanges with mediolaterally narrow proximal ends, like *P. cookei* and suspensory taxa (Boyer and Bloch, 2008). Although the aye-aye is adept at quadrumanus suspensory locomotion (personal observation of D. M. B.), it is not a 'suspensory animal' in the manner of a sloth or a dermopteran.

Finally, the claws of *P. cookei* are very similar overall to the claws of other plesiadapids. The features that differentiate the claws of *P. cookei* from those of smaller plesiadapids (slightly narrower and more hook-like shaft) could easily be related to allometric effects of body size differences (although this remains to be demonstrated).

Similarities to carpolestids

Our survey of the diversity of plesiadapids allowed

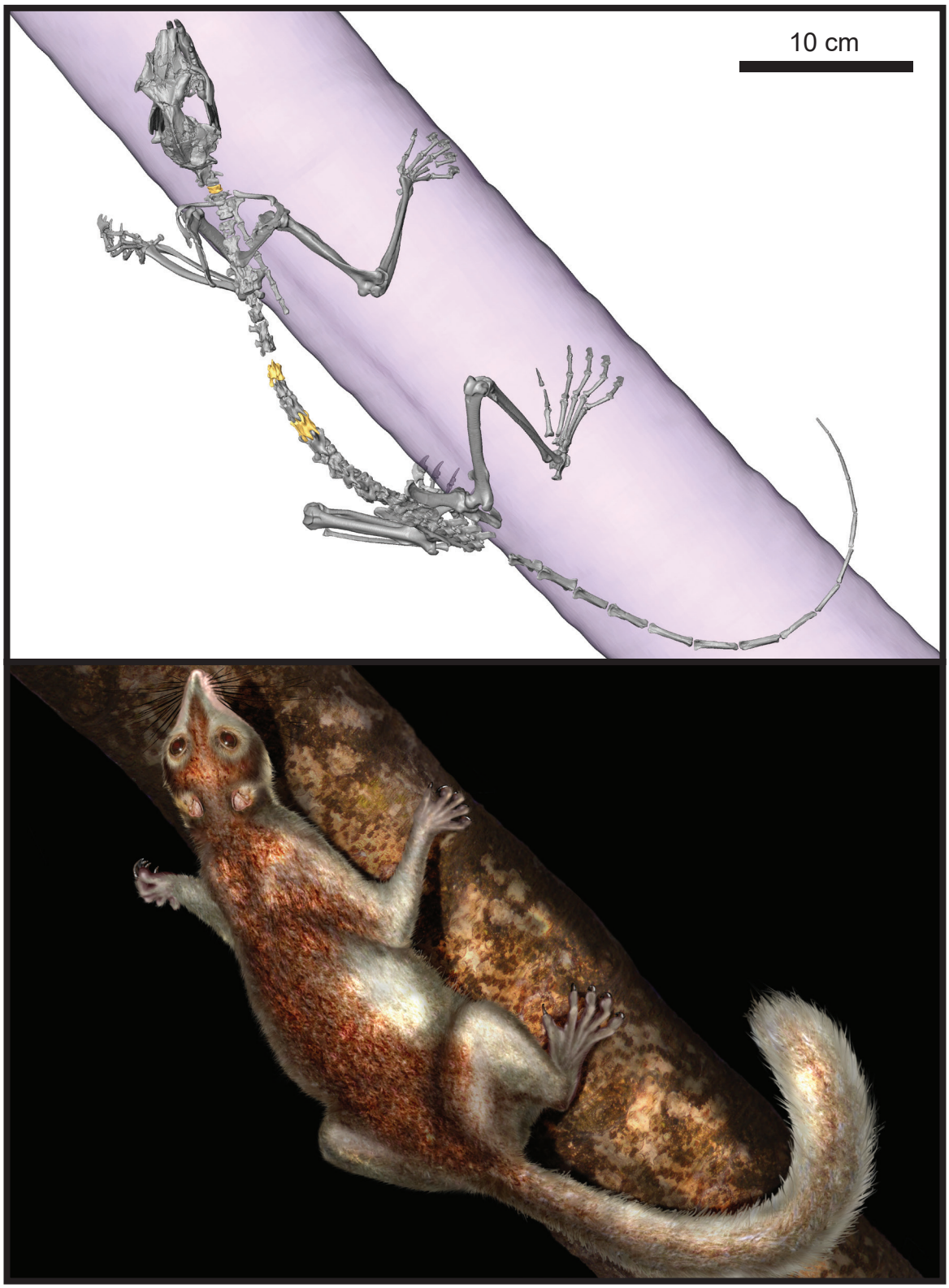

FIGURE 87.— Skeletal restoration and life reconstruction of *Plesiadapis cookei* (UM 87990). Both are shown in a representative antipronograde posture, based on our interpretation of *P. cookei* limb proportions, limb articulations, and falciform terminal phalanges.

resolution of polymorphic character state scorings and revision of others. Several characters previously scored as polymorphic now match carpolestids, including *p4* (deltopectoral crest orientation) and *p32* (buttressing of the acetabulum). Others characters were determined to not match carpolestids, (i.e., *p30* plantodistal process presence). Certain characters were revised to states that match carpolestids, including *p10* (ulnar trochlea lateral keel) and *p54* (pubic symphysis length). Others were revised to states that do not match carpolestids (*p21*, presence of nail-like distal phalanges). Revisions and disambiguations of character states resulted in an increase by 1 in the number of recognized similarities between carpoelstids and plesiadapids.

Interestingly, two of the postcranial traits that now appear to be shared by plesiadapids and carpolestids suggest specialized arboreality, rather than scansoriality, and might be the ancestral condition for these two groups. Specifically, presence of a lateral keel on the humerus suggests more specialized axial mobility of the forearm (e.g., Szalay and Dagosto, 1980; Boyer et al., 2010), and a short pubic symphysis suggests a more cautious locomotor repertoire that might emphasize bridging over bounding (e.g., Boyer and Bloch, 2008). This is consistent with the idea that many euprimate-like specializations of carpolestids might be homologous to those of euprimates even if carpolestids are the sister taxon of plesiadapids.

LIFE HISTORY

The life history characteristics of *P. cookei* that we are able to address from study of the UM 87990 skeleton and other dental remains are body weight, brain size and relative brain size (encephalization), sex of the skeleton, sequence of tooth eruption and rate of growth, and finally ontogenetic stage of development of the skeleton. More could be said if multiple skeletons and an ontogenetic growth series were available for study.

Body weight and encephalization

In Chapter V, we predicted the body weight of *P. cookei* and other plesiadapids. Three estimates of body weight for UM 87990 ranged from 1,799 to 2,052 g. The preferred weight based on multiple regression is 2,052 g. With a 5 g brain, we calculated an encephalization residual $ER_{TC} = -1.816$. The corresponding encephalization quotient is $EQ_{TC} = 0.284$. This residual and the corresponding quotient indicate a brain approaching two halvings or 28% of the size expected for an average living terrestrial mammal of the same body weight. To put these numbers in perspective, ER_{TC} values calculated from brain and body weights for Eocene euprimates published by Ramdarshan and Orliac (2016) start a full doubling larger than the value for *P. cookei*. Relative brain sizes for *Notharctus* and *Smilodectes* were published by Harrington et al. (2016) and disputed by Gilbert and Jungers (2017).

Evaluation of the argument that plesiadapiform brains were meaningfully smaller than early euprimate brains is best deferred until reliably comparable body mass predictions can be generated for samples including both plesiadapiforms and early euprimates. Such reliably comparable predictions will necessarily be based primarily on the postcranium, but must sample a larger number of postcranial bones from each species compared. Although the bones representing a species need not be from the same individual, they should come from a sample approximating a single biological population of individuals. If such analyses confirm different relative brain sizes, the implications of these differences will be easier to understand and less debatable if either the absolute brain sizes or absolute body sizes of the plesiadapiforms and euprimates being compared are similar. In other words, the sample should reflect "narrow allometry" as recommended by Gilbert and Jungers (2017).

Our prediction of body weight is based on long bone lengths and diameters because the postcranial skeleton as a whole should be more representative of body weight than the skull, dentition, or any individual postcranial bone. The postcranial skeleton is less likely to be influenced by brain size, chewing mechanics, and the mechanical properties of food (Yapuncich et al., 2015). Boyer et al. (2010a) showed that *P. cookei* and *P. tricuspidens* have cranial and dentary dimensions that are nearly identical, but molar sizes that are significantly different, meaning that body weight estimates from tooth size would suggest differences in weight, whereas estimates from cranial size would not. Looking at patterns in our body weight prediction data reveals interesting implications for the *bauplan* of *Plesiadapis*, the scaling of head and body proportions among plesiadapids, and estimates of relative brain size and EQ.

First, prediction of body weight using a reference sample based on a large range of extant mammals (Gingerich, 1990) indicated that *P. cookei* had relatively long limbs compared to an average mammal: body weight predictions based on long bone lengths are generally greater than average whereas those based on long bone diameters are less than average. *P. cookei* probably weighed somewhere in the range of 1–3 kg estimated from long bone lengths and diameters, but not as much as 5 kg suggested by regression of body weight on skull length in extant primates (Silcox et al., 2009a).

Second, allometry of head and body proportions among plesiadapids is revealed by comparing the interspecific range of weight predictions from crania with the range of weight predictions from postcrania for the same species (Table A-III-2). Proportional differences in body weight distinguishing *P. cookei* and other plesiadapids based on the postcranium are much smaller than proportional differences in body weight based on skull length. Postcranial measurements suggest that *P. cookei* is at most five times the weight of the smallest plesiadapid, *N. intermedius*, whereas the cranial measurements suggest that *P. cookei* was 9 to 16 times the weight of *N. intermedius*. This contradiction between postcranial and cranial estimates in plesiadapids shows that the relationship of skull length and postcranial dimensions is not isometric.

Phylogenetic hypotheses in Chapter VI add support to the idea that a low EQ is the ancestral condition for Euarchonta

and Plesiadapidae. Finding that *P. tricuspidens* and *P. cookei* are members of separate large-bodied lineages makes it more likely that *P. cookei* and *P. tricuspidens* inherited their low encephalization quotients (EQ) from a common ancestor with a low EQ, as suggested by Orliac et al. (2014). *P. cookei* and *P. tricuspidens* effectively bracket plesiadapids such as *P. dubius, P. fodinatus, P. churchilli, P. simonsi*, and *P. gingerichi* phylogenetically, so it is reasonable to expect that these species too had smaller EQ values than those of other plesiadapiforms. The broader implication of Orliac et al.'s (2014) hypothesis is that higher EQ values evolved in parallel in paromomyid and microsyopid lineages from values more similar to those of plesiadapids. Of course, a well-preserved skull of one of the bracketed taxa with a larger brain would refute the inference that all had low encephalization.

Sex and ontogeny

Relative width of the superior pubic ramus of the innominate led us to interpret the UM 87990 skeleton of *Plesiadapis cookei* as a male. This specimen retains no deciduous teeth and has all of the permanent teeth fully erupted but little worn. A referred specimen has P^3/P_3 and P^4/P_4 erupting late, placing the species in the category of rapidly-growing mammals. Epiphyseal fusion of postcranial bones is limited to the elbow joint (distal humerus and the proximal radius and ulna), leading us to interpret UM 87990 as an advanced and nearly full-grown subadult or a full-grown young adult. Rapid growth like that inferred for *P. cookei* is often associated with a relatively short life span, and the life history of *Plesiadapis* represents what is probably a widespread mammalian baseline condition. Information from dental histology would help test and build on this idea.

PHYLOGENETIC RELATIONSHIPS

Species level phylogeny of Plesiadapidae

In Chapter VI, the species-level cladistic and stratocladistic analyses of plesiadapids yielded strict consensus trees largely consistent with Gingerich's (1976) statophenetic hypotheses (Fig. 83A). The stratocladistic result shown in Figure 2A shows some important differences compared to Gingerich's (1976) hypothesis, as described in the results. Nonetheless, all of these results share some features in common with Gingerich's (1976) hypothesis that were lacking from more recent cladistic results published in Boyer et al. (2012a, b). This result may be somewhat surprising because the character matrix analyzed here was one updated from Boyer et al. (2012a, b). Updates include better representation of intraspecific variability with polymorphic codings, error corrections (Table A-IV-2), and addition of new characters representing features discussed as phylogenetically informative by earlier authors (see Table A-IV-1, ch70–71). These updates resulted in a topology that does not unambiguously support a sister-taxon relationship between the clade containing *P. dubius* and *P. fodinatus* and that containing *P. cookei* and *Platychoerops* to the exclusion of *P. simonsi*, *P. gingerichi*, *P. remensis*, and *P. tricuspidens*. Instead, the most resolved version of our stratocladistics results (Fig. 2A) suggests that *P. dubius* and *P. fodinatus* are sister taxon to a clade containing *P. simoni*, *P. gingerichi*, *P. remensis*, *P. tricuspidens*, *P. cookei* and *Platychoerops*, as also envisioned by Gingerich (1976).

The hypothesis that *P. simoni*, *P. gingerichi*, *P. remensis*, and *P. tricuspidens* are more closely related to *P. cookei* and *Platychoerops* than are *P. dubius* and *P. fodinatus* is interesting because it suggests a number of similarities in premolar morphology must have evolved convergently in the last two groups (Gingerich, 1976). The homoplasy in premolar morphology among *P. dubius* + *P. fodinatus* and *P. cookei* + *Platychoerops* are all expressions of greater molarization and probably relate to greater emphasis on a leafy diet (Boyer et al., 2010). These similarities include presence of a trigonid and paraconid on P_4 (Table A-IV-1, ch19-20), loss of a primitive paraconule, and the appearance of a 'molar-type' paraconule on P^4 (Table A-IV-1, ch23-24). In addition, these species all tend to have more 'crestiform' and complex molar teeth than *P. simonsi*, *P. gingerichi*, *P. remensis*, and *P. tricuspidens* (Boyer et al., 2010; 2012b). It may be that because many of the premolar traits are actually polymorphic (Table-IV-2), they do not add unambiguous support for topologies uniting *P. dubius* and *P. fodinatus* to *P. cookei* and *Platychoerops*.

One interesting result recovered by Boyer et al. (2012a, b) that is corroborated in our analysis is a sister-taxon relationship for *P. cookei* and *Platycheorops* (Fig. 83). This result contrasts with results of Gingerich (1976), which suggested *Platychoerops* was derived from something more like *P. triscuspidens*. However, Gingerich (1976) demonstrated his understanding of the evidence for this 'new' alternative hypothesis by his comparisons of North American *P. cookei* with European species of *Platychoerops*. Linking of *Platychoerops* to *P. cookei* here is supported by the following synapomorphies: an elongated crown of the central incisors (Table A-IV-1, ch1), a reduced I^1 laterocone and posterocone (Table A-IV-1, ch6–7), lack of a mediocone on I^1 (Table A-IV-1, ch8), presence of a trigonid on P_4 (Table A-IV-1, *ch19*), lack of premolar-type paraconules on $P^{3–4}$ (Table A-IV-1, ch22–23), and a zygomatic process of the maxilla that arises lateral to M^1 (Table A-IV-3, ch66).

One aspect of our results that may still trouble researchers familiar with plesiadapid morphology, geography, and stratigraphy is the separation of North American *P. gingerichi* and *P. cookei* by *P. remensis* and *P. tricuspidens* (Figs. 2A, 83). We are somewhat skeptical of this result because *P. gingerichi* and *P. cookei* share a P_3 that is longer than the P_4, a similar geographic range, and superposed stratigraphic relationships (Rose, 1981; but see Bloch and Gingerich, 1998). The main problem here is likely high levels of missing data in *P. gingerichi* (it is scored for 27 out of 67 craniodental characters). If its upper incisors, upper premolars (Table A-IV-1, ch22–23) and maxillary zygomatic process (Table A-IV-3, ch66) were eventually revealed to be most similar to those of *P. cookei*, this would probably lead to a topology more like what Rose (1981) suggested with *P. gingerichi* and *P. cookei* as sister taxa or anagenetically related.

We do not think this would change the finding that *P. cookei* and *Platychoerops* are closer relatives to each other than either is to *P. tricuspidens*, but this scenario is potentially congruent with the perspective of Gingerich (1976). That is, *P. gingerichi* has been proposed as a subspecies or regional variant of *P. tricuspidens* (Rose, 1981), and it was implied that *P. cookei* might be a subspecies or regional variant of *Pl. russelli* (Gingerich, 1976). Regardless, if the morphocline going from *P. gingerichi/P.tricuspidens* to *P. cookei/Pl. russelli* and then to later, more derived *Platychoerops* species describes an anagenetic process, then it is unlikely that the transition could have happened in central Europe since *Platychoerops* has now been found as a contemporary of *P. tricuspidens* there (Boyer et al., 2012b; Smith et al., 2014).

Boyer et al. (2012b) suggested that the evolution of more derived *Platychoerops* might have been catalyzed by character displacement after the migration of *P. cookei/Pl. russelli*-like populations into the territory of persistent lineages of more *P. gingerchi/P. tricuspidens*-like populations in central Europe during the late Paleocene. However, we remain cognizant of the possibility that there was more parallelism in plesiadapid evolution than we can currently detect using a strictly cladistic approach. That is, if multiple lineages became large-bodied, then it would not be surprising if other character complexes reflecting the same ecological transition also changed in parallel. In other words, multiple lineages may have evolved to become more *Platychoerops*-like and future investigations may discover that the traits diagnosing *Platychoerops* describe a polyphyletic taxon. Under such a scenario, the proposed relationship between *P. tricuspidens* and *Pl. daubrei* may still be correct, and *Pl. antiquus* could represent a parallel evolution of *Platychoerops*-like morphology, perhaps with *P. cookei* or some other undetermined taxon as its ancestral lineage. In order to entertain these more complex evolutionary scenarios, more specimens are needed to fill temporal gaps in lineages and to fill anatomical gaps in knowledge of particular species.

Although we do not find evidence of a sister-taxon relationship between *P. cookei* and *P. tricuspidens,* our results suggest they are more closely related to each other than to many smaller-bodied and earlier-occurring plesiadapids. Nevertheless, the two species differ craniodentally in a number of ways. In many respects, *P. cookei* remains more similar to other North American species. The most notable features in which *P. cookei* differs craniodentally from *P. tricuspidens* include: (1) relatively larger teeth, (2) a more molariform P^4, (3) the lack of P^2, (4) broader nasal bones, (5) a more anteriorly rooted zygomatic process, (6) smaller glenoid fossae, (7) a less expanded annular component to its ectotympanic bone, and (8) a more posteriorly projecting nuchal crest. Features 4 and 6-8 here make *P. cookei* more similar to earlier occurring North American plesiadapids such as *P. anceps, N. intermedius*, and *Pr. gaoi*.

Relationship of Plesiadapidae to other plesiadapiforms and Euprimates

Rescoring cranial and postcranial characters from Bloch and Silcox (2006) and Bloch et al. (2007) for individual plesiadapid species and optimizing the states on to the root of Plesiadapidae changes the character state distribution implied for a supraspecific Plesiadapidae OTU compared to that presented by Bloch and Silcox (2006) and Bloch et al. (2007). The plesiadapid species that differs most from all of the others and from the ancestral node reconstruction is *P. tricuspidens*. This result is important because previous cladistic analyses used features of *P. tricuspidens* as representative of the family (Kay et al., 1992; Wible, 1993; Silcox, 2001; Bloch and Silcox, 2006; Bloch et al., 2007). These results encouraged us to reevaluate the interrelationships of plesiadapids among other plesiadapiforms and euarchontans.

In particular, the relationship between carpolestids and plesiadapids within euprimates has strong implications for the patterns of morphological change involved in primate origins (e.g., Bloch and Boyer, 2002, 2003; Kirk et al., 2003; Bloch et al., 2007). In the matrix of Bloch and Silcox (2006), there are 17 cranial characters (out of 24) scored the same for plesiadapids and carpolestids. As discussed above, five are similarities to the exclusion of paromomyids (and potentially suggestive of a special relationship between carpolestids and plesiadapids). These include (in plesiadapids and carpolestids): presence of a posterior carotid foramen with a posteromedial position (c6), presence of a foramen rotundum (c21), orbital contact between the frontal and maxilla (c18), nasals that narrow mediolaterally from anterior to posterior (c16), and a petrosal bulla (c1). Evidence marshaled here suggests that Plesiadapidae is distinct from Carpolestidae in lacking the first two features and possibly the third. Only *P. tricuspidens* exhibits the fourth feature. A petrosal bulla characterizes plesiadapids, but we consider this feature uncertain in carpolestids until better fossil material is collected. Thus, none of the cranial features listed by Bloch et al. (2007) as characterizing both plesiadapids and carpolestids survived careful scrutiny and reanalysis of the relevant specimens.

Nevertheless, an additional four features, previously scored differently for carpolestids and plesiadapids were revised to be scored the same. Plesiadapids and carpolestids now appear to have been primitively similar in having a non-expanded external auditory meatus (c3), a groove on the promontorium demarcating the route of the internal carotid artery and/or nerve (c5), a lacrimal tubercle (c19), and no chambers within the tympanic cavity (c24). It should be noted, however, that none of these features is a similarity to the exclusion of the morphology exhibited by paromomyids (see discussion of cranial morphology above).

Modification and reanalysis of the Bloch et al. (2007) matrix to reflect this revised characterization of the Plesiadapidae yields no change to the topology recovered. Further, although the topology remained unchanged, treelength decreased, indicating a strengthening of the phylogenetic hypothesis of Bloch et al. (2007).

Although these results can likely be attributed to the fact that the total number of cranial and postcranial similarities between carpolestids and plesiadapids increased compared to earlier analyses, further consideration of the Bloch et al. (2007) matrix provides additional insight into why the

original topology is so stable: many of the features that link plesiadapids with carpolestids are dental features. In the Bloch et al. (2007) character matrix, there are at least 21 out of 80 (ca. 26%) dental characters shared by plesiadapids and carpolestids to the exclusion of paromomyid plesiadapiforms.

Results of the analysis of modified character matrices notwithstanding, the phylogenetic significance of the morphology of paromomyids, plesiadapids, and carpolestids is still not fully clear. Cranial and postcranial similarities uniting paromomyids and plesiadapids (e.g., a reduced carotid system, limited divergence of the hallux), and postcranial similarities uniting carpolestids and euprimates (e.g., a nail on pedal digit I, a broadly divergent and opposable hallux), may mean that carpolestids, along with some other 'plesiadapoids' (of Bloch et al., 2007), are closer to Euprimates within a 'plesiadapoid + euprimate' clade than to plesiadapids. In other words, Plesiadapoidea may be paraphyletic with respect to Euprimates. In this case, a topology similar to that depicted in Figure 85A or that recovered by the cladistic analysis of postcranial characters by Bloch and Boyer (2002) may be closer to the truth.

Clearly, there is much still to be learned regarding the phylogenetic relationships among various plesiadapiforms and extant euarchontan mammals including dermopterans, treeshrews and euprimates. New matrices that more intensively sample the anatomy of a broader array of relevant taxa, and the discovery of more plesiadapiform fossils are necessary to increase knowledge on this subject. An obvious next step would be analyze character matrices combining updated scorings from Bloch et al. (2016) with the observations presented here.

SUMMARY AND CONCLUSIONS

1. *Plesiadapis cookei* is a large-bodied plesiadapiform euarchontan and possible stem primate known from many localities of middle Clarkforkian age, late Paleocene, in the Clarks Fork Basin of northwestern Wyoming.

2. Most specimens of *P. cookei* are gnathic and dental remains, but one specimen, UM 87990, is a virtually complete skeleton preserving the cranium, dentaries, dentition, much of the axial skeleton, forelimbs, and hind limbs.

3. Description, measurement, and illustration of the UM 87990 complete skeleton of *P. cookei* provides new information enabling analysis of proportions within the skeleton and comparisons across a range of primates and related mammals.

4. The UM 87990 skull preserves much of the upper and lower dentition, rostrum, braincase, and basicranium. The dental formula is 2.0.2.3 / 1.0.2.3. Composition of the auditory bulla— petrosal, ectotympanic, or entotympanic— is uncertain. *P. cookei* had a very small posterior carotid foramen and lacked a functional internal carotid artery.

5. The UM 87990 postcranial skeleton preserves five cervical, 12 thoracic, and six lumbar vertebrae. The sacrum is complete with three vertebrae. There are 17 caudal vertebrae preserved, with at least three of the most proximal positions missing, implying at least 20 caudal vertebrae. We expect the full plesiadapid vertebral formula to have been 7.13.6.3.24, matching the formula in *Tupaia* and the median formula in primates. Caudal vertebrae show the tail of *P. cookei* to have been long. Seven sternebrae are preserved, possibly representing the complete series. Ribs are slender and lack any notable craniocaudal expansion.

6. The forelimb of UM 87990 preserves clavicles, much of a right scapula, humeri, ulnae, radii, and a number of carpal bones. Two sets of metacarpals, one set slightly longer and one set slightly shorter, were found with UM 87990. We interpret the slightly shorter set,'set-1,' as belonging to *P. cookei*. Manual and pedal phalanges are difficult to distinguish on any basis other than size. Distal phalanges are all relatively long, narrow and distinctly falciform. Forelimb joint morphology and cheirideal morphology is strongly suggestive of an arboreal habit.

7. The hind limb of UM 87990 includes well-preserved innominates, femora, tibae, incomplete fibulae, and most tarsal bones (navicular and entocuneiform excepted). Metatarsals are identified based on their size and form in comparison to those described for other plesiadapids. Joint morphologies of the hips, knees, and ankles suggest an emphasis on abduction-adduction and inversion-eversion as expected for a mobile limb and vertical arboreal postures.

8. Limb indices for *P. cookei* include a brachial index of 101, a crural index of 99, and an intermembral index of 88. Indices suggest that *P. cookei* may have been most like lorises in overall body proportions, however a more comprehensive principal components analysis of body proportions places *P. cookei* and other plesiadapiforms closer to *Tupaia*, sciurids, and callitrichid primates. *P. cookei* is not particularly close to *Nycticebus*, the one lorisine slow climber in our sample, nor is it near *Cynocephalus*.

9. The postcranial skeleton of *P. cookei* suggests that it was a forest-dwelling arboreal climber primarily adapted to and possibly constrained to large diameter vertical and horizontal supports. Headfirst descent of large supports was likely accomplished using claw-clinging with a reversed (supinated) foot. *P. cookei* would have been more cautious and less scansorial in its movements than smaller-bodied plesiadapids.

10. The body weight of *P. cookei*, estimated from multiple regression of 11 long bone lengths and diameters for UM 87990, was 2,052 g. Brain weight, estimated from

a partial endocast and three-dimensional model of the brain, was close to 5 g. Comparison of a 5g brain to the expected brain size for a terrestrial mammal the size of *P. cookei* yields an encephalization residual ER_{TC} of −1.801 and a corresponding encephaliation quotient EQ_{TC} of 0.284 (28% of expected size).

11. We interpret UM 87990 as a male individual of *P. cookei* because the innominate has a relatively wide superior pubic ramus like that of male individuals in a range of rodents and primates.

12. UM 87990 has a fully erupted adult dentition, little tooth wear, and long-bone epiphyseal fusion limited to the elbow. We have no independent means of determining sexual maturity, and thus can only interpret UM 87990 as an advanced and nearly full-grown subadult, or as a full-grown young adult *P. cookei*.

13. Cladistic analysis of 37 dental characters, 34 cranial characters and one geographic character indicates that Plesiadapidae is monophyletic with respect to two carpolestid genera. Though *Pronothodectes* is paraphyletic, it contains all of the most basal plesiadapid species. *Chiromyoides* and *Platychoerops* are monophyletic. *Nannodectes* is probably also paraphyletic. *Plesiadapis* itself appears polyphyletic, with *P. cookei* recovered as the sister taxon of *Platychoerops*, *P. walbeckensis* as the sister taxon of *Chiromyoides* (when including stratigraphic data), and still other *Plesiadapis* species as more basal.

    Our morphology-based and stratocladistic results are largely congruent with Gingerich's (1976) stratophenetic analysis. Differences may stem from the fact that Gingerich (1976) did not attempt to depict a cladogram uniting European and North American species, whereas we have. Nevertheless, combining these two radiations into a single phylogeny provides important indications as to where and when certain evolutionary transitions occurred. For instance, it argues against the possibility that *P. tricuspidens* evolved anagenetically into *Platychoerops* in the Paris basin based on the co-occurrence of *Pl. antiquus* with *P. tricuspidens*. Although our results are compatible with the possibility that a peripheral population of *P. tricuspidens* evolved into *Pl. antiquus*, this would not have been a strictly anagenetic process. Furthermore, under that scenario, the sister relationship recovered between *P. cookei* and *Platychoerops* requires that *P. cookei* branched from this lineage in Europe and migrated to North America.

    A less equivocal difference is resolution of *N. intermedius* as the common ancestor of non-*Pronothodectes* plesiadapids, whereas Gingerich (1976) suggested that *Pr. jepi* held this ancestral position. Our results are supported by the observation that *N. intermedius* lacks the narrow P_3 and P_4 that appear to be synapomorphies of other members of the genus, as well as the observation that earliest Tiffanian sites contain *N. intermedius*, but not *P. praecursor* or any other plesiadapids. Although *Pronothodectes* species are still recovered as basal to *N. intermedius* and other plesiadapids, there was not unanimous support for ancestor status of any of these *Pronothodectes* species.

14. Cladistic analysis of higher-level taxa was run with Plesiadapidae scorings revised through optimization of the ancestral node of the species-level phylogenies. Overall, our rescorings increased the number of character states shared between plesiadapids and carpolestids, revealed the original topologies to be robust, and increased the number of postcranial character states suggesting a specialized arboreal, rather than scanorial lifestyle for the common ancestor of plesiadapids and carpolestids.

    Reanalyzing the cranial matrix of Bloch and Silcox (2006) yielded the same three cladograms as analyses by the original authors. Strict consensus of these trees resolved Carpolestidae, Plesiadapidae, and Euprimates as an unresolved clade to the exclusion of other taxa included in the analysis. Reanalyzing the craniodental and postcranial matrix of Bloch et al. (2007) upheld their original linking of Plesiadapidae to Carpolestidae, followed by other plesiadapoids, as the sister to Euprimates and resulted in a shorter tree. Thus, the notion that carpolestids and plesiadapids are sister taxa and close to Euprimates, as suggested Bloch et al. (2007) among others, stands firm in light of new data presented here.

    The finding that primitive plesiadapids and carpolestids shared additional postcranial features suggesting a committed arboreal lifestyle is consistent with the notion that arboreal specializations shared by *Carpolestes* and Euprimates are also homologous (Bloch et al., 2007). Additional, more detailed investigation of the phylogenetic and functional significance of the fossils described here is warranted in the context of new data recently published on other plesiadapiforms (Bloch et al., 2016).

LITERATURE CITED

ALEXANDER, R. M., A. S. JAYES, G. M. O. MALOIY, and E. M. WATHUTA. 1979. Allometry of the limb bones of mammals from shrews (*Sorex*) to elephant (*Loxodonta*). Journal of Zoology, London, 189: 305–314.

ANEMONE, R. L. and W. DIRKS. 2009. An anachronistic Clarkforkian mammal fauna from the Paleocene Fort Union Formation (Great Divide Basin, Wyoming, USA). Geologica Acta, 7: 113–124.

ANKEL-SIMONS, F. A. 2007. Primate Anatomy, Third Edition. Academic Press, San Diego, 700 pp.

ARGOT, C. 2002. Functional-adaptive analysis of the hindlimb anatomy of extant marsupials and the paleobiology of the Paleocene marsupials *Mayulestes ferox* and *Pucadelphys andinus*. Journal of Morphology, 253: 76–108.

BEARD, K. C. 1989. Postcranial anatomy, locomotor adaptations, and palaeoecology of early Cenozoic Plesiadapidae, Paromomyidae, and Micromomyidae (Eutheria, Dermoptera). Ph.D. dissertation, Johns Hopkins University, Baltimore, 661 pp.

———. 1990. Gliding behavior and palaeoecology of the alleged primate family Paromomyidae (Mammalia, Dermoptera). Nature, 345: 340–341.

———. 1993a. Phylogenetic systematics of the Primatomorpha, with special reference to Dermoptera. In F. S. Szalay, M. J. Novacek, and M. C. McKenna (eds.), Mammal Phylogeny: Placentals, Springer-Verlag, New York, pp. 129–150.

———. 1993b. Origin and evolution of gliding in early Cenozoic Dermoptera (Mammalia, Primatomorpha). In R. D. E. MacPhee (ed.), Primates and Their Relatives in Phylogenetic Perspective, Plenum Press, New York, pp. 63–90.

BERNSTEIN, P. and E. S. CRELIN. 1967. Bony pelvic sexual dimorphism in the rat. Anatomical Record, 157: 517–525.

BLACK, E. S. 1970. Sexual dimorphism in the ischium and pubis of three species of South American monkeys. Journal of Mammalogy, 51: 794–796.

BLOCH, J. I. and D. M. BOYER. 2001. Taphonomy of small mammals in freshwater limestones from the Paleocene of the Clarks Fork Basin. In P. D. Gingerich (ed.), Paleocene–Eocene Stratigraphy and Biotic Change in the Bighorn and Clarks Fork Basins, Wyoming, University of Michigan Papers on Paleontology, 33: 185–198.

———. and ———. 2002. Grasping primate origins. Science, 298: 1606–1610.

———. and ———. 2003. Response to comment on ‘grasping primate origins’. Science, 300: 741c.

———. and ———. 2007. New skeletons of Paleocene–Eocene Plesiadapiformes: a diversity of arboreal positional behaviors in early primates. In M. Dagosto and M. J. Ravosa (eds.), Primate Origins: Adaptations and Evolution, Plenum Press, New York, pp. 535–581.

BLOCH, J. I., D. M. BOYER, P. D. GINGERICH, and G. F. GUNNELL. 2002. New primitive paromomyid from the Clarkforkian of Wyoming and dental eruption in Plesiadapiformes. Journal of Vertebrate Paleontology, 22: 366–379.

BLOCH, J. I., S. G. B. CHESTER, and M. T. SILCOX. 2016. Cranial anatomy of Paleogene Micromomyidae and implications for early primate evolution. Journal of Human Evolution, 96: 58–81.

BLOCH, J. I., D. C. FISHER, K. D. ROSE, and P. D. GINGERICH. 2001. Stratocladistic analysis of Paleocene Carpolestidae (Mammalia, Plesiadapiformes) with description of a new late Tiffanian genus. Journal of Vertebrate Paleontology, 21: 119–131.

BLOCH, J. I. and P. D. GINGERICH. 1998. *Carpolestes simpsoni*, new species (Mammalia, Proprimates) from the late Paleocene of the Clarks Fork Basin, Wyoming. Contributions from the Museum of Paleontology, University of Michigan, 30: 131–162.

BLOCH, J. I. and M. T. SILCOX. 2001. New basicrania of Paleocene–Eocene *Ignacius*: re-evaluation fo the plesiadapiform-dermopteran link. American Journal of Physical Anthropology, 116: 184–198.

———. and ———. 2006. Cranial anatomy of the Paleocene plesiadapiform *Carpolestes simpsoni* (Mammalia, Primates) using ultra high-resolution x-ray computed tomography, and the relationships of plesiadapiforms to Euprimates. Journal of Human Evolution, 50: 1–35.

BLOCH, J. I., M. T. SILCOX, D. M. BOYER, and E. J. SARGIS. 2007. New Paleocene skeletons and the relationship of plesiadapiforms to crown-clade primates. Proceedings of the National Academy of Sciences USA, 104: 1159–1164.

BOYER, D. M. 2009. New cranial and postcranial remains of late Paleocene Plesiadapidae (‘Plesiadapiformes,’ Mammalia) from North America and Europe: description and evolutionary implications. Ph.D., Stony Brook University, Stony Brook, 569 pp.

BOYER, D. M. and J. I. BLOCH. 2008. Evaluating the mitten-gliding hypothesis for Paromomyidae and Micromomyidae (Mammalia, ‘Plesiadapiformes’) using comparative functional morphology of new Paleogene skeletons. In E. J. Sargis and M. Dagosto (eds.), Mammalian Evolutionary Morphology: A Tribute to Frederick S. Szalay, Springer, Dordrecht, pp. 233–284.

BOYER, D. M., L. COSTEUR, and Y. LIPMAN. 2012b. Earliest record of *Platychoerops* (Primates, Plesiadapidae), a new species from Mouras Quarry, Mont de Berru, France. American Journal of Physical Anthropology, 149: 329–346.

BOYER, D. M., A. R. EVANS, and J. JERNVALL. 2010a. Evidence of dietary differentiation among late Paleocene–early Eocene plesiadapids (Mammalia, Primates). American Journal of Physical Anthropology, 142: 194–210.

BOYER, D. M., G. F. GUNNELL, S. KAUFMAN, and T. M. MCGEARY. 2016. MorphoSource — archiving and sharing digital specimen data. Paleontological Society Papers, 22: 157–181.

BOYER, D. M., B. A. PATEL, S. G. LARSON, and J. T. STERN JR. 2007. Telemetered electromyography of peroneus longus in *Varecia variegata* and *Eulemur rubriventer*: implications for the functional significance of a large peroneal process. Journal of Human Evolution, 53: 119–134.

BOYER, D. M., G. V. R. PRASAD, D. W. KRAUSE, M. GODINOT, A. GOSWAMI, O. VERMA, and J. J. FLYNN. 2010b. New postcrania of *Deccanolestes* from the Late Cretaceous of India and their bearing on the evolutionary and biogeographic history of euarchontan mammals. Naturwissenschaften, 97: 365–377.

BOYER, D. M., C. S. SCOTT, and R. C. FOX. 2012a. New craniodental material of *Pronothodectes gaoi* Fox (Mammalia, 'Plesiadapiformes') and relationships among members of Plesiadapidae. American Journal of Physical Anthropology, 147: 511–550.

BOYER, D. M., G. S. YAPUNCICH, S. G. B. CHESTER, J. I. BLOCH, and M. GODINOT. 2013. Hands of early primates. American Journal of Physical Anthropology, 57: 33–78.

BOYER, D. M., G. S. YAPUNCICH, S. G. B. CHESTER, J. I. BLOCH, and M. GODINOT. 2016. Hands of Paleogene Primates. In L. T. Kivell, P. Lemelin, G. B. Richmond, and D. Schmitt (eds.), The Evolution of the Primate Hand: Anatomical, Developmental, Functional, and Paleontological Evidence, Springer, New York, pp. 373–419.

BROWN, J. C. and G. I. TWIGG. 1969. Studies on the pelvis in British Muridae and Cricetidae (Rodentia). Journal of Zoology, 158: 81–132.

CARTMILL, M. 1974. Pads and claws in arboreal locomotion. In F. A. Jenkins (ed.), Primate Locomotion, Academic Press, Inc., New York, pp. 45–83.

CHESTER, S. G. B., J. I. BLOCH, D. M. BOYER, and W. A. CLEMENS. 2015. Oldest known euarchontan tarsals and affinities of Paleocene *Purgatorius* to Primates. Proceedings of the National Academy of Sciences USA, 112: 1487–1492.

CLEMENS, W. A. 2004. *Purgatorius* (Plesiadapiformes, Primates?, Mammalia), a Paleocene immigrant into northeastern Montana: stratigraphic occurrences and incisor proportions. Bulletin of the Carnegie Museum of Natural History, 36: 3–13.

COLEMAN, M. N. AND D. M. BOYER. 2012. Inner ear evolution in primates through the Cenozoic: implications for the evolution of hearing. Anatomical Record, 295: 615–631.

DAVIS, D. D. 1962. Mammals of the lowland rain-forest of North Borneo. Bulletin of the Singapore National Museum, 31: 1–129.

DAWSON, M. R. and K. C. BEARD. 1996. New late Paleocene rodents (Mammalia) from Big Multi Quarry, Washakie Basin, Wyoming. In M. Godinot and P. D. Gingerich (eds.), Paléobiologie et Evolution des Mammifères Paléogènes: Volume Jubilaire En Hommage à Donald E. Russell, Palaeovertebrata, Montpellier, 25 pp. 301–322.

DORR, J. A. and P. D. GINGERICH. 1980. Early Cenozoic mammalian paleontology, geologic structure, and tectonic history in the overthrust belt near La Barge, western Wyoming. Contributions to Geology, University of Wyoming, 18: 101–115.

DUNMIRE, W. W. 1955. Sex dimorphism in the pelvis of rodents. Journal of Mammalogy, 36: 356–361.

EISENBERG, J. F. 1981. The Mammalian Radiations: an Analysis of Trends in Evolution, Adaptation, and Behavior. University of Chicago Press, Chicago, 610 pp.

EVANS, H. E. 1993. Miller's Anatomy of the Dog. Saunders, Philadelphia, 1113 pp.

FLEAGLE, J. G. 1999. Primate Adaptation and Evolution, Second Edition. Academic Press, San Diego, 596 pp.

FLEAGLE, J. G. and F. C. ANAPOL. 1992. The indriid ischium and the hominid hip. Journal of Human Evolution, 22: 285–305.

FLOWER, W. H. and H. GADOW. 1885. An Introduction to the Osteology of the Mammalia, Third Edition. MacMillan and Co. London, 382 pp.

FOX, R. C. 1990. *Pronothodectes gaoi* n. sp. from the Late Paleocene of Alberta, Canada, and the early evolution of the Plesiadapidae (Mammalia. Journal of Paleontology, 64: 637–647.

———. 1991. Systematic position of *Pronothodectes gaoi* Fox from the Paleocene of Alberta: reply. Journal of Paleontology, 65: 700–701.

———. 1993. The primitive dental formula of the Carpolestidae (Plesiadapiformes, Mammalia) and its phylogenetic implications. Journal of Vertebrate Paleontology, 13: 516–524.

GAMBARYAN, P. P. 1974. How Mammals Run. Wiley, New York, 367 pp.

GAZIN, C. L. 1942. Fossil Mammalia from the Almy formation in western Wyoming. Journal of the Washington Academy of Sciences, 32: 219–220.

———. 1956. The upper Paleocene Mammalia from the Almy Formation in western Wyoming. Smithsonian Miscellaneous Collections, 131: 1–18.

GEORGE, R. M. 1977. The limb musculature of the Tupaiidae. Primates, 18: 1–34.

GERVAIS, P. 1877. Enumération de quelques ossements d'animaux vertébrés recueillis aux environs de Reims par M. Lemoine. Journal de Zoologie, Paris, 6: 74–79.

GILBERT, C. C. and W. L. JUNGERS. 2017. Comment on relative brain size in early primates and the use of encephalization quotients in primate evolution. Journal of Human Evolution, 109: 79–87.

GINGERICH, P. D. 1971. Cranium of *Plesiadapis*. Nature, 232: 566.

———. 1972. The development of sexual dimorphism in the bony pelvis of the squirrel monkey. Anatomical Record, 172: 589–596.

———. 1975a. Systematic position of *Plesiadapis*. Nature, 253: 111–113.

———. 1975b. New North American Plesiadapidae (Mammalia, Primates) and a biostratigraphic zonation of the middle and upper Paleocene. Contributions from the Museum of Paleontology, University of Michigan, 24: 135–148.

———. 1976. Cranial anatomy and evolution of early Tertiary Plesiadapidae (Mammalia, Primates). University of Michigan Papers on Paleontology, 15: 1–140.

———. 1983. Paleocene–Eocene faunal zones and a preliminary analysis of Laramide structural deformation in the Clarks Fork Basin, Wyoming. Wyoming Geological Association Guidebook, 34: 185–195.

———. 1989. New earliest Wasatchian mammalian fauna from the Eocene of northwestern Wyoming: composition and diversity in a rarely sampled high-floodplain assemblage. University of Michigan Papers on Paleontology, 28: 1–97.

———. 1990. Prediction of body mass in mammalian species from long bone lengths and diameters. Contributions from the Museum of Paleontology, University of Michigan, 28: 79–92.

———. 1991. Systematic position of *Pronothodectes gaoi* Fox from the Paleocene of Alberta. Journal of Paleontology, 65: 699.

———. 2000. Arithmetic or geometric normality of biological variation: an empirical test of theory. Journal of Theoretical Biology, 204: 201–221.

———. 2016. Body weight and relative brain size (encephalization) in Eocene Archaeoceti (Cetacea). Journal of Mammalian Evolution, 23: 17–31

GINGERICH, P. D. and G. F. GUNNELL. 1992. A new skeleton of *Plesiadapis cookei*. Display Case, Quarterly Newsletter of the Exhibit Museum, University of Michigan, 6: 1–3.

———. and ———. 2005. Brain of *Plesiadapis cookei* (Mammalia, Proprimates): surface morphology and encephalization compared to those of Primates and Dermoptera. Contributions from the Museum of Paleontology, University of Michigan, 31: 185–195.

GINGERICH, P. D., P. HOUDE, and D. W. KRAUSE. 1983. A new earliest Tiffanian (late Paleocene) mammalian fauna from Bangtail Plateau, western Crazy Mountain Basin, Montana. Journal of Paleontology, 57: 957–970.

GODINOT, M. and K. C. BEARD. 1991. Fossil primate hands: a review and an evolutionary inquiry emphasizing early forms. Human Evolution, 6: 307–354.

GODINOT, M. and G. V. R. PRASAD. 1994. Discovery of Cretaceous arboreal eutherians. Naturwissenschaften, 81: 79–81.

GOODENBERGER, K. E., D. M. BOYER, C. M. ORR, R. L. JACOBS, J. C. FEMIANI, and B. A. PATEL. 2015. Functional morphology of the hallucal metatarsal with implications for inferring grasping ability in extinct primates. American Journal of Physical Anthropology, 156: 327–348.

GRADSTEIN, F. M., J. G. OGG, and A. G. SMITH (eds.). 2004. A Geological Time Scale 2004, Cambridge University Press, Cambridge, 589 pp.

GRANATOSKY, M. C., P. LEMELIN, S. G. B. CHESTER, J. D. PAMPUSH, and D. SCHMITT. 2014. Functional and evolutionary aspects of axial stability in euarchontans and other mammals. Journal of Morphology, 275: 313–327.

GREGORY, W. K. 1920. On the structure and relations of *Notharctus*, an American Eocene primate. American Museum of Natural History Memoirs, 3: 49–243.

GUILDAY, J. E. 1951. Sexual dimorphism in the pelvic girdle of *Microtus pennsylvanicus*. Journal of Mammalogy, 32: 216–217.

GUNNELL, G. F. 1989. Evolutionary history of Microsyopoidea (Mammalia, ?Primates) and the relationship between Plesiadapiformes and Primates. University of Michigan Papers on Paleontology, 27: 1–157.

GUNNELL, G. F. and P. D. GINGERICH. 1987. Skull and partial skeleton of *Plesiadapis cookei* from the Clarks Fork Basin. American Journal of Physical Anthropology, 72: 206.

HAINES, R. W. 1955. The anatomy of the hand of certain insectivores. Proceedings of the Zoological Society of London, 125: 761–776.

HAMRICK, M. W. 1997. Functional osteology of the primate carpus with special reference to Strepsirhini. American Journal of Physical Anthropology, 104: 105–116.

———. 2001. Primate origins: evolutionary change in digital ray patterning and segmentation. Journal of Human Evolution, 40: 339–351.

HAMRICK, M. W., B. A. ROSENMAN, and J. A. BRUSH. 1999. Phalangeal morphology of the Paromomyidae (?Primates, Plesiadapiformes): the evidence for gliding behavior reconsidered. American Journal of Physical Anthropology, 109: 397–413.

HARRINGTON, A. R., M. T. SILCOX, G. S. YAPUNCICH, D. M. BOYER, and J. I. BLOCH. 2016. First virtual endocasts of adapiform primates. Journal of Human Evolution, 99: 52–78.

JANEČKA, J. E., W. MILLER, T. H. PRINGLE, F. WIENS, A. ZITZMANN, K. M. HELGEN, M. S. SPRINGER, and W. J. MURPHY. 2007. Molecular and genomic data identify the closest living relative of primates. Science, 318: 792–794.

JENKINS, F. A. 1970. Anatomy and function of expanded ribs in certain edentates and primates. Journal of Mammalogy, 51: 288–301.

———. 1974. Tree shrew locomotion and the origins of primate arborealism. In F. A. Jenkins (ed.), Primate Locomotion, Academic Press, New York, pp. 85–115.

JENKINS, F. A. and D. W. KRAUSE. 1983. Adaptations for climbing in North American multituberculates (Mammalia). Science, 220: 712–715.

JENKINS, F. A. and D. McCLEARN. 1984. Mechanisms of hind foot reversal in climbing mammals. Journal of Morphology, 182: 197–219.

JEPSEN, G. L. 1930. Stratigraphy and paleontology of the Paleocene of northeastern Park County, Wyoming. Proceedings of the American Philosophical Society, 69: 463–528.

JERISON, H. J. 1973. Evolution of the Brain and Intelligence. Academic Press, New York, 482 pp.

JUNGERS, W. L. 1976. Osteological form and function: the appendicular skeleton of *Megaladapis*, a subfossil prosimian from Madagascar (Primates, Lemuroidea). Ph.D., University of Michigan, Ann Arbor, 361 pp.

———. 1979. Locomotion, limb proportions, and skeletal allometry in lemurs and lorises. Folia Primatologica, 32: 8–28.

———. 1985. Body size and scaling of limb proportions in primates. In W. L. Jungers (ed.), Size and Scaling in Primate Biology, Springer, pp. 345–381.

JUNGERS, W. L., A. B. FALSETTI, and C. E. WALL. 1995. Shape, relative size, and size-adjustments in morphometrics. Yearbook of Physical Anthropology, 38: 137–161.

KAY, R. F. and E. C. KIRK. 2000. Osteological evidence for the evolution of activity pattern and visual acuity in primates. American Journal of Physical Anthropology, 113: 235–262.

KAY, R. F., J. G. M. THEWISSEN, and A. D. YODER. 1992. Cranial anatomy of *Ignacius graybullianus* and the affinities of the Plesiadapiformes. American Journal of Physical Anthropology, 89: 477–498.

KIRK, E. C., M. CARTMILL, R. F. KAY, and P. LEMELIN. 2003. Comment on 'Grasping primate origins'. Science, 300: 741.

KIRK, E. C., P. LEMELIN, M. W. HAMRICK, D. M. BOYER, and J. I. BLOCH. 2008. Intrinsic hand proportions of euarchontans and other mammals: Implications for the locomotor behavior of plesiadapiforms. Journal of Human Evolution, 55: 278–299.

KOENIGSWALD, W. v., J. HABERSETZER, and P. D. GINGERICH. 2012. Pedal distal phalanges of the Eocene adapoids *Europolemur* and *Darwinius* compared to phalanges of *Notharctus* and other primates. Palaeobiodiversity and Palaeoenvironments, 92: 539–565.

KRAUSE, D. W. and F. A. JENKINS. 1983. The postcranial skeleton of North American multituberculates. Bulletin of the Museum of Comparative Zoology, Harvard University, 150: 199–246.

KUNZ, T. H., C. M. WEMMER, and V. HAYSSEN. 1996. Sex, age, and reproductive condition of mammals. In D. E. Wilson, F. R. Cole, J. D. Nichils, R. Rudran, and M. S. Foster (eds.), Measuring and Monitoring Biological Diversity, Standard Methods for Mammals, Smithsonian Press, Washington, pp. 279–290.

LAUNAY, L. D. 1908. La fourrure d'un écureuil tertiaire. La Nature, Paris, 36: 393–395.

LE GROS CLARK, W. E. 1926. On the anatomy of the pen-tailed tree-shrew. Proceedings of the Zoological Society of London, 1179–1309.

LEMOINE, V. 1893. Étude sur les os du pied des mammifères de la faune cernaysienne et sur quelques pièces osseuses nouvelles de cet horizon paléontologique. Bulletin de la Société Géologique de France, Série 3, 21: 353–368.

LEUTENEGGER, W. 1973. Sexual dimorphism in the pelves of African lorises. American Journal of Physical Anthropology, 38: 251–254.

LINNAEUS, C. 1758. Systema Naturae, Tenth Edition (*Systema Naturae Per Regna Tria Naturae, Secundum Classes, Ordines, Genera, Species, Cum Characteribus, Differentiis, Synonymis, Locis. Tomus I. Editio Decima, Reformata*). Laurentii Salvii, Holmiae (Stockholm), 824 pp.

LOFGREN, D. L., J. A. LILLEGRAVEN, W. A. CLEMENS, P. D. GINGERICH, and T. E. WILLIAMSON. 2004. Paleocene biochronology: the Puercan through Clarkforkian land-mammal ages. In M. O. Woodburne (ed.), Late Cretaceous and Cenozoic Mammals of North America, Columbia University Press, New York, pp. 43–105.

MACPHEE, R. D. E. 1981. Auditory regions of primates and eutherian insectivores. Morphology, ontology, and character analysis. Contributions to Primatology, 18: 1–282.

MACPHEE, R. D. E. and M. CARTMILL. 1986. Basicranial structures and primate systematics. In D. R. Swindler and J. Erwin (eds.), Comparative Primate Biology. Volume 1: Systematics, Evolution, and Anatomy, Alan Liss, New York, pp. 219–275.

MACPHEE, R. D. E., M. CARTMILL, and P. D. GINGERICH. 1983. New Palaeogene primate basicrania and the definition of the order Primates. Nature, 301: 509–511.

MARCOT, J. D. and D. L. FOX. 2008. STRATAPHY: a new computer program for stratocladistic analysis. Palaeontologia Electronica, 11.1.5A: 1–16.

MARTIN, R. D. 1981. Relative brain size and basal metabolic rate in terrestrial vertebrates. Nature, 293: 57–60.

MATTHEW, W. D. 1917. The dentition of *Nothodectes*. Bulletin of the American Museum of Natural History, 37: 831–839.

MELDRUM, D. J., M. DAGOSTO, and J. WHITE. 1997. Hindlimb suspension and hind foot reversal in *Varecia variegata* and other arboreal mammals. American Journal of Physical Anthropology, 103: 85–102.

MOSIMANN, J. E. and J. D. MALLEY. 1979. Size and shape variables. In L. Orlóci, C. R. Rao, and W. M. Stiteler (eds.), Multivariate Methods in Ecological Work, International Cooperative, Fairland, Maryland, pp. 175–189.

MURPHY, W. J., E. EIZIRIK, S. J. O'BRIEN, O. MADSEN, M. SCALLY, C. J. DOUADY, E. TEELING, O. A. RYDER, M. J. STANHOPE, W. W. DE JONG, and M. S. SPRINGER. 2001. Resolution of the early placental mammal radiation using Bayesian phylogenetics. Science, 294: 2348–2351.

NAPIER, J. R. 1961. Prehensility and opposability in the hands of primates. Symposia of the Zoological Society of London, 5: 115–132.

NAPIER, J. R. and A. C. WALKER. 1967. Vertical clinging and leaping — a newly recognized category of locomotor behavior of primates. Folia Primatologica, 6: 204–219.

NI, X., D. L. GEBO, M. DAGOSTO, J. MENG, P. TAFFOREAU, J. J. FLYNN, and K. C. BEARD. 2013. The oldest known primate skeleton and early haplorhine evolution. Nature, 498: 60–64.

NI, X., Q. LI, L. LI, and K. C. BEARD. 2016. Oligocene primates from China reveal divergence between African and Asian primate evolution. Science, 352: 673.

NOMINA ANATOMICA. 1983. Nomina Anatomica, 5th Edition. Williams and Wilkins, Baltimore, 192 pp.

NOMINA ANATOMICA VETERINARIA. 1994. Nomina Anatomica Verterinaria, 4th Edition. World Association of Veterinary Anatomists, Zurich, 198 pp.

NOVACEK, M. J. 1980. Cranioskeletal features in tupaiids and selected Eutheria as phylogenetic evidence. In W. P. Luckett (ed.), Comparative Biology and Evolutionary Relationships of Tree Shrews, Plenum, New York, pp. 35–93.

———. 1986. The skull of leptictid insectivorans and the higher-level classification of eutherian mammals. Bulletin of the American Museum of Natural History, 183: 1–112.

NOVACEK, M. J. and A. R. WYSS. 1986. Higher-level relationships of the recent eutherian orders: morphological evidence. Cladistics, 2: 257–287.

ORLIAC, M. J., S. LADEVÈZE, P. D. GINGERICH, R. LEBRUN, and T. SMITH. 2014. Endocranial morphology of Palaeocene *Plesiadapis tricuspidens* and evolution of the early primate brain. Proceedings of the Royal Society of London. Series B, 281 (20132792): 1–7.

PIRLOT, P. and T. KAMIYA. 1982. Relative size of brain and brain components in three gliding placentals (Dermoptera: Rodentia). Canadian Journal of Zoology, 60: 565–572.

PISSINATTI, A., E. C. D. SILVA, A. F. COIMBRA-FILHOL, W. BERTOLAZZO, and J. B. D. CRUZ. 1992. Sexual dimorphism of the pelvis in *Leontopithecus* (Lesson, 1840). Folia Primatologica, 58: 204–209.

PITON, L. E. 1940. Paléontologie du gisement éocène de Menat (Puy-de-Dôme) (flore et faune). Mem. Soc. Hist. Nat. Auvergne, 1: 1–303.

RAMDARSHAN, A. and M. J. ORLIAC. 2016. Endocranial morphology of *Microchoerus erinaceus* (Euprimates, Tarsiiformes) and early evolution of the Euprimates brain. American Journal of Physical Anthropology, 159: 5–16.

ROSE, K. D. 1975. The Carpolestidae: early Tertiary primates from North America. Bulletin of the Museum of Comparative Zoology, Harvard University, 147: 1–74.

———. 1980. Clarkforkian land-mammal age: revised definition, zonation, and tentative intercontinental correlations. Science, 208: 744–746.

———. 1981. The Clarkforkian land-mammal age and mammalian faunal composition across the Paleocene–Eocene boundary. University of Michigan Papers on Paleontology, 26: 1–197.

———. 1990. Postcranial skeletal remains and adaptations in early Eocene mammals from the Willwood Formation, Bighorn Basin, Wyoming. Geological Society of America Special Papers, 243: 107–134.

———. 2001. Compendium of Wasatchian mammal postcrania from the Willwood Formation of the Bighorn Basin. In P. D. Gingerich (ed.), Paleocene–Eocene Stratigraphy and Biotic Change in the Bighorn and Clarks Fork Basins, Wyoming, University of Michigan Papers on Paleontology, 33: 157–183.

RUNESTAD, J. A. and C. B. RUFF. 1995. Structural adaptations for gliding in mammals with implications for locomotor behavior in paromomyids. American Journal of Physical Anthropology, 98: 101–119.

RUSSELL, D. E. 1959. Le crâne de *Plesiadapis*. Bulletin de la Société Géologique de France, 1: 312–315.

———. 1962. Essai de reconstitution de la vie Paléocène au Mont de Berru. Bulletin du Muséum National d'Histoire Naturelle, Paris, Série 2, 34: 101–106.

———. 1964. Les mammifères Paléocènes d'Europe. Mémoires du Muséum National d'Histoire Naturelle, Paris, Série C, 13: 1–324.

———. 1967. Sur *Menatotherium* et l'âge Paléocène du gisement de Menat (Puy-de-Dôme). Problèmes Actuels De Paléontologie, Evolution Des Vertébrés, Paris, Colloques Internationaux du Centre National de la Recherche Scientifique, 163: 483–490.

RUSSELL, D. E., P. LOUIS, and D. E. SAVAGE. 1967. Primates of the French early Eocene. University of California Publications in Geological Sciences, 73: 1–46.

SARGIS, E. J. 2001. A preliminary qualitative analysis of the axial skeleton of tupaiids (Mammalia, Scandentia): functional morphology and phylogenetic implications. Journal of Zoology, 253: 473–483.

———. 2002a. Functional morphology of the forelimb of tupaiids (Mammalia, Scandentia) and its phylogenetic implications. Journal of Morphology, 253: 10–42.

———. 2002b. Functional morphology of the hindlimb of tupaiids (Mammalia, Scandentia) and its phylogenetic implications. Journal of Morphology, 254: 149–185.

———. 2004. New views on tree shrews: the role of tupaiids in primate supraordinal relationships. Evolutionary Anthropology, 13: 56–66.

SARGIS, E. J., D. M. BOYER, J. I. BLOCH, and M. T. SILCOX. 2007. Evolution of pedal grasping in primates. Journal of Human Evolution, 53: 103–107.

SECORD, R. 2008. The Tiffanian Land-Mammal Age (middle and late Paleocene) in the northern Bighorn Basin, Wyoming. University of Michigan Papers on Paleontology, 35: 1–192.

SECORD, R., P. D. GINGERICH, M. E. SMITH, W. C. CLYDE, P. WILF, and B. S. SINGER. 2006. Geochronology and mammalian biostratigraphy of middle and upper Paleocene continental strata, Bighorn Basin, Wyoming. American Journal of Science, 306: 211–245.

SHAPIRO, L. J. and C. V. M. SIMONS. 2002. Functional aspects of strepsirrhine lumbar vertebral bodies and spinous processes. Journal of Human Evolution, 42: 753–783.

SHIGEHARA, N. 1980. Epiphyseal union, tooth eruption, and sexual maturation in the common tree shrew, with reference to its systematic problem. Primates, 21: 1–19.

SILCOX, M. T. 2001. A phylogenetic analysis of the Plesiadapiformes and their relationship to Euprimates and other archontans. Ph.D., Johns Hopkins University, Baltimore, 723 pp.

———. 2003. New discoveries on the middle ear anatomy of *Ignacius graybullianus* (Paromomyidae, Primates) from ultra high resolution x-ray computed tomography. Journal of Human Evolution, 44: 73–86.

SILCOX, M. T., J. I. BLOCH, D. M. BOYER, and P. HOUDE. 2010. Cranial anatomy of Paleocene and Eocene *Labidolemur kayi* (Mammalia: Apatotheria) and the relationships of the Apatemyidae to other mammals. Zoological Journal of the Linnean Society, 160: 773–825.

SILCOX, M. T., J. I. BLOCH, D. M. BOYER, M. GODINOT, T. M. RYAN, F. SPOOR, and A. WALKER. 2009a. Semicircular canal system in early primates. Journal of Human Evolution, 56: 315–327.

SILCOX, M. T., C. K. DALMYN, and J. I. BLOCH. 2009b. Virtual endocast of Ignacius graybullianus (Paromomyidae, Primates) and brain evolution in early primates. Proceedings of the National Academy of Sciences, 106: 10987–10992.

SILCOX, M. T. and G. F. GUNNELL. 2008. Plesiadapiformes. In C. M. Janis, G. F. Gunnell, and M. D. Uhen (eds.), Evolution of Tertiary Mammals of North America, Volume 2: Small Mammals, Xenarthrans, and Marine Mammals, Cambridge University Press, Cambridge, pp. 207–238.

SILCOX, M. T., D. W. KRAUSE, M. C. MAAS, and R. C. FOX. 2001. New specimens of *Elphidotarsius russelli* (Mammalia, ?Primates, Carpolestidae) and a revision of plesiadapoid relationships. Journal of Vertebrate Paleontology, 21: 132–152.

SIMONS, E. L. 1960. New fossil primates: a review of the past decade. American Scientist, 48: 179–192.

———. 1964. The early relatives of man. Scientific American, 211: 51–62.

———. 1967. Fossil primates and the evolution of some primate locomotor systems. American Journal of Physical Anthropology, 26: 241–254.

SIMPSON, G. G. 1935. The Tiffany fauna, upper Paleocene. II. Structure and relationships of *Plesiadapis*. American Museum Novitates, 816: 1–30.

———. 1937. Notes on the Clark Fork, upper Paleocene, fauna. American Museum Novitates, 954: 1–24.

———. 1948. *Menatotherium*, Eocene mammal from France. American Journal of Science, 246: 165–170.

SMITH, B. H. 1992. Life history and the evolution of human maturation. Evolutionary Anthropology, 1: 134–142.

———. 2000. 'Schultz's Rule' and the evolution of tooth emergence and replacement patterns in primates and ungulates. In M. F. Teaford, M. M. Smith, and M. W. J. Ferguson (eds.), Development, Function, and Evolution of Teeth, Cambridge University Press, Cambridge, pp. 212–227.

SMITH, T., F. QUESNEL, G. D. PLÖEG, D. DE FRANCESCHI, G. MÉTAIS, E. DE BAST, F. SOLÉ, A. FOLIE, A. BOURA, J. CLAUDE, C. DUPUIS, C. GAGNAISON, A. IAKOVLEVA, J. MARTIN, F. MAUBERT, J. PRIEUR, E. ROCHE, J.-Y. STORME, R. THOMAS, H. TONG, J. YANS, and E. BUFFETAUT. 2014. First Clarkforkian equivalent land mammal age in the latest Paleocene basal Sparnacian facies of Europe: fauna, flora, paleoenvironment and (bio)stratigraphy. PLoS One, 9: e86229.

SOKAL, R. R. and F. J. ROHLF. 1995. Biometry, Third Edition. W. H. Freeman, New York, 887 pp.

ST. CLAIR, E. M. 2007. Sexual dimorphism in the pelvis of *Microcebus*. International Journal of Primatology, 28: 1109–1122.

STAFFORD, B. J. 1999. Taxonomy and ecological morphology of the flying lemurs (Dermoptera, Cynocephalidae). Ph.D., City University of New York, New York, 464 pp.

STAFFORD, B. J. and R. W. J. THORINGTON. 1998. Carpal development and morphology in archontan mammals. Journal of Morphology, 235: 135–155.

STERN, J. T. 1988. Essentials of Gross Anatomy. F. A. Davis, Philadelphia, 795 pp.

STRAUS, W. L. 1930. The foot musculature of the highland gorilla (*Gorilla beringei*). Quarterly Review of Biology, 5: 261–317.

SWOFFORD, D. L. 2002. PAUP*: Phylogenetic Analysis Using

Parsimony and Other Methods, Version 4.0b10. Sinauer Associates, Sunderland, Massachusetts.

SZALAY, F. S. 1968. The beginnings of primates. Evolution, 22: 19–36.

———. 1971. Cranium of the ate Palaeocene primate *Plesiadapis tricuspidens*. Nature, 230: 324–325.

———. 1972a. Cranial morphology of the early Tertiary *Phenacolemur* and its bearing on primate phylogeny. American Journal of Physical Anthropology, 36: 59–76.

———. 1972b. Paleobiology of the earliest primates. In R. H. Tuttle (ed.), The Functional and Evolutionary Biology of Primates, Aldine-Atherton, Chicago, pp. 3–35.

———. 1984. Arboreality: is it homologous in metatherian and eutherian mammals? In M. K. Hecht, B. Wallace, and G. T. Prance (eds.), Evolutionary Biology, Volume 18, Plenum, New York, pp. 215–258.

SZALAY, F. S. and M. DAGOSTO. 1980. Locomotor adaptations as reflected on the humerus of Paleogene primates. Folia Primatologica, 34: 1–45.

———. and ———. 1988. Evolution of hallucial grasping in the primates. Journal of Human Evolution, 17: 1–33.

SZALAY, F. S. and R. L. DECKER. 1974. Origins, evolution, and function of the tarsus in late Cretaceous Eutheria and Paleocene primates. In F. A. Jenkins (ed.), Primate Locomotion, Academic Press Inc., New York, pp. 223–259.

SZALAY, F. S. and E. DELSON. 1979. Evolutionary History of the Primates. Academic Press, New York, 580 pp.

SZALAY, F. S. and G. M. DRAWHORN. 1980. Evolution and diversification of the Archonta in an arboreal milieu. In W. P. Luckett (ed.), Comparative Biology and Evolutionary Relationships of Tree Shrews, Plenum Press, New York, London, pp. 133–169.

SZALAY, F. S., A. L. ROSENBERGER, and M. DAGOSTO. 1987. Diagnosis and differentiation of the order Primates. Yearbook of Physical Anthropology, 30: 75–105.

SZALAY, F. S., I. TATTERSALL, and R. L. DECKER. 1975. Phylogenetic relationships of *Plesiadapis* — postcranial evidence. In F. S. Szalay (ed.), Approaches to Primate Paleobiology, Karger, Basel, Contributions to Primate Biology, 5: 136–166.

TAGUE, R. G. 2003. Pelvic sexual dimorphism in a metatherian, Didelphis virginiana: implications for eutherians. Journal of Mammalogy, 84: 1464–1473.

TEILHARD DE CHARDIN, P. 1922. Les mammifères de l'Éocène inférieur français et leurs gisements. Annales de Paléontologie, Paris, 11: 9–116.

THEWISSEN, J. G. M. 1990. Evolution of Paleocene and Eocene Phenacodontidae (Mammalia, Condylarthra). University of Michigan Papers on Paleontology, 29: 1–107.

TROTTER, S. 1885. The significance of the 'collar bone' in the Mammalia. American Naturalist, 19: 1172–1177.

TROUESSART, E.-L. 1897. *Catalogus Mammalium Tam Viventium Quam Fossilium, Tomus I*. Friedländer und Sohn, Berlin, 664 pp.

VAN VALEN, L. M. 1971. Adaptive zones and the orders of mammals. Evolution, 25: 420–428.

———. 1994. The origin of the plesiadapid primates and the nature of *Purgatorius*. Evolutionary Monographs, Chicago, 15: 1–79.

VANDENBERGHE, N., F. J. HILGEN, R. P. SPEIJER, J. G. OGG, F. M. GRADSTEIN, O. HAMMER, C. J. HOLLIS, and J. J. HOOKER. 2012. The Paleogene period. In F. M. Gradstein, J. G. Ogg, M. D. Schmitz, and G. M. Ogg (eds.), The Geological Time Scale 2012, Elsevier, Amsterdam, pp. 855–921.

WIBLE, J. R. 1993. Cranial circulation and relationships of the colugo *Cynocephalus* (Dermoptera, Mammalia). American Museum Novitates, 3072: 1–27.

WIBLE, J. R. and H. H. COVERT. 1987. Primates: cladistic diagnosis and relationships. Journal of Human Evolution, 16: 1–22.

WIBLE, J. R. and M. J. NOVACEK. 1988. Cranial evidence for the monophyletic origin of bats. American Museum Novitates, 2911: 1–19.

WILEY, E. O., D. SIEGEL-CAUSEY, D. R. BROOKS, and V. A. FUNK. 1991. The compleat cladist: a primer of phylogenetic procedures. University of Kansas Museum of Natural History, Special Publications, 19: 1–158.

WILF, P., K. C. BEARD, K. S. DAVIES-VOLLUM, and J. W. NOREJKO. 1998. Portrait of a late Paleocene (early Clarkforkian) terrestrial ecosystem: Big Multi quarry and associated strata, Washakie Basin, southwestern Wyoming. Palaios, 13: 514–532.

WOOD, A. E. 1962. The early Tertiary rodents of the family Paramyidae. Transactions of the American Philosophical Society, 52: 1–261.

WOOD, H. E., R. W. CHANEY, J. CLARK, E. H. COLBERT, G. L. JEPSEN, J. B. REESIDE, and C. STOCK. 1941. Nomenclature and correlation of the North American continental Tertiary. Bulletin of the Geological Society of America, 52: 1–48.

WOOD, R. C. 1967. A review of the Clark Fork vertebrate fauna. Breviora, Museum of Comparative Zoology, Harvard University, 257: 1–30.

WOODBURNE, M. O. (ed.). 2004. Late Cretaceous and Cenozoic Mammals of North America, Columbia University Press, New York, 391 pp.

YAPUNCICH, G. S., J. T. GLADMAN, and D. M. BOYER. 2015. Predicting euarchontan body mass: a comparison of tarsal and dental variables. American Journal of Physical Anthropology, 157: 472–506.

YOULATOS, D. and M. GODINOT. 2004. Locomotor adaptations of *Plesiadapis tricuspidens* and *Plesiadapis* n. sp. (Mammalia, Plesiadapiformes) as reflected in selected parts of the postcranium. Journal of Anthropological Sciences, 82: 103–118.

APPENDIX I — CRANIAL AND DENTAL FIGURES AND MEASUREMENTS

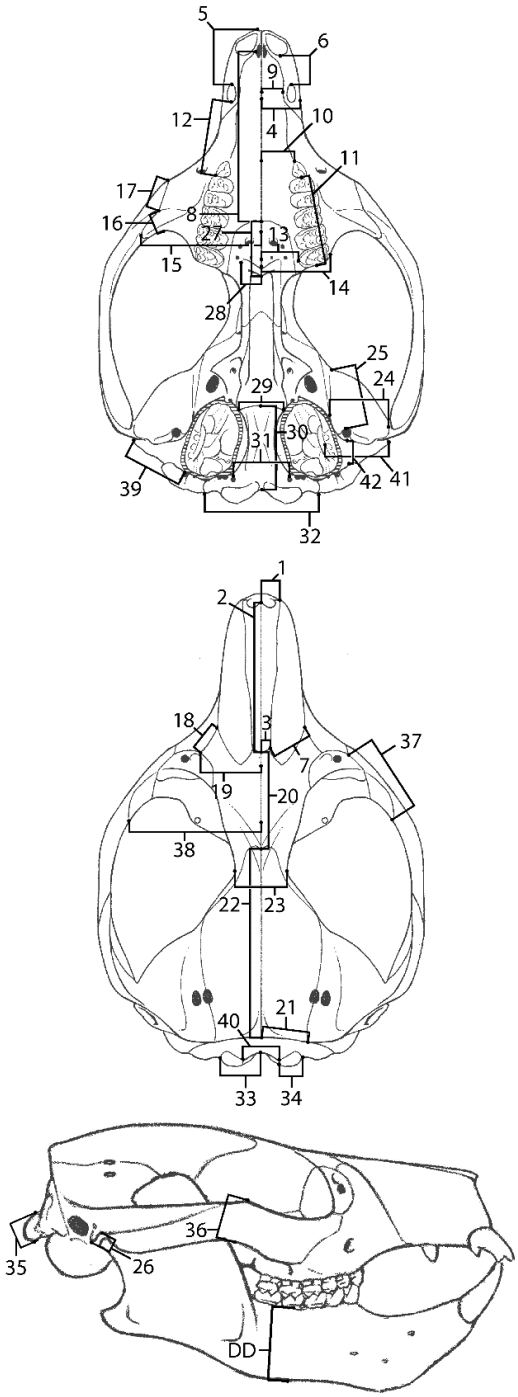

FIGURE A-I-1.— Cranial measurements used to compare the size and shape of the skull of *Plesiadapis cookei* (UM 87990) to other plesiadapids. See Table A-I-1 for a list and description of numbered measurements. Table A-I-2 is a table of measurement values. Figure is modified from Boyer et al. (2010a: fig. 1).

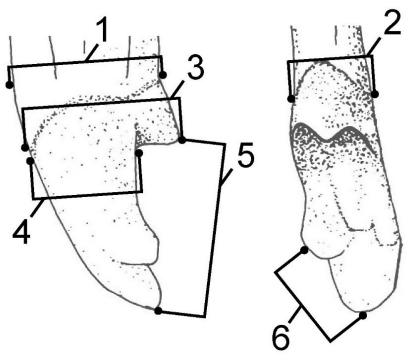

FIGURE A-I-2.— Incisor measurements used to compare size and shape of incisors of *Plesiadapis cookei* (UM 87990) to other plesiadapids. See Table A-I-1 for description of numbered measurements. See Table A-I-8 for measurements. Figure is modified from Boyer et al. (2010a: fig. 7).

TABLE A-I-1.— List of numbered measurements for the cranium shown in Figure A-I-1. This is equivalent to appendix table 2.4 of Boyer (2009). Similar tables in Boyer et al. (2010a, 2012a) leave out numbers 43–44 but use the same numbering scheme otherwise.

No.	Description
Nasal	
1	Maximum mediolateral width of anterior end
2	Maximum anteroposterior length
3	Maximum mediolateral width of posterior end (along frontal suture)
Premaxilla	
4	Maximum mediolateral width at anteroposterior level of juncture with maxilla
5	Distance to anterior margin of I^2, foramen measured from anterior margin of bone
6	Distance between I^1 and I^2 alveoli
Premaxilla–Frontal	
7	Length of suture on dorsum of skull
Maxilla	
8	Anteroposterior length in palate with measurement starting at anterior margin of suture with palatine
9	Mediolateral width in palate at level of I^2 alveolus
10	Mediolateral width in palate at anterior margin of P^2 or P^3 alveolus
11	Length of tooth row from P^3 to M^3
12	Distance between I^2 and P^3
13	One half mediolateral width of palate at level of M^3
14	Unilateral mediolateral width of maxilla at level of M^3, measurement starts at midline (not palatomaxillary suture) and ends at lateral edge of alveolar process
Maxilla–Zygomatic	
15	Maximum mediolateral width due to projection of maxillary zygomatic process
16	On zygomatic process, anteroposterior distance of expansion of maxilla for attachment of masseter
17	Length of suture on anterior surface of maxilla
Maxilla–Frontal	
18	Length of suture on dorsum of skull
Frontal	
19	Maximum unilateral mediolateral width from metopic suture to most lateral point of contact with lacrimal and maxilla
20	Maximum anteroposterior length along midline from nasal contact to parietal contact
Parietal	
21	Unilateral mediolateral width at posterior contact with squamosal along nuchal crest
22	Length of sagittal crest
23	Maximum bilateral mediolateral width at postorbital constriction
Squamosal	
24	Mediolateral width of glenoid
25	Anteroposterior length of glenoid, measured along medial margin, slightly obliquely going from ostglenoid foramen to most anterior point on glenoid
26	Dorsoventral projection of postglenid process
Palatine	
27	Anteroposterior length from anterior suture with maxilla to postpalatine torus
28	Unilateral mediolateral distance to outer margin of postpalatine torus
Basioccipital	
29	Bilateral mediolateral width at anteriormost point (spheno-occipital synchondrosis)
30	Maximum anteroposterior length
Exoccipital	
31	Bilateral mediolateral distance between hypoglossal foramina
32	Bilateral mediolateral width at posterior margin of skull (between tips of jugular processes)
33	Unilateral mediolateral distance from midline to outer margin of occipital condyle
34	Maximum mediolateral width of occipital condyle, measured laterally from lateral edge of foramen magnum
35	Dorsoventral height of occipital condyle, not including anteromedial projection of facet
Zygomatic	
36	Dorsoventral depth at lateral margin of excavation for orbits
37	Distance from anterior zygomatic/maxilla contact to lateral margin of excavation for orbits on zygomatic
Orbits	
38	Unilateral mediolateral distance between midline and lateral edge of excavation for orbit on zygomatic

TABLE A-I-1.— Cont'd.

No.	Description
Basicranium	
39	Distance from anterolateral margin of ectotympanic bone to stylomastoid foramen
40	Mediolateral width of foramen magnum
41	External auditory meatus mediolateral length, measured from lateral tip to medial margin of annular component of ectotympanic bone
42	External auditory meatus anteroposterior length, measured posterior to potglenoid foramen
43	Total skull length
44	Length from tip of maxillae to occipital condyle
Mean cranial size	
GM	Geometric mean of all measurements from 1–44 except 7, 41, and 42 (number of measurements available for calculation is given in parentheses)
Foramina	
45	Infraorbital foramen major diameter
46	Infraorbital foramen minor diameter
47	Optic foramen major diameter
48	Optic foramen minor diameter
49	Suboptic foramen major diameter
50	Suboptic foramen minor diameter
51	Sphenorbital fissure major diameter
52	Sphenorbital fissure minor diameter
53	Foramen ovale major diameter
54	Foramen ovale minor diameter
55	Hypoglossal foramen major diameter
56	Hypoglossal foramen minor diameter
57	Major diameter of MNHN CR 125 foramen *93*
58	Postpalatine foramen major diameter
59	Postpalatine foramen minor diameter
60	Jugular foramen major diameter
61	Length of internal carotid canal
Petrosal measurements	
Avl	Aperature of fenesta vestibuli length
Ccl	Cochlea length
Pd	Promontorium depth: height of the pars cochlearis measured perpendicular to the plane of the endocranial surface of the element
Pw	Promontorium width: mediolateral thickness of the petrosal measured perpendicular to the previous measurement
Shape variables	
Avl / GM	Fenestra vestibuli relative length, calculated as av / GM (= fv / GM)
Ccl / GM	Cochlea relative length, calculated as ccl / GM
EAM-S	External auditory meatus shape, calculated as measurement 41 / measurement 42
Gld / GM	Glenoid relative size, calculated as √(measurement 24 * measurement 25) / GM
N / F	Nasal length relative to frontal length, calculated as measurement 2 / measurement 20
N / Pmx	Nasal width relative to premaxilla, calculated as: measurement 3 / measurement 7
Nc / GM	Caudal nasal relative width, calculated as measurement 3 / GM
Nc / Nr	Nasal caudal width relative to rostral width, calculated as measurement 3 / measurement 1
Pcsa / GM	Petrosal relative cross-sectional area, calculated as = √ (pd * pw) / GM
Pmx / GM	Premaxilla relative width, calculated as measurement 7 / GM
Upper central incisor measurements and indices	
1	Mesiodistal length of root at base of crown
2	Mediolateral width of root at base of crown
3	Mesiodistal length of crown at posterocone
4	Mesiodistal length of crown immediately distal to posterocone
5	Distance between anterocone tip and posterocone tip
6	Distance between anterocone tip and laterocone tip (not applicable to Platychoerops)
Index 1	Ratio of measurement 3 to square root of product of measurements 1 and 2
Index 2	Ratio of measurement 4 to square root of product of measurements 1 and 2
Index 3	Ratio of measurement 5 to square root of product of measurements 1 and 2
Index 4	Ratio of measurement 6 to 5

TABLE A-I-2.— Measurements (mm) of eight plesiadapid crania. Numbered measurements in the left-hand column are described in Table A-I-1. See also Figure A-I-1. Column headings list the taxon, specimen number, element, and locality for each specimen.

	Plesiadapis tricuspidens	*Plesiadapis tricuspidens*	*Plesiadapis tricuspidens*	*Plesiadapis cookei*	*Pronothodectes gaoi*	*Nannodectes gidleyi*	*Nannodectes intermedius*	*Plesiadapis anceps*
	MNHN CR 125	Pellouin skull	MNHN CR 965	UM 87990	UALVP 46685	AMNH 17388	USNM 309902	YPM-PU 19642
	Skull	Skull	Skull base	Skull	Skull	Skull	Skull	Rostrum
	Berru	Berru	Berru	SC-117	DW-2	Mason Pocket	Bangtail	7 - up Butte
1	4.30	—	—	4.84	2.67	—	2.31	3.34
2	30.69	—	—	31.35	18.40	—	13.61	21.84
3	1.51	2.00	—	4.57	2.60	—	2.31	3.34
4	7.68	—	—	8.61	—	—	—	—
5	16.25	—	—	15.93	6.52	—	—	—
6	5.50	—	—	3.87	2.66	—	—	—
7	9.60	—	—	—	4.36	—	—	4.52
8	35.78	30.36	—	29.37	—	—	—	—
9	4.44	5.75	—	5.53	3.39	—	—	—
10	6.89	8.02	—	7.71	5.45	—	—	—
11	21.16	20.80	—	22.16	12.36	12.40	10.55	—
12	15.14	12.37	—	14.04	6.73	—	—	—
13	6.66	6.84	6.54	6.80	—	—	—	—
14	13.89	13.26	10.82	15.12	—	—	—	—
15	27.99	24.76	—	26.10	—	—	—	—
16	3.79	3.47	—	2.33	1.29	1.44	—	—
17	15.01	17.70	—	18.44	—	—	—	—
18	8.38	—	—	8.84	3.77	—	—	4.60
19	14.15	—	—	15.11	.	—	—	10.20
20	20.68	19.69	—	21.02	11.23	—	—	13.08
21	10.09	8.63	—	10.82	—	—	—	—
22	41.88	38.52	—	41.00	—	—	—	—
23	11.31	10.85	—	11.66	—	—	—	—
24	13.54	14.02	—	10.12	5.38	5.60	4.11	—
25	13.98	13.52	—	11.52	6.96	6.50	4.49	—
26	4.01	4.54	—	3.69	—	1.35	1.43	—
27	13.83	11.16	12.93	12.57	—	—	—	—
28	4.26	3.74	4.33	4.45	—	3.10	—	—
29	6.37	6.94	—	—	3.25	—	2.21	—
30	14.82	14.40	—	14.42	8.46	—	7.22	—
31	10.94	10.54	—	10.59	—	—	—	—
32	24.97	25.00	—	26.00	—	17.40	12.20	—
33	8.30	8.50	—	8.60	6.17	5.92	5.39	—
34	4.39	4.05	—	4.38	2.46	2.50	1.95	—
35	6.48	5.06	—	5.36	3.87	2.80	2.80	—
36	8.97	9.78	—	7.86	3.99	—	—	—
37	16.69	—	—	16.55	—	—	—	—

TABLE A-I-2.— Cont'd.

38	27.21	—	—	24.00	—	—	—	—
39	11.95	12.45	—	10.80	—	—	—	—
40	8.95	6.88	—	8.71	7.40	6.84	6.87	—
41	11.60	11.50	—	4.80	5.75	—	—	—
42	6.80	6.60	—	12.00	5.50	—	4.07	—
43	106.36	—	—	87.74	—	—	—	—
44	89.27	80.27	—	78.00	—	—	—	—
GM	10.60 (39)	10.28 (30)	—	10.71 (39)	4.91 (21)	4.45 (11)	4.32 (14)	—
45	2.80	2.34	—	2.73	2.12	2.22	2.20	—
46	1.30	1.79	—	1.52	1.26	—	1.15	—
47	1.36	—	1.21	—	—	—	—	—
48	0.84	—	1.02	—	—	—	—	—
49	1.45	—	1.64	—	—	—	—	—
50	1.17	—	~1.4	—	—	—	—	—
51	4.08		—	—	—	—	—	—
52	—	—	2.08	~2.00	—	—	—	—
53	2.61	—	3.12	—	—	—	—	—
54	1.49	—	1.42	—	—	—	—	—
55	1.52	~1.70	—	1.75	1.03	—	—	—
56	1.05	~1.40	—	1.60	0.86	—	—	—
57	0.72	—	—	—	—	—	—	—
58	2.53	—	2.97	—	—	—	—	—
59	1.81	—	—	—	—	—	—	—
60	2.38	—	—	2.86	—	—	—	—
61	2.80	2.70	—	—	~1.60	—	—	—

TABLE A-I-3.— Petrosal measurements (mm). Column heading abbreviations: *Avl*, maximum diameter of aperature of fenestra vestibuli; *Ccl*, cochlear length; *g**, grooves on promontorium: distinctions between *g1–g5* are explained in main text, Table 2 and the caption for Figure 14; *Pd*, petrosal depth (height of the pars cochlearis measured perpendicular to the plane of the endocranial surface of the element); *Pw*, petrosal width (mediolateral thickness of the petrosal measured perpendicular to the previous measurement); *p-s*, promontorium shape (*Pd / Pw*). Abbreviations in the body of the table: *a*, morphology absent or different; *n*, morphology cannot be assessed because it is not preserved; *nm*, not measured or not measureable; *p*, morphology is present and preserved; *pp*, in the case of *g1–g4* indicates the presence of a set of parallel grooves in the appropriate position; —, relevant anatomy for gauging the anatomical condition is preserved but obscured by other bone or matrix, or just difficult to interpret. Entry with superscript-a ([a]) was measured from an illustration in Russell (1964: p. 95, fig. 16). Entry with asterisk (*) is the maximum diameter of the stapes foot plate. Cochlear length measurements courtesy of M. Coleman.

Taxon	Specimen	*Ccl*	*Avl*	*Pd*	*Pw*	*p-s*	*g1*	*g2*	*g3*	*g4*	*g5*
Pronothodectes gaoi	UALVP 46685 R	nm	1.21	4.55	3.45	132	—	—	—	p	—
Pronothodectes gaoi	UALVP 46685 L	15.60	1.17	4.68	3.48	134	—	—	p	p	—
Pronothodectes gaoi	UALVP 46687 R	nm	1.20	4.29	3.73	115	pp	pp	p	p	p
Pronothodectes gaoi	UALVP 49105 L	15.30	1.03	4.61	3.84	120	pp	p	p	p	p
N. intermedius	USNM 309902 R	14.50	1.16	3.54	3.55	100	p	—	a	p	—
N. intermedius	USNM 309902 L	nm	1.19	~3.60	~3.80	95	p	n	a	—	a
N. gidleyi	AMNH 17388 R	nm	nm	nm	~3.50	nm	n	—	a	p	—
N. gidleyi	AMNH 17388 L	nm	nm	nm	~3.40	nm	n	—	a	p	—
P. tricuspidens	MNHN CR 125 R	nm	1.53[a]	nm	4.47	nm	p	a	a	p	p
P. tricuspidens	MNHN CR 125 L	nm	nm	nm	nm	nm	—	a	a	p	p
P. tricuspidens	Pellouin R	nm	nm	nm	nm	nm	—	a	pp	—	—
P. tricuspidens	Pellouin L	nm	nm	nm	4.31	nm	p	a	pp	p	p
P. tricuspidens	MNHN BR 1371	17.30	1.15	4.91	4.14	119	pp	p	pp	p	p
P. tricuspidens	MNHN BR 17414	nm	nm	4.86	4.16	117	n	n	n	n	—
P. tricuspidens	MNHN BR 17415	16.10	1.31	5.30	4.21	126	p	p	p	p	p
P. tricuspidens	MNHN BR 17416	17.20	1.2	4.98	4.43	112	p	a	a	a	p
P. tricuspidens	MNHN BR 17417	17.50	1.53	5.30	4.14	128	n	n	pp?	n	p
P. tricuspidens	MNHN BR 17418	17.00	1.36	4.95	4.52	110	p	—	a	a	p
P. tricuspidens	MNHN BR 17419	nm	nm	4.07	4.55	89	n	n	a	a	p
Plesiadapis cookei	UM 87990 R	21.03	1.32	~5.50	4.43	124	p	pp?	p	a	p
C. simpsoni	USNM 482354	8.64	nm	~2.00	~2.40	83	p	—	—	—	—
I. graybullianus	USNM 421608	nm	1.10*	3.28	3.04	108	p	n	n	n	—

TABLE A-I-4.— Additional petrosal measures (mm). In two cases, the posterior carotid foramen was not visible and had to be approximated ([a]) from the width of the groove for the internal carotid plexus on the petrosal. Where measureable, the value is given after the condition symbol. Abbreviations: *bs*, apparent suture separating pars cochlearis from bulla forming bone; *cc*, cochlear canaliculus; *lam*, several specimens exhibit what appeared to be two laminae of bone comprising the remnant of the rostral tympanic process; *pcf*, posterior cartid foramen (presence/absence: width in millimeters); *ps*, posterior septum of MacPhee (1981); *s**, septa of tympanic cavity (see main text, Table 2 and Figure 14 caption for distinguishing features of each septum); *tng*, tympanic nerve groove (whether there is a groove leading to a tympanic canaliculus on the ridge of the cochlear canaliculus). Other abbreviations: *a*, morphology absent/different; *n*, morphology cannot be assessed because it is not preserved; *nm*, not measured or not measureable; *p*, morphology is present/preserved; —, relevant anatomy for gauging the anatomical condition is preserved but obscured by other bone or matrix, or difficult to interpret.

Taxon	Specimen	s1	s2	s3	tng	cc	ps	pcf	lam	bs
Pronothodectes gaoi	UALVP 46685 R	p	p	p	—	p	p	n	p	a
Pronothodectes gaoi	UALVP 46685 L	p	p	p	p	p	p	p: nm	a	p?
Pronothodectes gaoi	UALVP 46687 R	n	n	n	p	—	p	p: nm	a	a
Pronothodectes gaoi	UALVP 49105 L	p	p	p	p	p	p	p: 0.28	p	a
N. intermedius	USNM 309902 R	—	p	n	n	p	n	n	—	—
N. intermedius	USNM 309902 L	p	p	a	—	—	n	n: 0.29[a]	—	a
N. gidleyi	AMNH 17388 R	—	p	a	p	p	—	n	—	a
N. gidleyi	AMNH 17388 L	—	p	a	p	p	—	n	—	a
P. tricuspidens	MNHN CR 125 R	p	p	a	p	p	p	p: 0.34	a	a
P. tricuspidens	MNHN CR 125 L	p	p	a	p	p	p	n	a	a
P. tricuspidens	Pellouin R	—	p	a	p	p	p	p: 0.31	p	p?
P. tricuspidens	Pellouin L	p	p	a	p	p	p	p: 0.29	p	p?
P. tricuspidens	MNHN BR 1371	p	p	a	n	p	n	n	n	n
P. tricuspidens	MNHN BR 17414	n	—	n	n	p	n	n	n	n
P. tricuspidens	MNHN BR 17415	p	p	a	—	p	n	n	p	a
P. tricuspidens	MNHN BR 17416	p	p	a	n	p	n	n	p	a
P. tricuspidens	MNHN BR 17417	n	p	—	n	p	n	n	p	a
P. tricuspidens	MNHN BR 17418	p	p	p	—	p	n	n	p	a
P. tricuspidens	MNHN BR 17419	p	p	n	—	p	n	n	p?	a
Plesiadapis cookei	UM 87990 R	p	p	a	p	p	n	n: 0.40[a]	n	p?
C. simpsoni	USNM 482354	—	—	—	—	—	p	p: 0.53	—	—
I. graybullianus	USNM 421608	p	—	—	—	p	p	p: 0.17	a	p?

TABLE A-I-5.— Dentary depth measurements (mm) of *Plesiadapis cookei*.

Specimen	Dentary depth at M_2	Tooth wear (relative age)
UM 65049	14.02	Moderate wear
UM 65720	17.00	Moderate wear
UM 66701	18.13	Light moderate wear
UM 66919	16.12	Light moderate wear
UM 67187	15.76	Moderate–heavy wear
UM 69265	13.25	Unworn
UM 69913	16.55	Slight wear
UM 71764	16.20	—
UM 73653	15.70	Slight wear
UM 73704	17.83	Heavy wear
UM 82364	13.96	Slight wear
UM 87990	14.04	Unworn
YPM-PU 13292	15.94	Moderate wear
YPM-PU 17973	19.70	—
YPM-PU 18097	18.12	—
YPM-PU 18312	15.83	Slight wear
YPM-PU 19551	19.36	—
YPM-PU 21589	19.48	—
Geometric Mean	16.50	

TABLE A-I-6.— Dentary measurements (mm) of *Plesiadapis tricuspidens* and *Platychoerops daubrei*.

Specimen	Taxon	Dentary depth at M_2
MNHN Berru L-S1	*P. tricuspidens*	14.82
MNHN Berru L-S2	*P. tricuspidens*	18.96
MNHN Berru L-S3	*P. tricuspidens*	17.17
MNHN BR 10119	*P. tricuspidens*	17.90
MNHN BR 10181	*P. tricuspidens*	14.51
MNHN BR 10198	*P. tricuspidens*	15.58
MNHN BR 13881	*P. tricuspidens*	13.26
MNHN R 129	*P. tricuspidens*	15.24
MNHN R 132	*P. tricuspidens*	14.61
MNHN R 401	*P. tricuspidens*	17.27
MNHN R 402	*P. tricuspidens*	18.46
MNHN R 403	*P. tricuspidens*	14.60
MNHN R 420	*P. tricuspidens*	16.06
MNHN R 421	*P. tricuspidens*	18.44
MNHN R 422	*P. tricuspidens*	17.63
MNHN R 423	*P. tricuspidens*	15.54
MNHN R 424	*P. tricuspidens*	20.32
MNHN R 431	*P. tricuspidens*	15.24
MNHN R 432	*P. tricuspidens*	17.62
MNHN R 433	*P. tricuspidens*	12.69
MNHN BR 11832	*P. tricuspidens*	14.76
MNHN BR 12498	*P. tricuspidens*	16.03
MNHN BR 12499	*P. tricuspidens*	16.62
MNHN BR 12500	*P. tricuspidens*	14.84
MNHN BR 12502	*P. tricuspidens*	19.52
MNHN BR 12504	*P. tricuspidens*	12.82
MNHN BR 12505	*P. tricuspidens*	17.50
MNHN BR 12506	*P. tricuspidens*	16.25
MNHN BR 12507	*P. tricuspidens*	15.91
MNHN BR 14053	*P. tricuspidens*	15.84
MNHN BR 14054	*P. tricuspidens*	15.01
MNHN BR 14062	*P. tricuspidens*	17.61
MNHN BR 14616	*P. tricuspidens*	15.41
Berru Divers A	*P. tricuspidens*	12.82
Berru Divers C	*P. tricuspidens*	12.35
Berru Divers D	*P. tricuspidens*	14.03
Berru Divers E	*P. tricuspidens*	14.75
Mean	P. tricuspidens	15.89
MNHN AL 5156	*Pl. daubrei*	14.38
MNHN Mu 12301	*Pl. daubrei*	11.77
MNHN Mu 12302	*Pl. daubrei*	12.53
Mean	Pl. daubrei	12.89

TABLE A-I-7.— P_4 characteristics of *Plesiadapis cookei*.

Specimen	P_4 trigonid basin	P_4 paraconid
UM 65031	No trigonid basin	No
UM 65720	Slit-like trigonid basin	No
UM 67187	Dimple-like trigonid basin	Yes
UM 69265	Expansive trigonid basin	No
UM 69995	Slit-like trigonid basin	Yes
UM 71764	No trigonid basin	Yes
UM 73653	No trigonid basin	No
UM 73704	Slit-like trigonid basin	Worn
UM 80270	Expansive, trigonid basin	No
UM 82364	Slit-like trigonid basin	No
UM 87990	Expansive trigonid basin	No
UM 88001	No trigonid basin	No
YPM-PU 13292	No trigonid basin	Yes
YPM-PU 17937	No trigonid basin	Worn
YPM-PU 17939	No trigonid basin	No
YPM-PU 17940	Slit-like trigonid basin	No
YPM-PU 21009	No trigonid basin	Yes

TABLE A-I-8.— Plesiadapid incisor measurements (mm) and shape variables. See appendix Table A-I-1 and Figure A-I-2 for descriptions and illustrations of measurements and indices. Abbreviations: *CA*, square root of cross-sectional area of incisor root respresented as the product of measurement 1 and measurement 2 from table A-I-1 (*M-1 * M-2*); *Ind*, index; *M-1* is upper incisor measurement 1, etc.

Specimen	Taxon	M-1	M-2	M-3	M-4	M-5	M-6	CA	Ind-1	Ind-2	Ind-3	Ind-4
YPM-PU 17977	*P. cookei*	7.46	4.36	8.69	5.78	11.58	2.73	5.70	1.52	1.01	2.03	0.24
YPM-PU 18118	*P. cookei*	6.76	3.92	—	5.44	10.80	2.67	5.15	—	1.06	2.10	0.25
YPM-PU 13292	*P. cookei*	6.85	4.48	6.97	5.79	12.90	3.10	5.54	1.26	1.05	2.33	0.24
UM 66725	*P. cookei*	6.72	4.28	7.30	5.45	9.83	2.69	5.36	1.36	1.02	1.83	0.27
UM 88183	*P. cookei*	6.66	3.93	7.04	5.57	—	—	5.12	1.38	1.09	—	—
UM 65049	*P. cookei*	7.13	3.68	7.76	4.83	—	2.14	5.12	1.51	0.94	—	—
UM 69265	*P. cookei*	7.12	4.60	8.00	6.52	—	2.19	5.72	1.40	1.14	—	—
UM 69995 (L)	*P. cookei*	—	—	—	—	—	3.07	—	—	—	—	—
UM 69995 (R)	*P. cookei*	—	—	—	—	—	3.22	—	—	—	—	—
MNHN CR 14359	*P. tricuspidens*	4.38	2.67	5.53	3.34	5.93	2.06	3.42	1.62	0.98	1.73	0.35
MNHN CR 14369	*P. tricuspidens*	—	—	5.44	3.37	7.30	2.04	—	—	—	—	0.28
MNHN Berru misc 01	*P. tricuspidens*	4.83	3.22	5.74	3.70	—	—	3.94	1.46	0.94	—	—
MNHN Berru misc 02	*P. tricuspidens*	5.13	3.14	6.21	3.14	6.23	2.21	4.01	1.55	0.78	1.55	0.35
MNHN Berru misc 03	*P. tricuspidens*	4.70	2.96	6.02	3.38	6.52	2.12	3.73	1.61	0.91	1.75	0.33
MNHN Berru misc 04	*P. tricuspidens*	5.40	3.16	6.47	3.68	6.99	1.96	4.13	1.57	0.89	1.69	0.28
MNHN Berru misc 05	*P. tricuspidens*	6.06	3.56	7.18	3.95	—	—	4.64	1.55	0.85	—	na
MNHN MUT 17158	*Pl. daubrei*	6.29	4.51	6.36	5.70	10.56	na	5.33	1.19	1.07	1.98	na
MNHN Mu 17076	*Pl. daubrei*	—	—	5.90	4.89	9.56	na	—	—	—	—	na
MNHN AL 5173A	*Pl. daubrei*	6.09	4.05	6.13	5.05	8.98	na	4.97	1.23	1.02	1.81	na
MNHN AL 5173B	*Pl. daubrei*	—	—	5.59	4.49	—	na	—	—	—	—	na
MNHN MU 5555	*Pl. daubrei*	5.91	4.36	5.64	5.18	9.76	na	5.08	1.11	1.02	1.92	na
MNHN Mu 6502	*Pl. daubrei*	5.41	—	5.29	4.36	7.96	na	—	—	—	—	na
MNHN Mu 6447	*Pl. daubrei*	5.04	3.77	5.05	4.15	8.54	na	4.36	1.16	0.95	1.96	na
MNHN AL 5172	*Pl. daubrei*	6.67	4.52	6.40	5.70	11.30	na	5.49	1.17	1.04	2.06	na

TABLE A-I-9.— Posterior carotid foramen (*PCF*) functionality and groove diameters, with skull lengths (mm), for selected mammals. Abbreviations: *Func*, functionality of internal carotid artery (1, supplies forebrain with blood; 2, does not contribute to blood supply of brain); *Le*, prosthion–inion length of skull. Superscript-a ([a]) indicates that value represents *g1* groove (Tables A-I-3 and A-I-4). Superscript-b ([b]) indicates that value is an estimate from Table 3.

Taxon	Func.	Reference or specimen	PCF	Le
Erinaceus sp.	1	Kay et al. (1992)	0.43	45.00
Tupaia glis	1	Kay et al. (1992)	0.62	49.10
Tupaia tana	1	Kay et al. (1992)	0.81	59.40
Nycticebus coucang	2	Kay et al. (1992)	0.45	59.20
Perodicticus potto	2	Kay et al. (1992)	0.18	61.90
Galago senegalensis	2	Kay et al. (1992)	0.16	40.66
Galago senegalensis	2	Kay et al. (1992)	0.20	46.80
Galago demidovii	2	Kay et al. (1992)	0.14	37.30
Eulemur fulvus	1	Kay et al. (1992)	0.68	87.30
Lemur sp.	1	Kay et al. (1992)	0.75	83.70
Tarsius sp.	1	Kay et al. (1992)	0.56	39.30
Callithrix argentata	1	Kay et al. (1992)	0.74	45.70
Callicebus sp. (Bolivia)	1	Kay et al. (1992)	1.05	59.00
Saguinus mystax	1	Kay et al. (1992)	0.99	50.70
Saimiri sciureus	1	Kay et al. (1992)	1.24	59.70
Aotus trivirgatus	1	Kay et al. (1992)	1.30	62.70
Cebus paella	1	Kay et al. (1992)	2.00	95.50
Pithecia pithecia	1	Kay et al. (1992)	1.37	82.60
Ateles geoffroyi	1	Kay et al. (1992)	2.42	102.90
Alouatta pigra	1	Kay et al. (1992)	2.50	104.40
Plesiadapis tricuspidens	?	MNHN CR 125	0.34	106.36
Plesiadapis tricuspidens	?	Pellouin skull	0.30	106.50[b]
Plesiadapis cookei	?	UM 87990	0.40[a]	105.80[b]
Nannodectes intermedius	?	USNM 309902	0.29[a]	50.40[b]
Pronothodectes gaoi	?	UALVP 49105	0.28	61.20[b]
Carpolestes simpsoni	?	Bloch and Silcox (2006)	0.53	39.56
Ignacius graybullianus	?	Kay et al. (1992)	0.17	48.20

APPENDIX II — POSTCRANIAL MEASUREMENTS

TABLE A-II-1.— Measurement abbreviations (*Abbrev*) for the postcranial skeleton, listed in alphabetical order by abbreviation. The measurements themselves are listed in the following tables.

Abbrev.	Measurement
AcD	Acetabulum (of innominate) anteroposterior depth (Sargis, 2002b, table 2, measurement 5)
AcL	Acetabulum (of innominate) superoinferior length (Sargis, 2002b, table 2, measurement 4)
AcV	Anticlinal vertebral position: first thoracic = 1, last lumbar = number of thoracic vertebrae + lumbar vertebrae
AD	Acromion (of scapula) superoinferior depth measured from superior tip of acromion to scapular spine, perpendicular to scapular spine
AFD	Auricular facet (of sacrum) maximum anteroposterior depth
AFL	Auricular facet (of sacrum) maximum superoinferior length
AfW	Accessory facet (of hamate) radioulnar width
AL	Acromion (of scapula) mediolateral length
AP	Projection of acromion (of scapula) lateral to glenoid fossa, measured perpendicular to inferior half of glenoid fossa
APL	Accessory process length (on thoracic and lumbar vertebrae; measured from apex of notch between postzygapophysis and accessory process to tip of accessory process
Br-I	Brachial index (100 H radius length/humerus length)
BSV	Base shape variable = PED / PEW
C-L	Length of cervical region of vertebral column
C%l	Index of cervical length as a proportion of trunk length (100 H cervix / (thorax + lumbus))
Ca-L	Length of first 10 caudal vertebrae
Ca#	Number of caudal vertebrae
Ca%l	Index of caudal length as a proportion of trunk length (100 H cauda / (thorax + lumbus))
CaH	Capitulum (of humerus) height (Sargis, 2002a, table 2, measurement 13)
CaIW	Caudal inter-facet mediolateral width (of atlas): measured between lateral edges of axis facets
CaL	Capitulum (of humerus) anteroposterior length (Szalay and Dagosto, 1980, CL)
CaW	Capitulum (of humerus) mediolateral width (Szalay and Dagosto, 1980, CW; Sargis, 2002a, table 2, measurement 11)
CfA	Calcaneum facet (of cuboid) angle with respect to metatarsal facet of cuboid
CfD	Capitate facet (of hamate) dorsoventral depth
CH	Dorsoventral height of vertebral canal
CL	Coracoid (of scapula) mediolateral length
Cr-I	Crural index (100 H tibia length/femur length)
CrIW	Cranial interfacet mediolateral width (of atlas): measured between lateral edges of occipital facets on lateral masses of atlas
CSV	Claw shape variable = ln (MSD / MSW) = ln MSD - ln MSW
CW	Mediolateral width of vertebral canal
DAL	Distal articular surface (of fibula) anteroposterior length (Sargis, 2002b, table 2, measurement 43)
DCL	Deltopectoral crest (of humerus) proximodistal length (Sargis, 2002a, table 2, measurement 17)
dCW	Dorsal vertebral canal (of atlas) mediolateral width, measured dorsal to articular facets for occiput and axis
DED	Distal end dorsoventral or anteroposterior depth of various elements (unless otherwise specified in table footnotes; Sargis, 2002a, table 2, measurement 32; Sargis, 2002b, table 2, measurement 45)
DEV	Distal end variable = DEW / DED
DEW	Distal end mediolateral or radioulnar width (unless otherwise specified in table footnotes; Sargis, 2002a, table 2, measurement 16, 31; Sargis, 2002b, table 2, measurement 19, 36)
DFT	Distance to flexor tubercle distal margin (from proximal end of distal phalanx)
DL	Dorsal side craniocaudal length (of posterior arch of atlas)
DpV	Diaphragmatic vertebral position in thoracic region of vertebral column

TABLE A-II-1.— Cont'd.

Abbrev.	Measurement
EEC	Entepicondyle (of humerus) mediolateral width
ETH	Extensor tubercle (of distal phalanx) height dorsal to proximal articular surface
FHL	Femoral head proximodistal length (Sargis, 2002b, table 2, measurement 10)
FHW	Femoral head mediolateral width (Sargis, 2002b, table 2, measurement 11)
FTH	Flexor tubercle height ventral to proximal articular surface (distal phalanx)
FTW	Flexor tubercle (of distal phalanx) mediolateral width
GD	Glenoid (of scapula) superoinferior depth (Sargis, 2002a, table 2, measurement 3)
GM	Geometric mean
GTL	Greater trochanter (of femur) proximodistal length (Sargis, 2002b, table 2, measurement 12)
GW	Glenoid (of scapula) anteroposterior width (Sargis, 2002a, table 2, measurement 4)
Hf-I	Humerofemoral index (100 H humerus length/femur length)
HfD	Hamate facet (of triquetrum) dorsoventral depth
HfW	Hamate facet (of triquetrum) radioulnar width
HMD	Head (of femur) maximum anteroposterior thickness, measured parallel to plane of rim of femoral head epiphysis
HMW	Head (of femur) maximum mediolateral width, measured parallel to plane of rim of femoral head epiphysis
HShV	Head to shaft shape variable = Le / √ (HMW*HMD)
HSV	Head shape variable = DEW / DED
ICW	Intercondylar notch (of femur) mediolateral width (Sargis, 2002b, table 2, measurement 26)
IL	Ilium superoinferior length (Sargis, 2002b, table 2, measurement 2)
InD	Ilium neck (between acetabulum and posterior inferior iliac spine) anteroposterior thickness
Int-I	Intermembral index (100 H (humerus length + radius length) / (femur length + tibia length))
InW	Ilium neck (between acetabulum and posterior inferior iliac spine) mediolateral width
IsD	Ischium anteroposterior depth (Sargis, 2002b, table 2, measurement 8)
IsL	Ischium superoinferior length (Sargis, 2002b, tabe 2, measurement 7)
IspL	Ischial spine (of ischium) distance inferior to inferior margin of acetabulum
IspV	Ischial spine (of ischium) position variable = AcL / IspL
IW	Ilium width (Sargis, 2002b, table 2, measurement 3)
L#	Number of lumbar vertebrae, using rib definition
L%l	Index of lumbar length as a proportion of trunk length = 100 H lumbus / (thorax + lumbus)
LCD	Lateral condyle (of femur) anteroposterior depth (Sargis, 2002b, table 2, measurement 21)
LCL	Lateral condyle (of femur or tibia) proximodistal length (Sargis, 2002b, table 2, measurement 25 and 30)
LCW	Lateral condyle (of femur or tibia) mediolateral width (Sargis, 2002b, table 2, measurement 23 and 32)
LD	Lateral deviation (of mediolateral axis on distal humerus) of coronal plane in degrees
Le	Maximum length (Sargis, 2002a: measurement 5, 18, 26; Sargis, 2002b, table 2, measurement 1, 9, 29, 42)
LL	Lumbar region (rib-less vertebrae of trunk) length
LML	Lamina (of vertebrae) craniocaudal length
LSH	Lunate surface (of scaphoid) proximodistal length, perpendicular to LSL
LSL	Lunate surface (of scaphoid) maximum dorsoventral length
LTL	Lesser trochanter (of femur) mediolateral length (Sargis, 2002b, table 2, measurement 13)
LTP	Lesser trochanter (of femur) proximodistal position (Sargis, 2002b, table 2, measurement 27)
LTPV	Lesser trochanter (of femur) position variable = LTP / femur length
Ltr-I	Limb-trunk index = 50 H (length of humerus + radius + femur + tibia) / trunk length
MCD	Medial condyle (of femur) anteroposterior depth (Sargis, 2002b, table 2, measurement 20)
MCL	Medial condyle (of femur or tibia) proximodistal length (Sargis, 2002b, table 2, measurement 24 and 31)
MCW	Medial condyle (of femur or tibia) mediolateral width (Sargis, 2002b, table 2, measurement 22 and 33)
MH	Maximum dorsoventral height (of atlas)

TABLE A-II-1.— Cont'd.

Abbrev.	Measurement
MML	Medial malleolus proximodistal length (Sargis, 2002b, table 2, measurement 37)
MMW	Medial malleolus mediolateral width (Sargis, 2002b, table 2, measurement 38)
MSD	Mid-shaft dorsoventral or anteroposterior depth (unless otherwise specified in table footnotes; Sargis, 2002b, table 2, measurement 16)
MSW	Mid-shaft mediolateral or radioulnar width (unless otherwise specified in table footnotes; Sargis, 2002a, table 2, measurement 8; Sargis, 2002b, table 2, measurement 15)
MW	Maximum mediolateral width (of atlas)
NcD	Notch (of ulna) dorsoventral depth (Sargis, 2002a, table 2, measurement 24)
NcL	Notch (of ulna) proximodistal length (Sargis, 2002a, table 2, measurement 25)
NkL	Neck (of rib) length, measured between lateral edge of tubercle and lateral edge of head
NL	Neck (of radius) proximodistal length (Sargis, 2002a, table 2, measurement 27)
NSV	Notch (of ulna) shape variable = Le / √ (PNW H NcL)
OL	Olecranon process (of ulna) proximodistal length (Sargis, 2002a, table 2, measurement 19)
PAW	Proximal articular surface (of humerus) mediolateral width (Sargis, 2002a, table 2, measurement 6)
PCD	Proximal carpal articular facet (of hamate) dorsoventral depth
PCV	Proximal carpal articular facet (of hamate) shape variable = PCW / PCD
PCW	Proximal carpal articular facet (of hamate) radioulnar width
PD	Pubis dorsoventral depth (Sargis, 2002b, table 2, measurement 6)
PED	Proximal end dorsoventral or anteroposterior depth (unless otherwise specified in table footnote; Sargis, 2002a, table 2, measurement 7, 33; Sargis, 2002b, table 2, measurement 35, 44)
PEW	Proximal end mediolateral or radioulnar width (unless otherwise specified in table footnotes; Sargis, 2002a, table 2, measurement 28; Sargis, 2002b, table 2, measurement 34)
PfD	Pisiform facet (of triquetrum) dorsoventral depth
PfW	Pisiform facet (of triquetrum) radioulnar width
PGL	Patellar groove (of femur) proximodistal length (Sargis, 2002b, table 2, measurement 17)
PgV	Peroneous longus tendon groove (of cuboid) variable = PtgW / GM
PGW	Patellar groove (of femur) mediolateral width (Sargis, 2002b, table 2, measurement 18)
PNW	Proximal end of notch (of ulna) mediolateral width
PtgW	Peroneous longus tendon groove (of cuboid) proximodistal width
PTW	Proximal end of trochlea (of ulna) mediolateral width (Sargis, 2002a, table 2, measurement 20)
RFL	Radial facet (of ulna) proximodistal length (Sargis, 2002a, table 2, measurement 21)
RFV	Radial facet (of ulna) variable = RFL / RFW
RFW	Radial facet (of ulna) mediolateral width (Sargis, 2002a, table 2, measurement 22)
RRL	Radial head rim proximodistal length (Sargis, 2002a, table 2, measurement 29)
RSD	Radial surface (of scaphoid) maximum dorsoventral depth
RSV	Radial head size variable = Le / √ (PEW H PED)
RSW	Radial surface (of scaphoid) maximum mediolateral width
Rt-I	Radiotibial index = 100 H radius length / tibia length
S-L	Sacrum length
S#	Number of sacral vertebrae
S%l	Index of sacral length as a proportion of trunk length = 100 H sacrum / (thorax + lumbus)
ScT	Scaphoid tubercle proximodistal length
SL	Scapula length measured along inferior margin of scapular blade between inferior angle and inferior border of glenoid fossa (Sargis, 2002a, table 2, measurement 1)
SND	Superoinferior thickness of scapula measured just medial to glenoid and coracoid at deepest point of scapular notch
SPL	Spinous process length measured parallel to process on ventral edge (if angled) starting from lamina
SSV	Shaft shape variable = Le / √ (MSW H MSD)

TABLE A-II-1.— Cont'd.

Abbrev.	Measurement
StL	Styloid process (of ulna and radius) proximodistal length (Sargis, 2002a, table 2, measurement 23 and 30)
T-L	Length of thoracic region (rib-bearing vertebrae)
T%l	Index of thorax length as a proportion of trunk length = 100 H thorax / (thorax + lumbus)
TAD	Tibial astragalar articular surface anteroposterior depth (Sargis, 2002b, table 2, measurement 40)
TAW	Tibial astraglar articular surface mediolateral width (Sargis, 2002b, table 2, measurement 39)
TbCL	Tibial crest proximodistal length (Sargis, 2002b, table 2, measurement 41)
TH	Trochlea (of humerus) proximodistal height (Szalay and Dagosto, 1980, TH; Sargis, 2002a, table 2, measurement 12)
Th#	Number of thoracic vertebrae (rib-bearing vertebrae)
TL	Trochlea (of humerus) anteroposterior length (Szalay and Dagosto, 1980, TL; Sargis, 2002a, table 2, measurement 14)
TPL	Transverse process of vertebra length: for atlas and other cervical vertebrae measured from edge of vertebral artery foramen (foramen transversarium); for other vertebrae measured from lateral edge of vertebral body
TrL	Triquetrum proximodistal length
TrL-V	Triquetrum proximodistal length variable = TrL / GM
TrW	Triquetrum maximum radioulnar width
TTL	Third trochanter (of femur) mediolateral length (Sargis, 2002b, table 2, measurement 14)
TTP	Third trochanter (of femur) proximodistal position (Sargis, 2002b, table 2, measurement 28)
TW	Trochlea (of humerus) mediolateral width (Szalay and Dagosto, 1980, TW; Sargis, 2002a, table 2, measurement 10)
UfD	Ulnar facet (of triquetrum) depth
UfW	Ulnar facet (of triquetrum) width
vCW	Ventral vertebral canal mediolateral width (of atlas) measured between articular facets for occiput and axis
VL	Ventral side, craniocaudal length (of anterior or ventral arch of atlas)

TABLE A-II-2.— Measurements (mm) and counts in the vertebral column of plesiadapiforms and select other mammals. Abbreviations are explained in Table A-II-1. These data are analyzed in Figure 68.

Taxon	Specimen	DpV	AcV	T#	L#	S#	Ca#	C-L	Th-L	L-L	S-L	Ca-L	C%l	T%l	L%l	S%l	Ca%l
Plesiadapis cookei	UM 87990	11?	12?	13?	6?	3	>20	43.7	113.9	92.5	31.6	154.7	21	55	45	15	75
Ignacius clarksforkensis	UM 82616	—	11?	12?	7?	3	>20	23.3	58.6	51.3	18.3	92.6	21	53	47	17	84
Tupaia glis	UMMZ 118389	10	9	13	6	3	24	15.4	43.9	41.5	13.1	56.7	18	51	49	15	66
Cynocephalus volans	USNM 56530	9	22	14	8	3-4	18	73.0	118.1	92.4	32.8	158.7	35	56	44	16	75
Cebuella pygmaea	UMMZ 160146	10	10	12	7	3	21	13.8	28.3	32.9	8.9	65.3	23	46	54	15	107
Saguinus mystax	UMMZ 160148	10	10	12	7	3	28	31.7	62.4	68.1	17.3	112.9	24	48	52	13	87
Saguinus oedipus	UMMZ 156437	10	10	12	7	3	32	23.9	62.6	67.5	16.9	117.1	18	48	52	13	90
Callimico goeldii	UMMZ 160149	—	10	12	8	3	29	28.6	59.9	79.2	16.9	106.1	21	43	57	12	76
Saimiri sciureus	UMMZ 122657	11	11	12	7	3	34	29.0	71.8	96.9	25.3	125.7	17	43	57	15	74
Eulemur fulvus	UMMZ 160910	10	11	12	7	3	19	46.5	102.5	104.7	31.8	198.1	22	49	51	15	96
Galago senegalensis	UMMZ 113351	11	11	12	6	3	26	23.1	45.5	40.0	14.9	100.5	27	53	47	17	118
Tarsius philippensis	UMMZ 95741	10	11	12	7	3	26	17.2	22.8	23.6	9.6	69.1	37	49	51	21	149
Sciurus niger	UMMZ TC 269	9	9	12	7	3	26	30.3	75.7	73.8	23.8	66.3	20	51	49	16	44
Spermophilus mexicanus	UMR 1716	9	9	11	7	3	22	15.0	37.6	35.7	11.7	35.4	20	51	49	16	48
Petaurus breviceps	UMMZ 160143	10	11	12	7	2	23	15.0	39.1	45.3	9.1	77.9	18	46	54	11	92
Trichosurus vulpecula	UMMZ 157192	10	11	13	6	2	27	52.0	140.9	109.2	26.2	134.7	21	56	44	10	54

TABLE A-II-3.— Measurements (mm) of plesiadapid atlantes. Abbreviations are explained in Table A-II-1. Number in parentheses following USNM 442229 is a unique identifier assigned by P. Houde during preparation. In cases where one half of an atlas is broken, the mediolateral width of the intact half was doubled to generate MW.

Taxon	Specimen	MW	MH	CH	vCW	dCW	crIW	caIW	DL	VL	TPL
P. cookei	UM 87990 (Fig. 29A)	24.50	12.60	7.80	6.03	8.44	17.20	12.38	4.70	4.40	5.40
N. intermedius	USNM 442229 (138)	13.12	6.99	5.65	3.36	5.21	10.22	6.37	2.21	1.38	2.66
N. gidleyi	AMNH 17388	—	—	—	—	—	10.65	7.15	—	1.83	—
N. gidleyi	AMNH 17379	16.40	8.52	6.13	4.39	6.36	11.55	7.67	2.76	2.08	3.75

TABLE A-II-4.— Measurements (mm) of plesiadapid cervical vertebrae. Abbreviations are explained in Table A-II-1. Numbers in parentheses following USNM 442229 are unique identifiers assigned by P. Houde during preparation. For vertebrae, '*P*' of PEW and PED refers to the cranial end of the element, whereas '*D*' of DEW and DED refers to the caudal end.

Taxon	Specimen	Position	Le	PEW[a]	PED	DEW	DED	CH	CW	LML	SPL	TPL
P. cookei	UM 87990 (Fig. 29B)	C2	11.90 (9.45)	11.16	4.20	7.12	3.62	5.56	5.40	—	4.92	—
P. cookei	UM 87990 (Fig. 29C)	C3?	6.33	6.74	3.11	7.92	3.75	4.27	5.27	5.05	1.05	5.78
P. cookei	UM 87990 (Fig. 29D)	C4?	5.92	7.43	2.57	7.99	3.13	—	—	—	—	—
P. cookei	UM 87990 (Fig. 29E)	C6	5.66	7.59	2.91	7.57	3.67	4.4	6.54	—	—	—
N. intermedius	USNM 442229 (134)	C2	6.70 (5.04)	6.49	2.05	4.66	2.25	3.62	4.32	—	—	3.29
N. intermedius	USNM 442229 (144)	C3?	3.27	3.72	1.70	3.88	1.92	2.85	4.5	—	0.70	—
N. intermedius	USNM 442229 (135)	C6	3.60	3.65	1.69	3.54	1.63	3.06	4.63	1.92	0.80	—
N. gidleyi	AMNH 17388	C2	? (5.39)	—	—	4.30	—	—	—	—	—	—
N. gidleyi	AMNH 17388	C3	3.86	—	—	4.50	—	—	—	—	—	—
N. gidleyi	AMNH 17388	C4	3.73	—	—	—	—	—	—	—	—	—
N. gidleyi	AMNH 17379	7?	5.01	4.19	1.95	4.97	2.58	—	—	—	—	—

TABLE A-II-5.— Measurements of plesiadapid thoracic and lumbar vertebrae. Abbreviations are explained in Table A-II-1. Numbers in parentheses following USNM 442229 are unique identifiers assigned by P. Houde during preparation. For vertebrae, '*P*' of PEW and PED refers to the cranial end of the element, while '*D*' of DEW and DED refers to the caudal end. Measurements are in mm.

Taxon	Specimen	Position	Le	PEW	PED	DEW	DED	CH	CW	LML	SPL	SPW	TPL	APL
P. cookei	UM 87990 (Fig. 30A)	T1?	6.59	7.45	3.07	9.24	3.46	—	—	—	—	—	—	—
P. cookei	UM 87990 (Fig. 30B)	T2?	—	6.14	2.80	—	—	3.90	4.30	5.93	—	—	—	—
P. cookei	UM 87990 (Fig. 30C)	T3?	8.45	6.11	3.25	8.00	3.32	—	4.65	7.44	—	—	—	—
P. cookei	UM 87990 (Fig. 30D)	T4?	9.01	—	—	7.34	4.57	—	—	—	—	—	—	—
P. cookei	UM 87990 (Fig. 30E)	T5?	8.80	6.80	5.20	7.90	5.24	—	—	—	—	—	5.50	—
P. cookei	UM 87990 (Fig. 30E)	T6?	8.55	6.40	4.70	7.71	5.35	—	—	—	—	—	5.30	—
P. cookei	UM 87990 (Fig. 30F)	T7?	8.00	5.67	4.69	—	5.25	—	4.77	—	—	—	—	—
P. cookei	UM 87990 (Fig. 30G)	T8?	8.94	5.86	4.80	—	4.78	—	6.00	—	—	—	5.00	—
P. cookei	UM 87990 (Fig. 30H)	T9?	8.86	5.88	4.94	7.24	4.54	—	5.39	6.62	—	3.62	5.10	—
P. cookei	UM 87990 (Fig. 30I)	T10?	9.13	6.30	4.34	8.53	4.19	4.00	4.04	7.60	4.90	4.14	3.51	—
P. cookei	UM 87990 (Fig. 30J)	T12?	10.13	—	—	8.34	5.79	—	4.60	8.45	—	—	—	—
P. cookei	UM 87990 (Fig. 30K)	T13?	10.29	7.57	4.62	8.29	—	3.78	—	7.86	4.80	6.46	—	—
N. intermedius	USNM 442229 (146)	T1?	—	—	—	3.62	1.95	2.60	—	2.45	—	1.62	—	—
N. intermedius	USNM 442229 (145)	T7?	4.20	3.15	1.93	3.63	1.93	2.73	3.43	3.16	>2.40	1.28	2.71	—
N. intermedius	USNM 442229 (136)	T12?	5.24	3.46	2.21	4.13	2.23	2.42	3.03	3.80	—	2.94	—	1.30
N. intermedius	USNM 442229 (148)	T13?	5.68	3.6	2.46	4.48	2.80	2.32	3.11	3.95	2.37	2.30	—	2.78
N. gidleyi	AMNH 17379	T1?	5.35	4.04	2.63	5.10	2.80	2.98	2.92	4.53	2.49	1.20	1.43	—
N. gidleyi	AMNH 17379	T2?	4.90	3.64	2.52	4.32	2.60	2.90	2.95	—	—	1.12	2.36	—
N. gidleyi	AMNH 17379	T12?	6.49	3.87	2.50	5.00	2.88	2.80	—	5.12	—	—	—	—
N. gidleyi	AMNH 17379	T13?	6.57	4.20	2.50	—	2.80	2.80	3.30	5.49	—	3.64	—	3.61
P. cookei	UM 87990 (Fig. 31A)	L1?	11.60	7.40	4.97	8.10	5.16	—	—	8.70	5.42	7.80	—	5.20
P. cookei	UM 87990 (Fig. 31B)	L3?	13.06	7.57	5.23	8.46	5.30	4.16	3.80	10.6	5.50	7.40	—	4.41
P. cookei	UM 87990 (Fig. 31C)	L4?	13.26	7.50	5.60	8.10	—	—	—	10.8	—	—	—	—
P. cookei	UM 87990 (Fig. 31D)	L5?	—	7.74	6.30	—	—	4.12	3.50	9.10	6.98	6.20	—	—
P. cookei	UM 87990 (Fig. 31E)	L6?	14.03	8.12	6.05	9.98	6.24	—	—	11.60	—	—	—	—
P. cookei	UM 87990 (Fig. 31F)	L7?	14.60	10.70	6.30	11.55	7.00	—	—	10.10	—	—	—	—
N. intermedius	USNM 442229 (137)	L1?	5.93	4.10	2.46	4.71	2.78	2.50	3.31	4.97	2.90	2.27	—	2.12
N. intermedius	USNM 442229 (107)	L7?	7.28	4.76	3.12	5.28	3.42	2.30	3.30	4.46	4.70	2.48	4.80	—
N. gidleyi	AMNH 17379	L1?	7.24	4.74	3.00	5.12	3.40	2.70	3.40	6.13	—	—	—	4.10
N. gidleyi	AMNH 17379	L2?	7.76	5.42	3.62	5.10	3.42	—	3.60	6.90	—	—	—	>2.70
N. gidleyi	AMNH 17379	L3?	8.30	5.20	3.13	5.46	3.26	2.53	3.75	7.35	3.10	~4.30	—	>2.50
N. gidleyi	AMNH 17379	L6?	9.30	5.63	3.93	5.42	3.75	2.94	3.90	7.56	—	—	—	—

TABLE A-II-6.— Measurements (mm) of plesiadapid sacral vertebrae. The sacrum of UM 87990 is illustrated in Figure 32. Abbreviations are explained in Table A-II-1. Number in parentheses following USNM 399898 is unique identifier assigned by P. Houde during preparation. For vertebrae, '*P*' of PEW and PED refers to the cranial end of the element, whereas '*D*' of DEW and DED refers to the caudal end.

Taxon	Specimen	Position	Le	PEW	PED	DEW	DED	CH	CW	LML	SPL	TPL
P. cookei	UM 87990	S1	11.80	10.70	4.12	7.90	—	—	—	8.20	>4.25	6.00
P. cookei	UM 87990	S2	9.60	8.30	—	7.60	—	—	—	9.50	—	5.60
P. cookei	UM 87990	S3	10.2	7.60	—	7.80	4.02	—	—	9.90	>4.50	4.60
N. intermedius	USNM 399898 (72)	S1	6.10	4.55	2.98	3.74	—	2.00	3.10	4.80	>2.65	3.60
N. intermedius	USNM 399898 (72)	S2	6.50	3.82	—	3.71	2.40	—	—	5.03	—	3.00
N. intermedius	USNM 399898 (72)	S3	6.10	3.71	2.60	3.90	2.74		1.30	—	—	1.90
N. gidleyi	AMNH 17379	S1	6.92	6.82	3.30	4.78	—	—	3.35	4.45	—	5.67
N. gidleyi	AMNH 17379	S2	7.17	4.84	—	4.64	—	—	—	6.98	—	4.69
N. gidleyi	AMNH 17379	S3	6.55	4.88	—	5.06	2.8	1.75	2.70	—	—	2.22

TABLE A-II-7 — Measurements (mm) of plesiadapid sacra. Abbreviations are explained in Table A-II-1. Number in parentheses following USNM 399898 is a unique identifier assigned by P. Houde during preparation. For vertebrae, '*P*' of PEW refers to the cranial end of the element, whereas '*D*' of DEW refers to the caudal end.

Taxon	Specimen	Le	PEW	DEW	LML	AFL	AFW
P. cookei	UM 87990	32.96	21.70	—	30.50	21.48	6.50
N. intermedius	USNM 399898 (72)	19.25	11.73	—	—	9.73	4.04
N. gidleyi	AMNH 17379	21.87	17.97	—	—	11.86	4.61

TABLE A-II-8.— Measurements (mm) of plesiadapid caudal vertebrae. Abbreviations are explained in Table A-II-1. Numbers in parentheses following USNM 442229 are unique identifiers assigned by P. Houde during preparation. For vertebrae, '*P*' of PEW and PED refers to the cranial end of the element, whereas '*D*' of DEW and DED refers to the caudal end.

Taxon	Specimen	Position	Le	PEW	PED	DEW	DED	CH	CW	LML	TPL
P. cookei	UM 87990 (Fig. 33A)	Ca1	9.70	—	—	—	—	1.40	2.70	7.57	6.90
P. cookei	UM 87990 (Fig. 33B)	Ca4?	13.80	5.60	5.60	5.26	5.55	—	2.02	—	—
P. cookei	UM 87990 (Fig. 33C)	Ca6	21.30	6.80	5.70	7.90	5.80	—	—	—	—
P. cookei	UM 87990 (Fig. 33D)	Ca7	24.72	7.30	5.96	7.98	5.70	—	—	—	2.18
P. cookei	UM 87990 (Fig. 33E)	Ca8?	>22.79	7.06	5.14	—	—	—	—	—	—
P. cookei	UM 87990 (Fig. 33F)	Ca9?	25.46	6.30	5.60	—	—	—	—	—	—
P. cookei	UM 87990 (Fig. 33G)	Ca10?	>25.41	—	—	—	—	—	—	—	—
P. cookei	UM 87990 (Fig. 33H)	Ca11?	26.70	5.30	4.60	—	—	—	—	—	1.38
P. cookei	UM 87990 (Fig. 33I)	Ca12?	27.80	5.89	4.95	5.27	4.90	—	—	—	0.83
P. cookei	UM 87990 (Fig. 33J)	Ca13?	26.00	—	—	4.93	4.14	—	—	—	—
P. cookei	UM 87990 (Fig. 33K)	Ca14?	>21.40	—	—	4.50	4.10	—	—	—	—
P. cookei	UM 87990 (Fig. 33L)	Ca15?	21.90	3.57	3.45	3.80	3.34	—	—	—	—
P. cookei	UM 87990 (Fig. 33M)	Ca16?	20.88	3.09	3.13	3.43	3.09	—	—	—	—
P. cookei	UM 87990 (Fig. 33N)	Ca17?	19.85	3.00	2.96	3.05	2.90	—	—	—	—
P. cookei	UM 87990 (Fig. 33O)	Ca18?	17.84	2.81	2.73	2.70	2.53	—	—	—	—
P. cookei	UM 87990 (Fig. 33P)	Ca19?	13.48	2.36	2.32	2.05	2.15	—	—	—	—
P. cookei	UM 87990 (Fig. 33Q)	Ca20?	11.48	2.12	1.97	1.84	1.63	—	—	—	—
N. intermedius	USNM 442229 (149)	Ca6	12.34	3.80	3.34	4.03	3.48	—	—	—	1.43
N. intermedius	USNM 442229 (138)	Ca7	12.84	3.80	3.67	3.53	3.97	—	—	—	1.17
N. intermedius	USNM 442229 (149)	Ca>7	12.60	—	—	—	—	—	—	—	—
N. intermedius	USNM 442229 (149)	Ca>7	8.12	1.70	1.70	—	—	—	—	—	—
N. intermedius	USNM 442229 (149)	Ca>7	12.40	—	—	—	—	—	—	—	—
N. intermedius	USNM 442229 (149)	Ca>7	—	—	—	2.30	2.70	—	—	—	—
N. intermedius	USNM 442229 (149)	Ca>7	—	2.12	2.50	—	—	—	—	—	—
N. gidleyi	AMNH 17379	Ca?1	6.32	3.99	2.98	4.37	3.35	1.48	2.08	4.50	—
N. gidleyi	AMNH 17379	Ca?2	6.35	4.20	2.90	4.80	2.67	1.43	1.99	5.83	—

TABLE A-II-9.— Measurements (mm) of *Plesiadapis cookei* sternebrae. Abbreviations are explained in Table A-II-1. Asterisk indicates an estimate.

Taxon	Specimen	Position	Le	PEW	PED	DEW	DED
P. cookei	UM 87990 (Fig. 34A)	Manubrium	17.27	18.60*	—	5.76	4.96
P. cookei	UM 87990 (Fig. 34B)	St2?	12.50	4.40	5.15	6.02	4.10
P. cookei	UM 87990 (Fig. 34C)	St3?	11.80	5.98	3.56	5.14	—
P. cookei	UM 87990 (Fig. 34D)	St4?	—	5.86	3.35	—	—
P. cookei	UM 87990 (Fig. 34E)	St5?	11.10	4.78	3.90	5.26	3.76

TABLE A-II-10.— Measurements (mm) of plesiadapid ribs. Abbreviations are explained in Table A-II-1. Length (*Le*) is measured between the rib tubercle and distal end. PEW refers to craniocaudal dimension of rib head. MSW refers to maximum diameter of rib shaft in vicinity of angle.

Taxon	Specimen	Number	Side	Le	PEW	PED	NkL	MSW	MSD	DEW	DED
P. cookei	UM 87990 (Fig. 35B)	a (2–9)	L	28.50	3.03	2.70	4.70	3.93	2.37	3.25	2.40
P. cookei	UM 87990	b (3–9)	L	>43.70	3.75	2.55	4.61	3.88	2.78	—	—
P. cookei	UM 87990	c (3–9)	L	—	3.67	3.60	3.83	>3.40	2.77	—	—
P. cookei	UM 87990	d (5–10)	L	—	3.38	2.63	3.10	—	—	—	—
P. cookei	UM 87990 (Fig. 35C)	e (6–10)	L	59.20	—	—	—	3.56	2.38	3.72	1.71
P. cookei	UM 87990	f (7–12)	L	>50.40	—	—	—	3.71	1.55	3.30	1.05
P. cookei	UM 87990 (Fig. 35A)	a (2–9)	R	—	3.23	2.80	4.85	3.86	2.44	—	—
P. cookei	UM 87990	g (?)	R	—	—	—	—	3.50	2.29	—	—
P. cookei	UM 87990	b (3–9)	R	—	3.50	2.27	4.40	—	—	—	—
P. cookei	UM 87990	c (3–9)	R	—	3.20	3.08	3.23	3.50	2.47	—	—
P. cookei	UM 87990	e (6–10)	R	—	3.09	1.80	2.87	—	—	—	—
P. cookei	UM 87990	h (11–13)	R	—	2.26	1.54	na	3.60	1.13	—	—
N. gidleyi	AMNH 17379	?	L	—	1.74	1.40	2.30	—	—	—	—
N. gidleyi	AMNH 17379	?	L	—	1.30	1.90	2.10	1.77	1.43	—	—
N. gidleyi	AMNH 17379	?	L	—	—	—	—	1.95	1.15	—	—
N. gidleyi	AMNH 17379	?	L	—	—	—	—	1.79	1.47	—	—
N. gidleyi	AMNH 17379	?	R	—	1.48	1.84	2.52	—	—	—	—

TABLE A-II-11.— Measurements (mm) of plesiadapid clavicles. Abbreviations are explained in Table A-II-1. UM 87990 is illustrated in Figure 36A. Width (e.g., *W* in PEW) is anteroposterior dimension of bone; depth (e.g., *D* in PED) is superior-inferior dimension of bone.

Taxon	Specimen	Le	PEW	PED	MSW	MSD	DEW	DED
P. cookei	UM 87990	32.50	3.60	4.30	2.90	4.90	3.50	6.80
N. gidleyi	AMNH 17388	17.09	—	1.62	—	2.44	—	3.45

TABLE A-II-12.— Measurements (mm) of plesiadapid scapulae. Abbreviations are explained in Table A-II-1. UM 87990 is illustrated in Figure 36B. Numbers in parentheses in column headers correspond to measurements in Sargis (2002a, table 2).

Taxon	Specimen	SL (1)	GW (4)	GD (3)	SND	CL	AD	AP	AL
P. cookei	UM 87990	49.00	7.70	10.70	11.70	3.90	11.10	5.80	4.50
cf. *P. churchilli*	SMM P77.33.517	—	4.61	7.69	—	—	—	—	—
N. intermedius	USNM 442229	—	3.42	5.10	5.03	2.17	4.73	0.00	3.31
N. gidleyi	AMNH 12379	—	4.13	—	6.05	—	—	—	—

TABLE A-II-13.— Measurements (mm) of the proximal end and shaft of plesiadapiform humeri. Abbreviations are explained in Table A-II-1. UM 87990 is illustrated in Figure 37. Numbers in parentheses in column headers correspond to measurements in Sargis (2002a, table 2). Asterisk indicates angle is probably distorted.

Taxon	Specimen	LD	Le (5)	PEW	PED (7)	PAW (6)	MSW (8)	MSD	DCL (17)	SSV
P. cookei	UM87990 (L)	32	75.24	13.90	10.80	10.50	7.85	6.73	29.70	2.34
P. cookei	UM87990 (R)	—	—	13.60	10.80	10.40	6.60	6.98	—	—
P. tricuspidens	MNHN BR 14522	—	—	—	—	—	7.10	7.69	—	—
P. tricuspidens	MNHN BR-03-L	34	70.40	13.43	11.45	9.91	8.96	8.02	30.25	2.12
P. tricuspidens	MNHN BR 12591	27	—	—	—	—	7.73	7.88	—	—
P. tricuspidens	MNHN BR 12590	29	—	—	—	—	8.09	7.05	—	—
P. tricuspidens	MNHN BR 12585	—	—	—	—	—	8.60	7.36	—	—
P. tricuspidens	MNHN R 405	55*	—	—	—	—	7.61	7.60	—	—
P. tricuspidens	Berru (M. Malfait)	34	—	—	—	—	—	8.99	—	—
P. tricuspidens	MNHN BR-04-L(a)	27	—	—	—	—	7.77	7.61	—	—
P. tricuspidens	MNHN BR-04-L(b)	37	71.93	12.04	10.50	9.61	8.58	7.66	26.78	2.18
P. tricuspidens	MNHN R 492	31	—	—	—	—	7.90	8.33		—
P. tricuspidens	MNHN R 442	22	—	—	—	—	7.60	6.96	—	—
P. tricuspidens	MNHN R 591	40	69.03	12.09	10.22	9.64	7.71	7.20	24.72	2.23
P. tricuspidens	MNHN R 148	23	—	—	—	—	7.91	7.11	—	—
cf. *P. remensis*	MNHN CR 208	23	—	—	—	—	—	—	—	—
cf. *Pl. daubrei*	UCMP 102829	28	—	—	—	—	8.59	—	—	—
P. rex	UM 64588	19	—	—	—	—	4.06	3.75	—	—
N. intermedius	USNM 42229	15	—	—	—	—	3.41	3.28	—	—
N. gidleyi	AMNH 17379	13	—	—	—	—	3.74	—	—	—
cf. *Pr. gaoi*	UALVP 49114	16	—	—	—	—	4.96	4.89	—	—
"*Nothodectes*"	AMNH 17379	19	38.71	7.98	5.45	~5.5	3.76	3.65	15.31	2.35
C. simpsoni	UM 101963	8	21.27	4.22	3.73	3.31	2.10	2.22	8.76	2.29

TABLE A-II-14.— Measurements (mm) of the distal end of plesiadapiform humeri. Abbreviations are explained in Table A-II-1. UM 87990 is illustrated in Figure 37. Numbers in parentheses in column headers correspond to measurements in Sargis (2002a, table 2). Capitulum width measurements (CaW) include the width of the lateral flange. Geometric mean (GM) is based on TW, TH, CaW, TL, CaL, and EEC only.

Taxon	Specimen	DEW (16)	CaH (13)	TW (10)	TH (12)	CaW (11)	TL (14)	CaL	EEC	GM
P. cookei	UM87990 (L)	22.80	6.40	5.84	4.33	8.75	6.63	6.35	8.05	6.49
P. cookei	UM87990 (R)	22.25	—	5.80	—	8.52	7.20	6.30	—	—
P. tricuspidens	MNHN BR 14522	18.25	5.54	4.65	3.99	6.51	5.59	4.16	6.00	5.06
P. tricuspidens	MNHN BR-03-L	20.35	5.52	4.60	3.16	8.16	7.09	4.85	7.68	5.61
P. tricuspidens	MNHN BR 12591	20.49	6.39	5.77	4.55	8.42	6.44	4.59	6.09	5.84
P. tricuspidens	MNHN BR 12590	—	5.63	4.53	3.87	8.66	6.56	4.88	—	—
P. tricuspidens	MNHN BR 12585	—	6.34	—	—	7.89	—	4.50	—	—
P. tricuspidens	MNHN R 405	23.75	5.67	6.65	5.40	9.47	7.19	4.47	7.22	6.55
P. tricuspidens	Berru (Mr Malfait)	20.38	5.69	6.03	4.94	7.68	6.70	4.14	6.65	5.90
P. tricuspidens	MNHN BR-04-L(a)	20.40	5.97	5.53	3.71	7.63	5.92	4.40	7.11	5.54
P. tricuspidens	MNHN BR-04-L(b)	19.29	—	6.40	4.20	—	7.07	—	6.13	—
P. tricuspidens	MNHN R 492	23.25	6.19	6.01	5.16	8.23	6.85	4.16	8.17	6.24
P. tricuspidens	MNHN R 442	20.71	5.76	5.39	4.26	8.51	—	4.36	6.28	—
P. tricuspidens	MNHN R 591	—	—	5.57	3.45	—	6.31	—	8.11	—
P. tricuspidens	MNHN R 148	—	—	5.22	3.57	—	6.47	—	7.01	—
cf. *P. remensis*	MNHN CR 208	16.74	5.02	4.17	3.73	7.03	5.81	3.42	5.80	4.82
cf. *Pl. daubrei*	UCMP 102829	22.92	6.55	6.51	5.06	8.87	6.81	6.13	7.84	6.76
P. rex	UM 64588	12.10	3.14	2.90	2.20	5.05	3.59	3.45	3.84	3.40
N. intermedius	USNM 442229	10.70	2.45	2.96	1.58	3.89	3.51	2.80	3.25	2.89
N. gidleyi	AMNH 17379	11.95	2.80	2.71	2.11	4.57	—	—	4.17	—
cf. *Pr. gaoi*	UALVP 49114	14.52	3.90	3.80	3.01	5.40	4.10	3.90	5.09	4.14
'*Nothodectes*'	AMNH 17379	11.21	3.25	3.30	2.97	3.95	3.84	3.42	3.80	3.53
C. simpsoni	UM 101963	7.23	1.69	1.55	1.09	2.60	1.88	1.34	3.12	1.80

TABLE A-II-15.— Measurements (mm) of the proximal end and shaft of plesiadapid radii. Abbreviations are explained in Table A-II-1. UM 87990 is illustrated in Figures 38A and 39. Numbers in parentheses in column headers correspond to measurements in Sargis (2002a, table 2).

Taxon	Specimen	PEW (28)	PED (33)	NL (27)	RRL (29)	Le (26)	MSD	MSW	BSV	SSV	RSV
P. cookei	UM 87990	8.60	6.73	10.10	3.56	76.30	3.56	5.62	0.25	2.84	2.31
N. intermedius	USNM 442229	4.05	3.10	4.45	1.90	32.84	1.82	2.69	0.27	2.70	2.23
N. gidleyi	AMNH 17379	4.45	3.59	4.80	1.92	—	1.91	2.69	0.21	—	—
Pr. gaoi	UALVP 49124 (DB 031)	4.89	3.77	5.74	2.87	—	—	—	0.26	—	—
P. tricuspidens	MNHN R 550	8.11	6.26	9.36	3.39	70.10	3.77	6.02	0.26	2.69	2.29
P. tricuspidens	MNHN BR 11399	7.51	5.50	9.70	3.33	—	—	—	0.31	—	—
P. tricuspidens	MNHN BR 5440	7.35	6.17	8.37	3.11	—	—	—	0.18	—	—
P. tricuspidens	MNHN R 597	7.55	6.22	8.70	3.23	—	—	—	0.19	—	—

TABLE A-II-16.— Measurements (mm) of the distal end of plesiadapid radii. Abbreviations are explained in Table A-II-1. UM 87990 is illustrated in Figures 38A and 39. Numbers in parentheses in column headers correspond to measurements in Sargis (2002a, table 2).

Taxon	Specimen	DEW (31)	DED (32)	StL (30)
P. cookei	UM 87990	9.09	6.82	1.57
N. intermedius	USNM 442229	~3.60	3.07	—
N. gidleyi	AMNH 17379	4.48	3.70	—
Pr. gaoi	UALVP 49124 (DB 031)	—	—	—
P. tricuspidens	MNHN R 550	8.69	6.27	0.99
P. tricuspidens	MNHN BR 11399	—	—	—
P. tricuspidens	MNHN BR 5440	—	—	—
P. tricuspidens	MNHN R 597	—	—	—

TABLE A-II-17.— Measurements (mm) and shape variables of plesiadapid ulnae. Abbreviations are explained in Table A-II-1. UM 87990 is illustrated in Figure 38B. Numbers in parentheses in column headers correspond to measurements in Sargis (2002a, table 2).

Taxon	Specimen	Le (18)	PTW (20)	RFL (21)	RFW (22)	NcL (25)	MSW	MSD	RFV	NSV	SSV
P. cookei	UM 87990 (L)	88.30	5.74	5.58	4.69	8.43	3.30	5.85	0.17	2.54	3.00
P. cookei	UM 87990 (R)	—	5.60	5.39	5.08	7.70	—	—	0.06	—	—
P. tricuspidens	MNHN BR-07-L	—	5.09	4.82	4.57	6.77	3.20	5.89	0.05	—	—
P. tricuspidens	MNHN BR 70713*	—	5.09	5.41	4.51	6.01	2.66	5.19	0.18	—	—
P. tricuspidens	MNHN R 411	—	5.43	5.94	5.49	8.34	3.11	6.61	0.08	—	—
P. tricuspidens	MNHN R 546	85.08	5.90	5.73	5.46	8.26	3.57	5.67	0.05	2.50	2.94
P. tricuspidens	MNHN R 443	—	5.81	5.42	4.78	7.78	3.39	6.46	0.12	—	—
P. tricuspidens	MNHN R 452	—	4.90	4.90	4.72	7.07	—	—	0.04	—	—
P. tricuspidens	MNHN R 1521*	—	4.28	4.60	4.27	6.88	2.35	4.41	0.08	—	—
P. tricuspidens	MNHN R 5196	—	4.61	4.40	4.19	6.80	—	—	0.05	—	—
P. tricuspidens	MNHN nn*	—	3.69	4.11	3.84	5.24	—	4.69	0.07	—	—
P. rex	UM 64588	—	3.00	2.87	2.54	4.30	1.49	3.35	0.12	—	—
N. intermedius	USNM 442229	41.20	2.72	2.30	2.06	3.74	1.30	2.94	0.11	2.56	3.05
N. gidleyi	AMNH 117379	—	3.22	2.80	2.31	4.96	1.49	3.16	0.19	—	—

TABLE A-II-18.— Measurements (mm) of plesiadapid ulnae. Abbreviations are explained in Table A-II-1. UM 87990 is illustrated in Figure 38B. Numbers in parentheses in column headers correspond to measurements in Sargis (2002a, table 2).

Taxon	Specimen	OL (19)	StL (23)	NcD (24)
P. cookei	UM 87990 (L)	—	2.80	3.80
P. cookei	UM 87990 (R)	—	—	3.30
P. tricuspidens	MNHN BR-07-L	7.32	—	2.48
P. tricuspidens	MNHN BR 70713	—	—	1.88
P. tricuspidens	MNHN R 411	—		2.47
P. tricuspidens	MNHN R 546	9.87	—	3.17
P. tricuspidens	MNHN R 443	—	—	2.54
P. tricuspidens	MNHN R 452	7.77	—	2.11
P. tricuspidens	MNHN R 1521	—	—	1.67
P. tricuspidens	MNHN R 5196	—	—	—
P. tricuspidens	MNHN nn	—	—	1.41
P. rex	UM 64588	6.16	—	1.94
N. intermedius	USNM 442229	5.13	1.21	1.60
N. gidleyi	AMNH 117379	4.54	—	1.74

TABLE A-II-19.— Measurements (mm) of plesiadapid scaphoids. Abbreviations are explained in Table A-II-1. UM 87990 is illustrated in Figures 40A and 41. Le* is the maximum length between the medial and lateral margins of the bone.

Taxon	Specimen	Le*	LSL	LSH	RSW	RSD	TL
P. cookei	UM 87990	9.78	4.03	1.42	5.62	4.1	5.03
N. intermedius	USNM 442229	4.21	1.72	0.72	2.44	1.65	1.90

TABLE A-II-20.— Measurements (mm) of plesiadapid triquetra. Abbreviations are explained in Table A-II-1. UM 87990 is illustrated in Figures 40C and 41. Asterisk (*) indicates measurement may be inaccurate because of a broken facet.

Taxon	Specimen	TrW	TrL	PfW	PrfD	PufD	UfW	UfD	HfW	HfD	GM	TrL-V
P. cookei	UM 87990	5.43	2.17	4.01	1.72	1.93	3.15	2.24	2.83	3.17	2.85	0.76
P. tricuspidens	MNHN R 5320	6.07	2.85	4.00	1.11	1.90	2.74	2.01*	3.06	2.90	2.99	0.95

TABLE A-II-21.— Measurements (mm) of plesiadapid pisiforms. Abbreviations are explained in Table A-II-1. UM 87990 is illustrated in Figure 40D.

Taxon	Specimen	Le	PEW	TfW	TrfD	TufD	UfD	MSW	MSD	DEW	DED	SSV	BSV
P. cookei	UM 87990	8.87	2.80	3.23	1.78	1.95	2.41	1.89	2.21	2.96	4.22	1.47	1.28
N. intermedius	USNM 442229	3.60	1.52	1.54	0.72	1.11	1.17	1.16	0.84	1.26	1.61	1.29	1.11

TABLE A-II-22.— Comparisons of UM 87990 carpal-metacarpal articular areas (mm^2). Carpal areas represent the trapezoid distal facet for metacarpal (*MC*) II, reconstructed capitate distal facet for metacarpal III, and hamate distal facet for metacarpal IV and V, respectively. These carpal areas are then compared to two different 'sets' of metacarpals preserved with UM 87990 that differ in size and morphology. The rationale for this comparison is that corresponding facets of a carpal and metacarpal should be closer in size (area) when both bones are from the same individual or species than if they come from two different individuals or species. Note that the absolute differences (*diff*) in articular area for 'set 1' metacarpals are less than the absolute differences in articular area for 'set 2' metacarpals, suggesting that 'set 1' metacarpals provide a better fit to the carpals attributed to *P. cookei*.

MC	Carpal area	'Set 1' area	'Set 1' diff	'Set 2' area	'Set 2' diff
II	8.2	7.7	0.5	9.5	1.3
III	~6.0	7.1	1.1	8.5	2.5
IV	10.7	6.8	2.1	8.5	5.3
V		6.0		7.5	

TABLE A-II-23.— Measurements (mm) of plesiadapid hamates. Abbreviations are explained in Table A-II-1. UM 87990 is illustrated in Figure 43C. Le* is proximodistal length measured on the radial side of the bone.

Taxon	Specimen	Le*	DEW	DED	PCW	PCD	CfD	AfW	DEV	PCV
P. cookei	UM 87990 (L)	3.30	3.92	3.42	4.15	2.52	2.07	1.38	1.15	1.65
P. tricuspidens	MNHN R 5321 (L)	3.46	3.84	3.22	3.57	2.15	2.06	—	1.19	1.66
N. intermedius	USNM 442229	1.93	2.26	1.54	2.29	1.4	1.4	0.57	1.47	1.64
N. intermedius	USNM 442229 (L)	1.97	2.24	1.43	2.35	1.38	1.23	0.55	1.57	1.70

TABLE A-II-24.— Measurements (mm) and shape variables of plesiadapid metacarpals. Abbreviations are explained in Table A-II-1. 'Set 1' metacarpals of UM 87990 are illustrated in Figure 41, and 'set 2' metacarpals of UM 87990 are illustrated in Figure 42. GM here is the geometric mean of Le, PEW, PED, MSW, MSD, DEW, and DED. Head shape variable HSV is DEW / DED. Shaft shape variable SSV is Le / √ (MSW * MSD).

Taxon	Specimen	Bone	Le	PEW	PED	MSW	MSD	DEW	DED	GM	HSV	SSV
P. cookei	UM 87990 set 1	L MC I	11.40	4.80	3.10	2.50	1.80	3.40	3.00	3.60	1.13	5.37
P. cookei	UM 87990 set 1	L MC II	17.00	2.70	4.00	2.50	2.20	3.90	3.50	3.90	1.11	7.25
P. cookei	UM 87990 set 1	R MC III	20.00	3.00	4.00	2.20	2.20	4.00	3.50	4.00	1.14	9.09
P. cookei	UM 87990 set 1	R MC IV	—	2.80	4.00	2.20	2.20	—	—	—	—	—
P. cookei	UM 87990 set 1	R MC V	15.65	3.32	2.82	2.18	2.10	4.23	3.52	3.73	1.20	7.31
P. cookei	UM 87990 set 2	L MC II	18.90	2.90	4.20	2.70	2.30	4.30	4.20	4.27	1.02	7.58
P. cookei	UM 87990 set 2	R MC III	23.20	2.70	4.40	2.30	2.10	4.20	4.00	4.18	1.05	10.56
P. cookei	UM 87990 set 2	L MC IV	23.70	3.00	4.20	2.30	2.10	4.20	4.00	4.23	1.05	10.78
P. cookei	UM 87990 set 2	R MC IV	23.80	3.10	4.40	2.40	2.10	4.30	4.10	4.34	1.05	10.60
P. cookei	UM 87990 set 2	R MC V	17.73	3.86	3.20	1.97	2.17	3.98	3.52	3.87	1.13	8.58
P. insignis	MNHN Menat	R MC III	11.70	—	—	—	—	—	—	—	—	—
P. insignis	MNHN Menat	R MC V	9.70	—	—	—	—	—	—	—	—	—
P. tricuspidens	MNHN R 5295	R MC III	21.10	2.70	4.10	2.50	2.30	4.40	3.70	4.17	1.19	8.80
P. tricuspidens	MNHN R 5364	R MC IV	24.70	3.20	3.80	2.70	2.40	4.50	3.50	4.37	1.29	9.70
P. tricuspidens	MNHN R 5305	R MC V	15.15	3.30	2.90	2.40	2.00	4.30	3.40	3.74	1.26	6.91
P. tricuspidens	MNHN R 5373	L MC V	13.00	3.30	2.70	2.20	1.80	3.60	2.80	3.34	1.29	6.53
P. tricuspidens	MNHN nn	L MC V	15.20	3.40	2.90	2.10	1.80	3.80	3.10	3.52	1.23	7.82
N. intermedius	USNM 442229	R MC I	6.64	2.54	1.61	1.27	1.03	1.84	1.71	1.96	1.08	5.81
N. intermedius	USNM 442229	R MC III	11.51	1.33	—	1.09	1.05	2.09	—	—	—	10.76
N. intermedius	USNM 442229	L MC V	8.70	1.93	1.58	1.08	1.01	2.13	1.75	1.95	1.22	8.33
N. gidleyi	AMNH 17379	L MC I	6.92	2.89	1.57	1.54	1.08	2.13	2.02	2.17	1.05	5.37
N. gidleyi	AMNH 17379	L MC III	12.02	1.61	1.88	1.13	1.02	2.14	1.63	2.04	1.31	11.20

TABLE A-II-25.— Shape variables of plesiadapid metacarpals expressed as proportional differences. Abbreviations are explained in Table A-II-1. Entries here are calculated from measurements in Table A-II-24. For example, variable 'V-Le' = Ln (Le / GM) = Ln (Le) - Ln (GM). Positive entries are larger than average for the bone in question, and negative entries are smaller than average.

Taxon	Specimen	Bone	V-Le	V-PEW	V-PED	V-MSW	V-MSD	V-DEW	V-DED
P. cookei	UM 87990 set 1	L MC I	1.153	0.288	-0.150	-0.365	-0.693	-0.057	-0.182
P. cookei	UM 87990 set 1	L MC II	1.472	-0.368	0.025	-0.445	-0.573	0.000	-0.108
P. cookei	UM 87990 set 1	R MC III	1.609	-0.288	0.000	-0.598	-0.598	0.000	-0.134
P. cookei	UM 87990 set 1	R MC V	1.434	-0.116	-0.280	-0.537	-0.574	0.126	-0.058
P. cookei	UM 87990 set 2	L MC II	1.488	-0.387	-0.017	-0.458	-0.619	0.007	-0.017
P. cookei	UM 87990 set 2	L MC III	1.714	-0.437	0.051	-0.597	-0.688	0.005	-0.044
P. cookei	UM 87990 set 2	L MC IV	1.723	-0.344	-0.007	-0.609	-0.700	-0.007	-0.056
P. cookei	UM 87990 set 2	R MC IV	1.702	-0.336	0.014	-0.592	-0.726	-0.009	-0.057
P. cookei	UM 87990 set 2	R MC V	1.522	-0.003	-0.190	-0.675	-0.579	0.028	-0.095
P. tricuspidens	MNHN R 5295	R MC III	1.621	-0.435	-0.017	-0.512	-0.595	0.054	-0.120
P. tricuspidens	MNHN R 5364	R MC IV	1.732	-0.312	-0.140	-0.482	-0.599	0.029	-0.222
P. tricuspidens	MNHN R 5305	R MC V	1.399	-0.125	-0.254	-0.444	-0.626	0.140	-0.095
P. tricuspidens	MNHN R 5373	L MC V	1.359	-0.012	-0.213	-0.418	-0.618	0.075	-0.176
P. tricuspidens	MNHN nn	L MC V	1.463	-0.035	-0.194	-0.517	-0.671	0.077	-0.127
N. intermedius	USNM 442229	R MC I	1.220	0.259	-0.197	-0.434	-0.643	-0.063	-0.136
N. intermedius	USNM 442229	L MC V	1.495	-0.010	-0.210	-0.591	-0.658	0.088	-0.108
N. gidleyi	AMNH 17379	L MC I	1.160	0.287	-0.324	-0.343	-0.698	-0.019	-0.072
N. gidleyi	AMNH 17379	L MC III	1.774	-0.237	-0.082	-0.591	-0.693	0.048	-0.224

TABLE A-II-26.— Measurements (mm) of plesiadapid proximal phalanges. Abbreviations are explained in Table A-II-1. Numbers in parentheses following USNM 442229 are unique identifiers assigned by P. Houde during preparation. Abbreviation: *Atd*, autopod (alternative states are 1, hand; or 2, foot).

Taxon	Specimen	Atd	Ray	Le	PEW	PED	MSW	MSD	DEW	DED	BSV	HSV	SSV
P. cookei	UM 87990 (Fig. 51A)	2	1	—	—	4.00	—	—	—	—	—	—	—
P. cookei	UM 87990 (Fig. 51B)	2	1	—	—	—	—	—	4.20	4.16	—	-0.01	—
P. cookei	UM 87990 (Fig. 51C)	2?	?	—	—	4.23	—	2.80	—	—	—	—	—
P. cookei	UM 87990 (Fig. 51D)	2?	?	—	4.69	3.90	2.17	2.85	—	—	-0.18	—	—
P. cookei	UM 87990 (Fig. 51E)	1?	?	—	—	—	—	—	3.36	2.37	—	—	—
P. cookei	UM 87990 (Fig. 51F)	2?	?	—	—	—	—	—	3.15	2.72	—	—	—
P. cookei	UM 87990 (Fig. 51G)	2?	?	—	—	—	—	—	—	2.81	—	—	—
P. cookei	UM 87990 (Fig. 52A)	1?	?	12.76	4.09	3.24	2.26	2.31	3.21	2.41	-0.23	0.29	1.72
P. cookei	UM 87990 (Fig. 52B)	1?	?	15.52	4.54	3.47	2.22	2.58	3.65	2.53	-0.27	0.37	1.87
P. cookei	UM 87990 (Fig. 52C)	2?	?	15.23	4.52	4.11	2.33	2.87	3.47	2.84	-0.09	0.20	1.77
P. cookei	UM 87990 (Fig. 52D)	2?	?	17.28	4.67	3.89	2.48	2.78	3.67	2.94	-0.18	0.22	1.88
P. cookei	UM 87990 (Fig. 52E)	2?	?	17.28	4.68	3.90	2.37	2.95	3.66	2.97	-0.18	0.21	1.88
P. cookei	UM 87990 (Fig. 52F)	2?	?	17.67	4.76	4.49	2.47	2.87	3.87	2.76	-0.06	0.34	1.89
?P .tricuspidens	MNHN R 503	2?	?	17.32	4.90	3.68	3.45	2.91	3.61	2.56	-0.29	0.34	1.70
P .tricuspidens	MNHN 'Divers Coll.'	1?	?	14.25	4.71	3.54	3.27	2.74	3.45	2.71	-0.29	0.24	1.56
P .tricuspidens	MNHN R 5303	1	?	14.17	4.57	3.37	2.65	2.25	3.58	2.61	-0.30	0.31	1.76
P .tricuspidens	MNHN R 5297	1	?	15.63	4.86	4.18	3.03	2.60	3.67	3.05	-0.15	0.18	1.72
P .tricuspidens	MNHN BR 14538	1?	1	12.87	4.40	3.72	2.38	2.58	3.01	2.66	-0.17	0.12	1.65
P .tricuspidens	MNHN R 5315	2?	1	12.41	4.81	4.18	2.42	2.58	3.47	3.12	-0.14	0.10	1.60
P .tricuspidens	Pellouin Coll (CM 091)	2?	?	16.97	4.57	3.51	2.73	2.56	3.31	2.33	-0.26	0.35	1.86
P .tricuspidens	Pellouin Coll. Nn	1?	?	14.23	4.54	3.73	2.79	2.51	3.23	2.43	-0.19	0.29	1.68
P.insignis	MNHN Menat specimen	1	3	8.60	—	—	—	—	—	—	—	—	—
P.insignis	MNHN Menat specimen	1	5	7.50	—	—	—	—	—	—	—	—	—
P.insignis	MNHN Menat specimen	2	3	9.70	—	—	—	—	—	—	—	—	—
P.insignis	MNHN Menat specimen	2	4	9.90	—	—	—	—	—	—	—	—	—
P.insignis	MNHN Menat specimen	2	5	9.20	—	—	—	—	—	—	—	—	—
N. intermedius	USNM 442229 (143a)	1?	?	7.76	2.43	1.96	1.38	1.22	1.95	1.19	-0.21	0.49	1.79
N. intermedius	USNM 442229 (143b)	2?	?	8.21	2.43	1.96	1.30	1.29	1.88	1.20	-0.21	0.45	1.85
N. intermedius	USNM 442229 (143c)	2?	?	8.73	2.40	1.81	1.30	1.20	1.83	1.26	-0.29	0.37	1.95
N. intermedius	USNM 442229 (143d)	2?	1	6.79	2.38	—	1.40	1.46	1.74	1.43	—	0.20	1.56
N. intermedius	USNM 442229a	2?	1	6.79	2.47	2.20	1.47	1.33	1.92	1.32	-0.11	0.37	1.58
N. intermedius	USNM 442229b	2?	?	9.21	2.58	2.16	1.43	1.38	1.87	1.18	-0.18	0.46	1.88
N. gidleyi	AMNH 17379	1	?	9.20	2.46	2.13	1.48	1.36	1.82	1.34	-0.15	0.30	1.87
N. gidleyi	AMNH 17379	1?	?	8.56	2.68	2.06	1.56	1.33	2.08	1.39	-0.27	0.41	1.78
N. gidleyi	AMNH 17379	?	1	6.24	2.04	1.63	0.98	1.12	1.53	1.31	-0.22	0.16	1.79

TABLE A-II-27.— Measurements (mm) of plesiadapid intermediate phalanges. Abbreviations are explained in Table A-II-1. Numbers in parentheses following USNM 442229 are unique identifiers assigned by P. Houde during preparation. Abbreviation: *Atd*, autopod (alternative states are 1, hand; or 2, foot).

Taxon	Specimen	Atd	Ray	Le	PEW	PED	MSW	MSD	DEW	DED	BSV	HSV	SSV
P. cookei	UM 87990 (Fig. 53A)	1?	?	—	3.65	4.06	1.73	2.93	—	—	0.11	—	—
P. cookei	UM 87990 (Fig. 53B)	1?	?	12.05	3.93	4.03	1.70	2.81	3.02	3.27	0.03	-0.08	1.71
P. cookei	UM 87990 (Fig. 53C)	1?	?	—	3.40	3.43	1.70	2.36	—	—	0.01	—	—
P. cookei	UM 87990 (Fig. 53D)	1?	?	—	3.45	3.53	1.69	2.54	—	—	0.02	—	—
P. cookei	UM 87990 (Fig. 53E)	2?	?	13.56	3.88	3.95	1.94	2.56	3.10	3.17	0.02	-0.02	1.81
P. cookei	UM 87990 (Fig. 53F)	2?	?	13.24	3.86	4.16	1.82	2.95	2.89	3.2	0.07	-0.10	1.74
P. cookei	UM 87990 (Fig. 53G)	2?	?	13.25	3.85	4.18	1.85	2.83	3.06	3.45	0.08	-0.12	1.76
P. tricuspidens	MNHN R 5296	2	?	13.88	4.17	3.85	2.10	2.82	2.87	3.49	-0.08	-0.20	1.74
P. tricuspidens	MNHN BR nn	2?	?	12.26	3.68	3.30	1.95	2.23	2.50	3.09	-0.11	-0.21	1.77
P. tricuspidens	MNHN BR 14536	2?	?	11.04	3.81	3.67	1.89	2.14	2.68	3.03	-0.04	-0.12	1.70
P. tricuspidens	MNHN CR nn	2?	?	12.56	3.38	3.62	1.95	2.38	2.47	3.07	0.07	-0.22	1.76
P. tricuspidens	MNHN R 5363	2	?	12.90	4.08	4.03	2.04	2.84	3.12	3.45	-0.01	-0.10	1.68
P. tricuspidens	MNHN R 5324	2	?	11.91	3.87	3.89	2.00	2.58	2.72	3.23	0.01	-0.17	1.66
P. tricuspidens	MNHN R 5341	2	?	11.10	3.70	3.41	1.49	2.08	2.44	3.01	-0.08	-0.21	1.84
P. tricuspidens	MNHN R 5360	1	?	9.08	3.32	3.10	1.59	1.99	2.18	2.64	-0.07	-0.19	1.63
P. tricuspidens	MNHN R 5330	2	?	12.28	3.19	3.19	1.79	2.20	2.45	2.72	0.00	-0.10	1.82
P. tricuspidens	MNHN R 5346	2	?	12.53	3.79	3.83	2.02	2.51	2.62	3.18	0.01	-0.19	1.72
P. tricuspidens	MNHN R 5342	1	?	9.64	3.14	3.24	1.87	2.32	2.41	2.85	0.03	-0.17	1.53
P. tricuspidens	MNHN R 5369	1	?	9.50	3.33	3.21	1.92	2.21	2.40	2.75	-0.04	-0.14	1.53
P. tricuspidens	Pellouin Coll. Nn	1?	1?	9.29	3.34	3.26	1.76	1.97	2.51	2.89	-0.03	-0.14	1.61
cf *P. churchilli*	SMM P77.33.517	1?	1?	8.40	2.48	2.15	1.27	1.31	1.70	1.87	-0.14	-0.10	1.87
P. insignis	MNHN Menat specimen	1	4	7.80	—	—	—	—	—	—	—	—	—
P. insignis	MNHN Menat specimen	1	5	5.60	—	—	—	—	—	—	—	—	—
N. intermedius	USNM 442229 (142)	1	?	6.56	2.18	1.92	1.08	1.31	1.46	1.54	-0.13	-0.06	1.71
N. intermedius	USNM 442229	2	?	7.28	2.14	1.76	1.04	1.20	1.31	1.59	-0.19	-0.19	1.88
N. intermedius	USNM 442229 (140)	2	?	6.97	2.14	1.72	0.97	1.18	1.31	1.65	-0.22	-0.23	1.87
N. intermedius	USNM 442229 (141)	2	?	7.02	2.11	1.76	1.04	1.33	1.35	1.71	-0.18	-0.24	1.79
N. gidleyi	AMNH 17379	1?	?	6.95	2.10	1.73	1.00	1.06	1.43	1.63	-0.20	-0.13	1.91
N. gidleyi	AMNH 17379	1?	?	7.10	2.28	1.92	0.99	1.14	1.39	1.73	-0.17	-0.22	1.90
N. gidleyi	AMNH 17379	2?	?	8.27	2.35	2.31	1.06	1.46	1.51	1.74	-0.02	-0.14	1.89

TABLE A-II-28.— Measurements (mm) of plesiadapid distal phalanges. Abbreviations are explained in Table A-II-1. PED only includes articular area. Numbers in parentheses following USNM 442229 are unique identifiers assigned by P. Houde during preparation.

Taxon	Specimen	Le	DFT	PEW	PED	ETH	FTW	FTH	MSW	MSD	CSV
P. cookei	UM 87990 (Fig. 54A)	—	4.81	3.11	3.50	0.80	2.32	2.55	1.31	3.93	1.10
P. cookei	UM 87990 (Fig. 54B)	~12.00	—	—	3.94	0.83	—	—	1.65	4.47	1.00
P. cookei	UM 87990 (Fig. 54C)	—	4.45	2.91	4.17	0.69	2.22	2.30	1.29	4.14	1.17
P. cookei	UM 87990 (Fig. 54D)	—	4.84	2.94	3.64	0.92	2.83	2.34	1.39	4.31	1.13
P. cookei	UM 87990 (Fig. 54E)	—	—	—	—	1.03	—	—	1.62	~4.50	1.02
P. cookei	UM 87990 (Fig. 54F)	12.50	4.82	3.02	3.76	0.74	1.85	2.79	1.54	4.66	1.11
P. cookei	UM 87990 (Fig. 54G)	13.81	4.85	3.25	3.95	0.74	2.28	2.60	1.59	4.50	1.04
P. cookei	UM 87990 (Fig. 54H)	—	4.78	3.09	3.77	0.79	2.27	2.98	1.68	4.47	0.98
P. cookei	UM 87990 (Fig. 54I)	—	4.76	2.91	—	—	2.15	~2.40	—	—	—
P. cookei	UM 87990 (Fig. 54J)	—	4.77	3.14	3.96	1.11	2.28	2.73	—	—	—
P. tricuspidens	Berru, divers (A)	—	5.07	2.81	3.64	0.85	1.89	3.18	1.55	4.48	1.06
P. tricuspidens	Berru, divers (B)	—	—	2.27	—	—	1.74	—	—	—	—
P. tricuspidens	MNHN R 5344	—		3.05	—	—	2.57	—		—	—
P. tricuspidens	MNHN R 539	—	6.53	2.84	3.28	0.76	2.01	2.99	1.59	3.77	0.86
P. tricuspidens	MNHN R 5379	—	—	1.93	—	—	1.74	—	—	—	—
P. tricuspidens	MNHN R 613	11.95	4.82	3.19	3.87	0.78	2.44	2.94	1.45	3.60	0.91
P. tricuspidens	MNHN R 612	—	4.67	2.76	3.10	0.88	2.46	2.85	1.41	3.85	1.00
P. tricuspidens	MNHN R 5361	—	3.53	2.13	3.03	0.66	1.99	2.07	1.09	2.86	0.97
P. tricuspidens	MNHN R 5309	—	4.88	3.46	3.87	0.72	2.61	2.36	1.47	3.38	0.83
P. tricuspidens	MNHN R 5313	—	—	3.24	—	—	2.35	—	—	—	—
P. tricuspidens	Berru, Pellouin (CM 091)	12.86	4.33	2.94	4.19	0.59	1.83	2.98	1.51	4.29	1.04
cf. *P. churchilli*	SMM P77.33.517 (A)	—	—	1.84	—	—	1.48	—	—	—	—
cf. *P. churchilli*	SMM P77.33.517 (B)	—	3.02	1.91	2.03	0.67	1.57	1.28	0.96	2.54	0.98
cf. *P. churchilli*	SMM P77.33.517 (C)	—	2.95	1.85	2.21	0.49	1.45	1.45	1.08	2.40	0.80
cf. *P. churchilli*	SMM P77.33.517 (D)	7.06	2.91	2.05	2.15	0.55	1.42	1.43	1.10	2.28	0.73
N. intermedius	USNM 442229 (142)	5.22	2.30	1.39	1.67	0.36	0.95	1.23	0.66	1.76	0.99
N. intermedius	USNM 442229 (assoc2)	5.41	1.77	1.35	1.78	0.41	0.97	0.96	0.71	1.88	0.98
N. intermedius	USNM 442229 (141)	4.53	2.02	1.43	1.61	0.39	0.93	1.19	0.69	1.80	0.96
N. intermedius	USNM 442229 (A)	—	2.16	1.47	1.79	0.35	1.09	1.01	0.65	2.01	1.13
N. intermedius	USNM 442229 (C)	—	2.18	1.39	1.71	0.47	1.28	1.20	0.74	1.90	0.95
Pr. gaoi	UALVP 49110	~6.70	2.80	1.52	1.99	0.31	1.30	1.21	0.89	2.16	0.89

TABLE A-II-29.— Measurements (mm) of plesiadapid innominates. Abbreviations are explained in Table A-II-1. UM 87990 is illustrated in Figure 55. Numbers in parentheses in column headers correspond to measurements in Sargis (2002a, table 2). Asterisk (*) is an estimate.

Taxon	Specimen	Le (1)	IL (2)	IW (3)	AcL (4)	AcD (5)	PD (6)	IsL (7)	IsD (8)	IspL	InD	InW	IspV
P. cookei	UM 87990 (R)	73.77	41.51	10.34	11.16	11.77	24.60	19.89	13.54	3.46	7.17	4.85	0.31
P. cookei	UM 87990 (L)	72.50	38.90	7.95*	10.92	—	—	19.90	13.33	3.90	7.00	4.94	0.36
P. tricuspidens	MNHN R 448	—	—	—	13.46	12.34	—	21.90	—	3.73	8.59	6.20	0.28
P. tricuspidens	MNHN R 409	—	—	10.87	—	—	—	—	—	—	7.12	7.03	—
P. tricuspidens	MNHN R 413	—	—	12.79	—	—	—	—	—	—	9.27	8.18	—
P. tricuspidens	Pellouin Coll. Nn	—	—	—	—	—	—	18.47	—	4.54	—	—	—
N. gidleyi	AMNH 17409	—	—	—	7.35	—	—	13.99	—	3.32	3.85	3.57	0.45
N. gidleyi	AMNH 17379	—	—	4.57	6.88	—	—	—	—	3.58	3.67	3.57	0.52
N. gidleyi	AMNH 17379	—	—	4.57	6.52	—	—	—	—	3.82	3.27	3.02	0.59

TABLE A-II-30.— Measurements (mm) of the proximal end of plesiadapid femora. UM 87990 is illustrated in Figure 56. Abbreviations are explained in Table A-II-1. Numbers in parentheses in column headers correspond to measurements in Sargis (2002a, table 2).

Taxon	Specimen	FHL (10)	FHW (11)	GTL (12)	LTL (13)	TTL (14)	TTP (28)
P. cookei	UM 87990 (R)	9.40	8.99	—	8.30	1.73	23.50
P. cookei	UM 87990 (L)	8.77	8.67	2.78	8.90	1.95	24.97
P. tricuspidens	MNHN BR 14523	7.88	7.57	—	8.29	2.18	20.39
P. tricuspidens	MNHN BR-15-L	7.84	8.42	2.34	8.19	1.99	23.48
P. tricuspidens	MNHN Br-13-L	—	—	—	8.57	2.03	—
P. tricuspidens	MNHN BR 13856	8.89	8.77	5.04	8.61	1.75	23.40
P. tricuspidens	MNHN BR 11865	8.19	7.79	3.16	7.68	1.36	22.00
P. tricuspidens	MNHN BR 11866	8.58	8.52	—	9.32	2.23	23.31
P. tricuspidens	MNHN BR 12569	—	—	—	8.08	1.82	—
P. tricuspidens	MNHN BR-12-L	—	—	—	7.70	1.31	—
P. tricuspidens	MNHN BR-16-L	8.56	10.15	3.62	10.06	2.34	25.78
P. tricuspidens	MNHN R 444	8.89	9.17	2.69	8.62	2.73	23.61
P. tricuspidens	MNHN R 450	7.78	7.38	2.22	8.28	1.41	23.40
P. tricuspidens	MNHN R 445	—	—	—	—	1.74	—
P. tricuspidens	MNHN R 440	8.23	8.95	—	9.12	2.83	24.05
P. tricuspidens	MNHN R 438	8.71	8.37	—	5.91	2.22	21.60
P. tricuspidens	MNHN R 446	8.55	8.78	2.79	9.36	1.91	26.32
P. tricuspidens	MNHN R 408	9.00	9.31	3.93	9.93	1.50	24.04
P. tricuspidens	MNHN R 407	—	—	—	—	—	—
P. tricuspidens	MNHN BR 5454	6.62	7.62	2.13	—	—	—
P. tricuspidens	MNHN R 523	—	7.68	7.65	3.30	1.57	20.73
P. tricuspidens	MNHN R 578	—	—	—	8.87	1.45	—
P. churchilli	P78.14.93	5.67	6.10	2.11	5.99	1.59	17.60
N. gidleyi	AMNH 17379	5.13	5.34	2.57	6.06	1.27	14.73
N. gidleyi	AMNH 17409	—	—	—	—	—	—
N. intermedius	USNM 309895	—	—	—	—	—	—

TABLE A-II-31.— Measurements (mm) of the distal end of plesiadapid femora. UM 87990 is illustrated in Figure 56. Abbreviations are explained in Table A-II-1. Numbers in parentheses in column headers correspond to measurements in Sargis (2002a, table 2).

Taxon	Specimen	PGL (17)	PGW (18)	DEW (19)	MCD (20)	LCD (21)	MCW (22)	LCW (23)	MCL (24)	LCL (25)	ICW (26)
P. cookei	UM 87990 (R)	9.22	5.73	15.60	11.83	10.87	5.37	4.84	7.55	7.26	4.48
P. cookei	UM 87990 (L)	8.59	6.09	15.23	12.02	10.67	4.93	4.01	7.72	7.23	4.62
P. tricuspidens	MNHN BR 14523	—	—	13.57	—	—	—	4.85	6.54	6.82	3.62
P. tricuspidens	MNHN BR-15-L	9.23	5.96	14.47	11.68	10.28	4.92	4.84	7.41	7.08	3.60
P. tricuspidens	MNHN Br-13-L	9.36	5.87	15.20	11.73	10.88	5.17	5.16	8.01	7.21	3.33
P. tricuspidens	MNHN BR 13856	9.32	6.49	15.68	12.02	10.32	5.68	5.29	7.61	7.08	3.09
P. tricuspidens	MNHN BR 11865	—	—	—	—	—	—	—	—	—	—
P. tricuspidens	MNHN BR 11866	—	—	—	—	—	—	—	—	—	—
P. tricuspidens	MNHN BR 12569	10.22	6.8	15.08	12.39	11.68	5.66	5.39	8.72	8.23	3.36
P. tricuspidens	MNHN BR-12-L	—	—	—	—	—	—	—	—	—	—
P. tricuspidens	MNHN BR-16-L	10.7	6.62	16.44	13.04	12.04	5.64	5.62	8.60	7.86	3.87
P. tricuspidens	MNHN R 444	8.70	5.48	13.86	11.20	10.69	4.74	4.56	7.50	6.96	3.34
P. tricuspidens	MNHN R 450	7.72	5.41	12.96	10.44	—	3.92	3.79	7.13	6.34	3.57
P. tricuspidens	MNHN R 445	—	—	—	—	—	—	—	—	—	—
P. tricuspidens	MNHN R 440	—	—	—	—	—	—	—	—	—	—
P. tricuspidens	MNHN R 438	—	7.33	15.14	—	—	5.36	5.30	—	7.11	3.46
P. tricuspidens	MNHN R 446	10.51	7.21	15.49	12.54	11.34	5.85	5.11	8.13	6.99	3.01
P. tricuspidens	MNHN R 408	9.81	7.01	15.74	11.20	—	5.28	5.08	7.63	7.24	3.80
P. tricuspidens	MNHN R 407	10.01	8.08	16.75	12.82	11.75	5.80	5.50	8.45	7.68	4.26
P. tricuspidens	MNHN BR 5454	—	—	—	—	—	—	—	—	—	—
P. tricuspidens	MNHN R 523	—	—	—	—	—	—	—	—	—	—
P. tricuspidens	MNHN R 578	—	—	—	—	—	—	—	—	—	—
P. churchilli	SMMP 78.14.93	—	—	—	—	—	—	—	—	—	—
N. gidleyi	AMNH 17379	—	—	—	—	—	—	—	—	—	—
N. gidleyi	AMNH 17409	4.70	3.77	8.51	7.54	6.37	2.83	2.80	4.72	4.11	2.05
N. intermedius	USNM 309895	5.10	3.68	8.38	6.57	6.50	2.80	2.96	4.34	—	1.89

TABLE A-II-32.— Measurements (mm) and shape variables of plesiadapid femora. UM 87990 is illustrated in Figure 56. Abbreviations are explained in Table A-II-1. Numbers in parentheses in column headers correspond to measurements in Sargis (2002a, table 2).

Taxon	Specimen	Le (9)	MSW (15)	MSD (16)	LTP (27)	HMW	HMD	SSV	HShV	LTPV
P. cookei	UM 87990 (R)	85.70	7.21	6.69	17.66	9.49	9.10	2.51	2.22	1.58
P. cookei	UM 87990 (L)	87.50	7.20	6.36	18.01	9.47	9.37	2.56	2.23	1.58
P. tricuspidens	MNHN BR 14523	69.81	6.35	5.74	15.35	8.28	8.11	2.45	2.14	1.51
P. tricuspidens	MNHN BR-15-L	74.65	7.95	6.19	18.84	9.05	9.28	2.36	2.10	1.38
P. tricuspidens	MNHN Br-13-L	—	7.62	6.06	—	—	—	—	—	—
P. tricuspidens	MNHN BR 13856	77.18	8.00	7.36	17.93	9.18	9.63	2.31	2.11	1.46
P. tricuspidens	MNHN BR 11865	—	7.03	5.62	18.02	8.45	8.49	—	—	—
P. tricuspidens	MNHN BR 11866	—	7.27	Nm	18.95	9.96	10.33	—	—	—
P. tricuspidens	MNHN BR 12569	—	7.77	6.24	—	—	—	—	—	—
P. tricuspidens	MNHN BR-12-L	—	6.48	5.41	—	—	—	—	—	—
P. tricuspidens	MNHN BR-16-L	84.30	8.18	7.01	20.74	10.49	10.18	2.41	2.10	1.40
P. tricuspidens	MNHN R 444	74.70	7.71	6.01	17.48	9.69	9.34	2.40	2.06	1.45
P. tricuspidens	MNHN R 450	71.46	6.53	5.39	18.70	8.88	9.35	2.49	2.06	1.34
P. tricuspidens	MNHN R 445	—	7.32	6.69	—	—	—	—	—	—
P. tricuspidens	MNHN R 440	—	6.99	6.23	18.79	9.41	9.56	—	—	—
P. tricuspidens	MNHN R 438	75.89	7.56	6.04	17.20	—	9.92	2.42	—	—
P. tricuspidens	MNHN R 446	81.44	8.20	6.44	18.77	10.08	10.39	2.42	2.07	1.47
P. tricuspidens	MNHN R 408	80.44	7.66	6.46	17.86	9.71	9.98	2.44	2.10	1.50
P. tricuspidens	MNHN R 407	—	8.12	6.51	—	—	—	—	—	—
P. tricuspidens	MNHN BR 5454	—	—	—	—	8.45	8.35	—	—	—
P. tricuspidens	MNHN R 523	—	—	—	—	8.34	—	—	—	—
P. tricuspidens	MNHN R 578	—	—	—	—	—	—	—	—	—
P. churchilli	P78.14.93	—	5.20	4.94	12.75	6.30	6.50	—	—	—
N. gidleyi	AMNH 17379	—	—	—	10.96	5.82	6.09	—	—	—
N. gidleyi	AMNH 17409	—	4.26	4.22	—	—	—	—	—	—
N. intermedius	USNM 309895	—	3.98	3.69	—	—	—	—	—	—

TABLE A-II-33.— Measurements (mm) of the length and proximal end of plesiadapid tibiae. UM 87990 is illustrated in Figure 57. Abbreviations are explained in Table A-II-1. Numbers in parentheses in column headers correspond to measurements in Sargis (2002a, table 2).

Taxon	Specimen	Le (29)	LCL (30)	MCL (31)	LCW (32)	MCW (33)	PEW (34)	PED (35)
P. cookei	UM 87990	86.10	9.66	8.45	6.00	5.67	14.20	10.70
P. cookei	UM 87990 (L)	—	—	—	—	—	—	—
P. tricuspidens	MNHN BR 218	—	6.82	7.64	4.95	5.06	11.92	8.78
N .gidleyi	AMNH 17379	—	4.99	4.89	3.83	~2.70	~8.30	6.52
N. intermedius	USNM 442229	44.80	—	4.87	—	3.47	—	6.88
N. intermedius	USNM 309900	—	4.60	4.96	3.16	3.64	7.90	6.88

TABLE A-II-34.— Measurements (mm) of the distal end of plesiadapid tibiae. UM 87990 is illustrated in Figure 57. Abbreviations are explained in Table A-II-1. Numbers in parentheses in column headers correspond to measurements in Sargis (2002a, table 2).

Taxon	Specimen	DEW (36)	MML (37)	MMW (38)	TAW (39)	TAD (40)	TbCL (41)	MSW	MSD
P. cookei	UM 87990	8.56	2.04	3.33	4.76	7.36	~17.00	4.64	5.71
P. cookei	UM 87990 (L)	—	—	—	—	—	—	4.90	5.70
P. tricuspidens	MNHN BR 218	—	—	—	—	—	—	—	—
N .gidleyi	AMNH 17379	4.60	1.70	1.84	2.46	3.60	~11.00	2.39	3.36
N. intermedius	USNM 442229	4.30	—	—	2.25	—	—	2.46	2.88

TABLE A-II-35.— Measurements (mm) of the fibulae of *Plesiadapis cookei*. UM 87990 is illustrated in Figures 58 and 59. Abbreviations are explained in Table A-II-1. Numbers in parentheses in column headers correspond to measurements in Sargis (2002a, table 2). Asterisk (*) indicates measurement does not include epiphyses.

Taxon	Specimen	Le (42)	DAL (43)	PED (44)	DED (45)	MSW	MSD
P. cookei	UM 87990 (L)	—	—	—	5.90	3.00	3.60
P. cookei	UM 87990 (R)	75.90*	—	7.55	—	2.90	3.50

TABLE A-II-36.— Measurements (mm) of the astragali of plesiadapiforms and select other mammals (see Fig. 61; measurements here are continued in Tables A-II-37 and A-II-38). Astragalus (*Ast*) measurements 1–10 and the neck length variable (*NVar*) are: 1, maximum proximodistal length; 2, body proximodistal length; 3, head and neck proximodistal length; 4, fibular facet maximum dorsoplantar height; 5, fibular facet proximodistal length; 6, lateral tibial facet maximum proximodistal length; 7, lateral tibial facet maximum mediolateral width; 8, medial tibial facet maximum dorsoplantar height; 9, medial tibial facet maximum proximodistal length; 10, ectal (posterior calcaneoastragalar) facet proximodistal length; NVar, neck length variable (Ast-3 / Ast-1).

Higher taxon	Taxon	Specimen	Ast-1	Ast-2	Ast-3	Ast-4	Ast-5	Ast-6	Ast-7	Ast-8	Ast-9	Ast-10	NVar
Adapisoriculidae	*Deccanolestes hislopi*	VPL/JU/NKIM/52	1.73	1.04	0.67	0.83	0.80	1.07	0.74	0.61	1.31	0.66	0.39
Adapisoriculidae	*Deccanolestes robustus*	VPL/JU/NKIM/51	2.52	1.34	0.89	1.10	1.20	1.51	0.94	1.02	1.95	0.98	0.35
Cimolestidae	*Procerberus formicarum*	AMNH 117454	6.78	3.39	3.33	2.60	3.74	5.17	3.72	2.57	4.32	3.39	0.49
Condylarthra	*Protungulatum donnae*	AMNH 118260	6.72	4.02	2.68	2.66	3.59	4.01	3.52	2.42	4.78	3.05	0.40
Condylarthra	*Protungulatum donnae*	AMNH 11878	6.83	4.53	2.21	2.58	3.43	3.91	3.64	2.66	4.99	3.87	0.32
Dermoptera	*Cynocephalus volans*	USNM 144662	10.51	7.35	2.48	3.98	5.66	6.80	4.70	4.33	10.48	4.79	0.24
Dermoptera	*Cynocephalus volans*	USNM 578084	10.84	9.18	1.67	3.78	6.24	7.19	5.52	4.39	10.74	5.12	0.15
Dermoptera	*Cynocephalus volans*	USNM 317118	11.07	8.63	2.55	4.23	5.73	7.00	5.67	3.70	10.08	4.56	0.23
Omomyoidea	*Hemiacodon gracilis*	AMNH 12613A	8.21	4.32	3.89	2.71	3.73	6.38	3.66	3.77	6.59	3.06	0.47
Omomyoidea	*Omomys carteri*	UM 98648	6.66	3.17	3.44	2.39	3.35	4.03	2.61	2.66	4.26	2.72	0.52
Omomyoidea	*Omomys carteri*	UM 38321	6.91	3.50	3.39	2.36	3.26	4.46	2.69	2.41	4.00	2.87	0.49
Haplorhini	*Cebuella pygmaea*	SBU-C01	4.97	2.91	2.01	1.53	2.50	3.48	2.25	1.64	3.21	2.14	0.40
Haplorhini	*Cebus apella*	SBU-NCb04	18.47	11.82	6.66	6.51	10.94	14.61	7.68	6.72	14.72	8.46	0.36
Haplorhini	*Saguinus oedipus*	SBU-NSg06	8.84	5.17	3.53	2.84	4.81	7.11	3.77	2.50	6.56	3.79	0.40
Haplorhini	*Saimiri sciureus*	SBU-Nsm06	11.19	6.46	4.52	3.33	5.87	6.88	5.38	3.81	7.91	5.06	0.40
Haplorhini	*Tarsius syrichta carbonarius*	AMNH 203296	6.38	3.76	2.65	1.68	3.01	3.74	3.22	2.29	5.12	3.07	0.42
Plesiadapiformes	*Carpolestes simpsoni*	UM 101963	4.70	2.97	1.86	1.95	2.44	2.83	2.14	1.25	3.09	2.17	0.40
Plesiadapiformes	*Dryomomys szalayi*	UM 41870	1.79	1.16	0.74	0.76	1.10	1.10	0.73	0.63	1.40	0.87	0.41
Plesiadapiformes	*Ignacius graybullianus*	USNM 442235	4.57	2.88	1.71	1.80	2.54	2.85	2.20	1.46	2.78	1.94	0.37
Plesiadapiformes	*Nannodectes gidleyi*	AMNH 17379	6.84	5.02	2.37	2.43	3.33	3.66	2.92	1.99	4.63	3.25	0.35
Plesiadapiformes	*Plesiadapis cookei*	UM 87990	13.02	8.14	4.64	4.90	6.80	7.25	5.62	3.40	8.40	5.47	0.36
Plesiadapiformes	*Plesiadapis rex*	UM 94816	7.94	5.51	2.46	3.39	4.10	5.43	3.86	3.01	6.32	3.49	0.31
Plesiadapiformes	*Plesiadapis tricuspidens*	MNHN BR 14537	11.05	7.24	4.16	4.54	6.52	7.35	5.51	3.17	8.42	5.48	0.38
Plesiadapiformes	*Plesiadapis tricuspidens*	MNHN nn	9.97	7.47	3.00	4.07	5.82	6.75	4.89	4.24	7.75	4.95	0.30
Plesiadapiformes	*Plesiadapis tricuspidens*	MNHN R 5347	10.88	7.58	3.45	5.22	6.54	7.07	5.56	3.80	8.68	5.22	0.32
Plesiadapiformes	*Plesiadapis tricuspidens*	MNHN R 610	10.96	7.80	3.22	4.69	6.61	8.01	5.65	4.00	9.33	5.44	0.29
Plesiadapiformes	*Purgatorius*	UCMP 197509	3.34	2.31	1.25	1.46	1.75	2.25	1.53	1.13	2.57	1.65	0.37
Plesiadapiformes	*Purgatorius*	UCMP 197507	3.41	2.27	1.33	1.46	1.72	2.30	1.52	1.21	2.62	1.58	0.39
Plesiadapiformes	*Tinimomys graybulliensis*	USNM 461201	2.42	1.29	1.16	0.92	1.40	1.55	0.93	0.78	1.80	1.14	0.48
Scandentia	*Ptilocercus lowii*	USNM 488067	4.28	1.96	2.17	1.31	2.03	2.71	1.49	1.32	3.34	1.58	0.51
Scandentia	*Ptilocercus lowii*	USNM 488072	4.23	1.95	2.14	1.32	2.03	2.80	1.43	1.34	3.42	1.56	0.51
Scandentia	*Ptilocercus lowii*	USNM 488055	4.36	2.07	2.17	1.39	2.11	2.81	1.44	1.36	3.55	1.47	0.50
Scandentia	*Tupaia belangeri*	AMNH 113135	6.05	3.27	2.68	1.72	2.84	4.68	2.85	1.67	3.90	2.64	0.44
Scandentia	*Tupaia glis*	SBU coll.	6.06	3.69	2.20	1.67	2.59	4.02	3.09	1.70	3.59	2.47	0.36
Scandentia	*Urogale everetti*	AMNH 203293	6.83	3.66	3.18	2.28	2.28	4.66	3.22	1.76	4.02	2.91	0.47
Adapoidea	*Leptadapis magnus*	AMNH 127411	25.21	17.30	7.58	9.55	12.02	13.45	10.65	7.71	19.74	10.80	0.30
Adapoidea	*Notharctus tenebrosus*	AMNH 11474	16.64	10.70	5.96	6.23	7.97	8.79	7.33	5.77	14.81	7.20	0.36
Adapoidea	*Adapis parisiensis*	AMNH 111935	10.64	7.15	3.61	4.09	5.85	6.85	5.29	4.11	8.71	5.23	0.34
Strepsirrhini	*Cheirogaleus medius*	DPC 0142	7.06	3.87	2.68	2.25	3.08	3.83	2.45	1.96	5.60	2.93	0.38
Strepsirrhini	*Eulemur fulvus*	DPC 095	14.83	9.23	4.78	4.66	8.20	9.66	5.91	4.51	12.31	6.58	0.32
Strepsirrhini	*Galago senegalensis*	AMNH 86502	7.90	4.41	3.43	2.33	4.15	5.82	2.90	3.03	5.57	3.09	0.43
Strepsirrhini	*Galago senegalensis*	AMNH 83299	8.51	4.59	3.86	2.68	4.46	5.89	2.81	3.34	5.61	3.26	0.45
Strepsirrhini	*Loris tardigradus*	HTB 750	6.59	4.69	1.91	2.34	2.79	4.55	2.98	1.53	4.63	2.25	0.29
Strepsirrhini	*Loris tardigradus*	AMNH 150038	7.84	5.05	2.89	2.90	3.50	5.21	3.29	2.27	6.01	2.65	0.37
Strepsirrhini	*Loris tardigradus*	AMNH 165931	6.87	4.80	2.38	2.66	2.97	4.74	3.10	1.97	4.75	2.58	0.35
Strepsirrhini	*Otolemur crassicaudatus*	SBU1163	13.67	8.25	4.75	4.26	7.76	10.76	5.79	4.70	11.85	5.71	0.35
Strepsirrhini	*Propithecus sp.*	DPC 051	22.21	12.97	6.80	6.12	10.52	12.04	7.83	6.18	18.89	8.70	0.31
Strepsirrhini	*Varecia variegata*	DPC049	20.31	11.98	7.13	7.32	10.23	12.35	7.65	6.13	17.37	8.04	0.35

TABLE A-II-37.— Measurements (mm) of the astragali of plesiadapiforms and select other mammals (see Fig. 61; measurements here were initiated in Table A-II-36 and are continued in Table A-II-38). Astragalus (*Ast*) measurements 11–18 are: 11, ectal (posterior calcaneoastragalar) facet mediolateral width; 12, flexor fibularis groove mediolateral width; 13, flexor fibularis groove proximodistal length; 14, sustentacular (anterior calcaneoastragalar) facet proximodistal length; 15, sustentacular (anterior calcaneoastragalar) facet mediolateral width; 16, sustentacular (anterior calcaneoastragalar) facet width of contact with navicular facet; 17, maximum mediolateral diameter of astragalar head; 18, maximum dorsoplantar height of astragalar head. *GM*, geometric mean of Ast-1, 4–15, and 17–18.

Higher taxon	Taxon	Specimen	Ast-11	Ast-12	Ast-13	Ast-14	Ast-15	Ast-16	Ast-17	Ast-18	GM
Adapisoriculidae	*Deccanolestes hislopi*	VPL/JU/NKIM/52	0.45	0.77	0.61	0.73	0.41	0.50	0.80	0.41	0.73
Adapisoriculidae	*Deccanolestes robustus*	VPL/JU/NKIM/51	0.64	1.28	0.93	1.00	0.59	0.58	1.20	0.81	1.10
Cimolestidae	*Procerberus formicarum*	AMNH 117454	1.78	2.31	1.91	2.04	2.04	0.92	3.67	2.26	2.98
Condylarthra	*Protungulatum donnae*	AMNH 118260	1.78	3.15	2.23	2.64	1.85	0.99	4.28	2.33	3.06
Condylarthra	*Protungulatum donnae*	AMNH 11878	1.86	2.81	2.00	2.81	2.20	1.43	4.14	2.60	3.15
Dermoptera	*Cynocephalus volans*	USNM 144662	2.09	4.25	4.27	3.65	2.14	2.45	4.59	3.64	4.58
Dermoptera	*Cynocephalus volans*	USNM 578084	2.02	3.65	3.96	3.88	2.64	2.94	5.38	3.89	4.77
Dermoptera	*Cynocephalus volans*	USNM 317118	2.19	2.87	3.77	3.65	2.22	2.40	4.78	4.00	4.52
Omomyoidea	*Hemiacodon gracilis*	AMNH 12613A	1.65	1.68	1.72	3.95	1.75	2.73	3.47	2.82	3.25
Omomyoidea	*Omomys carteri*	UM 98648	1.45	1.07	1.43	2.74	1.32	1.48	2.91	2.27	2.50
Omomyoidea	*Omomys carteri*	UM 38321	1.45	1.11	1.35	2.77	1.01	1.85	2.66	2.17	2.43
Haplorhini	*Cebuella pygmaea*	SBU-C01	1.00	1.05	1.14	1.90	1.16	1.59	2.27	1.65	1.91
Haplorhini	*Cebus apella*	SBU-NCb04	4.24	4.46	3.21	7.77	4.03	6.53	7.95	6.12	7.42
Haplorhini	*Saguinus oedipus*	SBU-NSg06	1.93	2.01	2.12	4.03	2.12	2.64	3.69	2.75	3.50
Haplorhini	*Saimiri sciureus*	SBU-Nsm06	2.57	2.36	1.82	5.59	2.09	2.53	4.04	3.14	4.17
Haplorhini	*Tarsius syrichta carbonarius*	AMNH 203296	1.09	1.46	0.66	2.29	1.93	1.92	2.80	1.85	2.34
Plesiadapiformes	*Carpolestes simpsoni*	UM 101963	1.13	1.30	1.27	2.31	1.30	1.58	2.64	1.57	1.97
Plesiadapiformes	*Dryomomys szalayi*	UM 41870	0.44	0.66	0.38	0.62	0.35	0.39	0.98	0.43	0.73
Plesiadapiformes	*Ignacius graybullianus*	USNM 442235	1.21	1.28	0.94	1.91	0.98	1.32	2.64	1.43	1.86
Plesiadapiformes	*Nannodectes gidleyi*	AMNH 17379	1.57	2.11	1.53	2.43	1.95	2.46	3.86	2.03	2.72
Plesiadapiformes	*Plesiadapis cookei*	UM 87990	2.92	4.96	4.47	5.72	2.90	3.50	6.94	3.68	5.31
Plesiadapiformes	*Plesiadapis rex*	UM 94816	2.71	2.97	2.44	2.98	2.39	2.99	4.79	2.27	3.61
Plesiadapiformes	*Plesiadapis tricuspidens*	MNHN BR 14537	3.08	3.48	3.08	4.21	2.78	2.91	6.45	3.54	4.81
Plesiadapiformes	*Plesiadapis tricuspidens*	MNHN nn	2.92	3.20	3.06	3.91	2.81	2.46	5.35	3.58	4.56
Plesiadapiformes	*Plesiadapis tricuspidens*	MNHN R 5347	3.42	4.01	3.97	4.55	3.23	3.72	6.25	3.45	5.12
Plesiadapiformes	*Plesiadapis tricuspidens*	MNHN R 610	3.23	3.86	3.32	3.87	3.45	4.47	6.34	3.50	5.08
Plesiadapiformes	*Purgatorius*	UCMP 197509	1.03	1.32	0.86	1.27	0.96	1.12	1.93	0.95	1.48
Plesiadapiformes	*Purgatorius*	UCMP 197507	0.86	1.19	0.78	1.59	0.74	1.14	1.74	0.88	1.43
Plesiadapiformes	*Tinimomys graybulliensis*	USNM 461201	0.61	0.87	0.48	0.69	0.50	0.54	1.10	0.53	0.94
Scandentia	*Ptilocercus lowii*	USNM 488067	0.96	0.72	1.08	1.61	0.99	1.08	1.65	1.14	1.55
Scandentia	*Ptilocercus lowii*	USNM 488072	0.98	0.71	1.08	1.64	1.03	1.12	1.63	1.17	1.56
Scandentia	*Ptilocercus lowii*	USNM 488055	0.92	0.78	0.87	1.60	1.00	1.17	1.74	1.17	1.55
Scandentia	*Tupaia belangeri*	AMNH 113135	1.72	1.30	1.31	2.43	1.18	1.64	2.67	1.79	2.30
Scandentia	*Tupaia glis*	SBU coll.	1.67	0.99	1.48	2.47	1.02	1.69	2.79	1.69	2.21
Scandentia	*Urogale everetti*	AMNH 203293	1.93	1.44	1.55	2.27	1.44	1.29	3.30	2.12	2.52
Adapoidea	*Leptadapis magnus*	AMNH 127411	5.51	6.18	6.02	8.84	4.80	4.85	12.33	9.04	9.73
Adapoidea	*Notharctus tenebrosus*	AMNH 11474	2.81	3.96	2.60	5.55	3.00	3.24	6.95	5.52	6.10
Adapoidea	*Adapis parisiensis*	AMNH 111935	2.38	2.53	2.31	3.89	2.33	2.41	5.39	4.05	4.41
Strepsirrhini	*Cheirogaleus medius*	DPC 0142	1.30	0.48	1.93	3.54	1.74	2.74	2.93	2.01	2.44
Strepsirrhini	*Eulemur fulvus*	DPC 095	2.75	3.09	3.91	5.15	3.83	3.39	5.73	5.09	5.71
Strepsirrhini	*Galago senegalensis*	AMNH 86502	1.54	1.92	0.56	3.91	1.86	2.49	3.10	2.23	2.82
Strepsirrhini	*Galago senegalensis*	AMNH 83299	2.18	2.03	0.57	4.35	1.66	2.75	3.51	2.41	3.02
Strepsirrhini	*Loris tardigradus*	HTB 750	1.31	1.74	1.54	2.32	1.62	2.23	3.53	1.80	2.47
Strepsirrhini	*Loris tardigradus*	AMNH 150038	1.48	2.04	1.59	3.25	1.83	2.05	2.89	2.37	2.92
Strepsirrhini	*Loris tardigradus*	AMNH 165931	1.27	1.99	1.32	2.68	1.74	2.62	4.03	2.15	2.68
Strepsirrhini	*Otolemur crassicaudatus*	SBU1163	2.97	3.29	2.70	6.32	3.44	3.95	5.62	4.61	5.52
Strepsirrhini	*Propithecus sp.*	DPC 051	4.53	5.31	5.01	7.76	5.86	6.91	8.88	6.72	8.13
Strepsirrhini	*Varecia variegata*	DPC049	3.82	3.90	4.33	7.76	4.99	7.46	8.79	6.67	7.65

TABLE A-II-38.— Measurements (degrees) of the astragali of plesiadapiforms and select other mammals (see Fig. 61; measurements here were initiated in Tables A-II-36 and A-II-37). Astragalus (*Ast*) measurements 19–23 are angular: 19, angle between fibular facet and lateral tibial facet; 20, angle between fibular facet and medial tibial facet; 21, angle between medial and lateral tibial facets; 22, angle between ectal (posterior calcaneoastragalar) facet and fibular facet; 23, angle between major axis of head and plane of lateral tibial facet.

Higher taxon	Taxon	Specimen	Ast-19	Ast-20	Ast-21	Ast-22	Ast-23
Adapisoriculidae	*Deccanolestes hislopi*	VPL/JU/NKIM/52	97	45	97	91	5
Adapisoriculidae	*Deccanolestes robustus*	VPL/JU/NKIM/51	118	58	102	93	-9
Cimolestidae	*Procerberus formicarum*	AMNH 117454	84	27	103	125	-10
Condylarthra	*Protungulatum donnae*	AMNH 118260	96	38	107	108	-5
Condylarthra	*Protungulatum donnae*	AMNH 11878	98	40	92	111	-11
Dermoptera	*Cynocephalus volans*	USNM 144662	103	18	95	105	8
Dermoptera	*Cynocephalus volans*	USNM 578084	108	13	92	112	7
Dermoptera	*Cynocephalus volans*	USNM 317118	99	14	97	113	12
Omomyoidea	*Hemiacodon gracilis*	AMNH 12613A	81	7	72	106	-8
Omomyoidea	*Omomys carteri*	UM 98648	74	6	68	99	2
Omomyoidea	*Omomys carteri*	UM 38321	72	6	74	102	-9
Haplorhini	*Cebuella pygmaea*	SBU-C01	70	13	87	112	-5
Haplorhini	*Cebus apella*	SBU-NCb04	78	8	85	117	-16
Haplorhini	*Saguinus oedipus*	SBU-NSg06	70	17	85	115	-10
Haplorhini	*Saimiri sciureus*	SBU-Nsm06	77	11	72	114	-11
Haplorhini	*Tarsius syrichta carbonarius*	AMNH 203296	83	16	61	110	6
Plesiadapiformes	*Carpolestes simpsoni*	UM 101963	82	34	80	86	27
Plesiadapiformes	*Dryomomys szalayi*	UM 41870	105	56	112	86	15
Plesiadapiformes	*Ignacius graybullianus*	USNM 442235	80	38	88	89	22
Plesiadapiformes	*Nannodectes gidleyi*	AMNH 17379	78	27	112	93	17
Plesiadapiformes	*Plesiadapis cookei*	UM 87990	84	22	115	93	14
Plesiadapiformes	*Plesiadapis rex*	UM 94816	92	43	116	93	18
Plesiadapiformes	*Plesiadapis tricuspidens*	MNHN BR 14537	81	40	119	87	16
Plesiadapiformes	*Plesiadapis tricuspidens*	MNHN nn	89	35	116	91	21
Plesiadapiformes	*Plesiadapis tricuspidens*	MNHN R 5347	87	53	132	93	11
Plesiadapiformes	*Plesiadapis tricuspidens*	MNHN R 610	77	37	131	92	20
Plesiadapiformes	*Purgatorius*	UCMP 197509	99	49	114	88	14
Plesiadapiformes	*Purgatorius*	UCMP 197507	93	46	107	88	17
Plesiadapiformes	*Tinimomys graybulliensis*	USNM 461201	118	50	113	85	18
Scandentia	*Ptilocercus lowii*	USNM 488067	95	36	123	90	7
Scandentia	*Ptilocercus lowii*	USNM 488072	100	39	121	91	11
Scandentia	*Ptilocercus lowii*	USNM 488055	101	32	126	93	5
Scandentia	*Tupaia belangeri*	AMNH 113135	94	-1	56	105	-15
Scandentia	*Tupaia glis*	SBU coll.	72	6	87	105	-9
Scandentia	*Urogale everetti*	AMNH 203293	95	-5	62	104	2
Adapoidea	*Leptadapis magnus*	AMNH 127411	89	20	85	109	17
Adapoidea	*Notharctus tenebrosus*	AMNH 11474	93	18	80	94	15
Adapoidea	*Adapis parisiensis*	AMNH 111935	90	23	89	102	2
Strepsirrhini	*Cheirogaleus medius*	DPC 0142	92	16	83	101	18
Strepsirrhini	*Eulemur fulvus*	DPC 095	98	26	75	111	-8
Strepsirrhini	*Galago senegalensis*	AMNH 86502	75	32	89	107	21
Strepsirrhini	*Galago senegalensis*	AMNH 83299	78	37	96	103	23
Strepsirrhini	*Loris tardigradus*	HTB 750	84	15	79	100	17
Strepsirrhini	*Loris tardigradus*	AMNH 150038	93	38	83	93	12
Strepsirrhini	*Loris tardigradus*	AMNH 165931	76	27	81	97	15
Strepsirrhini	*Otolemur crassicaudatus*	SBU1163	92	27	69	103	14
Strepsirrhini	*Propithecus sp.*	DPC 051	98	26	67	102	-21
Strepsirrhini	*Varecia variegata*	DPC049	91	20	70	103	14

TABLE A-II-39.— Measurements (mm) of the calcanea of plesiadapiforms and select other mammals (see Fig. 62; measurements here are continued in Tables A-II-40 and A-II-41). Calcaneum (*Cc*) measurements 1–10 and the distal end length variable (*DVar*) are: 1, maximum proximodistal length; 2, tuber proximodistal length; 3, distal calcaneum length; 4, tuber maximum dorsoplantar depth; 5, tuber proximal end dorsoplantar height; 6, tuber proximal end mediolateral width; 7, ectal facet proximodistal length; 8, maximum length of arc of ectal facet; 9, ectal facet mediolateral width; 10, medial projection of sustentaculum from ectal facet lateral margin. DVar, distal end length variable (Cc 3 / Cc 1).

Higher taxon	Taxon	Catalogue number	Cc-1	Cc-2	Cc-3	Cc-4	Cc-5	Cc-6	Cc-7	Cc-8	Cc-9	Cc-10	DVar
Adapisoriculidae	*Deccanolestes hislopi*	VPL/JU/NKIM/52	2.52	1.74	0.78	1.12	0.91	0.64	0.77	1.25	0.54	1.14	0.31
Cimolestidae	*Procerberus formicarum*	AMNH 117455	9.48	6.37	3.03	4.08	3.45	2.57	3.10	3.41	1.51	4.11	0.32
Cimolestidae	*Procerberus formicarum*	AMNH 119802	9.61	6.42	3.29	4.06	3.06	3.03	2.95	3.56	1.96	4.45	0.34
Condylarthra	*Protungulatum donnae*	AMNH 118060	11.93	8.95	2.89	4.72	3.45	3.41	3.28	3.75	1.50	5.09	0.24
Dermoptera	*Cynocephalus volans*	USNM 144662	12.07	6.89	5.23	4.64	4.98	2.87	4.66	4.85	1.93	5.64	0.43
Dermoptera	*Cynocephalus volans*	USNM 317118	14.69	7.46	7.00	5.05	5.90	4.16	4.99	5.51	2.57	6.24	0.48
Dermoptera	*Cynocephalus volans*	USNM 578084	13.66	7.34	6.56	5.46	5.82	3.21	5.26	5.17	2.26	5.48	0.48
Omomyoidea	*Omomys carteri*	UCM 69303	17.38	7.87	9.76	5.04	4.75	3.07	3.17	4.33	2.07	4.52	0.56
Omomyoidea	*Omomys carteri*	UCM 69065	16.38	7.51	8.89	5.18	4.87	3.01	3.24	4.57	2.02	4.56	0.54
Omomyoidea	*Omomys carteri*	UCM 68745	16.29	7.15	9.00	4.73	4.59	2.90	2.78	4.02	2.05	4.69	0.55
Haplorhini	*Cebuella pygmaea*	AMNH 244101	7.15	3.94	3.42	2.85	2.12	1.82	2.18	2.84	1.2	2.88	0.48
Haplorhini	*Cebuella pygmaea*	AMNH 244365	7.56	3.98	3.20	2.90	2.55	1.89	2.18	2.90	1.21	2.88	0.42
Haplorhini	*Cebuella pygmaea*	SBU NC1	7.66	4.12	3.25	3.12	2.76	1.64	2.25	3.10	1.24	2.83	0.42
Haplorhini	*Cebus apella*	AMNH 133606	28.57	14.47	12.86	10.36	9.30	9.07	7.43	10.97	5.48	10.58	0.45
Haplorhini	*Cebus apella*	AMNH 133608	24.8	12.78	11.42	9.06	8.46	7.33	6.88	9.75	5.05	9.00	0.46
Haplorhini	*Cebus apella*	AMNH 133764	24.27	12.82	11.29	9.11	8.80	7.43	6.90	9.85	4.36	9.26	0.47
Haplorhini	*Saguinus mystax*	AMNH 188177	11.77	6.15	5.45	4.69	3.88	2.84	3.16	3.99	1.94	4.44	0.46
Haplorhini	*Saimiri boliviensis*	AMNH 211613	17.11	9.18	7.89	6.27	5.64	4.34	4.84	6.07	2.59	6.01	0.46
Haplorhini	*Tarsius spectrum*	AMNH 109369	27.11	5.91	18.84	3.61	3.27	2.31	3.03	3.58	1.14	3.15	0.69
Plesiadapiformes	*Carpolestes simpsoni*	UM 101963	6.79	4.03	2.78	2.98	2.30	1.65	2.52	3.50	1.38	3.48	0.41
Plesiadapiformes	*Dryomomys szalayi*	UM 41870	3.32	2.20	1.12	1.42	1.08	0.80	1.03	1.51	0.62	1.48	0.34
Plesiadapiformes	*Ignacius graybullianus*	USNM 442240	7.28	4.80	2.46	3.08	2.26	1.91	2.75	3.67	1.30	3.19	0.34
Plesiadapiformes	*Nannodectes gidleyi*	AMNH 17379	10.43	6.48	3.49	4.10	3.84	2.84	3.20	4.60	1.85	4.53	0.33
Plesiadapiformes	*Phenacolemur simonsi*	USNM 442238	6.65	4.26	2.38	2.54	1.93	1.37	2.21	3.08	1.10	2.72	0.36
Plesiadapiformes	*Plesiadapis churchilli*	UM 118271	12.30	7.94	4.09	4.67	4.39	2.96	4.00	4.93	2.14	5.10	0.33
Plesiadapiformes	*Plesiadapis cookei*	UM 87990	18.80	11.80	6.50	7.50	6.70	5.50	6.80	7.90	3.31	7.90	0.35
Plesiadapiformes	*Plesiadapis tricuspidens*	MNHN R 414	18.39	12.22	6.10	7.40	6.57	5.20	6.43	7.78	3.25	7.53	0.33
Plesiadapiformes	*Plesiadapis tricuspidens*	MNHN R 611	16.99	10.88	5.68	6.41	5.46	4.55	5.66	7.05	2.91	7.45	0.33
Plesiadapiformes	*Purgatorius*	UCMP 197517	5.30	3.87	1.46	2.04	1.47	1.40	1.69	2.22	0.78	2.15	0.28
Plesiadapiformes	*Tinimomys graybulliensis*	USNM 461201	3.39	2.36	1.06	1.30	1.06	0.87	1.08	1.56	0.68	1.55	0.31
Scandentia	*Ptilocercus lowii*	YPM 6873	5.26	3.11	2.11	1.78	1.66	1.21	1.60	2.21	0.70	2.45	0.40
Scandentia	*Tupaii belangeri*	AMNH 113135	9.27	5.33	3.62	3.56	3.01	2.22	2.62	3.28	1.29	4.31	0.39
Scandentia	*Tupaii sp.*	SBU coll.	9.02	5.21	3.67	3.27	2.79	2.14	2.46	3.87	1.57	4.03	0.41
Scandentia	*Urogale everetti*	AMNH 203293	10.22	5.72	4.14	3.79	3.12	2.55	2.96	3.97	1.51	4.69	0.41
Adapoidea	*Adapis parisiensis*	AMNH 111937	19.50	12.73	6.92	6.52	5.91	5.05	5.60	7.55	3.53	7.32	0.35
Adapoidea	*Adapis parisiensis*	NMB QE741	17.13	11.99	4.94	6.33	6.81	4.48	5.46	5.39	2.21	6.99	0.29
Adapoidea	*Notharctus tenebrosus*	AMNH 131945	25.55	13.99	11.4	10.37	9.85	6.32	7.46	8.66	3.87	9.44	0.45
Adapoidea	*Notharctus tenebrosus*	AMNH 131766	23.56	13.56	10.17	8.37	8.03	6.21	7.11	8.23	2.91	8.99	0.43
Adapoidea	*Notharctus tenebrosus*	AMNH 11474	23.07	13.19	9.89	8.60	8.32	5.23	6.87	8.78	3.12	7.96	0.43
Adapoidea	*Leptadapis magnus*	NHMB QF 421	33.2	23.07	9.52	11.59	11.53	11.98	10.09	12.66	3.98	13.24	0.29
Strepsirrhini	*Cheirogaleus medius*	DPC 031	10.08	4.95	5.16	3.30	2.74	2.32	2.99	4.23	1.56	3.41	0.51
Strepsirrhini	*Cheirogaleus medius*	DPC 1023	10.53	5.03	5.43	3.47	2.93	3.12	2.81	4.22	1.44	3.30	0.52
Strepsirrhini	*Cheirogaleus medius*	AMNH 80072	12.59	6.15	6.40	4.42	2.24	3.52	3.29	4.84	1.56	4.14	0.51
Strepsirrhini	*Eulemur fulvus*	AMNH 170717	23.64	12.55	10.57	8.67	7.20	6.09	6.97	8.40	2.43	8.44	0.45

TABLE A-II-39.— Cont'd.

Higher taxon	Taxon	Catalogue number	Cc-1	Cc-2	Cc-3	Cc-4	Cc-5	Cc-6	Cc-7	Cc-8	Cc-9	Cc-10	DVar
Strepsirrhini	*Eulemur fulvus*	AMNH 100528	25.85	14.14	11.57	9.01	6.51	6.30	6.65	8.37	2.13	8.99	0.45
Strepsirrhini	*Eulemur fulvus*	DPC 095	22.95	11.78	11.00	8.83	7.50	6.58	6.24	7.17	2.32	7.93	0.48
Strepsirrhini	*Galago senegalensis*	AMNH 86502	27.03	7.38	19.55	4.25	4.09	2.76	2.87	2.89	1.52	3.64	0.72
Strepsirrhini	*Loris tardigradus*	AMNH 34256	9.61	4.68	4.90	3.60	1.96	1.32	2.76	3.70	1.53	2.77	0.51
Strepsirrhini	*Loris tardigradus*	AMNH 150038	9.94	5.24	4.65	4.19	2.52	1.65	3.30	4.26	1.48	3.29	0.47
Strepsirrhini	*Loris tardigradus*	HTB 750	8.62	4.82	3.63	3.64	2.57	1.60	3.57	5.17	1.70	3.54	0.42
Strepsirrhini	*Otolemur crassicaudatus*	SBU coll.	34.66	12.69	22.10	8.24	7.01	4.15	5.68	8.19	3.57	6.56	0.64
Strepsirrhini	*Otolemur crassicaudatus*	AMNH 216240	33.09	9.87	22.26	7.32	6.13	4.38	4.91	7.2	2.48	6.64	0.67
Strepsirrhini	*Propithecus verreauxi*	AMNH 170471	25.61	14.22	11.24	9.67	9.05	6.26	7.53	9.13	1.65	9.23	0.44
Strepsirrhini	*Varecia variegate*	AMNH 201384	27.70	15.44	11.76	10.68	8.61	7.07	7.92	9.77	3.88	10.38	0.42

TABLE A-II-40.— Measurements (mm) of the calcanea of plesiadapiforms and select other mammals (see Fig. 62; measurements here were initiated in Table A-II-39 and are continued in Table A-II-41). Calcaneum (*Cc*) measurements 11–19 are: 11, proximodistal length from sustentaculum medial apex to distal end; 12, sustentacular facet proximodistal length; 13, sustentacular facet mediolateral width; 14, lateral projection of peroneal tubercle from ectal facet lateral margin; 15, proximodistal length from peroneal tubercle lateral apex to distal end; 16, dorsoplantar depth of peroneal tubercle; 17, diameter of calcaneocuboid facet perpendicular to sustentacular facet; 18, diameter of calcaneocuboid facet parallel to sustentacular facet; 19, distance from proximal margin of peroneal tubercle to distal end. GM is geometric mean of measurements Cc-1, 4–7, 9–11, and 17–18.

Higher taxon	Taxon	Catalogue Number	Cc-11	Cc-12	Cc-13	Cc-14	Cc-15	Cc-16	Cc-17	Cc-18	Cc-19	GM
Adapisoriculidae	*Deccanolestes hislopi*	VPL/JU/ NKIM/52	0.64	0.85	0.50	0.69	0.38	0.48	0.64	0.74	0.73	0.87
Cimolestidae	*Procerberus formicarum*	AMNH 117455	3.03	3.08	1.56	1.21	1.42	1.42	2.29	2.42	1.77	3.19
Cimolestidae	*Procerberus formicarum*	AMNH 119802	2.60	3.17	1.46	1.44	0.86	1.26	2.28	2.34	1.54	3.25
Condylarthra	*Protungulatum donnae*	AMNH 118060	3.89	3.18	1.98	1.74	1.74	1.46	2.89	2.43	2.67	3.68
Dermoptera	*Cynocephalus volans*	USNM 144662	4.88	5.55	2.18	1.53	2.25	1.16	4.05	4.08	3.32	4.48
Dermoptera	*Cynocephalus volans*	USNM 317118	5.66	5.68	2.16	2.35	2.48	1.00	3.32	4.67	3.74	5.14
Dermoptera	*Cynocephalus volans*	USNM 578084	6.29	5.19	2.65	2.08	2.48	1.21	3.60	4.74	3.51	5.00
Omomyoidea	*Omomys carteri*	UCM 69303	9.29	6.96	1.91	0.69	10.17	1.32	3.68	3.07	12.25	4.57
Omomyoidea	*Omomys carteri*	UCM 69065	8.27	6.07	1.91	0.95	9.41	1.15	3.26	3.06	11.09	4.45
Omomyoidea	*Omomys carteri*	UCM 68745	8.50	6.36	1.71	0.36	9.03	1.18	2.77	2.94	11.16	4.24
Haplorhini	*Cebuella pygmaea*	AMNH 244101	2.86	2.97	0.84	0.71	3.30	0.66	2.15	1.83	4.32	2.41
Haplorhini	*Cebuella pygmaea*	AMNH 244365	3.13	3.03	0.86	0.73	3.36	0.73	2.00	1.84	4.30	2.49
Haplorhini	*Cebuella pygmaea*	SBU NC1	3.23	3.06	0.90	0.71	3.40	0.65	1.97	1.71	4.35	2.49
Haplorhini	*Cebus apella*	AMNH 133606	10.89	11.97	4.18	4.01	12.61	3.71	8.55	5.60	16.26	9.44
Haplorhini	*Cebus apella*	AMNH 133608	11.66	11.13	3.55	3.43	13.20	3.45	7.96	4.67	16.88	8.46
Haplorhini	*Cebus apella*	AMNH 133764	10.97	10.42	3.44	2.96	11.32	2.92	7.41	6.34	15.13	8.54
Haplorhini	*Saguinus mystax*	AMNH 188177	4.94	4.98	1.53	1.00	5.58	0.87	3.22	2.25	6.19	3.78
Haplorhini	*Saimiri boliviensis*	AMNH 211613	7.65	7.76	2.78	1.53	8.20	1.22	5.11	2.99	9.14	5.45
Haplorhini	*Tarsius spectrum*	AMNH 109369	20.02	2.09	1.25	0.46	21.31	0.75	2.07	2.48	22.34	3.91
Plesiadapiformes	*Carpolestes simpsoni*	UM 101963	2.40	2.78	1.29	1.11	0.86	0.95	1.71	2.12	2.22	2.46
Plesiadapiformes	*Dryomomys szalayi*	UM 41870	1.00	1.30	0.72	0.67	0.49	0.68	0.84	0.72	1.10	1.09
Plesiadapiformes	*Ignacius graybullianus*	USNM 442240	2.20	2.52	1.46	0.94	1.16	1.07	2.12	2.00	2.86	2.52
Plesiadapiformes	*Nannodectes gidleyi*	AMNH 17379	3.60	3.54	2.07	1.37	3.26	1.13	2.03	2.45	3.92	3.43
Plesiadapiformes	*Phenacolemur simonsi*	USNM 442238	2.03	2.25	1.37	1.11	1.19	0.74	1.68	1.53	2.67	2.08
Plesiadapiformes	*Plesiadapis churchilli*	UM 118271	4.61	4.29	2.67	2.18	3.01	1.79	2.52	3.30	4.25	4.07
Plesiadapiformes	*Plesiadapis cookei*	UM 87990	8.75	7.00	3.65	3.34	4.67	2.19	5.14	5.19	7.63	6.81
Plesiadapiformes	*Plesiadapis tricuspidens*	MNHN R 414	6.81	6.43	3.90	3.11	4.20	2.34	4.67	5.26	6.35	6.44
Plesiadapiformes	*Plesiadapis tricuspidens*	MNHN R 611	5.52	5.43	3.11	3.00	4.70	2.11	4.23	4.33	6.36	5.66
Plesiadapiformes	*Purgatorius*	UCMP 197517	1.56	1.79	0.81	1.00	0.75	0.78	1.41	1.33	1.69	1.68
Plesiadapiformes	*Tinimomys graybulliensis*	USNM 461201	0.92	1.27	0.54	0.65	0.50	0.65	0.90	0.79	0.93	1.12
Scandentia	*Ptilocercus lowii*	YPM 6873	2.04	1.68	0.80	0.80	2.44	0.85	1.32	1.12	2.77	1.66
Scandentia	*Tupaii belangeri*	AMNH 113135	2.88	3.08	1.35	1.26	3.58	0.99	2.44	1.77	4.83	2.89
Scandentia	*Tupaii sp.*	SBU coll.	2.81	2.98	1.36	0.74	3.90	0.53	1.59	1.99	4.88	2.75
Scandentia	*Urogale everetti*	AMNH 203293	3.93	3.84	1.64	1.72	3.41	0.83	2.79	2.21	4.82	3.31

TABLE A-II-40.— Cont'd.

Higher taxon	Taxon	Catalogue Number	Cc-11	Cc-12	Cc-13	Cc-14	Cc-15	Cc-16	Cc-17	Cc-18	Cc-19	GM
Adapoidea	*Adapis parisiensis*	AMNH 111937	5.39	7.09	2.99	0.44	8.47	1.28	5.74	3.72	10.12	6.03
Adapoidea	*Adapis parisiensis*	NMB QE741	5.38	6.99	3.08	1.13	8.86	1.38	5.28	4.57	10.07	5.70
Adapoidea	*Notharctus tenebrosus*	AMNH 131945	10.29	10.75	3.93	1.81	10.95	2.24	7.33	6.02	12.58	8.53
Adapoidea	*Notharctus tenebrosus*	AMNH 131766	8.75	9.02	3.53	1.99	9.32	2.29	6.42	5.07	11.62	7.44
Adapoidea	*Notharctus tenebrosus*	AMNH 11474	9.49	8.63	3.68	1.83	9.42	1.86	6.34	5.05	11.42	7.33
Adapoidea	*Leptadapis magnus*	NHMB QF 421	9.41	11.99	4.26	3.17	14.35	3.97	9.76	7.29	19.99	10.66
Strepsirrhini	*Cheirogaleus medius*	DPC 031	5.34	4.79	1.53	0.58	6.51	0.72	2.68	1.97	7.17	3.15
Strepsirrhini	*Cheirogaleus medius*	DPC 1023	5.73	5.14	1.61	0.51	6.72	0.85	2.66	2.05	7.22	3.27
Strepsirrhini	*Cheirogaleus medius*	AMNH 80072	5.89	5.95	1.91	0.50	7.56	0.74	2.79	2.41	8.33	3.60
Strepsirrhini	*Eulemur fulvus*	AMNH 170717	10.61	9.99	3.45	0.79	14.53	2.13	6.46	4.52	16.10	7.24
Strepsirrhini	*Eulemur fulvus*	AMNH 100528	12.1	10.36	3.65	0.70	17.04	1.80	6.80	4.60	18.40	7.36
Strepsirrhini	*Eulemur fulvus*	DPC 095	10.57	9.85	3.19	0.59	16.01	2.04	6.27	4.62	17.44	7.15
Strepsirrhini	*Galago senegalensis*	AMNH 86502	19.13	4.22	1.27	0.65	21.31	0.78	2.51	2.48	26.34	4.35
Strepsirrhini	*Loris tardigradus*	AMNH 34256	4.22	4.22	1.50	0.71	4.62	0.61	3.14	2.04	5.15	2.79
Strepsirrhini	*Loris tardigradus*	AMNH 150038	3.94	4.03	1.56	0.97	4.31	0.59	3.35	2.53	5.77	3.14
Strepsirrhini	*Loris tardigradus*	HTB 750	3.44	3.41	1.66	0.63	4.49	0.67	2.87	2.35	5.87	3.03
Strepsirrhini	*Otolemur crassicaudatus*	SBU coll.	22.13	8.31	3.57	1.57	24.83	1.42	6.16	4.94	25.83	7.72
Strepsirrhini	*Otolemur crassicaudatus*	AMNH 216240	20.75	2.94	2.73	0.48	24.39	1.74	5.48	4.21	25.71	6.92
Strepsirrhini	*Propithecus verreauxi*	AMNH 170471	12.01	11.44	4.03	1.04	18.17	2.18	7.31	5.28	18.68	7.71
Strepsirrhini	*Varecia variegate*	AMNH 201384	11.61	10.93	3.64	0.41	18.08	2.62	8.83	5.81	19.82	8.98

TABLE A-II-41.— Measurements (degrees) of the calcanea of Plesiadapiformes and select other mammals (see Fig. 62; measurements here were initiated in Tables A-II-39 and A-II-40). Calcaneum (*Cc*) measurements 20–25 are angular: 20, angle between ectal facet surface (parallel to its axis) and proximal part of sustentacular facet surface (parallel to its axis); 21, angle between ectal facet axis and tuber; 22, angle between peroneal tubercle and sustentaculum; 23, mediolateral angle between calcaneocuboid facet and tuber axis; 24, dorsoplantar angle between calcaneocuboid facet and tuber axis; 25, angle between surface of proximal part of sustentacular facet (parallel to its axis) and distal part of sustentacular facet (parallel to its axis).

Higher taxon	Taxon	Specimen	Cc-20	Cc-21	Cc-22	Cc-23	Cc-24	Cc-25
Adapisoriculidae	*Deccanolestes hislopi*	VPL/JU/NKIM/52	142	61	166	86	104	32
Cimolestidae	*Procerberus formicarum*	AMNH 117455	141	55	168	76	103	48
Cimolestidae	*Procerberus formicarum*	AMNH 119802	147	40	167	77	107	43
Condylarthra	*Protungulatum donnae*	AMNH 118060	147	50	175	72	122	19
Dermoptera	*Cynocephalus volans*	USNM 144662	138	74	180	76	105	47
Dermoptera	*Cynocephalus volans*	USNM 317118	142	70	166	76	106	37
Dermoptera	*Cynocephalus volans*	USNM 578084	146	77	168	68	110	34
Omomyoidea	*Omomys carteri*	UCM 69303	137	71	139	98	108	10
Omomyoidea	*Omomys carteri*	UCM 69065	123	72	144	93	114	10
Omomyoidea	*Omomys carteri*	UCM 68745	136	70	146	98	106	7.5
Haplorhini	*Cebuella pygmaea*	AMNH 244101	129	58	165	86	105	13
Haplorhini	*Cebuella pygmaea*	AMNH 244365	134	60	163	86	100	10
Haplorhini	*Cebuella pygmaea*	SBU NC1	135	58	168	82	102	12
Haplorhini	*Cebus apella*	AMNH 133606	133	61	166	85	90	46
Haplorhini	*Cebus apella*	AMNH 133608	130	58	165	85	91	46
Haplorhini	*Cebus apella*	AMNH 133764	148	63	174	87	91	47
Haplorhini	*Saguinus mystax*	AMNH 188177	111	58	161	89	130	28
Haplorhini	*Saimiri boliviensis*	AMNH 211613	104	62	151	87	122	40
Haplorhini	*Tarsius spectrum*	AMNH 109369	141	82	160	87	100	37
Plesiadapiformes	*Carpolestes simpsoni*	UM 101963	141	68	162	79	107	44
Plesiadapiformes	*Dryomomys szalayi*	UM 41870	129	67	166	80	103	35
Plesiadapiformes	*Ignacius graybullianus*	USNM 442240	125	59	165	79	109	42
Plesiadapiformes	*Nannodectes gidleyi*	AMNH 17379	145	69	175	81	105	20
Plesiadapiformes	*Phenacolemur simonsi*	USNM 442238	124	63	171	78	99	44
Plesiadapiformes	*Plesiadapis churchilli*	UM nn	152	75	173	75	104	25
Plesiadapiformes	*Plesiadapis cookei*	UM 87990	148	73	162	75	103	32
Plesiadapiformes	*Plesiadapis tricuspidens*	MNHN R 414	146	68	172	73	94	21
Plesiadapiformes	*Plesiadapis tricuspidens*	MNHN R 611	150	73	166	73	100	21
Plesiadapiformes	*Purgatorius*	UCMP 197517	129	64	164	71	107	44
Plesiadapiformes	*Tinimomys graybulliensis*	USNM 461201	132	63	165	81	106	30
Scandentia	*Ptilocercus lowii*	YPM 6873	126	84	160	78	97	50
Scandentia	*Tupaii belangeri*	AMNH 113135	123	53	156	85	91	34
Scandentia	*Tupaii sp.*	SBU coll.	141	61	158	83	89	9
Scandentia	*Urogale everetti*	AMNH 203293	125	60	150	82	91	35
Adapoidea	*Adapis parisiensis*	AMNH 111937	167	76	180	102	104	42
Adapoidea	*Adapis parisiensis*	NMB QE741	143	84	154	89	111	17
Adapoidea	*Notharctus tenebrosus*	AMNH 131945	147	82	162	91	104	23
Adapoidea	*Notharctus tenebrosus*	AMNH 131766	145	81	163	92	97	17

TABLE A-II-41.— Cont'd.

Higher taxon	Taxon	Specimen	Cc-20	Cc-21	Cc-22	Cc-23	Cc-24	Cc-25
Adapoidea	*Notharctus tenebrosus*	AMNH 11474	158	82	160	90	94	16
Adapoidea	*Leptadapis magnus*	NHMB QF 421	143	83	147	90	113	28
Strepsirrhini	*Cheirogaleus medius*	DPC 031	129	86	161	86	107	36
Strepsirrhini	*Cheirogaleus medius*	DPC 1023	148	84	157	83	110	39
Strepsirrhini	*Cheirogaleus medius*	AMNH 80072	136	78	152	85	110	43
Strepsirrhini	*Eulemur fulvus*	AMNH 170717	145	83	142	88	97	23
Strepsirrhini	*Eulemur fulvus*	AMNH 100528	144	84	148	85	105	22
Strepsirrhini	*Eulemur fulvus*	DPC 095	140	79	144	89	108	26
Strepsirrhini	*Galago senegalensis*	AMNH 86502	157	81	166	86	114	26
Strepsirrhini	*Loris tardigradus*	AMNH 34256	149	79	175	87	135	13
Strepsirrhini	*Loris tardigradus*	AMNH 150038	157	84	176	86	125	13
Strepsirrhini	*Loris tardigradus*	HTB 750	160	90	180	93	114	9
Strepsirrhini	*Otolemur crassicaudatus*	SBU coll.	157	78	180	91	100	42
Strepsirrhini	*Otolemur crassicaudatus*	AMNH 216240	121	78	141	88	129	33
Strepsirrhini	*Propithecus verreauxi*	AMNH 170471	99	85	172	84	102	45
Strepsirrhini	*Varecia variegata*	AMNH 201384	137	79	153	83	101	12

TABLE A-II-42.— Measurements (mm) and shape variables of plesiadapid cuboids. UM 87990 is illustrated in Figure 63A. Abbreviations are explained in Table A-II-1. GM is the geometric mean of Le, PEW, PED, PtgW, DEW, and DED.

Taxon	Specimen	Le	PEW	PED	PtgW	DEW	DED	CfA	GM	PgV
P. cookei	UM 87990	8.22	6.22	4.98	2.04	5.01	5.16	58	4.88	0.42
P. tricuspidens	MNHN R 415	7.95	5.83	5.48	1.90	4.74	4.74	59	4.71	0.40
P. tricuspidens	Pellouin coll.	8.24	6.16	5.11	1.83	4.60	4.60	41	4.65	0.39
N. intermedius	USNM 442229	4.64	3.17	2.76	0.96	2.36	2.54	51	2.48	0.39

TABLE A-II-43.— Measurements (mm) and shape variables of plesiadapid metatarsals. Metatarsals of UM 87990 'set 1' are illustrated in Figure 65. Metatarsals of UM 87990 'set 2' are illustrated in Figure 67. Head shape variable HSV is ln (DEW / DED). Shaft shape variable SSV is ln (Le / √ (MSW H MSD)). Abbreviations are explained in Table A-II-1.

Taxon	Specimen	Bone	Le	PEW	PED	MSW	MSD	DEW	DED	HSV	SSV
P. cookei	UM 87990 set 1	R MT I	17.80	5.80	4.20	2.70	2.50	4.40	4.10	0.071	1.924
P. cookei	UM 87990 set 1	L MT II	—	3.30	4.80	—	—	—	—	—	—
P. cookei	UM 87990 set 1	R MT II	—	—	—	2.80	2.70	5.10	4.30	0.171	—
P. cookei	UM 87990 set 1	L MT III	—	3.20	5.10	2.80	2.40	—	—	—	—
P. cookei	UM 87990 set 1	R MT III	29.10	3.50	5.10	2.40	2.50	4.30	4.00	0.072	2.475
P. cookei	UM 87990 set 1	R MT IV	31.50	3.30	—	2.50	2.30	4.60	—	—	2.575
P. cookei	UM 87990 set 2	L MT IV	32.30	3.30	—	2.50	2.40	4.80	—	—	2.579
P. cookei	UM 87990 set 2	R MT V	—	6.40	3.60	3.30	2.40	—	—	—	—
P. n. sp.	MNHN no no.	R MT I	16.60	6.00	3.90	2.90	2.60	4.30	—	—	1.799
P. n. sp.	MNHN no no.	L MT II	24.10	—	—	2.70	2.20	—	—	—	2.291
P. n. sp.	MNHN no no.	R MT III	24.70	3.30	—	2.70	2.30	3.90	—	—	2.294
P. n. sp.	MNHN no no.	R MT IV	25.70	4.00	—	2.70	2.30	3.90	—	—	2.333
P. n. sp.	MNHN no no.	R MT V	19.00	5.20	—	1.90	—	3.70	—	—	—
cf. *P. churchilli*	UM 118270	L MT I	12.88	4.15	3.20	2.11	1.81	3.05	2.60	0.160	1.886
cf. *P. churchilli*	SMM P77.33.517	L MT III	—	2.08	3.40	1.85	1.68	—	—	—	—
cf. *P. churchilli*	SMM P77.33.517	R MT IV	—	2.24	3.26	1.65	1.54	—	—	—	—
cf. *P. churchilli*	SMM P77.33.517	L MT V	17.54	—	2.84	1.65	1.40	2.93	2.58	0.127	2.446
N. intermedius	USNM 442229	L MT I	11.38	3.12	2.70	1.66	1.64	2.29	2.03	0.121	1.931
N. intermedius	USNM 442229	L MT II	—	1.71	2.78	1.61	1.21	—	—	—	—
N. intermedius	USNM 442229	?L MT II	—	—	—	—	—	2.67	1.98	0.299	—
N. intermedius	USNM 442229	L MT III	—	1.72	3.00	—	—	—	—	—	—
N. intermedius	USNM 442229	?L MT III	—	—	—	1.73	1.41	2.40	2.01	0.177	—
N. intermedius	USNM 442229	L MT IV	—	—	2.61	1.38	1.20	—	—	—	—
N. intermedius	USNM 442229	?L MT IV	—	—	—	1.65	1.38	2.34	1.98	0.167	—
N. intermedius	USNM 442229	L MT V	—	2.80	2.30	—	—	—	—	—	—
N. intermedius	USNM 442229	L MT V	—	—	—	1.30	1.27	2.47	1.98	0.221	—

TABLE A-II-44.— Measurements (mm) of the distal humerus of *Plesiadapis cookei*, Plesiadapidae, and comparative taxa (augmented from Table A-II-14). Abbreviations are explained in Table A-II-1. The principal components analysis illustrated in Figure 71 compares these measurements as shape variables. Asterisks indicate specimens for which CaL was not available, with CaL being approximated by CaH.

Code	Taxon	Specimen	TW	TH	CaW	TL	CaL	EEC
1	*Plesiadapis cookei*	UM 87990	5.84	4.33	8.75	6.63	6.35	8.05
2	cf. *Pronothodectes gaoi*	UALVP 49114	3.80	3.01	5.40	4.10	3.90	5.09
3	*Nannodectes intermedius*	USNM 42229	2.96	1.58	3.89	3.51	2.80	3.25
4	cf. *Plesiadapis rex*	UM 64588	2.90	2.20	5.05	3.59	3.45	3.84
5	*Plesiadapis walbeckensis*	Walbeck (Szalay and Dagosto, 1980)	3.40	3.10	5.80	3.55	3.50	3.70
6	cf. *P. remensis*	MNHN CR 208	4.17	3.73	7.03	5.81	3.42	5.80
7	*Plesiadapis tricuspidens*	MNHN BR 14522	4.65	3.99	6.51	5.59	4.16	6.00
8	*Plesiadapis tricuspidens*	MNHN BR-03-L	4.60	3.16	8.16	7.09	4.85	7.68
9	*Plesiadapis tricuspidens*	MNHN BR 12591	5.77	4.55	8.42	6.44	4.59	6.09
10	*Plesiadapis tricuspidens*	MNHN R 405	6.65	5.40	9.47	7.19	4.47	7.22
11	*Plesiadapis tricuspidens*	Berru (Mr Malfait)	6.03	4.94	7.68	6.70	4.14	6.65
12	*Plesiadapis tricuspidens*	MNHN BR-04-L	5.53	3.71	7.63	5.92	4.40	7.11
13	*Plesiadapis tricuspidens*	MNHN R 492	6.01	5.16	8.23	6.85	4.16	8.17
14	cf. *Pl. daubrei*	UCMP 102829	6.51	5.06	8.87	6.81	6.13	7.84
15	cf. *Saxonellla crepaturae*	Walbeck	0.91	0.60	1.21	0.75	0.75	1.09
16	*C. simpsoni*	UM 101963	1.55	1.09	2.60	1.88	1.34	3.12
17	*'Nothodectes'*	AMNH 17379	3.30	2.97	3.95	3.84	3.42	3.80
18	Omomyid Bridger Basin	AMNH29126 (Szalay and Dagosto, 1980)	3.00	1.45	3.95	2.55	2.20	2.60
19	Omomyid Bitter Creek	AMNH113301 (Szalay and Dagosto, 1980)	1.21	0.75	1.50	1.42	1.20	1.51
20	Microchoerine omomyid 1	Basel QD 328 (Szalay and Dagosto, 1980)	2.90	2.10	3.25	2.75	2.40	2.60
21	Microchoerine omomyid 2	Basel QJ 620 (Szalay and Dagosto, 1980)	3.70	2.65	4.10	3.05	3.15	1.95
22	Microchoerine omomyid 3	Basel QV 18 (Szalay and Dagosto, 1980)	2.20	1.55	2.40	1.90	1.90	1.75
23	Microchoerine omomyid 4	Basel QK 989 (Szalay and Dagosto, 1980)	2.00	1.65	2.75	1.70	1.65	2.10
24	*Smilodectes gracilis*	AMNH11484 (Szalay and Dagosto, 1980)	4.90	5.20	8.90	5.00	5.05	5.55
25	*Adapis parisiensis*	Basel QW 1481 (Szalay and Dagosto, 1980)	5.65	4.25	8.55	6.40	6.50	4.60
26	*Adapis parisiensis*	Basel QW 1482 (Szalay and Dagosto, 1980)	4.80	3.80	7.75	5.20	5.30	4.70
27	*Adapis parisiensis*	AMNH 81001 (Szalay and Dagosto, 1980)	5.15	3.85	7.30	5.20	6.15	3.65
28	*Leptadapis magnus*	Basel QD 663 (Szalay and Dagosto, 1980)	10.10	7.90	15.15	9.20	9.40	10.20
29	*Leptadapis magnus*	Basel QD 664 (Szalay and Dagosto, 1980)	9.35	8.20	15.50	10.10	10.10	7.05
30	*Leptadapis magnus*	Basel QD 681 (Szalay and Dagosto, 1980)	10.60	6.80	16.10	10.40	10.10	10.40
31	*Deccanolestes* cf. *hislopi*	VPL/JU/NKIM/79	0.57	0.84	1.08	0.95	0.80	1.06
32	*Protungulatum donnae*	UMinn 1836 (Szalay and Dagosto, 1980)	2.33	3.01	4.18	3.80	2.13	3.78
33	Actocyonidae indet.	USNM 9999 (Szalay and Dagosto, 1980)	2.65	3.45	7.60	5.35	3.85	5.70
34	Mason Pocket taxon	AMNH 89519 (Szalay and Dagosto, 1980)	1.16	0.57	1.60	1.21	1.00	1.22
35	*Ptilocercus lowii*	Means (Sargis, 2002a)*	1.45	1.41	1.55	1.46	1.19	1.90
36	*Tupaia minor*	Means (Sargis, 2002a)*	1.16	1.51	1.77	1.93	1.62	1.60
37	*Tupaia glis*	Means (Sargis, 2002a)*	1.55	2.22	2.29	2.63	2.19	1.99
38	*Cynocephalus volans*	UF 5969	3.39	4.59	5.92	5.96	4.97	4.02

TABLE A-II-45.— Plesiadapiform limb indices. Abbreviations: *Ltr-I*, limb-trunk index; *Br-I*, brachial index; *Cr-I*, crural index; *Int-I*, intermembral index; *Hf-I*, humerofemoral index; *Rt-I*, radiotibial index. See Table A-II-1for explanations of indices.

Taxon	Specimen	Ltr-I	Br-I	Cr-I	Int-I	Hf-I	Rt-I
P. cookei	UM 87990	79	101	99	88	87	89
P. tricuspidens	Various	—	99	—	—	92	—
P. insignis	Gingerich (1976)	58	84	94	71	75	67
N. intermedius	USNM 442229	—	—	—	73	—	73
C. simpsoni	UM 101963	—	112	—	—	74	—
I. clarkforkensis	UM 82616	89	94	104	80	84	76
Micromomyidae	Various	—	117	127	93	97	90

TABLE A-II-46.— Body segment lengths of *Plesiadapis cookei* and other plesiadapiforms. Abbreviations: *Trk*, trunk (thorax + lumbus); *H*, humerus; *U*, ulna; *R*, radius; *MC III*, third metacarpal; *F*, femur; *T*, tibia; *MT III*, third metatarsal.

Taxon	Specimen	Le Trk	Le H	Le U	Le R	Le MC III	Le F	Le T	Le MT III
P. cookei	UM 87990	206.00	75.24	88.30	76.30	20.00	86.60	86.10	29.10
P. tricuspidens	Various	—	70.50	85.08	70.10	21.10	76.60	—	—
P. n. sp.	Various	—	—	—	—	19.70	77.80	—	24.70
P. insignis	Gingerich (1976)	140.00	36.73	36.00	31.00	11.70	49.00	46.00	—
N. intermedius	USNM 442229	—	—	41.20	32.84	11.51	—	44.80	—
N. gidleyi	Various	—	—	—	—	12.02	—	—	—
C. simpsoni	UM 101963	57.92	21.60	28.12	~24.10	7.18	29.12	~30.00	7.40
I. clarkforkensis	Various	109.00	44.70	44.00	41.82	10.32	53.00	55.00	15.30
Micromomyidae	Various	—	14.58	—	17.13	3.72	15.02	19.03	5.09

TABLE A-II-47.— Body segment lengths for comparison with those of plesiadapids in Table A-II-46. Abbreviations: *Trk*, trunk (thorax +lumbus); *H*, humerus; *U*, ulna; *R*, radius; *MC III*, third metacarpal; *F*, femur; *T*, tibia; *MT III*, third metatarsal.

Taxon	Specimen	Le Trk	Le H	Le R	Le MC III	Le F	Le T	Le MT III
Petaurus breviceps	UMMZ 160143	84.40	33.54	41.06	7.34	41.04	44.90	7.14
Trichosurus vulpecula	UMMZ 157192	250.08	80.20	92.90	18.53	104.06	102.02	22.50
Choloepus hoffmani	UMMZ 64940	308.50	125.40	140.00	29.00	126.50	117.54	29.00
Bradypus tridactylus	UMMZ 64943	236.00	170.00	152.00	19.05	97.42	90.25	19.76
Cynocephalus volans	USNM 56530	210.49	105.40	121.90	28.39	122.96	120.17	24.58
Tupaia glis	UMMZ 118389	85.38	28.98	27.20	9.60	37.00	37.00	15.90
Eulemur fulvus	UMMZ 160910	207.23	86.19	102.78	22.15	135.53	128.73	31.24
Galago senegalensis	UMMZ 113351	85.54	35.50	35.70	8.82	70.10	62.50	11.02
Nycticebus coucang	UMMZ 113355	166.68	69.70	67.80	12.00	81.70	76.90	14.30
Tarsius philippensis	UMMZ 95741	46.39	27.60	35.10	10.49	55.46	53.36	11.63
Cebuella pygmaea	UMMZ 160146	61.21	30.12	28.40	8.18	34.58	36.70	14.08
Callimico goeldii	UMMZ 160149	139.95	56.70	53.50	16.00	77.50	77.50	29.00
Saguinus mystax	UMMZ 160148	147.70	54.14	50.78	15.02	70.28	71.94	26.26
Ateles geoffroyi	UMMZ 63171	202.50	194.00	207.00	47.30	200.00	187.00	54.60
Glaucomys volans	UMMZ 168356	56.70	26.41	30.34	5.21	31.20	35.34	12.08
Citellus mexicanus	UMR 1716	73.33	24.30	21.43	8.06	31.46	33.70	13.46
Sciurus niger	UMMZ TC 29	149.45	48.00	46.20	13.90	62.40	67.90	24.90
Ptilocercus lowii	Le Gros Clark (1926)	—	21.53	22.93	6.12	27.16	28.73	8.90
Tupaia glis	SBU specimen	—	29.85	26.62	9.33	37.72	38.69	16.14
Varecia variegata	UMMZ 172669	—	105.74	122.01	29.57	157.79	140.22	36.65
Otolemur crassicandatus	UMMZ mean of 2	—	55.66	68.44	13.21	92.03	85.22	16.15
Nycticebus coucang	UMMZ mean of 3	—	69.84	76.52	13.66	81.52	79.22	15.90
Galago senegalensis	UMMZ mean of 2	—	35.50	35.70	8.82	70.10	62.50	11.02
Cebuella pygmaea	SBU NC-01	—	34.70	32.01	9.34	38.68	38.97	15.28
Callicebus m. pallesceus	UMMZ 125576	—	67.60	64.80	9.13	79.65	83.09	24.95
Saguinus goeffroyi	UMMZ 160147	—	52.94	55.52	15.27	66.56	69.40	25.58
Saguinus oedipus	SBU NSg-06	—	51.46	45.83	14.22	65.28	65.18	24.63
Saguinus oedipus	UMMZ 157195	—	52.18	52.85	14.81	63.56	64.27	25.18
Saimiri s. sciureus	UMMZ 46414	—	67.68	66.06	15.66	80.91	82.13	27.18
Saimiri sciureus	UMMZ 122657	—	74.44	79.97	8.22	92.27	92.46	30.53
Cebus capucinus	UMMZ 77296	—	100.91	104.99	22.53	123.72	118.02	37.50
Ateles geoffroyi	UMMZ mean of 2	—	194.71	223.43	50.10	195.89	187.73	54.60
Alouatta caraya	UMMZ 124690	—	136.01	144.30	30.34	145.60	126.30	37.70
Alouatta p. aequatorialis	UMMZ mean of 2	—	148.77	160.53	34.20	154.70	136.15	40.46
Alouatta p. mexicana	UMMZ mean of 2	—	149.79	157.65	31.00	148.61	136.54	38.32
Cercopithecus cephus	UMMZ 39508	—	111.32	123.85	28.64	140.88	137.78	42.20
Macaca f. mindanensis	UMMZ 161308	—	119.50	137.20	31.54	141.98	131.85	43.14
Macaca mulatta	UMMZ 98651	—	125.84	139.40	30.65	145.40	137.15	37.27
Hylobates hoolock	UMMZ 160908	—	220.80	255.10	61.44	203.60	182.00	46.64
Pan troglodytes	UMMZ 167199	—	285.60	286.68	87.01	281.30	252.10	74.70
Pan troglodytes	UMMZ 76276	—	247.00	238.40	75.00	226.40	200.70	65.24
Sciurus carolinensis	SBU MRd-10	—	42.03	40.16	12.59	54.69	61.06	23.00

TABLE A-II-48.— List of specimens from MNHN collection mentioned by Beard (1989). Fig. # - figure in Beard (1989), Relocated? – whether DMB was able to relocate the specimen in the MNHN collection in Paris in 2006.

Specimen #	Identification	Fig. #	Relocated?
MNHN R 415	R. cuboid	—	Y
MNHN R 416	L. entocuneiform	—	Y
MNHN R 5295	R. metatarsal III	—	Y
MNHN R 5296	Ped. intermediate phalanx	—	Y
MNHN R 5297	Man. proximal phalanx	—	Y
MNHN R 5298	L. metatarsal IV	—	N
MNHN R 5300	R. metatarsal III	—	N
MNHN R 5301	Man. proximal phalanx	—	N
MNHN R 5303	Man. proximal phalanx	—	Y
MNHN R 5305	L. metacarpal II	—	Y
MNHN R 5306	R. metatarsal I, epiphysis	—	N
MNHN R 5309	Ped. distal phalanx	—	Y
MNHN R 5310	Ped. distal phalanx, frag.	—	N
MNHN R 5312	Man. intermediate phalanx	—	N
MNHN R 5313	Ped. distal phalanx	—	Y
MNHN R 5315	proximal phalanx, pollex	—	Y
MNHN R 5317	Ped. distal phalanx, frag.	—	N
MNHN R 5318	L. mesocuneiform	—	N
MNHN R 5319	right capitate	20	N
MNHN R 5320	right triquetrum	19	Y
MNHN R 5321	left hamate	21	N
MNHN R 5372	R. navicular & proximal phalanx	—	N
MNHN R 5373	R. metacarpal II	—	Y
MNHN R 5342	Man. proximal phalanx	—	N
MNHN R 5355	Man. proximal phalanx	—	N
MNHN R 5365	Man. proximal phalanx	—	N
MNHN R 5371	Man. proximal phalanx	—	N
MNHN R 5352	Man. intermediate & distal phalanx	—	N
MNHN R 5360	Man. intermediate phalanx	—	Y
MNHN R 5366	Man. intermediate phalanx	—	N
MNHN R 5369	Man. intermediate phalanx	—	Y
MNHN R 5361	Man. distal phalanx	—	Y
MNHN R 5331	L. entocuneiform	—	Y
MNHN R 5359	R. entocuneiform	—	Y
MNHN R 5340	metacarpal, frag.	—	N
MNHN R 5350	metacarpal, frag.	—	Y
MNHN R 5353	metacarpal, frag.	—	Y
MNHN R 5358	metacarpal, frag.	—	N

TABLE A-II-48.— Cont'd.

Specimen #	Identification	Fig. #	Relocated?
MNHN R 5323	R. metatarsal IV	—	Y
MNHN R 5325	L. metatarsal II	—	N
MNHN R 5326	L. metatarsal IV	—	N
MNHN R 5336	metatarsal, frag.	—	N
MNHN R 5337	L. metatarsal II, frag.	—	N
MNHN R 5345	R. metatarsal II, frag	—	N
MNHN R 5351	R. metatarsal II, frag	—	N
MNHN R 5368	L. metatarsal II, frag.	—	N
MNHN R 5370	metatarsal, frag.	—	N
MNHN R 503	Ped. proximal phalanx	—	Y
MNHN R 5328	Ped. proximal phalanx	—	N
MNHN R 5329	Ped. proximal phalanx	—	N
MNHN R 5324	Ped. intermediate phalanx	—	Y
MNHN R 5330	Ped. intermediate phalanx	—	Y
MNHN R 5341	Ped. intermediate phalanx	—	Y
MNHN R 5346	Ped. intermediate phalanx	—	Y
MNHN R 5363	Ped. intermediate phalanx	—	Y
MNHN R 589	Ped. distal phalanx	—	Y
MNHN R 612	Ped. distal phalanx	—	Y
MNHN R 613	Ped. distal phalanx	—	Y
MNHN R 5344	Ped. distal phalanx	—	Y
MNHN R 5377	Ped. distal phalanx	—	N
MNHN R 5379	Ped. distal phalanx	—	Y
MNHN R 5381	Ped. distal phalanx	—	N

APPENDIX III — BODY WEIGHT

Body weight can be estimated from mammalian long bone lengths and diameters using the following R script (R Core Team. 2015. R: a language and environment for statistical computing. R Foundation for Statistical Computing, Vienna (http://www.R-project.org/). The reference sample is from Alexander et al. (1979).

Input data are listed in tabular form in Table A-III-1 below. Results for *Plesiadapis cookei* and other plesiadapids are tabulated in Table 6 in the text.

```
#=========================================================================
#Rewritten R version of 1990 'BodyMass' program.  Univ. Mich.  Dec. 29, 2017
#See original for details:  Gingerich, P. D. 1990.  Prediction of body mass
#in mammalian species from long bone lengths and diameters.  Contrib.
#Mus. Paleont., Univ. Mich. 28:79-92.  http://hdl.handle.net/2027.42/48540
print (date()) #session run date
#=========================================================+ Input data file
#list.files("C://R_BodyMass",pattern=".csv")
Brain=TRUE  #FALSE
m.mm<-vector(length=12)
#m.mm=c(76.6,92.0,24.1,88.8,87.0,32.4,7.8,5.6,2.3,6.6,6.2,2.8)
#  m.l='Plesiadapis cookei (Gingerich 1990 measurements)'
m.mm=c(75.6,88.3,20,86.6,86.1,29.1,6.86,5.85,2.2,6.53,5.71,2.5)
  m.l='Plesiadapis cookei (Boyer 2009 measurements)'
#m.mm=c(70.5,85.08,21.1,76.6,NA,NA,7.65,5.56,2.30,6.21,NA,NA)
#  m.l='Plesiadapis tricuspidens (Boyer 2009)'
#m.mm=c(NA,NA,NA,NA,NA,NA,3.75,3.35,NA,NA,NA,NA)
#  m.l='Plesiadapis rex (Boyer 2009)'
#m.mm=c(NA,NA,NA,NA,NA,NA,NA,NA,NA,4.94,NA,1.68)
#  m.l='Plesiadapis churchilli (Boyer 2009)'
#m.mm=c(36.73,36,11.7,49,46,NA,NA,NA,NA,NA,NA,NA)
#  m.l='Plesiadapis insignis (Boyer 2009)'
#m.mm=c(NA,41.2,11.51,NA,44.8,NA,3.28,2.94,1.05,3.69,2.88,1.41)
#  m.l='Nannodectes intermedius (Boyer 2009)'
#m.mm=c(NA,NA,12.02,NA,NA,NA,NA,3.16,1.02,4.22,3.36,NA)
#  m.l='Nannodectes gidleyi (Boyer 2009)'
#m.mm=c(NA,NA,15.61,NA,NA,NA,4.89,NA,1.51,NA,NA,2)
#  m.l='Pronothodectes gaoi (Boyer 2009)'

#================================================ Alexander 1979 statistics
#total species: 36; non-artiodactyls: 26; artiodactyls: 10
A<-matrix(nrow=12,ncol=8)
  rownames(A)=c('H.L','U.L','MC.L','F.L','T.L','Mt.L',
    'H.D','U.D','MC.D','F.D','T.D','Mt.D')
  colnames(A)=c('N','Slope','Intcpt','R2','Xbar','S2yx','Sb','T05nm2')
A[1,]=c( 41, 2.6752, -1.5579, 0.969, 1.9154, 0.06655, 0.07726,  2.021)
A[2,]=c( 40, 2.7162, -1.8459, 0.972, 1.9787, 0.05931, 0.07499,  2.022)
A[3,]=c( 29, 2.4746, -0.0636, 0.918, 1.3217, 0.14524, 0.14218,  2.052)
A[4,]=c( 40, 2.6544, -1.7511, 0.965, 2.0104, 0.07524, 0.08196,  2.022)
A[5,]=c( 41, 3.0581, -2.6904, 0.964, 2.0459, 0.07640, 0.09486,  2.021)
A[6,]=c( 30, 3.0604, -1.3562, 0.922, 1.4612, 0.15419, 0.16846,  2.048)
A[7,]=c( 41, 2.5984,  1.2061, 0.992, 0.9083, 0.01593, 0.03627,  2.021)
A[8,]=c(  0,     NA,      NA,    NA,     NA,      NA,      NA,     NA)
```

```
A[9,]=c( 26, 2.7377,  2.1836, 0.985, 0.3515, 0.03348, 0.06817,  2.064)
A[10,]=c(40, 2.7418,  1.0632, 0.991, 0.9199, 0.01855, 0.04147,  2.022)
A[11,]=c(41, 2.6828,  1.1929, 0.981, 0.8846, 0.03933, 0.05917,  2.021)
A[12,]=c(27, 2.9932,  1.7879, 0.966, 0.4529, 0.07449, 0.11213,  2.060)
#A

#================================================================== Labels
labels<-vector(length=12)
labels=c("Humerus length","Ulna length","Metacarpal length","Femur length",
  "Tibia length","Metatarsal length","Humerus diameter","Ulna diameter",
  "Metacarpal length","Femur diameter","Tibia diameter",
  "Metatarsal diameter")
#================================================================ Functions
wgt.est<-function(m.mm){
  wgt.est=10^(A[,2]*log10(m.mm)+A[,3])
}
syhat<-function(m.mm,A){                              #prediction interval
  syhat=sqrt( A[,6] + A[,6]/A[,1] + A[,7]^2 * (log10(m.mm)-A[,5])^2 )
}
geomean<-function(x, na.rm=TRUE){
  exp(sum(log(x[x > 0]), na.rm=na.rm) / length(x[!is.na(x)]))
}
#================================================ Single-variable regression
w.g<-vector(length=12);w.g=wgt.est(m.mm)        #'weight in grams'
syh<-vector(length=12);syh=syhat(m.mm,A)        #'Sy-hat'
hpi<-vector(length=12);hpi=abs(A[,8]*syh)       #'half prediction interval'
svr<-matrix(nrow=12,ncol=0);rownames(svr)=labels[1:12]
svr=cbind(svr,m.mm)
svr=cbind(svr,round(w.g,digits=0))
svr=cbind(svr,round(10^(log10(w.g)-hpi),digits=0))
svr=cbind(svr,round(10^(log10(w.g)+hpi),digits=0))
colnames(svr)=c('m.mm','w.g','pmin','pmax')
Nwgts=length(w.g[!is.na(w.g)])
Geomean=geomean(w.g)
maxmin=max(svr[,3],na.rm=TRUE)
minmax=min(svr[,4],na.rm=TRUE)
#print(m.l)
#svr
#print(paste("N geomean max min",
#Nwgts,round(Geomean,digits=0),maxmin,minmax))
#========================================== Alexander 1979 MR coefficients
Amr<-matrix(nrow=12,ncol=4)
Amr[1,]= c( 1.12630,  1.14940,  1.36900,  2.08050)
Amr[2,]= c(-0.34705,  0.54825, -0.53119, -0.82606)
Amr[3,]= c(-0.42902, -0.01596, -0.06522,  0.16526)
Amr[4,]= c( 0.14743,  1.66070,  0.87466,  1.66470)
Amr[5,]= c(-0.51599, -1.76350, -1.01270, -1.12290)
Amr[6,]= c( 0.41567,  0.93805,  0.13456,  0.38280)
Amr[7,]= c( 0.67837,       NA,  0.61230,       NA)
Amr[8,]= c(      NA,       NA,       NA,       NA)
Amr[9,]= c( 0.83146,       NA,  0.90372,       NA)
Amr[10,]=c( 0.97864,       NA,  0.73021,       NA)
Amr[11,]=c(-0.27735,       NA, -0.46398,       NA)
Amr[12,]=c( 0.05630,       NA, -0.09818,       NA)
#Amr
#================================================== Multiple regression
Plength=m.mm[1]*m.mm[2]*m.mm[3]*m.mm[4]*m.mm[5]*m.mm[6]
Pdiameter=m.mm[7]*m.mm[9]*m.mm[10]*m.mm[11]*m.mm[12]
```

```
if(isTRUE(Plength>0 && Pdiameter>0)){           #all species
  Amr1<-vector(length=12);Amr1=Amr[,1]*log10(m.mm)
  MRa11=10^(1.0539+sum(Amr1,na.rm=TRUE))
}else{
  MRa11=NA
}
if(isTRUE(Plength>0)){
  Amr2<-vector(length=6);Amr2=Amr[1:6,2]*log10(m.mm[1:6])
  MRa06=10^(-1.0061+sum(Amr2,na.rm=TRUE))
}else{
  MRa06=NA
}
if(isTRUE(Plength>0 && Pdiameter>0)){           #partial no artio.
  Amr3<-vector(length=12);Amr3=Amr[,3]*log10(m.mm)
  MRp11=10^(0.90053+sum(Amr3,na.rm=TRUE))
}else{
  MRp11=NA
}
if(isTRUE(Plength>0)){                         #all species
  Amr4<-vector(length=6);Amr4=Amr[1:6,4]*log10(m.mm[1:6])
  MRp06=10^(-0.81709+sum(Amr4,na.rm=TRUE))
}else{
  MRp06=NA
}
print(m.l)
svr
print(paste("N geomean max min",Nwgts,round(Geomean,digits=0),maxmin,minmax))
print(paste("MR all species—    11 L&D: ",round(MRa11,digits=0),"   6L: ",
  round(MRa06,digits=0)))
print(paste("MR no artiodactyls—11 L&D: ",round(MRp11,digits=0),"   6L: ",
  round(MRp06,digits=0)))
#========================================================= Relative brain size
if(Brain==TRUE){
Brainw.g=5
ERtc=log2(Brainw.g)-(0.740*log2(Geomean)-4.004)
ERtc1=log2(Brainw.g)-(0.740*log2(MRp11)-4.004)
ERtc2=log2(Brainw.g)-(0.740*log2(MRp06)-4.004)
EQtc=2^ERtc;EQtc1=2^ERtc1;EQtc2=2^ERtc2;
cat(paste(m.l),'\n')
cat(paste('Body wgt (g), 11 L&D, 6 L:','\t',round(Geomean,digits=0),
  '\t\t',round(MRp11,digits=0),'\t\t',round(MRp06,digits=0)),'\n')
cat('Brain weight (g):','\t\t',format(round(Brainw.g,digits=1),nsmall=1),
  '\t\t',format(round(Brainw.g,digits=1),nsmall=1),
  '\t\t',format(round(Brainw.g,digits=1),nsmall=1),'\n')
cat(paste("ERtc:",'\t\t\t\t',format(round(ERtc,digits=3),nsmall=3),
  '\t',format(round(ERtc1,digits=3),nsmall=3),
  '\t',format(round(ERtc2,digits=3),nsmall=3),'\n'))
cat(paste("EQtc:",'\t\t\t\t',format(round(EQtc,digits=3),nsmall=3),
  '\t\t',format(round(EQtc1,digits=3),nsmall=3),
  '\t\t',format(round(EQtc2,digits=3),nsmall=3),'\n'))
}
#============================================================================
```

TABLE A-III-1.— Long bone lengths and diameters used to estimate the plesiadapid body weights reported in Table 6 in the text. Long bone lengths and diameters for *P. cookei* differ slightly from those reported by Gingerich and Gunnell (2005), principally in metacarpal length, metatarsal length and diameter, and humerus diameter. These changes mean the weight estimates for *P. cookei* differ slightly as well. Long bone diameters for *P. insignis* (parentheses) are not included in calculating body weight for the species because the diameters are distorted by compression. Abbreviations: *H*, humerus; *U*, ulna; *R*, radius; *Mc*, third metacarpal; *F*, femur; *T*, tibia; and *Mt*, third metatarsal. For each bone: *L*, length; and *D*, parasagittal (anteroposterior) diameter.

Taxon	H-L	U-L	Mc-L	F-L	T-L	Mt-L	H-D	U-D	Mc-D	F-D	T-D	Mt-D
P. cookei	75.60	88.30	20.00	86.60	86.10	29.10	6.86	5.85	2.20	6.53	5.71	2.50
P. tricuspidens	70.50	85.08	21.10	76.60	—	—	7.65	5.56	2.30	6.21	—	—
P. rex	—	—	—	—	—	—	3.75	3.35	—	—	—	—
P. churchilli	—	—	—	—	—	—	—	—	—	4.94	—	1.68
P. insignis	36.73	36.00	11.70	49.00	46.00	—	(6.00)	(4.00)	—	(6.00)	(5.00)	—
N. intermedius	—	41.20	11.51	—	44.80	—	3.28	2.94	1.05	3.69	2.88	1.41
N. gidleyi	—	—	12.02	—	—	—	—	3.16	1.02	4.22	3.36	—
Pr. gaoi	—	—	15.61	—	—	—	4.89	—	1.51	—	—	2.00

TABLE A-III-2.— Summary of body weight estimates (grams) for plesiadapid species calculated from long bone lengths and diameters in the mammal sample of Alexander et al. (1979) (see Gingerich, 1990). Weights are compared for predictions from long bone lengths alone, long bone diameters alone, and both combined. Then weight predictions for each species are expressed as a percentage of the weight estimated for *P. cookei*. Finally, body weights estimated from skull length are normalized to those for *P. cookei* assuming isometric scaling and allometric scaling ('horizontal primate' sample of Silcox et al., 2009a). Note that long bone lengths yield substantially greater weight estimates for *P. cookei* compared to those for long bone diameters, whereas the remaining species show greater agreement where these estimates can be compared. Note also that normalizing by size for *P. cookei* yields substantial discrepancies in body size estimates based on postcranial measurements and skull length in some other species. Abbreviations: *L*, length; *D*, parasagittal (anteroposterior) diameter; *A*, all (lengths and diameters combined); *N*, sample size; *CV*, coefficient of variation (100 H stdev / mean). Superscript-a ([a]) indicates skull length estimates from Table 4 were cubed and divided by the cubed skull length of *P. cookei*. The resulting ratio was multiplied by 100. Superscript-b ([b]) indicates body masses were predicted from estimated skull lengths of Table 4 using the horizontal equation from Silcox et al. (2009a) and then each species' predicted body mass was divided by that of *P. cookei*. This ratio was multiplied by 100.

	P. cookei	*P. tricuspidens*	*P. rex*	*P. churchilli*	*P. insignis*	*N. intermedius*	*N. gidleyi*	*Pr. gaoi*
Mammal sample								
Length N	6	4	0	0	5	3	1	1
Length mean	2100	2084	—	—	368	314	406	776
Length CV	33	21	—	—	35	24	—	—
Diameter N	5	3	1	2	0	5	3	3
Diameter mean	1665	2133	498	607	—	276	388	651
Diameter CV	34	43	—	—	—	39	57	46
All N	11	7	1	2	5	8	4	4
All mean	1902	2105	498	607	368	290	392	682
All CV	34	29	—	—	35	32	46	37
Species means normalized to *P. cookei* size								
% *P. cookei* (All)	100	111	26	32	19	15	21	36
Estimates from skull length								
% *P. cookei* (isometry[a])	100	102	—	—	11	11	21	19
% *P. cookei* (allometry[b])	100	102	—	—	6	6	13	13

APPENDIX IV — CLADISTIC EVALUATION OF NEW OBSERVATIONS

TABLE A-IV-1.— Dental character list for species-level analysis of Plesiadapidae (Characters 1–32 match Boyer et al., 2012a, b; characters 67–69 are from Boyer et al., 2012b; characters 70–71 are new to this study). Taxon scorings are given in Table A-IV-2. Characters 33-66 are not dental characters and appear in other tables (Table A-IV-3, 4).

Incisors

1 Incisor proportions: (0) occlusal height short compared with area in occlusal plane, (1) occlusal height intermediate, (2) occlusal height high. Ordered.

Lower incisors

2 Basal cusp on lingual cingulum of I1: (0) absent, (1) present. Character 4 of Bloch et al. (2001).

3 I_1: with squared tip: (0) absent, (1) present.

4 I_2: (0) present, (1) absent.

5 I_3: (0) present, (1) absent. Character 6 of Bloch et al. (2001).

Upper Incisors

6 I^1 laterocone: (0) present, (1) reduced, (2) absent. Ordered.

7 I^1 posterocone: (0) twinned (1) present, (2) reduced, (3) absent. Ordered.

8 I^1 mediocone: (0) present, (1) reduced or absent.

9 I^1 centroconule: (0) present, (1) reduced or absent.

Canines

10 C^1: (0) present, (1) absent.

11 C_1: (0) present, (1) absent.

Premolars

12 Diastemata between premolars and more anterior teeth: (0) absent, (1) present.

13 P_1 or P_1: (0) present, (1) absent.

Lower premolars

14 P_2: (0) large, (1) small, (2) absent. Ordered.

15 Form of P_2: (0) premolariform with talonid heel, (1) button shaped.

16 Metaconid on P_4: (0) absent, (1) present. Modified from character 14 of Bloch et al. (2001).

17 (d25 of Silcox, 2001) Paraconid on P_4: (0) present, (1) absent.

18 Entoconid on P_4: (0) present, (1) absent.

19 Trigonid of P_4: (0) present, (1) absent.

20 P_4 shape (ratio of mesiodistal length to buccolingual width): (0) ratio < 0.9, (1) 0.9 < ratio < 1.06, (2) 1.06 < ratio < 1.2. (3) ratio > 1.2. Unordered.

Upper premolars

21 P^2: (0) present, (1) absent.

22 P^3 paraconule: (0) present, (1) reduced, (2) absent. Ordered

23 P^4 paraconule: (0) present, (1) reduced, (2) absent. Ordered

24 P^4 molar-type paraconule: (0) absent, (1) present

Lower molars

25 Entoconid of M_{1-2}: (0) squared and lacking crest (1) curved with crest

26 Length of M_1: (0) species sample mean less than 3.5 mm, (1) greater than or equal to 3.5 mm.

27 Postvallid of M_1: (0) flush, (1) stepped. Character d80 of Silcox (2001).

28 Size of M_3 hypoconulid: (0) small relative to talonid, (1) large. Modified from d75 of Silcox (2001).

29 Shape of M_3 hypoconulid: (0) rounded and unfissured, (1) squared and fissured.

Upper molars

30 M^{1-2} mesostyles: (0) absent, (1) weakly present, (2) strong. Ordered.

General

31 Incisor size relative to molars: (0) slightly larger, (1) greatly enlarged (M_1 area / I_1 area 0.85).

32 Premolar and/or molar form: (0) cuspidate, (1) blunt, (2) crestiform, Unordered.

Additional out-of-sequence dental characters

67 M_3 posterior cingulid: (0) present, (1) absent.

68 P_3 metaconid: (0) absent, (1) present.

69 M_3 size: (0) smaller than in *Plesiadapis cookei*, (1) as larger or larger than *P. cookei.*

70 P_3 shape (ratio of mesiodistal length to buccolingual width): (0) ratio < 1.0, (1) 1.0 < ratio < 1.15, (2) ratio > 1.15. Unordered.

71 P_3/P_4 length ratio: (0) ratio < 1.05, (1) ratio > 1.05.

Table A-IV-2.— Dental character matrix for species-level analysis of Plesiadapidae. See Table A-IV-1 for descriptions of numbered dental characters. Characters 1–32 are from Boyer et al. (2012a), characters 67–69 are from Boyer et al. (2012b), and 70–71 are new to this study. Gray cells have states modified from previous studies that published or analyzed a version of this matrix (Boyer et al., 2012a,b). Character 20 was redefined and re-scored: no states compare to previous matrices. Cells with two states represent polymorphisms identified in intraspecific samples.

	1	2	3	4	5	6	7	8	9	10	11	12	13	14	15	16	17	18	19	20	21	22	23	24	25	26	27	28	29	30	31	32	67	68	69	70	71
Purgatorius	1	0	0	0	0	0	1	0	1	?	0	0	0	1	0	0	1	0	1	3	0	1	1	0	0	0	0	0	0	0	0	0	0	0	0	2	0
Elphidotarsius sp.	1	0	0	0	1	0	0	0 1	1	1	0	0	0	1	1	1	1	1	1	3	0	0	0	0	0	0	0	1	1	0	0	0	0	0	0	0	0
Carpolestes simpsoni	1	0	0	0	1	0	0	1	1	0	0	0	1	2	?	1	1	1	1	3	0	0	0	0	0	0	0	1	1	0	0	0	0	0	0	?	0
Plesiadapis tricuspidens	1	0	0	1	1	0	1	0	0	1	1	1	1	2	?	0 1	**0 1**	1	1	1	0	**1 2**	0	0	1	1	1	1	1	2	0	0	0 1	0	0	1	0
Plesiadapis cookei	2	0	0	1	1	1	2	1	1	1	1	1	1	2	?	0	0 1	0	**0 1**	1	1	2	2	0	1	1	1	1	1	2	0	2	0	0	1	2	1
Plesiadapis rex	1	1	0	1	1	0	1	0	0	0	1	1	1	1	?	0	0	1	1	1	0	0	0	0	0	0	1	1	1	1	0	0	0	0	0	1	0
Plesiadapis anceps	1	1	0	1	1	0	1	0	1	0	0 1	1	1	1	?	0	0	1	1	1	0	0	0	0	0	0	1	1	0	0	0	0	0	0	0	1	0
Nannodectes intermedius	1	1	0	1	1	0	1	0	1	0	0	0	1	1	1	0	0	1	1	1	0	0	0	0	0	0	1	1	0	0	0	0	0	0	0	2	0
Nannodectes gidleyi	1	1	0	1	1	0	1	?	1	0	1	1	1	1	1	0	0	1	1	2	0	1 2	0	0	0	0	1	1	0	1	0	0	0	0	0	2	0
Pronothodectes gaoi	1	1	0	0	1	0	1	0	1	0	0	0	1	1	0	0	0	1	1	1	0	0	0	0	0	0	1	1	**0 1**	0	0	0	0	0	0	2	0
Platychoerops daubrei	2	0	0	1	1	2	3	1	1	1	1	1	1	2	?	1	1	0	0	2	**0**	2	2	1	1	1	1	1	1	2	0	2	1	1	0	2	0
Plesiadapis churchilli	1	1	0	1	1	0	1	0	0	0	1	1	1	1 2	?	0	0	0	1	1	0	0	0	0	0	0	1	1	1	2	0	0	0	0	0	1	0
Plesiadapis insignis	1	1	0	1	1	0	1	0	1	0	1	1	1	0	?	?	0	1	1	?	0	?	?	0	0	0	1	1	0	0	?	0	0	0	0	?	0
Plesiadapis walbeckensis	1	1	0	1	1	0	1	0	1	0	1	1	1	1 2	?	0	0	1	1	1	0	0	0	0	0	0	1	1	0	1	**1**	0	0	0	0	?	0
Plesiadapis remensis	1	1	0	1	1	0	1	0	0	?	1	1	1	2	?	0	**0**	1	1	1	0	**1 2**	0	0	1	1	1	1	1	2	0	0	0	0	0	?	0
Plesiadapis praecursor	1	1	0	1	1	0	1	0	1	0	0 1	1	1	1	**?**	0	0	1	1	1	0	0	0	0	0	0	1	1	0	0	0	0	0	0	0	2	1
Pronothodectes matthewi	1	1	0	0	1	0	1	0	1	0	0	0	1	1	0	0	0	1	1	1	0	0	0	0	0	0	1	1	0	0	0	0	0	0	0	1	0
Pronothodectes jepi	1	1	0	0	1	0	1	0	1	0	0	0	1	1	?	0	0	1	1	1	0	0	0	0	0	0	1	1	0	0	0	0	0	0	0	1	0
Plesiadapis dubius	1	1	0	1	1	0	1	0	1	0	1	1	1	2	?	**0 1**	0 1	0	1	3	0	**2**	**1 2**	**0 1**	1	0	1	1	1	2	0	2	0	0	0	?	?
Plesiadapis simonsi	?	?	?	?	?	?	1	?	?	?	?	?	?	?	?	?	?	?	?	?	?	?	?	0	1	1	1	1	1	2	?	0	?	?	0	?	?
Plesiadapis gingerichi	1	?	?	?	?	0	1	0	1	?	1	1	1	2	?	0	0	0	1	1	?	?	?	0	1	1	1	1	1	2	?	0	0	0	0	2	1
Plesiadapis fodinatus	1	1	0	1	1	0	1	0	0	0	1	1	1	**1 2**	?	**0 1**	0 1	0	1	2	0	**1 2**	**1 2**	**1 0**	1	0	1	1	1	2	0	2	0	0	0	2	0
Nannodectes gazini	1	1	0	1	1	0	1	0	1	0	0	0	1	1	?	0	0	1	1	2	0	**1 2**	0	0	0	0	1	1	0	0	0	0	0	0	0	2	0
Nannodectes simpsoni	1	1	0	1	1	?	?	?	?	0	0	1	1	1	?	0	0	1	1	2	0	2	0	0	0	0	1	1	0	1	0	0	0	0	0	2	0
Chiromyoides minor	0	1	0	1	1	0	1	0	1	?	1	0	?	2	?	?	?	?	?	?	?	?	?	?	?	0	?	?	?	?	1	1	?	?	?	?	?
Chiromyoides potior	0	1	1	1	1	0	1	0	1	?	1	1	?	2	?	?	?	?	?	?	?	?	0	0	0	0	?	?	?	?	1	1	?	?	?	?	?
Chiromyoides caesor	0	?	?	?	?	0	1	0	1	?	?	?	?	?	?	?	?	?	?	?	?	?	?	?	0	0	0	1	0	1	1	1	?	?	?	?	?
Chiromyoides major	0	1	1	1	1	0	1	0	1	?	1	1	?	2	?	?	?	**?**	**?**	?	?	?	?	?	?	?	?	?	?	?	1	1	?	?	?	?	?
Chiromyoides campanicus	0	1	0	1	1	0	1	0	1	?	1	0	1	2	?	0	0	1	1	0	0	?	0	0	0	0	1	1	0	1	1	1	0	0	0	0	0
Platychoerops russelli	2	?	?	**?**	**?**	1	2	**?**	1	**?**	**?**	?	**?**	**?**	?	?	?	?	?	?	?	2	2	1	?	1	?	1	1	2	0	2	1	0	1	1	0
Platychoerops richardsoni	?	?	?	?	?	?	?	?	?	1	1	1	1	?	?	?	2	?	?	3	1	?	2	1	1	1	1	1	1	2	0	2	1	?	1	2	0
Platychoerops antiquus	**2**	**0**	?	**1**	**1**	?	?	?	?	?	1	1	?	2	?	1	**2**	1	0	3	?	?	?	?	1	1	1	1	1	?	**0**	**2**	0	1	0	2	0

Table A-IV-3.— Cranial and postcranial characters for optimization. All characters are unordered. More extensive discussion of most characters is available in Bloch et al. (2007) and Silcox (2001). Characters 1–23 are the same as those in Bloch and Silcox (2006) and Bloch et al. (2007). Character 24 of Bloch and Silcox (2006) is not represented here. Sources for characters in this dataset include Szalay (1975), Wible and Covert (1987), Kay et al. (1992), Wible (1993), Beard and MacPhee (1994), and Silcox (2001).

This study	Bloch et al. (2007)	Boyer et al. (2012)	DESCRIPTION
			Cranial characters
c1	83	33	Structure of auditory bulla: membranous, or bony but non-petrosal in origin (0), or no suture separating bulla from petrosal and/or no developmental evidence for additional elements (1). Character is modified from Beard and MacPhee (1994) and is designed to best employ the data that are available from fossils (i.e., under this definition microsyopids can be scored in spite of uncertainty about the composition of their bullae).
c2	84	34	Relations of entotympanic: no entotympanic present (0), entotympanic contacts petrosal medially (1), entotympanic contacts basioccipital medially (2), or no medial contact (3). This character is modified from Kay et al. (1992) and was scored only in taxa for which an entotympanic could be positively identified.
c3	85	35	Form of external auditory meatus: not expanded into bony tube (0), or expanded into bony tube (1). As defined here, this character does not differentiate between tubular external auditory meati that are formed from different bones. This reflects the difficulty of accurately reconstructing the contribution of all of the bones making up the auditory bulla in fossils.
c4	86	36	Presence of subtympanic recess (between tympanic ring and bulla): subtympanic recess absent and ectotympanic does not include distinct ring-like element (0), or subtympanic recess present and ectotympanic includes ring-like element separated by annular bridge, membrane or gap between it and bulla (1). This character is modified from a character relating to the annular bridge employed by Beard and MacPhee (1994). See discussion in Silcox (2001). As configured here, this character allows the recognition of the basic similarity of a ring-like ectotympanic even if this is all that is preserved (i.e., as is the case for *Ignacius*; Bloch and Silcox, 2001).
c5	87	37	Presence of branches of internal carotid artery: grooves for at least promontorial branch, no tubes (0), tubes present for one or both arteries (1), or internal carotid artery absent (2).
c6	88	38	Posterior carotid foramen position (or position of entry of internal carotid artery and/or nerves into middle ear): posteromedial (0), or posterolateral (1).
c7	89	39	Subsquamosal foramen: present and large (0), or very small or absent (1). Note that this feature refers to a foramen located at the distal end of the zygomatic arch, making it equivalent to the opening called a suprameatal foramen by Kay et al. (1992); see discussion in Beard and MacPhee (1994).
c8	90	40	Width of central stem and relative size of hypotympanic sinus: broad with hypotympanic sinus restricted (0), or narrow with hypotympanic sinus expansive (1). Beard and MacPhee (1994: p. 79) define the central stem as "the midline keel of the posterior basicranium normally composed of the basisphenoid and basioccipital bones." Taxa with highly inflated bullae (i.e., an expansive hypotympanic sinus) also by necessity have a central stem, so the expanse of the hypotympanic sinus was not included as a separate character here (by contrast, it was employed as a character by MacPhee and Cartmill, 1986).
c9	91	41	Snout: relatively long (0), or short (1). To score this character, the length of the snout was measured from the ventral base of the anterior extent of the zygomatic arch to the front of the premaxilla. This was then compared to total skull length, measured from the caudal-most point on the occiput to the front of the premaxilla. A least-squares regression was performed of snout length on cranial length using SPSS 10.05, with the constraint that it pass through the origin (Silcox, 2001). The resulting line had this equation: snout length=0.039(cranial length). This line was a good fit to the data (r2=0.971). Character state 1 was assigned to any taxon with a residual more negative than –5.0. This indicates that the snout is at least 5 mm shorter than would be predicted by the equation.

Table A-IV-3.— Cont'd.

This study	Bloch et al. (2007)	Boyer et al. (2012)	DESCRIPTION
c10	92	42	Presence of postorbital bar: absent (0), postorbital process of frontal present but does not meet zygomatic (1), or complete postorbital bar present (2). Although it can be difficult to rule out absolutely the presence of a postorbital bar in damaged specimens, the absence of a process on either the zygomatic or the frontal can demonstrate that there was no complete bar.
c11	93	43	Presence of mastoid process: no strong tubercle or inflation in mastoid region (0), or strong tubercle or inflation in mastoid region (1). This character was scored somewhat differently than in Kay et al. (1992) in that it was considered likely that an inflated mastoid region was on the same morphocline as a strong tubercle, rather than being most similar to the complete absence of any expansion of the mastoid.
c12	94	44	Number of jugular (=posterior lacerate) foramina: single (0), or dual (1).
c13	95	45	Position of caudal midsagittal margin of palate: near M3 (0), well rostral to M3 (1), or well caudal to M3 (2). The states for this character differ somewhat from those used by Kay et al. (1992), who based the character on small variations in the position of the midsagittal margin of the palate.
c14	96	46	Number of pterygoid plates: two (0), or one (1).
c15	97	47	Supraorbital foramen: absent (0), or present (1).
c16	98	48	Nasals: flare laterally at caudal extent with wide contact with frontal (0), or nasals do not flare laterally at caudal extent with narrow contact with frontal (1).
c17	99	49	Diameter of infraorbital foramen: large (0), or small (1). For this analysis two measurements were taken from the infraorbital foramen, following Kay et al. (1992): the greatest diameter, and the maximum length perpendicular to the first measurement. These two measurements were then multiplied together to give an approximation of the area of the foramen. A least squares regression analysis was performed of the infraorbital foramen area vs. the logarithm of M1 (calculated as buccal length * width). Taxa that fell outside the 99% confidence limit for this analysis were grouped together in the 'small' category (Silcox, 2001).
c18	100	50	Contact between lacrimal and palatine in orbit: present (0), obscured by maxillofrontal contact (1).
c19	101	51	Lacrimal tubercle: absent (0), or present (1).
c20	102	52	Size of optic foramen: small (0), moderate (1), or large (2). Scoring for this character followed the ranges employed by Kay et al. (1992).
c21	103	53	Foramen rotundum: absent (0), or present (1).
c22	104	54	Position of lacrimal foramen: on orbital rim (0), on face (1), or in orbit (2).
c23	105	55	Cochlear window: not shielded (0), shielded by arterial tube (1), or shielded by bony septum (2).
c24	106	56	Orientation of fenestra rotunda (=cochlear window): directed posterolaterally (0), or directed posteriorly (1). Although there is some slight variation in the orientation of the fenestra rotunda, the situation in dermopterans and chiropterans, where this opening points directly posteriorly, is particularly distinctive. The derived state of this character has been cited frequently as a volitantian synapomorphy (Novacek, 1986; Novacek and Wyss, 1986; Wible and Novacek, 1988).
c25	107	57	Septae in middle ear cavity formed by entotympanic: absent (0), or present (1). The 'present' state was only recognized in scandentians, in which the entotympanic forms a dorsal cover to petrosal structures on the roof of the middle ear cavity (MacPhee, 1981).
c26	108	58	Fattened area on medial promontorium: absent (0), or present (1). This character was suggested by Szalay (1975). The '1' state represents a rounded, bulging promontorium, contrasting with the 'deflated' appearance of taxa that exhibit the '0' state.
c27	—	59	Expansiveness of premaxillary contact with frontal: absent (0), narrow (1), or broad (2).
c28	—	60	Relative size of annular component of ectotympanic: small, not flaring greatly beyond bony struts by which it is connected to bullar part of ectotympanic (0), or large, flaring well beyond bony struts by which it is connected to bullar part of ectotympanic (1).

Table A-IV-3.— Cont'd.

This study	Bloch et al. (2007)	Boyer et al. (2012)	DESCRIPTION
c29	—	61	Exposure of maxillary tooth roots in orbit: present (0), reduced to only distobuccal root of M3 or absent (1).
c30	—	62	Glenoid fossa relative size: small (0), or large (1).
c31	—	63	Nuchal crest length: projects posteriorly (0), or restricted (1).
c32	—	64	Internal carotid artery functionality: functional (0), or non-functional (1).
c33	—	65	Presence of s3 septum on promontorium: present (0), absent (1).
c34	—	66	Position of zygomatic process of maxilla: lateral to M2 (0), lateral to M1 (1).
			Postcranial characters
p1	109	—	Greater tuberosity on humerus small (0), or prominent (1).
p2	110	—	Lesser tuberosity on humerus gracile (0), or protrudes medially away from humeral shaft (1).
p3	111	—	Deltopectoral crest of humerus more than 33% total length of the bone (0), or less than 33% total length of bone (1).
p4	112	—	Deltopectoral crest of humerus positioned anteriorly (0), or laterally (1).
p5	113	—	Radial and/or olecranon fossa of humerus distinct (0), or indistinct to absent (1).
p6	114	—	Breadth of medial epicondyle (=entepicondyle) of humerus 30% or more of total distal breadth (0), or less than 30% of total distal breadth (1).
p7	115	—	Supinator crest of humerus broad and well developed (0), or reduced to absent (1).
p8	116	—	Capitulum of humerus spindle-shaped (0), or ball-like (1).
p9	117	—	Attachment for m. teres major on humerus not distinct (0), or present as distinct protrusion on crest leading down from lesser tuberosity (1).
p10	118	—	Trochlea of humerus only medial edge present (0), or both medial and lateral edges present and trochlea and capitulum well separated by distinct gap (1).
p11	119	—	Bicipital tuberosity on radius clearly distinct from rest of shaft (0), or absent (1).
p12	120	—	Radial head ovoid with ratio of mediolateral breadth/anteroposterior breadth greater than 1.26 (0), or round with ratio of mediolateral breadth/anteroposterior breadth less than 1.26 (1).
p13	121	—	Radial head with central fossa flat (0), or deeply excavated (1).
p14	122	—	Lateral lip on radial head broad but limited to lateral side (0), or narrow and more extensive (1).
p15	123	—	Ridge on distal end of anterior radius absent (0), or present, raised and canted (1).
p16	124	—	Ulnocarpal articulation mediolaterally and dorsopalmarly extensive, occurring in transverse plane (0), or limited to radial and palmar aspects of distal ulna, lying in proximodistal plane (1).
p17	125	—	Olecranon process of ulna similar in length to height of semilunar notch, with ratio of olecranon process length/semilunar notch height greater than 0.8 (0), or very reduced with ratio of olecranon process length/semilunar notch height less than 0.75 (1).
p18	126	—	Distal radioulnar articulation unfused (0), or fused (1).
p19	127	—	Scaphoid and lunate unfused (0), or fused (1).
p20	128	—	Relative length of intermediate phalanges short (0), or long (1).
p21	129	—	Nails absent (0), or present on at least one digit (1).
p22	130	—	Flexor sheath ridges on manual proximal phalanges absent (0), present but poorly demarcated (1), or present and very well demarcated (2).
p23	131	—	Groove for tendon of the flexor fibularis muscle on the astragalus on the midline (0), shifted laterally (1), or absent (2).
p24	132	—	Astragalar body shallowly grooved (0), narrow and more deeply grooved (1), not grooved at all, medial and lateral guiding ridges absent (2).
p25	133	—	Height of borders of astragalar trochlea subequal (0), or lateral border much higher than medial (1).

Table A-IV-3.— Cont'd.

This study	Bloch et al. (2007)	Boyer et al. (2012)	DESCRIPTION
p26	134	—	Length of astragalar neck less than 30% of total length of bone (0), or more than 30% of total length of bone (1).
p27	135	—	Secondary articulation between posterior side of sustentaculum tali and astragalus absent (0), present (1), similar facet on sustentaculum contacts medial malleolus rather than astragalus (2), or sustentaculum reduced or absent (3).
p28	136	—	Calcaneocuboid articulation with distal calcaneus flat (0), or with concave pit (1).
p29	137	—	Distal end of calcaneus not elongate (0), or elongate (1).
p30	138	—	Plantodistal process on entocuneiform strong (0), or reduced to absent (1).
p31	139	—	Acetabular shape circular with ratio of craniocaudal length/dorsoventral breadth less than 1.1 (0), or with ratio of craniocaudal length/dorsoventral breadth more than 1.1 (1).
p32	140	—	Pattern of acetabular bony buttressing even around the entire rim (0), or markedly more emphasized cranially (1).
p33	141	—	Greater trochanter on femur taller than femoral head (0), comparable in proximal extent to femoral head (1), or markedly shorter than femoral head (2).
p34	142	—	Lesser trochanter on femur not enlarged and not extensive medially (0), or enlarged and extended medially beyond level of head (1).
p35	143	—	Third trochanter on femur distal to lesser trochanter (0), or on same level as lesser trochanter (1).
p36	144	—	Patellar groove on femur triangular and narrow mediolaterally relative to its distal extent (0), or rectangular and wide mediolaterally relative to its distal extent (1).
p37	145	—	Distal femur deep with no anterior extension of patellar ridges (0), very deep with anterior extension of patellar ridges (1), or shallow (2).
p38	146	—	Trochanteric fossa on femur deep (0), or shallow to absent (1).
p39	147	—	Tibial tuberosity robust (0) or small to absent (1).
p40	148	—	Medial malleolus on tibia long (0), or short (1).
p41	149	—	Tibial plateau with lateral condyle projecting further proximally than medial condyle (0), or medial and lateral condyles projecting to similar extent proximally (1).
p42	150	—	Humerofemoral index [=(humerus length/femoral length)*100)] between 70 and 150 (0), greater than 150 (1), or less than 70 (2).
p43	151	—	Brachial index [=(radius length/humerus length)*100] less than 120 (0), or greater than 120 (1).
p44	152	—	Centrale unfused (0), or postnatal ossification between scaphoid or lunate and centrale in adults (1).
p45	153	—	Capitular tail on humerus present (0), or very reduced to absent (1).
p46	154	—	Cross-sectional shape of radial shaft rounded (0), or flattened (1).
p47	155	—	Manual intermediate phalanges short and broad (0), or tall and narrow (1).
p48	156	—	Non-hallucial terminal phalanges shallow proximally and distally (0), deep proximally and shallow distally (1), deep proximally and distally (2), or mediolaterally wide and dorsoventrally flattened (3).
p49	157	—	Manual proximal phalanges longer than intermediate phalanges (0), or shorter than intermediate phalanges (1).
p50	158	—	Metatarsal I facet on entocuneiform mediolaterally narrow (0), mediolaterally broad (1), or saddle-shaped (2).
p51	159	—	Peroneal process on metatarsal I small (0) or extensive (1).
p52	160	—	Medial process of metatarsal I small, medially rather than proximally extended (0), or large, mediolaterally restricted and proximally extended (1).
p53	161	—	Ilium blade-like (0), or rod-like (1).
p54	162	—	Pubic symphysis long (0), or short (1).
p55	163	—	Anterior inferior iliac spine large (0), or very small to absent (1).
p56	164	—	Ribs craniocaudally narrow (0), or wide (1).

Table A-IV-3.— Cont'd.

This study	Bloch et al. (2007)	Boyer et al. (2012)	DESCRIPTION
p57	165	—	Atlas craniocaudally narrow (0), or wide (1).
p58	166	—	Axis spinous process oriented caudally (0), or cranially (1).
p59	167	—	Thoracic spinous processes long and narrow (0), or short and wide (1).
p60	168	—	Lumbar transverse processes long and projecting ventrally beyond centrum (0), or short and lateral to centrum, not projecting ventrally beyond centrum (1).
p61	169	—	Third trochanter on femur large (0), small (1), or very small to absent (2).
p62	170	—	Proximal end of fibula large (0), or reduced (1).
p63	171	—	Height of ridges on patellar groove on femur subequal (0), medial higher than lateral ridge (1), or lateral higher than medial ridge (2).
p64	172	—	Prehensile hand proportions absent, with proximal phalanx short relative to metacarpal (0), or present, with proximal phalanx long relative to metacarpal (1).
p65	173	—	Metatarsal I torsion absent, with distal condyle anteroposterior direction equal to proximal anteroposterior direction (0), or present, with distal condyle anteroposterior direction rotated 90 degrees laterally relative to that of proximal end (1).

Table A-IV-4.— Cranial characters for Plesiadapidae adapted from Bloch et al. (2007). Characters 33–58 here correspond to 33–58 in Boyer et al. (2012a, b), to 83–108 in Bloch et al. (2007), and c1–c26 in Table A-IV-3. Bold cells in the 'ancestor' bottom row represent scorings that differ from those of 'Plesiadapidae' in Bloch and Silcox (2006) and Bloch et al. (2007). Only taxa with at least one known state are included.

Taxon	33	34	35	36	37	38	39	40	41	42	43	44	45	46	47	48	49	50	51	52	53	54	55	56	57	58
Carpolestes simpsoni	1	?	0	?	0	0	1	1	0	0	0	0	0	0	1	1	1	1	0	0	1	2	2	0	?	1
Plesiadapis tricuspidens	1	0	1	1	0	1	1	1	0	0	1	0	0	1	0	1	0	?	1	0	0	1	1	0	0	1
Plesiadapis cookei	1	0	1	1	0	1	?	1	0	0	1	0	0	?	?	0	0	?	?	?	?	?	?	0	0	1
Plesiadapis rex	?	?	?	?	?	?	?	?	?	?	?	?	0	?	?	?	0	?	?	?	?	?	?	?	?	?
Plesiadapis anceps	?	?	?	?	?	?	?	?	0	?	?	?	?	?	?	0	?	?	?	?	?	?	?	?	?	?
Nannodectes intermedius	1	0	0	1	0	1	?	1	0	0	1	?	0	?	?	0	0	?	?	?	?	?	?	0	0	1
Nannodectes gidleyi	1	0	?	?	?	?	?	1	0	?	1	?	0	1	?	?	0	?	?	?	?	?	?	0	0	1
Pronothodectes gaoi	1	0	0	1	0	1	?	1	0	0	1	0	?	?	0	0	0	?	?	?	?	1	1	0	0	1
Ancestor	1	**0**	**0**	1	**0**	**1**	1	1	0	0	1	0	0	1	0	**0**	0	**?**	**1**	0	**0**	1	**1**	0	0	1

Table A-IV-5.— Other cranial characters for Plesiadapidae. Characters 27–34 here correspond to c27–c34 in Table A-IV-3. Codings for *P. rex* are based on two maxillary specimens (YPM-PU 21448, YPM-PU 21347) from Cedar Point Quarry. Only taxa with at least one known state are included. Bold-face type indicates states that were modified from previous studies. Cells with two states represent polymorphisms identified in intraspecific samples.

	59	60	61	62	63	64	65	66
Elphidotarsius sp.	?	?	?	?	?	?	?	0
Carpolestes simpsoni	0	0	**1**	0	0	0	1	0
Plesiadapis tricuspidens	2	1	1	1	1	0	1	**0**
Plesiadapis cookei	1	0	1	0	0	0	1	1
Plesiadapis rex	?	?	**0 1**	?	?	?	?	0
Plesiadapis anceps	1	?	0	?	?	?	?	0
Nannodectes intermedius	1	0	0	0	0	0	1	0
Nannodectes gidleyi	?	?	?	1	?	0	1	0
Pronothodectes gaoi	1	0	0	0	0	0	0	0
Plesiadapis churchilli	?	?	1	?	?	?	?	0
Plesiadapis insignis	?	?	?	?	?	?	?	0
Plesiadapis praecursor	?	?	?	?	?	?	?	0
Pronothodectes matthewi	?	?	?	?	?	?	?	0
Pronothodectes jepi	?	?	?	?	?	?	?	0
Plesiadapis dubius	?	?	?	?	?	?	?	0
Plesiadapis simonsi	?	?	?	?	?	?	?	0
Plesiadapis fodinatus	?	?	?	?	?	?	?	0
Nannodectes gazini	?	?	?	?	?	?	?	0
Nannodectes simpsoni	?	?	?	?	?	?	?	**0**
Chiromyoides caesor	?	?	?	?	?	?	?	**1**
Chiromyoides campanicus	?	?	?	?	?	?	?	1
Platychoerops richardsoni	?	?	?	?	?	?	?	1

Table A-IV-6.— Postcranial characters for Plesiadapidae adapted from Bloch et al. (2007). Characters 1–65 correspond to p1–p65 in Table A-IV-3. *P. anceps* scorings are based on AMNH 92011, which is an entocuneiform from the Bison Bason saddle locality described by Szalay and Dagosto (1988). Bold cells in the 'ancestor' bottom row represent scorings that differ from those of Bloch et al. (2007). Cells with two states represent polymorphisms identified in intraspecific samples.

Taxon	1	2	3	4	5	6	7	8	9	10	11	12	13	14	15	16	17	18	19	20	21	22	23	24	25	26	27	28	29	30
Pr. gaoi	?	?	?	1	0	0	0	1	?	1	0	1	1	1	?	?	?	?	?	?	?	?	1	0	1	0	1	?	?	?
N. intermedius	?	?	?	1	0	0	0	1	1	0	0	1	1	1	0	0	0	0	0	0	?	1	?	?	?	?	?	?	?	?
N. gidleyi	?	?	?	1	0	0	0	1	?	?	0	1	1	1	0	0	0	0	?	0	?	1	1	0	1	0	1	1	0	?
P. insignis	?	?	?	?	?	?	?	?	?	?	?	?	?	?	?	?	?	0	?	0	0	?	?	?	?	?	?	?	?	?
P. churchilli	?	?	?	?	?	?	?	?	?	?	?	?	?	?	?	?	?	?	?	?	?	?	?	?	?	?	1	1	0	?
P. rex	?	?	?	1	0	0	0	1	1	1	?	?	?	?	?	?	0	?	?	?	?	?	1	0	1	0	1	?	?	?
P. anceps	?	?	?	?	?	?	?	?	?	?	?	?	?	?	?	?	?	?	?	?	?	?	?	?	?	?	?	?	?	0
P. walbeckensis	?	?	?	1	0	0	0	1	1	1	?	?	?	?	?	?	?	?	?	?	?	?	?	?	?	?	?	?	?	?
Pl. daubrei	?	?	?	?	0	0	0	1	?	1	?	?	?	?	?	?	?	?	?	?	?	?	?	?	?	?	?	?	?	?
P. tricuspidens	1	1	0	1	0	0	0	1	1	1	0	1	1	1	0	0	0	0	?	0	?	1	1	0	1	0	1	1	0	0
P. cookei	1	1	0	0	0	0	0	1	1	0	0	1	1	1	0	0	?	0	0	0	?	1	1	0	1	0	1	1	0	?
P. remensis	?	?	?	?	0	0	0	1	?	1	?	?	?	?	?	?	?	?	?	?	?	?	?	?	?	?	?	?	?	?
Ancestor	1	1	0	**1**	0	0	0	1	1	**1**	0	1	1	1	0	0	0	0	0	0	**0**	1	1	0	1	0	1	1	0	**0**

Table A-IV-6.— Cont'd.

Taxon	31	32	33	34	35	36	37	38	39	40	41	42	43	44	45	46	47	48	49	50	51	52	53	54	55	56	57	58	59	60	61	62	63	64	65
Pr. gaoi	?	?	?	?	?	?	?	?	?	?	?	?	?	?	0	1	1	1	?	?	?	?	?	?	?	?	?	?	?	?	?	?	?	?	?
N. intermedius	?	?	?	?	?	1	2	?	0	1	0	?	?	0	0	1	1	1	0	?	0	0	?	?	?	?	0	1	0	?	?	?	1	0	0
N. gidleyi	1	1	1	1	0	1	2	0	0	1	0	?	?	?	0	1	1	?	0	?	?	?	?	?	1	0	0	?	0	?	1	?	1	0	?
P. insignis	?	?	?	?	?	?	?	?	?	?	?	0	0	?	?	?	1	1	0	?	?	?	?	?	?	?	?	?	?	?	?	1	?	0	?
P. churchilli	?	?	1	1	0	?	?	0	?	?	?	?	?	?	?	?	?	1	?	?	0	0	?	?	?	?	?	?	?	?	1	?	?	?	0
P. rex	?	?	?	?	?	?	?	?	?	1	?	?	?	?	0	?	?	?	?	?	?	?	?	?	?	?	?	?	?	?	?	?	?	?	?
P. anceps	?	?	?	?	?	?	?	?	?	?	?	?	?	?	?	?	?	?	?	1	?	?	?	?	?	?	?	?	?	?	?	?	?	?	?
P. walbeckensis	?	?	?	?	?	?	?	?	?	?	?	?	?	?	0	?	?	?	?	?	?	?	?	?	?	?	?	?	?	?	?	?	?	?	?
Pl. daubrei	?	?	?	?	?	?	?	?	?	?	?	?	?	?	0	?	?	?	?	?	?	?	?	?	?	?	?	?	?	?	?	?	?	?	?
P. tricuspidens	0	1	1	1	0	1	2	0	0	1	0	0	0	?	0	1	1	1	0	1	?	?	?	?	0	?	?	?	?	?	1	?	1	0	?
P. cookei	0	1	1	1	0	1	2	0	0	1	0	0	0	0	0	1	1	1	0	?	0	0	0	1	0	0	0	?	0	?	1	1	1	0	0
P. remensis	?	?	?	?	?	?	?	?	?	?	?	?	?	?	0	?	?	?	?	?	?	?	?	?	?	?	?	?	?	?	?	?	?	?	?
Ancestor	0 1	**1**	1	1	0	1	2	0	0	1	0	0	0	0	0	1	1	1	0	1	0	0	0	**1**	0 1	0	0	**1**	0	?	1	1	1	0	0

Table A-IV-7.— Scoring changes for plesiadapiform characters.

Matrix	Taxon	Character	Original	Final
Bloch and Silcox (2006)	Plesiadapidae	3	1	0
Bloch and Silcox (2006)	Plesiadapidae	5	2	0
Bloch and Silcox (2006)	Paromomyidae	5	0,1	0
Bloch and Silcox (2006)	Plesiadapidae	6	0	1
Bloch and Silcox (2006)	Plesiadapidae	16	1	0
Bloch and Silcox (2006)	Plesiadapidae	18	1	?
Bloch and Silcox (2006)	Plesiadapidae	19	1	0
Bloch and Silcox (2006)	Plesiadapidae	21	1	0
Bloch and Silcox (2006)	Plesiadapidae	23	2	1
Bloch and Silcox (2006)	Paromomyidae	23	1,2	1
Bloch and Silcox (2006)	Carpolestidae	23	2	1
Bloch and Silcox (2006)	Carpolestidae	24	1	0
Bloch et al. (2007)	Plesiadapidae	c2	?	0
Bloch et al. (2007)	Plesiadapidae	c3	1	0
Bloch et al. (2007)	Plesiadapidae	c5	2	0
Bloch et al. (2007)	Paromomyidae	5	1	0
Bloch et al. (2007)	Plesiadapidae	c6	0	1
Bloch et al. (2007)	Plesiadapidae	c16	1	0
Bloch et al. (2007)	Plesiadapidae	c18	1	?
Bloch et al. (2007)	Plesiadapidae	c19	0	1
Bloch et al. (2007)	Plesiadapidae	c21	1	0
Bloch et al. (2007)	Plesiadapidae	c23	2	1
Bloch et al. (2007)	Paromomyidae	c23	2	1
Bloch et al. (2007)	Carpolestidae	c23	2	1
Bloch et al. (2007)	Plesiadapidae	p4	0,1	1
Bloch et al. (2007)	Plesiadapidae	p10	0	1
Bloch et al. (2007)	Plesiadapidae	p21	?	0
Bloch et al. (2007)	Plesiadapidae	p30	0,1	0
Bloch et al. (2007)	Plesiadapidae	p32	0,1	1
Bloch et al. (2007)	Plesiadapidae	p54	0	1
Bloch et al. (2007)	Plesiadapidae	p58	0	1

Table A-IV-8.— Most parsimonious tree parameters. Note that Chester et al. (2015) is Bloch et al.'s (2007) matrix with tarsal scores for *Purgatorius* added.

Variable	Matrix	Original	Final
Tree length	Bloch and Silcox (2006)	60	59
Consistency Index	Bloch and Silcox (2006)	63	59
Retention Index	Bloch and Silcox (2006)	61	55
Tree length	Chester et al. (2015)	472	469
Consistency Index	Chester et al. (2015)	48	47
Retention Index	Chester et al. (2015)	60	52

APPENDIX V — CRANIA OF OTHER NORTH AMERICAN AND EUROPEAN PLESIADAPIDAE

In the course of this investigation, we studied plesiadapid crania that have not been adequately described and illustrated. Here we provide detailed element-by-element descriptions of crania of *Nannodectes intermedius* based on USNM 309902, *Nannodectes gidleyi* based on AMNH 17388, and *Plesiadapis anceps* based on YPM-PU 19642. Brief comparisons among them enable us to address persistent questions of basic plesiadapid anatomy.

The remaining discussion includes taxa and specimens that have been described in a comprehensive and detailed fashion previously. We are able to present new information (in the form of both observations and illustrations) on these specimens. The new information is focused on three topics for each specimen: (1) cranial sutures; (2) cranial foramina; (3) more general aspects of cranial morphology.

Table A-V-1 (below) is a numbered list of anatomical features of interest. The numbered features are cited in the text following reference to a particular figure. Numbered features are also listed in the captions to figures where each feature is illustrated.

***Nannodectes intermedius* (USNM 309902)**

USNM 309902 has been illustrated in previous publications, but most of the morphology of this specimen remains undescribed and inadequately illustrated. Furthermore, some aspects of the petrosal description by MacPhee et al. (1983) are incorrect, due to what appears to have been an editorial error. Here we augment and revise previous descriptions, assisted by access to High Resolution X-ray Computed Tomography (HRxCT) imagery.

Nasal.— Remnants of both the right and left nasals are preserved (Fig. A-V-1). The tip of the left element measures 2.31 mm mediolaterally (Fig. A-V-1: *32*). The anteroposterior length of the right counterpart is 13.61 mm (Fig. A-V-1: *33, 34*).

Premaxilla.— Right and left premaxillae are preserved, although the latter is extremely fragmentary (Fig. A-V-1). The right element has its dorsoventral depth (8.33 mm), palatal length (7.75 mm), and maxillary suture preserved (Fig. A-V-1: *35*). The dorsal margin clearly had a posteriorly projecting process that most likely contacted the frontal. No teeth remain in the right premaxilla, however, Gingerich et al. (1983: fig. 5) showed that right and left I^1 and right I^2 were preserved nearby.

Lacrimal.— A fragment of the lacrimal appears to be preserved (Fig. A-V-1) but none of its sutures, the lacrimal foramen, or the lacrimal tubercle are observable.

Maxilla.— The maxillae are preserved bilaterally. The anterior portion is broken on both sides so that the canine is missing. On the right side $P^{2–3}$ are missing. On the left all teeth are present (Fig. A-V-1) and the P^2 to M^3 distance is 12.04 mm. On the left side, the roots of the posterior molars, including $M^{2–3}$ are exposed in the orbit (Fig. A-V-1: *36)*. None of the sutures of the maxilla is preserved except a small segment of the premaxillary suture on the right side (Fig. A-V-1). The infraorbital foramen is preserved and measures 2.20 mm by 1.15 mm (Fig. A-V-1: *37*).

Zygomatic.— A fragment of the left zygomatic bone is preserved (Fig. A-V-1). It seems that most of its ventral anteroposterior length is present, measuring 9.70 mm. However the dorsal margin is broken, especially anteriorly, so that the maxillary contact is not visible.

Palatines, sphenoids, frontals, and parietals.— These bones may be visible, but if so, they are too fragmentary to allow certain identification or meaningful description. A delicately preserved foramen that has been pushed into the palate through deformation may represent the optic foramen, because it is similar in proportional size and morphology to optic foramina of European plesiadapid specimens (Fig. A-V-1: *38*).

Squamosal.— The right glenoid of the squamosal (Fig. A-V-2: *39*) and its postglenoid process (Fig. A-V-2: *40*) are nearly completely preserved. The glenoid is flat. Its anteroposterior length is 4.49 mm, whereas its mediolateral width is 4.11 mm. Due to broken anterior and medial margins and a missing entoglenoid process, these values are likely to underestimate the dimensions of the pristine element. The postglenoid process projects straight ventrally by 1.43 mm. On the left side, some of the zygomatic process of the squamosal is preserved (Fig. A-V-1), but not enough to warrant description.

Petrosal.— Both petrosals are preserved, including regions of pars cochlearis and canalicularis (Figs. A-V-3 through A-V-6). Remains of both ectotympanics and a substantial portion of the left auditory bulla also exist. The maximum diameter of the aperture for the fenestra vestibuli is 1.16–1.19 mm (left–right). The left spiral cochlea measures 14.5 mm in length (Fig. A-V-2H) and completes 2.5 turns. The width of the pars cochlearis is 3.6–3.8 mm, whereas its dorsoventral depth as measured from the endocranial surface is 3.5–3.6 mm. The promontorium has only two visible grooves on its surface (Figs. A-V-2 through A-V-4). The identification of some of these requires consideration of how they relate to the preserved bony septa that buttress the promonotory. Four bony septa are preserved. The left promontorium visibly preserves the posterior septum (Figs. A-V-3, A-V-4) and the *s1* (Fig. A-V-4A–C, C', E). HRxCT data shows that it additionally preserves the *s2*, and cochlear canaliculus, but no *s3*, arising from the medial tympanic process (Fig. A-V-4E). This medial process appears to have a smooth, edge. It projects medially from the promontorium an average distance of 1.2 mm. The right promontorium preserves the cochlear canaliculus, but is broken on the medial side more anteriorly (Fig. A-V-2).

Table A-V-1.— Numerical list of anatomical features illustrated in figures of selected cranial specimens of Plesiadapidae (equivalent to table 2.1 of Boyer, 2009; and, in part, table 1 of Boyer et al., 2012a).

No.	Feature
Pronothodectes gaoi (UALVP 46685, 49105, 46687)	
1	Nasal/premaxilla suture (Boyer et al., 2012a, fig. 8)
2	Nasal/frontal suture (Boyer et al., 2012a, fig. 8)
3	Premaxilla/maxillary suture (Boyer et al., 2012a, figs. 8–10)
4	Premaxilla/frontal suture (Boyer et al., 2012a, fig. 8)
5	Lacrimal/frontal suture (Boyer et al., 2012a, fig. 8)
6	Lacrimal/maxillary suture (Boyer et al., 2012a, fig. 8)
7	Lacrimal orbital process (Boyer et al., 2012a, fig. 8)
8	Lacrimal foramen (Boyer et al., 2012a, fig. 8)
9	Maxilla/frontal suture (Boyer et al., 2012a, fig. 8)
10	Infraorbital foramen (Boyer et al., 2012a, figs. 9, 11, and 12)
11	Point on jugal where anteroposterior width was measured (Boyer et al., 2012a, fig. 8)
12	Metopic suture (Boyer et al., 2012a, fig. 8)
13	Frontal/parietal suture (Boyer et al., 2012a, fig. 8)
14	Frontal temporal ridge (Boyer et al., 2012a, fig. 8)
15	Zygomatic process of squamosal (Boyer et al., 2012a, figs. 8 and 9)
16	Glenoid of squamosal (Boyer et al., 2012a, figs. 8 and 9)
17	Postglenoid foramen (Boyer et al., 2012a, fig. 9D)
18	Entoglenoid process (Boyer et al., 2012a, fig. 9E)
19	Point on zygomatic process of squamosal where width was measured (Boyer et al., 2012a, fig. 9D)
20	Medial and rostral tympanic processes of petrosal (Boyer et al., 2012a, figs. 11 and 12)
21	Tympanic nerve foramen (Boyer et al., 2012a, figs. 11, 13, and 14)
22	Tympanic nerve groove (Boyer et al., 2012a, figs. 11 and 13)
23	Broken facial canal (Boyer et al., 2012a, figs. 11–13)
24	Remnants of bulla (Boyer et al., 2012a, figs. 8–10, 12)
25	Dorsal (petrosal?) layer of bone on rostral process of petrosal (Boyer et al., 2012a, figs. 11–13)
26	Ventral (nonpetrosal?) layer of bone on rostral process of petrosal (Boyer et al., 2012a, figs. 11–13)
27	Anterior end of basioccipital (Boyer et al., 2012a, figs. 9 and 10)
28	Occipital condyle (Boyer et al., 2012a, figs. 9 and 10)
29	Hypoglossal foramen (Boyer et al., 2012a, figs. 9 and 10)
30	Foramen magnum (Boyer et al., 2012a, figs. 9 and 10)
31	Nuchal crest (Boyer et al., 2012a, figs. 9 and 10)
Nannodectes intermedius (USNM 309902)	
32	Left nasal anterior end (Fig. A-V-1)
33	Right nasal anterior end (Fig. A-V-1)
34	Right nasal posterior end (Fig. A-V-1)
35	Right maxilla/premaxilla suture (Fig. A-V-1)
36	M2–3 roots exposed in orbit (Fig. A-V-1)
37	Infraorbital foramen (Fig. A-V-1)
38	Possible optic foramen (Fig. A-V-1)
39	Glenoid of squamosal (Fig. A-V-2)
40	Postglenoid process (Fig. A-V-2)
41	Facial canal (Fig. A-V-2)
42	Semicircular canal (Figs. A-V-2, A-V-4)
43	Epitympanic recess (Fig. A-V-2)
44	Crista tympanica (Figs. A-V-2, A-V-5)
45	Bony ridges of annular bridge (Fig. A-V-2)
46	Midline ridge of basioccipital (Figs. A-V-3, A-V-4, A-V-6)
47	Ventrally projecting lateral processes of basioccipital (Figs. A-V-3, A-V-4, A-V-6)
48	Right occipital condyle (Figs. A-V-3, A-V-4, A-V-6)
49	Foramen magnum (Figs. A-V-3, A-V-4, A-V-6)
50	Jugular process of exoccipital (Fig. A-V-6)
51	Nuchal crest (Figs. A-V-4, A-V-6)
52	Exoccipital/petrosal suture (Fig. A-V-6)

Table A-V-1.— Cont'd.

No.	Feature
Nannodectes gidleyi (AMNH 17388).	
53	Root of zygmatic process of maxilla (Fig. A-V-8)
54	Infraorbital foramen (Fig. A-V-8)
55	Pterygoid process of palatine (Fig. A-V-8)
56	Pterygoid process of basisphenoid (Fig. A-V-8)
57	Pterygoid process of alisphenoid (Fig. A-V-8)
58	Palatine postpalatine torus (Fig. A-V-8)
59	Postpalatine spine (Fig. A-V-8)
60	Glenoid of squamosal (Fig. A-V-8)
61	Postglenoid process (Fig. A-V-8)
62	Zygomatic process of squamosal (Fig. A-V-8)
63	Postglenoid foramen of squamosal (Fig. A-V-8)
64	Stylomastoid foramen (Figs. A-V-8, A-V-9)
65	Possible posterior carotid foramen and internal carotid canal (Figs. A-V-8, A-V-9)
66	Occipital condyle (Fig. A-V-8)
67	Jugular process of exoccipital (Fig. A-V-8)
68	Foramen magnum (Fig. A-V-8)
Plesiadapis tricuspidens (MNHN CR 125)	
69	Nasal/premaxilla suture (Fig. A-V-10)
70	Nasal/frontal suture (Fig. A-V-10)
71	Maxilla/frontal suture (Fig. A-V-10)
72	Premaxilla/frontal suture (Fig. A-V-10)
73	Lacrimal/frontal suture (Fig. A-V-10)
74	Lacrimal/maxilla suture (Fig. A-V-10)
75	Lacrimal/zygomatic suture (Fig. A-V-10)
76	Parietal/frontal suture (Fig. A-V-10)
77	Parietal/squamosal suture (Fig. A-V-10)
78	Premaxilla/maxilla suture in palate (Fig. A-V-10)
79	Palatine/maxilla suture (Fig. A-V-11)
80	Palatine/sphenoid suture (Figs. A-V-12, A-V-13)
81	Occipital/petrosal suture (Fig. A-V-12)
82	Petrosal/ectotympanic suture (Fig. A-V-11)
83	Ectotympanic/squamosal suture (Fig. A-V-11)
84	Parietal/frontal suture (Fig. A-V-10)
85	Maxilla/zygomatic suture (Figs. A-V-10, A-V-12)
86	Alisphenoid/squamosal suture (Fig. A-V-11)
87	Dorsal orbitosphenoid/frontal suture (Fig. A-V-13)
88	Infraorbital foramen (Fig. A-V-12)
89	Foramen ovale (Fig. A-V-13)
90	Sphenorbital fissure (Fig. A-V-13)
91	Suboptic foramen (Fig. A-V-13)
92	Optic foramen (Fig. A-V-13)
93	Possible superior orbital fissure (Fig. A-V-13)
94	Tympanic canaliculus foramen (tca; Fig. A-V-14)
95	Tympanic canaliculus groove (tca; Fig. A-V-14)
Plesiadapis tricuspidens (MNHN CR 965)	
96	Palatine/frontal suture in the postpalatine canal (Fig. A-V-16)
97	Frontal/orbitosphenoid suture just anterior to the optic foramen (Figs. A-V-16, A-V-17)
98	Orbitosphenoid/palatine contact running anteroposteriorly (Fig. A-V-17)
99	Palatine–alisphenoid suture (Fig. A-V-17)
100	Dorsal margin of orbitosphenoid (Figs. A-V-16, A-V-17)
101	Alisphenoid/orbitosphenoid suture (Fig. A-V-17)
102	'Dished' surface on alisphenoid for broken out orbitosphenoid (Fig. A-V-17)
103	Foramen ovale (Figs. A-V-15, A-V-18)

Table A-V-1.— Cont'd.

No.	Feature
104	Sphenorbital fissure (Figs. A-V-15 – A-V-17, A-V-18)
105	Optic foramen (Figs. A-V-15, A-V-17, A-V-18)
106	Various foramina representing blood sinus drainage (Figs. A-V-16, A-V-17)
107	Suboptic foramen (Figs. A-V-15, A-V-17)
108	Remnants of optic canals on broken orbitosphenoid (Fig. A-V-16)
109	Basisphenoid sinus space (Figs. A-V-16, A-V-18)
Plesiadapis tricuspidens (Pellouin skull)	
110	Palatine/alisphenoid suture (Figs. A-V-19, A-V-22)
111	Squamosal/alisphenoid (Fig. A-V-19)
112	Premaxillary sutural surface of frontal (Fig. A-V-20)
113	Nasal sutural surface of frontal (Fig. A-V-20)
114	Palatine/maxilla suture on palate (Fig. A-V-19)
115	Frontal/parietal suture (Fig. A-V-20)
116	Parietal/squamosal suture (Fig. A-V-20)
117	Squamosal foramina (Fig. A-V-20)
118	?Parietal/occipital suture (Fig. A-V-20)
119	Squamosal/tympanic suture (Fig. A-V-19)
120	Tympanic/petrosal suture (Fig. A-V-19)
121	Tympanic ring with annular bridge (Figs. A-V-21, A-V-22)
122	Palatal palatine foramina (Fig. A-V-19)
123	Sphenorbital fissure (Fig. A-V-22)
124	Foramen ovale fragment (Fig. A-V-22)
125	Foramen in scaphoid fossa (Fig. A-V-19)
126	Tubal canal of right bulla (Fig. A-V-22)
127	Posterior carotid foramen and carotid canal (Figs. A-V-21, A-V-22)
128	Foramen for tympanic canaliculus (tca; Fig. A-V-21)
129	Jugular foramen (Fig. A-V-21)
130	Hypoglossal foramen (Fig. A-V-21)
131	Possible suture along medial side of left promontorium (Fig. A-V-22)
Plesiadapis tricuspidens (MNHN CR 126)	
132	Frontal/maxilla suture in orbit (Fig. A-V-24)
133	Crack or maxilla/palatine suture? (Fig. A-V-24; also labeled on Fig. A-V-20)
134	Region of palatine/frontal contact in postpalatine canal (broken; Fig. A-V-24)
135	Lacrimal foramen (Fig. A-V-24)
136	Lacrimal/frontal suture (Fig. A-V-24)
137	Lacrimal/maxilla suture (Fig. A-V-24)

FIGURE A-V-1.— *Nannodectes intermedius* (USNM 309902). **A**, stereophotographs of rostrum in left lateral view. **B**, left lateral view of rostrum; also note inset of infraorbital foramen (*37*) in anterior view, with dorsal end up and medial on left. **C**, lateral view of right premaxilla. **D**, dorsolateral view of left maxilla showing molar roots. **E**, ventrolateral view of left maxilla showing foramina of questionable attribution. **F**, stereophotograph of left maxillary dentition in occlusal view. Anterior is to the left in A–B, D–F; to the right in C. Numbers (Table A-V-1) and abbreviations: *32*, left nasal anterior end; *33*, right nasal anterior end; *34*, right nasal posterior end; *35*, right maxilla/premaxilla suture; *36*, M^{2-3} roots exposed in orbit; *37*, infraorbital foramen; *38*, possible optic foramen; *De*, dentary; *Lc*, lacrimal; *Mx*, maxilla; *Ns*, right (r) and left (l) nasal; *Pmx*, right (r) and left (l) premaxilla; *Sq*, squamosal; *Zy*, zygomatic.

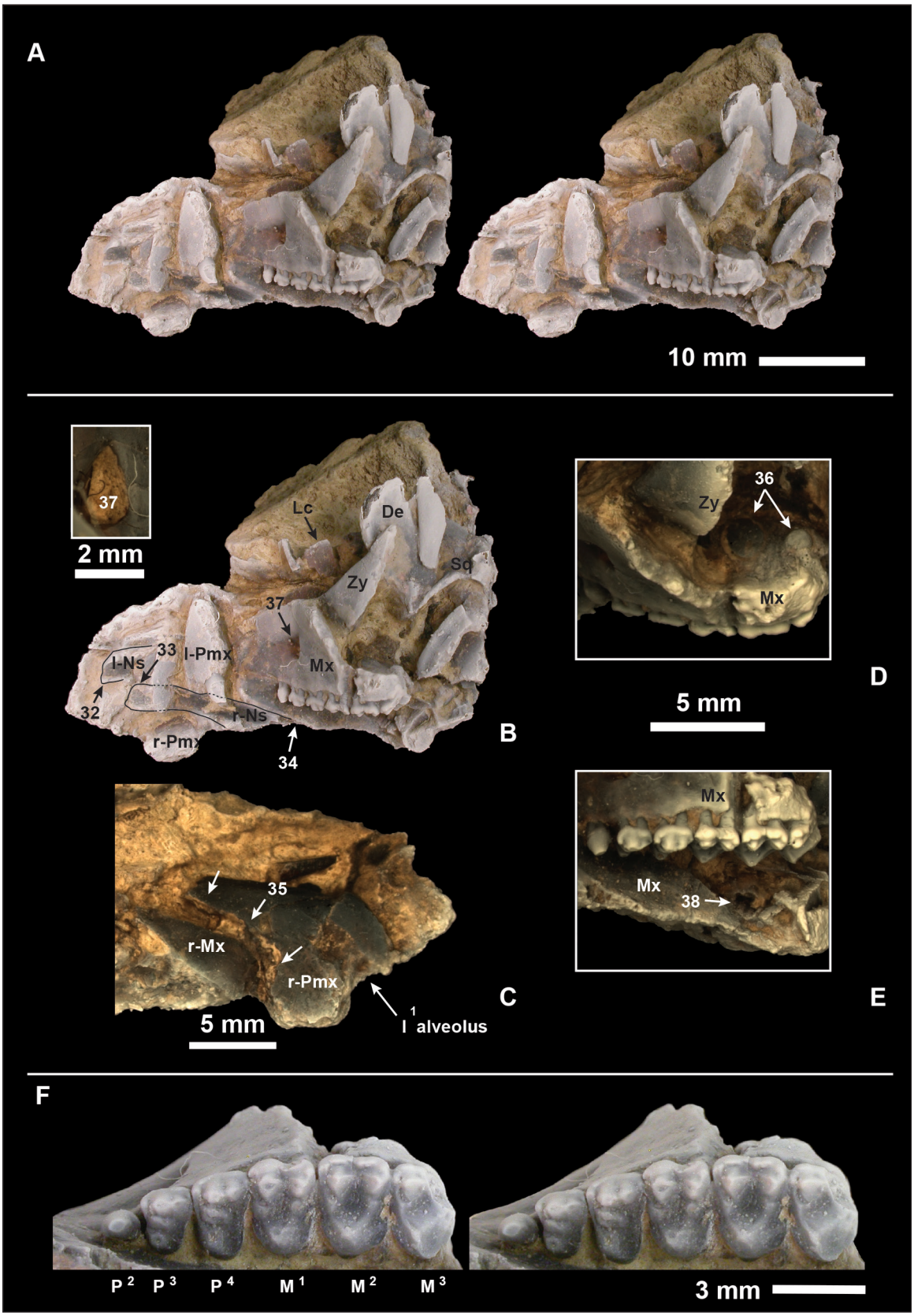
A
10 mm
37
2 mm
Lc
De
Sq
Zy
37
l-Ns
33
l-Pmx
Mx
32
r-Ns
r-Pmx
34
B
36
Zy
Mx
5 mm
D
Mx
Mx
38
E
35
r-Mx
r-Pmx
5 mm
C
I 1 alveolus
F
P 2 P 3 P 4 M 1 M 2 M 3
3 mm

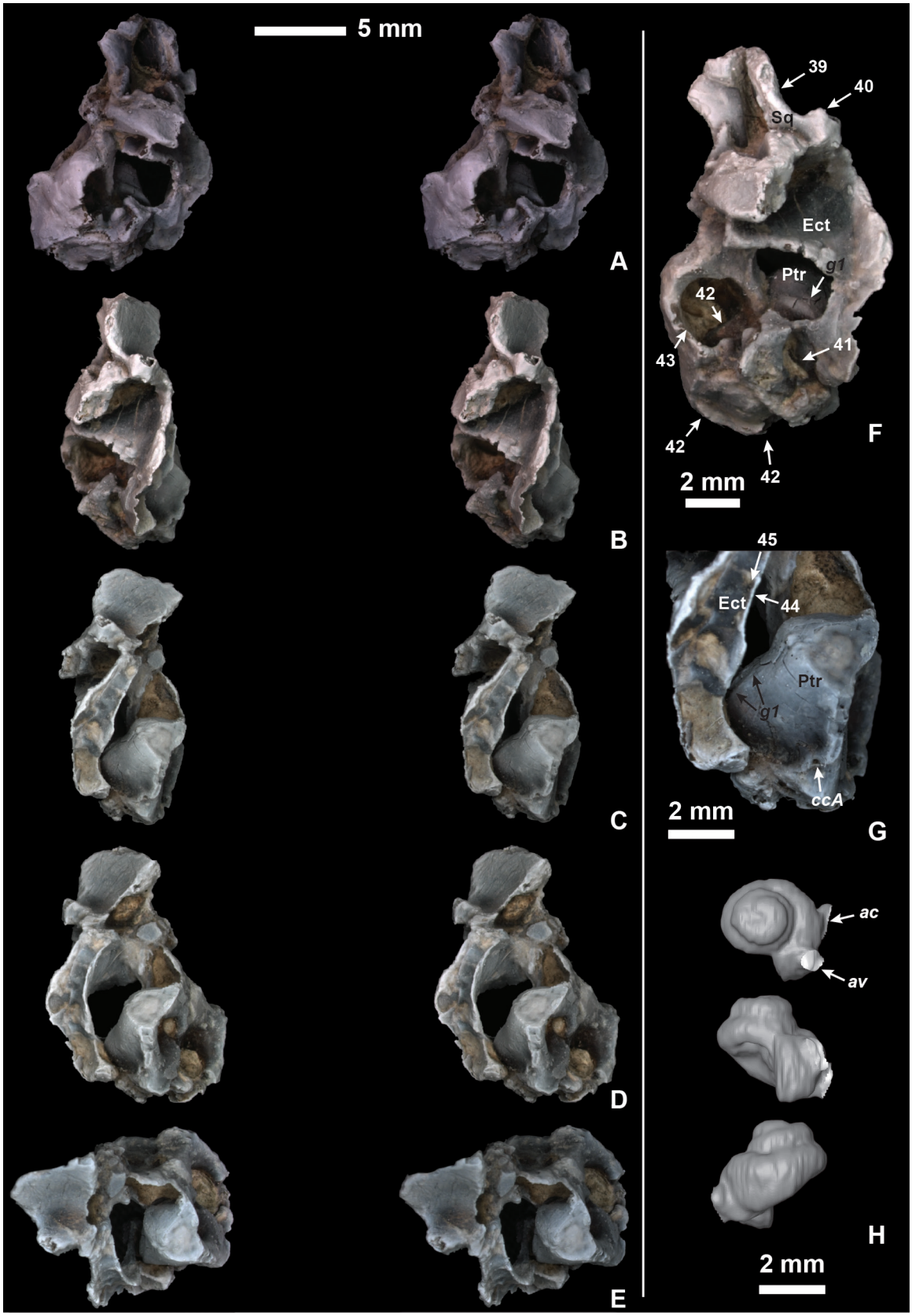
5 mm
A
B
C
D
E
39
40
Sq
Ect
Ptr
g1
42
43
41
42
42
F
2 mm
45
Ect
44
Ptr
g1
ccA
2 mm
G
ac
av
H
2 mm

The *g1* groove is present on the ventrolateral aspect of the promontorium. It actually grooves the ventral part of the posterior septum anteriorly; however, more posteriorly, it diverges to the lateral side of the posterior septum (Figs. A-V-2 through A-V-4). The *g1* groove measures about 0.29 mm in diameter. This is the groove that MacPhee et al. (1983: fig. 1) labeled as 's2.' In their figure caption they attributed this morphology to AMNH 17388, and described USNM 309902 as possessing the morphology of the former specimen. MacPhee et al. (1983: 509) stated that this groove has a blind end, posteriorly against a "bridge of bone uniting the promontory to the posterior wall of the bulla." This description, however, did not reveal that the specimen is broken in some critical areas. How the bulla and promontory connected can actually only be inferred, because the whole bulla is shifted anteriorly and the posterior part of the bulla is broken out where the posterior carotid foramen would have been located on both ears (Figs. A-V-2 through A-V-5 and A-V-6). This is especially observable with the CT scan. The portion of the pars cochlearis of the petrosal bone in which the *g2* and *g5* grooves are expressed when present is not preserved. Therefore, whether these grooves were present in USNM 309902 is unknown.present. The *g4* groove may be present on the right ear where the medial side of the promontorium is best exposed. A groove running mediolateraly on the left promontorium appears to be the *g3* groove (Fig. A-V-4: *g3*), because HRxCT data reveal that it leads toward *s2*.

Both ears preserve the bone-enclosed facial nerve canals (Fig. A-V-2: *41*). Semicircular canals are also preserved (Figs. A-V-2: *42*). Their diameters are provided in Silcox et al. (2009a). The right ear preserves a large epitympanic recess (Fig. A-V-2: *43*), a bone-enclosed chamber dorsolateral to the fenestra vestibuli and posterior to the epitympanic crest.

The left bulla, although shifted relative to the promontorium, is fairly undistorted (Figs. A-V-3 through A-V-6). As indicated above, the posterior wall of the bulla is missing, however, the limestone that fills it creates a natural cast, which allows visualization of its intact form. The bulla measures 11.23 mm in anteroposterior length. There is no obvious suture with the ectotympanic (Figs. A-V-3 through A-V-5).

FIGURE A-V-2.— *Nannodectes intermedius* (USNM 309902). **A–E**, stereophotograph of the right petrosal and other basicranial fragments, in lateral (A), ventral (B), ventromedial (C), medial (D), and anterior (E) views. Because of deformation, the glenoid is seen in ventral view in C, revealing its mediolateral dimensions. **F**, right petrosal in ventrolateral view. **G**, right petrosal in ventromedial view. **H**, three views (lateral, dorsal, and ventral) of the cochlea extracted from the HRxCT dataset. Anterior is at the top in A–D and F–G. Lateral is to the left in E. Numbers (Table A-V-1) and abbreviations: *39*, glenoid of squamosal; *40*, postglenoid process; *41*, facial canal; *42*, semicircular canal; *43*, epitympanic recess; *44*, crista tympanica; *45*, bony ridges of annular bridge; *ac*, aperture of cochlear fenestra; *av*, aperture of fenestra vestibuli; *ccA*, aperture of cochlear canaliculus; *Ect*, ectotympanic; *g1*, groove for internal carotid plexus; *Ptr*, petrosal; *Sq*, squamosal.

Ectotympanic.— The left ectoympanic is missing most of the external auditory meatus (*eam*). The crista tympanica and its concentric, inward projection are visible (Figs. A-V-4, 12: *44*). On the right side, some of the *eam* is preserved (Fig. A-V-2). It was 4.07 mm in mediolateral projection. Its anteroposterior width is not preserved well enough to allow measurement; however, it can at least be stated that the *eam* was not tubular. The crista tympanica is not as well preserved on this side (Fig. A-V-2: *44*), but more of it is visible. The connection between the crista tympanica and the bulla is solid and marked by subtly raised ridges (Fig. A-V-2: *45*), rather than prominent bony struts as in *P. tricuspidens*. The diameter of the crista tympanica is 5.3 mm (although it may be slightly distorted), giving an indication of the tympanic membrane diameter. As with other plesiadapids there is no telling how much of the *eam* and bulla were comprised of ectotympanic.

Occipital.— The occipitals are fairly well preserved (Figs. A-V-3, A-V-4, A-V-6). The basioccipital is a narrow element 7.22 mm in anteroposterior length and 2.21 mm in width at the spheno-occipital synchondrosis (Figs. A-V-3, A-V-4). At the anteroposterior midpoint the width is 2.04 mm. The width of the posterior margin cannot be measured reliably due to breakage. There is only faint development of a sagittally positioned longitudinal ridge on the element (Figs. A-V-3, A-V-4, A-V-6: *46*). The lateral margins project ventrally and would have braced the edge of the bulla in the pristine specimen (Figs. A-V-4, A-V-6: *47*).

The preserved parts of the exoccipitals include the right occipital condyle (Figs. A-V-3, A-V-4, A-V-6: *48*), foramen magnum diameter (Fig. A-V-6: *49*), and jugular process (Fig. A-V-6: *50*). The suture with the supraoccipital is difficult to locate due to fusion; however, it appears that the supraoccipital was very narrow ventrally and comprised only a narrow median segment of the foramen magnum's dorsal margin. The occipital condyle measures 2.83 mm in dorsoventral depth by 1.95 mm mediolaterally. The foramen magnum is 6.87 mm by 4.51 mm. The jugular process projects laterally by 1.30 mm. The bilateral distance between jugular processes can be reconstructed by measuring laterally from the midpoint of the foramen magnum. The value would have been roughly 12.2 mm. The contribution of the supra-exoccipital complex to the posterior margin of the skull is concave in dorsoventral profile due to posterior projection of the nuchal crest (Figs. A-V-4, A-V-6: *51*). The dorsoventral depth of the supraoccipital along the midline from the top of the foramen magnum to the top of the nuchal crest is 6.02 mm. The right lateral edge of this complex (Fig. A-V-6: *52*) seems to correspond to the sutural margin with the pars canalicularis of the petrosal, which has been displaced. Thus the unilateral distance from the midline to the most lateral point on the right exoccipital is 8.71 mm.

Dentary.— The left dentary was also preserved with the skull. Some pieces of the ramus are visible underneath the zygomatic (Fig. A-V-3). The dentary and mandibular dentition were described by Gingerich et al. (1983), but neither was figured. Thus, the mandibular teeth are shown here in various views (Fig. A-V-7).

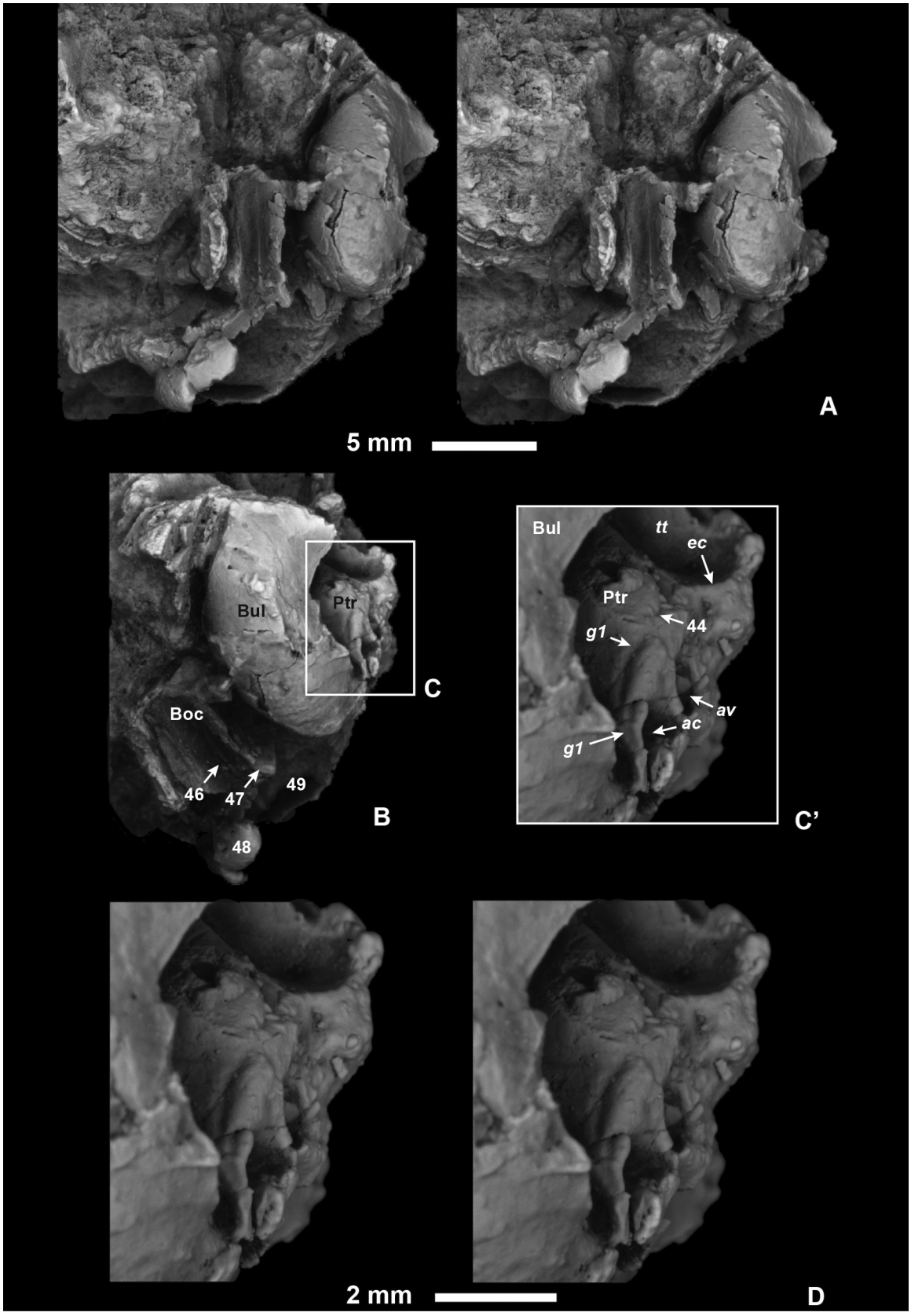
A
5 mm
Bul
Ptr
C
Boc
46
47
49
48
B
Bul
tt
ec
Ptr
44
g1
av
ac
g1
C'
2 mm
D

***Nannodectes gidleyi* AMNH 17388**

No aspect of this specimen has ever been illustrated except a schematic diagram in MacPhee et al. (1983). However, as indicated above, its morphology is incorrectly attributed to USNM 309902. Furthermore, both Simpson's (1935) and MacPhee et al.'s (1983) descriptions are brief and contain inaccuracies and omissions. Simpson (1935: p. 9) misinterpreted the exposed promontorium as a bulla that "is completely ossified, but is remarkably small and relatively little inflated."

Thus, much of the morphology of this specimen is illustrated and described for the first time here. This specimen could not be HRxCT-scanned because of an x-ray opaque naturally deposited/precipitated mineral infilling the petrosals. The skull is crushed flat and only the ventral aspect is visible (Figs. A-V-8 and A-V-9). The dorsal aspect is embedded in matrix and a composite, or plaster, that has been applied, apparently in order to stabilize the specimen. The skull is articulated with a cervical vertebral series. Lying parallel to the vertebral series is a clavicle. Just behind this accumulation is what appears to be part of a radius shaft.

Maxilla.— The nasals, premaxillae, and lacrimals are not visible. The maxillae are preserved bilaterally. Left P^3–M^3 and right $M^{1–3}$ are present, still in their alveoli. One P^2 (probably left) is out of its alveolus and lying on the palate (Fig. A-V-8). The length of the tooth row from P^2–M^3 is 14.00 mm (Fig. A-V-8). The heavy wear on these teeth reveals that the animal was probably senescent. Neither element preserves any sutures except possibly the zygomatic contact on the right side. The zygomatic process of the maxilla arises at the level of M^2 (Fig. A-V-8: *53*). The infraorbital foramen is visible on the right side at the level of P^3 (Fig. A-V-8: *54*). Its dorsoventral depth is roughly 2.22 mm.

Zygomatic.— The right zygomatic bone is visible (Fig. A-V-8) but fragmentary; no morphology of significance is apparent.

Palatine.— Fragments of both palatines are preserved (Fig. A-V-8). The posterior end of the palatal part of the bone and the anterior bases of both pterygoid processes are preserved (Fig. A-V-8: *55*). In fact, the right pterygoid process is continuous with the basisphenoid (Fig. A-V-8: *56*) and alisphenoid (Fig. A-V-8: *57*; see below). On the palate, the right palatine terminates at the choanae in a swollen rim of bone, also referred to as a postpalatine torus (Fig. A-V-8: *58*). The outer (anterior) margin of the torus reaches the lateral margin of the pterygoid processes. Furthermore, the outer margin of the torus is angular, with the anterior part following a straight, transversely-to-slightly-posteriorly-running course (so that the right and left margins together form a 'v' with its tip pointing posteriorly), and the lateral part following a straight, anteroposteriorly-running course (thus, together the lateral and anterior margins of the postpalatine torus would form an 'm'). The inner margin of the torus, which forms the inferoposterior margin of the choanae, is biconcave, with a midline postpalatine spine present (Fig. A-V-8: *59*), prior to shifting of the contralateral palatines. The level of the posterior termination to the palatal part of the palatine bone is ambiguous because the palatines have been thrust anteriorly and to the left.

Sphenoids.— The alisphenoid is visible as the right ectopterygoid process, whereas the basisphenoid is visible by its contribution to the right entopterygoid process (Fig. A-V-8: *56, 57*).

Squamosal.— The right and left squamosals are preserved (Fig. A-V-8). The right side is relatively complete and includes the glenoid (Fig. A-V-8: *60*), postglenoid process (Fig. A-V-8: *61*), and a fragment of zygomatic process (Fig. A-V-8: *62*). The glenoid is flat with the condyle of the dentary still resting in it. It measures 6.5 mm in anteroposterior length and 5.6 mm in mediolateral width. The postglenoid process is oriented transversly and projects straight ventrally by 1.35 mm. It is lateral to the postglenoid foramen (Fig. A-V-8: *63*).

Petrosal.— The pars cochlearis of both petrosals are preserved, as well as some of the septa and tympanic processes that attach to them (Figs. A-V-8 and A-V-9). On the right side, a bit of the pars canalicularis is visible. The posterior septum is either broken, or differently configured than in other plesiadapid specimens, such that no evidence of the *g1* groove is present. Because the posterior septum actually appears fairly complete, it may be that the internal carotid plexus took a different route in this taxon and did not go through the middle ear (see further discussion below). The lateral aspects of the promontoria are obscured so that the presence of the *g2* and *g5* grooves and anterior septum cannot be evaluated. The medial aspect on the right element preserves a groove that begins near the cochlear canaliculus and arches laterally to where the posterior septum meets the promontorium (i.e., where the *g1* groove would also normally reach the promontorium; Fig. A-V-9A–C). There is no evidence of a foramen located on the cochlear canaliculus and leading into the promontory on this side. The groove thus has the anatomical relationships of the *g4* groove of other specimens. This is the groove referred to by MacPhee et al. (1983) as the 's1' groove. They suggested it held fibers of the tympanic plexus of nerves. However, as noted above, this morphology was referred to USNM 309902 in their figure caption. The left side is differently configured. The groove and foramen relating to the tympanic canaliculus are present on the septum housing the cochlear canaliculus (Fig. A-V-9A–C). However, the more ventromedial aspect of the promontorium is free of any marks. There is no groove that matches MacPhee et al.'s (1981) 's1' from the other side. Ventral to the fenestra vestibuli at the base of the posterior

FIGURE A-V-3.— *Nannodectes intermedius* (USNM 309902). **A**, stereophotographs of the basicranial fragment in ventral view. **B**, basicranial fragment with left auditory bulla intact in ventrolateral view. **C**, inset of left petrosal. C', enlargement of inset from C. **D**, stereophotographic of left petrosal in ventrolateral view. Anterior is at the top in all images. Numbers (Table A-V-1) and abbreviations: *44*, crista tympanica; *46*, midline ridge of basioccipital; *47*, ventrally projecting lateral processes of basioccipital; *48*, right occipital condyle; *49*, foramen magnum; *ac*, aperture of cochlear fenestra; *av*, aperture of fenestra vestibuli; *Boc*, basioccipital; *Bul*, auditory bulla; *ec*, epitympanic crest; *g1*, groove for internal carotid plexus; *Ptr*, petrosal; *tt*, tegmen tympani.

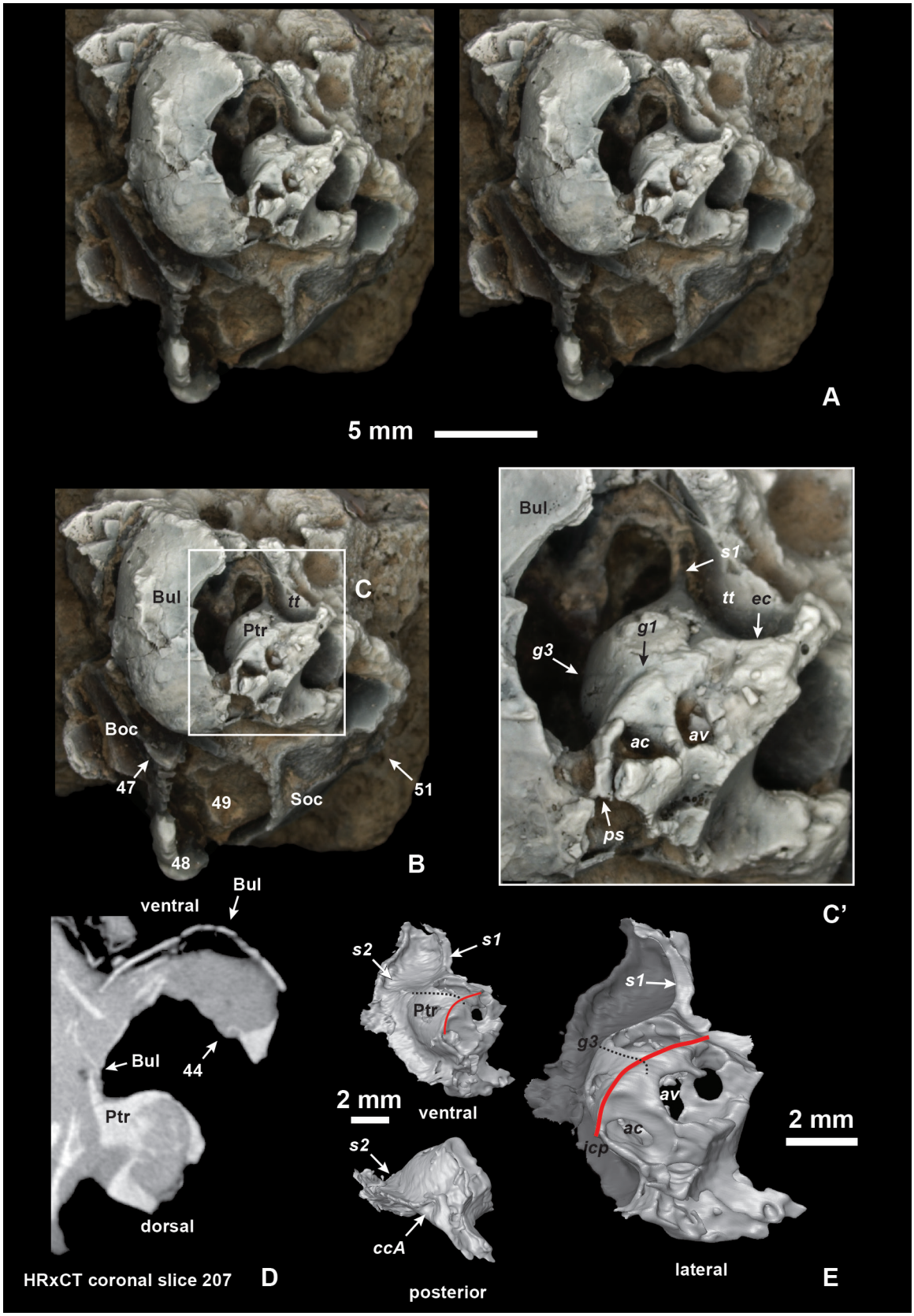
A
5 mm
Bul
tt
C
Ptr
Boc
47
49
Soc
51
48
B
Bul
s1
tt
ec
g1
g3
ac
av
ps
C'
ventral
Bul
Bul
44
Ptr
dorsal
HRxCT coronal slice 207
D
s2
s1
Ptr
2 mm
ventral
s2
ccA
posterior
s1
g3
av
ac
icp
2 mm
lateral
E

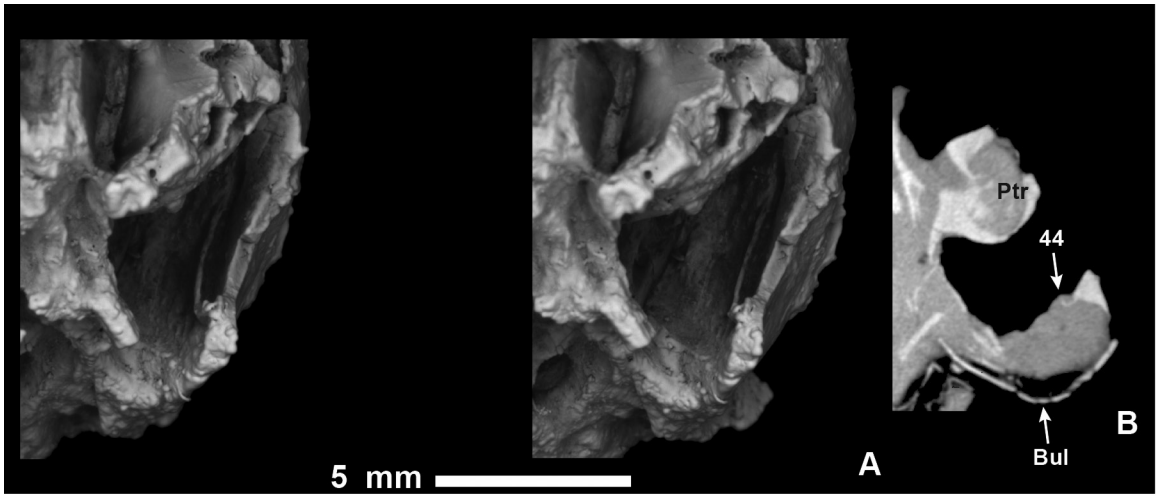

Figure A-V-5.— *Nannodectes intermedius* (USNM 309902). A, stereophotographs of left ear region in anterolateral view. B, HRxCT coronal slice number 207 (lateral to the right). Numbers (Table A-V-1) and abbreviations: *44*, crista tympanica; *Bul*, auditory bulla; *Ptr*, petrosal.

septum, a deeply incised canal stems anterodorsally from an apparent foramen (Fig. A-V-9C: *g4*). Both promontoria also have a groove that crosses from medial to lateral, approaching the *s2*. It thus appears to be the *g3* groove. However, the morphology of this groove on the left side looks suspiciously as though it could be due to postmortem damage (i.e., like a crack, the edges of which have become beveled by weathering).

Medial tympanic processes flare out from the medial side of both promontories. These processes measure 1.5–1.6 mm in width, on average. The stylomastoid foramina are preserved on both sides (Fig. A-V-9: *64*) and circular. They measure roughly 0.80–0.90 mm in diameter. Interestingly, there is a foramen wedged medial to these facial nerve foramina, and lateral to the posterodorsal base of the posterior septum on both sides (Fig. A-V-9B, C: *65*). This foramen appears to lead to a canal and may have transmitted the internal carotid plexus. If so, it means that the route of the internal carotid plexus has migrated dorsally, and slightly laterally from its position in other plesiadapids. The diameter of this possible posterior carotid foramen is about 0.29 mm, comparable to the posterior carotid foramen and internal carotid groove (*g1*) on other plesiadapids (Tables A-I-3 and A-I-4).

Occipital.— The left occipital condyle and the jugular process are preserved (Fig. A-V-8: *66, 67*). The dorsoventral height of the condyle is roughly 2.8 mm; the mediolateral width is 2.5 mm. The jugular process projects 2.64 mm laterally from the edge of the condyle. The mediolateral width of the foramen magnum (Fig. A-V-8: *68*), although possibly slightly distorted owing to dorsoventral crushing, is 6.84 mm.

Plesiadapis anceps YPM-PU 19642

The illustration of this specimen in Gingerich (1976: fig. 32) is adequate to show major morphological features; new illustrations are not necessary. Some details can be added to the description – mainly dimensions (see Tables A-I-1 through A-I-5). The nasals measure 21.84 mm in length, with anterior and posterior mediolateral widths that are equal (3.34 mm). At the anteroposterior midpoint, the bone is mediolaterally narrower (2.30 mm). The premaxilla/frontal suture measures 4.52 mm. The premaxilla is 9.51 mm in dorsoventral depth. The maxilla/frontal suture measures 4.6 mm. The entire anteroposterior length of the frontals is preserved as well as the anterior margin of the parietal/frontal suture. Thus, the length of the metopic suture can also be given: 13.08 mm.

Plesiadapis tricuspidens MNHN CR 125

Cranial sutures.— As indicated in the introduction, Russell (1964: figs. 13, 14, 19) provided reconstructions of the skull of *P. tricuspidens* showing cranial sutures, but did not provide photographic evidence for most of the drawings. Thus, images of major sutures are provided here (Figs. A-V-10 through A-V-13: *69–87*). In addition to sutures recognized by Russell

FIGURE A-V-4.— *Nannodectes intermedius* (USNM 309902). **A**, stereophotographs of the left basicranial fragment in lateral view. **B**, basicranial fragment in lateral view. **C**, inset of left petrosal. C', enlargement of inset C. **D**, HRxCT coronal slice number 207. **E**, three views of HRxCT renderings of left petrosal. Nerves reconstructed in yellow represent components of tympanic plexus. Neurovasculature reconstructed in red shows components of the internal carotid plexus. Anterior is at the top in all images. Fine dashed line is g3 groove. Numbers (Table A-V-1) and abbreviations: *44*, crista tympanica; *47*, ventrally projecting lateral processes of basioccipital; *48*, right occipital condyle; *49*, foramen magnum; *51*, nuchal crest; *ac*, aperture of cochlear fenestra; *av*, aperture of fenestra vestibuli; *Boc*, basioccipital; *Bul*, auditory bulla; *ccA*, aperture of cochlear canaliculus; *ec*, epitympanic crest; *g1*, groove for internal carotid plexus; *g3*, groove that leads to s2 (for a small vein?); *ps*, posterior septum; *Ptr*, petrosal; *s1*, first (anterior) septum; *s2*, second septum; *Soc*, supraoccipital; tt, tegmen tympani.

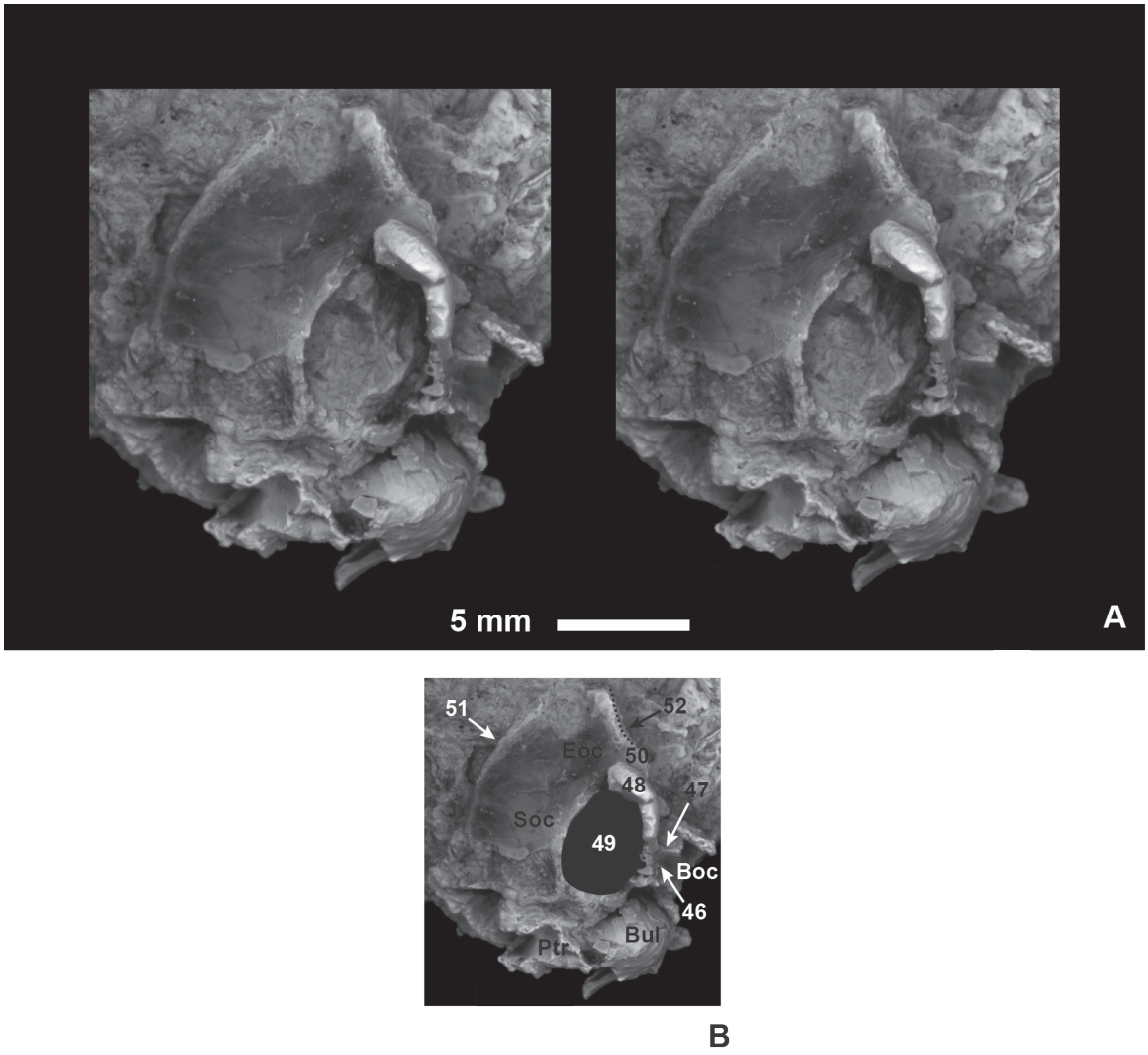

FIGURE A-V-6.— *Nannodectes intermedius* (USNM 309902). **A**, stereophotographs of basicranial fragment in posterior view. **B**, labeled image of basicranial fragment in posterior view (dorsal is to the left in A and B). Numbers (Table A-V-1) and abbreviations: *46*, midline ridge of basioccipital; *47*, ventrally projecting lateral processes of basioccipital; *48*, right occipital condyle; *49*, foramen magnum; *50*, jugular process of exoccipital; *51*, nuchal crest; *52*, exoccipital–petrosal suture; *Boc*, basioccipital; *Bul*, auditory bulla; *Eoc*, exoccipital; *Ptr*, petrosal; *Soc*, supraoccipital.

(1964), there seems to be evidence of an orbitosphenoid/frontal suture (Fig. A-V-13: *87*); observation of MNHN CR 965 helps strengthen interpretation of the presence of this suture.

Cranial foramina.— Infraorbital foramina are well preserved in MNHN CR 125 (Fig. A-V-12E: *88*). The foramen ovale is clearly present, contained within the alisphenoid (Fig. A-V-13B, D: *89*). As indicated in the introduction, the presence of foramen rotundum in *P. tricuspidens* has been debated. The large foramen posterior to the optic foramen and dorsal to the split of the ecto- and entopterygoid crests (Fig. A-V-13D: *90*) must be considered either the foramen rotundum (Russell, 1964) or the sphenorbital fissure (Kay et al., 1992). This interpretation depends on the identity of another foramen (Fig. A-V-13B, D, E: *91*), which is located directly posteroventral to the optic foramen (Fig. A-V-13B, D, E: *92*) and best preserved in MNHN CR 965. It has been interpreted as the 't.d.a.' (superior orbital fissure) by Russell (1964), Gingerich (1976), and Bloch and Silcox (2006) and as the suboptic foramen by Kay et al. (1992). The logic of the Kay et al. (1992) interpretation is as follows: if Russell (1964) were incorrect, and this smaller foramen is not the superior orbital fissure, then it did not transmit the ophthalmic division of the trigeminal nerve, and the more posterior foramen must have carried both the ophthalmic and maxillary divisions. In this case, no foramen devoted solely to the maxillary division of

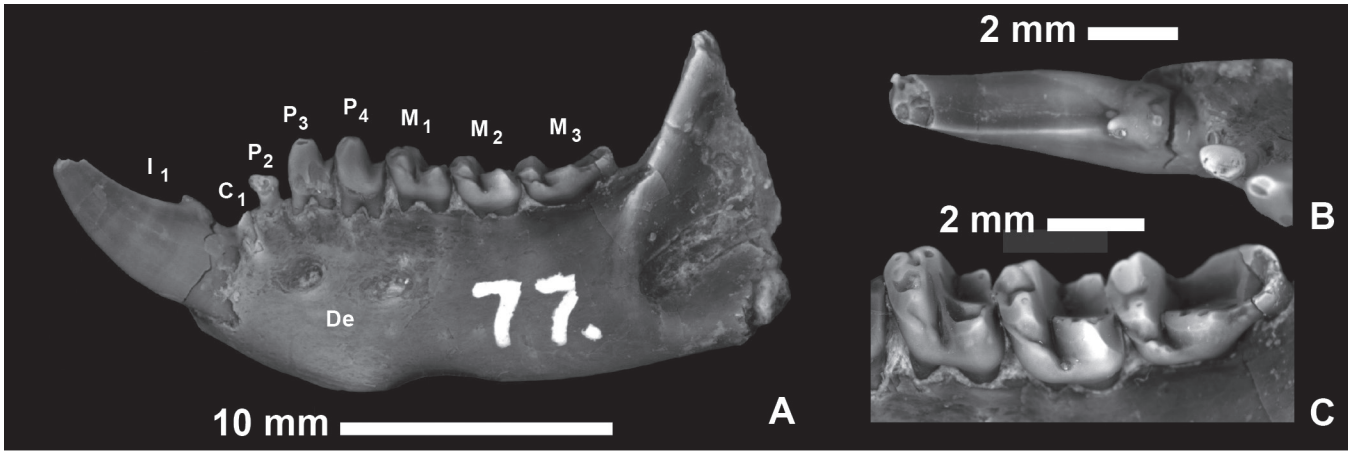

FIGURE A-V-7.— *Nannodectes intermedius* (USNM 309902). **A**, left dentary in buccal view. **B**, left anterior teeth in occlusal view. **C**, left M_{1-3} in oblique bucco-occlusal view. Abbreviation: *De*, dentary.

the trigeminal would have existed, and thus a foramen rotundum did not exist.

Our observations of the original material lead us to conclude that there is no foramen rotundum. That is, the structure Russell called the 't.d.a.' is in fact the suboptic foramen, as Kay et al. (1992) suggested. However, the evidence for this conclusion must partly be gleaned from MNHN CR 965, as discussed below. One point that can be made on MNHN CR 125, however, is that the 'suboptic foramen' appears to be entirely within the orbitosphenoid, unlike the superior orbital fissure, which falls between the orbitosphenoid and alisphenoid. Notably, MNHN CR 125 has a different small foramen just posterior to the optic foramen and anterior to the 'sphenorbital fissure.' This small foramen could also plausibly be considered a superior orbital fissure because it appears to open anteriorly through the junction of the alisphenoid and orbitosphenoid (Fig. A-V-13': *93*). However, this foramen is not bilaterally present and it is absent from MNHN CR 965, suggesting that it is simply another, variably present opening. It does, however, serve to reveal the alisphenoid/orbitosphenoid suture, which connects the foramen (*93*) and the sphenorbital fissure (*90*).

Interpretations of foramina of the basicranium have also been contentious. As discussed in the introduction, Bloch and Silcox (2001) implied that this specimen was lacking evidence of a posterior carotid foramen. However, Figure A-V-12B' shows the posterior carotid foramen perpendicular to its canal and illustrates its caliber and shape. There is no doubt regarding the interpretation of this feature, given the consistency of its presence in other specimens of this species, as well as in other species (see above). The canal leading from the posterior carotid foramen through the base of the posterior septum is roughly 2.8 mm long. Medial to the promontorium is a groove leading to a foramen that perforates the medial process of the bulla at its medial point of termination, and one that perforates the promontorium itself at its lateral point of termination. This feature has been interpreted as the vestibular aqueduct by Szalay et al. (1987), but it is clearly the tympanic canaliculus foramen and groove, as discussed for other specimens earlier (MacPhee, 1981; Fig. A-V-14C': *94–95*). This morphology is clearly present in most other plesiadapid specimens preserving the relevant anatomy, as discussed and illustrated above. The hypoglossal canal appears septate and split into two foramina, as in *Pronothodectes*.

Morphology of cranial bones.— Some of the most critical information relating to the structure of the basicranium in this specimen has been lost. What remained of the medial process of the left petrosal when Gingerich (1976: Pl. 8c) photographed the specimen sometime prior to 1974 is now gone. However, a cast recently made from an old mold housed in the MNHN, retains the medial process. This cast also reveals that MNHN CR 125 was broken at the junction of the medial tympanic process and pars cochlearis even before the medial process was lost (demonstrating that this specimen was never substantially better preserved than the Pellouin skull anyway).

The promontoria of MNHN CR 125 conform well to the description by Gingerich (1976). As noted above, however, neither the posterior carotid foramen nor the laterally positioned *g1* groove for the internal carotid plexus has been photographically illustrated previously. Figure A-V-14B shows this morphology. Unlike other *P. tricuspidens* promontoria (see below) and unlike many other plesiadapid petrosals (see above), MNHN CR 125 does not express the *g2–3* grooves. However, the *g4–5* grooves are present (Fig. A-V-14).

Plesiadapis tricuspidens MNHN CR 965

This specimen appears frustratingly incomplete on preliminary inspection, being represented by only sphenoids, a palatine, and parts of maxillae with teeth. However, it provides the most solid evidence available for deducing the pattern of cranial foramina in *P. tricuspidens*. In fact, reconstructions of cranial foraminal patterns have been based primarily on MNHN CR 965 (Russell, 1964; Kay et al., 1992), of which little of the dorsal aspect of the orbitosphenoid or alisphenoid

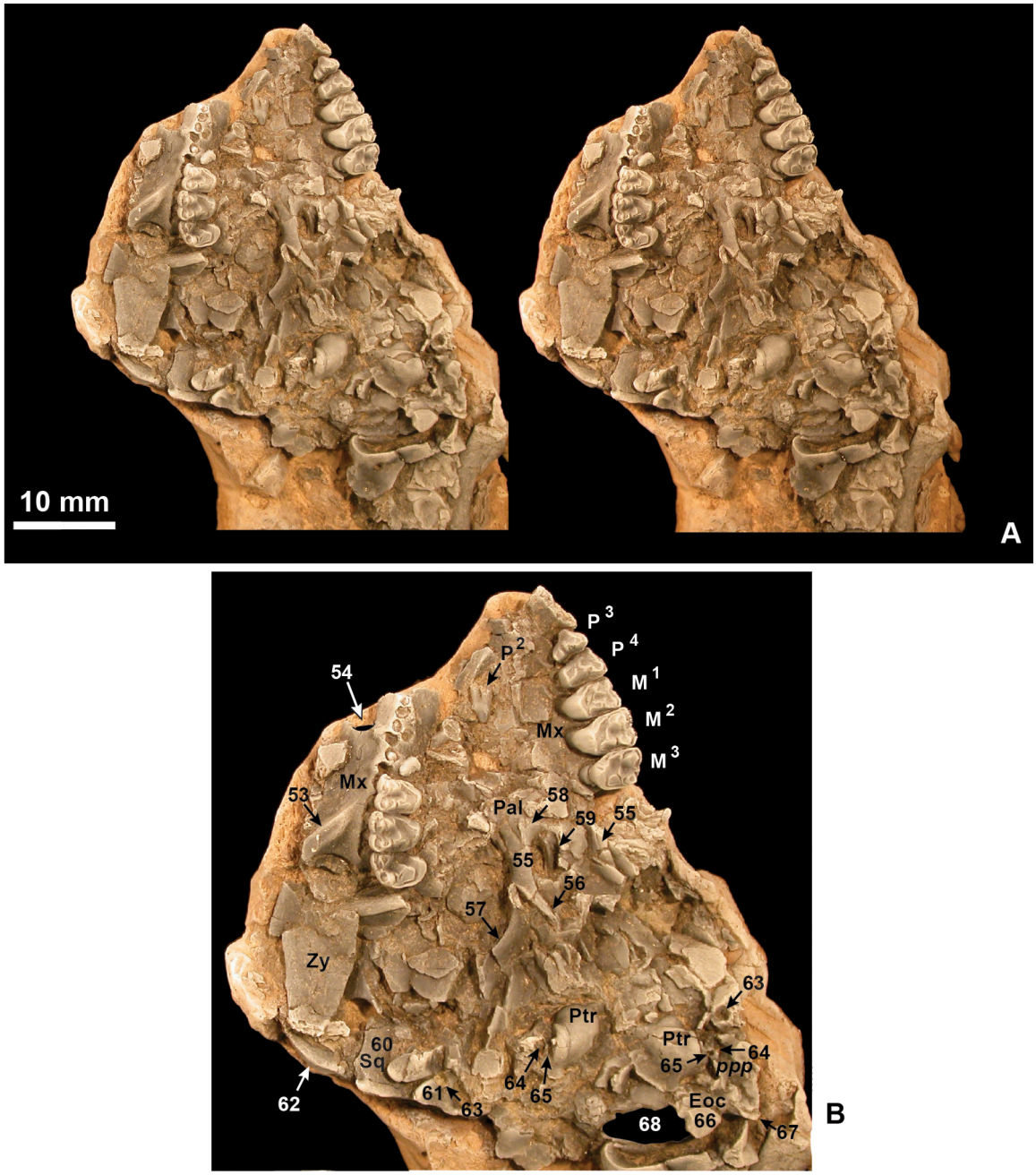

FIGURE A-V-8.— *Nannodectes gidleyi* (AMNH 17388). **A**, stereophotographs of base of skull in ventral view. **B**, enlarged ventral view. Anterior is at the top in A and B. Numbers (Table A-V-1) and abbreviations: *53*, root of zygmatic process of maxilla; *54*, infraorbital foramen; *55*, pterygoid process of palatine; *56*, pterygoid process of basisphenoid; *57*, pterygoid process of alisphenoid; *58*, palatine postpalatine torus; *59*, postpalatine spine; *60*, glenoid of squamosal; *61*, postglenoid process; *62*, zygomatic process of squamosal; *63*, postglenoid foramen of squamosal; *64*, stylomastoid foramen; *65*, possible posterior carotid foramen and internal carotid canal; *66*, occipital condyle; *67*, jugular process of exoccipital; *68*, foramen magnum; *Eoc*, exoccipital; *Mx*, maxilla; *Pal*, palatine; *ppp*, paroccipital process of petrosal; *Ptr*, petrosal; *Sq*, squamosal; *Zy*, zygomatic.

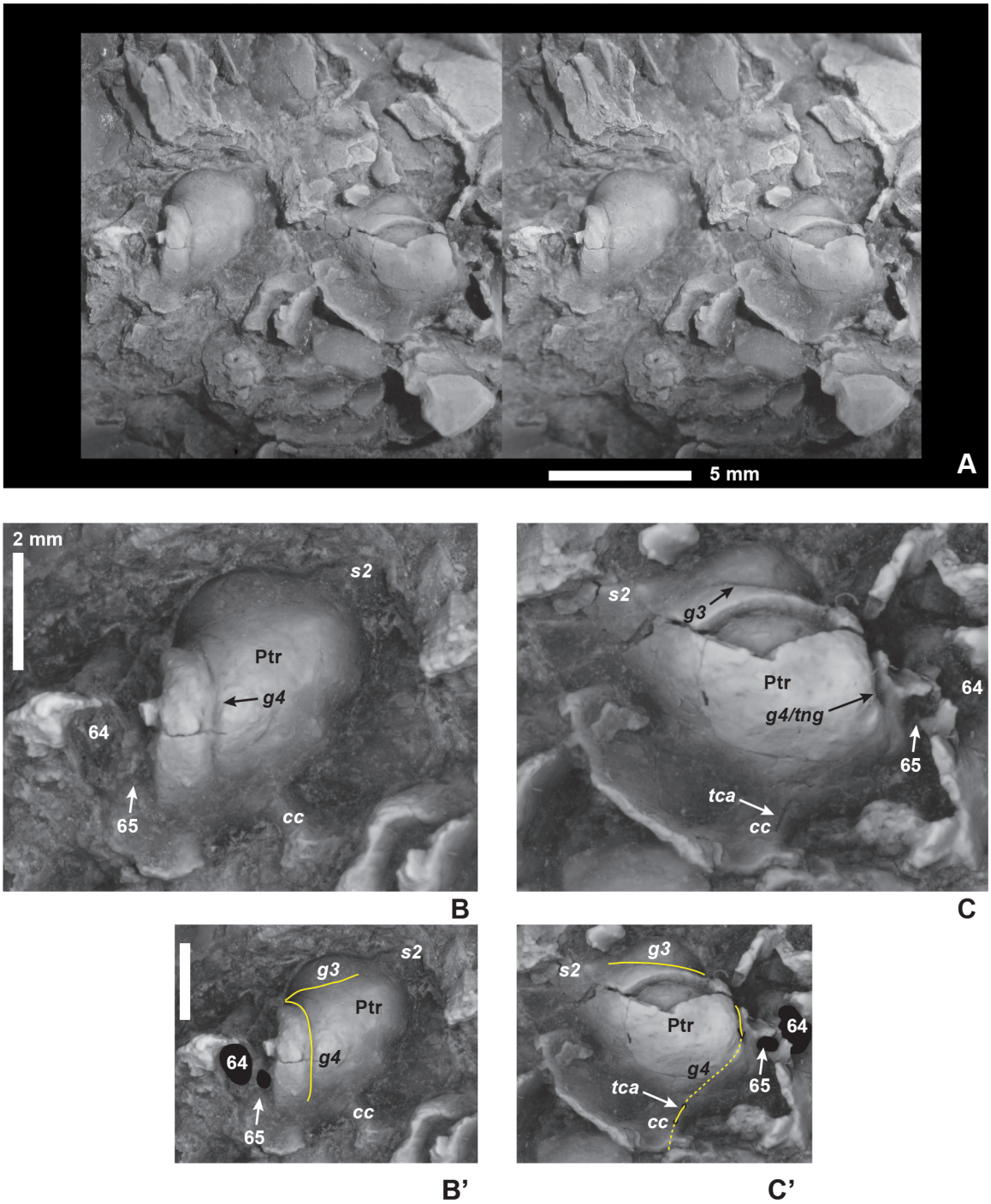

FIGURE A-V-9.— *Nannodectes gidleyi* (AMNH 17388). **A**, stereophotographs of basicranium in ventral view. **B**, right petrosal in ventral view with limited labeling. B', right petrosal in ventral view with augmented labeling. **C**, left petrosal in ventral view with limited labeling. C', left petrosal in ventral view with augmented labeling. Anterior is at the top in all images. Solid white lines represent the course of nerves relating to the tympanic plexus. Dashed white line represents the nerve course passing through a canal in the promontorium. Numbers (Table A-V-1) and abbreviations: *64*, stylomastoid foramen; *65*, possible posterior carotid foramen and internal carotid canal; *cc*, cochlear canaliculus; *g3*, groove that leads to s2 (for a small vein?); *g4*, groove for tympanic plexus fibers to reach routes g1–3; *Ptr*, petrosal; *s2*, second septum; *tca*, tympanic canaliculus; *tng*, tympanic nerve groove.

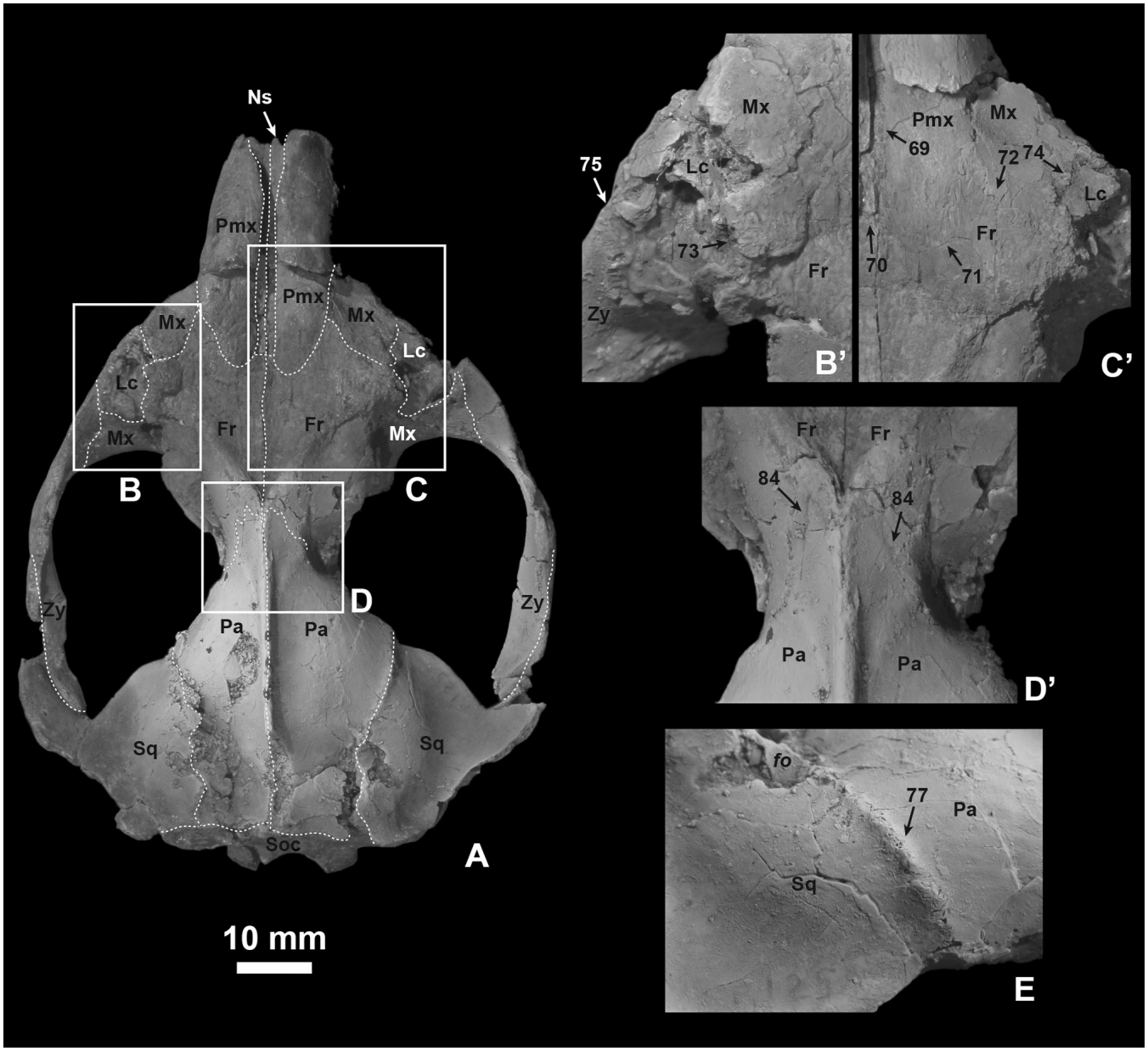

FIGURE A-V-10.— *Plesiadapis tricuspidens* (MNHN CR 125). **A**, cranium in dorsal view; sutures are shown as dashed white lines. **B**, inset of left anterior orbit in dorsal view. B', enlargement of inset B. **C**, inset of right anterior orbit in dorsal view. C' enlargement of inset C. **D** inset of orbitotemporal constriction in dorsal view. D', enlargement of inset D. Anterior is at the top in images A–D. **E**, right neurocranium showing squamosal/parietal suture in lateral view (anterior is at the right). Numbers (Table A-V-1) and abbreviations: *69*, nasal/premaxilla suture; *70*, nasal/frontal suture; *71*, maxilla/frontal suture; *72*, premaxilla/frontal suture; *73*, lacrimal/frontal suture; *74*, lacrimal/maxilla suture; *75*, lacrimal/zygomatic suture; *77*, parietal/squamosal suture; *84*, parietal/frontal suture; *fo*, foramen; *Fr*, frontal; *Lc*, lacrimal; *Mx*, maxilla; *Ns*, nasal; *Soc*, supraoccipital; *Sq*, squamosal; *Zy*, zygomatic.

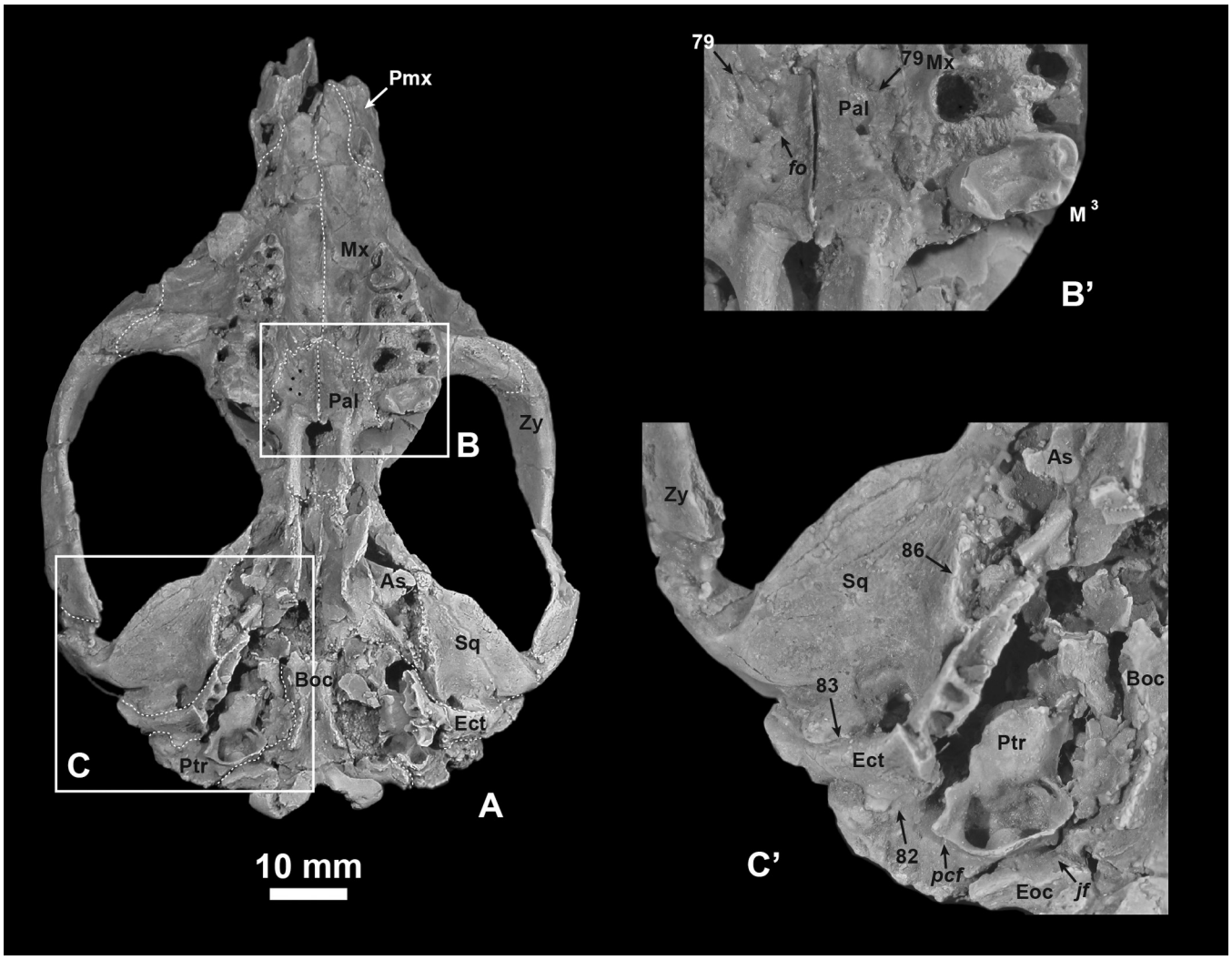

FIGURE A-V-11.— *Plesiadapis tricuspidens* (MNHN CR 125). **A**, cranium in ventral view; sutures are shown as dashed white lines. **B**, inset of posterior palate in ventral view. B', enlargement of inset B. **C**, inset of right basicranium in ventral view. C', enlargement of inset C. Anterior is at the top in all images. Numbers (Table A-V-1) and abbreviations: *79*, palatine/maxilla suture; *82*, petrosal/ectotympanic suture; *83*, ectotympanic/squamosal suture; *86*, alisphenoid/squamosal suture; *As*, alisphenoid; *Boc*, basioccipital; *Ect*, ectotympanic; *Eoc*, exoccipital; *fo*, foramen; *jf*, jugular foramen; *Mx*, maxilla; *Pal*, palatine; *pcf*, posterior carotid foramen; *Pmx*, premaxilla; *Ptr*, petrosal; *Sq*, squamosal.

remains. Only the ventral portions of those bones are intact, but this is helpful in some ways that we discuss below (Fig. A-V-15).

Cranial sutures.— For the most part the sutural patterns in the orbitotemporal region depicted by Russell (1964: fig. 19) are based on this specimen and can easily be observed, as documented here with photographs for the first time (Figs. A-V-16 and A-V-17: *96–99*).

There are two sutures that were not previously discussed or illustrated by Russell (1964): the orbitosphenoid-frontal suture and the alisphenoid-orbitosphenoid suture. The dorsal margin of the orbitosphenoid actually appears to be an intact sutural edge that represents the dorsal boundary with the frontal bone. This suture appears to be preserved in a consistent position in MNHN CR 125 as well (Figs. A-V-16 and A-V-17A: *100*). Additionally, the alisphenoid/orbitosphenoid suture is evident (Fig. A-V-17: *101*). It passes through, or just above, the sphenorbital fissure, such that the medial aspect of the foramen is probably formed of orbitosphenoid, whereas the lateral aspect is alisphenoid. Although on superficial inspection this boundary resembles a crack, because it is not convoluted like many other sutures, the contact between these particular bones frequently looks this way in various other taxa (e.g., tenrecs). Furthermore, two features (only one could be photo-documented) of this contact strongly suggest it is a suture: (1) the form of the discontinuity between the alisphe-

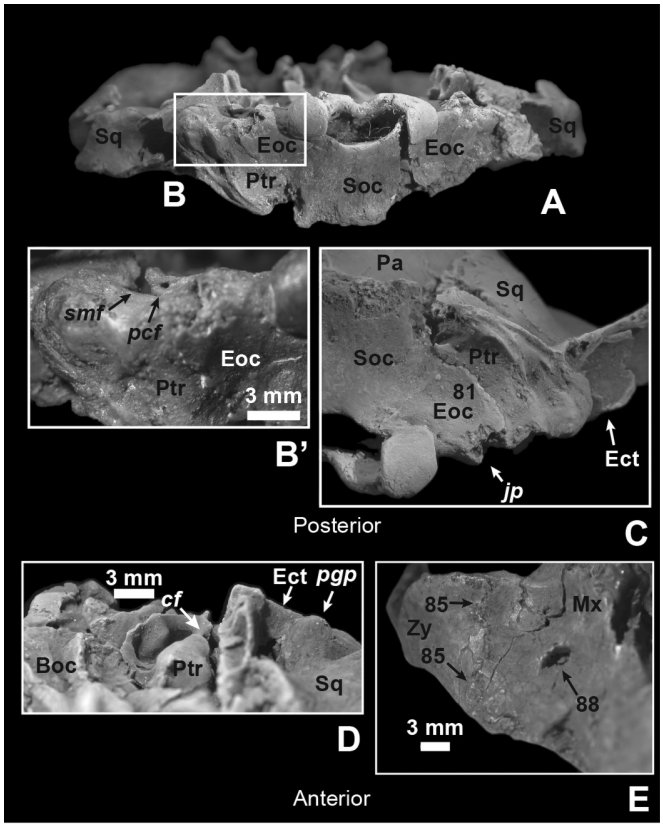

FIGURE A-V-12.— *Plesiadapis tricuspidens* (MNHN CR 125). **A**, cranium in posterior view. **B**, inset of right side of cranium in posterior view. B', enlargement of inset B showing the posterior carotid foramen (*pcf*). **C**, close-up of right side in posterior view, with the dorsal surface facing upward. **D**, right petrosal in anterior view, showing the anterior end of the carotid canal (*cf*). **E**, right maxilla in anterior view. Dorsal is up in image C, but down in all other images. Numbers (Table A-V-1) and abbreviations: *81*, occipital/petrosal suture; *85*, maxilla/zygomatic suture; *88*, infraorbital foramen; *89*, foramen ovale; *Boc*, basioccipital; *Ect*, ectotympanic; *Eoc*, exoccipital; *jp*, jugular process of exoccipital; *Mx*, maxilla; *Pa*, parietal; *pcf*, posterior carotid foramen; *Ptr*, petrosal; *smf*, stylomastoid foramen; *Soc*, supraoccipital; *Sq*, squamosal; *Zy*, zygomatic.

noid and orbitosphenoid is revealed by the absence (i.e., broken condition) of the orbitosphenoid in the region of interest. Instead of appearing 'crack-like' and planar, the discontinuity is dished like a sutural contact (Fig. A-V-17: *102*). (2) Even though the discontinuity is not convoluted like some other sutures, it is still more complex than would be expected for a crack created by brittle deformation. Identification of this suture helps interpret cranial foraminal patterns. Having recognized this suture on MNHN CR 965, it becomes apparent that it has a slightly different course than that preserved on the left side of MNHN CR 125 connecting foramina *90* and *93* (Fig. A-V-13D'). The latter suture would likely have resulted in the orbitosphenoid forming most of the medial wall of the sphenorbital fissure.

Cranial foramina.— Foramina for the mandibular division of the trigeminal nerve (Figs. A-V-15, A-V-18: *103*), for the combined maxillary and ophthalmic divisions of the trigeminal nerve (Figs. A-V-15 through A-V-18: *104*), and for the optic nerve (Figs. A-V-15, A-V-17, A-V-18: *105*) are clearly visible and traceable to endocranial space. There are a number of small foramina venous representing sinus drainage from the lateral aspect of the alisphenoid and the lateral aspect of the orbitosphenoid (Fig. A-V-16, A-V-17: *106*). These cannot be mistaken for cranial nerve foramina because they are not bilaterally present in some cases and do not lead to the endocranium in other cases. This is also true for the 'suboptic foramen' located posteroventral to the optic foramen (Figs. A-V-15, A-V-17: *107*). It appears to lead into the trabecular space of the orbitosphenoid and probably communicates directly with the blood sinus foramina on the opposite side.

Bloch and Silcox (2006) argued that communicating suboptic foramina are not expected in a taxon with such broad interorbital spacing; however, despite broad interorbital spacing, the postorbital constriction of the neurocranium in *Plesiadapis* is substantial and results in a sphenoid region as narrow as that of many euprimates. It thus seems unlikely that previous interpretations of the suboptic foramen as the 't.d.a.' are correct. It is acknowledged that the left side of the orbitosphenoid has been displaced substantially, which prevents complete confidence in the interpretation. However, the right side is more intact, and the remnants of the optic canal can be traced to the dorsal (endocranial) aspect of the orbitosphenoid (Fig. A-V-16: *108*). There is no comparable canal that could represent the ophthalmic branch of the trigeminal running ventrolateral to this. Moreover, given the identification of the orbitosphenoid/alisphenoid suture above, Russell's (1964) 't.d.a.' and ophthalmic canal would have run within the orbitosphenoid, which would be an unusual pattern for a eutherian mammal, as discussed above.

Morphology of cranial bones.—The only previously unmentioned aspect of this specimen is the existence of pneumatization of the alisphenoid (Figs. A-V-15A, A-V-16C, A-V-18: *109*). This is consistent with observation by MacPhee and Cartmill (1986) that the Pellouin skull is enervated by empty 'celluoles.'

Plesiadapis tricuspidens Pellouin skull

Cranial sutures.—The Pellouin skull preserves perhaps the best example of a remnant of the palatine/alisphenoid suture (Figs. A-V-19C–C', A-V-22B–B': *110*) and the only squamosal/alisphenoid suture (Fig. A-V-19E–E': *111*). Furthermore, it increases confidence in descriptions based on other specimens by preserving similar sutural patterns. Specifically, there is a clear sutural surface for a large wing of premaxilla on the frontal (Fig. A-V-20B–B': *112*). The sutural surface for the nasals on the frontal is preserved, showing that the nasal was morphologically similar to MNHN CR 125 in this region (Fig. A-V-20B–B': *113*).

In the palate, the transverse palatine suture is similar to that in other *P. tricuspidens* specimens (Fig. A-V-19B–B': *114*) in

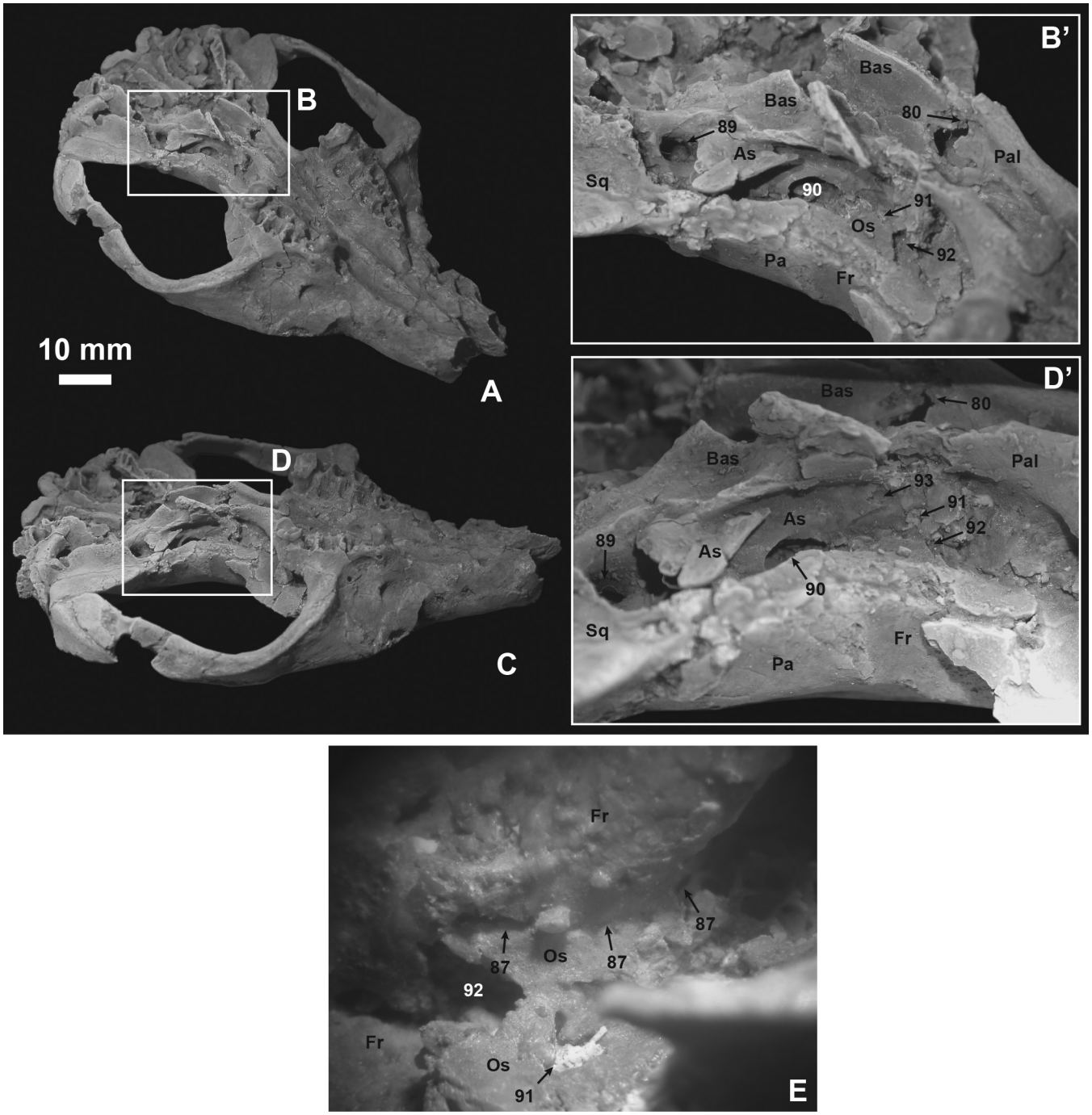

FIGURE A-V-13.— *Plesiadapis tricuspidens* (MNHN CR 125). **A**, cranium in anteroventrolateral view. **B**, inset of orbitotemporal region. B', enlargement of inset B. **C**, cranium in ventrolateral view. **D**, inset of orbitotemporal region. D', enlargement of inset C. Dorsal is down and ventral up in images A–D. **E**, enlargement of frontal/orbitosphenoid contact. Dorsal is up and ventral down in image E. Numbers (Table A-V-1) and abbreviations: *80*, palatine/sphenoid suture; *87*, dorsal orbitosphenoid/frontal suture; *89*, foramen ovale; *90*, sphenorbital fissure; *91*, suboptic foramen; *92*, optic foramen; *93*, possible superior orbital fissure; *As*, alisphenoid; *Bas*, basisphenoid; *Fr*, frontal; *Os*, orbitosphenoid; *Pa*, parietal; *Pal*, palatine; *Sq*, squamosal.

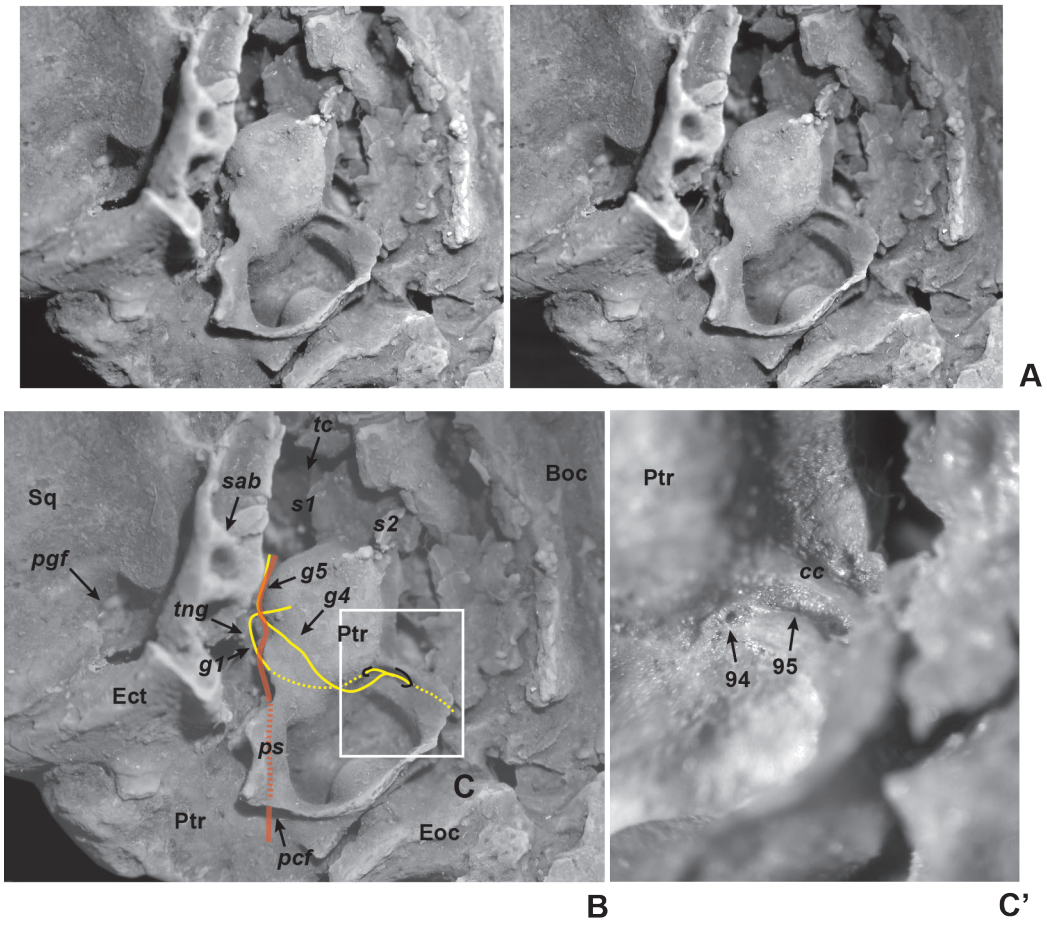

FIGURE A-V-14.— *Plesiadapis tricuspidens* (MNHN CR 125). **A**, stereophotographs of right promontorium in ventral view. **B**, right promontorium in ventral view. **C**, ventral view of inset of right promontorium showing the tympanic canaliculus groove. C', enlargement of inset C showing the tympanic canaliculus groove (95) and foramina relating to the tympanic nerve (canal edges are out of focus). Anterior is at the top in all images. Nerves reconstructed in yellow represent components of the tympanic plexus. Neurovasculature reconstructed in red represents components of the internal carotid plexus. Numbers (Table A-V-1) and abbreviations: *94*, tympanic canaliculus foramen; *95*, tympanic canaliculus groove; *Boc*, basioccipital; *cc*, cochlear canaliculus; *Ect*, ectotympanic; *Eoc*, exoccipital; *g1*, a lateral route that begins at the posterior carotid foramen and proceeds through a short canal to the lateral aspect of the promontorium (this likely held the internal carotid plexus and possibly a remnant of the internal carotid artery); *g4*, groove for tympanic plexus fibers to reach routes g1–3; *g5*, groove that leads toward epitympanic crest; *pgf*, postglenoid foramen; *ps*, posterior septum; *ptr*, petrosal; *s1*, first (anterior) septum; *s2*, second septum; *sab*, strut from annular part to bullar part; *Sq*, squamosal; *tc*, tubal canal; *tng*, tympanic nerve groove. Compare to figure 14 for further clarification.

its convoluted shape and in reaching the level of M^1. There appears to be a nearly obliterated palatine/frontal suture in the postpalatine canal. Unfortunately, neither the frontal/orbitosphenoid contact nor the alisphenoid/orbitosphenoid suture is visible.

The frontal/parietal contact is visible at the anterior apex of the dorsum of the skull (Fig. A-V-20D–D': *115*), but barely evident elsewhere. The parietal/squamosal contact is most distinct anteriorly (Fig. A-V-20A, E–E': *116*) and broken in the region of squamosal foramina (Fig. A-V-20E–E': *117*). Note that there are two squamosal foramina, one at the boundary between squamosal and parietal and one completely within the squamosal (Fig. A-V-20E–E'). A suture between what appears to be parietal and occipital is visible along the nuchal crest (Fig. A-V-20F–F': *118*). Sutures are clear between the tubular external auditory meatus and postglenoid process anteriorly, and the external auditory meatus and mastoid posteriorly (Fig. A-V-19F–F': *119–120*). The tympanic annulus of the ectotympanic, holding the crista tympanica, projects well beyond the bony struts of the annular bridge. It even appears that there is a gap between the bridge and the annulus suspended from it, but it is unclear whether this is a suture or due to breakage (Figs. A-V-21B–B' and A-V-22C–C': *121*).

Cranial foramina.— The infraorbital foramen is well preserved and measures 2.34 mm by 1.79 mm. The palatine in the palate has three main foramina, unlike MNHN CR 125,

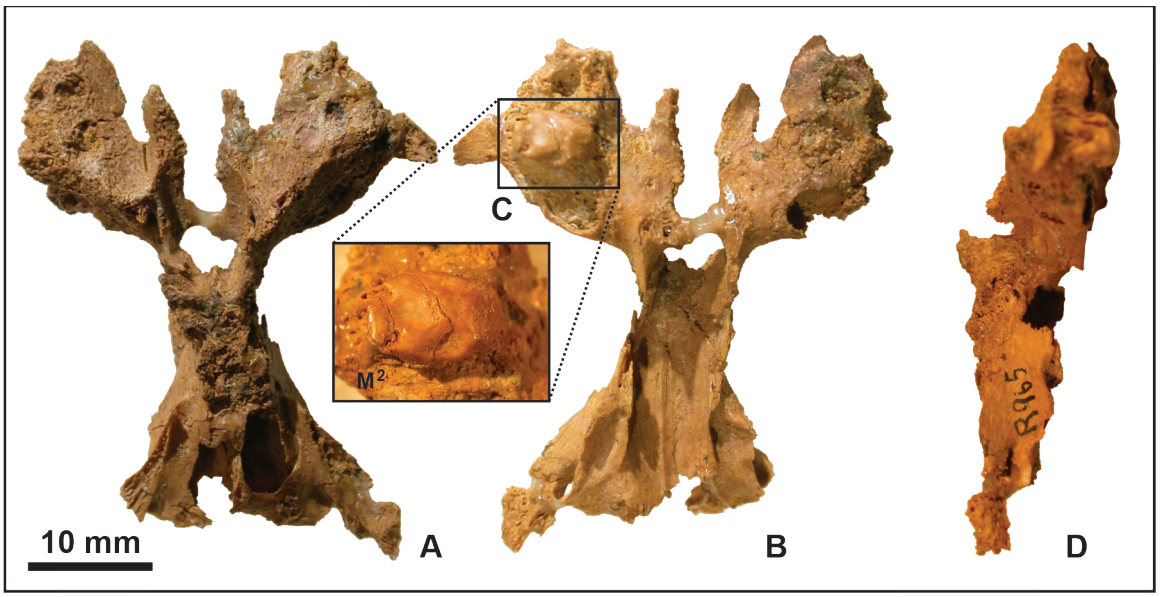

FIGURE A-V-15.— *Plesiadapis tricuspidens* (MNHN CR 965). **A**, cranial fragment in dorsal view. **B**, same in ventral view. **C**, inset and enlargement of M^2. **D**, cranial fragment in right lateral view. This specimen is identified as *P. tricuspidens* on the basis of size, the morphology of M^2, and details of cranial morphology.

which has four (as illustrated in Gingerich, 1976: pl. 9a; Fig. A-V-19B–B': *122*). As indicated above, the postpalatine foramen is visible on the left side. The optic and 'suboptic' foramina are obscured by crushing. However, the base of the 'sphenorbital fissure' is visible in a way similar to that in MNHN CR 125 (Fig. A-V-22B–B': *123*). The foramen ovale is visible, but barely so because it is obscured by matrix and broken (Fig. A-V-22B–B': *124*). There is a foramen within the left scaphoid fossa (Fig. A-V-19D–D': *125*), which may represent the vidian foramen. This appears to be that which Gingerich (1976) mentions (but does not illustrate).

Relating to the ear, a tubal canal is present on the right bulla (Fig. A-V-22C–C': *126*). Regarding the promontoria of the pars cochlearis of the petrosal, both *ac*, but neither *av*, are visible. Arching over the *ac*, the posterior septum holds an actual carotid canal that is visible on both sides: the ventral half is sheared away on the left side, but the canal is intact on the right side and the posterior carotid foramen is both visible and measureable (0.31 mm on right side, 0.29 mm on left side; Figs. A-V-21, A-V-22C–C': *127*). On the medial aspect of both promontoria, the opening of the tympanic canaliculus is present on the septum for the cochlear canaliculus (Fig. A-V-21C'', E: *128*). On the posterior side of the left caudal tympanic process of the petrosal (posterior wall of the bulla), the jugular foramen is clearly visible, formed between the bulla and the exoccipital. It measures roughly 2.13 mm in maximum diameter. As in MNHN CR 125, it is clearly divided into two regions for the internal jugular vein laterally and cranial nerves IX–XI medially (Fig. A-V-21C'': *129*). The hypoglossal canal is also well preserved on the left side (Fig. A-V-21C'': *130*) and, as for MNHN CR 125, it is split into two foramina. A small, laterally oriented foramen is present anterior to the *eam*.

Morphology of cranial bones.— The only region that requires additional description in light of new information on other plesiadapids is the pars cochlearis. As indicated above, the posterior septum with a carotid canal and *g1* groove is visible on the lateral aspect of the promontorium, as it is in other plesiadapids. No laterally coursing *g2* groove is visible on this specimen although, admittedly, this region is obscured, at least on the right side. Medial to the posterior septum, the septum for the cochlear canaliculus is visible with the tympanic canaliculus foramen on it. Moving anteriorly from the cochlear canaliculus along the medial side of the bulla, there is no third septum, and thus the second septum is eventually encountered (Figs. A-V-21 and A-V-22: *s2*). On both promontoria, a set of parallel grooves begins from the lateral side of the promontorium, near the posterior septum. This set of grooves arches medially and anteriorly, approaching the second septum, and thereby reveals itself as a set of *g3* grooves (Figs. A-V-21 and A-V-22: *g3*). Arching ventrolaterally, away from the tympanic canaliculus, is the *g4* groove (Fig. A-V-21: *g4*).

Neither promontorium is continuous with its medial tympanic process, apparently due to breakage. The breakage appears to have happened in the same way on both sides, with the pars cochlearis having been shifted ventrally away from the surrounding bulla (Fig. A-V-21). Additionally, the caudal and rostral processes are broken on the right promontorium. On the left, the caudal process is intact, the medial process is broken even closer to the pars cochlearis, and rostral processes, although broken, are more visible and intact than on the right side.

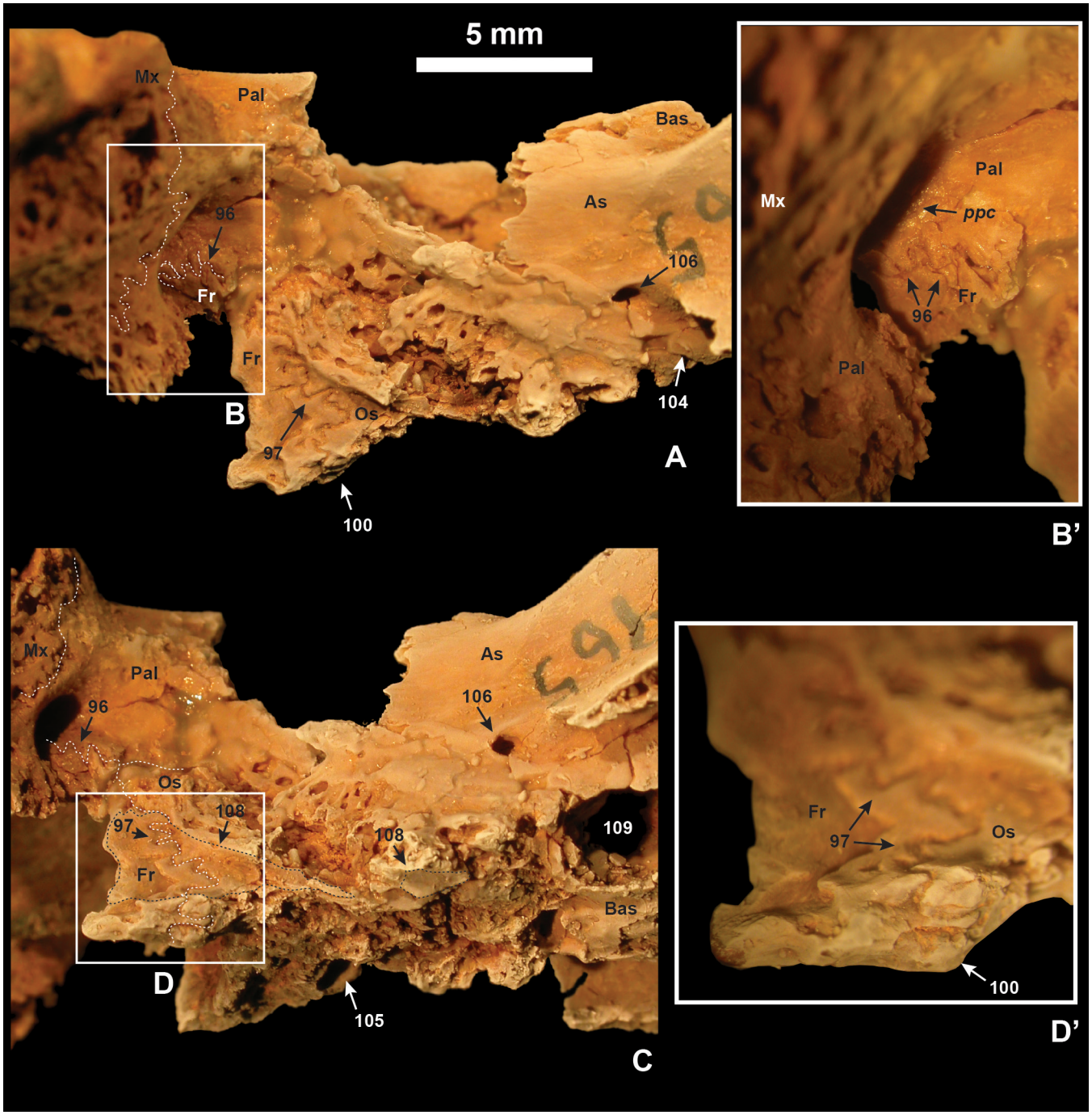

FIGURE A-V-16.— *Plesiadapis tricuspidens* (MNHN CR 965). **A**, orbitotemporal region of cranium in right lateral view. **B**, inset of right postpalatine foramen. B', enlargement of inset B. **C**, right dorsolateral view of orbitotemporal region. **D**, inset of frontal and orbitosphenoid fragment. D', enlargement of inset D. Sutures are shown as dashed white lines. Anterior is to the left and dorsal is down in all images. Numbers (Table A-V-1) and abbreviations: *96*, palatine/frontal suture in postpalatine canal; *97*, frontal/orbitosphenoid suture just anterior to optic foramen; *100*, dorsal margin of orbitosphenoid; *104*, sphenorbital fissure; *105*, optic foramen; *106*, various foramina representing blood sinus drainage; *108*, remnants of optic canals on broken orbitosphenoid (surrounded by dashed black line and shaded lightly); *109*, basisphenoid sinus space; *As*, alisphenoid; *Bas*, basisphenoid; *Fr*, frontal; *Mx*, maxilla; *Os*, orbitosphenoid; *Pal*, palatine; *ppc*, postpalatine canal.

The broken edges of the bullar walls just ventral to the ectotympanic ring and medial to the pars cochlearis of the petrosal on the right side are clearly comprised of two layers of bone (Fig. A-V-23E–G). The outer (more superficial) layer is generally thinner near the ectotympanic and of a deeper amber color than the deep layer. On the medial bullar wall, the superficial layer is thicker than the deep layer.

Evidence against a petrosal composition to the bulla (contrary to the evidence above – see discussion) is that the left ear has a distinct color change between the edge of the pars cochlearis and the posterior septum, as well as between the pars cochlearis and the very base of the medial tympanic process. Associated with this color change is what also looks like a groove that invites interpretation as a sutural margin or bone boundary (Fig. A-V-21E: *131*). However, closer inspection of this juncture reveals the presence of a thin crack at its posterior end that accentuates the distinction between these two regions of the petrosal.

***Plesiadapis tricuspidens* MNHN CR 126**

Cranial sutures.— This specimen shows superficially convincing evidence of frontal/maxilla contact in the orbit. The sutures are generally sinuous (or convoluted) there. There are two anteroposteriorly running discontinuities along the medial orbital wall. The more dorsally positioned one is clearly a suture given its sinuous form (Fig. A-V-24: *132*). It appears to separate the frontal from a second bone, possibly (probably?) maxilla. The second discontinuity (Fig. A-V-24: *133*), ventral to the sinuous suture (*132*), may represent another suture, although it has apparently always been interpreted as a crack due to its very straight contour. It would be easy to continue to discount this feature as a crack except for the presence of a similarly positioned ridge of bone on the maxilla of the Pellouin skull (Fig. A-V-20A). If this straight 'crack-like' feature is actually a suture, then it would seem to represent the palatine-maxilla suture, whereas *132* would represent the maxilla-palatine suture. CT data for this specimen could help resolve the question.

Although not easily visible on this specimen, it is still possible to tell that the palatine foramen is not completely formed by the palatine (as mentioned for MNHN CR 125 and MNHN CR 965 above) and that the frontal contributes to it (Fig. A-V-24: *134*).

This is the only specimen to effectively illustrate the size, form, and number of lacrimal foramina: there is a single large lacrimal foramen (Fig. A-V-24: *135*) – an apparent second is formed by glue.

Morphology of cranial bones.— Measurements on the mediolateral breadth of the maxillae and medial-most point of frontal-lacrimal contact in this essentially undistorted specimen are similar to the same measurements in MNHN CR 125. This suggests that MNHN CR 125 is also basically undistorted in the transverse plane, even though it is crushed dorsoventrally. The posterolateral root of M^3 is exposed on the orbital surface of the maxilla, similar to the condition apparent in the Pellouin skull. The lacrimal foramen is located on the rostrum, just beyond the orbital rim. Furthermore, medial and dorsal to the lacrimal foramen the lacrimal bone bulges (Fig. A-V-24E, F). This bulge appears to represent the lacrimal tubercle.

***Plesiadapis tricuspidens* MNHN BR 17414–17419, 1371**

These specimens represent isolated petrosals from Berru identified by M. Godinot. In all cases one of us (DMB) assessed the morphology independently and confirmed the attribution to *P. tricuspidens*. The specimens have been measured from HRxCT scans generated at Pennsylvania State University at a resolution of 0.0500 mm for pixel dimensions, and 0.0581 mm for slice spacing. MNHN BR 17418 includes a stapes that has fallen into the cochlea. This element was digitally extracted and measured, which helps confirm that *P. tricuspidens* did not have a functional stapedial artery. The area of the obturator foramen of the stapes is small relative to its footplate length, which makes it like modern primates that lack stapedial arteries (Coleman and Boyer, 2008, 2012).

Tables A-I-3 and A-I-4 are codified descriptions of these specimens and other petrosal specimens studied here. The presence/absence and measurements of various features is documented therein. None of these specimens reveals an apparent suture at the boundary between the medial tympanic process and the promontorium, as in the case of the Pellouin skull.

Select quantitative differences between *P. tricuspidens* and other plesiadapids

As mentioned in the Introduction of Part 1, features thought to be distinctive for plesiadapids, as based on observations of *P. tricuspidens*, include a nasal bone that is narrow at its caudal extent, a premaxilla that has a broad contact with the frontal, and a tubular-shaped ectotympanic (e.g., Bloch et al., 2007). Table A-I-2 provides measurements of these and other features. Table 4 provides natural log ratio variables quantifying their shape (see Table A-I-1 for descriptions of variables). Although sample sizes are too small for statistical confidence of any sort, it is interesting to note that *P. tricuspidens* has substantially proportionally narrower nasals (Table 4: N/GM), wider premaxillae (Table 4: N/Pmx, Pmx/GM), and a more tubular external auditory meatus (Table 4: EAM-S) than any of the other plesiadapids. Thus other plesiadapids are not *as distinctive* in these features as is *P. tricuspidens*. Another interesting difference between *P. tricuspidens* and other plesiadapids is its proportionally larger glenoid fossae (Table 4: Gld/GM). Finally, it appears that the largest plesiadapids (mainly *P. tricuspidens*) have the proportionally shortest cochleae (Table 4: Cl/GM), smallest petrosals (Table 4: Pcsa/GM) and smallest fenestra vestibulae (Table 4: ac/GM).

New evidence bearing on the composition of the plesiadapid bulla

As mentioned in the introduction, the morphological prediction for a non-petrosal bulla is the presence of a suture separating the bulla from the pars cochlearis of the petrosal bone. However, whether and when this suture would have been obliterated by remodeling, and what the physical evidence

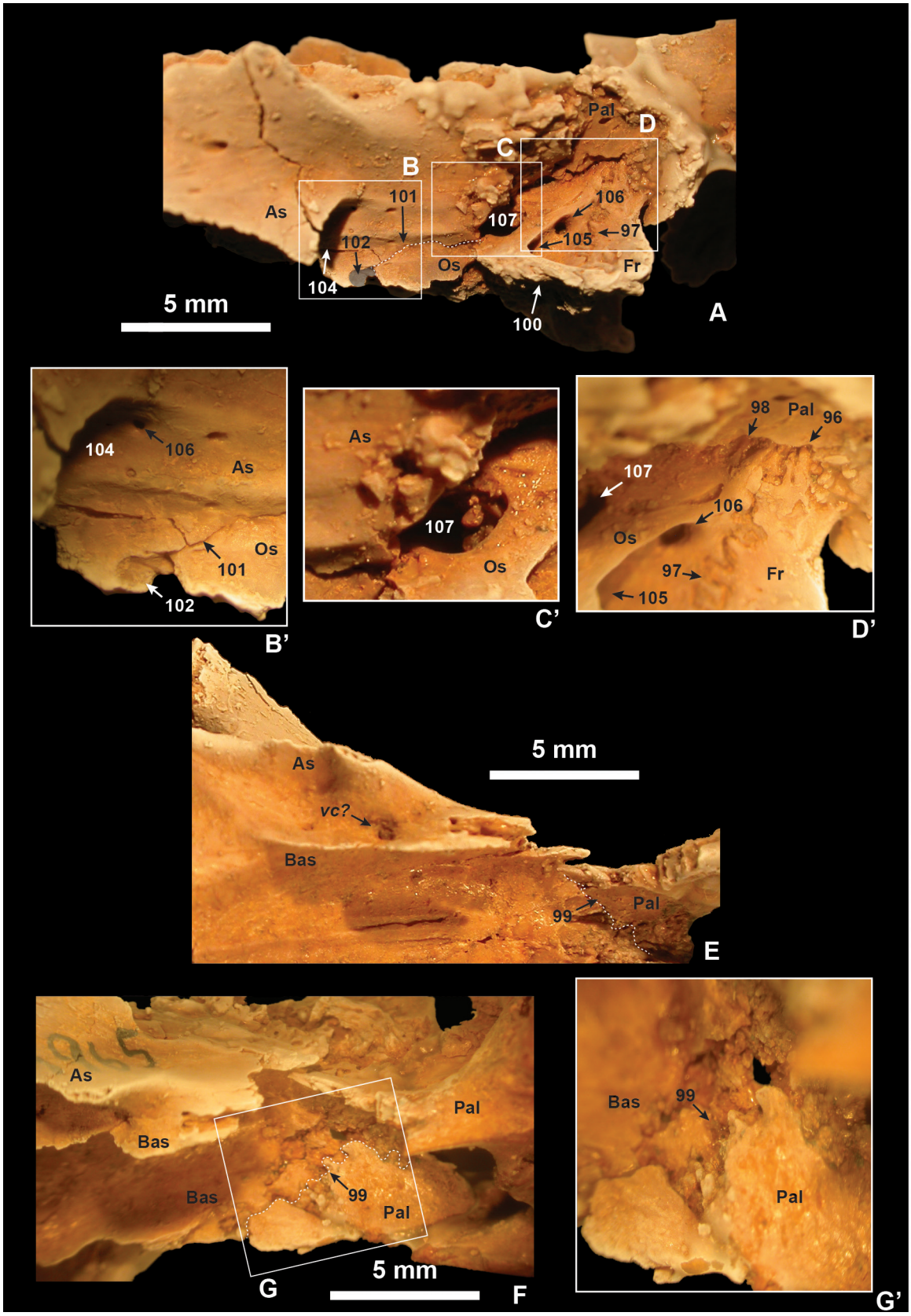
Pal
D
C
B
As
101
106
107
105
97
102
Os
Fr
104
5 mm
100
A
104
106
As
Os
101
102
B'
As
107
Os
C'
98
Pal
96
107
106
Os
97
Fr
105
D'
5 mm
As
vc?
Bas
99
Pal
E
As
Pal
Bas
Bas
99
Pal
G
5 mm
F
Bas
99
Pal
G'

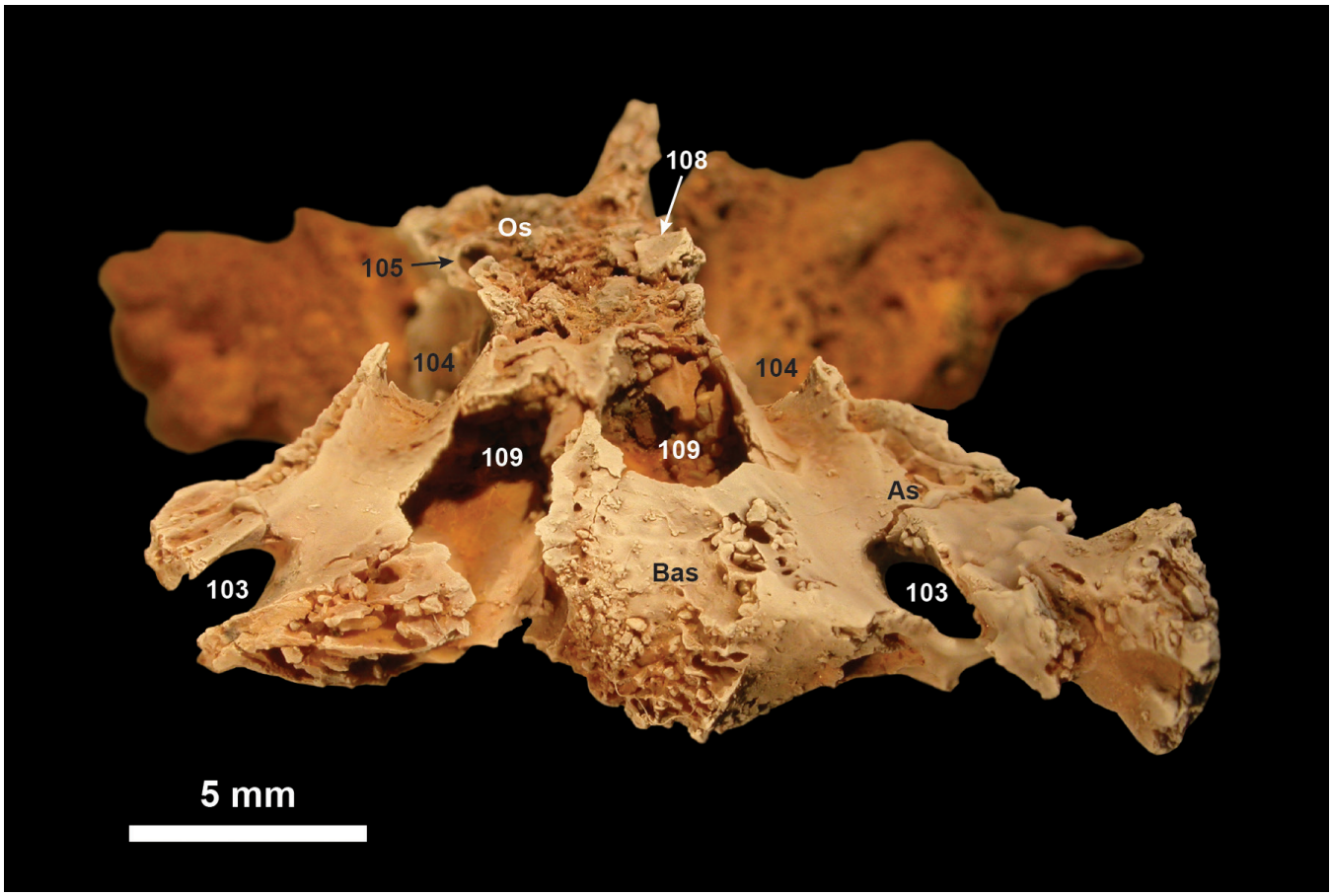

FIGURE A-V-18.— *Plesiadapis tricuspidens* (MNHN CR 965). Broken cranium in posterior view showing various foramina. Dorsal is at the top. Numbers (Table A-V-1) and abbreviations: *103*, foramen ovale; *104*, sphenorbital fissure; *105*, optic foramen; *108*, remnants of optic canals on broken orbitosphenoid; *109*, basisphenoid sinus space; *As*, alisphenoid; *Bas*, basisphenoid; *Os*, orbitosphenoid.

FIGURE A-V-17.— *Plesiadapis tricuspidens* (MNHN CR 965). **A**, left lateral view of orbitotemporal region of cranium (ventral up). **B**, inset of sphenorbital fissure and alisphenoid/orbitosphenoid suture. B', enlargement of inset B. **C**, inset of suboptic foramen. C', enlargement of inset C. **D**, inset of sphenoid/palatine and palatine/frontal sutures. D', enlargement of inset D. **E**, ventral view of right sphenoidal region. **F**, orbitotemporal region in right ventrolateral view. **G**, inset of sphenoid/palatine suture. G', enlargement of inset G. Sutures are shown as dashed white lines. Anterior is at the right in all images. Dorsal is down in images A–D.' Dorsal is up in images G and F. Numbers (Table A-V-1) and abbreviations: *96*, palatine/frontal suture in postpalatine canal; *97*, frontal/orbitosphenoid suture just anterior to optic foramen; *98*, orbitosphenoid/palatine contact running anteroposteriorly; *99*, palatine/alisphenoid suture; *100*, dorsal margin of orbitosphenoid; *101*, alisphenoid/orbitosphenoid suture; *102*, 'dished' surface on alisphenoid for broken out orbitosphenoid; *104*, sphenorbital fissure; *105*, optic foramen; *106*, various foramina representing blood sinus drainage; *107*, suboptic foramen; *As*, alisphenoid; *Bas*, basisphenoid; *Fr*, frontal; *Os*, orbitosphenoid; *Pal*, palatine; *vc*, vidian canal.

for its presence should look like have not been outlined. A preliminary survey of mammals with basicranial forms similar to those of plesiadapids and basal euprimates includes several rodents, treeshrews, and two paromomyids. These taxa have large inflated bullar cavities with bony septa buttressing the bulla. In *Sciurus carolinensis* and *Tupaia glis* the promontoria have modest medial and rostral tympanic processes. In *Sciurus*, the ectotympanic forms the bulla and septa, which contact the medial and rostral tympanic processes of the petrosal in an externally on-lapping, squamous suture. The overlap is extensive and can easily be visualized in HRxCT data (Fig. A-V-25). In *Tupaia*, the condition is similar except that the bulla-forming bone is the entotympanic, and the overlap is not so extensive, because the rostral and medial processes of its promonotorium are relatively smaller (MacPhee, 1981; Fig. A-V-26). In some rodents with this basic pattern (e.g., *Marmota*; Fig. 20), foramina for neurovasculature relating to the tympanic and internal carotid plexuses can be observed to enter the tympanic cavity at the sutural boundary between the ectotympanic and petrosal on the medial aspect of the

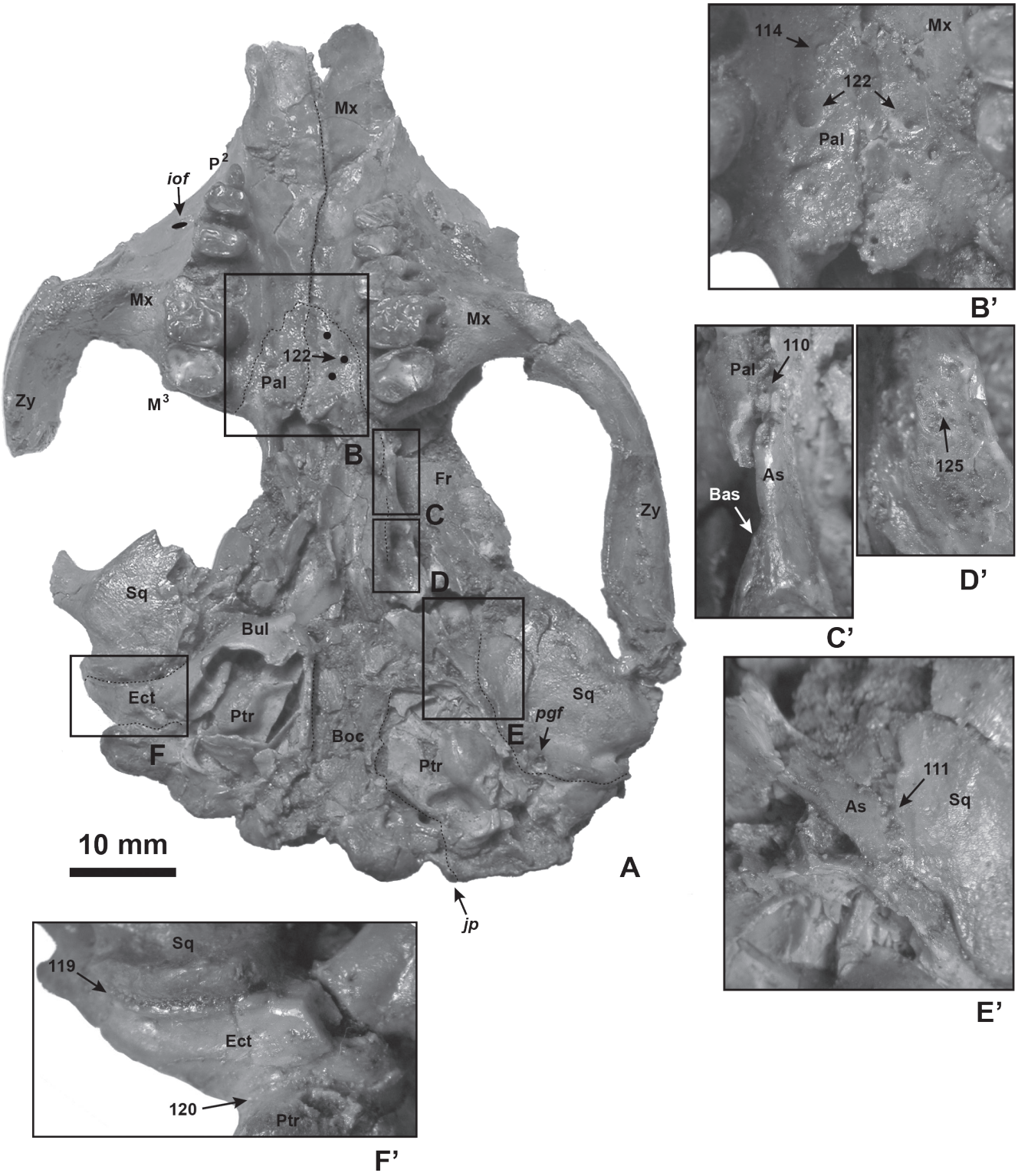
Mx
P2
iof
Mx
Mx
Zy
M3
122
Pal
B
Fr
C
D
Zy
Sq
Bul
Ect
Ptr
F
Boc
Ptr
E
pgf
Sq
10 mm
A
jp
Sq
119
Ect
120
Ptr
F'
114
Mx
122
Pal
B'
110
Pal
As
Bas
C'
125
D'
111
As
Sq
E'

promontorium. Other rodents, specifically *Lagostomus* (Figs. 21, 22) and *Dipodomys*, fuse the suture between the ectotympanic and petrosal (and thus superficially appear to have a petrosal bulla), but still preserve evidence of this suture via the canals for tympanic plexus nerves that reach the middle ear cavity through this sutural conduit (Fig. 22). Thus, if plesiadapids have a non-petrosal bulla, one might expect the suture to be expressed as overlapping laminae of bones on the tympanic processes, as in *Sciurus* and *Tupaia*, or by the planar organization of canals for neurovasculature along a previously unfused suture.

Almost all the plesiadapid specimens that preserve part of the medial tympanic process show it to be comprised of two layers of bone. In fact, *Pronothodectes gaoi* (UALVP 49105) looks nearly identical to a *Sciurus carolinensis* ear that has been prepared in a way so as to mimic the inferred breakage on the fossil (Fig. A-V-25). This fact, combined with the observation of what appears to be a suture on the medial aspect of the promontorium of the Pellouin skull (Fig. A-V-21), strongly suggest a suture in this vicinity. HRxCT scans of UALVP 49105 do not, however, strengthen the support for this interpretation because they do not reveal any separation between these bony layers, and furthermore, do not show any 'planes of canals' along a possibly previously unfused boundary (Boyer et al., 2012a).

A further test of the significance of the apparent similarity in the medial tympanic process morphology between plesiadapids and mammals known to have non-petrosal bullae is to examine the cross-sectional morphology of more ventral and lateral components of the bullar wall. If plesiadapids do in fact have a bullar construction similar to that of *Sciurus*, for instance, then these more ventral regions of the bullar wall should be thin and comprised of a single lamina of bone as they are in *Sciurus*. This test was not possible in the UALVP specimens. However, it is possible in the Pellouin skull of *P. tricuspidens*.

The cross-sectional morphology of the more ventral and lateral parts of the bullar wall in the Pellouin skull exhibit two distinct layers. This is contrary to the prediction of the hypothesis that the two layers of bone on the medial tympanic process represent two different bones (Fig. A-V-23). Furthermore, the broken open bulla in the otherwise intact skull of the euprimate *Adapis* looks extremely similar to the condition in *P. tricuspidens* in having two layers comprising the bulla (Fig. A-V-23). Finally, the morphology of a petrosal specimen of the euprimate *Indri indri* contradicts the most straightforward interpretation of the significance of multiple bony layers on the medial process of the promontorium. *Indri* also exhibits the double layer morphology at the lateral margin of the medial process extending from the promontorium (Fig. 23).

Thus, despite the presence of suture-like morphologies on the medial tympanic process of plesiadapid specimens described here, there is still no solid morphological evidence for an entotympanic or ectotympanic bulla. There are, however, some surprisingly detailed similarities in bullar wall construction among existing plesiadapid specimens and some euprimates. In this context it is worth considering the morphology of various paromomyid plesiadapiforms, in which evidence for a suture (squamous) between promontorium and bulla is generally accepted (Bloch and Silcox, 2001). This suture is unique in that the hypothesized entotympanic has an edge that inserts dorsal to the medial tympanic process of the petrosal, the opposite of the condition in treeshrews and rodents (as well as carnivorans, e.g., Klaauw, 1931; pholidotans, Gaudin and Wible, 1999; and macroscelideans, Novacek, 1977, and MacPhee, 1981; Fig. 24A–B').

Interestingly, there are several features of the paromomyid 'medial tympanic process' that would seem to indicate even the medial tympanic process is not petrosally-derived. Specifically, there are a series of distinct, ventrally raised ridges on the medial process, which continue laterally onto the promontorium and then stop abruptly along an anteroposteriorly running boundary (Fig. 24C–F: *bs*). This boundary appears to be a sutural edge because lateral to it, the ridges are nonexistent and the promontorium is smooth. Second, the dorsal surface of the promontorium seems to show the other side of this same suture (Fig. 24B: *bs?*). Finally, an HRxCT scan (8 µm resolution) of a juvenile individual of the paromomyid *Acidomomys hebeticus* (UM 108207) reveals that the bone forming the cochlea is distinct in its density and porosity from the bone forming the medial tympanic process as well as other contiguous regions (Fig. 25). The hazy boundary between bone forming the promontorium itself and its medial tympanic process seen on the HRxCT scan is expressed as a distinctly visible discontinuity on the medial aspect of the promontorium under a light microscope. However, the HRxCT image also shows that bones on either side of the apparent dorsal expression of this suture (*bs?*) are two separate processes of the same bone.

Presence and position of a posterior carotid foramen and canal

The evidence for an internal carotid plexus going through the middle ear has recently been considered limited (MacPhee

FIGURE A-V-19.— *Plesiadapis tricuspidens* (Pellouin skull). **A**, ventral view. **B**, inset of palate. B', labeled enlargement of inset B. **C**, inset of pterygoid process. C', enlargement of inset C (note the discontinuity between the ento- and ectopterygoid processes, likely indicating a pterygoid/alisphenoid suture). **D**, inset of scaphoid fossa of pterygoid process. D', enlargement of inset D. **E**, inset of alisphenoid/squamosal suture. E', labeled enlargement of inset E. **F**, inset of posterolateral basicranium. F', enlargement of inset F. Anterior is at the top in all images. Sutures are shown as dashed black lines. Numbers (Table A-V-1) and abbreviations: *110*, palatine/alisphenoid suture; *111*, squamosal/alisphenoid suture; *114*, palatine/maxilla suture on palate; *119*, squamosal/tympanic suture; *120*, tympanic/petrosal suture; *122*, palatal palatine foramina; *125*, foramen in scaphoid fossa; *As*, alisphenoid; *Bas*, basisphenoid; *Boc*, basioccipital; *Bul*, auditory bulla; *Ect*, ectotympanic; *Fr*, frontal; *iof*, infraorbital foramen; *jp*, jugular process of exoccipital; *Mx*, maxilla; *Pal*, palatine; *pgf*, postglenoid foramen; *Ptr*, petrosal; *Sq*, squamosal.

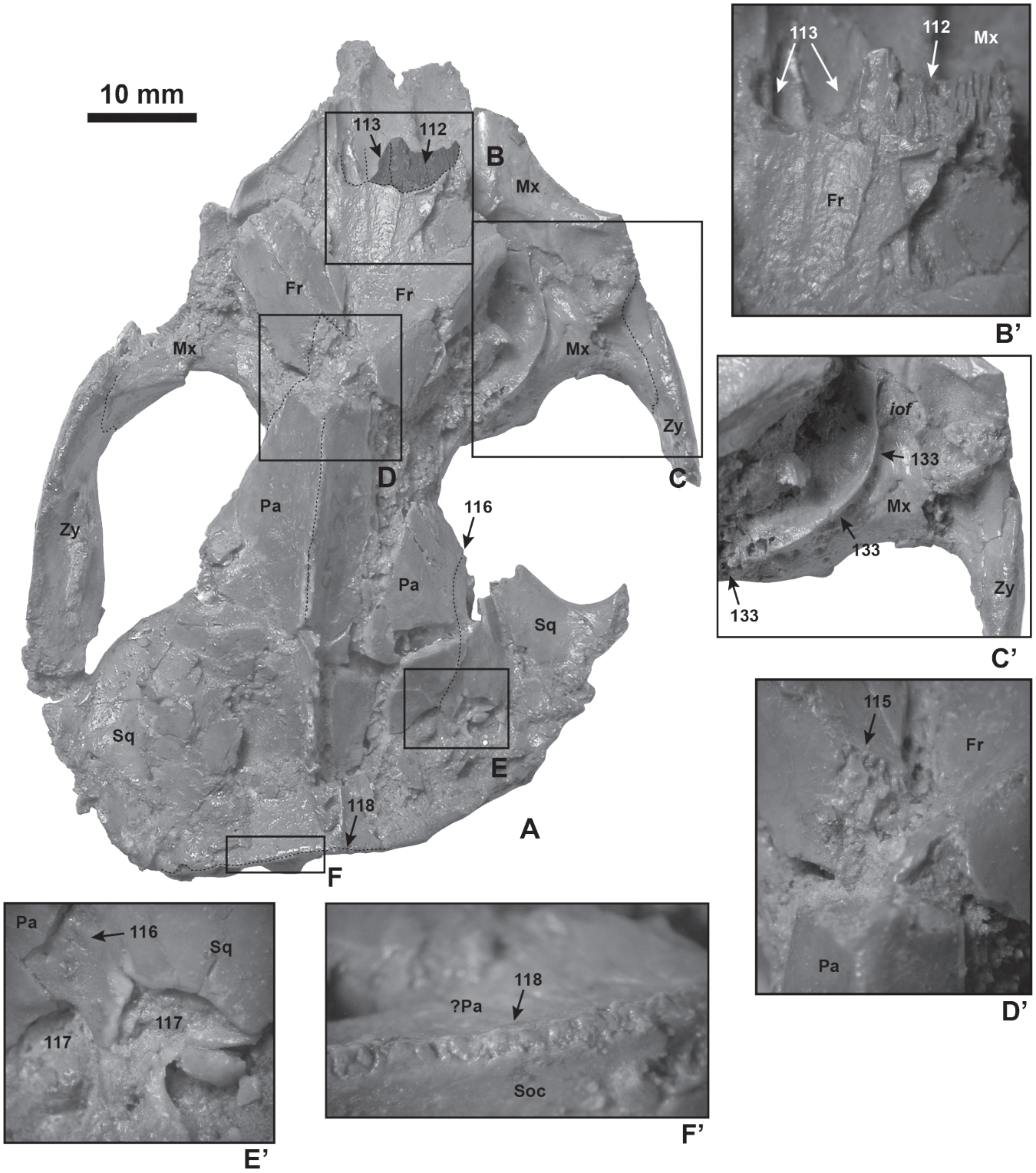

FIGURE A-V-20.— *Plesiadapis tricuspidens* (Pellouin skull). **A**, dorsal view. **B**, inset of rostrum. B', enlargement of inset B. **C**, inset of dorsal aspect of maxilla. C', enlargement of inset C. **D**, inset of orbitotemporal region. D', enlargement of inset D. **E**, inset of lateral neurocranium. E' enlargement of inset E. **F**, inset of nuchal crest. F' enlargement of inset F. Anterior is at the top in all images. Sutures shown as dashed black lines. Numbers (Table A-V-1) and abbreviations: *112*, premaxillary sutural surface of frontal. *113*, nasal sutural surface of frontal; *115*, frontal/parietal suture; *116*, parietal/squamosal suture; *117*, squamosal foramina; *118*, parietal/occipital suture ?; *133*, crack or maxilla/palatine suture?; *Fr*, frontal; *iof*, infraorbital foramen; *Mx*, maxilla; *Pa*, parietal; *Soc*, supraoccipital; *Sq*, squamosal.

et al., 1983; Bloch and Silcox, 2001, 2006). However, as shown in descriptions above, all but one of the specimens that are well enough preserved show a posterior carotid foramen and/or the remnants of its canal on the posterior septum. In all of these specimens the posterior carotid foramen and/or the remnants of its canal show it to have had a posterolateral entrance into the tympanic cavity. This differs from the interpretation of some recent authors (e.g., MacPhee et al., 1983; Silcox, 2001; Bloch and Silcox, 2006). On the other hand this finding agrees with Wible (1993), who considered both plesiadapids and paromomyids to exhibit a 'posterolateral' entrance. The morphology of *Nannodectes gidleyi* AMNH 17388 is clearly different from that of other plesiadapid taxa preserving this region, in that the internal carotid plexus route, although still adjacent to the stylomastoid foramen, was not intratympanic. It seems likely that this difference is the result of a more dorsal location of the internal carotid plexus route. Even if this is incorrect, the earlier occurring more basal *N. intermedius* (Gingerich, 1976) has morphology like that of other plesiadapiforms (Tables A-I-3 and A-I-4) indicating that the morphology of *N. gidleyi* is derived, whatever the correct interpretation may be.

Absence of the foramen rotundum in *Plesiadapis tricuspidens*

New observations of the specimens of interest show that Russell's (1964) 't.d.a.' is clearly formed within the orbitosphenoid on MNHN CR 125 (Fig. A-V-13B',A-V-13D': *91*). On MNHN CR 965 it appears to have been present only on the left side and, as in MNHN CR 125, contained within the orbitosphenoid. Fig. A-V-17C shows a ridge of the alisphenoid positioned where the posterior rim of the foramen should be, but this appears to be an artifact of breakage. Furthermore, in MNHN CR 965 it seems clear that this foramen simply did not connect to the endocranium through any sort of canal (Figs. A-V-16, A-V-18). What Russell (1964) identified as the foramen rotundum ('t.r.') appears to be formed at the boundary between the alisphenoid and orbitosphenoid, instead of within the alisphenoid. This interpretation is based on observation of an apparent suture that spans from this foramen (Fig. A-V-13B', A-V-13D': *90*) to a tiny foramen located ventral to the suboptic foramen (Fig. A-V-13B', A-V-13D': *93*) in MNHN CR 125. The reasons why foramen *93* is not a candidate for a superior orbital fissure (t.d.a.) are that (1) it is too small and (2) it is definitively absent from the other side of MNHN CR 125 and all other specimens. This suggests that it is not a major conduit for branches of cranial nerves III–VI, as it is in other taxa with a superior orbital fissure. In MNHN CR 965, the location of the alisphenoid/orbitosphenoid suture is located more dorsally such that, given the breakage, it is possible that the orbitosphenoid did not reach the sphenorbital fissure. These variations introduce some uncertainty to the interpretation. Even so, in light of the above observations, it seems that 'suboptic foramen' is a better-supported designation for Russell's 't.d.a.' and that Russell's 't.r.' should be considered the sphenorbital fissure. This conclusion is illustrated in Figure A-V-27.

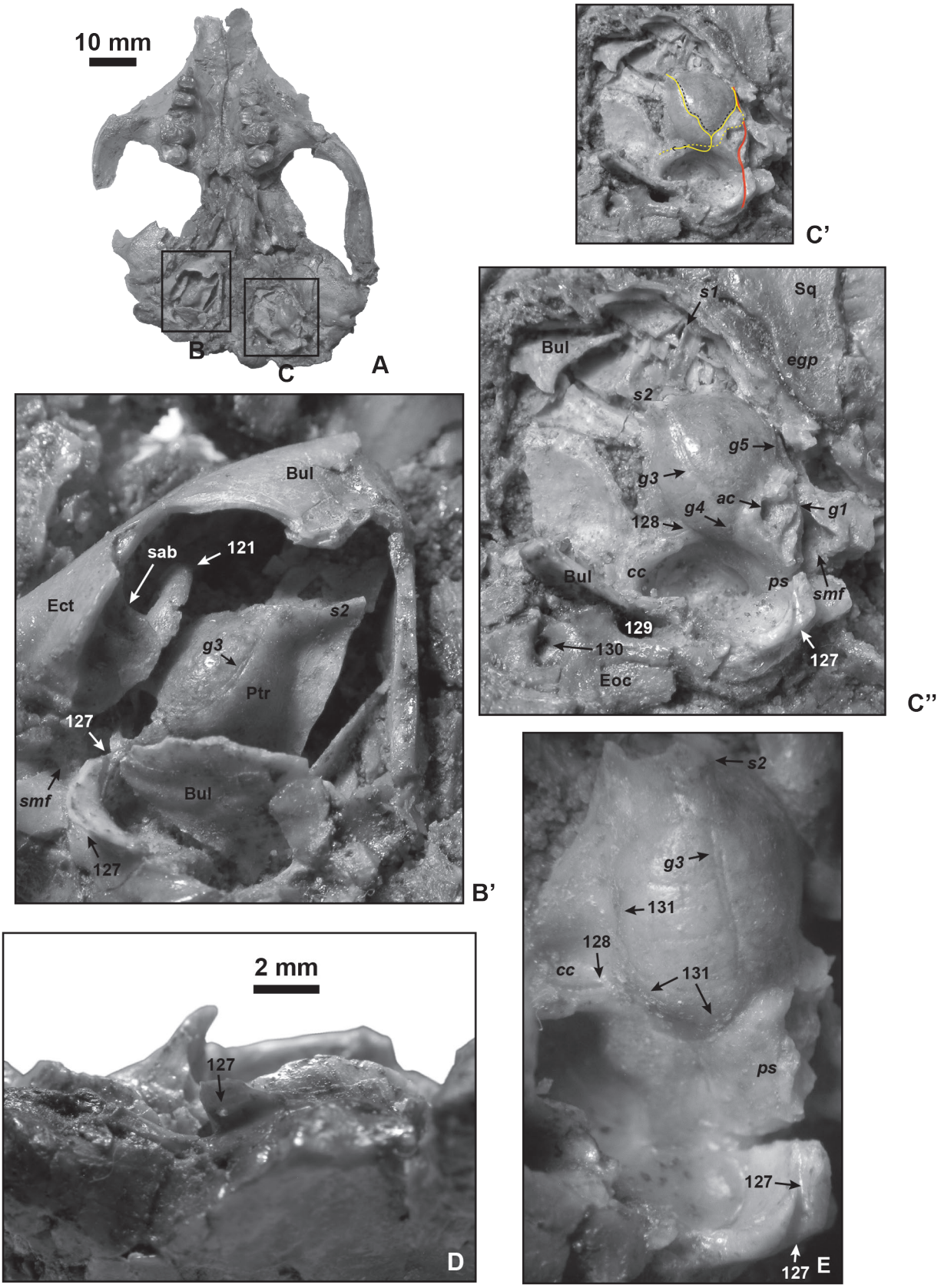

FIGURE A-V-21.— See figure description page 260.

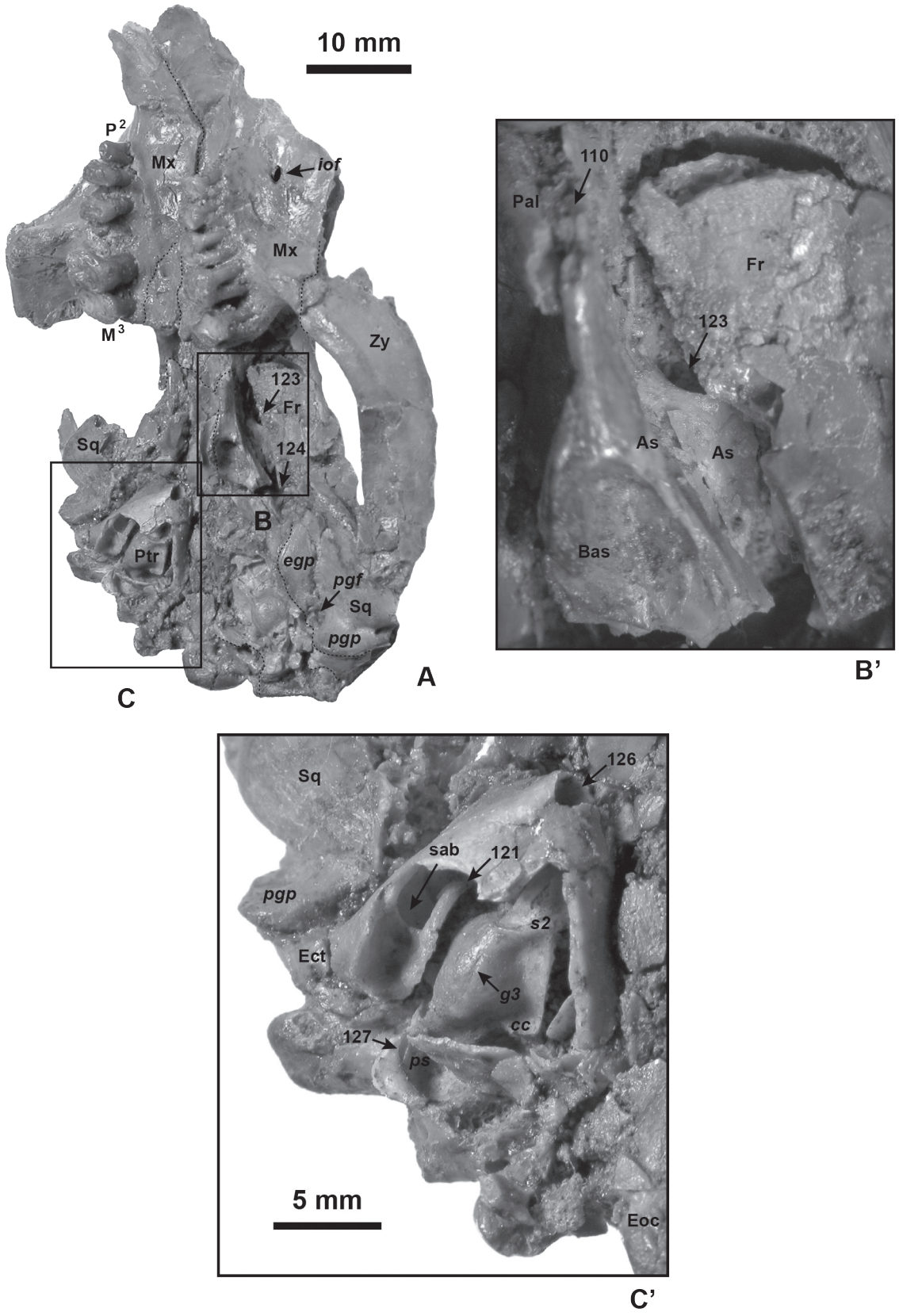

FIGURE A-V-22.— See figure description page 260.

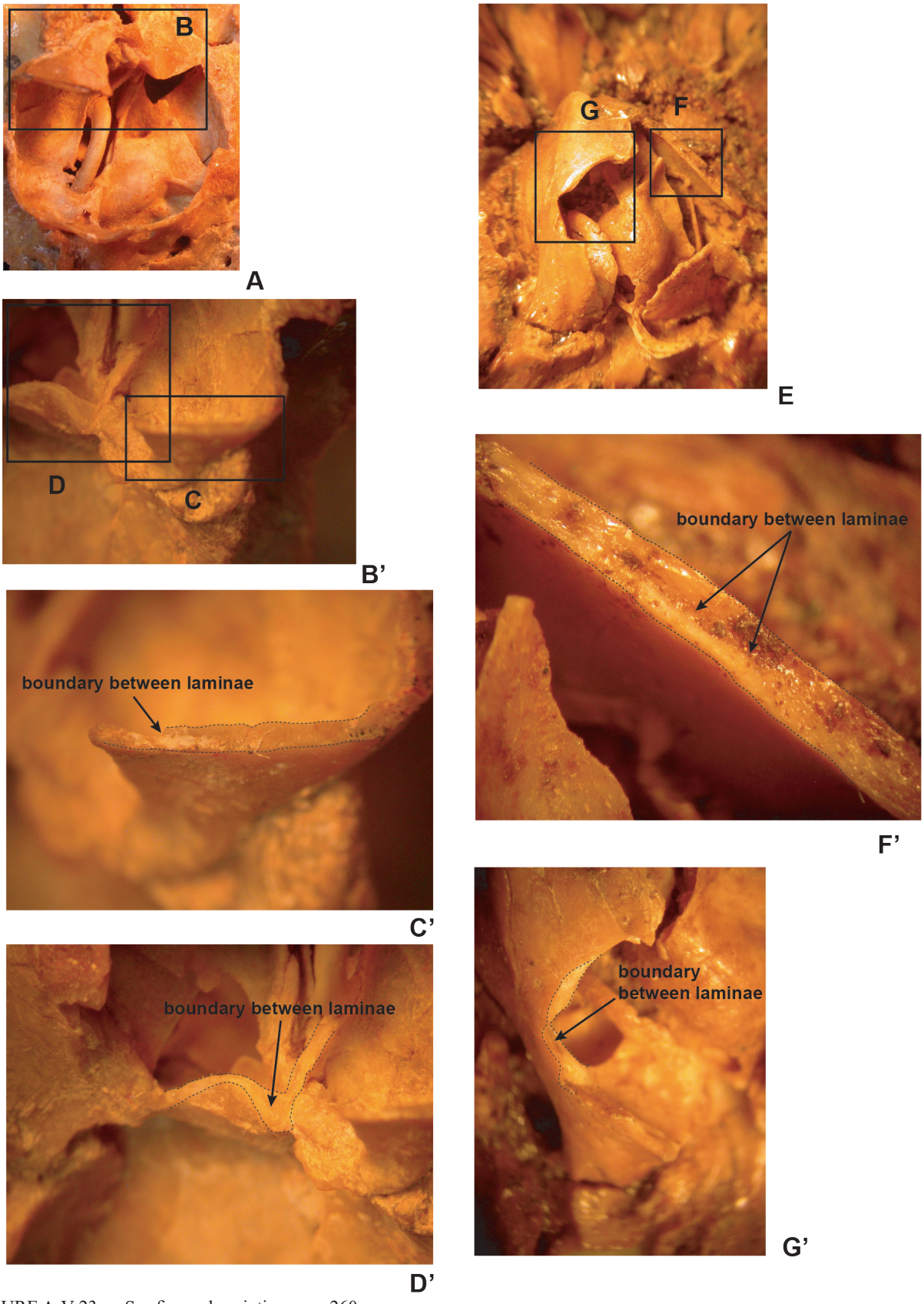

FIGURE A-V-23.— See figure description page 260.

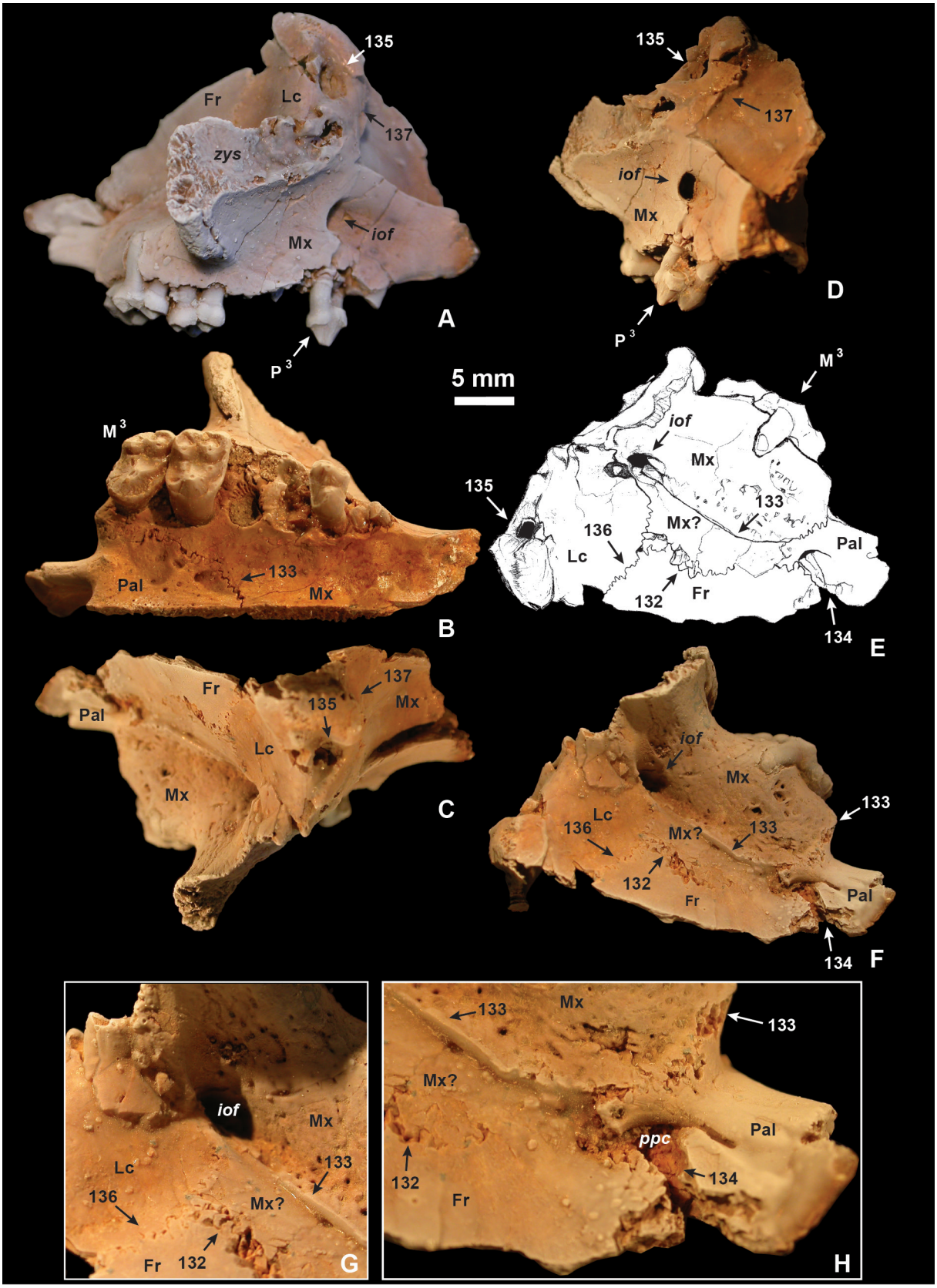

FIGURE A-V-24.— See figure description page 260.

FIGURE A-V-21.— *Plesiadapis tricuspidens* (Pellouin skull). **A**, ventral view. **B**, inset of right petrosal and bulla. B', labeled enlargement of inset B. **C**, inset of left petrosal and bullar fragments. C', enlargement of inset C with reconstructed vasculature. C'', labeled enlargement of inset C. **D**, posterior view of skull showing the right posterior carotid foramen (*127*). **E**, labeled ventromedial view of left petrosal, showing grooves (*g3*), foramina (*127–128*), and apparent suture (*131*). Anterior is at the top in images A–C and E. Ventral is at the top in image D. Nerves reconstructed in yellow represent components of the tympanic plexus. Neurovasculature reconstructed in red represents components of the internal carotid plexus. Fine dashed line, g3 groove. Numbers (Table A-V-1) and abbreviations: *121*, tympanic ring with annular bridge; *127*, posterior carotid foramen and carotid canal; *128*, foramen for tympanic and mastoid canaliculus; *129*, jugular foramen; *130*, hypoglossal foramen; *131*, possible suture along medial side of left promontorium; *ac*, aperture of cochlear fenestra; *Bul*, auditory bulla; *cc*, cochlear canaliculus; *ps*, posterior septum; *Ect*, ectotympanic; *egp*, entoglenoid process; *Eoc*, exoccipital; *g1*, groove for internal carotid plexus; *g3*, groove that leads to s2 (for a small vein?); *g4*, groove for tympanic plexus fibers to reach routes g1–3; *g5*, groove that leads toward epitympanic crest; *Ptr*, petrosal; *s1*, first (anterior) septum; *s2*, second septum; *sab*, strut connecting annular and bullar part of ectotympanic; *smf*, stylomstoid foramen; *Sq*, squamosal.

FIGURE A-V-22.— *Plesiadapis tricuspidens* (Pellouin skull). **A**, cranium in left ventrolateral view. **B**, inset of left orbitotemporal region. B', enlargement of inset B showing sphenorbital fissure (*123*). Optic foramen is not visibly preserved. **C**, inset of right petrosal and bullar fragments. C', enlargement of inset C, showing tubal canal (126) opening. Anterior is at the top in all images. Numbers (Table A-V-1) and abbreviations: *110*, palatine/alisphenoid suture; *121*, tympanic ring with annular bridge; *123*, sphenorbital fissure; *124*, foramen ovale fragment; *126*, tubal canal of right bulla; *127*, posterior carotid foramen and carotid canal; *As*, alisphenoid; *Bas*, basisphenoid; *Bul*, auditory bulla; *cc*, cochlear canaliculus; *Ect*, ectotympanic; *egp*, entoglenoid process; *Eoc*, exoccipital; *Fr*, frontal; *g3*, groove that leads to s2 (for a small vein?); *iof*, infraorbital foramen; *Mx*, maxilla; *Pal*, palatine; *pgf*, postglenoid foramen; *pgp*, postglenoid process; *ps*, posterior septum; *Ptr*, petrosal; *s1*, first (anterior) septum; *s2*, second septum; *sab*, strut connecting annular to bullar part of ectotympanic; *Sq*, squamosal.

FIGURE A-V-23.— *Adapis parisiensis* (MaPhQ 33y) (A–D) and *Plesiadapis tricuspidens* (Pellouin skull) (E–G). **A**, ventral view of right petrosal and bulla (anterior up). **B**, inset of broken edges of bulla. B', enlargement of inset B rotated 180 degrees (anterior down). **C**, inset of lateral part of broken edge of bulla. C', enlargement of inset C with lateral flange of bulla showing double laminae. **D**, inset of more medial part of broken edges of bulla. D', enlargement of inset D with anterior part of bulla showing double laminae. **E**, ventral view of right petrosal and bulla. F, inset of broken medial process. F', enlargement of inset F with medial flange of bulla showing double laminae. **G**, inset of broken lateral process. G', enlargement of inset G with lateral edge of bulla showing double laminae. Broken edges are highlighted with dashed lines. The two laminae comprising the bony wall of the bulla may be derived from two, or more likely, a single cranial bone. The bulla is probably petrosal-derived in both taxa shown here.

FIGURE A-V-24.— *Plesiadapis tricuspidens* (MNHN CR 126). Right cranial mid-face fragment in lateral (**A**), ventral (**B**), dorsal (**C**), anterior (**D**), and dorsolateral (**E**, **F**) views. E is a drawing, and **G** and **H** are enlargements of the anterior and posterior parts of image F. Note that the bone labeled 'Mx?' can only be considered as part of the maxilla if: (1) there is a suture spanning between *132* and *133* close to the *ppc*; (2) the labeled, more anterior part of *133* actually represents a crack. A suture spanning *132* and *133* is not clearly visible. The existence of a ridge of bone on the Pellouin skull that would correspond to the anterior part of the maxillary process of *133* suggests that *133* may *not* be a crack in this region. If neither (1) or (2) are true then Mx? must actually correspond to the palatine. If only (1) is true then Mx? may represent an ethmoid os planum. Numbers (Table A-V-1) and abbreviations: *132*, Frontal/maxilla suture in orbit; *133*, crack or maxilla/palatine suture?; *134*, region of palatine/frontal contact in postpalatine canal (broken); *135*, lacrimal foramen; *136*, lacrimal/frontal suture; *137*, lacrimal/maxilla suture; *Fr*, frontal; *iof*, infraorbital foramen; *Lc*, lacrimal; *Mx*, maxilla; *Mx?*, possible fragment of maxilla; *Pal*, palatine; *zys*, sutural surface on maxilla for zygomatic.

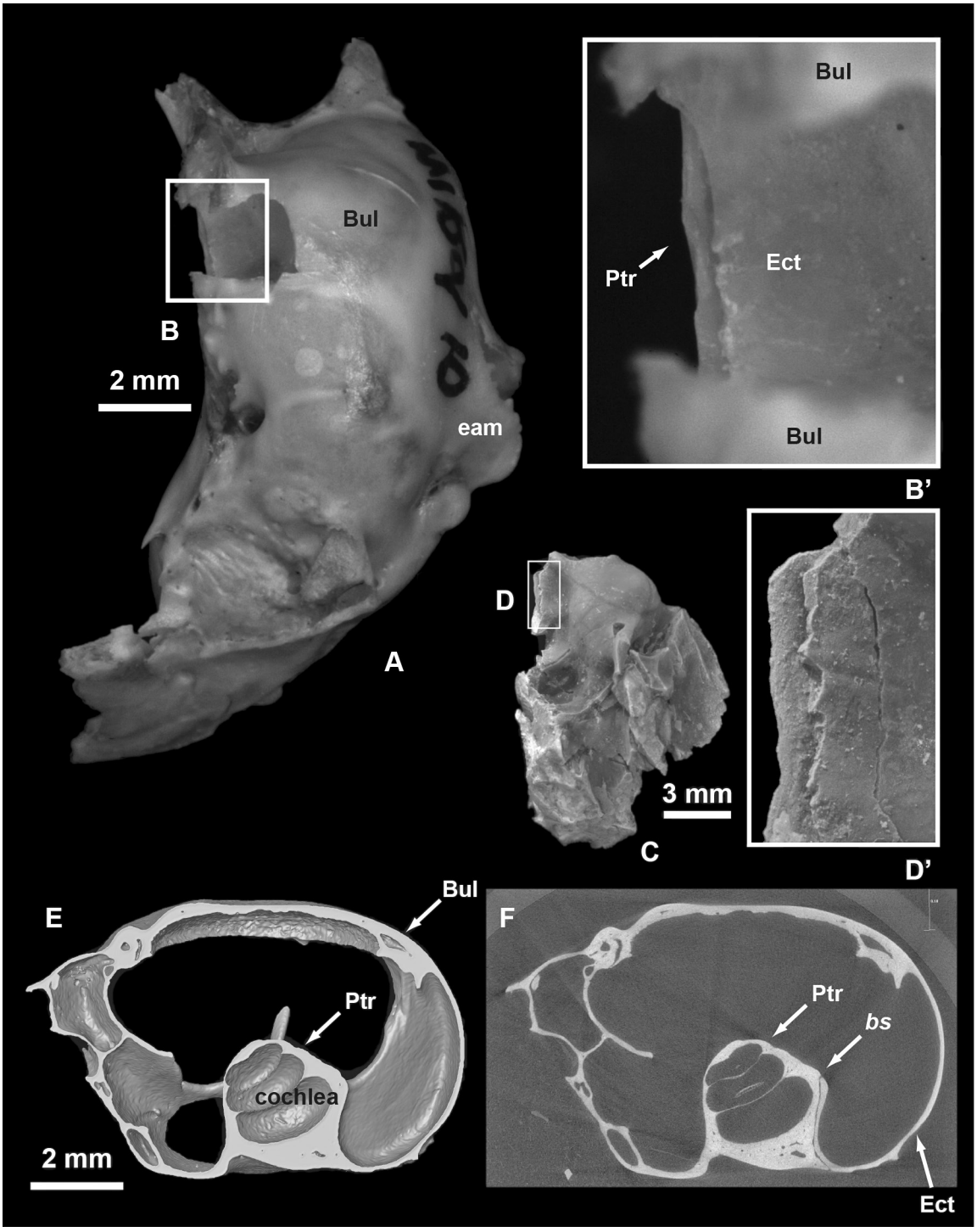

FIGURE A-V-25.— *Sciurus caroliniensis* (SBU MRd-12) (A–B, E–F), and *Pronothodectes gaoi* (UALVP 49105) (C–D). **A**, left petrosal and ectotympanic bulla in ventral view. **B**, inset of medial region of bulla. B', enlargement of inset B. **C**, left petrosal in ventral view. **D**, inset of medial tympanic process. D', enlargement of inset D. **E**, surface reconstruction of HRxCT data in anterior view. **F**, HRxCT slice in anterior view. Anterior is at the top in images A–D; lateral is to the left in images E and F. Note the appearance of a medial process of the petrosal projecting beyond the ventrally located, broken lamina of the ectotympanic in B', and also similarity of the broken medial process in D' to that in B'. The ectotympanic/petrosal bullar suture is clearly visible in F. Abbreviations: *bs*, bullar suture; *Bul*, auditory bulla; *eam*, external auditory meatus; *Ect*, ectotympanic; *Ptr*, petrosal.

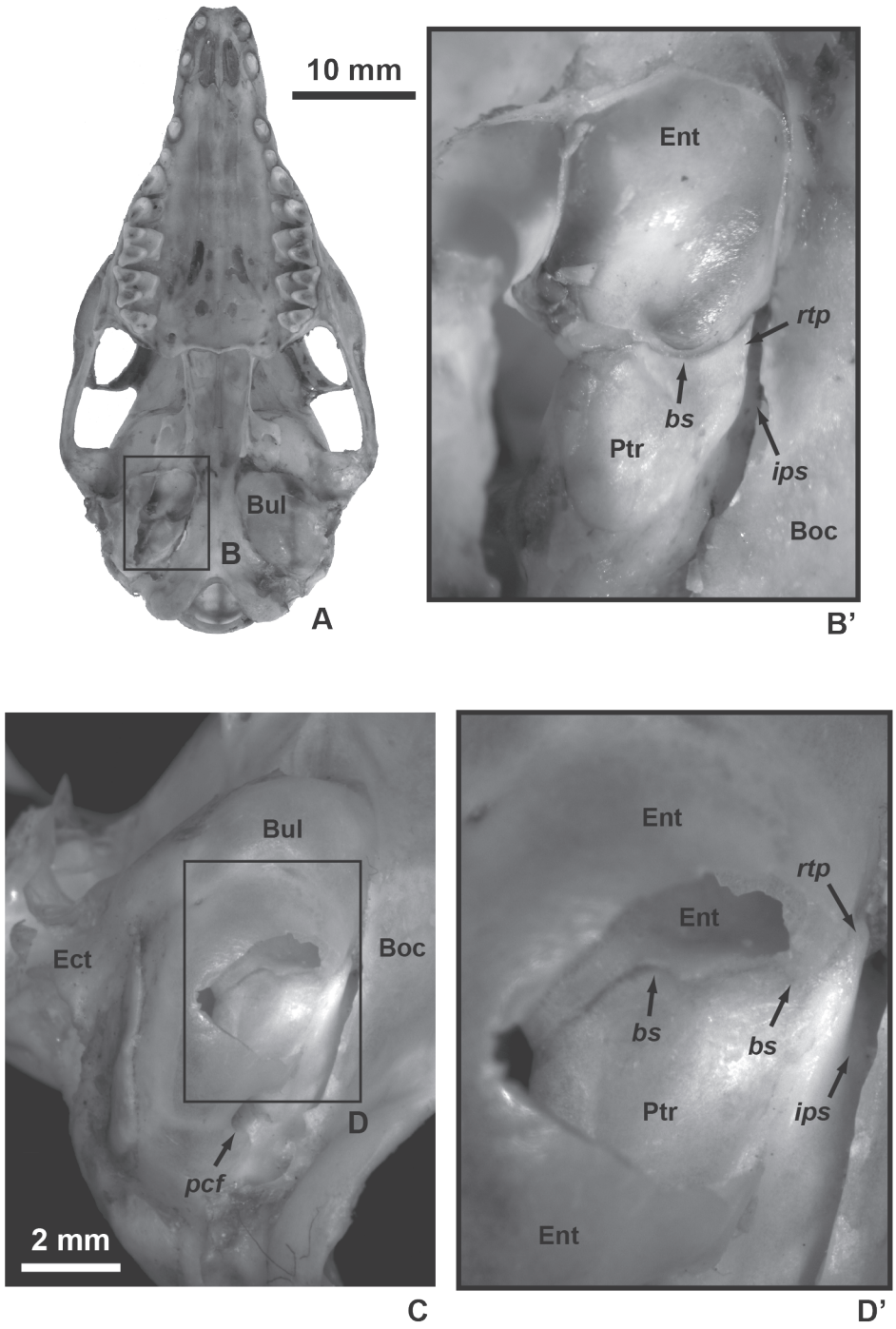

FIGURE A-V-26.— *Tupaia glis* (UMMZ 58983) (A, B), and *Tupaia glis* (SBU collection) (C, D). **A**, ventral view of skull. **B**, inset of right basicranium. B', enlargement of inset B. **C**, ventral view of right basicranium. **D**, inset of suture in right basicranium. D', enlargement of inset D. Anterior is at the top in all images. Note that the bony ear morphology of this taxon is generally similar to that in *Sciurus* (Fig. 2.35). The medial process of the petrosal is not well-developed, however a rostral process is present just anterior to where medial process would be. The rostral process buttresses the lamina of entotympanic bone that lies ventral to it. Abbreviations: *bs*, bullar suture; *Boc*, basioccipital; *Bul*, auditory bulla; *Ent*, entotympanic; *Ect*, ectotympanic; *ips*, inferior petrosal sinus; *pcf*, posterior carotid foramen; *rtp*, rostral process of petrosal.

APPENDIX VI — CT SCAN DOCUMENTATION

TABLE A-VI-1.— Cranial specimens scanned for this study. Facility abbreviations: *CQI-PSU*, Center for Quantitative Imaging, Pennsylvania State University; *HRxCT*, *UT*, High-Resolution X-ray CT Facility at the University of Texas at Austin, *SBU CBT*, Stony Brook University Center for Biotechnology, and *SMiF*, Shared Materials Instrumentation Facility, Duke. Resolution (*res*) and 'z-spacing' are in microns (µm). MorphoSource DOI links provided.

Taxon	Specimen	Figure	Description	Side	Facility	Scanner make/mod	x/y res	z res	MorphoSource DOI
Pronothodectes gaoi	UALVP 46685	—	cranium	na	PSU CQI	Varian BIR HD-600 OMNI-X	0.0439	0.0491	https://doi.org/10.17602/M2/M64276
Pronothodectes gaoi	UALVP 49105	—	petrosal bone	L	PSU CQI	Varian BIR HD-600 OMNI-X	0.04	0.0491	https://doi.org/10.17602/M2/M64984
Pronothodectes gaoi	UALVP 49105	—	petrosal bone	L	SBU CB	Scanco uCT40	0.006	0.006	https://doi.org/10.17602/M2/M65903
Pronothodectes gaoi	UALVP 46687	—	petrosal bone	R	PSU CQI	Varian BIR HD-600 OMNI-X	0.04	0.0491	https://doi.org/10.17602/M2/M65333
Nannodectes intermedius	USNM 309902	A-V-3,4,5	basicranium	na	SMiF	Nikon XTH 225 ST	0.02026	0.02026	https://doi.org/10.17602/M2/M44337
Nannodectes intermedius	USNM 309902	A-V-1	rostrum	na	SMiF	Nikon XTH 225 ST	0.02379	0.02379	https://doi.org/10.17602/M2/M44740
Nannodectes intermedius	USNM 309902	A-V-2	tympanic region	R	SMiF	Nikon XTH 225 ST	0.0106	0.0106	https://doi.org/10.17602/M2/M44742
Nannodectes intermedius	USNM 309902	—	P2	R	SMiF	Nikon XTH 225 ST	0.0106	0.0106	https://doi.org/10.17602/M2/M44744
Nannodectes intermedius	USNM 309902	—	C1	R	SMiF	Nikon XTH 225 ST	0.0106	0.0106	https://doi.org/10.17602/M2/M44746
Nannodectes intermedius	USNM 309902	A-V-7	dentary	L	SMiF	Nikon XTH 225 ST	0.01604	0.01604	https://doi.org/10.17602/M2/M44766
Nannodectes intermedius	USNM 309902	—	I1	R	SMiF	Nikon XTH 225 ST	0.01604	0.01604	https://doi.org/10.17602/M2/M44768
Nannodectes intermedius	USNM 309902	—	maxilla	R	SMiF	Nikon XTH 225 ST	0.01604	0.01604	https://doi.org/10.17602/M2/M44770
Plesiadapis tricuspidens	MNHN BR 1371	—	petrosal bone	R	PSU CQI	Varian BIR HD-600 OMNI-X	0.05	0.05811	https://doi.org/10.17602/M2/M64292
Plesiadapis tricuspidens	MNHN BR 17414	—	petrosal bone	L	PSU CQI	Varian BIR HD-600 OMNI-X	0.05	0.05811	https://doi.org/10.17602/M2/M64298
Plesiadapis tricuspidens	MNHN BR 17415	—	petrosal bone	L	PSU CQI	Varian BIR HD-600 OMNI-X	0.05	0.05811	https://doi.org/10.17602/M2/M64306
Plesiadapis tricuspidens	MNHN BR 17416	—	petrosal bone	L	PSU CQI	Varian BIR HD-600 OMNI-X	0.05	0.05811	https://doi.org/10.17602/M2/M64309
Plesiadapis tricuspidens	MNHN BR 17417	—	petrosal bone	L	PSU CQI	Varian BIR HD-600 OMNI-X	0.05	0.05811	https://doi.org/10.17602/M2/M64312
Plesiadapis tricuspidens	MNHN BR 17418	—	petrosal bone	L	PSU CQI	Varian BIR HD-600 OMNI-X	0.05	0.05811	https://doi.org/10.17602/M2/M64314
Plesiadapis tricuspidens	MNHN BR 17419	—	petrosal bone	R	PSU CQI	Varian BIR HD-600 OMNI-X	0.05	0.05811	https://doi.org/10.17602/M2/M64316
Plesiadapis cookei	UM 87990	6	cranium	na	SMiF	Nikon XTH 225 ST	0.0397	0.0397	https://doi.org/10.17602/M2/M30540
Plesiadapis cookei	UM 87990	18	dentary	R	SMiF	Nikon XTH 225 ST	0.04455	0.04455	https://doi.org/10.17602/M2/M56414
Plesiadapis cookei	UM 87990	—	dentary	L	SMiF	Nikon XTH 225 ST	0.04455	0.04455	https://doi.org/10.17602/M2/M56415
Ignacius graybullianus	USNM 482353	26	petrosal bone	R	SBU CB	Scanco uCT40	0.006	0.006	https://doi.org/10.17602/M2/M65906
Ignacius graybullianus	USNM 482353	—	stapes	R	SBU CB	Scanco uCT40	0.006	0.006	https://doi.org/10.17602/M2/M65909
Acidomomys hebeticus	UM 108207	27	petrosal bone	L	SBU CB	Scanco uCT40	0.006	0.006	https://doi.org/10.17602/M2/M65904
Sciurus caroliniensis	SBU MRd-12	A-V-25	petrosal bone	L	SBU CB	Scanco uCT40	0.008	0.008	https://doi.org/10.17602/M2/M65910
Lagostomus maximus	AMNH-M-41527	23,24	petrosal bone	L	SBU CB	Scanco uCT40	0.01	0.01	https://doi.org/10.17602/M2/M65912
Peromyscus leucopus	AMNH-M-30836	—	petrosal bone	L	SBU CB	Scanco uCT40	0.006	0.006	https://doi.org/10.17602/M2/M65914

TABLE A-VI-2.— HRxCT bones of UM 87990 (*Plesiadapis cookei*) with DOI links on MorphoSource.org. The "Fig." column gives the main text figure number in which a photograph of the bone can be found. Each bone has two DOIs: one is associated with the 'raw' CT image stack; the other links to a polygonal mesh file derived from the image stack. All image stacks have cubic voxels. Thus, x, y, and z dimensions are equal. Units for the voxel value (x/y/z res) is millimeters. Double dashes (--) in the Figure column mean the bone was not figured. Abbreviations: *SMiF* – Shared Materials Instrumentation Facility, Duke University; *SBU-CB* – Stony Brook University Center for Biotechnology.

Fig.	Description/element	Side	Facility	Scanner make/mod	x/y/z res	DOI
6	cranium	midline	SMiF	Nikon XTH 225 ST	0.03970	https://doi.org/10.17602/M2/M30540 stack https://doi.org/10.17602/M2/M30542 mesh
18	dentary	Right	SMiF	Nikon XTH 225 ST	0.04455	https://doi.org/10.17602/M2/M56414 stack https://doi.org/10.17602/M2/M56413 mesh
--	dentary	left	SMiF	Nikon XTH 225 ST	0.04455	https://doi.org/10.17602/M2/M56415 stack https://doi.org/10.17602/M2/M56416 mesh
29A	atlas	midline	SMiF	Nikon XTH 225 ST	0.03619	https://doi.org/10.17602/M2/M41394 stack https://doi.org/10.17602/M2/M41395 mesh
29B	axis	midline	SMiF	Nikon XTH 225 ST	0.03619	https://doi.org/10.17602/M2/M41396 stack https://doi.org/10.17602/M2/M41397 mesh
29C	cervical vertebra	midline	SMiF	Nikon XTH 225 ST	0.03619	https://doi.org/10.17602/M2/M41398 stack https://doi.org/10.17602/M2/M41399 mesh
29D	cervical vertebra	midline	SMiF	Nikon XTH 225 ST	0.03619	https://doi.org/10.17602/M2/M41400 stack https://doi.org/10.17602/M2/M41401 mesh
29E	cervical vertebra	midline	SMiF	Nikon XTH 225 ST	0.03619	https://doi.org/10.17602/M2/M41402 stack https://doi.org/10.17602/M2/M41403 mesh
30A	thoracic vertebra	midline	SMiF	Nikon XTH 225 ST	0.03619	https://doi.org/10.17602/M2/M41404 stack https://doi.org/10.17602/M2/M41405 mesh
30B	thoracic vertebra	midline	SMiF	Nikon XTH 225 ST	0.03470	https://doi.org/10.17602/M2/M43261 stack https://doi.org/10.17602/M2/M43262 mesh
30C	thoracic vertebra	midline	SMiF	Nikon XTH 225 ST	0.03470	https://doi.org/10.17602/M2/M43263 stack https://doi.org/10.17602/M2/M43264 mesh
30D	thoracic vertebra	midline	SMiF	Nikon XTH 225 ST	0.03619	https://doi.org/10.17602/M2/M41406 stack https://doi.org/10.17602/M2/M41407 mesh
30E	thoracic vertebra	midline	SMiF	Nikon XTH 225 ST	0.03619	https://doi.org/10.17602/M2/M41408 stack https://doi.org/10.17602/M2/M41409 mesh
30F	thoracic vertebra	midline	SMiF	Nikon XTH 225 ST	0.03470	https://doi.org/10.17602/M2/M43265 stack https://doi.org/10.17602/M2/M43266 mesh
30G	thoracic vertebra	midline	SMiF	Nikon XTH 225 ST	0.03470	https://doi.org/10.17602/M2/M43267 stack https://doi.org/10.17602/M2/M43268 mesh
30H	thoracic vertebra	midline	SMiF	Nikon XTH 225 ST	0.03470	https://doi.org/10.17602/M2/M43269 stack https://doi.org/10.17602/M2/M43270 mesh
30I	thoracic vertebra	midline	SMiF	Nikon XTH 225 ST	0.03470	https://doi.org/10.17602/M2/M43271 stack https://doi.org/10.17602/M2/M43272 mesh
30J	thoracic vertebra	midline	SMiF	Nikon XTH 225 ST	0.03642	https://doi.org/10.17602/M2/M44792 stack https://doi.org/10.17602/M2/M44793 mesh
30K	thoracic vertebra	midline	SMiF	Nikon XTH 225 ST	0.03470	https://doi.org/10.17602/M2/M43273 stack https://doi.org/10.17602/M2/M43274 mesh
31A	lumbar vertebra	midline	SMiF	Nikon XTH 225 ST	0.03470	https://doi.org/10.17602/M2/M43275 stack https://doi.org/10.17602/M2/M43276 mesh
31B	lumbar vertebra	midline	SMiF	Nikon XTH 225 ST	0.03642	https://doi.org/10.17602/M2/M44786 stack https://doi.org/10.17602/M2/M44787 mesh
31C	lumbar vertebra	midline	SMiF	Nikon XTH 225 ST	0.03642	https://doi.org/10.17602/M2/M44788 stack https://doi.org/10.17602/M2/M44789 mesh
31D	lumbar vertebra	midline	SMiF	Nikon XTH 225 ST	0.03642	https://doi.org/10.17602/M2/M44847 stack https://doi.org/10.17602/M2/M44848 mesh

TABLE A-VI-2.— Cont'd.

Fig.	Description/element	Side	Facility	Scanner make/mod	x/y/z res	DOI
31E	lumbar vertebra	midline	SMiF	Nikon XTH 225 ST	0.03642	https://doi.org/10.17602/M2/M44790 stack https://doi.org/10.17602/M2/M44791 mesh
31F	lumbar vertebra	midline	SMiF	Nikon XTH 225 ST	0.03642	https://doi.org/10.17602/M2/M44849 stack https://doi.org/10.17602/M2/M44850 mesh
32	sacrum	midline	SMiF	Nikon XTH 225 ST	0.04466	https://doi.org/10.17602/M2/M38121 stack https://doi.org/10.17602/M2/M38122 mesh
33A	caudal vertebra	midline	SMiF	Nikon XTH 225 ST	0.03470	https://doi.org/10.17602/M2/M54487 stack https://doi.org/10.17602/M2/M54488 mesh
33B	caudal vertebra	midline	SMiF	Nikon XTH 225 ST	0.03642	https://doi.org/10.17602/M2/M55138 stack https://doi.org/10.17602/M2/M55139 mesh
33C	caudal vertebra	midline	SMiF	Nikon XTH 225 ST	0.03642	https://doi.org/10.17602/M2/M55140 stack https://doi.org/10.17602/M2/M55141 mesh
33D	caudal vertebra	midline	SMiF	Nikon XTH 225 ST	0.03642	https://doi.org/10.17602/M2/M55142 stack https://doi.org/10.17602/M2/M55143 mesh
33E	caudal vertebra	midline	SMiF	Nikon XTH 225 ST	0.03642	https://doi.org/10.17602/M2/M55144 stack https://doi.org/10.17602/M2/M55145 mesh
33F	caudal vertebra	midline	SMiF	Nikon XTH 225 ST	0.03642	https://doi.org/10.17602/M2/M55146 stack https://doi.org/10.17602/M2/M55147 mesh
33G	caudal vertebra	midline	SMiF	Nikon XTH 225 ST	0.03642	https://doi.org/10.17602/M2/M55148 stack https://doi.org/10.17602/M2/M55149 mesh
33H	caudal vertebra	midline	SMiF	Nikon XTH 225 ST	0.03642	https://doi.org/10.17602/M2/M55150 stack https://doi.org/10.17602/M2/M55151 mesh
33I	caudal vertebra	midline	SMiF	Nikon XTH 225 ST	0.03642	https://doi.org/10.17602/M2/M55152 stack https://doi.org/10.17602/M2/M55153 mesh
33J	caudal vertebra	midline	SMiF	Nikon XTH 225 ST	0.03642	https://doi.org/10.17602/M2/M55154 stack https://doi.org/10.17602/M2/M55155 mesh
33L	caudal vertebra	midline	SMiF	Nikon XTH 225 ST	0.04044	https://doi.org/10.17602/M2/M44853 stack https://doi.org/10.17602/M2/M44854 mesh
33M	caudal vertebra	midline	SMiF	Nikon XTH 225 ST	0.04044	https://doi.org/10.17602/M2/M44855 stack https://doi.org/10.17602/M2/M44856 mesh
33N	caudal vertebra	midline	SMiF	Nikon XTH 225 ST	0.04044	https://doi.org/10.17602/M2/M44857 stack https://doi.org/10.17602/M2/M44858 mesh
33O	caudal vertebra	midline	SMiF	Nikon XTH 225 ST	0.04044	https://doi.org/10.17602/M2/M44859 stack https://doi.org/10.17602/M2/M44860 mesh
33P	caudal vertebra	midline	SMiF	Nikon XTH 225 ST	0.04044	https://doi.org/10.17602/M2/M44861 stack https://doi.org/10.17602/M2/M44862 mesh
33Q	caudal vertebra	midline	SMiF	Nikon XTH 225 ST	0.04044	https://doi.org/10.17602/M2/M44863 stack https://doi.org/10.17602/M2/M44864 mesh
34A	manubrium	midline	SMiF	Nikon XTH 225 ST	0.03642	https://doi.org/10.17602/M2/M44851 stack https://doi.org/10.17602/M2/M44852 mesh
34B	sternebra	midline	SMiF	Nikon XTH 225 ST	0.04044	https://doi.org/10.17602/M2/M44867 stack https://doi.org/10.17602/M2/M44868 mesh
34C	sternebra	midline	SMiF	Nikon XTH 225 ST	0.04044	https://doi.org/10.17602/M2/M44869 stack https://doi.org/10.17602/M2/M44870 mesh
34D	sternebra	midline	SMiF	Nikon XTH 225 ST	0.04044	https://doi.org/10.17602/M2/M44871 stack https://doi.org/10.17602/M2/M44872 mesh
34E	sternebra	midline	SMiF	Nikon XTH 225 ST	0.04044	https://doi.org/10.17602/M2/M44873 stack https://doi.org/10.17602/M2/M44874 mesh
34F	sternebra	midline	SMiF	Nikon XTH 225 ST	0.04044	https://doi.org/10.17602/M2/M44875 stack https://doi.org/10.17602/M2/M44876 mesh
34G	xiphoid	midline	SMiF	Nikon XTH 225 ST	0.04044	https://doi.org/10.17602/M2/M44877 stack https://doi.org/10.17602/M2/M44878 mesh

TABLE A-VI-2.— Cont'd.

Fig.	Description/element	Side	Facility	Scanner make/mod	x/y/z res	DOI
35A	rib	Unknown	SMiF	Nikon XTH 225 ST	0.04044	https://doi.org/10.17602/M2/M44865 stack https://doi.org/10.17602/M2/M44866 mesh
--	rib	Unknown	SMiF	Nikon XTH 225 ST	0.04044	https://doi.org/10.17602/M2/M44879 stack https://doi.org/10.17602/M2/M44880 mesh
--	rib	Unknown	SMiF	Nikon XTH 225 ST	0.04044	https://doi.org/10.17602/M2/M44881 stack https://doi.org/10.17602/M2/M44882 mesh
--	rib	Unknown	SMiF	Nikon XTH 225 ST	0.04044	https://doi.org/10.17602/M2/M44883 stack https://doi.org/10.17602/M2/M44884 mesh
--	rib	Unknown	SMiF	Nikon XTH 225 ST	0.03782	https://doi.org/10.17602/M2/M54667 stack https://doi.org/10.17602/M2/M54668 mesh
--	rib	Unknown	SMiF	Nikon XTH 225 ST	0.03782	https://doi.org/10.17602/M2/M54669 stack https://doi.org/10.17602/M2/M54670 mesh
--	rib	Unknown	SMiF	Nikon XTH 225 ST	0.03782	https://doi.org/10.17602/M2/M54671 stack https://doi.org/10.17602/M2/M54672 mesh
--	rib	Unknown	SMiF	Nikon XTH 225 ST	0.03782	https://doi.org/10.17602/M2/M54673 stack https://doi.org/10.17602/M2/M54674 mesh
--	rib	Unknown	SMiF	Nikon XTH 225 ST	0.03782	https://doi.org/10.17602/M2/M54675 stack https://doi.org/10.17602/M2/M54676 mesh
--	rib	Unknown	SMiF	Nikon XTH 225 ST	0.03782	https://doi.org/10.17602/M2/M54677 stack https://doi.org/10.17602/M2/M54678 mesh
--	rib	Unknown	SMiF	Nikon XTH 225 ST	0.03782	https://doi.org/10.17602/M2/M54679 stack https://doi.org/10.17602/M2/M54680 mesh
--	rib	Unknown	SMiF	Nikon XTH 225 ST	0.03782	https://doi.org/10.17602/M2/M54681 stack https://doi.org/10.17602/M2/M54682 mesh
--	rib	Left	SMiF	Nikon XTH 225 ST	0.03782	https://doi.org/10.17602/M2/M54683 stack https://doi.org/10.17602/M2/M54684 mesh
36A	clavicle	Left	SMiF	Nikon XTH 225 ST	0.03470	https://doi.org/10.17602/M2/M54489 stack https://doi.org/10.17602/M2/M54490 mesh
--	clavicle	Right	SMiF	Nikon XTH 225 ST	0.03470	https://doi.org/10.17602/M2/M54491 stack https://doi.org/10.17602/M2/M54492 mesh
36B	scapula	Left	SMiF	Nikon XTH 225 ST	0.03470	https://doi.org/10.17602/M2/M54497 stack https://doi.org/10.17602/M2/M54498 mesh
37	humerus	Left	SMiF	Nikon XTH 225 ST	0.05375	https://doi.org/10.17602/M2/M37089 stack https://doi.org/10.17602/M2/M37090 mesh
37	humerus	Right	SMiF	Nikon XTH 225 ST	0.05375	https://doi.org/10.17602/M2/M37278 stack https://doi.org/10.17602/M2/M37279 mesh
38A	radius	Right	SMiF	Nikon XTH 225 ST	0.05105	https://doi.org/10.17602/M2/M54240 stack https://doi.org/10.17602/M2/M54241 mesh
--	radius	Left	SMiF	Nikon XTH 225 ST	0.03470	https://doi.org/10.17602/M2/M54495 stack https://doi.org/10.17602/M2/M54496 mesh
38B	ulna	Right	SMiF	Nikon XTH 225 ST	0.05105	https://doi.org/10.17602/M2/M54246 stack https://doi.org/10.17602/M2/M54247 mesh
--	ulna (proximal frag.)	Left	SMiF	Nikon XTH 225 ST	0.03470	https://doi.org/10.17602/M2/M54499 stack https://doi.org/10.17602/M2/M54500 mesh
--	ulna (frag.)	Left	SMiF	Nikon XTH 225 ST	0.03470	https://doi.org/10.17602/M2/M54493 stack https://doi.org/10.17602/M2/M54494 mesh
40A	scaphoid	Right	SMiF	Nikon XTH 225 ST	0.01690	https://doi.org/10.17602/M2/M54216 stack https://doi.org/10.17602/M2/M54217 mesh
40B	lunate	Right	SMiF	Nikon XTH 225 ST	0.01690	https://doi.org/10.17602/M2/M54212 stack https://doi.org/10.17602/M2/M54213 mesh
40C	triquetrum	Right	SMiF	Nikon XTH 225 ST	0.01690	https://doi.org/10.17602/M2/M54222 stack https://doi.org/10.17602/M2/M54223 mesh
--	triquetrum	Left	SMiF	Nikon XTH 225 ST	0.01517	https://doi.org/10.17602/M2/M55176 stack https://doi.org/10.17602/M2/M55177 mesh

TABLE A-VI-2.— Cont'd.

Fig.	Description/element	Side	Facility	Scanner make/mod	x/y/z res	DOI
40D	pisiform	Right	SMiF	Nikon XTH 225 ST	0.01690	https://doi.org/10.17602/M2/M54214 stack https://doi.org/10.17602/M2/M54215 mesh
43A	trapezium	Left	SMiF	Nikon XTH 225 ST	0.01690	https://doi.org/10.17602/M2/M54218 stack https://doi.org/10.17602/M2/M54219 mesh
43B	trapezoid	Right	SMiF	Nikon XTH 225 ST	0.01690	https://doi.org/10.17602/M2/M54220 stack https://doi.org/10.17602/M2/M54221 mesh
--	trapezoid	Left	SMiF	Nikon XTH 225 ST	0.01517	https://doi.org/10.17602/M2/M55169 stack https://doi.org/10.17602/M2/M55171 mesh
43C	hamate	Left	SMiF	Nikon XTH 225 ST	0.01690	https://doi.org/10.17602/M2/M54210 stack https://doi.org/10.17602/M2/M54211 mesh
46A	metacarpal I (MC1)	Left	SMiF	Nikon XTH 225 ST	0.02268	https://doi.org/10.17602/M2/M38927 stack https://doi.org/10.17602/M2/M38929 mesh
--	metacarpal I (MC1)	Right	SMiF	Nikon XTH 225 ST	0.02095	https://doi.org/10.17602/M2/M54473 stack https://doi.org/10.17602/M2/M54474 mesh
46B	metacarpal II (MC2)	Right	SMiF	Nikon XTH 225 ST	0.01776	https://doi.org/10.17602/M2/M54226 stack https://doi.org/10.17602/M2/M54227 mesh
--	MC2 (proximal frag.)	Left	SMiF	Nikon XTH 225 ST	0.01776	https://doi.org/10.17602/M2/M54224 stack https://doi.org/10.17602/M2/M54225 mesh
46C	metacarpal III (MC3)	Right	SMiF	Nikon XTH 225 ST	0.01776	https://doi.org/10.17602/M2/M54228 stack https://doi.org/10.17602/M2/M54229 mesh
46D	metacarpal IV (MC4)	Right	SMiF	Nikon XTH 225 ST	0.01776	https://doi.org/10.17602/M2/M54232 stack https://doi.org/10.17602/M2/M54233 mesh
--	MC4 (proximal frag.)	Left	SMiF	Nikon XTH 225 ST	0.01776	https://doi.org/10.17602/M2/M54230 stack https://doi.org/10.17602/M2/M54231 mesh
46E	metacarpal V (MC5)	Right	SMiF	Nikon XTH 225 ST	0.01776	https://doi.org/10.17602/M2/M54234 stack https://doi.org/10.17602/M2/M54235 mesh
47A	metacarpal II (MC2)	Left	SMiF	Nikon XTH 225 ST	0.02095	https://doi.org/10.17602/M2/M54471 stack https://doi.org/10.17602/M2/M54472 mesh
47B	metacarpal III (MC3)	Left	SMiF	Nikon XTH 225 ST	0.02268	https://doi.org/10.17602/M2/M38932 stack https://doi.org/10.17602/M2/M38934 mesh
--	metacarpal IV (MC4)	Left	SMiF	Nikon XTH 225 ST	0.02268	https://doi.org/10.17602/M2/M38945 stack https://doi.org/10.17602/M2/M38948 mesh
47C	metacarpal IV (MC4)	Right	SMiF	Nikon XTH 225 ST	0.02095	https://doi.org/10.17602/M2/M54475 stack https://doi.org/10.17602/M2/M54476 mesh
47D	metacarpal V (MC5)	Right	SMiF	Nikon XTH 225 ST	0.02268	https://doi.org/10.17602/M2/M55712 stack https://doi.org/10.17602/M2/M55713 mesh
--	metacarpal V (MC5)	Left	SMiF	Nikon XTH 225 ST	0.02095	https://doi.org/10.17602/M2/M54459 stack https://doi.org/10.17602/M2/M54460 mesh
--	metacarpal	Unknown	SMiF	Nikon XTH 225 ST	0.02095	https://doi.org/10.17602/M2/M54467 stack https://doi.org/10.17602/M2/M54468 mesh
51A	proximal phalanx, proximal frag.	Unknown	SMiF	Nikon XTH 225 ST	0.02095	https://doi.org/10.17602/M2/M54479 stack https://doi.org/10.17602/M2/M54480 mesh
51B	proximal phalanx, distal frag.	Unknown	SMiF	Nikon XTH 225 ST	0.02095	https://doi.org/10.17602/M2/M54481 stack https://doi.org/10.17602/M2/M54482 mesh
51C	proximal phalanx frag.	Unknown	SMiF	Nikon XTH 225 ST	0.02246	https://doi.org/10.17602/M2/M40674 stack https://doi.org/10.17602/M2/M40675 mesh
51D	proximal phalanx	Unknown	SMiF	Nikon XTH 225 ST	0.02268	https://doi.org/10.17602/M2/M38966 stack https://doi.org/10.17602/M2/M38968 mesh
51E	proximal phalanx frag.	Unknown	SMiF	Nikon XTH 225 ST	0.02268	https://doi.org/10.17602/M2/M38975 stack https://doi.org/10.17602/M2/M38977 mesh
51F	proximal phalanx frag.	Unknown	SMiF	Nikon XTH 225 ST	0.02268	https://doi.org/10.17602/M2/M38972 stack https://doi.org/10.17602/M2/M38974 mesh
51G	proximal phalanx frag.	Unknown	SMiF	Nikon XTH 225 ST	0.02268	https://doi.org/10.17602/M2/M38969 stack https://doi.org/10.17602/M2/M38971 mesh

TABLE A-VI-2.— Cont'd.

Fig.	Description/element	Side	Facility	Scanner make/mod	x/y/z res	DOI
52A	proximal phalanx, manual	Unknown	SMiF	Nikon XTH 225 ST	0.02095	https://doi.org/10.17602/M2/M54485 stack https://doi.org/10.17602/M2/M54486 mesh
52B	proximal phalanx, manual	Unknown	SMiF	Nikon XTH 225 ST	0.02268	https://doi.org/10.17602/M2/M38963 stack https://doi.org/10.17602/M2/M38965 mesh
52C	proximal phalanx, pedal	Unknown	SMiF	Nikon XTH 225 ST	0.02246	https://doi.org/10.17602/M2/M40701 stack https://doi.org/10.17602/M2/M40702 mesh
52D	proximal phalanx, pedal	Unknown	SMiF	Nikon XTH 225 ST	0.02246	https://doi.org/10.17602/M2/M40703 stack https://doi.org/10.17602/M2/M40704 mesh
52E	proximal phalanx, pedal	Unknown	SMiF	Nikon XTH 225 ST	0.02246	https://doi.org/10.17602/M2/M40705 stack https://doi.org/10.17602/M2/M40706 mesh
52F	proximal phalanx, pedal	Unknown	SMiF	Nikon XTH 225 ST	0.02246	https://doi.org/10.17602/M2/M40708 stack https://doi.org/10.17602/M2/M40709 mesh
--	proximal phalanx, digit 1	Unknown	SMiF	Nikon XTH 225 ST	0.02095	https://doi.org/10.17602/M2/M54477 stack https://doi.org/10.17602/M2/M54478 mesh
--	proximal phalanx, proximal frag.	Unknown	SMiF	Nikon XTH 225 ST	0.02095	https://doi.org/10.17602/M2/M54483 stack https://doi.org/10.17602/M2/M54484 mesh
53A	intermediate phalanx, manual	Unknown	SMiF	Nikon XTH 225 ST	0.02095	https://doi.org/10.17602/M2/M54465 stack https://doi.org/10.17602/M2/M54466 mesh
53B	intermediate phalanx, manual	Unknown	SMiF	Nikon XTH 225 ST	0.02095	https://doi.org/10.17602/M2/M54463 stack https://doi.org/10.17602/M2/M54464 mesh
53C	intermediate phalanx, manual	Unknown	SMiF	Nikon XTH 225 ST	0.02095	https://doi.org/10.17602/M2/M54461 stack https://doi.org/10.17602/M2/M54462 mesh
53D	intermediate phalanx, manual	Unknown	SMiF	Nikon XTH 225 ST	0.02095	https://doi.org/10.17602/M2/M54469 stack https://doi.org/10.17602/M2/M54470 mesh
53E	intermediate phalanx, pedal	Unknown	SMiF	Nikon XTH 225 ST	0.02246	https://doi.org/10.17602/M2/M40695 stack https://doi.org/10.17602/M2/M40696 mesh
53F	intermediate phalanx, pedal	Unknown	SMiF	Nikon XTH 225 ST	0.02246	https://doi.org/10.17602/M2/M40697 stack https://doi.org/10.17602/M2/M40698 mesh
53G	intermediate phalanx, pedal	Unknown	SMiF	Nikon XTH 225 ST	0.02246	https://doi.org/10.17602/M2/M40699 stack https://doi.org/10.17602/M2/M40700 mesh
54A	distal phalanx	Unknown	SBU-CB	vivaCT 75	0.02500	https://doi.org/10.17602/M2/M34534 stack https://doi.org/10.17602/M2/M34536 mesh
54B	distal phalanx	Unknown	SBU-CB	vivaCT 75	0.02500	https://doi.org/10.17602/M2/M34538 stack https://doi.org/10.17602/M2/M34540 mesh
54C	distal phalanx	Unknown	SBU-CB	vivaCT 75	0.02500	https://doi.org/10.17602/M2/M34568 stack https://doi.org/10.17602/M2/M34570 mesh
54D	distal phalanx	Unknown	SBU-CB	vivaCT 75	0.02500	https://doi.org/10.17602/M2/M34573 stack https://doi.org/10.17602/M2/M34575 mesh
54E	distal phalanx	Unknown	SBU-CB	vivaCT 75	0.02500	https://doi.org/10.17602/M2/M34578 stack https://doi.org/10.17602/M2/M34580 mesh
54F	distal phalanx	Unknown	SBU-CB	vivaCT 75	0.02500	https://doi.org/10.17602/M2/M34581 stack https://doi.org/10.17602/M2/M34583 mesh
54G	distal phalanx	Unknown	SBU-CB	vivaCT 75	0.02500	https://doi.org/10.17602/M2/M34584 stack https://doi.org/10.17602/M2/M34586 mesh
54H	distal phalanx	Unknown	SBU-CB	vivaCT 75	0.02500	https://doi.org/10.17602/M2/M34588 stack https://doi.org/10.17602/M2/M34590 mesh
54I	distal phalanx	Unknown	SBU-CB	vivaCT 75	0.02500	https://doi.org/10.17602/M2/M34591 stack https://doi.org/10.17602/M2/M34593 mesh
54J	distal phalanx	Unknown	SBU-CB	vivaCT 75	0.02500	https://doi.org/10.17602/M2/M34594 stack https://doi.org/10.17602/M2/M34596 mesh
55	innominate	Left	SMiF	Nikon XTH 225 ST	0.04466	https://doi.org/10.17602/M2/M37532 stack https://doi.org/10.17602/M2/M37533 mesh

TABLE A-VI-2.— Cont'd.

Fig.	Description/element	Side	Facility	Scanner make/mod	x/y/z res	DOI
55	innominate	Right	SMiF	Nikon XTH 225 ST	0.04466	https://doi.org/10.17602/M2/M38123 stack https://doi.org/10.17602/M2/M38124 mesh
56	femur	Left	SMiF	Nikon XTH 225 ST	0.05375	https://doi.org/10.17602/M2/M37087 stack https://doi.org/10.17602/M2/M37088 mesh
56	femur	Right	SMiF	Nikon XTH 225 ST	0.05375	https://doi.org/10.17602/M2/M37091 stack https://doi.org/10.17602/M2/M37092 mesh
--	patella	Unknown	SMiF	Nikon XTH 225 ST	0.01517	https://doi.org/10.17602/M2/M55164 stack https://doi.org/10.17602/M2/M55165 mesh
--	patella	Unknown	SMiF	Nikon XTH 225 ST	0.01517	https://doi.org/10.17602/M2/M55166 stack https://doi.org/10.17602/M2/M55167 mesh
57A	tibia	Left	SMiF	Nikon XTH 225 ST	0.05105	https://doi.org/10.17602/M2/M54242 stack https://doi.org/10.17602/M2/M54243 mesh
57B	tibia	Right	SMiF	Nikon XTH 225 ST	0.05105	https://doi.org/10.17602/M2/M54244 stack https://doi.org/10.17602/M2/M54245 mesh
58A	fibula	Unknown	SMiF	Nikon XTH 225 ST	0.05105	https://doi.org/10.17602/M2/M54236 stack https://doi.org/10.17602/M2/M54237 mesh
58B	fibula	Unknown	SMiF	Nikon XTH 225 ST	0.05105	https://doi.org/10.17602/M2/M54238 stack https://doi.org/10.17602/M2/M54239 mesh
60	astragalus	Right	SMiF	Nikon XTH 225 ST	0.00979	https://doi.org/10.17602/M2/M22012 stack https://doi.org/10.17602/M2/M56417 mesh
--	astragalus	Left	SMiF	Nikon XTH 225 ST	0.02268	https://doi.org/10.17602/M2/M38797 stack https://doi.org/10.17602/M2/M38799 mesh
60	calcaneus	Right	SMiF	Nikon XTH 225 ST	0.01182	https://doi.org/10.17602/M2/M30517 stack https://doi.org/10.17602/M2/M30522 mesh
--	calcaneus	Left	SMiF	Nikon XTH 225 ST	0.02268	https://doi.org/10.17602/M2/M38800 stack https://doi.org/10.17602/M2/M38802 mesh
63A	cuboid	Right	SMiF	Nikon XTH 225 ST	0.02268	https://doi.org/10.17602/M2/M38978 stack https://doi.org/10.17602/M2/M38980 mesh
--	entocuneiform	Left	SMiF	Nikon XTH 225 ST	0.02268	https://doi.org/10.17602/M2/M38957 stack https://doi.org/10.17602/M2/M38959 mesh
63C	mesocuneiform	Right	SMiF	Nikon XTH 225 ST	0.02268	https://doi.org/10.17602/M2/M38981 stack https://doi.org/10.17602/M2/M38983 mesh
64C	ectocuneiform	Left	SMiF	Nikon XTH 225 ST	0.02268	https://doi.org/10.17602/M2/M38954 stack https://doi.org/10.17602/M2/M38956 mesh
65A	first metatarsal	Right	SBU-CB	uCT 40	0.01800	https://doi.org/10.17602/M2/M5176 stack https://doi.org/10.17602/M2/M5177 mesh
65B	metatarsal II (MT2)	Left	SMiF	Nikon XTH 225 ST	0.02189	https://doi.org/10.17602/M2/M38987 stack https://doi.org/10.17602/M2/M38989 mesh
65C	metatarsal II (MT2)	Right	SMiF	Nikon XTH 225 ST	0.02268	https://doi.org/10.17602/M2/M38984 stack https://doi.org/10.17602/M2/M38986 mesh
65D	metatarsal III (MT3)	Right	SMiF	Nikon XTH 225 ST	0.02189	https://doi.org/10.17602/M2/M38999 stack https://doi.org/10.17602/M2/M39001 mesh
--	metatarsal III (MT3)	Left	SMiF	Nikon XTH 225 ST	0.02189	https://doi.org/10.17602/M2/M38990 stack https://doi.org/10.17602/M2/M38992 mesh
65E	metatarsal IV MT4)	Right	SMiF	Nikon XTH 225 ST	0.02189	https://doi.org/10.17602/M2/M39003 stack https://doi.org/10.17602/M2/M39005 mesh
67A	metatarsal IV MT4)	Left	SMiF	Nikon XTH 225 ST	0.02189	https://doi.org/10.17602/M2/M38993 stack https://doi.org/10.17602/M2/M38995 mesh
67B	metatarsal V (MT5)	Left	SMiF	Nikon XTH 225 ST	0.02268	https://doi.org/10.17602/M2/M38960 stack https://doi.org/10.17602/M2/M38962 mesh
--	metatarsal head	Unknown	SMiF	Nikon XTH 225 ST	0.02189	https://doi.org/10.17602/M2/M38996 stack https://doi.org/10.17602/M2/M38998 mesh